UNIVERSITÄT LEIPZIG

REPORT
Institute für Physik
The Physics Institutes

2012

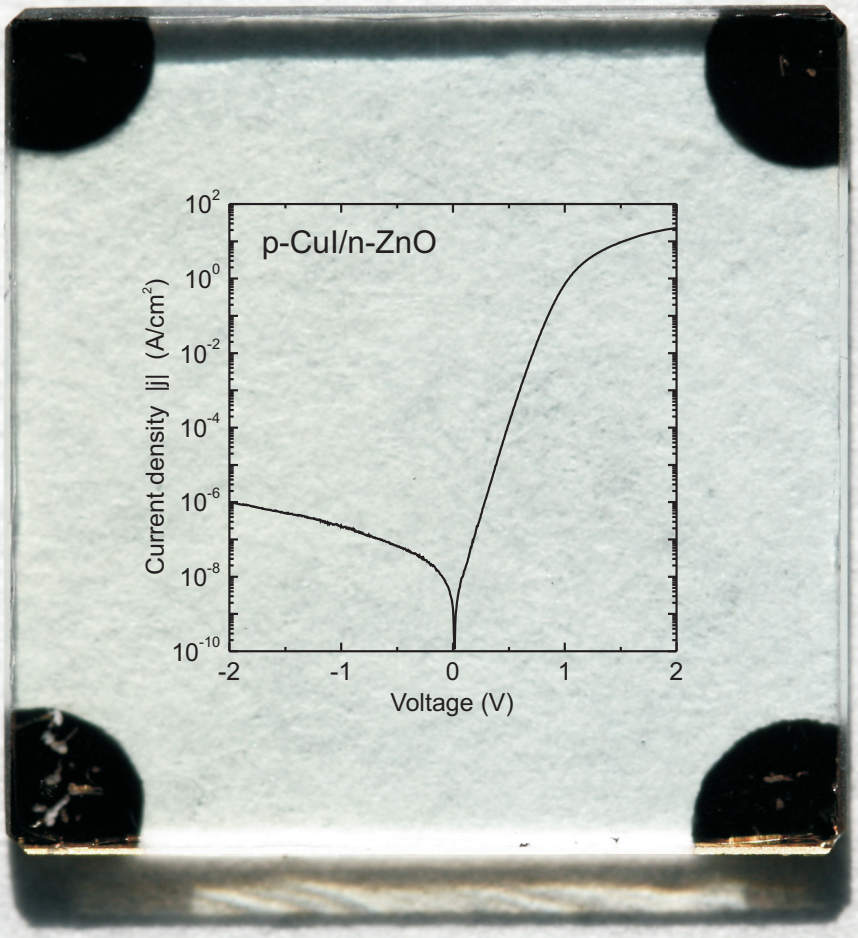

Karl Wilhelm Bädeker (1877-1914)

The Leipzig born Karl Bädeker, grandson of the founder of the Baedeker tour guides, reported 1907 in his Habilitationsschrift at Universität Leipzig the first transparent, conductive thin films, namely from cadmium oxide and copper iodide. He also achieved the first doping of semiconductors via variation of the iodine concentration in CuI. He died one hundred years ago in WWI in the battle around Liége.

Up-to-date Information on the scientific program, location, how to reach us and accomodation can be found at

www.uni-leipzig.de/~hlp/TCO2014

Registration
www.buildmona.de/TCO2014

UNIVERSITÄT LEIPZIG

TCO2014

Transparent Conductive Oxides – Fundamentals and Applications

in honor of the 100th anniversary of the death of
Prof. Dr. Karl Bädeker

29.9.-2.10.2014
Universität Leipzig
Institut für
Experimentelle Physik II
Linnéstr. 5, 04103 Leipzig

Program Committee

Pedro Barquinha, CENIMAT, Lissabon
Klaus Ellmer, HZB, Berlin
Roberto Fornari, IKZ, Berlin
Marius Grundmann, Universität Leipzig
Thomas Riedl, Universität Wuppertal
Tim Veal, University of Liverpool
Holger von Wenckstern, Universität Leipzig

The Physics Institutes of Universität Leipzig, Report 2012
M. Grundmann (Ed.)

Technical Editor: Anja Heck

Printed in Germany

online available at
http://www.uni-leipzig.de/~exph2/report_2012.pdf

Front cover
Optical image of cuprous iodide (CuI) thin film on zinc oxide (ZnO) thin film on sapphire wafer ($10 \times 10\,\mathrm{mm}^2$). At the corners are sputtered gold Hall contacts. The ZnO has been deposited by pulsed laser deposition; the CuI has been deposited by thermal evaporation of CuI powder. Inset: Current-voltage characteristics of fully transparent bipolar CuI/ZnO diode with high rectification (2×10^7 at $\pm2\,\mathrm{V}$). The transparent conductors CuI and CdO have been reported by Karl Bädeker in 1907 at Universität Leipzig for the first time.

Back covers
Recent book publications.

Institut für Experimentelle Physik I
Institut für Experimentelle Physik II
Institut für Theoretische Physik

Fakultät für
Physik und Geowissenschaften

Universität Leipzig

Institute for Experimental Physics I
Institute for Experimental Physics II
Institute for Theoretical Physics

Faculty of Physics and Earth Sciences

Universität Leipzig

Report 2012

Addresses

Institute for Experimental Physics I

Linnéstraße 5
D-04103 Leipzig, Germany
Phone: +49 341 97-32551
Fax: +49 341 97-32599
WWW: http://www.uni-leipzig.de/~physik/exp1.html
Mailing address: Postfach 100 920, D-04009 Leipzig, Germany

Institute for Experimental Physics II

Linnéstraße 5
D-04103 Leipzig, Germany
Phone: +49 341 97-32650
Fax: +49 341 97-32668
WWW: http://www.uni-leipzig.de/~physik/exp2.html
Mailing address: Postfach 100 920, D-04009 Leipzig, Germany

Institute for Theoretical Physics

Vor dem Hospitaltore 1
D-04103 Leipzig, Germany
Phone: +49 341 97-32420
Fax: +49 341 97-32548
WWW: http://www.uni-leipzig.de/~physik/thph.html
Mailing address: Postfach 100 920, D-04009 Leipzig, Germany

Preface

Welcome to the 2012 Report of the Physics Institutes of the Universität Leipzig presenting to you an overview of our research in numerous projects. We have enjoyed research and interaction with colleagues and partners worldwide. We are grateful to our guests for enriching our academic year with their contributions in the colloquium and within the work groups.

We are happy to welcome three new colleagues, one in each of the three institutes. In the winter term 2012/13 the Institute for Theoretical Physics welcomed Prof. Stefan Hollands working in the field of elementary particle physics with special emphasis on cosmology and structure formation (clusters, galaxies, etc.) in the early universe. He will closely cooperate with the Max Planck Institute for Mathematics in the Sciences (MPI MIS). Mrs Prof. Claudia Mierke has started in October 2012 in the Institute for Experimental Physics I. She leads the new Department of Biological Physics. Her expertise is on cellular biological physics in the field of maligant progression of cancer due to motility of cancer cells in connective tissue and their ability to transmigrate through the endothelium into blood or lymph vessels. Prof. Jan Meijer has started in January 2013 as head of the nuclear solid state physics group in the Institute for Experimental Physics II. He is reknown for high precision implantation and the creation and investigation of NV centers in diamond. He will expand activities with the LIPSION ion accelerator and also closely cooperate with the Leibniz-Institute for Surface Modification (IOM).

After several years of interim solutions and moving labs, the Technikum/Analytikum (Linnéstr. 3) is fully renovated and has been reopened, offering great conditions regarding infrastructure, media and safety. Also close cooperation with colleagues from chemistry is facilitated. In July/August 2012 the Institute for Theoretical Physics moved into the new office building in Brüderstr. 16, offering a good infrastructure (including the kindergarten "Einsteinchen" in the ground floor).

The BuildMoNa 2012 Minisymposium on 'Quantum Coherent Structures' focused on Bose-Einstein condensation of exciton-polaritons, topological insulators and hybrid structures, and coherent transport in graphene. Theoretical and experimental experts discussed at the symposium how quantum coherence in systems with restricted geometry or topology can lead to novel quantum phases and offers exciting new perspectives for the applications of low-energy and soft modes in hard condensed matter.

Work in the newly established DFG Forschergruppe 1616 'Dynamics and Interactions of Semiconductor Nanowires for Optoelectronics' has started in July 2012; the semiconductor physics group contributes with fabrication and investigation of nanowires conformally coated with Bragg mirrors. Also Mrs Dr. Helena Franke received a young investigator position in the research unit. Cooperation of the Institute for Experimental Physics II with the Leibniz-Institute for Surface Modification (IOM)

is intensified in the framework of a joint project on nanoscopic mechanical surface properties awarded within the Senatsausschuss Wettbewerb (competition) by the Wissenschaftsgemeinschaft Gottfried Wilhelm Leibniz. A new Institute Partnership of the computational physics group with the Institute for Condensed Matter Physics of the National Academy of Sciences of Ukraine in Lviv commenced its work in April 2012 and will be funded by the Alexander von Humboldt Foundation until 2015.

The extent of our activities is only possible with the generous support from various funding agencies for which we are very grateful and which is individually acknowledged in the brief reports.

Leipzig,
June 2013

M. Grundmann
W. Janke
K. Käs
Directors

Contents

1

Structure and Staff of the Institutes

1.1 Institute for Experimental Physics I

1.1.1 Office of the Director

Prof. Dr. Josef A. Käs (director)
Prof. Dr. Frank Cichos (vice director)

1.1.2 Molecular Nano-Photonics, Molekulare Nanophotonik [MON]

Prof. Dr. Frank Cichos

Technical staff

Dipl.-Phys. Uwe Weber

PhD candidates

Subhasis Adhikari
Nicole Amecke
Marco Braun
Andreas Bregulla
André Heber
Lars Heerklotz
Selmke Markus
Nils Neubauer
David Plotzki
Martin Pumpa
Romy Schachoff
Rebecca Wagner

1.1.3 Molecular Physics, Molekülphysik [MOP]

Prof. Dr. F. Kremer

Secretary

Karin Girke (till March 2012)
Kerstin Lohse

Technical staff

Hartmut Domröse (till October 2012)
Dipl.-Phys. Cordula Bärbel Krause
Dipl.-Ing. Jörg Reinmuth
Dipl.-Phys. Viktor Skokow

Academic staff

Dr. Mahdy Elmahdy
Dr. Christof Gutsche
Dr. Ciprian Ghiorghita Iacob
Dr. Malgorzata Jasiurkowska (till June 2012)
Dr. Joshua Rume Sangoro (till March 2012)

PhD candidates

Dipl.-Phys. Markus Anton
Wycliffe Kiprop Kipnusu, M.Sc.
Dipl.-Phys. Wilhelm Kossack
Emmanuel Urandu Mapesa, M.Sc.
Dipl.-Phys. Nils Neubauer
Ilya Semenov, M.Sc. (till August 2012)
Dipl.-Phys. Tim Stangner
Dipl.-Phys. Martin Treß
Dipl.-Phys. Olaf Ueberschär
Dipl.-Phys. Carolin Wagner

Students

Ludwig Popp
Lisa Schade
Benjamin Suttner

1.1.4 Physics of Interfaces, Grenzflächenphysik [GFP]

PD. Dr. Frank Stallmach
Prof. Dr. Jörg Kärger (retired)
Prof. Dr. Dieter Freude (retired)

Academic staff

Dr. Christian Chmelik
Dr. Rustem Valiullin

PhD candidates

Dipl.-Phys. Steffen Beckert
Dipl.-Phys. Tomas Binder
Dipl.-Phys. Carsten Horch
Dipl.-Math. Daria Kondrashova
Alexander Lauerer, M.Sc.
Mgr. Mikulas Peksa
Dipl.-Phys. Anne-Kristin Pusch
Dipl.-Phys. Christian Reichenbach
Dipl.-Phys. Alexander Shakhov
Dipl.-Phys. Tobias Titze
Dipl.-Phys. Philipp Zeigermann

1.1.5 Soft Matter Physics, Physik der weichen Materie [PWM]

Prof. Dr. Josef A. Käs

Secretary

Claudia Brück

Technical staff

Dr. Undine Dietrich
Dipl.-Phys. Bernd Kohlstrunk
Ing. Elke Westphal

Academic staff

Dr. Claus Fütterer
Dr. Mareike Zink

PhD candidates

Silke Agte, M.Sc.
Uta Allenstein, M.Sc. (zusammen mit Prof. Mayr, IOM)
Dipl.-Phys. Anatol Fritsch
Dipl.-Phys. Tina Händler
Paul Heine, M.Sc.
Thomas Fuhs, M.Sc.
Markus Gyger, M.Sc.
Dipl.-Phys. Chris Händel Dipl.-Phys. Florian Huber
Dipl.-Phys. Tobias Kießling
Dipl.-Math. Melanie Knorr
Kenechukwu David Nnetu, M.Sc.
Dipl.-Phys. Steve Pawlizak
Saddam Moyazur Rahman, M.Sc. (BBZ, Forschergruppe M. Zink)
Dipl.-Phys. Philipp Rauch
Susanne Rönicke, M.Sc.
Dipl.-Phys. Sebastian Schmidt
Dipl.-Phys. Jörg Schnauß
Dipl.-Phys. Carsten Schuldt
Dipl.-Ing. Roland Stange
Dipl.-Phys. Dan Strehle
Dipl.-Phys. Enrico Warmt
Dipl.-Phys. Franziska Wetzel
Dipl.-Phys. Lydia Woiterski

Students

Dave Ahrens
Hendrik Brehme
Tobias Eggebrecht
Julia Fischer
Sabrina Friebe
Martin Glaser
Tom Golde
Steffen Grosser
Nico Herbig
Tim Hohmann
Maximilian Ilse
Bernd Käßemodel
Michael Krahe
Hans Kubitschke, M. Sc.
Tom Kunschmann
Tony Kurth
Kao-Nung Lin
Jürgen Lippoldt
Erik Morawetz

Peter Palm
Wolfram Pönisch
Stefanie Puder
Florian Rämisch
Lydia Reuter
Markus Sommerfeld
Tobias Thalheim
Astrid Weidt
Iris Wenzel
Benjamin Winkler

1.2 Institute for Experimental Physics II

1.2.1 Office of the Director

Prof. Dr. Marius Grundmann (director)
Prof. Dr. Pablo Esquinazi (vice director)

1.2.2 Magnetic Resonance of Complex Quantum Solids, Magnetische Resonanz Komplexer Quantenfestkörper [MQF]

Prof. Dr. Jürgen Haase

Secretary

Sophie Kirchner

Technical staff

Dipl.-Phys. Gert Klotzsche
Dipl.-Ing. Kathrin Koch
Benno Krüger

Academic staff

Dr. Marko Bertmer
apl. Prof. Dr. Andreas Pöppl
Dr. Damian Rybicki

PhD candidates

Dipl.-Phys. Ingo Hilschenz
Dipl.-Phys. Benno Meier
Dipl.-Phys. Thomas Meißner
Dipl.-Phys. Gregor Thörmer
Dipl.-Phys. Alexander Jäger

Dipl.-Chem. Bettina Jee
Dipl.-Phys. Jonas Kohlrautz
Dipl.-Phys. Sebastian Sambale
Dipl.-Phys. Matthias Mendt
Farhana Gul-E-Noor, M.Sc.
Anusree Viswanath Kuttatheyil, M.Sc.
Michael Jurkutat, M.Sc.
Steven Reichardt, M.Sc.
Dimo Ivanov, M.Sc.
Kathrin Lorenz, M.Sc.
Nataliya Georgieva, M.Sc.
Thomas Meier, M.Sc.
Emmanouil Veroutis, M.Sc.

Students

Stefan Friedländer
Robin Gühne
Tobias Herzig
Richard Lange

1.2.3 Nuclear Solid State Physics, Nukleare Festkörperphysik [NFP]

Dr. Daniel Spemann

Technical staff

Carsten Pahnke
Dipl.-Ing. Joachim Starke

Academic staff

Dr. Daniel Spemann
Dr. Jürgen Vogt

PhD candidates

Dipl.-Phys. Tobias Andrea
Nirav Barapatre, M.Sc.
Dipl.-Inf. B.Sc. Markus Jäger
Dipl.-Phys. Steffen Jankuhn
Dipl.-Phys. Martin Rothermel

Students

Sascha Becker
David Diering

Nico Klingner
Michael Mensing
Olga Naumov
Pan Zhichao
Jeremy Perez
Annemarie Sickert
Ralf Wunderlich

1.2.4 Semiconductor Physics, Halbleiterphysik [HLP]

Prof. Dr. Marius Grundmann

Secretary

Anja Heck Birgit Wendisch

BuildMoNa Office

Dr. Alexander Weber (Officer)
Birgit Wendisch (Secretary)

Technical staff

Sascha Bader
Dipl.-Phys. Gabriele Benndorf
Dr. Jens Gabke
Monika Hahn
Dipl.-Ing. Holger Hochmuth
Dipl.-Phys. Jörg Lenzner
Dipl.-Phys. Axel Märcker
Gabriele Ramm
Roswitha Riedel

Academic staff

Dr. Heiko Frenzel
Prof. Dr. Michael Lorenz
Dr. Alexander Müller
PD. Dr. Rainer Pickenhain
Prof. Dr. Bernd Rheinländer (retired)
Dr. Rüdiger Schmidt-Grund
Dr. Chris Sturm
Dr. Alexander Weber
Dr. Holger von Wenckstern

PhD candidates

Henner Bieligk, M.Sc.
Dipl.-Phys. Tammo Böntgen
Michael Bonholzer, M.Sc.
Dipl.-Phys. Kerstin Brachwitz
Dipl.-Phys. Christof Peter Dietrich
Dipl.-Phys. Helena Franke
Robert Karsthof, M.Sc.
Sherzod Khujanov, M.Sc.
Dipl.-Phys. Fabian Klüpfel
Dipl.-Phys. Christian Kranert
Dipl.-Phys. Alexander Lajn
Dipl.-Phys. Martin Lange
Dipl.-Phys. Michael Lorenz
Abdurashid Mavlonov, M.Sc.
Dipl.-Phys. Stefan Müller
Anna Reinhardt, M.Sc.
Dipl.-Phys. Friedrich-Leonhard Schein
Dipl.-Phys. Florian Schmidt
Dipl.-Phys. Matthias Schmidt
Peter Schwinkendorf, M.Sc.
Dipl.-Phys. Marko Stölzel
Martin Thunert, M.Sc.
Tao Wang, M.Sc.
Zhang Zhipeng, M.Sc.

Students

Sofie Bitter
Eike Lennart Fricke
Christian Heinrichs
Sören Herath
Markus Jenderka
Max Kneiß
Oliver Kramer
Hannes Krauß
Silvia Kunz
Stefan Lange
Tobias Lühmann
Tom Michalsky
Markus Purfürst
Steffen Richter
Katharina Rudisch
Michael Scheibe
Peter Schlupp
Daniel Splith

Robert Staacke
Markus Winter
Vitaly Zviagin

1.2.5 Solid State Optics and Acoustics, Festkörperoptik und -akustik [FKO]

Prof. Dr. Wolfgang Grill

Secretary

Annette Käthner

Technical staff

PTA Hans-Joachim vom Hofe
Dipl.-Ing. (FH) Ulrike Teschner

Academic staff

Dr. Mieczyslaw Pluta

PhD candidates

Amro Abdelrahman, M.Sc.
Esam Eldin Ahmed Mohamed, M. Sc.
Dipl.-Phys. Erik von der Burg
Dipl.-Phys. Moritz von Buttlar
Albert Kamanyi, M.Sc. Zakir Hossain Muhammad, M.Sc.

1.2.6 Superconductivity and Magnetism, Supraleitung und Magnetismus [SUM]

Prof. Dr. Pablo Esquinazi

Secretary

Sandy Ehlers

Technical staff

Dr. Winfried Böhlmann
Klaus Grünwald
Dipl.-Krist. Annette Setzer

Academic staff

Dr. José Barzola-Quiquia
Mr. Mohtashim Ahmad Bukhari
Dr. Israel Villalba-Lorite
Dr. Prasanta Kumar Muduli
PD Dr. Michael Ziese

PhD candidates

Ana Ballestar, M.Sc.
Francis Bern, M.Sc.
Srujana Dusari, M. Sc.
Muhammad Khalid, M.Sc.
Chunhai Yin, M.Sc.

Students

Julia Tesch
Mahsa Zoraghi
Justus Krüger
Tobias Lehmann
Manuel Lindel
Axel Molle
Thomas Scheike
Johann Schmidt
Markus Stiller

1.3 Institute for Theoretical Physics

1.3.1 Office of the Director

Prof. Dr. Wolfhard Janke

Secretary

Susan Hussack
Gabriele Menge
Lea Voigt

1.3.2 Computational Quantum Field Theory, Computerorientierte Quantenfeldtheorie [CQT]

Prof. Dr. Wolfhard Janke

Technical staff

–

Academic staff

Dr. Stefan Schnabel
Prof. Dr. Handan Arkın-Olgar

PhD candidates

Dipl.-Phys. Mathias Aust
Dipl.-Phys. Rainer Bischof
Dipl.-Phys. Mario Collura (jointly with Nancy Université)
Dipl.-Phys. Niklas Fricke
Dipl.-Phys. Martin Marenz
Dipl.-Phys. Monika Möddel
Dipl.-Phys. Marco Müller
Dipl.-Phys. Hannes Nagel
Dipl.-Phys. Andreas Nußbaumer
Dipl.-Phys. Jeremi Ochab (jointly with Jagiellonian University Krakow)
Dipl.-Phys. Sebastian Schöbl
Dipl.-Phys. Micha Wiedenmann
M.Sc. Johannes Zierenberg

Students

Eugen Ehrenpreis
Johannes Bock
Max Gerlach
Momchil Ivanov
Thomas Peschel
Benjamin Schott
Felix Schramm
Arnd Tretbar
Christoph Vogelsberg
Andreas Wagner
Robert Wiesen

1.3.3 Molecular Dynamics / Computer Simulation, Moleküldynamik / Computersimulation [MDC]

PD Dr. S. Fritzsche (Speaker)

Academic staff

PD Dr. S. Fritzsche

PhD candidates

P. Pilvar, M.Sc.
U. Arsawang, M.Sc.

Students

P. Schierz

1.3.4 Quantum Field Theory and Gravity, Quantenfeldtheorie und Gravitation [QFG]

Prof. Dr. Gerd Rudolph (Speaker)
Prof. Dr. Rainer Verch

Academic staff

PD Dr. Michael Bordag
Dr. Gandalf Lechner
Dr. José M. Muñoz-Castañeda
Dr. Matthias Schmidt

Retired

Prof. em. Bodo Geyer
Prof. em. Armin Uhlmann

PhD candidates

Zhirayr Avetisyan, M.Sc.
Dipl.-Phys. Marcus Borris
Dipl.-Phys. Benjamin Eltzner
Erik Fuchs, M.Sc.
Michael Gransee, M.Sc.
Dipl.-Phys. Thomas Ludwig
Dipl.-Phys. Jan Zschoche

Students

Andreas Andersson
Richard Busch
Tobias Diez
Mathias Hänsel
Danny Krause

Thomas Ludwig
Adam Reichold
Johannes Zähle

1.3.5 Statistical Physics, Statistische Physik [STP]

Prof. Dr. Bernd Rosenow

Academic staff

Dr. Mats Horsdal
Dr. Timo Hyart
Dr. Daniel. D. Scherer
Dr. Tony Wright

PhD candidates

Dipl. Phys. Alexander Janot
Lukas Kimme, M. Sc.
Mirco Milletari, M. Sc.
Martin Treffkorn, M. Sc.
Dipl. Phys. Björn Zocher

Students

Christoph Lehmann
Christian Scheidler
Alexander Schneider
Alexander Uhlig
Heinrich-Gregor Zirnstein

1.3.6 Theory of Condensed Matter, Theorie der kondensierten Materie [TKM]

Prof. Dr. Ulrich Behn (Speaker)
Prof. Dr. Klaus Kroy

Prof. Dr. Dieter Ihle (retired)
Prof. Dr. Adolf Kühnel (retired)

PhD candidates

Dipl.-Phys. Jakob Tómas Bullerjahn
Gianmaria Falasco, M.Sc.
Dipl.-Phys. Andrea Kramer
Rüdiger Kürsten, M.Sc.

Dipl.-Phys. Marc Lämmel
Dipl.-Phys. Holger Schmidtchen
Dipl.-Phys. Sebastian Sturm
Guillermo Zecua, M.Sc.

Students

Sven Auschra, B.Sc.
Matti Gralka, B.Sc.
Marc Höll
Michaela Kettner, B.Sc.
Rüdiger Kürsten, B.Sc.
Anne Meiwald, B.Sc.
Richard Pfaller, B.Sc.
Heinz Sachsenweger, B.Sc.
Robert Schulz, M.A.
Andreas Hübner

1.3.7 Theory of Elementary Particles, Theorie der Elementarteilchen [TET]

Prof. Dr. Klaus Siboldt (retired)

Academic staff

Dr. Meinulf Göckeler
PD Dr. Roland Kirchner
Dr. Yi Liao
PD Dr. Arwed Schiller

PhD candidates

Dipl.-Phys. Christoph Dehne
Dipl.-Phys. Alexander Ivanov

Students

Tobias Reichenbach
Robert Feldmann

I

Institute for Experimental Physics I

2

Molecular Nano-Photonics

2.1 Introduction

The challenge of experimental physics on the nanoscale is to access local phenomena, that occur for example at interfaces, at specific molecular sites or at certain places within nano-structured materials. These local phenomena may control molecular dynamics, drive self-organization, cause charge separation or alter light propagation. Their importance extends to almost every field involved in future nanotechnology. The research of the molecular nano-photonics group thus aims at the development and application of optical techniques to access nanoscale (dynamical) processes in various fields such as chemical physics, biology or semiconductor physics. The understanding of these dynamical processes shall ultimately lead to a control over single molecules and other nano-objects by applying heat, flow, shear forces, electric fields or current.

The main experimental tool within our research is optical single molecule detection by ultra-sensitive microscopic techniques including time-resolved confocal microscopy, wide-field fluorescence or photothermal microscopy. Single molecules, semiconductor quantum dots or single metallic nanoparticles provide ideal local probes to access nanoscale physical properties inside materials while keeping the information on the heterogeneity of the system. Using these techniques recent projects focused on the

- Photothermal detection of single gold nanoparticles and nanorods
- Thermally propelled particles and micromachines
- Nanometric phase transitions in liquid crystalline systems
- Heat conduction at the nanoscale
- Electrochemical manipulation of the emission of colloidal semiconductor nanocrystals
- Angle resolved spectroscopy of photonic crystals

During the year 2012 the Molecular Nanophotonics Group has celebrated a number of achievements. Among them are:

- The groups student and their results have been awarded with several poster prizes on national and international conferences (Frühjahrstagung der Deutschen

Physikalischen Gesellschaft, International Conference on Holeburning and Single Molecule Spectroscopy, European Optical Society Meeting)

- The group has successfully participated in the first national short film festival for nanoscience ãNanospotsÒ funded by the Martin Luther University Halle and the Gesellschaft für Wissenschaftskommunikation science2public.

Collaborations with the group of Prof. Dr. Klaus Kroy (Universität Leipzig), Prof. Dr. Michael Mertig (TU Dresden) and Prof. Dr. Haw Yang (Princeton University) have been very fruitful. Collaborative measurements with the groups of Prof. Dr. Friedrich Kremer and Prof. Dr. Marius Grundmann have been carried out.

Frank Cichos

2.2 Individually Tunable Micromachines Driven by Laser-induced Self-propelled Thermophoresis

A. Bregulla, F. Cichos

Temperature gradients along the surface of micro- and nanoparticles in solution cause an interfacial liquid flow, which leads to a phoretic motion of particles. Such temperature gradients can either be created externally by heat sources or by the particle itself. The latter case has been explored in this project by coating polystyrene particles partly with a thin gold layer (so called Janus particles). This thin gold layer can be heated optically via its plasmon resonance. It has been shown in previous experiments by the group, that this temperature gradient leads to a self-propelled motion of the particles with a velocity of several micrometers per second. The particle moves with the uncoated side forward but its motion is randomized by rotational diffusion. In collaboration with the group of Prof. Haw Yang at the Princeton University, we have demonstrated that a simple optical feedback mechanism can be applied to exploit the rotational diffusion to trap or steer the particles in solution without optical gradient forces. This feedback mechanism is termed photon nudging and analyzes the orientation and position of a Janus particle in real time. If the particle direction is pointing towards a target, a laser is switched on to drive the self-propelled motion towards the target. Thus the rotational diffusion is used to stochastically drive the particle at the right times. Thereby, trapping and steering have been achieved (see Figure 2.1). The localization accuracy achieved is about the particle diameter and scales with the particle radius. Thus is shall be possible to achieve even better localization accuracies for smaller particles. This is a considerable advantage as compared to optical tweezers, since they require extremely high trapping intensities for small particles. This method is extendable to multiple particles which can be steered simultaneously on individual trajectories. In summary, this switchable self-propelled motion of Janus particles delivers new ways to control particle motion by feedback mechanisms. Thus new studies of the interaction and dynamics of swarming particles will become possible.

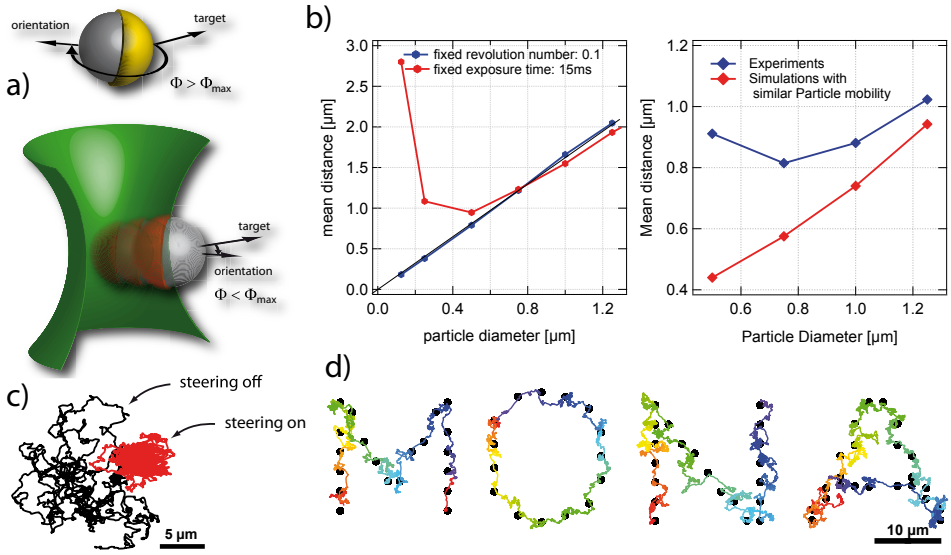

Figure 2.1: *a)* Principle of the Janus particle steering. The particle position and orientation is analyzed in real time. If the particle orientation points towards the target, the gold cap of the particle is heated to cause a directed motion. *b)* (left) Mean distance from the target obtained out of simulations as a function different Janus particles sizes. In the case of a fixed exposure time, the mean distance diverges for smaller particle sizes. For an exposure time which scales with the rotation correlation time of the rotational diffusion a linear dependence on the particle size is achieved. (right) Comparison between experimentally obtained data and simulated trajectories. *c)* example trajectory for a steered particle (red) and an unheated particle (black). *d* Steered particle with a series of targets (black points).

2.3 Gold Nanostructure Assisted Thermophoretic Trapping of Single Nanoobjects

M. Braun, F. Cichos

The manipulation and trapping of nano-objects that undergo Brownian motion are of increasing interest in soft-matter sciences. Optical tweezing is the most common technique for the trapping of individual particles in solution and is based on the optical gradient force. Hence, a sufficiently high polarizability of the particle in the solution is required. While it is thus easy to trap single dielectric particles larger than 100 nm, a trapping of smaller objects such as single molecules by means of optical forces can hardly be realized. Molecular trapping can be achieved e.g. by a technique called Anti-Brownian Electrokinetic trap (ABEL trap), which exploits the feedback controlled electric field of four electrodes. However, the latter technique requires electrical contacts, which introduce difficulties when fabricating multiple traps. In this project we develop an all-optical technique which replaces the electric fields by highly localized thermal fields. The so-called thermophoretic trap exploits thermophoretic interactions of a particle placed in a temperature gradient in solution, which locally distorts the screening of the surface charges and by that induces a particle drift. In our approach, the temperature field is generated by an optically heated Au nanostructure. Due to the small dimensions of the heat sources, even a small temperature increase introduces

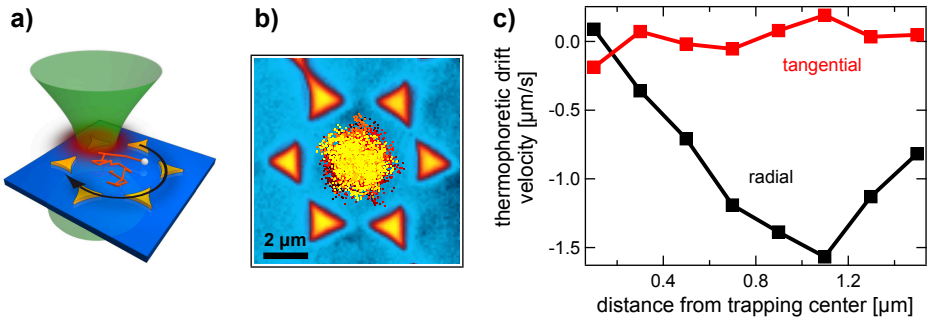

Figure 2.2: *a)* Sketch of the focused heating beam, only one gold island of the open structure is heated at a time. *b)* Trajectory points of a 200 nm PS sphere thermally trapped within an open gold structure. *c)* Dependence of the radial (black) and tangential (red) thermophoretic drift on the distance to the center of the trap for a laser rotation frequency of 18.9 rev/s.

large temperature gradients causing a strong thermophoretic drift through which the motion of a diffusing particle can be manipulated.
Therefore, hexagonal arrays of Au islands (50 nm in height) are manufactured by microsphere lithography, where gold is thermally evaporated onto a monolayer of polystyrene microspheres, which are later removed by ultra-sonification. Diffusing nanoparticles are then confined between a cover slide carrying the gold array and a blank cover slide, but undergo free diffusion in lateral directions. By means of a resonant laser beam the gold islands are heated and the Brownian motion of a particle can be restricted to a small trapping region as shown in fig. 2.2, b). For this purpose, the focused laser beam is rapidly steered in a circle over the gold structure (e.g. about 19 rev/s), such that the particle experiences a mean temperature field with a local minimum in the center. The temperature gradient induces a thermophoretic drift of the particle in radial direction, see fig. 2.2, c). The strength of the confinement can be adjusted by the heating beam intensity.

This new all-optical technique for the manipulation of nano-objects enables long-time observations of not only single but also multiple nano-objects without applying strong optical or electric fields. Also, with the hexagonal array, it is easily possible to set up many nearby traps, which can be individually controlled by the heating laser beam.

2.4 Photothermal Rutherford Scattering

M. Selmke, F. Cichos

The study of the thermal properties and the absorption of light by liquid or solid samples and interfaces has been the subject of photothermal spectroscopy. For more than 50 years, several versions of the macroscopic pump probe approach have been developed. The absorption of a heating (pump) laser leads to a well-defined temperature and thereby also to a corresponding refractive index field in the sample. This refractive index perturbation is probed via a second laser either interferometrically, via beam lensing or beam deflection [1]. Over the past decade, the first two approaches have been adapted to optical far-field microscopy setups [2, 3], where diffraction limited

beams have been used to generate and probe even individual absorbing molecules. The refractive index perturbations in these photothermal detection schemes exhibit a characteristic radially symmetric profile $n(r) = n_0 + \Delta n R r^{-1}$, decaying with the inverse distance r from the absorber and to half its value at twice the radius R of the absorber, typically a few nanometers only and thereby well below the wavelength of the light used.
In a series of recent publications, the group has characterized and quantified the electromagnetic scattering in photothermal single particle microscopy. A clear physical picture of the signal was hereby acquired. While geometrical optics concepts have been commonly used to describe the macroscopic probing schemes, the intrinsically nano-scopic nature of the refractive index change in the microscopy variants seemed to disallow for the application of such concepts. The rigorous analysis however showed, that many similarities connect the two disciplines and that the picture of a thermal lens well describes the entire phenomenology of the photothermal signal of singe nanoparticles.

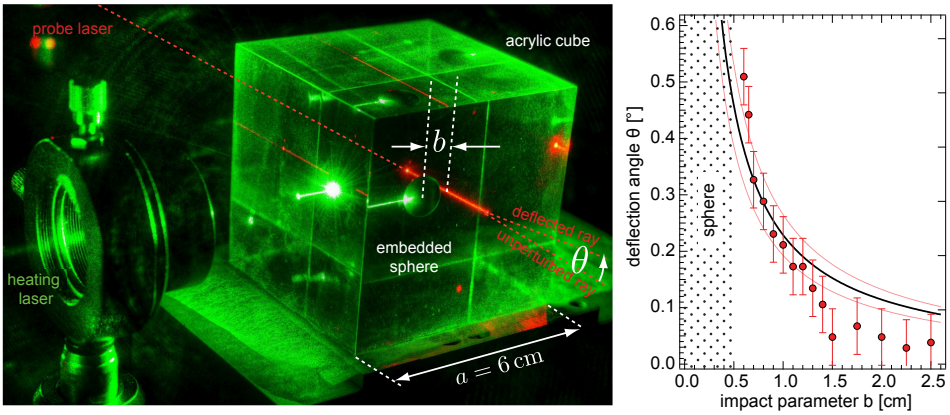

Figure 2.3: Macroscopic experimental realization of photonic Rutherford scattering. A metal sphere of radius $R = 0.5\,\text{cm}$ is embedded in an acrylic cube of side length $a = 6\,\text{cm}$. A green laser with power $P = 1\,\text{W}$ is focused into a small hole drilled into the sphere. The probing laser in the refractive index field $n(r)$ follows the classical hyperbolic Rutherford trajectory and is deflected by an angle θ.

Within this project, an analogy between the probe beam scattering by the thermal lens and the scattering of charged particles, known as Rutherford scattering, has been investigated. While the Coulomb potential $\propto r^{-1}$ leads to the well-known hyperbolic trajectories of particles and their characteristic deflections, the thermal lens $n(r)$ acts as a photothermal potential for the light of the probing laser beam. In the geometrical optics limit, a ray of light is refracted accordingly, see Fig. 2.3, and the phenomenon has been termed photonic Rutherford scattering. For a given impact parameter b, the ray is deflected by an angle θ determined by an adopted version of Rutherford's original result $\cot(\theta/2) = -n_0 b/\Delta n R$.
This analogy has been extended to wave-optics appropriate for photothermal microscopy. To this end, the inhomogeneous wave-equation for the thermal lens field has been solved along the lines of the quantum mechanical Coulomb scattering of wave-packets. This more rigorous description of light scattering by the thermal lens entails the geometrical description as the zero-wavelength limit $\lambda \to 0$, see Fig. 2.4a).

However, it further shows that even for tightly focused beams in photothermal microscopy experiments, a similar deflection may be observed, Fig. 2.4b). Experimentally, this deflection was measured using a quadrant photodiode in an otherwise unaltered transmission photothermal microscopy setup, see Fig. 2.4c,d,e). This detection scheme represents a novel microscopic counterpart to the macroscopic deflection or mirage spectroscopy.

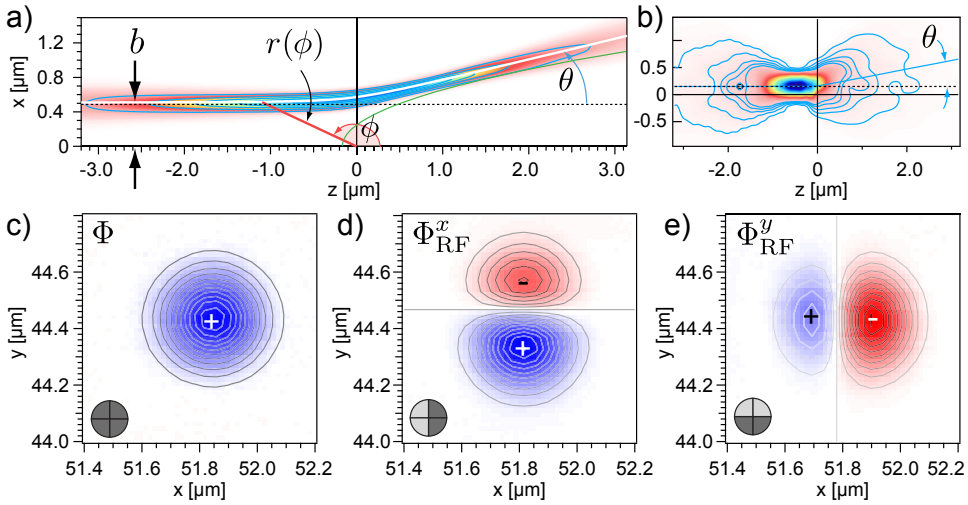

Figure 2.4: *a)* A weakly focused beam which is scattered by the photothermal potential closely follows the Rutherford trajectory $r\left(\phi\right)$. *b)* Under realistic conditions in photothermal microscopy the probe beam is strongly focused and aberrated. Still, the wave-mechanical solution shows that the beam is deflected approximately by the classical angle θ. *c)* Photothermal lens signal of conventional PT microscopy. *d,e)* Photothermal deflection signal in Rutherford scattering microscopy. The deflection is measured by the appropriate difference channels of a quadrant photodiode.

[1] S.E. Bialkowski, *Photothermal Spectroscopy Methods for Chemical Analysis*, John Wiley and Sons, Inc. (1996).

[2] S. Berciaud, L. Cognet, G.A. Blab, B. Lounis: *Photothermal Heterodyne Imaging of Individual Non-fluorescent Nano-objects*, Phys. Rev. Lett. **93**(25), 257402 (2004).

[3] A. Gaiduk, M. Yorulmaz, P.V. Ruijgrok, M. Orrit: *Room-temperature Detection of a Single Molecule's Absorption by Photothermal Contrast*, Science **330**(6002), 353-356 (2010).

2.5 Photothermal Signal Distribution Analysis

M. Braun, M. Selmke, R. Schachoff, F. Cichos

Our analysis of the signal generation mechanism in photothermal microscopy has shown, that the detection volume of this far field optical microscopy method is split into two sub-volumes, constituting a twin-focus. In these two sub-volumes, the photothermal signal is either positive or negative, respectively, see Fig. 2.5a). The twin-focal

volume is the direct consequence of the lensing action of the refractive index profile around a heated nanoparticle. This feature was previously shown to be advantageous in photothermal correlation spectroscopy (PhoCS), which has a great potential as a local probe for applications in biophysics similar to the well known fluorescence correlation spectroscopy (FCS). We have further advanced this promising method by a supple-

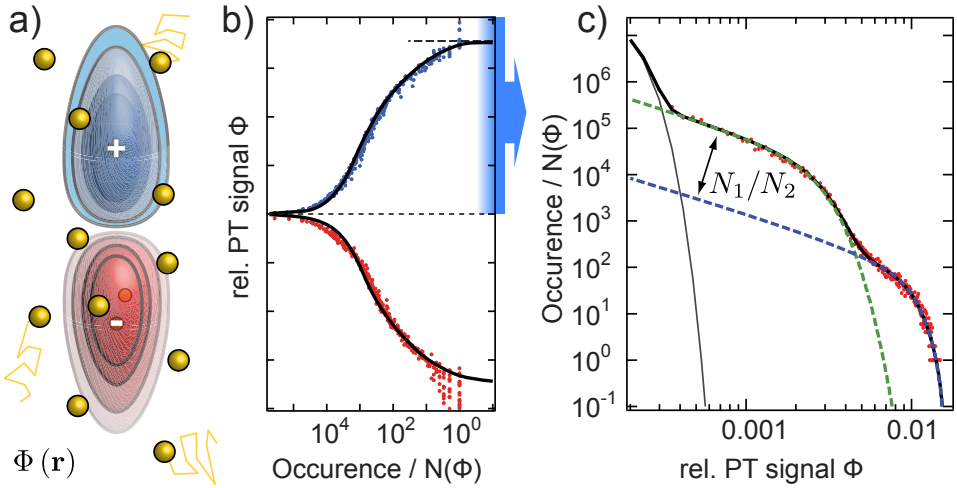

Figure 2.5: *a)* Photothermal signal detection volume for absorbing nanoparticle showing two sub-volumes. Particles diffusing through it cause a corresponding signal which is recorded over time. *b)* Exemplary histogram of such a signal time-trace for $R = 30\,\text{nm}$ gold nanoparticles diffusing in water. *c)* Binary mixture of $R = 20\,\text{nm}$ and $R = 30\,\text{nm}$ gold nanoparticles showing a characteristic step-feature.

menting signal distribution analysis framework. Using the statistics of the photothermal signal recorded for diffusing absorbing tracer particles, heterogeneous mixtures of different particle species and their size-distributions can be characterized. Figure 2.5b,c) exemplarily show experimental histograms of a signal time-trace recorded of a single species with a a finite size-distribution and the histogram of just the positive signal for a mixture of two species. The distinct features introduced by size-heterogeneities and mixtures can be readily analyzed and yield information which is otherwise unattainable through correlation analysis alone.

2.6 Photothermal Single Particle Microscopy in Liquid Crystals

A. Heber, M. Braun, M. Selmke, M. Pumpa, F. Cichos

Photothermal single particle microscopy is based on a refractive index change induced by a local temperature rise. This temperature rise is the result of nonradiative processes in the absorber which cause the release of heat into the local environment. While the temperature rise around such an absorber can be adjusted by changing the amount of absorbed optical power, the refractive index change with temperature is largely limited by the material's volumetric expansion coefficient and typically of the order of $10^{-4}\,\text{K}$. To achieve a high signal to noise ratio a lock-in detection scheme is used in which the

optical heating power is modulated. Its influence on the optical properties is detected by a second nonresonant laser being demodulated by a lock-in amplifier.

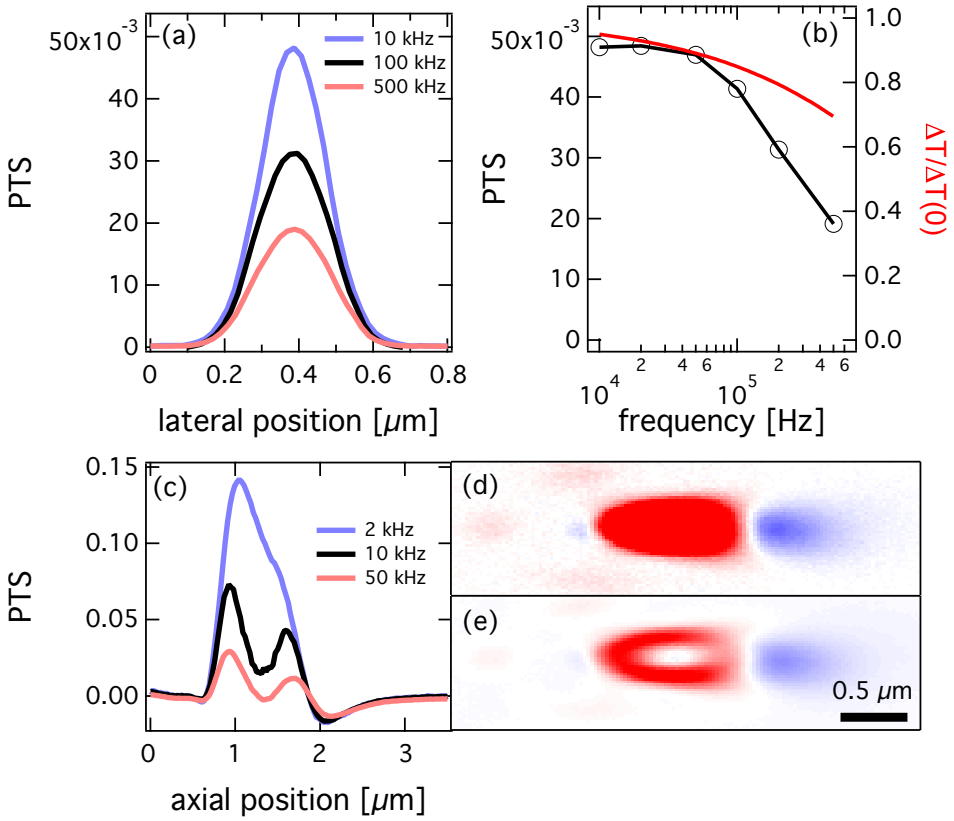

Figure 2.6: *a)* Lateral line profiles of the photothermal signal at different modulation frequencies. *b)* As the modulation frequencies increases, the amplitude of the photothermal signal decreases as the temperature profile around the particle is not completely modulated. The decrease of the signal and the theoretically predicted temperature are plotted against the modulation frequency. *c)* At a temperature closer to the phase transition the frequency dependence of the photothermal signal increases significantly. *d)* At a modulation frequency of 2 kHz the phase transition of the liquid crystal is completely modulated. *e)* Whereas at 50 kHz the liquid crystal remains locally in the isotropic phase and the signal is significantly lowered. In the center of the halo only the isotropic phase is probed. The large refractive index change from the nematic to isotropic phase transition does not contribute to the photothermal signal.

Liquid crystal show a much higher change of the refractive index if the phase transition between the ordered nematic and the disordered isotropic phase takes place, where the refractive index change can be 3 orders of magnitude larger than in common materials. This large change of the refractive index increases the photothermal signal by more than one order of magnitude. But the signal depends sensitively on frequency and sample temperature due to the phase transition in which latent heat is taken up.

The frequency dependence of the photothermal signal is investigated at two different temperatures. At 10 K below the phase transition temperature no qualitative changes occur (see fig. 2.6 *a)*). The photothermal signal drops comparable to the temperature shown in figure 2.6 *b)*. At 2 K below the phase transition temperature the photothermal signal changes drastically if the modulation frequency is increased from

2 to 50 kHz. At 2 kHz the signal exhibits a single large signal peak. At a modulation frequency of 50 kHz the peak splits (see figure 2.6 *c)* and compare figure 2.6 *d)* and 2.6 *e)*). This significant change is attributed to the nonlinearity in the refractive index due to the phase transition and the latent heat that has to be transformed. At high modulation frequency the phase transition is not modulated and the signal drops. The results indicate that photothermal microscopy is well suited to study the phase transition of liquid crystals from the ordered nematic to the disordered isotropic phase.

2.7 Electrochemical Manipulation of CdSe/ZnS Quantum Dots

N. Amecke, D. Plotzki, F. Cichos

CdSe/ZnS semiconductor quantum dots (QDs) are very efficient, photostable, wavelength-tunable sources of light in the visible range. They show interrupted emission (blinking) with spectral diffusion and fluctuating lifetime. Those interruptions and shifts are generally assumed to originate from charges tunneling in and out of the QD core or simply residing and diffusing in its close vicinity. They can lead to non-radiative exciton decay channels (e.g. Auger processes or trap assisted decay) and transition energy shifts (Stark effect). However, which charge (electron or hole) is more likely to be ejected and if this is really what intermittently quenches the fluorescence, still needs to be determined. This research project is devoted to the study of CdSe/ZnS QDs with externally injected and extracted charges. For this purpose we have constructed an electrochemical cell with a transparent thin electrode, which consists of an ITO coated glass cover slip with a 20 nm ZnO spacer deposited in the HLP group. Ensemble or single QD concentrations where spin coated on the electrode to be investigated with a confocal microscope while its potential is varied. We find high luminescence only at a preferred potential region close to the conduction band (CB) edge (see (B) in Fig. 2.7). At more negative potentials, electrons are injected in the CB and the fluorescence is quenched due to Auger processes (A). At more positive potentials, electrons are extracted from the environment, creating electron traps for the CB electron, which lead to non-radiative decay (C). The observation of single QDs suggests that at positive potentials the intensity decrease stems from increased blinking events. We thus find strong evidence for a connection of blinking with electron tunneling to trap states, which is a currently highly debated subject and a key question for a better understanding of the blinking process.

2.8 Back Focal Plane Spectroscopy of Photonic Crystals

R. Wagner, F. Cichos

Photonic Crystals (PCs) are materials in which the dielectric constant varies periodically. This causes a photonic band structure that can also contain stop bands. These stop bands inhibit the propagation of light with a certain wavelength for some directions in the PC. The spectral dependence of the stop band position on the direction can for example be probed by angle dependent fluorescence spectroscopy. Usually, this

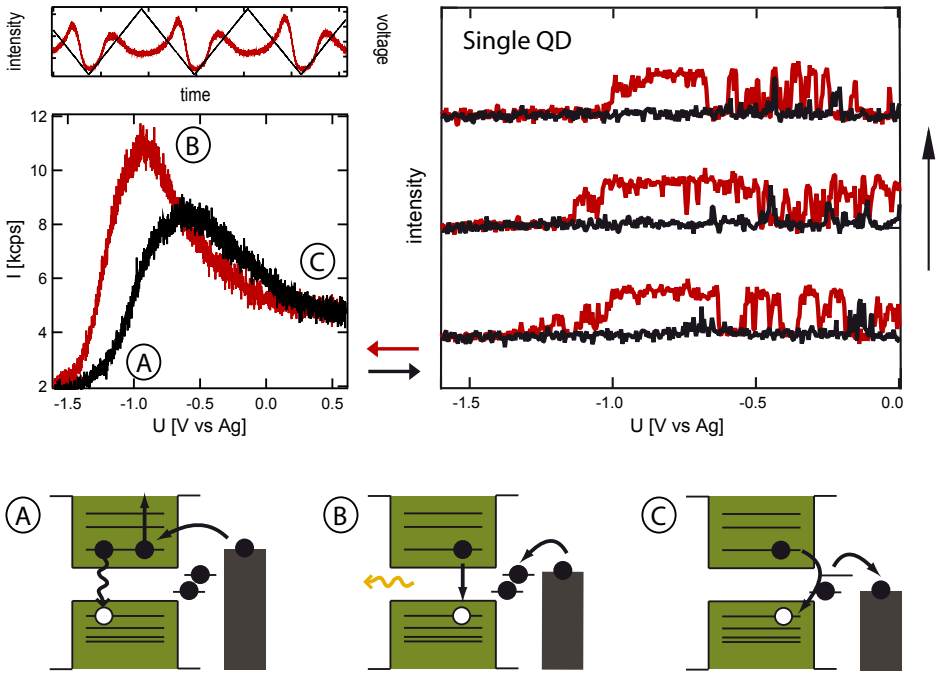

Figure 2.7: *Top left:* Intensity and voltage vs. time and corresponding cyclic voltammogram at scan rate 10 mV/s. *Top right:* Three consecutive cycles for a single QD. *Bottom:* Model to the voltage dependent increase and decrease of fluorescence intensity. A) Electron injection into the CB and Auger quenching. B) Complete electron trap passivation at the intensity maximum. C) Electron trap creation due to extraction of electrons leading to non-radiative decay.

requires a movement of the detector for every measurement, which is time consuming and poses a challenge when successive measurements are to be performed at a fixed sample position. Further, typically large sample areas are excited which causes an averaging over domains with defects like cracks or different order of the dielectric constituents of the PC. To probe the optical properties with spatial resolution requires methods that excite only small sample volumes. We developed a method that allows to detect fluorescence spectra for many directions in a single measurement (Fig. 2.8).[1] The fluorescence from the sample is collected by a microscope objective lens. All light that was emitted into the same direction is focused into one point in the objective's back focal plane (BFP). Every point in the BFP therefore corresponds to a certain emission direction. The distance r of this point from the optical axis is related to the emission angle ϑ_0 by

$$\sin(\vartheta_0) = \frac{r\mathrm{NA}}{r_{\max} n_0}$$

where NA is the numerical aperture of the objective, $r_{\max}$ the maximum radius of the BFP and n_0 the effective refractive index of the PC. The BFP is imaged onto the entrance slit of a spectrometer. This entrance slit selects light from some directions, which is then spectrally dispersed and imaged onto a CCD chip. This chip possesses 100 lines, each of which detects a spectrum from a different emission direction. This method was applied to PCs created by self-assembly of 260 nm polystyrene beads, which form a close packed fcc lattice. The fluorescence of the polystyrene beads was excited locally by a focused

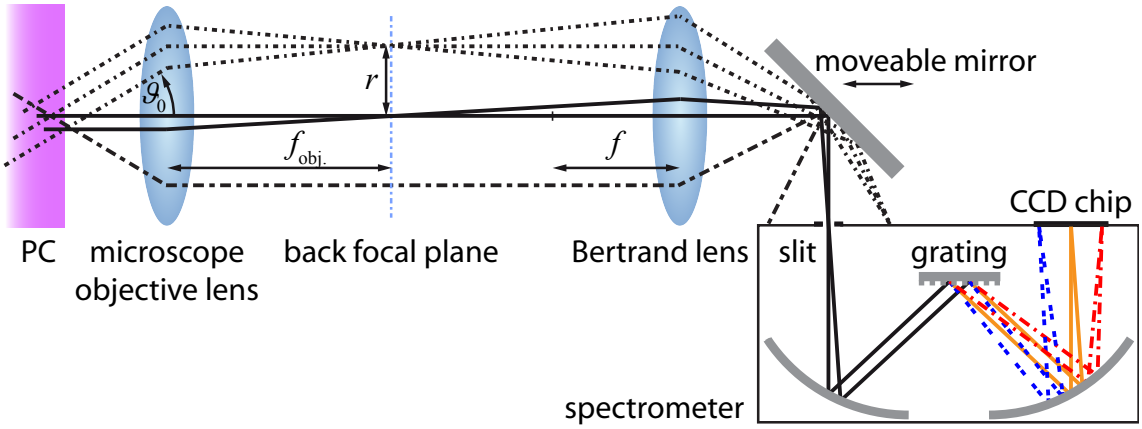

Figure 2.8: Scheme of the back focal plane spectroscopy setup. Light emitted into one direction is focused into one spot in the BFP of the objective lens. The BFP is imaged to the entrance slit (perpendicular to drawing plane) of a spectrometer using a Bertrand lens. Light passing through this slit is spectrally dispersed and imaged onto a CCD chip. Fig. adapted from [1].

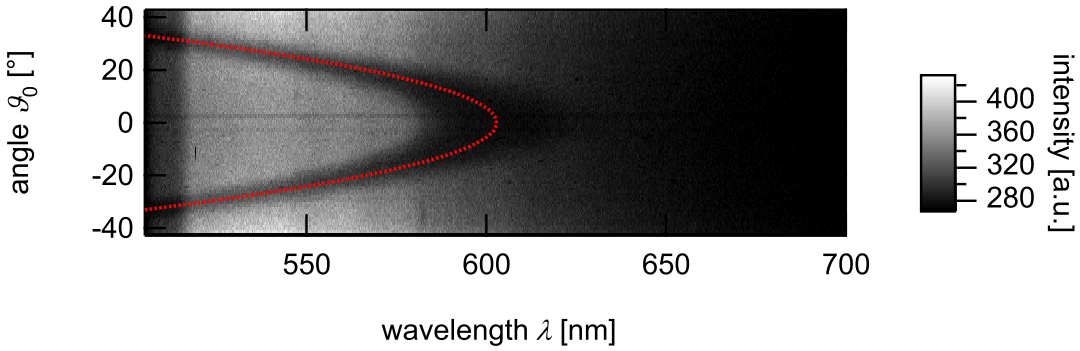

Figure 2.9: Emission spectra from a PC made of 260 nm polystyrene beads for different emission angles ϑ_0. The dark arc is caused by the stop band of the (111) lattice planes of the fcc lattice. The red dotted line indicates the theoretical position of this stop band.

laser. Fig. 2.9 shows as an example 100 spectra obtained in a single measurement when the slit was placed over the center of the BFP image. By shifting the mirror in Fig. 2.8 spectra from different directions can be detected.

[1] R. Wagner, L. Heerklotz, N. Kortenbruck, and F. Cichos, *Appl. Phys. Lett.*, 101, 081904,(2012)

2.9 Heterogeneous Single Molecule Dynamics in Polymers near T_g

S. Adhikari F. Cichos

The dynamics in polymers close to the glass transition temperature (T_g) becomes drastically slow and deviates from homogeneous liquid behavior such as non-Arrhenius

temperature dependence and non-exponential relaxation. Recently, single molecule experiments in polymers have shown that the dynamics of a single probe molecule is both spatially and temporally heterogeneous. The understanding of heterogeneous dynamics in polymers is expected to provide detailed insight into the glass transition phenomenon. The heterogeneous dynamics in the polymers poly (methyl acrylate)

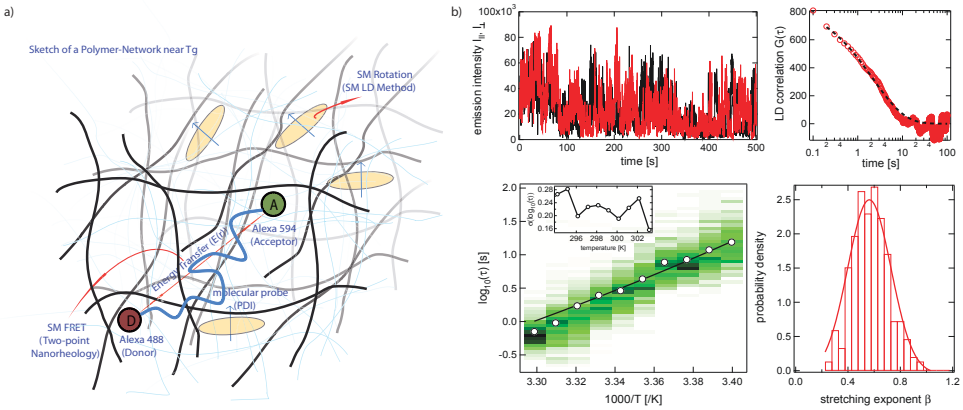

Figure 2.10: a) A sketch of polymer near T_g is shown. SM linear dichroism (LD) and SM-FRET methods are used to study heterogeneous dynamics in polymers. b) SM results from rotational studies in PMA using LD method are shown. (top left) The intensities in two polarization channels (black and red lines) fluctuate due to the rotational diffusion of the transition dipole of a single molecule. (top right) The autocorrelation of the linear dichroism calculated from intensity traces shown in the left is well fitted by a stretched exponential. (bottom left) The rotational times are log-normally distributed and mean rotational times closely follow the temperature dependence predicted by the Debye-Stokes-Einstein (DSE) relation using the polymer's bulk viscosity. (bottom right) A Gaussian distribution of stretching exponents are shown at temperature of 301 K.

(PMA) and poly (vinyl acetate) (PVAc) have been studied close to their glass transition temperatures (Tg) using single molecule (SM) techniques. The SM linear dichroism (LD) method has been applied to study diffusive rotational dynamics of single perylene-dimide (PDI) dye molecules over an extended temperature range of 10K. The autocorrelation function of the fluctuating LD of a single PDI molecule is found to be described well by a stretched exponential relaxation. Rotational times (τ) and stretching exponents (β) are broadly distributed at each temperature. The stretched exponential LD autocorrelation decay implies that the dynamics of a single PDI molecule is temporally heterogeneous. All SM results are discussed using a simple model of dynamical heterogeneity based on a Gaussian distribution of activation energies. SM results are compared to the results from dielectric experiments and viscosity data. The mean rotational times follow the Debye-Stokes-Einstein (DSE) relation using the bulk polymer viscosity but decouple from segmental motions. Further information on the heterogeneous dynamics is expected from an extension of two-point nanorheology to single molecule optical studies based on fluorescence resonance energy transfer (FRET). We have therefore synthesized a dual dye-labeled (Alexa 488 and Alexa 594) polystyrene polymer. A very high energy transfer efficiency (0.7) is observed in solution.

2.10 Funding

Light Emission of Single Emitters in 3-dimensional Photonic Crystals
Frank Cichos
CI 33/5-2

Ortsaufgelöste Detektion von Struktur und Dynamik in nematischen Phasen biaxialer Moleküle
Frank Cichos
CI 33/6-1

FG 877: Constrained Single Molecule Dynamics in Glassy Polymer Systems
Frank Cichos
CI 33/7-1

FG 877: Hot Brownian Motion
Frank Cichos
CI 33/7-2

FG 877: Static and dynamic properties of DNA-based polymer structures under constraints and confinement
Frank Cichos
CI 33/11-2

FG 877: From Local Constraints to Macroscopic Transport
Frank Cichos
CI 33/12 -1

BuildMONA, ESF-NFG: Funktionale multiskalige Strukturen

BuildMONA, ESF-NFG: Effiziente Energienutzung: Neue Konzepte und Materialien

SFB TRR102, Interaction of Single Polymer Chains in a Thermophoretic Trap

2.11 Organizational Duties

Frank Cichos

- Speaker of the DFG Research Unit 877 "From Local Constrainst to Macroscopic Transport"
- Head of the Eignungsfeststellungskommission Fakultät für Physik und Geowissenschaften
- Vice head Promotionsausschuss
- Member of the Prüfungsausschuss
- Organizer of the Physik-Kolloquium der Fakultät für Physik und Geowissenschaften
- Referee: Phys. Rev. B, Phys. Rev. Lett., Nature, Chem. Phys. Lett., Appl. Phys. Lett., ACS Petroleum Research Fund; Medical Research Council

2.12 External Cooperations

Academic

- TU Dresden
  Prof. Dr. Michael Mertig
- TU Dresden
  Dr. Ralf Seidel
- TU Chemnitz
  Prof. Dr. Christian von Borczyskowski
- TU Chemnitz
  Dr. Harald Graaf
- Universität Mainz
  Prof. Dr. T. Basché
- Princeton University
  Prof. Dr. H. Yang
- MPI Kohleforschung Mühlheim
  Dr. Frank Marlow

2.13 Publications

Journals

M. Selmke, M. Braun, F. Cichos, *Photothermal Single Particle Microscopy: Detection of a Nanolens* ACS Nano 6, (2012) 2714.

M. Selmke, M. Braun, F. Cichos, *Gaussian beam photothermal single particle microscopy*, JOSA A 29, (2012) 2237.

R. Wagner, L. Heerklotz, N. Kortenbruck, F. Cichos, *Back Focal Plane Imaging Spectroscopy of Photonic Crystals* Appl. Phys. Lett. 101, (2012) 081904.

M. Pumpa, F. Cichos, *Slow Single Molecule Diffusion in Liquid Crystals* Phys. Chem. B 116, (2012) 14487.

A. Issac, C. Krasselt, F. Cichos, C. von Borczyskowski, *Influence of the Dielectric Environment on the Photoluminescence Intermittency of CdSe Quantum Dots*, ChemPhysChem 13, (2012) 3223.

M. Selmke, M. Braun, F. Cichos *Nanolens Diffraction around a Single Heated Nanoparticle*, Optics Express 7, (2012) 8055.

T. Blaudeck, E. Zenkevich, M. Abdel-Mottaleb, K. Szwaykowska, D. Kowerko, F. Cichos, C. von Borczyskowski, *Formation Principles and Ligand Dynamics of Nanoassemblies of CdSe Quantum Dots and Functionalized Dye Molecules*, ChemPhysChem 13, (2012) 959.

Talks

F. Cichos: Thermophoretic Trapping and Steering of Janus Particles, International Meeting on Thermodiffusion, IMT 10, Brüssel, Belgien, 4.6.-8.6. 2012

F. Cichos: Thermophoretic Trapping and Steering of Janus Particles, IOP Topical Research Meeting on Physics: Swimming and Complexity at low Reynolds number, London/UK, 7.6.-8.6. 2012

F. Cichos: Thermophoretic Trapping and Steering of Janus Particles, Graduiertenkolleg "Stucture formation and transport in complex systems", Saarbr"ucken, 18.9.2012

M. Selmke, M. Braun, F. Cichos: Nano-lensing in Photothermal single particle microscopy, EOSAM 2012, European Optical Society, Annular Meeting 2012, Aberdeen, UK, 25.-28. September 2012

M. Selmke: Visualization in science, SFG-Meeting for doctoral researchers, Meissen, 20.-22. Jun. 2012

M. Selmke, M. Braun, R. Schachoff, F. Cichos: Twin-Focus Photothermal Correlation Spectroscopy, 76. DPG Spring Meeting, Berlin, 25.-30. March 2012

M. Braun, R. Schachoff, F. Cichos: Gold nanoparticle assisted thermophoretic trapping of single nano-objects, 76. DPG Spring Meeting, Berlin, 25.-30. March 2012

M. Braun, F. Cichos: Gold nanostructure assisted thermophoretic trapping of single nano-objects, EOS Annual Meeting 2012, Aberdeen, Scotland, UK, 25.-28. September 2012 R. Wagner, L. Heerklotz, F. Cichos: Fast Structural Analysis of Photonic Crystals, 76. DPG Spring Meeting, Berlin, 25.-30. March 2012

A. Bregulla, M. Braun, H. Yang, F. Cichos: Photon nudging of Janus Particles , EOSAM 2012, European Optical Society, Annular Meeting 2012, Aberdeen, UK, 25.-28. September 2012

L. Heerklotz, R. Wagner, F. Cichos: Influence of cracks on photonic stop bands, DPG spring meeting, Berlin, HL 21.3, (March 26, 2012)

Posters

M. Selmke, M. Braun, F. Cichos: Diffraction around a Single Heated Nanoparticle, 76. DPG Spring Meeting, Berlin, 25.-30. March 2012

A. Heber, M. Pumpa, M. Selmke, M. Braun, N. Amecke, and F. Cichos: Photothermal spectroscopy studies of quantum dots in liquid crystals, 76. DPG Spring Meeting, Berlin, 25.-30. March 2011

M. Braun, A. Bregulla, F. Cichos: Gold nanostructure assisted thermophoretic trapping of single nano-objects, Fifth BuildMoNa Symposium, Leipzig, 12. March 2012

S. Adhikari, M. Selmke, F. Cichos: SM rotational study and FRET in polymer: A detailed study of heterogeneous dynamics, HBSM12, Tübingen, 27.-30. August 2012

S. Adhikari, M. Selmke, F. Cichos: Single molecule dynamics in glassy polymer systems, SFG-Meeting for doctoral researchers, Meissen, 20. -22. June, 2012

S. Adhikari, M. Selmke, F. Cichos: Two-Point nanorheology based on single molecule FRET in polymer PMA, 76. DPG Spring Meeting, Berlin, 25.-30. March 2012

A. Bregulla, R. Seidel, K. Klaus, M. Mertig, F. Cichos: Rotational behavior of thermophoretically driven Janus particles at a hard wall, 76. DPG Spring Meeting, Berlin, 25.-30. March 2012

D. Plotzki, N. Amecke, F. Cichos: Motion and Fluorescence of Charged Single CdSe/ZnS Quantum Dots in an Electric Field, 76. DPG Spring Meeting, Berlin, Germany, 25.-30. March 2012

N. Amecke, F. Cichos: Optical Detection of a Surface Charge on CdSe/ZnS Quantum Dots in Apolar Solvents, 76. DPG Spring Meeting, Berlin, Germany, 25.-30. March 2012

N. Amecke, F. Cichos: Fluorescence of Surface-Charged CdSe/ZnS Quantum Dots in Apolar Solvents, NaNaX 5, Fuengirola, Spain, 7.-11. May 2012

2.14 Graduations

Master

- Jonas Buchmann
  Investigating Hot Brownian Motion of Gold Nanoparticles by Photothermal Correlation Spectroscopy
  December 2012
- Thomas Heyn
  Dynamics of gold particles under thermal gradients
  December 2012
- André Heber
  Photothermal Microscopy in Liquid Crystals
  December 2012

Bachelor

- Sascha Loebel
  Detektion einzelner Patikel in Flüssigkristallen
  November 2011
- Nikolai Kortenbruck
  Konoskopie an fluoreszenzdotierten photonischen Kristallen
  December 2011

2.15 Guests

- Frank Jülicher
  MPI für komplexe Systeme, Dresden
  6.November 2012
- Markus Lippitz
  MPI für intelligente Systeme, Stuttgart
  17. July 2012
- Joachim Rädler
  LMU München
  10. July 2012

3

Molecular Physics

3.1 Introduction

In 2012 we organized the "7th International Conference on Broadband Dielectric Spectroscopy and its Applications", in short BDS 2012. There were many things to celebrate: (i) one hundred years ago P. Debye published (Phys. Zeitschrift 13, 97 (1912)) for the first time his famous formula, which is still the basis for analysing dielectric relaxation processes; (ii) the International Dielectric Society (IDS) has developed since its foundation in 2002 in a splendid manner. International conferences were organized in 2001 (Jerusalem), 2002 (Leipzig), 2004 (Delft), 2006 (Poznan), 2008 (Lyon) and 2010 (Madrid) with increasing attendence; (iii) the "Peter Debye Prize for Young Investigators for Excellence in Dielectric Research" has been recognized as an extraordinary distinction in the field with Anatoli Serghei as prize winner in 2006, Periklis Papadopoulos and Daniele Prevosto in 2008, Catalin Gainaru in 2010 and Simone Napolitano in 2012; (iv) the equipment has developed strongly, covering typically 8-10 decades (or more) in frequency or time; (v) temperature- and pressure-dependent measurements can be carried out readily with commercially available systems; (vi) the amount of sample material required for dielectric measurements can be reduced down to the limit of monomolecular layers and of isolated polymer coils. The scope of the conferences has widened enormously covering nowadays hot topics like "Scaling of relaxation frequencies", "Terahertzspectroscopy", "Charge transport and glassy dynamics", "The interrelationship between Impedance Spectroscopy, Electrochemical measurements and Broadband Dielectric Spectroscopy", "Biological systems" to mention a few. Dielectric methods have gained increasing interest in modern technology. It was for me, as chairman of IDS, a pleasure to have had the chance to outline and organize this conference again in Leipzig. I am deeply obliged to my coworkers, without their extraordinary engagement the conference would have not been possible.

January 2013

Prof. Dr. Friedrich Kremer

3.2 Glassy dynamics of condensed isolated polymer coils

M. Treß, E.U. Mapesa, M. Reiche, F. Kremer

The glassy dynamics of randomly distributed, condensed isolated and semi-isolated poly(2-vinylpyridine) (P2VP) polymer chains is studied by means of Broadband Dielectric Spectroscopy (BDS). For this purpose, a recently developed nano-structured electrode arrangement is refined to achieve an electrode-to-electrode distance of only 40 nm. The P2VP polymer coils are deposited from solution on one of the ultra-flat, highly conductive silicon electrodes and a thorough annealing procedure applied to remove the solvent. Atomic Force Microscopy scans of the identical samples studied in the BDS measurements reveal that the mean volume of the coils resembles 1 to 2 times the volume expected for a single chain (Fig. 3.1). Accordingly, the measurement averages over single (or sometimes two) polymer chains; for two molecular weights also the semi-isolated case, where coil volumes correspond to 5 to 15 times the estimated single chain volume, is investigated [1].
The experiments show, that even isolated condensed polymer chains exhibit glassy dynamics. Further, in the case of P2VP on silicon, the mean relaxation time corresponds to the bulk (Fig. 3.2). An extensive analysis of the relaxation time distribution function reveals a broadening due to the occurrence of new relaxation modes mostly at longer times. This is attributed to interfacial interactions of chain segments with the substrate in their direct vicinity (Fig. 3.1).

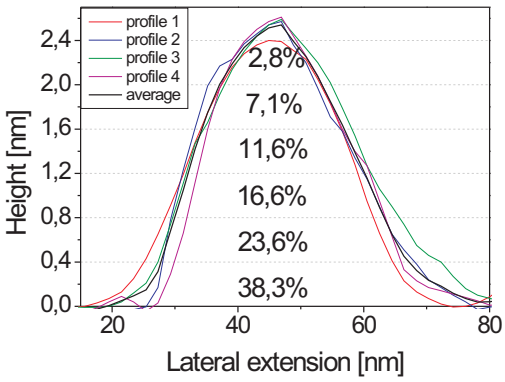

Figure 3.1: Height profiles of a single condensed P2VP chain, the separation of horizontal lines corresponds to the segment thickness and the percent figures represent the coil volume in each of these layers.

[1] M. Tress, E.U. Mapesa, M. Reiche and F. Kremer, Nature Materials (submitted).

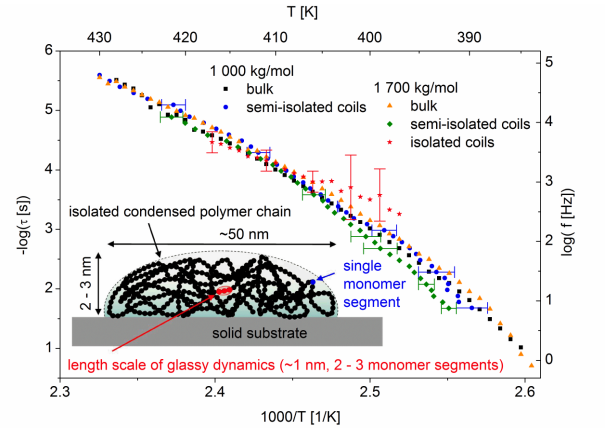

Figure 3.2: Mean relaxation time of the segmental relaxation time vs. inverse temperature for P2VP bulk, semi-isolated and isolated condensed polymer coils of different molecular weight as indicated. The scheme visualizes why a single polymer chain can still exhibit glassy dynamics.

3.3 Nanometric sample capacitors

M. Tress, E.U. Mapesa, M. Reiche, F. Kremer

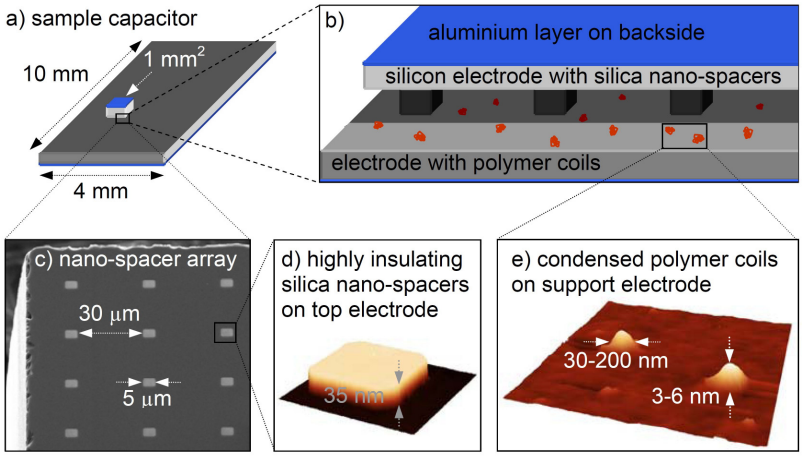

Figure 3.3: a) Schematic sample arrangement. b) Close-up scheme of a) showing the nano-structures which serve as spacers between the electrodes. c) TEM image of the regular nano-structure array. d) AFM height image of a single nano-structure of a height of only 35 nm. e) Condensed isolated polymer chains on a silicon surface can be measured with the refined set-up.

Recently, a novel method has been introduced to study thin polymer layers with a free upper interface by means of BDS [1]. With the aid of highly conductive ultra-flat silicon electrodes which are covered with strongly insulating silica nano-structures as spacers glassy dynamics in different polymers were investigated [2–4]. Due to a low filling fraction of the capacitor (and the resulting small signal to noise ratio) this technique was limited to layers thicker than ~5 nm [5].
To push this limitation, we refined this technique in several ways. First of all, the cleaning procedure has been improved significantly; the previous sonication in solvent

(which possibly breaks conductive silicon particles from the edges and transfers these contaminants to the flat surface) is replaced by a plasma treatment followed by a particle removal with a snow-jet gun. Second, the height of the spacers was reduced from previously 100 nm [4, 5] to only 35 nm. A third modification concerns the fabrication of the electrodes itself; to counterbalance the increasing capacity due to reduced electrode distance we decreased the area of the counter electrode from initially 3 x 8 mm^2 to 1 x 1 mm^2. Besides the geometric adjustment of the capacity, this step improves the realization of electrode separations in the range of the spacer height (which previously has been off by factors of 2 or mostly much more). Finally, sample capacitors of a thickness of only 40 nm were realized and enabled the investigation of the glassy dynamics of condensed isolated polymer chains).

[1] A. Serghei and F. Kremer, Rev. Sci. Inst. **79**, 026101 (2008)
[2] A. Serghei, H. Huth, C. Schick and F. Kremer, Macromolecules **41**, 3636 (2008)
[3] M. Erber, M. Tress, M. Mapesa, A. Serghei, K.-J. Eichhorn, B. Voit and F. Kremer, Macromolecules **43**, 7729 (2010)
[4] M. Tress, M. Erber, E.U. Mapesa, H. Huth, J. Müller, A. Serghei, C. Schick, K.-J. Eichhorn, B. Voit and F. Kremer, Macromolecules **43**, 9937 (2010)
[5] E.U. Mapesa, M. Erber, M. Tress, K.-J. Eichhorn, A. Serghei, B. Voit and F. Kremer, European Physical Journal: Special Topics. **189**, 173 (2010)

3.4 Segmental and chain dynamics in thin layers of poly(cis-1,4-isoprene)

E.U. Mapesa, M. Tress, F. Kremer

Broadband Dielectric Spectroscopy (BDS) - in combination with a nanostructured electrode arrangement - is used to study thin layers of poly(*cis*-1,4-isoprene) (PIP). Being a Type *A* polymer, PIP enables the investigation of two distinct relaxation modes taking place at two different length scales: the segmental motion which involves structures of about one nanometer in size and the normal mode which represents the global dynamics of the chain [1]. For molecular weights (24.5, 44.5, 53 and 75 kg/mol) much greater than M_c (the critical molecular weight, $M_c = 10^4$g/mol), down to thicknesses comparable to the respective radii of gyration, it is observed (see Fig. 3.4) that: (i) the segmental mode as a local relaxation process is unaffected by the confinement in thin layers - consistent with our previous results [2]; (ii) the normal mode becomes faster with decreasing layer thickness, and (iii) this change in the normal mode is molecular-weight dependent. For M~M_c, it is shown that both the segmental and normal modes remain unaffected by changes in layer thickness.

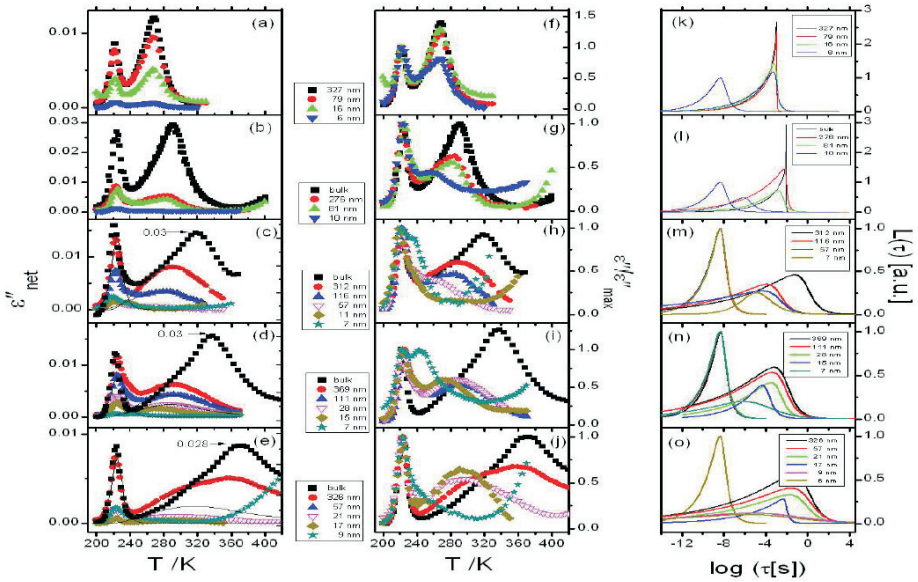

Figure 3.4: Temperature dependence of the dielectric loss ϵ''_{net} at 80 Hz for (a) PIP-11.6, (b) PIP-24.5, (c) PIP-44.5, (d) PIP-53, and (e) PIP-75 kg/mol. For graphical reasons, Havriliak-Negami fits (assumimg Vogel-Fulcher-Tammann VFT temperature-dependence) for some data are shown by lines. In (f), (g), (h), (i) and (j) respectively, the same dielectric data is shown normalized w.r.t. the maximum loss value of the segmental mode. (k), (l), (m), (n) and (o) show the respective relaxation time distribution functions as obtained from the HN fit parameters at 312 K.

[1] I. Bahar, B. Erman, F. Kremer, E.W. Fischer, Macrom. **25**, 816 (1992)
[2] E.U. Mapesa et al. Eur.Phys. J.-ST. **189**, 173 (2010)

3.5 Dynamics of poly(cis-1,4-isoprene) in 1- and 2D geometrical confine-ment

E.U. Mapesa, W.K. Kipnusu, M. Tress, F. Kremer

A current study addresses the question: How does the dimensionality of geometric confinement affect the dynamics of the constrained material? For the same material, 1- and 2-D confinements are attained by preparing thin films and by infilling unidirectional nanopores, respectively. Poly(*cis*-1,4-isoprene) (PIP), being a Type A [1] polymer, is the apt candidate for this study because both the local and global dynamics of the chain can be accessed by Broadband Dielectric Spectroscopy (BDS). BDS measurements on thin films are carried out using a state-of-the-art nano-structured silicon electrode arrangement where highly insulating silica structures are employed as spacers. For the polymer in anodized aluminium oxide (AAO) pores, a fractionated filling procedure (from solution) has been developed achieving filling factors better than 70% in seven days. First results (Fig. 3.5) show that, compared to bulk, the mean relaxation rate of the segmental mode is independent of the dimensionality of confinement. Further, it is clearly evident that both 1- and 2-D confinement affect the normal mode, that is, the conformation of the chains; this effect is more pronounced in the latter case. This study is being extended to different molecular weights of PIP.

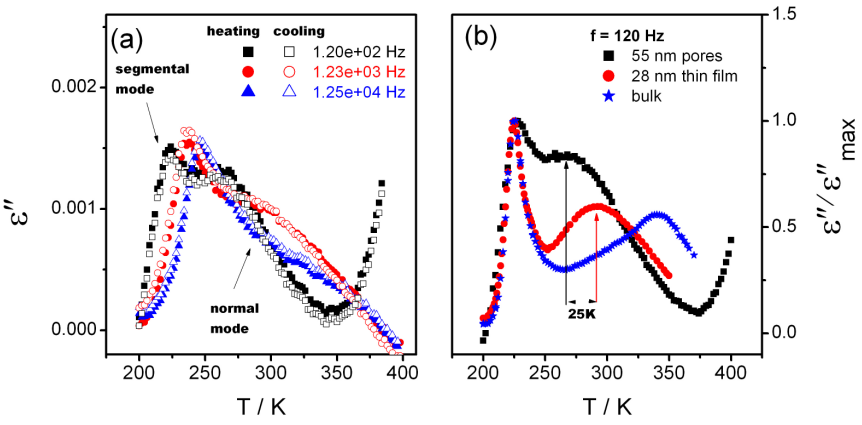

Figure 3.5: (a) Typical spectra showing dielectric loss (both heating and cooling cycles) as a function of temperature for PI (M_W = 53 000 g/mol) in AAO pores of mean diameter 55 nm. In (b), comparison is made at 120 Hz, between PI in bulk and the confined cases; the temperature position of the normal mode is shifted by about 25 K for the case of PIP in pores relative to PIP in thin layers of comparable size.

[1] W. H. Stockmayer, Pure Appl. Chem. **15**, 539 (1967)

3.6 Dynamics of poly(styrene-block-isoprene-1.4) diblock copolymers in nanometer thin layers using novel nano-structured electrodes

M.M. Elmahdy, M. Fuchs, M. Tress, E.U. Mapesa, F. Kremer

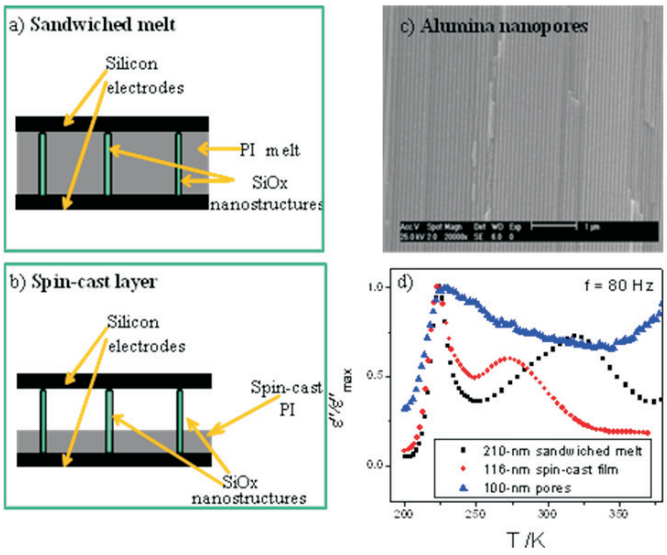

Figure 3.6: Optical microscope image showing representative regions of the surface topography of the spin-coated PS-b-PI films with f_{PI}=0.53 and film thickness of ~200 nm. The films are annealed under oil-free high vacuum (10^{-6} mbar) at 423 K for 48 h. (b) Tapping mode AFM-height image (scan size 40×40 μm^2) of the white square highlighted area in the microscope image. Differences in the terrace thickness are visible due to white light interference. (c) Height profile extracted from the AFM-height image shown in (b). This profile is plotted from a single scan line across the film (The red-dotted arrow) and shows terraces of well-defined thickness ranges between ~30-40 nm.

Broadband Dielectric Spectroscopy (BDS) using the novel nano-structured electrodes arrangement is employed to investigate the molecular dynamics of poly(styrene-block-isoprene-1.4) (PS-b-PI) diblock copolymers in nanometer thin layers with different PI volume fraction (f_{PI}) and identical molecular weight of the PS blocks [1]. Three relaxation processes are observed, which can be assigned to the two segmental modes of the styrene and isoprene blocks and a relaxation process related to the normal mode of the PI chain (Fig. 3.7). The dynamic glass transition related to the segmental mode of the styrene and isoprene blocks is independent of the layer thickness, while the normal mode of the PI chains becomes slightly faster with decreasing the layer thickness. The ordered state morphology, studied by Tapping mode AFM, revealed the formation lamellar structure (Fig. 3.6) in good agreement with the literature [2].

[1] M.M. Elmahdy, M. Fuchs, M. Tress, E. Mapesa and F. Kremer, in preparation
[2] Khandpur et al., Macromolecules **28**, 8796 (1995)

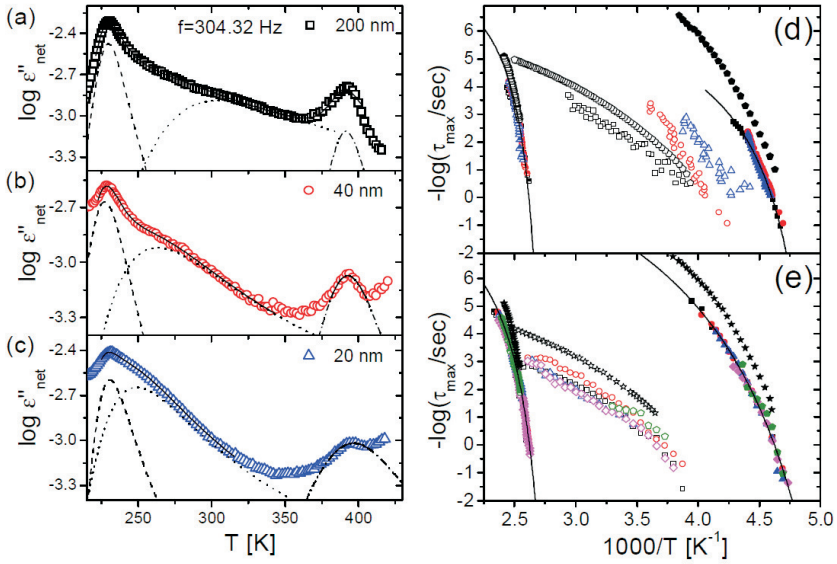

Figure 3.7: (a, b and c) are the dielectric loss (ϵ''_{net}) spectra under "isochronal" conditions of the PS-b-PI with f_{PI}=0.53 and film thicknesses of 200 nm, 40 nm and 20 nm obtained at frequency of 304.32 Hz. The dashed and dotted lines in are the fitted curves corresponding to the PI segmental and normal modes, respectively. The solid lines represent theoretical fit with two HN function (assuming Vogel-Fulcher-Tammann (VFT) temperature-dependence). The dasheddotted lines in are the HN fit to the PS segmental mode. (d and e) temperature dependence of the relaxation times corresponding to the PI-segmental mode (filled symbols), PI-normal mode (open symbols) and PS-segmental mode (halffilled symbols) of PS-b-PI diblock copolymer with f_{PI}=0.53 (d) and 0.66 (e). (d) Relaxation map of PS-b-PI with f_{PI}=0.53 and film thicknesses of 200 nm (squares), 40 nm (circles) and 20 nm (triangles). The bulk PI and PS-homopolymers with M_w=24500 and 58900 gram/mol, respectively, are included for comparison (pentagon). (b) Corresponding Arrhenius plot of PS-b-PI diblock copolymer with f_{PI}=0.66 and film thicknesses of 430 nm (squares), 247 nm (circles), 103 nm (up triangles), 21 nm (diamond) and 12 nm (pentagon). For comparison, the bulk PI and PS-homopolymers with M_w=44500 and 58900 gram/mol, respectively, are included (stars). The solid lines are Vogel-Fulcher-Tammann (VFT) fits to the experimental data.

3.7 The interplay between inter- and intra-molecular dynamics in a series of alkylcitrates

W.K. Kipnusu, W. Kossack, C. Iacob, P. Zeigermann, J.R. Sangoro, R. Valiullin, F. Kremer

The inter- and intra-molecular dynamics in a series of glass-forming alkylcitrates is studied by a combination of Broadband Dielectric (BDS), Pulsed Field Gradient Nuclear Magnetic Resonance (PFG NMR), Fourier-Transform Infrared (FTIR) Spectroscopy and Differential Scanning calorimetry (DSC). Analyzing the temperature dependencies of specific IR absorption bands in terms of their spectral position and the corresponding oscillator strengths enables one to unravel the intra-molecular dynamics of specific molecular moieties and to compare it with the (primarily dielectrically) determined intermolecular dynamics. With decreasing temperature, the IR band positions of carbonyls (part of the core units) and H-bonded moieties of citrates, show a red shift with

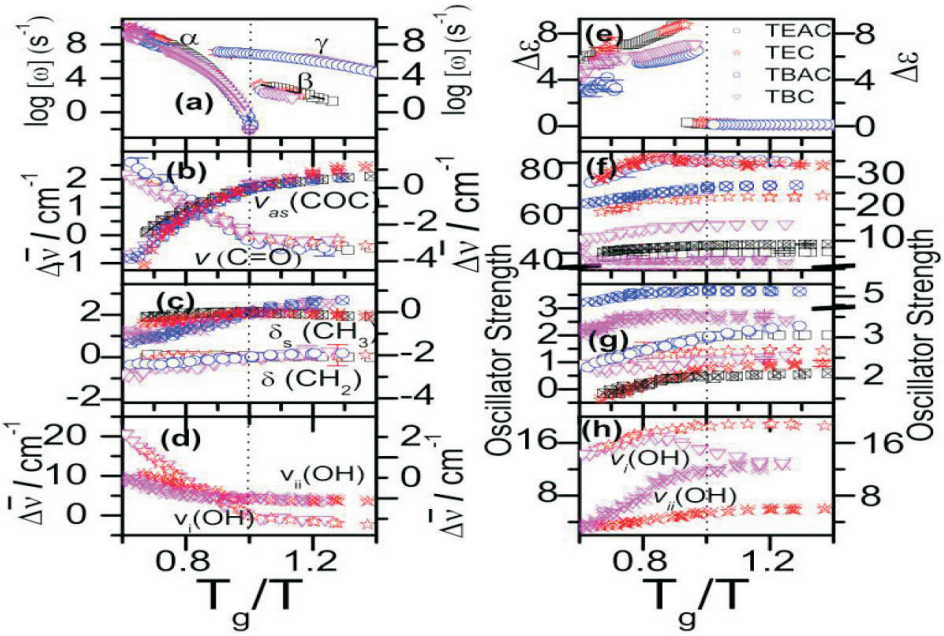

Figure 3.8: Comparison of dynamics (from BDS) and IR vibrational properties of the alkylcitrates as a function of scaled T. (a) , α, β and γ relaxation rates are compared with IR bandshifts for different moieties shown in (b-d). (e) dielectric relaxation strengths for α, β and γ processes compared with the oscillator strength for (f): ν(C=O)(open symbols, left-Y axis), ν_{as}(O-C-O) (crossed symbols, right-Y axis), (g): δ(CH3) (crossed symbols, right-Y axis) and δ(CH2) (open symbols, left-Y axis), (h): ν_i(OH) and ν_{ii}(OH) vibrations of H-bonds

a kink at the calorimetric glass transition temperature (T_g) while other moieties whose dynamics are decoupled from those of the core units, exhibit a blue shift with nominal changes at T_g. The oscillator strength of all units in citrates depict stronger temperature dependencies above T_g and in some, the ester linkage and H-bonded units show a change of slope at a temperature where structural and faster secondary relaxations merge. By that, a wealth of novel information is obtained proving the fundamental importance of intramolecular mobility in the process of glass formation, beyond coarse-grained descriptions.

[1] P. Papadopoulos, W. Kossack and F. Kremer. Soft Matter **9** (5), 1600 (2013)
[2] W.K Kipnusu et al., submitted Soft Matter (2013)

3.8 Decoupling of ionic conduction from structural dynamics in polymerized ionic liquids

C. Iacob, J.R. Sangoro, S. Berdzinski, V. Strehmel, A.P. Sokolov, F. Kremer

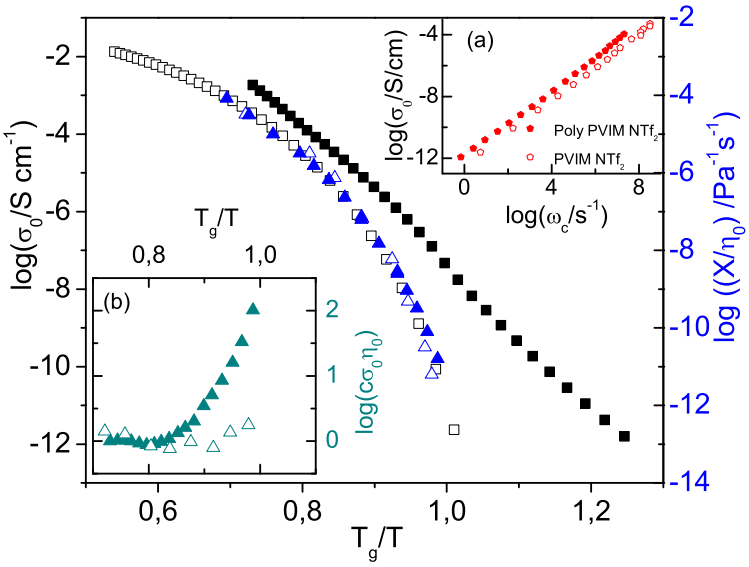

Figure 3.9: The dc conductivity, σ_0 (black symbols), as well as the inverse shear viscosity $1/\eta_0$ (blue symbols) versus T_g/T for the polymerized ionic liquid (poly (PVIM) NTf_2 - full symbols) and the low molecular weight ionic liquid PVIM NTf_2 (open symbols). The constant X with values 1 and $10^{4.43}$ is employed for a low molecular weight and polymerized ionic liquid, respectively, for direct comparison of the temperature dependence of $1/\eta_0$. The disparity in the values of X presumably stems from the differences in the molecular weights of the two materials. Inset: (a) BNN plot; dc conductivity, σ_0, versus the characteristic frequency, ω_c, for the materials under study as indicated, and, (b) product of the dc conductivity and the zero shear viscosity normalized with respect to the high temperature values for the materials investigated versus T_g/T. This quantifies the degree of decoupling of ion transport from structural dynamics in the two classes of ionic liquids probed.

Ionic conduction and structural dynamics in neat and polymerized bis(trifluoromethylsulfonyl)imide-based ionic liquids (IL) are investigated by a combination of Broadband Dielectric Spectroscopy, dynamic mechanical spectroscopy and differential scanning calorimetry. While in the low-molecular weight IL rotational and translational diffusion follow Einstein and Einstein-Smoluchowski equations, for the polymerized system a decoupling between charge transport and structural dynamics by up to two orders of magnitude at low temperatures is found. If rescaled to the calorimetric glass transition temperature T_g, charge transport is more efficient for the polymeric IL [1–4].

[1] J. R. Sangoro et al., Soft Matter **7**, 1678(2011)
[2] C Iacob et al., Soft Matter **8**, 289(2012)
[3] F. Kremer, A. Schönhals, Broadband Dielectric Spectroscopy, Berlin: Springer (2003).
[4] J. R. Sangoro et al., submitted to PRL.

3.9 Enhanced charge transport in nano-confined ionic liquids

C. Iacob, J.R. Sangoro, W.K. Kipnusu, J. Kärger, F. Kremer

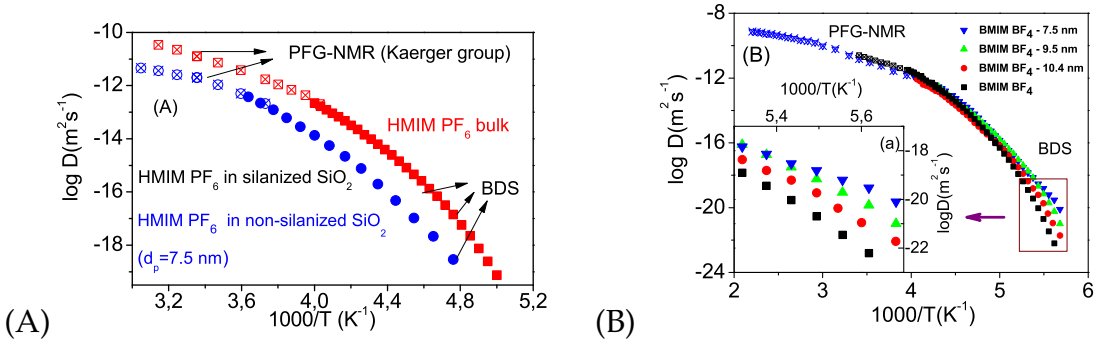

Figure 3.10: (A) Diffusion coefficient determined by applying the Einstein-Smoluchowski equation to the dielectric spectra of HMIM PF_6 in bulk (red squares), untreated nanopores (blue circles) and silanized nanopores (black triangles) versus inverse temperature. The respective values obtained by PFG-NMR are shown by crossed symbols. (B) Diffusion coefficients versus inverse temperature as obtained by PFG-NMR (crossed open symbols) and BDS measurements (?lled symbols) for bulk and con?ned BMIM BF_4 as indicated. Inset: (a) enlargement of the spectra at lower temperatures.

Charge transport and glassy dynamics of several classes of ionic liquids confined in uni-directional nanoporous silica membranes are investigated in a wide frequency and temperature range by a combination of Broadband Dielectric Spectroscopy (BDS), Pulsed Field Gradient Nuclear Magnetic Resonance (PFG NMR) and Fourier Transform Infrared spectroscopy (FTIR). Two opposite effects are observed: (i) surface effects and (ii) confinement effects. More than 10-fold systematic decrease in the effective diffusion coefficient (for $HMIM^+$-based ionic liquids with PF_6^-, I^-, Cl^-, Br^- anions) from the bulk value is observed in the silica nanopores. For a second category of ILs including BF_4 and NTf_2 -based ionic liquids, it is experimentally demonstrated that the ionic mobility at lower temperatures is enhanced by more than two decades under nano-confinement in comparison to the bulk value. In summary, the resultant macroscopic transport properties of glass-forming ionic liquids in silica nanopores are controlled by a subtle counterbalance between surface- and confinement-effects [1–4].

[1] C. Iacob et al., Soft Matter **8**, 289(2012)
[2] C. Iacob et al., Phys. Chem. Chem. Phys. **12**, 13798 (2010)
[3] F. Kremer, A. Schönhals, Broadband Dielectric Spectroscopy., Berlin: Springer (2003).
[4] C. Iacob et al., J. Chem. Phys. **129** (23), 234511 (2008)

3.10 Electrode polarisation at the interface between a metal and an ionic liquid

L. Popp, W.K. Kipnusu, C. Iacob, M. Tress, F. Kremer

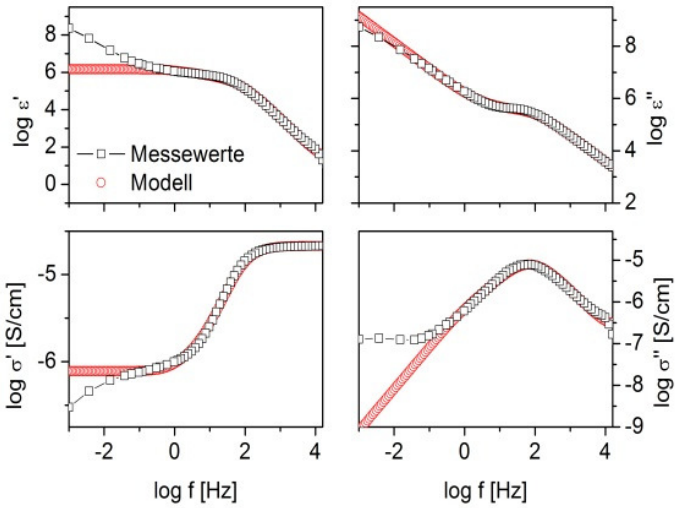

Figure 3.11: Comparison of the experimental data curves to the curves calculated by the model for the ionic liquid [HMIM][I] measured with platinum electrodes at 276 K.

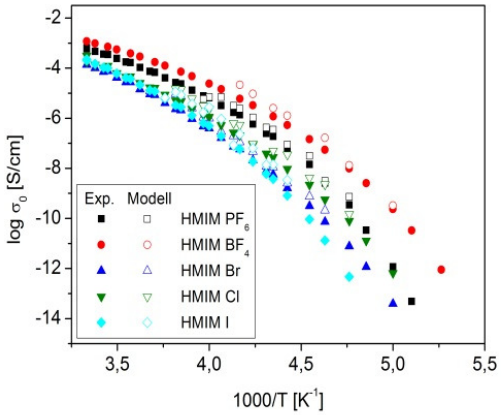

Figure 3.12: "dc" conductivity σ_0: Comparison of (i) the data measured directly with BDS (Exp.) and (ii) the values calculated by the model for the indicated ILs and platinum electrodes.

Charge transport and electrode polarization phenomena are investigated in a homologous series of imidazolium-based ionic liquids by Broadband Dielectric Spectroscopy (BDS) [4] in a large temperature (190 – 300 K) and frequency range (10^{-3} – 10^{5} Hz). The dielectric spectra are dominated – on the low frequency side – by electrode polarization, while, for higher frequencies, charge transport (in a disordered matrix) is the underlying physical mechanism [2]. The absolute values of the dc conductivity vary

over 5 decades upon systematic variation of ILs structure and electrode material [3]. A microscopic model is applied to quantitatively describe the electrode polarization [1]. The applicability of the model to the experimental data in a broad frequency range is discussed in more detail.

[1] A. Serghei et al. Phys. Rev. B **80** (18), 184301-5 (2009)
[2] J. C. Dyre, Phys. Rev. B **37** (17), 10143 (1988)
[3] J. R. Sangoro, Ph.D. Thesis (2010), University of Leipzig
[4] F. Kremer, A. Schönhals, Broadband Dielectric Spectroscopy, Springer, Berlin (2003)

3.11 Comparative study on the molecular dynamics of a series of polypropylene glycols

K. Kaminski, W.K. Kipnusu, K. Adrjanowicz, E.U. Mapesa, C. Iacob, M. Jasiurkowska, P. Wlodarczyk, K. Grzybowska, M. Paluch, F. Kremer,

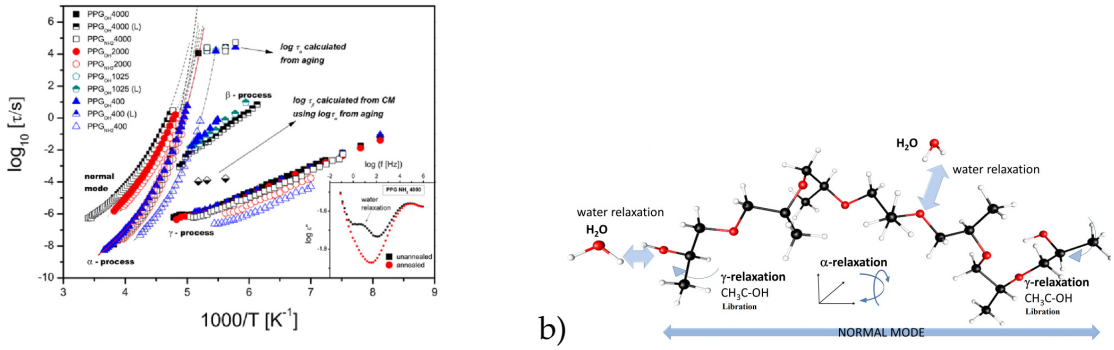

Figure 3.13: (a) Relaxation times versus inverse temperature for the PPG samples studied in the current work. Some data from literature (L) [1] is also included in this relaxation map. Inset: dielectric loss spectra of PPG NH_2 showing water relaxation which is removed after annealing (b) Scheme 3 PPG hydroxyl terminated with degree of polymerization n=6 with the assignments of the normal mode, α, β and γ- relaxations.

Broadband Dielectric Spectroscopy (BDS) is employed to study the molecular dynamics of hydroxyl (OH)- and amino (NH_2)-terminated polypropylene glycols (PPG) of varying molecular weight. Besides the dynamic glass transition (α-relaxation), a normal mode process and a secondary γ-relaxation is observed, the latter being assigned to librational fluctuations of the polar COC moiety. Additionally a further process is found and proven in two independent experiments (annealing PPGs at high temperatures and physical aging) to originate from residual H_2O impurities in the sample and not being related to the dynamics of PPG. It is occasionally discussed in the literature incorrectly as Johari-Goldsten (JG) relaxation. Furthermore aging in the systems under study is analyzed and found to follow the Nagel- Leheny equation.

[1] C. Gainaru, W. Hiller and R. Bohmer, Macromolecules **43**, 1907(2010)
[2] K. Kamil et al. accepted for publication in Macromolecules (2013)

3.12 Molecular dynamics and morphology in confined 4-heptan-4′-isothiocyanato-biphenyl liquid crystals

M. Jasiurkowska, W. Kossack, R. Ene, C. Iacob, W.K. Kipnusu, P. Papadopoulos*, J.R. Sangoro, F. Kremer

*Max-Planck-Institute for Polymer Research, Postfach 3148, D-55021 Mainz, Germany

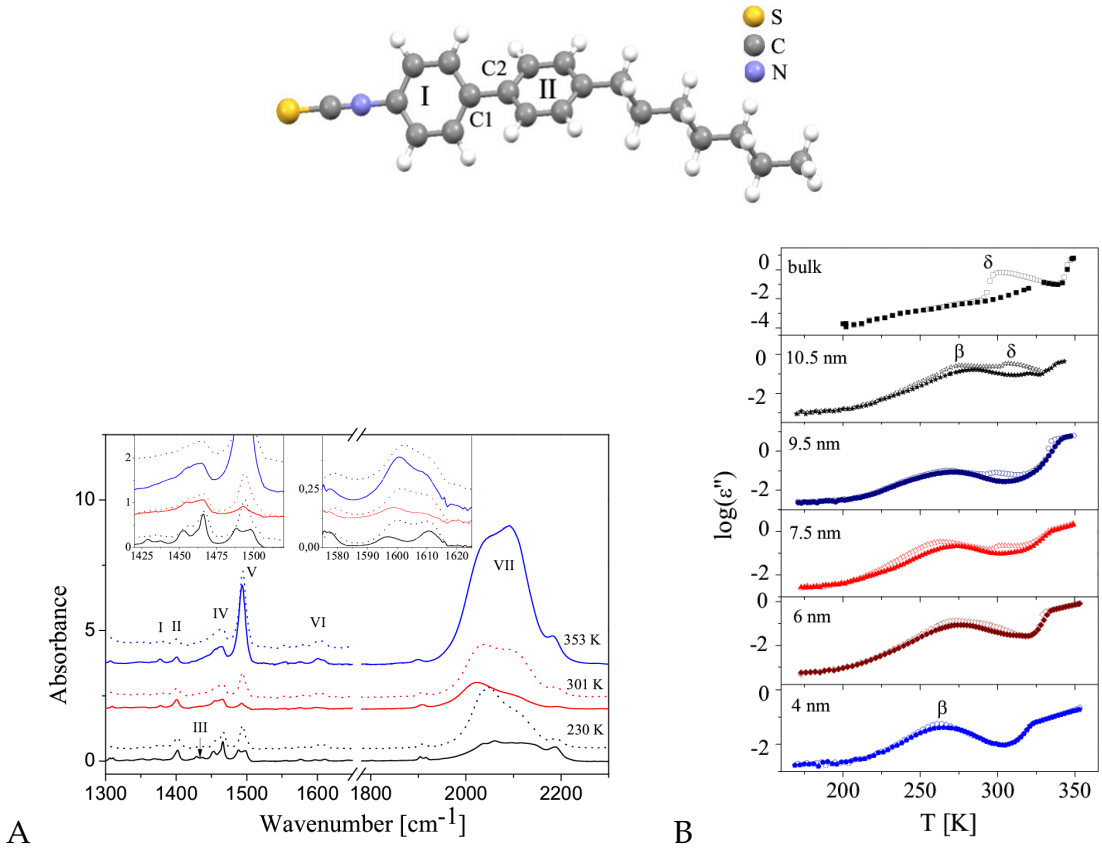

Figure 3.14: (A) Infrared absorption spectra of 7BT obtained on cooling for the bulk (solid lines) and in 6 nm pores (dotted lines) at the indicated temperatures. In the bulk one has the following phases: isotropic at 353 K, SmE at 301 K and the crystalline phase at 230 K. The spectra are normalized with respect to the band at 1400 cm^{-1}. The roman numerals denote the following vibrations: I: CH_2 twisting mode and deformation of CH aromatic, II: CH_3 deformation and CH_2 wagging, III: CH_3 deformation modes, IV: CH_2 scissoring, CH_3 deformation modes, C-C aromatic stretching, CH aromatic deformation, V: C-C aromatic stretching C1-C2, stretching CH aromatic deformation, VI: C-C aromatic stretching, CH aromatic, VII: NCS stretching. (B) Dielectric loss ϵ'' measured at 1.218 kHz as a function of temperature on cooling (empty symbols) and subsequent heating (solid symbols) of the sample in the bulk and in pores.

Broadband Dielectric and Fourier Transform Infrared Spectroscopy are combined to study the mobility and orientation of 4-heptyl-4′-isothiocyanatobiphenyl (7BT) mesogen confined in nano-pores of mean diameters from 4 nm to 10.5 nm [1]. The smectic E phase observed in bulk 7BT is replaced by short-range molecular order imposed by the surface potential within the pores. Transition Moment Orientational Analysis is

employed to explore the orientational order of molecules in pores. The highest degree of molecular order of the mesogenic cores is found for 7BT confined in 6 nm pores.

[1] M. Jasiurkowska, W. Kossack, R. Ene, C. Iacob, W. Kipnusu, P. Papadopoulos, J. Rume Sangoro, M. Massalska-Arodź, F. Kremer, Soft Matter **8**, 5194(2012).

3.13 Intra and inter-molecular dynamics in glass forming low molecular polymeric systems

M. Jasiurkowska, W. Kossack, W.K. Kipnusu, J.R. Sangoro, C. Iacob, F. Kremer

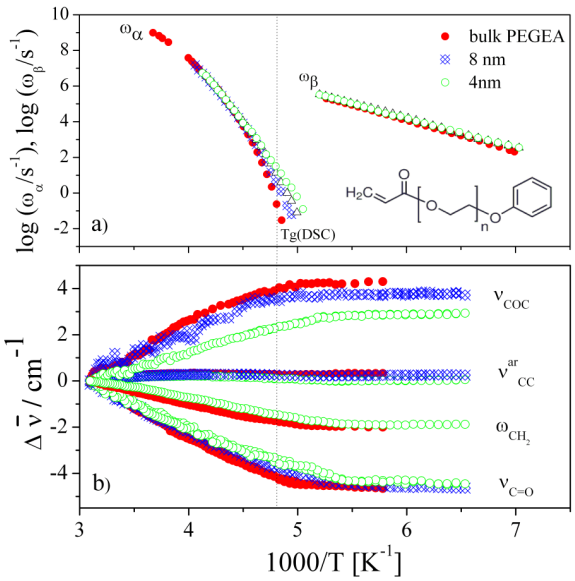

Figure 3.15: Comparison of intra- and inter-molecular dynamic of PEGEA in bulk and confined in nanopores of mean diameters of 4 nm, and 8 nm: Relaxation rates of the segmental (α) and the local (β) processes a) and the shift of the absorption bands of PEGEA with respect to the spectral position at 323 K b).

Broadband Dielectric Spectroscopy (BDS) and Fourier-Transform Infrared Spectroscopy (FTIR) are employed to study the inter- and intra-molecular interaction of two low molecular systems: poly(ethylene glycol) phenyl ether acrylate (PEGEA) and poly(ethyleneglycol) dibenzoate (PEGD), confined in non-intersecting nano-pores. The temperature dependencies of various IR absorption bands are analyzed in term of their spectral position and corresponding oscillator strength and compared with intermolecular dynamic properties obtained by BDS. The conformational changes of the OCC group accompanying the glass transition become less pronounced with the decreasing pore size. The results for PEGEA are presented in Fig. 3.15.

3.14 Physical Aging in glassy systems as reflected in inter- and intramolecular dynamics

W. Kossack, K. Kaminski, F. Kremer

Physical aging of fucose was studied by measuring the time dependence of Fourier-transform infrared (FTIR) and Broadband Dielectric (BDS) spectra in between 30 K to 4 K below the calorimetric glass transition temperature (T_g=305 K). Relaxation times were determined by fitting the spectral position (FTIR) and the dielectric loss (BDS)

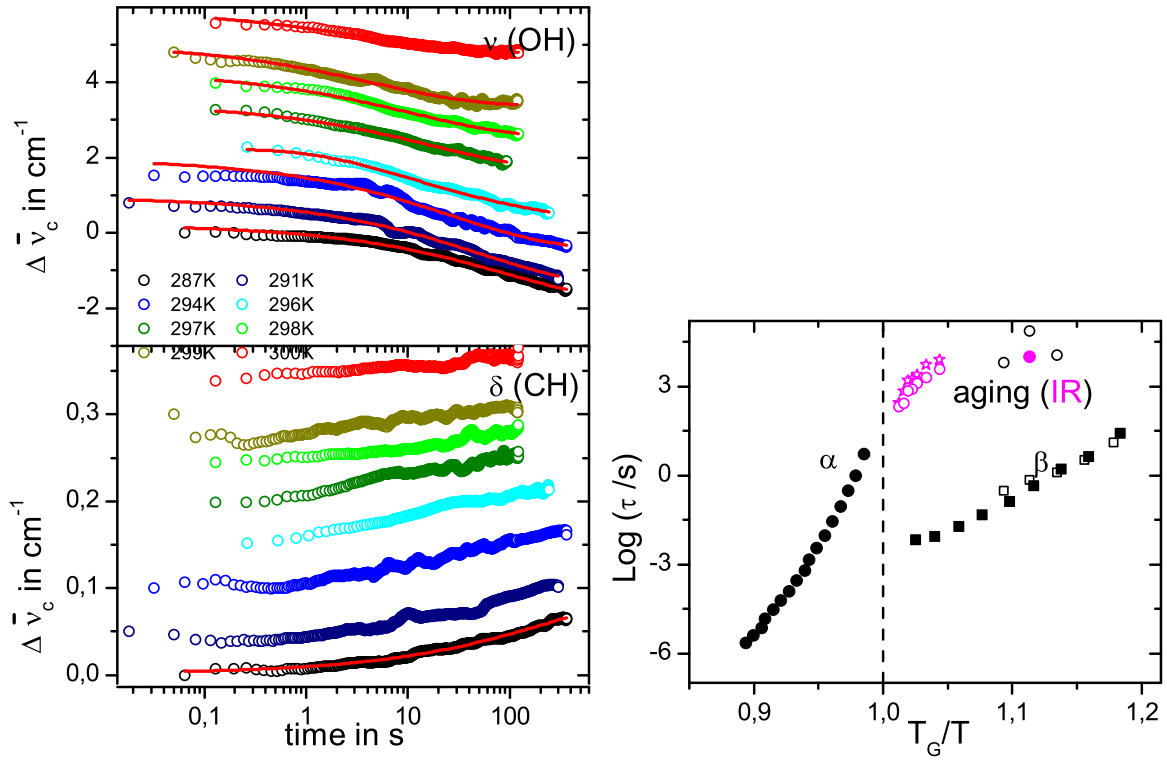

Figure 3.16: The shift of spectral position of the OH stretching (top left) and CH deformation band (bottom left) are shown depending on time for different temperatures. Red lines depict exemplary fits according to a stretched exponential function. The different dependencies are shifted vertically for graphical reasons. In (right) the BDS results of the segmental (α, black circles) and secondary (β, black squares) relaxation times are depicted together with the isostructural (aging) relaxation times from infrared (magenta) and BDS (black). Stars refer to the relaxation rate of oscillator strength and circles to spectral position, whereas filled symbols depict data from D and hollow ones data from L-fucose.

with respect to time by a stretched exponential function [1, 2]. Comparing the results to frequency and temperature dependent BDS measurements above T_g, it turns out that of the OH stretching band interlinks segmental ($T > T_g$) and isostructural ($T < T_g$) relaxation times from BDS. This indicates the fundamental role of the hydrogen bonding network in structure formation below T_g. Furthermore, subtle changes of spectral shape and position appear for a CH deformation vibration with a characteristic time being approximately 1/3 of τ(OH). Hereby, the different behavior of the different molecular moieties is emphasized linking up to molecular flexibility and individualism.

[1] MR. Casalini, C.M. Roland. J. Non-Cryst. Solids. **357** 2, 282 (2011)
[2] P. Papadopoulos, W. Kossack and F. Kremer. Soft Matter **9** (5), 1600 (2013)

3.15 Pressure-dependent FTIR-spectroscopy on the counterbalance between external and internal constraints in spider silk of Nephila pilipes

M. Anton, W. Kossack, R. Figuli, P. Papadopoulos, C. Gutsche, F. Kremer

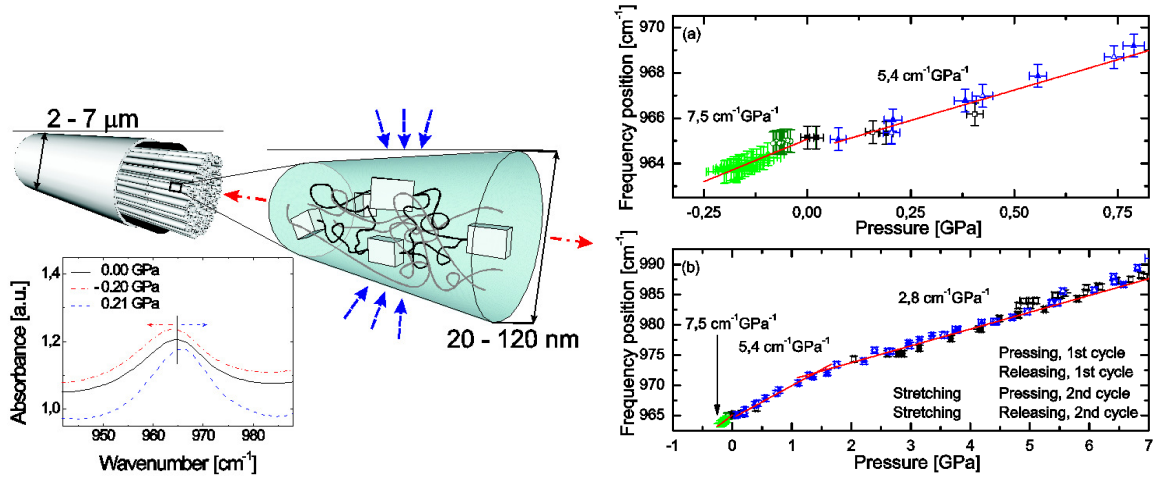

Figure 3.17: Illustration of the structure of spider silk. A fiber is made of fibrils which are composed of pre-stressed nanocrystals embedded in an amorphous matrix. The application of uniaxial stress induce a red shift of the vibration at $\bar{\nu}$=965 cm^{-1}, whereas hydrostatic pressure causes a blue shift. It is evident that the red shift is linear, while the blue shift is preceded by a small plateau and exhibit two linear regimes.

Spider silk exhibits outstanding mechanical properties elevating it to a promising new material for mechanically highly loaded applications, e.g. bullet-proof vests [1]. The reason for that lies in spider silk's unique structure of a glycine-rich amorphous, glassy matrix reinforced by nanocrystals mainly composed of β-sheet polyalanine nanocrystals, which are, additionally, in serial connection by pre-strained chains. FTIR-spectroscopy in combination with external mechanical fields (uniaxial stress and hydrostatic pressure) is a suitable tool to gain insight into this structural organization. Since both stretching and pressing experiments are performed on the same material, the way the nanocrystals are connected with the amorphous phase can be better understood. Unidirectional stress was produced while stretching the sample controlled by micrometer screws and monitored with a force sensor, while hydrostatic pressure was applied by means of a diamond anvil cell (DAC) and determined through the pressure-dependent ruby fluorescence [2]. The non-overlapping $N_C\alpha$ polyalanine stretching vibration $\bar{\nu}$=965 cm^{-1} can be used as molecular sensor of relative force changes within the β-sheet nanocrystals [1]. Hence, one is able to study the microscopic response to external mechanical fields through the observation of shifts of this vibration. In the case of applied unidirectional stress a linear red shift and for applied hydrostatic pressure a blue shift with a preceding plateau of the vibration is observed. The linear dependence of the blue shift bends off for hydrostatic pressure greater than 1.4 GPa and is fully reversible up to 7 GPa. The seamless connection of negative and positive pressure

regimes corroborate quantitatively our structural model of spider silk as composed of pre-stressed alanine-rich nanocrystals embedded in a glycine-rich amorphous matrix. It is also confirmed that nanocrystals withstand high pressures without undergoing structural transition or deteriorating their mechanical properties. Preliminary measurements in collaboration with Jihaan Ebad-Allah and Prof. Dr. Christine Kuntscher from the University of Augsburg are highly acknowledged.

[1] P. Papadopoulos et al., Eur. Phys. J. E **24**, 193(2007); P. Papadopoulos et al., Colloid. Polym. Sci. **287**, 231(2009); R. Ene et al., Soft Matter **5**, 4568 (2009)
[2] Ruby under pressure, K. Syassen, High Press. Res. **28**, 75 (2008)

3.16 Time-dependent FTIR-spectroscopy on fibrillization of Amyloid-β(1-40) protein

M. Anton, W. Kossack J. Adler, D. Huster, F. Kremer

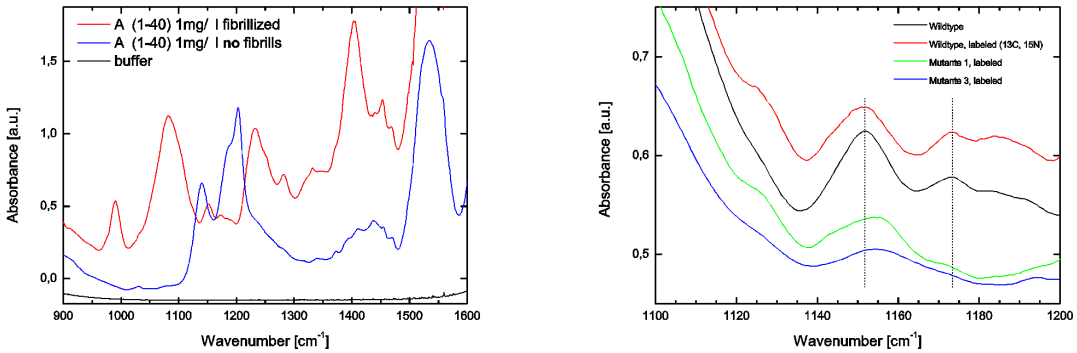

Figure 3.18: The left panel shows the fingerprint region of non-fibrillized and fibrillized Aβ(1-40) and the drastic changes coming from fibrillization. The right panel depicts an enlargement of the fingerprint region. Effects due to exchange of isotopes and amino acids are visible.

The fibrillization of peptides is a subject of great current interest. On the one hand, the formation of fibrils is symptomatic of many diseases, Alzheimer's, Parkinson's, or Creutzfeld-Jacob disease for instance, on the other hand these structures are of interest for novel applications in terms of nanotechnology [1]. Amyloid-β(1-40) protein is a naturally occurring peptide in human brains and is believed to play a crucial role in Alzheimer's disease. It forms a cross-β structure resulting in a rigid fibril. It is known that toxic forms of this and other proteins share the identical chemical structure than non-toxic forms, which led to the hypothesis that the physical state determines the possible toxicity of the protein [2]. It is believed that amyloid formation is not a matter of amino acid sequence; instead it is an aspect of polymer dynamics. Interestingly not only the protein parts incorporated in β-sheets exhibit a high order parameter, also the motion of the N-terminus of a peptide chain integrated into a fibril is somewhat suppressed [3]. FTIR-spectroscopy combines the specificity of vibration spectroscopy with fast data acquisition. Therefore it is suitable to investigate the dynamics during fibrillization in situ. Infrared studies are commonly focused on the amide I band, which is associated with C=O stretching vibration and, hence, the -sheet content of a structure. Unfortunately, this band results from a superposition of up to 12 different single peaks [4]. Consequently, the extraction of unambiguously spectral information is difficult. To extract reliable information, we concentrate our study on the fingerprint region. In preliminary measurements we found a drastic change in vibrational spectra from non-fibrillized to the fibrillized state. Additionally, the spectra of ^{13}C and ^{15}N labeled wildtype Aβ(1-40) peptide and labeled mutants of it show differences due to isotopic effects and varied amino aid sequence.

[1] I. W. Hamley, Angew. Chem. Int. (2007) 46, 8128; T. Scheibel et al., Handb. Exp. Pharmacol. **199** (2006)

[2] S. B. Prusiner, Proc. Natl. Acad. Sci. USA. (1998) 95, 13363; M. Fändrich, J. Mol. Biol. **421**, 427 (2012)
[3] H. A. Scheldt et al., J. Biol. Chem. **287**, 2017 (2012)
[4] H. Hiramatsu et al., Biochim. Biopyhs. Acta (2005) 1753, 100; X. Hu et al., Macromol. **39**, 6161 (2006)

3.17 The interaction between HPT-101 and tau-peptides with different phosphorylation patterns investigated by optical tweezers

C. Wagner, D. Singer, T. Stangner, C. Gutsche, R. Hoffmann, F. Kremer

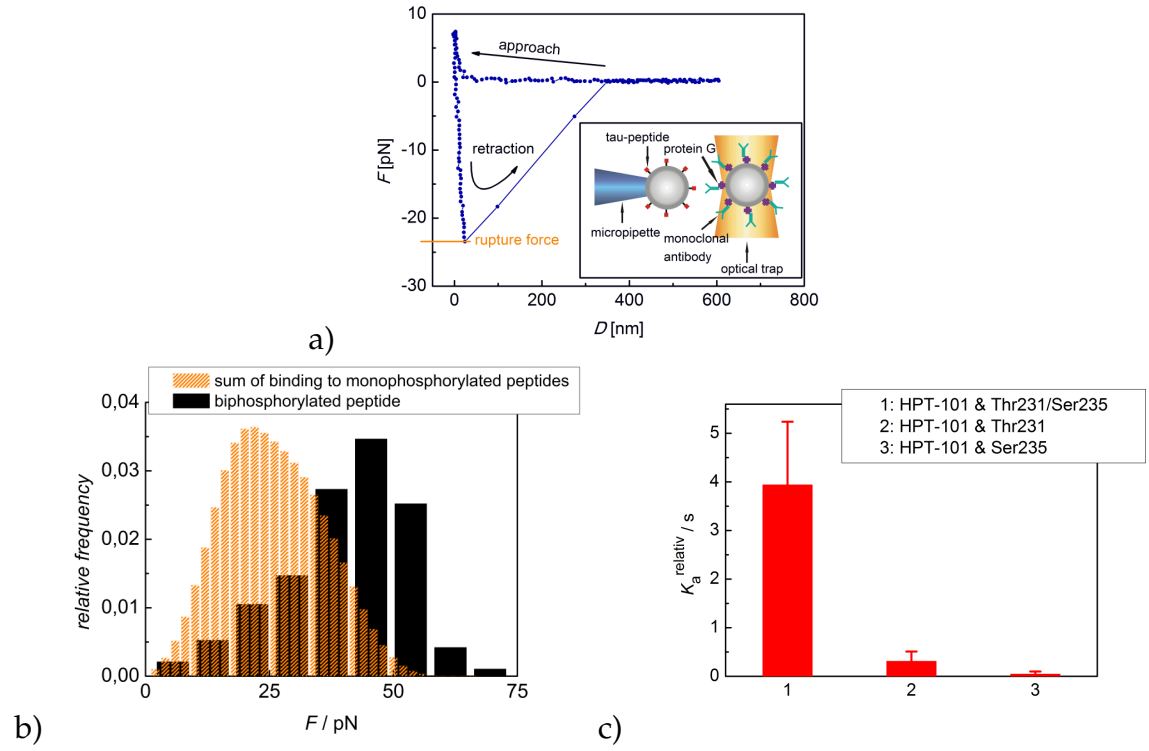

Figure 3.19: a) A typical force-distance dependence is shown. The beads are brought in contact and pulled apart with a preset velocity. Due to an individual binding between the tau-peptide and the mAb the particle in the optical trap is shifted out of the equilibrium position. Inset: The experimental configuration. b) The black histogram shows the experimentally observed rupture-force distribution of HPT-101 binding to the biphosphorylated peptide. The orange histogram corresponds to the theoretically calculated sum of the binding to the monophosphorylated peptides. The strong specific interaction cannot be explained by the summation of the binding to single phosphorylation sites. c) Relative affinity of the binding to peptides with different phosphorylation pattern. The specific binding to the biphosphorylated peptide shows the highest affinity.

Optical tweezers-assisted dynamic force spectroscopy is employed to investigate specific receptor/ligand bindings on the level of single binding events [1]. Here, the specific binding of the anti-human tau monoclonal antibody (mAb) HPT-101 to synthetic tau-peptides with 2 potential phosphorylation (Thr231 and Ser235) sites is analyzed (Fig. 3.19a). The binding parameters bond lifetime τ_0, the characteristic length x_{ts} and the free energy of activation ΔG are determined for the interactions to the biphosphorylated as well as to the two monophosphorylated peptides. It is shown that the specific binding to the biphosphorylated peptide is much stronger than expected from the summation

of the interactions to each monophosphorylated peptide (Fig. 3.19b). Calculating the relative affinity from the single-molecule data reveals a significantly higher value for the binding to the biphosphorylated peptide (Fig. 3.19c).

[1] C. Wagner et al., Soft Matter **7** (9), 4370 - 4378(2011)

3.18 Investigating the interactions between GPCRs and ligands on a single-contact level

C. Wagner, T. Stangner, C. Gutsche, U. Reibetanz, M. Göse, P. Schmidt, D. Huster, F. Kremer

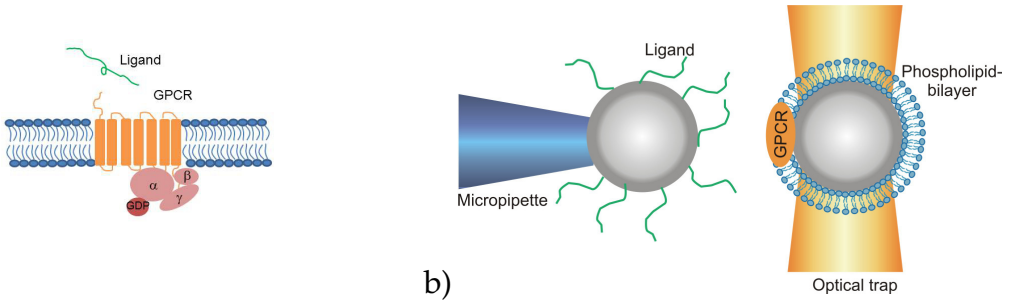

a) b)

Figure 3.20: (a) The G-protein coupled receptor consists of extra-, intracellular and transmembrane domains. A ligand binding from the extracellular side causes a structural change of the receptor. (b) Experimental setup to measure the interaction between GPCRs and ligands on a single-contact level. The colloid in the optical trap is covered by phospholipid bilayers containing GPCRs. The ligands are immobilized on the surface of the colloid in the micropipette.

Optical tweezers provide an extraordinary technique for the investigation of the interactions between biological macromolecules on a single-molecule level as they allow for positioning a micron-sized particle with nanometer resolution and measuring the forces acting on it with an accuracy of ~50 fN. In this project, the system of interest is the interaction between G-protein coupled receptors (GPCRs) and ligands. GPCRs are receptors, which transduce signals through the cell membrane. They consist of extra- and intracellular loops as well as transmembrane segments (Fig. 3.20a). The binding of a ligand causes a structural change of the receptor. To measure the binding between the Y2 receptor and its ligand neuropeptide Y by means of optical tweezers, the colloid held in the optical trap is covered with phospholipid bilayers mimicking the cell membrane. The GPCRs will then be inserted into this membrane. Also, the ligand will be immobilized on the surface of a microparticle, which is attached to the tip of a micropipette (Fig. 3.20b). In a first step, control experiments have to be carried out to investigate the interaction between membrane-covered particles as well as between a membrane covered particle and a blank one.

[1] Walther C, Mörl K, Beck-Sickinger AG. Neuropeptide Y receptors: ligand binding and trafficking suggest novel approaches in drug development. J Pept Sci. 233 (2011)

3.19 FACS-sorted particles reduce the data variance in Optical Tweezers assisted Dynamic Force Spectroscopy measurements

T. Stangner, D. Singer, C. Wagner, O. Ueberschär, C. Gutsche, R. Hoffmann, F. Kremer

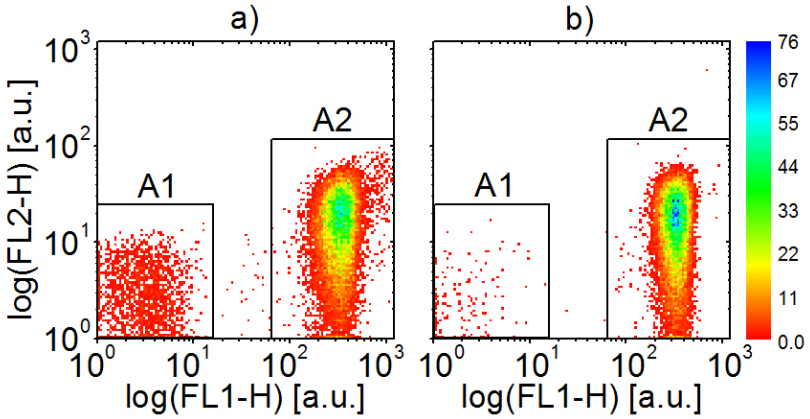

Figure 3.21: 2D-density plot of tau-peptide labeled MF-particles (diameter: 2.3 μm) in dependence on intensity signal of channel FL2-H vs. FL1-H. a) FACS data before the selection process. Two populations are visible: A1 contains uncoated colloids and A2 contains the fluorescence tagged tau-particles. It is apparent that both populations can be distinguished. b) Same batch of colloids as in a), but after sorting. Population A1 is sorted out, only the target population A2 remains with a significant reduction in width and a pronounced increase in density (blue color).

By Optical Tweezers assisted dynamic force spectroscopy experiments combined with fluorescence activated cell sorting (FACS), we demonstrate a new approach to reduce the data variance in measuring receptor-ligand-interactions on a single molecule level by ensuring similar coating densities. Therefore, the carboxyfluorescein-labeled monophosphorylated peptide tau226-240[pThr231] is anchored on melamine resin beads and these beads are sorted by FACS to achieve a homogeneous surface coverage (Fig. 3.21). To quantify the impact of the fluorescence dye on the bond parameters between the phosphorylated peptide and the corresponding phosphorylation specific anti-human tau monoclonal antibody HPT-104, we perform dynamic force spectroscopy and compare the results to data using unsorted beads covered with the non-fluorescence peptide analogue. Finally, we demonstrate that the data variance of the relative binding frequency is significantly decreased by a factor of 3.4 using presorted colloids with a homogeneous ligand coating compared to unsorted ones.

[1] C. Wagner, D. Singer, T. Stangner, O. Ueberschär, C. Gutsche, R. Hoffmann, F. Kremer, Soft Matter **7**, 4370 (2011)
[2] T. Stangner, D. Singer, C. Wagner, C. Gutsche, O. Ueberschär, R. Hoffmann, F. Kremer, Phys.Biol. **10** (2013), 046004

3.20 Amino acid sequence dependent interactions between receptors and ligands studied with Optical Tweezers

T. Stangner, D. Singer, C. Wagner, C. Gutsche, R. Hoffmann, F. Kremer

Sequence	V	A	V	V	R	pT	P	P	K	pS	P	S	S	A	K
HPT-101 (pT & pS)	V	A	V	V	R	pT	P	P	K	pS	P	S	S	A	K
HPT-104 (pT)	V	A	V	V	R	pT	P	P	K	pS	P	S	S	A	K
HPT-110 (pS)	V	A	V	V	R	pT	P	P	K	pS	P	S	S	A	K

Figure 3.22: Epitop mapping of monoclonal antibody HPT-101, HPT-104 and HPT-110. The antibody specific phosphorylation sites are underlined (abbreviation: p = phosphorylation) and essential amino acids are shown in red. Secondary amino acids, which contribute to binding, are highlighted in orange. White fields are not significant for the specific interaction between antigen and antibody.

For diagnostic procedures that rely on monoclonal antibodies (mAb), it is imperative to know whether the antibody (e.g. HPT-101) recognize the epitope of its target peptide/protein (e.g. tau-protein) specific or whether possible cross-reactivity may occur with other forms of the protein. In Wagner et al. [1] non-specific interactions of two antibodies with the tau-peptide were detected. Based on this result, an epitope mapping was generated. By means of the so called alanine-scan, it is possible to identify essential as well as secondary amino acids for the interaction between the tau-peptide and four different monoclonal antibodies (Table 1, performed by Dr. D. Singer with ELISA, BBZ Leipzig). It is apparent that the specificity of the antibody refers not only to a specific isolated phosphorylation site, but to the surrounding amino acid sequence in the tau peptide. First Optical Tweezers assisted measurements show that the dynamic force spectroscopy approach can make qualitative statements about the existence of essential amino acids and secondary amino acids and identify them, respectively.

[1] C. Wagner, D. Singer, T. Stangner, O. Ueberschär, C. Gutsche, R. Hoffmann, F. Kremer, Soft Matter **7**, 4370 (2011)

3.21 Electrophoretic mobility and charge inversion of a colloidal particle studied by SCE and MD simulations

I. Semenov, S. Raafatnia, M. Sega, V. Lobaskin, C. Holm, F. Kremer

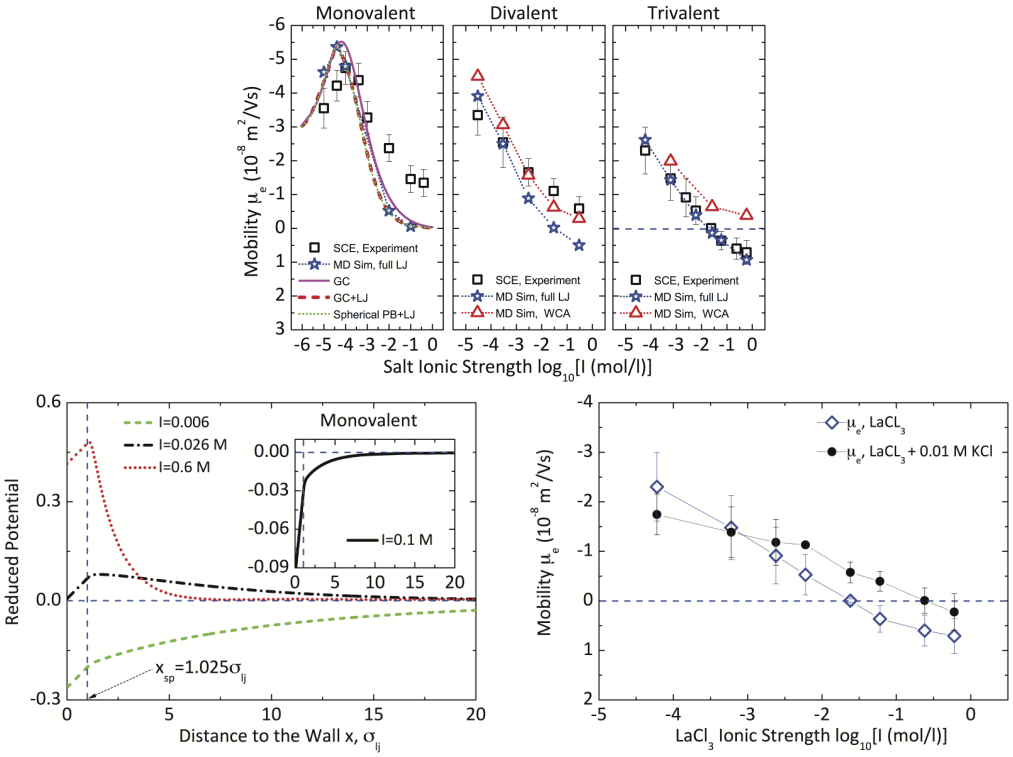

Figure 3.23: (top) electrophoretic mobility versus salt ionic strength of aqueous solutions of varying valency (KCl, $CaCl_2$, and $LaCl_3$). The measurements for each valency are carried out with the very same negatively charged PS colloid (diameter: 2.23 μm). (bottom left) Reduced electric potential profiles at different ionic strengths obtained from the MD simulations of the trivalent case. The shear plane is taken to be at $x_{sp} = 1.025\sigma_{lj}$ from the solid surface. Above ionic strengths I > 10^{-2} mol/l, the ζ-potential changes sign and, consequently, the mobility is reversed. In the inset, the reduced potential profile is shown for the monovalent case at ionic strength 10^{-1} mol/l with no mobility reversal observed. (bottom right) Electrophoretic mobility versus salt ionic strength of $LaCl_3$ aqueous solution with added monovalent screening salt.

A novel experimental method and computer simulations are used to examine the ion-surface interactions and the structure of the ionic double layer as a function of added KCl, $CaCl_2$, and $LaCl_3$ salt [1, 2]. Mobility reversal of a negatively charged latex colloid is observed in the presence of trivalent La^{3+} ions (Fig. 3.23(top)). Moreover, these observations are corroborated by the results of molecular dynamics (MD) simulations of the restricted primitive model [3], which are used to calculate the electric double layer structure and the ζ-potential (Fig. 3.23(middle)), and then, augmented by the standard electrokinetic model [4], the colloid mobility. It is shown that the experimental mobilities in mono- and divalent salts can be well reproduced with the electrostatic mechanism alone, whereas for the trivalent La^{3+} ions an additional attractive term between ions

and colloid surface is essential to reproduce the observed mobilities. The importance of electrostatic correlations in the observed electrophoretic mobility reversal, is confirmed with the measurements in the presence of trivalent salt ($LaCl_3$) are repeated with 10^{-2} mol/l of added KCl. Since the monovalent salt screens the Coulomb interactions, a shift of the isoelectric point to higher ionic strengths is observed as expected (Fig. 3.23(bottom)) [5].

[1] I. Semenov et al., J. Phys. Cond. Matter **22**, 494109(2010)
[2] I. Semenov et al., J Col. Int. Sci. **337**, 260(2009)
[3] O. Lenz and C. Holm, Euro Phys J. E **26**, 191(2008)
[4] R. W. O'Brien and L. R. White, J. Chem Soc. **74**, 1607(1978)
[5] I. Semenov et al., Phys. Rev. E (2012)

3.22 Microfluidic mobility of single (DNA-grafted) colloids in dilute DNA suspensions

O. Ueberschär, M. Krüger, C. Gutsche, T. Stangner, C. Wagner, K. Kühne, F. Kremer

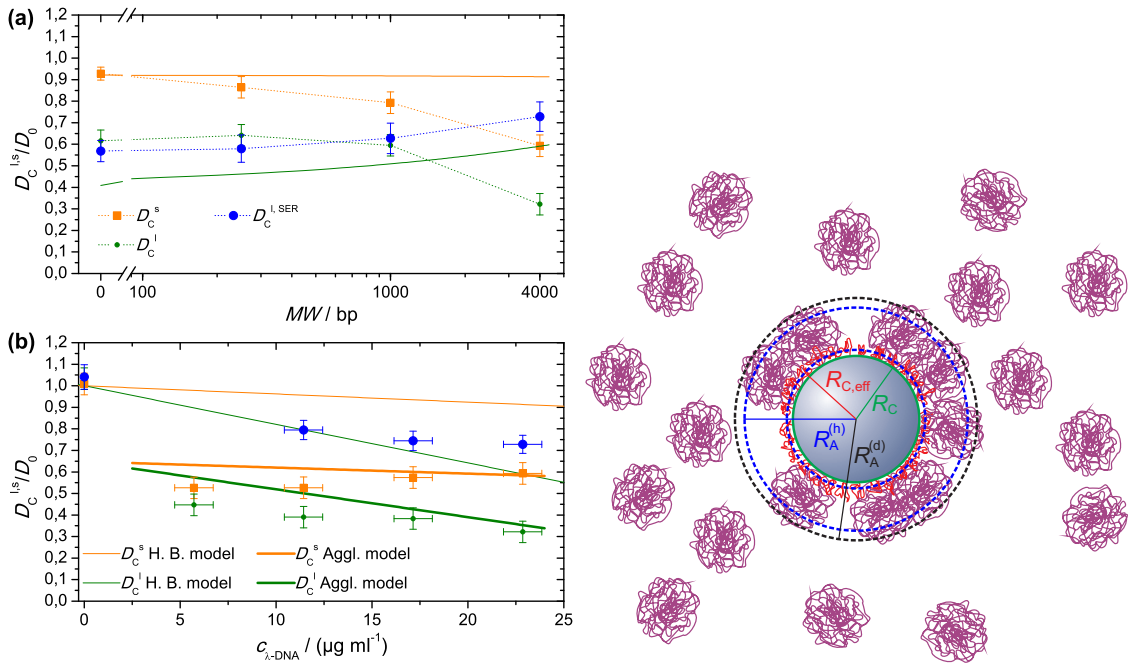

Figure 3.24: left: Short and long time diffusion coefficients of grafted microspheres. (a) Comparison of the directly measured diffusion coefficients D_C^s and D_C^l to the corresponding $D_C^{l,SER}$ values derived from drag measurements as function of the molecular weight MW. For **MW**=4000 bp , a clear discrepancy of $D_C^l \approx 0.4 D_C^{l,SER}$ is observed. The predictions of the hydrodynamic brush (H. B.) model are depicted as thin solid lines whereas the agglomeration (Aggl.) model results are plotted as thick solid lines. The agglomeration model yields a correct prediction for D_C^s and D_C^l. right: Schematic of agglomerate formation. Entanglements between grafted DNA molecules (4000 bp, orange) on the tracer microsphere core (grey) with λ-DNA coils (purple) from the suspension lead to the formation of a diffusing agglomerate. The (effective) hydrodynamic radii of the bare core (R_C), of the grafted microsphere ($R_{C,eff} = R_C + H_B$, black circle) and the agglomerate ($R_A^{(h)} \approx R_{C,eff} + 2R_H$, blue circle) are depicted schematically.

By employing single particle tracking on the basis of fast video microscopy, we directly measure the equilibrium short and long time diffusion coefficients of blank and DNA-grafted (molecular weight of 250, 1000 and 4000 base pairs (bp)) tracer colloids in dilute λ-DNA solutions. We compare these results to recently reported microfluidic mobilities under non-equilibrium steady state flow and to the predictions of quantitative theoretical models. A pronounced discrepancy between the measured equilibrium and non-equilibrium mobilities is observed for colloids grafted with 4000 bp DNA molecules, revealing the inapplicability of the Stokes-Einstein relation under these conditions. We demonstrate that this deviation may be interpreted as a strong micro-shear-thinning effect that is caused by the formation of entanglements between the grafted DNA brush and λ-DNA coils from the suspension.

[1] O. Ueberschär, M. Krüger, C. Gutsche, T. Stangner, C. Wagner, K. Kühne, F. Kremer. Polymer **53**, 5760 (2012)

3.23 Funding

FOR 877: " From local constraints to macroscopic transport" TP 7 "Electric field driven motion of single polyelectrolyte grafted colloids" TP3 "Dynamics of DNA under tension and confinement"
Prof. Dr. F. Kremer and Prof. Dr. K. Kroy
KR 1138/21-1 (2007-2011)

FOR 877: " From local constraints to macroscopic transport" TP 7 "Electric field driven motion of single polyelectrolyte grafted colloids"
Prof. Dr. F. Kremer
KR 1138/21-2 (2011-2014)

SPP 1191 "Ionic Liquids" TP "Charge transport and glassy dynamics in ionic liquids"
Prof. Dr. F. Kremer
KR 1138/18-3 (2010-2012)

SPP 1369 "Polymer-Solid Contacts: Interfaces and Interphases" TP "Interfacial dynamics of polymers in interaction with solid substrates"
Prof. Dr. F. Kremer
KR 1138/23-1 (2008-2011), KR 1138/23-2 (2011-2014)

Graduate School "Leipzig School of Natural Sciences -Building with Molecules and Nano-objects" BuildMoNa, TP 15 "Dynamics of DNA under tension and in confinement"
Prof. Dr. F. Kremer
GSC 185/1 (2008-2012)
Prof. Dr. F. Kremer is Principal Investigator and Lecturer in the International Research Training Group "Diffusion in Porous Materials" headed by Prof. Dr. R. Gläser and Prof. Dr. F. Kapteijn.

IRTG "Diffusion in Porous Materials" TP "Molecular Dynamics in Intentionally Tailored Nanopores"
Prof. Dr. F. Kremer
GRK 1056/02 (2009-2013)
Prof. Dr. F. Kremer is Principal Investigator and Lecturer in the International Research Training Group "Diffusion in Porous Materials" headed by Prof. Dr. R. Gläser and Prof. Dr. F. Kapteijn.

SFB/TRR 102 " Polymers under multiple constraints: restricted and controlled molecular order and mobility" TP B05 "Structural levels of organisation in spider-silk - a combined mechanical and IR-spectroscopic study" (2011-2015) TP B08 "Broadband Dielectric Spectroscopy to study the molecular dynamics in nanometer thin layers of block copolymers" (2011-2015)
Prof. Dr. F. Kremer

Prof. Dr. F. Kremer is deputy chairman of the SFB-TRR 102 on "Polymers under multiple constraints: resticted and controlled molecular order and mobility"of the Universities of Halle and Leipzig.

3.24 Organizational Duties

Hartmut Domröse
- electronic technician

Kerstin Lohse
- secretary

Dipl.-Phys. Cordula Bärbel Krause
- secretary

Karin Girke
- secretary

Dipl.-Ing. Jörg Reinmuth
- technician

Dipl.-Phys. Wiktor Skokow
- technician

3.25 External Cooperations

Industry

- Novocontrol, Hundsangen, Germany
- BOREALIS Polyolefine GmbH, Linz, Austria
- IST METZ GmbH
- Süd-Chemie AG

3.26 Publications

Journals

Iacob, C., J. R. Sangoro, W. K. Kipnusu, J. Kärger, F. Kremer "Enhanced charge transport in nano-confined ionic liquids" Soft Matter 8, 289-293 (2012) DOI:10.1039/C1SM06581E

Ueberschär, O., C. Wagner, T. Stangner, C. Gutsche, F. Kremer "A novel video-based microsphere localozation algorithm for low contrast silica particles under white light illumination" Optics & Lasers in Engineering 50, 423-439 (2012) DOI: 10.1016/j.optlaseng.-2011.10.012

Sangoro, J.R., F. Kremer "Charge transport and glassy dynamics in ionic liquids" Acc. Chem. Res. 45 (4), 525-532 (2012) DOI: 10.1021/ar2001809

Jasiurkowska, M., W. Kossack, R. Ene, C. Iacob, W. K. Kipnusu, P. Papadopoulos, J. R. Sangoro, M. Massalska-Arodz, F. Kremer "Molecular dynamics and morphology in confined 4-heptyl-4-isothiocyanoatobiphenyl liquid crystals" Soft Matter 8, 5194-5200 (2012) DOI: 10.1039/C2SMO7258K

Sangoro, J. R., M. Mierzwa, C. Iacob, M. Paluch, F. Kremer "Brownian dynamics determine the universality of charge transport in ionic liquids" RSC Adv. 2, 5047-5050 (2012) DOI: 10.1039/C2RA20560B

Kipnusu, W. K., W. Kossack, C. Iacob, M. Jasiurkowska, J. R. Sangoro, F. Kremer "Molecular Order and Dynamics of Tris(2-ethylhexyl)phosphate Confined in Uni-Directional Nanopores" Z. Phys. Chem.; Vol. 226 No. 7-8, 797-805 (2012) DOI: 10.1524/-zpch.2012.0287

Ene, R., C. Krywka, S.-G. Kang, P. Papadopoulos, M. Burghammer, E. Di Cola, M. Müller, F. Kremer "Structure changes in Nephila dragline: The in?uence of pressure" Polymer 53, 5507-5512 (2012) DOI: 10.1016/j.polymer.2012.09.045

A. Schönhals, F. Kremer "Amorphous Polymers" in: "Polymer Science: A Comprehensive Reference" Vol. 1, pp. 201-226, Matyjaszewski K. and Möller M. (Eds) Elsevier B.V., Amsterdam (2012) ISBN: 978-0-444-53349-4

Serghei A., J. R. Sangoro, F. Kremer "Broadband Dielectric Spectroscopy on electrode polarization and its scaling" in: "Electrical Phenomena at Interfaces and Biointerfaces: Fundamentals in Nano- Bio- and Environmental Sciences", Chapter 15, Hiroyuki Ohshima (Eds.) John Wiley&Sons, Inc. New York (2012) DOI: 10.1002/9781118135440.ch15

Semenov, I., S. Raafatnia, M. Sega, V. Lobaskin, C. Holm, F. Kremer "Electrophoretic mobility and charge inversion of a colloidal particle studied by single-colloid electrophoresis and molecular dynamics simulations" Phys. Rev. E (2012) pre.aps.org/accepted/-1b07dY3cE9e15c25784a84737ca6d950ab1d3a109

Ueberschär O., M. Krüger, C. Gutsche, T. Stangner, C. Wagner, K. Kühne, F. Kremer "Microfluidic mobility of single (DNA-grafted) colloids in dilute DNA suspensions" Polymer 53, 5760-5770 (2012) DOI: 10.1016/j.polymer.2012.09.045

Papadopoulos P., W. Kossack, F. Kremer "Intra- and inter-molecular dynamics in glass-forming liquids" Soft Matter 9, 1600-1613 (2013) DOI: 10.1039/c2sm27249k

Books

A.R. Khokhlov, F. Kremer "Basic Concepts and Polymer Properties" in: Polymer Science: A Comprehensive Reference Vol. 1, pp. 1-2, Matyjaszewski K. and Möller M. (Eds.), Elsevier B.V., Amsterdam (2012), ISBN: 978-0-444-53349-4

Kremer F., E. U. Mapesa, M. Treß, M. Reiche "Molecular Dynamics of Polymers at Nanometric Length Scales: From Thin Layers to Isolated Coils" in: "Recent Advances in Broadband Dielectric Spectroscopy", Y. P. Kalmykov (Eds.) NATO Science for Peace and Security Series B: Physics and Biophysics, Chapter 12, Springer (2012) DOI 10.1007/978-94-007-5012-8, ISBN: 978-9-400-75011-1

3.27 Graduations

Doctorate

- M. Sc. Ciprian Iacob
  Rotational and Translational Diffusion of Glass-Forming Ionic Liquids Confined in Nanoporous Silica

Master

- Markus Fuchs
  Molelulare Dynamik in sub-Mikrometer dünnen Block-Copolymer Schichten

Bachelor

- Benjamin Schott
  Untersuchung photophysikalischer Eigenschaften des Photosenibilisators THPTS

3.28 Guests

- Dr. Kamil Krystian Kaminski
  University of Silesia, Poland

4

Physics of Interfaces

4.1 Introduction

The department of Physics of Interfaces (Grenzflächenphysik, GFP) is in a transition state since April 2009. From the 16 scientists employed in the group at the end of 2012, 14 were financed as PhD students or post-docs via third party funding and one received a grant as Heisenberg fellow of the DFG. The good situation with respect to third party funding allowed us to successfully contribute to research and teaching within the Institute of Experimental Physics I. Teaching obligations in several main courses of Experimental Physics were taken over by scientists of the group. After finishing their Ph.D studies within the International Research Training Group "Diffusion in Porous Materials", Marcel Gratz, Markus Wehring and Florian Hibbe obtained their Ph.D degrees in 2012, left our group and continued their careers elsewhere.

PD Dr. F. Stallmach

4.2 ^{7}Li, ^{13}C and ^{133}Cs NMR self-diffusion studies in mesoporous silica foam and microporous MOF CuBTC

St. Schlayer, A.-K. Pusch, C. Horch, St. Beckert, M. Peksa, F. Pielenz, W.-D. Einicke* F. Stallmach

*Institut für Technische Chemie, Universität Leipzig

A standard WB 400 NMR probe (Bruker, Germany) was equipped with a *z*-gradient coil to enable high-sensitivity pulsed field gradient NMR diffusion studies of Li^+ and Cs^+ cations of aqueous salt solutions in a high-porosity mesocellular silica foam (MCF) and of CO_2 adsorbed in metal-organic frameworks (MOF). The gradient coil was designed using finite element simulations and constructed in the workshop of the Physics Institutes (see Fig. 4.1). It yields pulsed field gradients of up to $\pm 16.2\,\mathrm{Tm}^{-1}$. The gradient system was calibrated at ^{2}H resonance frequency using deuterated water as reference and up to now successfully applied for diffusion studies at ^{7}Li, ^{23}Na, ^{13}C and ^{133}Cs frequencies [1].

The diffusivities of the cations in $LiCl_{ac}$ and $CsCl_{ac}$ solution are significantly reduced if introduced into MCF pore network. By comparison of this diffusion behavior with

that of the bulk solutions, a tortuosity of the silica foam of 4.5 ± 0.6 was determined [1]. Single component self-diffusion of CO_2 and CH_4 (measured by ^{1}H NMR) as well as self-diffusion of the individual components in CO_2/CH_4 mixtures was studied in the MOF CuBTC. The experimental results confirm high mobilities of the adsorbed gases and trends for diffusion separation factors predicted by MD simulations [1, 2].

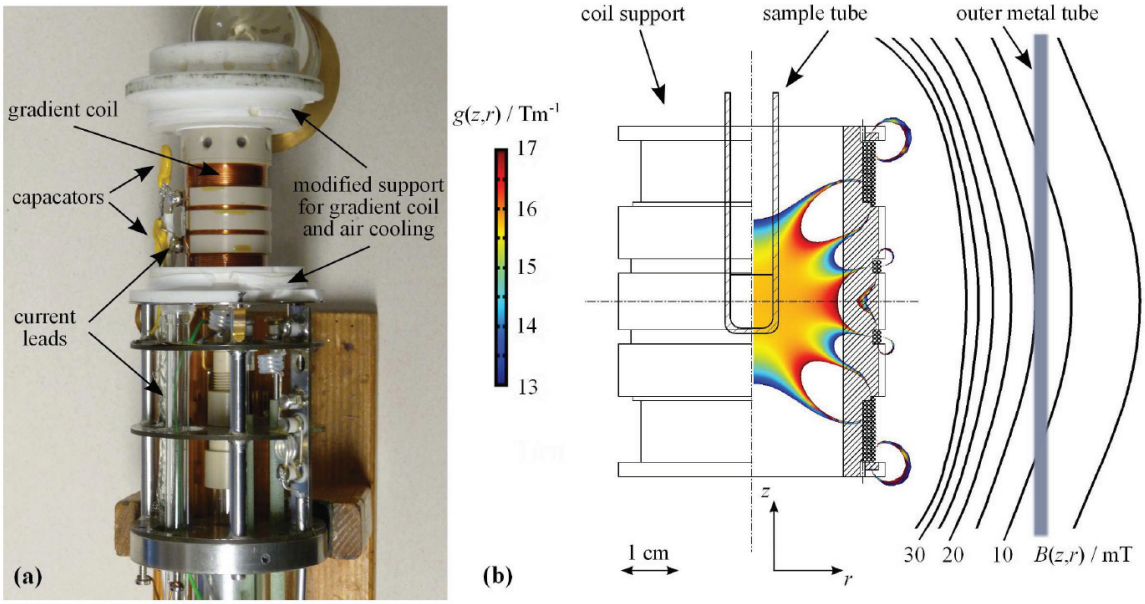

Figure 4.1: Design of the modified z-gradient probe for NMR diffusion studies: Photograph of the uncovered probe (a) and drawing of the gradient coil (b) including the 2d plots of the resulting magnetic field gradient $g(z, r)$ and the stray field $B(z, r)$ at 100 A gradient current.

[1] St. Schlayer, A.-K. Pusch, F. Pielenz, St. Beckert, M. Peksa, C. Horch, L. Moschkowitz, W.-D. Einicke, F. Stallmach, Materials **5**, 617 (2012)
[2] S. Keskin, J. Liu, J. K. Johnson, D. S. Sholl: Microporous Mesoporous Mater. **125** 125, 101 (2009)

4.3 NMR studies of carbon dioxide and methane self-diffusion in ZIF-8 at elevated gas pressures

A.-K. Pusch, T. Splith, St. Schlayer, F. Pielenz, R. Biniwale [*], G.B. Suffritti [†], J. Cravillon [‡], G. Papadopoulos [§], F. Stallmach

[*]National Environmental Engineering Research Institute, Nagpur, India
[†]Department of Chemistry, University of Sassari, Italy
[‡]Institute of Inorganic Chemistry, University Hannover, Germany
[§]School of Chemical Engineering, National Technical University of Athens, Greece

Self-diffusion measurements with methane and carbon dioxide adsorbed in the Zeolitic Imidazolate Framework-8 (ZIF-8) were performed by ^{1}H and ^{13}C pulsed field gradient

nuclear magnetic resonance [1]. The experiments were conducted at 298 K and variable pressures of 7 to 15 bar in the gas phase above the ZIF-8 bed. The self-diffusion coefficients of carbon dioxide are in good agreement with results from molecular dynamic (MD) simulations and resume the trend previously found by IR microscopy at lower loadings [2]. Methane diffuses in ZIF-8 only slightly slower than carbon dioxide. Its experimentally obtained self-diffusion coefficients are about a factor of two smaller than the corresponding values determined by MD simulations using flexible frameworks.

[1] A.-K. Pusch, T. Splith, L. Moschkowitz, S. Karmakar, R. Biniwale, M. Sant, G. B. Suffritti, P. Demontis, J. Cravillon, E. Pantatosaki, F. Stallmach, Adsorption **18**, 359 (2012)
[2] E. Pantatosaki, G. Megariotis, A.-K. Pusch, Ch. Chmelik, F. Stallmach, G. Papadopoulos, J. Phys. Chem. **116**, 201 (2012)

4.4 Understanding molecular transport in hierarchical porous materials

P. Zeigermann, A. Shakhov, J. Kärger, R. Valiullin,

Performance of many technological processes involving porous solids ultimately depends on their transport properties. In recent years, an increasing interest is attracted by porous materials with hierarchical organization of the pore spaces providing a good combination of high mass transfer rate and chemical functionality [1]. Although enhanced transport in these materials has already been supported by experimental evidence, better understanding of the structure-dynamics relationships still remains a challenging problem. In our work, we have combined theoretical modeling and experiments using nuclear magnetic resonance diffusometry to describe microscopic transport in bi-porous glasses with well-ordered pore structures. In this way, we have derived a two-phase exchange model, allowing to quantify mass transfer in materials with multiple porosities [2]. Nice agreement between the experimental findings and theoretical predictions validates the applicability of the model developed and provides a basis for its generalization to porous materials with more complex geometries of the pore spaces.

[1] J. Perez-Ramirez, C. H. Christensen, K. Egeblad, J. C. Groen, Chem. Soc. Rev. **37**, 2530 (2008).
[2] P. Zeigermann, S. Naumov, S. Mascotto, J. Kärger, B.M. Smarsly, R. Valiullin, Langmuir **28**, 3621 (2012)

4.5 IR Micro-Imaging of Mesoporous Silicon as a Model System for the Investigation of Hysteresis Phenomena

A. Lauerer, P. Zeigermann, J. Lenzner*, C. Chmelik, R. Valiullin, J. Kärger

*Department of Experimental Physics II, University of Leipzig, Germany

Ensembles of molecules confined to mesopore spaces reveal features which may notably deviate from their behavior both in the bulk phase and under dominating host-guest interaction. A previous detailed investigation of molecular dynamics in Vycor porous glass with a pore diameter of 6 nm using pulsed field gradient nuclear magnetic resonance (PFG NMR) indicated that under identical external conditions (temperature, pressure), the "histories" of sample preparation may give rise to differences in their microdynamics [1–3]. The occurrence of history-dependent states in mesoporous host-guest systems may be rationalized by a geometric disorder-induced rugged landscape in the free energy.

To get deeper insight into this phenomenon, novel options provided by the development of time-resolved IR micro-imaging [4] have been used. Electrochemically etched mesoporous silicon with a spatially ordered pore system was prepared. Focused ion beam milling of the freshly etched porous silicon film enabled the preparation of a sample with the pore channels open on both sides and aligned perpendicular to the incident IR beam. The pore system itself cosits of 5 nm pores with 55 μm length continued by channels of about 10 nm diameter with a length of 45 μm.

Successive benzene adsorption was performed at room temperature from 0 mbar up to saturated vapour pressure. Concentration profiles were observed by IR microscopy using the the focal plane array (FPA) detector. The obtained isotherm showed a clear hysteresis loop. The kinetics of the concentration equilibration following each pressure step were studied separately using a single element detector. In particular, at the onset of the hysteresis the uptake kinetics were found to be slowed down. In summary, we succeeded in developing the potential of IR micro-imaging for the application to mesoporous silicon and, thus, provided the basis for further in-depth studies on similar model systems for both ad- and desorption studies of benzene.

[1] R. Valiullin, S. Naumov, P. Galvosas, J. Kärger, H. J. Woo, F. Porcheron, P. A. Monson, Nature 2006, 443, 965-968.
[2] S. Naumov, R. Valiullin, P. A. Monson, J. Kärger, Langmuir 2008, 24, 6429-6432.
[3] R. Valiullin, J. Kärger, R. Gläser, Physical Chemistry Chemical Physics 2009, 11, 2833-2853.
[4] J. Kärger, D. M. Ruthven, D. N. Theodorou, Diffusion in Nanoporous Materials, Wiley-VCH, Weinheim, 2012.

4.6 Intra-Crystalline Diffusion Study of Light Hydrocarbons in Zeolite ZSM-58

T. Binder, F. Hibbe, C. Chmelik, J. Kärger, A. Martinez-Joaristi*, F. Kapteijn*, D.M. Ruthven†,

*Delft University of Technology, The Netherlands
†University of Maine, Orono, USA

Recent investigations of the sorption behavior of small molecules in 8-ring zeolites reveal potential industrial applications of zeolite ZSM-58 (structure type DDR) for

the separation of CO_2/CH_4 or propane/propylene. With large and well-shaped crystals being available from different labs, the single-crystal analysis by means of Interference Microscopy (IFM) now allows a detailed study of the intra-crystalline diffusion of light hydrocarbons in the two-dimensional channel structure of ZSM-58 [1]. With the approximately cylindrical symmetry and no diffusion in axial direction, the analysis of intra-crystalline concentration profiles provided by IFM is straightforward.

Experimental data for adsorption and desorption of light hydrocarbons were obtained at room temperature yielding both, single-crystal uptake curves and two-dimensional transient concentration profiles. The former allow the immediate comparison with sorption kinetic studies of a powder sample, e.g. by Zero Length Column or thermogravimetric uptake experiments. Furthermore, the wealth of intra-crystalline concentration profiles is explored by analyzing e.g. the shape of concentration profiles, the centre line concentration or the profiles at short times, the latter approach leading to the concentration dependence of diffusivity using cylindrical symmetry and Fujita's diffusion solution.

[1] T. Binder et al., J. Chem. Phys. 137 (2012) 164704.

4.7 Enhancing diffusion selectivities in FER-type structures by molecular traffic control

F. Hibbe, A. Lauerer, J. Kärger, J.M. vanBaten*, R. Krishna*, V.R.R. Marthala†, J. Weitkamp†, C. Chmelik

*University of Amsterdam, The Netherlands
†University of Stuttgart, Germany

Detailed understanding how molecular transport in nanoporous materials is influenced by various features of the host structure can provide new insights towards further optimization of their performance in technical applications, such as catalysis, separations, molecular storage and sensing. "Molecular traffic control" has been discussed as a concept to enhance selectivities and reactivities. It is based on the assumption that different molecular species are preferentially accommodated in different types of channels of the pore system. As a consequence, the mutual hindrance of the molecules on their diffusion paths through the pore network is reduced and differences in the mobilities can be enhanced. The importance of another phenomenon for adsorption and diffusion has been recently highlighted, viz. molecular clustering. "Clustering effects" are observed in systems where the guest-guest interaction exceeds the host-guest interaction, which is often the case for polar molecules in hydrophobic structures.

We have used siliceous ferrierite [1] as a model system to study the diffusion of small alkanes and alcohols. The pore structure of ferrierite consists of a network of mutually intersecting channels of two different sizes. Offering, in this way, two different types of diffusion paths, ferrierite provides the option to benefit from molecular traffic control effects for enhancing diffusion selecitivities. In fact, results of configurational-biased Monte-Carlo (CBMC) simulations suggest that, at lower loadings, methanol preferably occupies the larger 10-ring channels, while ethanol favors filling of the 8-ring windowed

cavities. The preference of the 10-ring channels for methanol originates, most likely, from its clustering tendency. Molecular clustering is energetically favorable only in these larger channels and not in the smaller 8-ring cavities. Consequently, the 10-ring channels are first populated by methanol. On the contrary, ethanol benefits from an increased host-guest interaction in the 8-ring cavities resulting in a clear preference of these sites.

This tendency to occupy different pores in the channel network leads to a particularly high difference in the diffusivity of methanol and ethanol. The ratio of the overall zero-loading diffusivities of methanol and ethanol $D_{\mathrm{MeOH}}/D_{\mathrm{EtOH}} = 25,000$ is by about three orders of magnitude larger than compared to a reference system. The major conclusion of our study can be summarized in two points: (i) molecular traffic control effects can be facilitated by molecular clustering and (ii) their combination provides a powerful option for enhancing diffusion selectivities.

[1] F. Hibbe, V. R. R. Marthala, C. Chmelik, J. Weitkamp, J. Kärger, J. Chem. Phys. 135 (2011) 184201.

4.8 Exploring diffusion and reaction in nanoporous catalysts by IR micro-imaging

T. Titze, C. Chmelik, J. Kärger, D. Enke*, R. Gläser*, J. Kullmann*, L. Prager†, J. Weitkamp‡

*Institute of Chemical Technology, University of Leipzig, Germany
†Leibniz Institute of Surface Modification, Leipzig, Germany
‡University of Stuttgart, Germany

Though PFG NMR has been successfully employed for the in-situ measurement of the diffusivities of the various components during chemical reactions [1] it fails to provide any information about the location of these components. Recent progress in the development of in-situ techniques for the characterization of solid catalysts [2] has overcome this limitation and provided us, with IR micro-imaging [3], with a technique offering best prospects for the recording of transient concentration profiles of the involved components during chemical reactions. The present contribution introduces into these options.

As an alternative to diffusion-reaction studies in zeolites with two-dimensional channel networks, we have cared for the option of similar investigations with three-dimensional pore networks. For this type of measurement, the catalyst is applied in the shape of small platelets, with the two large faces covered with a suitable layer which is impenetrable for the guest molecules but IR transparent at the relevant frequency. Hence, by observing perpendicular to the plane of the platelets, any diffusion in observation direction is excluded and IR micro-imaging directly yields the concentration profiles, simultaneously for each individual component!

First results of this type of measurement in a nanoporous glass [4] are shown in Fig. 4.2. In order to show the potentials of our model-system in combination with IR micro-imaging we performed a so called counter-diffusion experiment. The sample is thereby pre-loadedFig. 1. Concentration of benzene (a,b) and cyclohexane (c,d) before

(a,c) and 20 s after (b,d) the replacement of benzene by cyclohexane in a counter-diffusion experiment with benzene and then suddenly exposed to a cyclohexane atmosphere. In Figure 1 the benzene concentration in the sample is clearly seen to decrease (a, b) while, at the same time, the concentration of cyclohexane is increasing (c, d). Concentration profiles can be recorded because the coating of the glass plates ensures that the molecules can only enter from the open side on the right and not through the surfaces on top or bottom.

We are presently performing experiments for demonstrating these potentials by recording the spatial distribution of the components involved in simple model reactions like the reduction of benzene to cyclohexane.

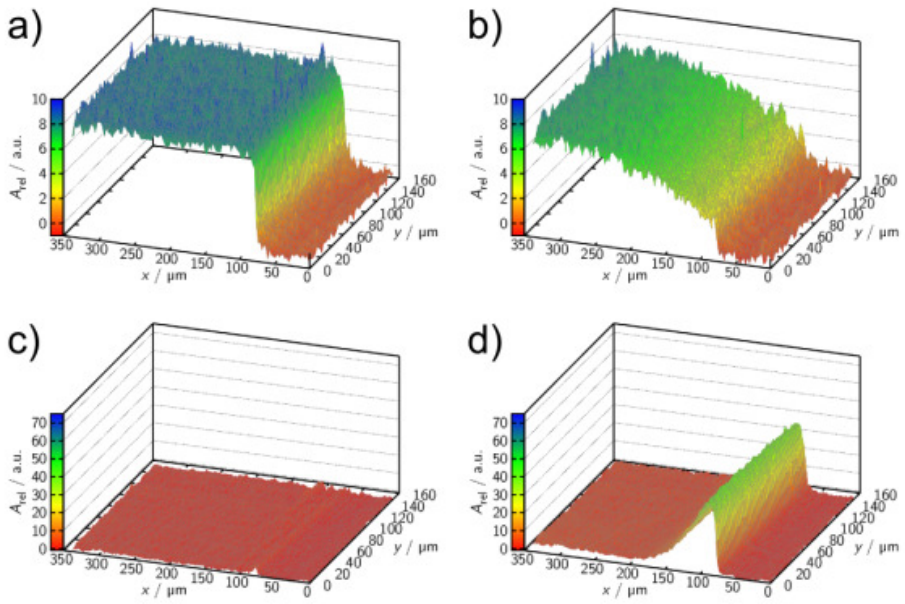

Figure 4.2: Concentration of benzene (a, b) and cyclohexane (c, d) before (a, c) and 20 s after (b, d) the replacement of benzene by cyclohexane in a counter-diffusion experiment

[1] U. Hong, J. Kärger, B. Hunger, N. N. Feoktistova, S. P. Zhdanov, J. Catal. 137 (1992) 243.
[2] B. M. Weckhuysen, Ed., In-situ characterization of heterogeneous catalysts, Chem. Soc. Rev. 39, 2010.
[3] C. Chmelik, J. Kärger, Chem. Soc. Rev. 39 (2010) 4864.
[4] C. Chmelik et al., ChemPhysChem 12 (2011) 1130.

4.9 Funding

Advanced Materials as CO_2 *Removers: A Computational Study of* CO_2 *Sorption Thermodynamics and Kinetics*
PD Dr. F. Stallmach
EU project CP-FP 233502 AMCOS

Fundamental Host-Guest Interactions in Porous Metal Organic Frameworks. A Combined Experimental and Theoretical Approach.
PD Dr. F. Stallmach
DFG-Projekt STA 648/1-2, SPP 1362 MOFs

International Research Training Group Diffusion in porous Materials
PD Dr. F. Stallmach, Prof. Dr. J. Kärger, Dr. R. Valiullin
DFG IRTG GK 1056/2

Diffusion and phase transitions under conditions of spatial confinements
Dr. R. Valiullin
DFG VA 463/1-2

Assessing pore structure via diffusion measurements
Dr. R. Valiullin
DFG VA 463/4-1

Driven diffusion in nanoscaled materials
Dr. R. Valiullin
DFG VA 463/5-2

Study of microscopic parameters of the translation of molecules in beds of nanoporous particles by PFG NMR and MC simulation
Prof. Dr. J. Kärger
DFG KA 953/19-2

Correlating diffusion processes in complementary pore spaces using NMR and theoretical modelling
Prof. Dr. J. Kärger, Prof. Dr. A. Bunde, Dr. R. Valiullin
DFG KA 953/30-1

Measuring Intracrystalline Profiles of Diffusion and Reactions in Zeolites by IR Microscopy
Dr. Ch. Chmelik
DFG KA 953/20-2

Knowledge-based development of supported ZIF membranes for liquid mixture separation by pervaporation
Dr. Ch. Chmelik, Prof. Dr. J. Kärger,
DFG KA 953/29-1 and CH 778/1-2, within SPP 1362 MOFs

Separating mixutures of chiral anesthetic gases by modified porous glasses
Dr. Ch. Chmelik
DFG CH 778/2-1, within SPP 1570

NMR-Porosimetrie an Sedimentproben
PD Dr. F. Stallmach
GFZ Potsdam

NMR-Untersuchungen an verstrangten Katalysatoren
PD Dr. F. Stallmach
BASF SE Ludwigshafen

4.10 Organizational Duties

Frank Stallmach

- deputy chair and member of the steering committee of the Porous Media Devision of the Groupement AMPERE; conference series "Magnetic Resonance in Porous Media" (MRPM)
- faculty board member, member of several commissions of the faculty board
- referee: Micropor. Mesopor. Mat., Angewandte Chemie, J. Magn. Res., J. Phys. Chem.
- Project Reviewer: Deutsche Forschungsgemeinschaft, National Science Foundation (USA)

Jörg Kärger

- Membership in the Programme Committee "Diffusion Fundamentals V" (Leipzig, 2013) and "FEZA conference (Leipzig, 2014)
- Editor: Diffusion Fundamentals; Membership in Editorial Boards: Adsorption, Micropor.Mesopor.Mat.
- Referee: Nature, Phys. Rev., Phys. Rev. Lett., Angew. Chem., Europhys. Lett., J. Chem. Phys., J. Phys. Chem., Langmuir, Micropor. Mesopor. Mat., Phys. Chem. Chem. Phys., J. Magn. Res.
- Project Reviewer: Deutsche Forschungsgemeinschaft

Rustem Valiullin

- Editorial Board Online Journal "Diffusion Fundamentals", Editorial Board "Dataset Papers in Physical Chemistry"
- Referee: J. Phys. Chem., J. Am. Chem. Soc., Adsorption, Micropor. Mesopor. Mat., Phys. Rev. B, Phys. Rev. E, Phys. Rev. Lett., Langmuir, Soft Matter, Chem. Soc. Rev.

Christian Chmelik

- Editorial Board Online Journal "Diffusion Fundamentals"
- Referee: J. Phys. Chem., Micropor. Mesopor. Mat.

4.11 External Cooperations

Academic

- Delft University, Inst.Chem. Tech., Delft, The Netherlands
  Prof. Kapteijn
- Institut de Recherches sur la Catalyse, CNRS, Villeurbanne, France
  Dr. Jobic
- Max Planck Institut für Kohlenforschung, Mülheim
  Dr. Schmidt, Prof. Schüth

- Ruhr-Universität Bochum, Lehrstuhl für Anorganische Chemie 2, Organometallics and Materials Chemistry
  PD Dr. Schmid
- Universität Hannover, Dept. Phys. Chem., Hannover
  Prof. Caro, Prof. Wiebcke
- Universität Leipzig, Institut für Technische Chemie, Leipzig
  Prof. Einicke, Prof. Gläser, Prof. Enke
- Universität Leipzig, Institut für Anorganische Chemie, Leipzig
  Prof. Krautscheid
- Universität Leipzig, Institut für Medizinische Physik und Biophysik, Leipzig
  Prof. Huster
- TU Dresden, Inst. Biophysik, Dresden
  Prof. Brunner
- Universität Stuttgart, Institut für Technische Chemie, Stuttgart
  Prof. Klemm, Prof. Hunger
- University Athens, Dept Chem. Engn., Athens, Greece
  Prof. Theodorou, Prof. Papadopoulos
- University of Amterdam, Faculty of Science, The Netherlands
  Prof. Krishna
- University of Maine, Dept. Chem. Eng., USA
  Prof. Ruthven
- Victoria University of Wellington, MacDiarmid Institute for Advanced Materials and Nanotechnology, School of Chemical and Physical Sciences, New Zealand
  Dr. Galvosas
- LMU München, Dept. Chemistry and Biochemistry
  Prof. Bräuchle, Dr. C. Jung
- University of Massachusetts, Dept. of Chemical Engineering, Amherst, USA
  Prof. P.A. Monson
- Northwestern University, Dept. of Chem. Eng., Evanston, USA
  Prof. Snurr
- University of Florida, Dept. of Chem. Eng., Gainesville (FL), USA
  Prof. Vasenkov
- University College London, UK
  Prof. Coppens
- Otto-von-Guericke-Universität Magdeburg, Institut für Verfahrenstechnik, Magdeburg
  Prof. Seidel-Morgenstern

Industry

- BASF SE, Ludwigshafen, Germany
  Dr. U. Müller

- Baker Hughes INTEQ GmbH, Celle, Germany
  Dr. Th. Kruspe, Dr. H. Thern,
- SINTEF, Oslo, Norway
  Prof. Stöcker
- Südchemie, Berlin, Germany
  Dr. Clariant-Tissler, Dr. Tufar, Dr. Lutz, Dr. Rakoczy

4.12 Publications

Journals

St. Schlayer, A.-K. Pusch, F. Pielenz, St. Beckert, M. Peksa, C. Horch, L. Moschkowitz, W.-D. Einicke, F. Stallmach: *X nuclei NMR self-diffusion studies in mesoporous silica foam and microporous MOF CuBTC*, Materials **5**, 617 - 633 (2012)

A.-K. Pusch, T. Splith, L. Moschkowitz, S. Karmakar, R. Biniwale, M. Sant, G. B. Suffritti, P. Demontis, J. Cravillon, E. Pantatosaki, F. Stallmach: *NMR studies of carbon dioxide and methane self-diffusion in ZIF-8 at elevated gas pressures*, Adsorption **18**, 359 - 366 (2012)

D. C. Ford, D. Dubbeldam, R. Q. Snurr, V. Künzel, M. Wehring, F. Stallmach, J. Kärger, U. Müller: *Self-Diffusion of chain molecules in the metal-organic framework IRMOF-1*, Phys. Chem. Letters **3**, 930 - 933 (2012)

E. Pantatosaki, G. Megariotis, A.-K. Pusch, Ch. Chmelik, F. Stallmach, G. Papadopoulos: *On the Impact of Sorbent Mobility on the Sorbed Phase Equilibria and Dynamics: A Study of methane and carbon dioxide within the zeolite imidazolate framework-8*, J. Phys. Chem. **116**, 201 - 207 (2012)

J. Lincke, D. Lässig, K. Stein, J. Moellmer, A. V. Kuttatheyil, C. Reichenbach, A. Moeller, R. Staudt, G. Kalies, M. Bertmer, H. Krautscheid: *A Novel Zn4O-Based Triazolyl Benzoate MOF: Synthesis, Crystal Structure, Adsorption Properties and Solid State 13C NMR Investigations*, Daltons Trans. **41**, 817 - 824 (2012)

P. Zeigermann, S. Naumov, S. Mascotto, J. Kärger, B.M. Smarsly, R. Valiullin: *Diffusion in hierarchical mesoporous materials: Applicability and generalization of the fast-exchange diffusion model*, Langmuir **28**, 3621 - 3632 (2012)

A. Shakhov, R. Valiullin, J. Kärger: *Tracing molecular propagation in dextran solutions by pulsed field gradient nmr*, J. Phys. Chem. Lett. **3**, 1854 - 1857 (2012)

D. Mehlhorn, R. Valiullin, J. Kärger, K. Cho, R. Ryoo: *Exploring the hierarchy of transport phenomena in hierarchical pore systems by nmr diffusion measurement*, Microporous Mesoporous Mat. **164**, 273-279 (2012)

D. Mehlhorn, R. Valiullin, J. Kärger, K. Cho, R. Ryoo: *Exploring mass transfer in mesoporous zeolites by nmr diffusometry*, Materials **5**, 699 - 720 (2012)

D. Mehlhorn, R. Valiullin, J. Kärger, K. Cho, R. Ryoo: *Intracrystalline diffusion in mesoporous zeolites*, ChemPhysChem **13**, 1495 - 1499 (2012)

T. Kirchner, A. Shakhov, P. Zeigermann, R. Valiullin, J. Kärger: *Probing mesopore connectivity in hierarchical nanoporous materials*, Carbon **50**, 4804 - 4808 (2012)

C. Iacob, J. R. Sangoro, W. K. Kipnusu, R. Valiullin, J. Kärger, F. Kremer: *Enhanced charge transport in nano-confined ionic liquids*, Soft Matter **8**, 289 - 293 (2012)

F. Hibbe, J. Caro, C. Chmelik, A. Huang, T. Kirchner, D. Ruthven, R. Valiullin, J. Kärger: *Monitoring molecular mass transfer in cation-free nanoporous host crystals of type alpo-lta*, J. Am. Chem. Soc. **134**, 7725 - 7732 (2012)

F. Feil, S. Naumov, J. Michaelis, R. Valiullin, D. Enke, J. Kärger, C. Bräuchle: *Single-particle and ensemble diffusivities - test of ergodicity*, Angew. Chem. **124**, 1178 - 1181 (2012)

K. Ulrich, P. Galvosas, J. Kärger, F. Grinberg: *Pore-Like" Effects of Super-Molecular Self-Assembly on Molecular Diffusion of Poly(Ethylene Oxide)-Poly(Propylene Oxide)-Poly(Ethylene Oxide) in Water*, Materials **5**, 966 (2012)

T. Binder, F. Hibbe, C. Chmelik, J. Kärger, A. Martinez-Joaristi, J. Gascon, F. Kapteijn, D.M. Ruthven: *Micro-imaging of transient guest profiles in nanoporous host systems of cylindrical symmetry*, J. Chem. Phys. **137**, 164704 (2012)

C. Chmelik, J.M. van Baten, R. Krishna: *Hindering effects in diffusion of CO2/CH4 mixtures in ZIF-8 crystals*, J. Membr. Sci. **87**, 397 - 398 (2012)

J. Kärger: *The Beauty of the Different Views on Diffusion*, Defect and Diffusion Forum **326-328**, 1 (2012)

L. Gueudre, T. Binder, C. Chmelik, F. Hibbe, D.M. Ruthven, J. Kärger: *Micro-Imaging by Interference Microscopy: A Case Study of Orientation-Dependent Guest Diffusion in MFI-Type Zeolite Host Crystals*, Materials **5**, 721 (2012)

C. Chmelik, D. Freude, H. Bux, J. Haase: *Ethene/ethane mixture diffusion in the MOF sieve ZIF-8 studied by MAS PFG NMR diffusometry* Micropor. Mesopor. Mater. **147**, 135 (2012)

Books

P. Lura, K. Friedemann, F. Stallmach, S. Mönning, L. P. Esteveves: *Kinetics of water migration in cement-based systems containing super absorbent polymers*, Chap. 4 in Application of Superabsorbent Polymers, V. Mechtcherin und H.-W. Reinhardt (Eds.), Springer, p. 21 - 37, 2012

J. Kärger, D. M. Ruthven, D. N. Theodorou: *Diffusion in Nanoporous Materials* (Wiley-VCH, Weinheim, 2012)

Talks

F. Stallmach: *NMR porosimetry and diffusometry in porous materials*, Baker Hughes INTEQ GmbH, Celle, Germany, February 23, 2012

C. Reichenbach, G. Kalies, D. Enke, D. Klank: *Cavitation and Pore Blocking in Nanoporous Glasses*, 24. Deutsche Zeolith-Tagung, Magdeburg, Germany, March 07 - 09, 2012

T. Binder, F. Hibbe, J. Kärger, A. Martinez-Joaristi, F. Kapteijn, D. M. Ruthven: *Intra-Crystalline diffusion study of light hydrocarbons in zeolite ZSM-58*, 24. Deutsche Zeolith-Tagung, Magdeburg, Germany, March 07 - 09, 2012.

T. Titze, C. Chmelik, D. Enke, R. Gläser, J. Kärger, J. Kullmann, L. Prager, J. Weitkamp: *The potentials of IR micro-imaging for in-situ studies of chemical reactions in nanoporous catalysts*, Jahrestreffen Deutscher Katalytiker, Weimar, Germany, March 14 - 16, 2012.

F. Stallmach: *Transport and storage of gases, liquids and electrolytes in porous media studied by NMR diffusometry*, Invited lecture, BASF SE, Ludwigshafen, Germany, March 22, 2012

M. Peksa: *NMR spectroscopy of anisotropic interactions of* $^{13}CO_2$ *and* $CDCl_3$ *in MOFs*, 15^{th} IRTG Workshop: Spectroscopy and mobility of confined molecules, Leipzig, Germany, April 2 - 4, 2012.

S. Beckert: *Enhanced Li-Ion Self-Diffusion in Porous Glasses*, 15^{th} IRTG Workshop: Spectroscopy and mobility of confined molecules, Leipzig, Germany, April 2 - 4, 2012.

A. Lauerer: *Deconvolution of transient concentration profiles measured by IR micro-imaging*, 15^th IRTG Workshop: Spectroscopy and mobility of confined molecules, Leipzig, Germany, April 2 - 4, 2012.

T. Binder: *Intra-crystalline diffusion study of light hydrocarbons in zeolite ZSM-58*, 15^th IRTG Workshop: Spectroscopy and mobility of confined molecules, Leipzig, Germany, April 2 - 4, 2012.

A.-K. Push, T. Splith, S. Schlayer, F. Stallmach: *NMR studies of carbon dioxide and methane self-diffusion in ZIF-8 at elevated pressures*, 6th Pacific Basin Conference on Adsorption Science and Technology (PBAST 6), Taipei, Taiwan, May 20 - May 23, 2012.

T. Binder, F. Hibbe, J. Kärger, A. Martinez-Joaristi, F. Kapteijn, D. M. Ruthven: *Intra-Crystalline Diffusion in Zeolite ZSM-58: An Interference Microscopy Study*, 6th Pacific Basin Conference on Adsorption Science and Technology (PBAST 6), Taipei, Taiwan, May 20 - 23, 2012.

F. Stallmach: *Generation and Application of Intensive Field Gradient Pulses for NMR diffusion studies*, Invited lecture, Annual GERM meeting, Domoine de St Hilaire, Roiffe, France, 29 May - 01 June 2012

T. Titze, C. Chmelik, D. Enke, R. Gläser, J. Kärger, J. Kullmann, L. Prager, J. Weitkamp: *The potentials of IR micro-imaging for in-situ studies of chemical reactions in nanoporous catalysts*, International Congress on Catalysis, Munich, Germany, July 1 - 6, 2012.

J. Kärger: *Potentials and Benefit of "Microscopic" Techniques of Diffusion Measurement in Nanoporous Materials*, Invited lecture, ETH-Micromeritics Symposium on Advanced porous materials, Zürich, Switzerland, August 22, 2012.

R. Valiullin: *Transport properties of hierarchical porous materials*, MRPM 11 Conference on Magnetic Resonance in Porous Media, Guildford, UK, September 9 - 13, 2012.

J. Kärger, R. Valiullin: *Exploring Pore Space and Molecular Dynamics: The Twofold Benefit of NMR Diffusometry*, GDCH-Fachgruppentagung Magnetresonanz, Halle, Germany, September 19, 2012.

F. Stallmach: *NMR studies of carbon dioxide and methane self-diffusion in ZIF-8 at elevated pressures*, Invited lecture, XVI. POROTEC Workshop über die Charakterisierung von feinteiligen und porösen Festkörpern, Bad Soden, Germany, November 13 - 14, 2012.

R. Valiullin: *Assessing the Hierarchy of Transport Resistances in Porous Materials by Experimental Evidence*, Invited lecture, XVI. POROTEC Workshop über die Charakterisierung von feinteiligen und porösen Festkörpern, Bad Soden, Germany, November 13 - 14, 2012.

M. Peksa, S. Bureekaew, R. Schmid, J. Lang, F. Stallmach: *NMR Measurements of Adsorption and Diffusion of CO_2 in the MOF $Zn(bdc)_2(dabco)$*, XVI. POROTEC Workshop über die Charakterisierung von feinteiligen und porösen Festkörpern, Bad Soden, Germany, November 13 - 14, 2012.

T. Titze, C. Chmelik, D. Enke, R. Gläser, J. Kärger, J. Kullmann, L. Prager, J. Weitkamp: *Exploring intra-particle diffusion and reaction by IR micro-imaging*, XVI. POROTEC Workshop über die Charakterisierung von feinteiligen und porösen Festkörpern, Bad Soden, Germany, November 13 - 14, 2012.

S. Beckert, F. Stallmach: *NMR Self-Diffusion Studies of Metal Cations Confined to Nanoporous Materials*, XVI. POROTEC Workshop über die Charakterisierung von feinteiligen und porösen Festkörpern, Bad Soden, Germany, November 13 - 14, 2012.

M. Peksa, S. Bureekaew: *Carbon dioxide mobility in Zn2(bdc)2(dabco) studied by NMR and MD*, DFG Status report meeting SPP 1632 Porous Metall-Organic Frameworks, Dresden, Germany, November 28, 2012.

Posters

J. Kullmann, T. Titze, C. Chmelik, J. Kärger, D. Enke, L. Prager: *The potentials of IR micro-imaging for in-situ studies of chemical reactions in nanoporous catalyst*, 24. Deutsche Zeolith-Tagung, Magdeburg, Germany, March 7 - 9, 2012.

T. Titze, C. Chmelik, D. Enke, R. Gläser, J. Kärger, J. Kullmann, L. Prager, J. Weitkamp: *The potentials of IR micro-imaging for in-situ studies of chemical reactions in nanoporous catalysts*, 6th Pacific Basin Conference on Adsorption Science and Technology (PBAST 6), Taipei, Taiwan, May 20 - 23, 2012.

M. Peksa, J. Lang, P. Capek, M. Vesely, V. Hejtmanek, L. Brabec, M. Kocirik, F. Stallmach, O. Solcova: *Measurements and theoretical prediction of water self-diffusion in macroporous media*, EUROMAR 2012, Dublin, Ireland, July 1 - 7, 2012.

S. Beckert, M. Peksa, F. Stallmach, J. Kullmann, D. Enke: *Description of the concentration dependent self-diffusivity of aqueous electrolytes in mesoporous glasses*, MRPM11, Guildford, UK, September 9 - 13, 2012.

A. Shakhov, J. Kärger, R. Valiullin: *Tracing Molecular propagation in Dextran Solutions by Pulsed Field Gradient NMR*, MRPM11 Conference, University of Surrey, Guildford, UK, September 09 - 13, 2012

P. Zeigermann, Rustem Valiullin: *Self-Diffusion of CO_2 - Expanded Toluene in Mesoporous Glasses*, Magnetic Resonance in Porous Materials 11, Guildford, UK, Sep 09 - 13, 2012

C. Chmelik, H. Bux, J. Caro, J.M. van Baten, R. Krishna: *Hindering effects in diffusion of CO_2/CH_4 mixtures in ZIF-8 crystals*, 3rd International Conference on Metal-Organic Frameworks and Open Framework Compounds, Edinburgh, UK, September 16 - 19, 2012.

T. Binder, F. Hibbe, C. Chmelik, J. Kärger, A. Martinez-Joaristi, F. Kapteijn, D.M. Ruthven: *Intra-Crystalline Diffusion in Zeolite ZSM-58: An Interference Microscopy Study*, XVI. POROTEC Workshop über die Charakterisierung von feinteiligen und porösen Festkörpern, Bad Soden, Germany, November 13 - 14, 2012.

A. Shakhov, C. Reichenbach, D. Enke and R. Valiullin: *NMR characterisation of nanoporous glasses*, XVI. POROTEC Workshop über die Charakterisierung von feinteiligen und porösen Festkörpern, Bad Soden, Germany, November 13 - 14, 2012

4.13 Graduations

Doctorate

- Marcel Gratz
  Strukturuntersuchungen an porösen Materialien mit ein- und mehrdimensionalen NMR-Experimenten
  January 2012
- Markus Wehring
  High-resolution PFG NMR diffusion studies in nanoporous materials
  April 2012
- Florian Hibbe
  Micro Imaging Employed to Study Diffusion and Surface Permeation in Porous Materials
  December 2012

Master

- Alexander Lauerer
  Artefakte bei der Messung transienter Konzentrationsprofile mittels IR-Imaging
  März 2012
- Tino Raßloff
  Charakterisierung des Stofftransports in DDR-Zeolithen mittels mikroskopischer Messverfahren
  Oktober 2012
- Tino Viertel
  NMR-Untersuchungen von Methan in der metallorganischen Gerüstverbindung ZIF-8
  October 2012
- André Müller
  Untersuchung des Einflusses nanoporöser Wirtsstrukturen auf den Stofftransport von Gastmolekülen mittels IR-Mikroskopie
  November 2012

Bachelor

- Kevin Woost
  Untersuchung der Methanol-Diffusion in Ferrierit mittels IR-Mikroskopie
  Januar 2012
- Christian Wesemann
  Untersuchungen der Diffusion von Elektrolytlösungen in porösen Materialien mittels NMR
  March 2012
- Stefan-Johannes Reich
  Temperaturkalibrierung eines NMR-Spektrometers mittels Fest-Flüssig-Phasenübergängen
  November 2012

4.14 Guests

- Dr. Petrik Galvosas
  Victoria University of Wellington, New Zealand
  January 01 - 04, 2012
- Prof. Vilas Gaikar
  ICT Mumbai, India
  February 22 - 25, 2012
- Prof. George Papadopoulos
  National Technical University Athens, Greece
  April 24 - 26, 2012
- Prof. Pierfranco Demontis
  University of Sassari, Italy
  April 24 - 26, 2012

- Dr. Herve Jobic
  IRCELYON, Villeurbanne, France,
  April 24 - 26, 2012
- Dr. Rajesh Biniwale
  National Environmental Engineering Research Institute Nagpur, India
  April 24 - 26, 2012
- Prof. Rajamani Krishna
  University of Amsterdam, Netherlands
  May 15 - 17, 2012
- Dipl. NanoSc. Alexander Mundstock
  Leibniz University of Hannover
  November 7, 2012
- Dr. Sareeya Bureekaew
  RU Bochum, Germany
  November 26 - 27, 2012
- Dipl.-Ing. Dennys Dressel
  Bauhaus Universität Weimar
  December 11, 2012
- Prof. Christoph Arns
  University of New South Wales, Sydney, Australia
  December 17 - 19, 2012

5

Soft Matter Physics

5.1 Introduction

Material science can offer a truly new perspective on neuronal growth and tumor progression by using active soft matter physics and vice versa moving cells are prototypical active soft matter. Active soft matter defines the emerging physics of cancer. While tumor cells are optimized to invade the body, the material properties of neurons are so designed that after development neuronal growth can only occur within the central nervous system (CNS) thus contrasting tumor progression and limiting nerve regeneration. In view of the fact that our work aims at the unique combination of soft condensed matter physics and medicine we hope for a redefining impact in both areas.

Do cells care about physics? As expressed by Erwin Schrödinger's famous quote "The working of an organism requires exact physical laws". Physicists strive to explain nature by precise mathematical equations, which could bring a truly new perspective to cancer research and has triggered worldwide efforts to begin to understand the potential physical underpinnings of cancer. Cancer is not a single disease with one etiology and one cure. In addition to the enormously complex molecular networks required for the functioning of normal cells, tumors have an inherently high molecular diversity due to the stochastic nature of the mutations that cause cancer. However, one should not get the wrong impression that cancer cannot be explained via physics, which strives to describe nature by precise laws. Statistical physics has identified laws behind the stochastic events underlying thermodynamics and nonlinear dynamics and has even uncovered what governs chaotic behavior in nature.

The "hallmarks of cancer"- uncontrolled proliferation, growth against the surrounding tissue matrix, and tumor cell migration - are functions that the cell has to fulfill and they may show molecular redundancy and diversity. However, from a physicist point of view, these functions require that the cancer cell has particular material properties to perform specific physical processes. In other word, the same unifying physics is needed for the intracellular functional modules to work. Thereby, the physical laws underlying solid tumor progression are rooted in soft condensed matter physics and will help define what unifies cancer despite tumor diversity. The concept of functional modules developed in biological physics will greatly facilitate our understanding of the laws that govern cancer. The functional modules of a tumor cell may not show identical molecular architectures, but the same physical principals are essential for

their functions. For instance, changes in a tumor cell's active and passive biomechanics are required for the working of the functional modules that are involved in metastasis. During tumor progression, the proportion of cancer cells with a high compliance under small deformations increases. Moreover these softer cells show an increased contractile behavior. These cells are capable of squeezing through narrow spaces which allows them to perform optimal mesenchymal or amoeboid motion to invasively migrate through the body.

Moreover, all cells in a tissue can be motile and are viscous on long time scales, behaving very much like a liquid droplet. Consequentially, tissue boundaries are comparable to fluid boundaries. Tissues can be described as a new form of fluid matter, which is a significant topic in the novel research area of active soft matter physics. If all cells are motile why does a tumor initially grow as a collective mass? What stabilizes the tumor boundaries? According to Malcolm Steinberg's famous differential adhesion hypothesis, compartment boundaries between tissues are stabilized through a new type of surface tension, which is not solely determined by intercellular adhesion (through molecules such as cadherins) but also through cell contractility. Additionally, cells in tissues are very similar to soft colloids and thus have difficulties passing by each other at higher packing densities. In this context, tissues can be thought of as being in a glass-like state, which may help stabilize tumor boundaries.

The physics of cancer is still in its infancy and it may need a decade until a translational impact will become truly visible. Nevertheless, in diagnosis, single tumor cell biomechanics provides some unparalleled advantages. Deformability of cells obtained from cytobrushes of the mouth may serve as a screening test for oral cancer. Moreover, biomechanical characterization could solve a dilemma in the staging of breast cancer. Biomechanical measurements may provide the first direct detection of metastatic cells from resected tumors. In terms of a more long term translational perspective, cancer therapy would benefit tremendously from this new perspective of physics of cancer. The most common chemotherapy agents act by killing cells that divide rapidly, one of the main properties of most cancer cells. Newer anticancer drugs act directly against abnormal proteins in cancer cells - this is termed targeted therapy - or inhibit tumor angiogenesis. In all these cases the goal is to destroy the solid tumor. Although in most cases the primary tumor can be removed by surgery and radiation without chemotherapy, it is the remaining tumor cells as well as their ability to transgress boundaries that have to be hindered since those properties determine long-term survival. Changes in tumor cells physical and material properties that disrupt the functional modules required for metastasis could provide a broad spectrum of cancer treatment. In addition, therapies that target the physical and material properties of the cancer cell do not exert much selective pressure on the cell since their goal is not to kill the cell but to criple it. This in turn would not lead to the development of resistant and more aggressive tumors which is the main issue with most current cancer therapies.

In 1999, the National Institutes of Health Director, Harold Varmus highlighted the role of physics for cell biology in his speech at the Centennial Meeting of the American Physical Society by stating, "Biology is rapidly becoming a science that demands more intense mathematical and physical analysis than biologists have been accustomed to, and such analysis will be required to understand the workings of cells." In this spirit our research sheds some new light on biological cells by approaching this problem from

a functional, materials perspective. In brief, soft matter science can learn from cells the design principles for active, multifunctional systems and provide a quantitative understanding of cellular processes.

Josef A. Käs

5.2 Tuning the biocompatibility of single crystalline $Fe_{70}Pd_{30}$ ferromagnetic shape memory films for cell sensing

U. Allenstein,Y. Ma*, A. Arabi-Hashemi*, F. Szillat*, S.G. Mayr*, M. Zink

*Leibniz-Institut für Oberflächenmodifizierung, Translationszentrum für Regenerative Medizin

Ferromagnetic shape memory alloys (FSMAs) have received great attention recently as an exciting class of smart functional materials. They exhibit large reversible strains of several percent at moderate stresses due to an external magnetic field induced reorientation of twin variants in the martensitic phase. External controllability at constant temperatures and sufficiently high strains thus make them excellent candidates for biomedical actuation devices, such as surgical implant materials or drug delivery systems. In comparison to conventional shape memory alloys, FSMA bear the significant potential for miniaturized devices for single cell actuation which is capable of yielding magnetically controllable shear strains and/or volume dilations of several percent, thus perfectly matching the requirements of cell investigations. However, biocompatibility of this material remains to be confirmed. Corrosion resistance of single crystalline $Fe_{70}Pd_{30}$ FSMA films on MgO substrates was obtained employing simulated body fluid (SBF) tests. Calcium-phosphate aggregates with granular microstructure were detected on the film surface after soaking in SBF. The adhesive properties as well as the viability and proliferation of different cell types, such as fibroblast, osteoblast and epithelial cells, were tested on the substrates and tuned by coating the substrates with different adhesive materials. We obtained that cells spread and proliferate well on Fe-Pd thin films even in the absence of adhesive agents such as fibronectin, laminin and poly-L-lysin, which can be coated to the substrate to enhance cell adhesion. Additionally, the cytoskeletal arrangements, as well as focal contacts of the cells were examined using confocal laser scanning microscopy. It turned out that all cell types express a well-pronounced actin cytoskeleton and focal contact sites, while the formation of focal adhesion sites increases with culture time. Rapidly splat-quenched Fe-Pd films with roughness graded surfaces were employed to furthermore investigate possible influences of substrate morphology on cell adhesion and viability. Our results show that osteoblasts, epithelial cells and fibroblasts can adapt to different surface roughness with time and spread well on these polycrystalline substrates. Since adhesion and spreading is mediated by the interaction of the amino acid sequence RGD which binds to integrin receptors on the cell surface, we further employed the interaction of RGD molecules with Fe-Pd by ad initio simulation, delamination and cell tests. Good adhesion of RGD to Fe-Pd is a prerequisite for bioactivity of the surface since the molecule must not

get ripped of substrate when the cell pulls on it during spreading and migration. Our simulation in comparison to experimental assessments demonstrate that the adhesion force of RGD with Fe-Pd is larger compared to the binding strength of RGD with integrin receptors. Moreover, on the FSMA side it is the iron which constitutes the binding partner for oxygen and nitrogen atoms within the RGD molecule. Taken together, Fe-Pd is a promising candidate for a new class of smart functional materials which shows good biocompatibility and bioactivity, a prerequisite for biomedical applications.

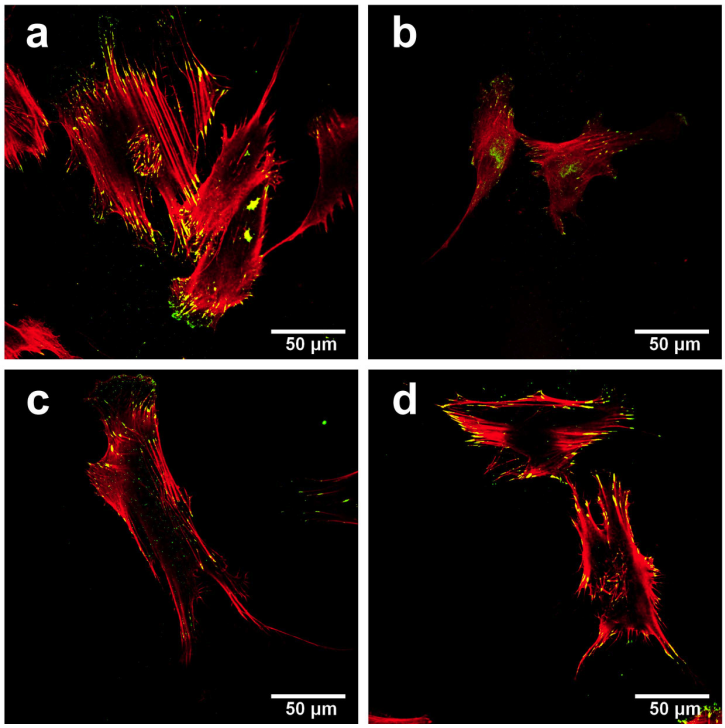

Figure 5.1: Confocal laser scanning microscopy images of single primary human osteoblast (HOB) cells with 63x magnification after 4 days incubation on $Fe_{70}Pd_{30}$ with (a) fibronectin, (b) laminin, (c) no and (d) poly-L-lysine coatings. The red TRITC channel shows actin fibers, the green FITC channel shows focal contacts..

5.3 Microtubule Deformability and Growth Cone Motility

P. Rauch, P. Heine, B. Goettgens, J.A. Käs

The directed motility of growth cones at the tip of neuronal processes is a key function in neuronal path-finding and relies on a complex system of interacting cytoskeletal components. Neurite navigation is primarily accomplished through the detection, integration, and tracking of a multitude of guidance cues, which are then translated into cytoskeletal rearrangements that yield directional deviations. Even though tremendous effort has been put into researching this interesting process, not all aspects of the involved cytoskeletal dynamics have been identified. Especially the function of microtubules has been largely underestimated, as most force-generating mechanisms are attributed to

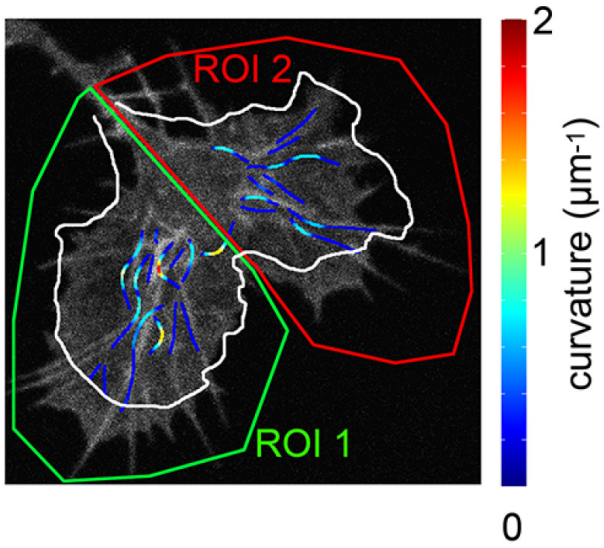

Figure 5.2: Figure 1 A: Different ROIs of the growth cone show different motility behavior. White lines indicate the lamellipodium at the beginning of recording. The actin signal (grayscale) and MT curvature data (color coded) underneath represent the last observation frame

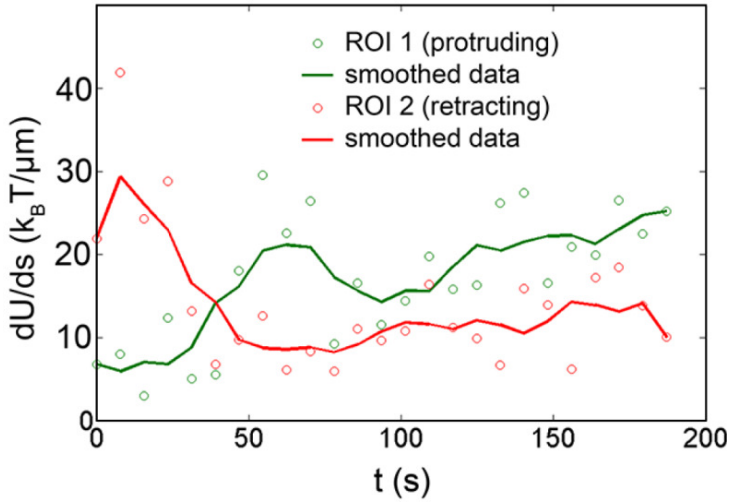

Figure 5.3: Figure 1 B: The bending energy per unit length dU/ds in ROI1 increases over time while in the stationary region it remains constant at a lower level (after initially dropping off). Solid lines in represent the data smoothed with a Þvefold moving average.

actin-myosin based structures and processes. We were able to implement a combination of custom written MATLAB algorithms to semi-automatically detect microtubule contours in laser scanning microscope image series. Armed with these tools it was now possible to analyze microtubule buckling and deformation in spreading growth cones. The analysis revealed that extending microtubules contribute significantly to the overall protrusion force of the growth cone [1]. Additionally we established a relationship of the local variations in stored bending energy to growth cone morphology and retrograde actin flow (fig. 5.2, 5.3). This indicates the importance of microtubule pushing and deformation to neurite outgrowth as well as path-finding processes. Furthermore we investigated cytoskeletal dynamics underlying growth cone collapse and retraction

mechanisms in transiently transfected NG108-15 growth cones. We could classify two discrete modes of growth cone collapse leading either to neurite retraction or to a controlled halt of neurite outgrowth [2]. In the latter case, lateral movement and folding of filopodia confine microtubule probing and constrict microtubule-based expansion processes without requiring continuous actin turnover. We term this previously unreported second type fold collapse and suggest that it marks an intermediate-term mode of growth regulation closing the gap between full retraction and small scale fluctuations.

[1] P. Rauch et al.: New Journal of Physics **15**, 015007, doi:10.1088/1367-2630/15/1/015007, (2013)
[2] P. Rauch et al.: submitted to European Biophysics Journal

5.4 Collective migration of weakly interacting cells

K.D. Nnetu, M. Knorr, D. Strehle, M. Zink, J.A. Käs

Cell migration is a prerequisite for many biological processes such as wound healing, embryologic development and metastasis. While the latter is characterized by single cell migration, usually in an amoeboid-like motion, collective cell migration is crucial for tumor development, as well as the formation of organs in the embryo. However, it still remains unclear why epithelial cells usually migrate collectively as an intact cell sheet in two dimensions and how epithelial-to-mesenchymal transition influences cell motion that single cell migration becomes possible. Considering cells as a liquid-like soft material, a two-dimensional cell sheet is supposed to form a line tension, similar to a surface tension in three dimensions, which prevents single cell escape out of the sheet. How physical properties come into play to describe cell migration from a materials science perspective, we performed extensive migration assays of the epithelial cell lines MCF-10A (benign breast epithelial cells), MCF-7 (cancerous breast epithelial cells) and NIH-3t3 fibroblast cells.

Employing an *ibidi* migration assay in which cell monolayers can migrate into free space, we observed that epithelial cells migrate as an entire cell sheet. Interestingly, for that weakly interacting MCF-10A cells adhesion forces to the substrate and the formation of a line tension at the edge of the sheets are not the origin of sheet integrity as always assumed by the biophysics community before. Instead, we could clearly show for the first time that single cell dynamics within the cell monolayer determine sheet integrity: Cells move collectively in the same direction (ballistic motion), while cells that leave the monolayer start to migrate as random walkers. These random walk results in a slowed-down velocity compared to ballistic motion into the direction of motion of the monolayer. To this end, the cell monolayer catches up with single cells that escaped the monolayer and an intact cell front is established Ð even in the absence of liquid-like surface tension effects. In contract, fibroblasts were shown to migrate as random walkers which suppress the formation of stable cell monolayers.

These results surprisingly demonstrate that only dynamical properties of cells have to be taken into account to understand why single cells might be able to leave a stable formation of cells which is supposed to have a great impact on the understanding of

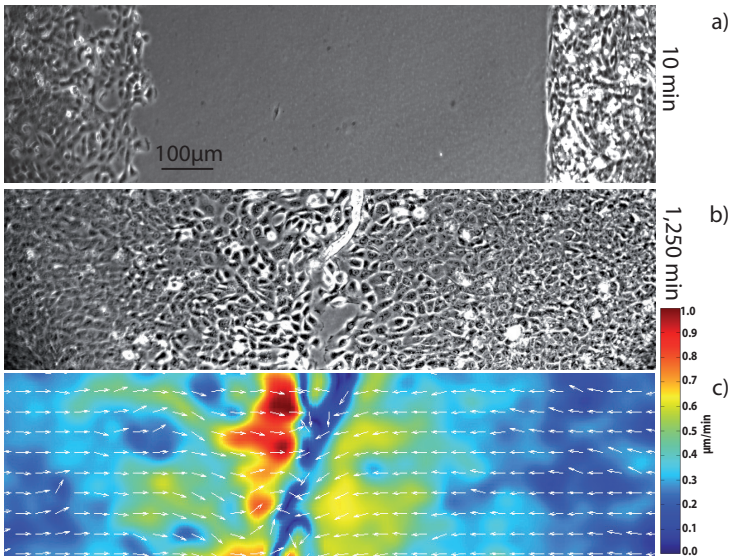

Figure 5.4: Phase contrast images of two oppositely migrating cell monolayers at times 10 min (a) and 1,250 min (b), respectively. At the lower cell density (left monolayer), single cells escape the monolayer. Color-coded spatial velocity distribution of the monolayers after 1,250 min (c). The velocities are both spatially heterogeneous, while single cells migrate uni-directionally.

metastasis when cells suddenly leave the solid tumor. On the other hand, the formation of compartment boundaries as well as solid tumor boundaries is still an open question which might be explained by similar mechanisms. To this end, we further studied the dynamics of cells within a monolayer in more detail by letting two monolayers migrate towards each other until they meet. Surprisingly cells did not mix when two sheets of MCF-10A and MCF-7 monolayers met. Instead a stable border was obtained. Considering the classical picture of cells as fluid material, surface tension differences can explain this observation.

However, when two monolayers of the same cell type (MCF-10A) cells met, also no mixing was obtained and all cells remained within their initial sheet, contradicting the explanation that line tension differences are the driving force for the formation of stable borders. Evaluation to determine the cellular dynamics in terms of velocity and direction of every single cell within the sheet showed that also here the dynamics of the epithelial cells and their ballistic motion can explain the observations: As long as the monolayer can migrate into free space, cell motion remains ballistically, while cells start to jam when the monolayers meet. Interestingly, jamming and slowed-down dynamics can cause the formation of stable borders without considering strong intracellular interactions. This jamming occurrence can also be understood in terms of glass-like behavior by considering typical features important for glass-forming materials. Although cells are active soft matter which have been supposed not to form a stable glass-like configuration, our study demonstrate for the first time that active processes and cellular dynamics can cause cell stabilization between monolayers without taking cellular interactions via signaling and adhesion into account.

5.5 Tailoring substrates for long-term organotypic culture of adult neuronal tissue

V. Dallacasagrande, M. Zink, A. Jakob*, A. Reichenbach†, J.A. Käs, S.G. Mayr*

*Leibniz-Institut für Oberflächenmodifizierung, Translationszentrum f. Regenerative Medizin
†Paul-Flechsig-Institut für Hirnforschung

The crucial role of organotypic cultures in studying the complex structure of neuronal tissue is widely known. The conventional way to obtain long-term culture is employing embryonic tissue explants or slices since these do not degenerate as quickly as adult tissue in vitro. However, it is a major challenge to maintain organotypic cultures of adult neuronal tissue to obtain reliable results, e.g. in drug testing. We successfully established a new experimental setup for long-term organotypic adult neuronal tissue cultures by using substrates based on titanium and its oxides. The excellent biocompatibility of TiO_2 and titania nanotubes structured surfaces makes these materials great candidates for novel biomedical applications. By employing TiO_2 nanotube arrays prepared by electrochemical anodization, we show for the first time that these substrates can be employed for successful organotypic culture of adult guinea pig retinae and adult mice brain slices for 14 days. A prerequisite for successful cultivation is ensuring a free oxygen and CO_2 exchange as well as adequate medium supply. Since the nanotube arrays exhibit an intrinsic superhydrophilicity, fresh medium in contact with the bottom side of the array is automatically transported to the upper surface without application of perfusion systems.

To study the tissue structure and possible changes after two weeks culture, the morphology of the neuronal tissue was analyzed by immunostaining. We obtained that tissue preservation is highly dependent on the underlying nanotube structure such as tube diameter, wall thickness and surface roughness. It turned out that for nanotube diameters ranging from about 50-80 nm, retinal wholemounts were maintained organotypic for 14 days. In detail, the arrangement of the nuclei within the inner and outer nuclear layers was unchanged compared to freshly isolated retinae. Even the sensitive photoreceptor cells, that are usually the first group of cells subjected to degeneration, maintain their shape - a certain indication for the vitality of the tissue. To further confirm the preservation and viability of the retinal tissue, we performed an immunohistochemical demonstration of glutamine synthetase, which is a key enzyme in glutamate recycling, and is commonly used as a specific marker of Müller cells to demonstrate their morphological and functional integrity. In turned out that even after long-term culture, the Müller cells still span the entire retina as seen in control experiments with freshly extracted tissue.

To further validate our new culture method, organotypic culture of adult murine brain slices on TiO_2 nanotube arrays was investigated. In contrast to retinal tissue culture, here larger nanotube diameters around 100 nm are important for tissue preservation. Even after 14 days culture, the neurofilaments and the cell nuclei were well maintained and the neuronal network showed the typical organization with long axons. Altogether these results confirm that our new substrate material could be the breakthrough for in vitro studies in tissue engineering and regeneration, as well as investigation of neuroplasticity, tissue-specific gene expression and drug testing.

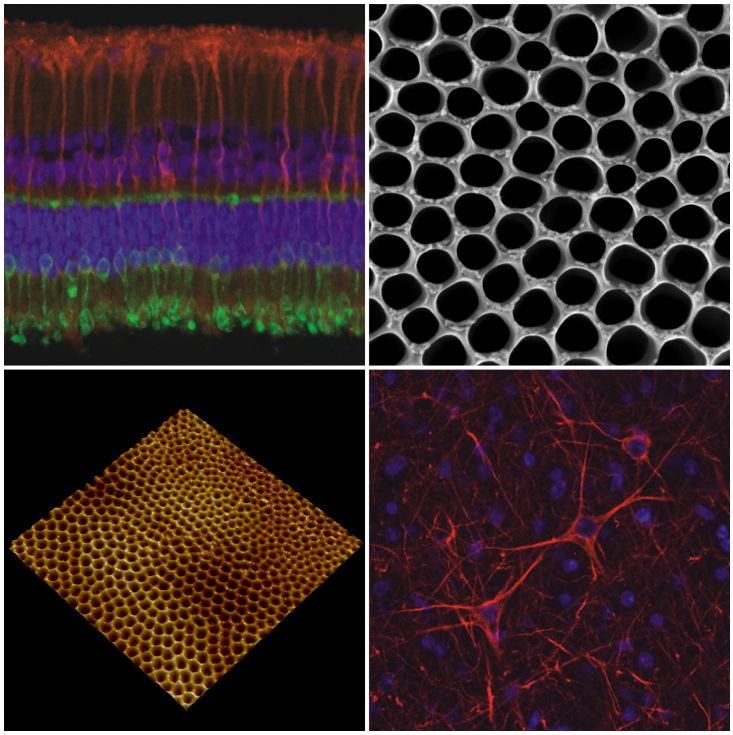

Figure 5.5: Up left and down right: Immunohistochemical staining of adult guinea pig retina and adult murine brain slice after 14 days culture, respectively. Up right and down left: Scanning electron microscopy image and atomic force microscopy map of TiO_2 nanotube surface. Nanotube diameter: ~ 100 nm.

5.6 Inherently slow and weak forward forces of neuronal growth cones measured by a drift-stabilized atomic force microscope

T. Fuhs, L. Reuter, I. Vonderhaid, J.A. Käs

The vertebrate brain does not start fully wired, but rather with single unconnected cells. To fulfill their functions, central nerve cells have to establish connections with other neurons, sensory, or muscle cells. For this, each nerve cell sends out axons and dendrites, while the cell body stays rather fixed. When an axon of one cell encounters the dendrite of another nerve cell, they can form a synapse, connecting the two cells. Still both types of neurites, axons and dendrites, advance using the same machinery. The growth cone (GC) at the tip of an outgrowing neurite has a double role: it is responsible for advancement, as well as path finding.

Here we present precise force measurements using a scanning force microscope (SFM) technique. We use the vertical and lateral deflection of a modified cantilever that allows direct measurements of the forces exerted by the cell [1]. A polystyrene bead glued to a cantilever-tip of an SFM is positioned on the substrate in front of an advancing neuronal growth cone [2]. The growth cone moves, perpendicular to the cantilever's long axis, towards the bead, and pushes against the bead, which leads to a twist of the cantilever and is detected as lateral deflection. The cantilever can be treated as a torsional spring, thus the lateral deflection gives the force acting on the cantilever.

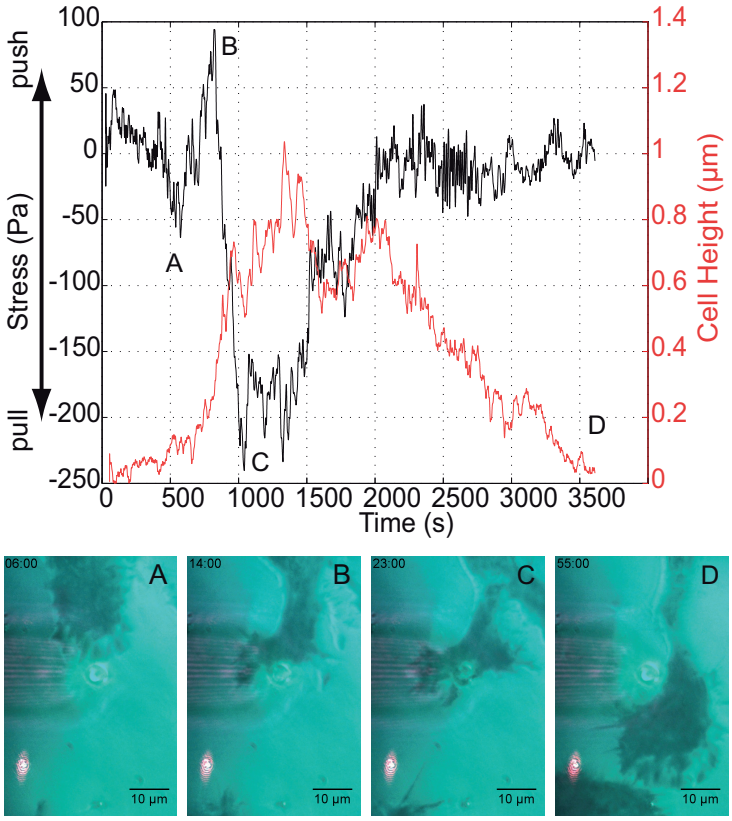

Figure 5.6: SFM forward force measurement of a growth cone of a NG 108 neurite. Left: force curve (black) and height of the cell (red), starting at time point a the cell pushes against the cantilever; at time point b the force peaks and the cantilever is lifted, while the growth cone migrates underneath the cantilever; at time d the growth cone has moved past the cantilever. Right: Interference reflection microscopy images

Normal outgrowth of neuronal growth cones only happens at 37°C, and even then is quite slow. Constant heating of the system is therefore required. However, heating leads to thermally induced drifts. Therefore, we incorporated an optical trap into our SFM-setup to measure, and correct for, the substrate's drift. Yet the scan head of the SFM does not allow using the forward scattered signal of the optical trap. To get position information nonetheless, we use the backscattered light of our marker bead. With this we can still reduce the drift of the SFM scan head with respect to the substrate to less than 50 nm/h in all 3 dimensions. Using this stabilization we can realize the necessary observation times of 1h and even longer, while still being sensitive in the pN force range.

We complemented the forward force measurements with traction force and elasticity measurements to obtain an overview of the mechanics in the neuronal growth cone. Measuring these forces for neuronal growth cones will give new insights into neuronal path finding during embryogenesis and nerve regeneration, as these occur in a crowded environment and not in wide open space.

5.7 Digital detection and analysis of branching and cell contacts in neural cell cultures

K. El-Laithy*, M. Knorr, J.A. Käs, M. Bogdan*

*Faculty of Mathematics and Computer Science

Far from being hard-wired and static, the brain is capable of dramatic reorganization. As we learn new skills or are subjected to novel experiences, our brain cells alter the way in which they respond to the outside world to reflect our changing environment and gained experience.On a biological level, these changes comprise the formation of new synapses and the elimination of existing synapses aside from the modulation of connecting properties within other ones. Due to the technical difficulties in integrating the methodologies of synaptic labeling and continuous observation of branching, only limited data is available on the normal time frame of cell contacting dynamics in general.

In our studies we developed a set of methods to detect, describe and analyze the dynamics attributed to the process of cell contacting in cell cultures *in vitro*. This involves the dynamics of branching and seeking for synaptic partners. Our developed image processing technique is able to formally distinguish between the actual formed synapses and the potential synaptic sites, i.e. where cell contacts are likely. The introduced tools are based on morphological image processing algorithms to automatically detect the sites of interest. With this at hand we investigated the dynamic behavior of these potential synaptic sites within the process of seeking for contacts in neuronal cell cultures. Our results indicate that the introduced tools can reliably describe experimentally observed branching and seeking for contacts dynamics. Being straightforward in terms of implementation and analysis, our framework represents a solid method for studying the neural preparation phases of synaptic formation via cell contacting in random networks using standard phase contrast microscopy.

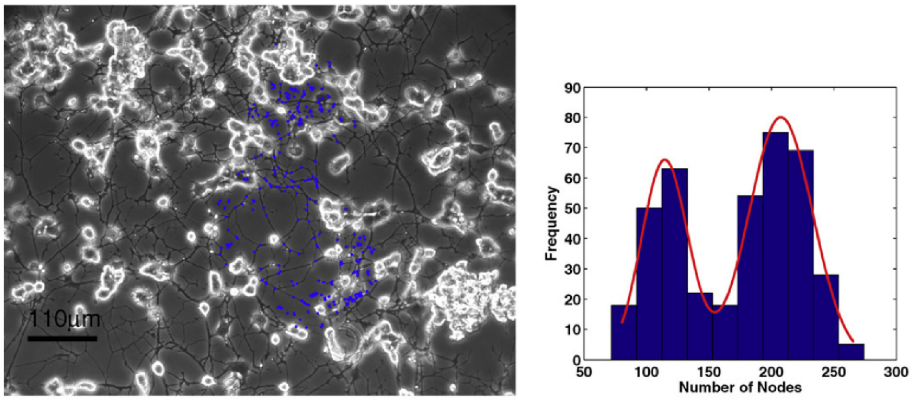

Figure 5.7: Left: Phase contrast image of developing neuronal network. Nodes detected with our tools are shown in blue. Right. Analysis of the timeseries of neuronal network developement shows a bimodal distribution of the number of detected nodes.

5.8 Oriented Confined Water Induced by Cationic Lipids

L. Woiterski, D.W. Britt*, J.A. Käs, C. Selle

*Department of Biological Engineering, Utah State University

Liquid water has outstanding properties which arise from the dynamic intermolecular hydrogen-bonding network. Water molecules form between two to four hydrogen bonds (HBs) to neighboring molecules that give rise to the broad and strong stretching vibration absorption. Assignment of the bands is still controversial as vibrational stretching modes involve complex intra- and intermolecular couplings. A particular interest persists in the interactions between biomolecules and water. Interfacial water strongly differs from the bulk liquid. It has a profound effect on the folding of proteins and DNA as well as on structure and function of biological membranes. Dimethyldioctadecylammonium (DODA) halides belong to the cationic lipids whose biophysical properties are widely studied due to their potential application in gene therapy. DODAX (X = Cl, Br, I) multilayers feature a low water capacity of few water molecules per lipid. Thus, our system allows a study on the structure and orientation of purely interfacial water adhered to DODAX model membranes.

We present a detailed attenuated total reflection (ATR) Fourier transform infrared (FTIR) spectroscopy study of the lipid associated water structure as a function of the counterion allowing us to resolve and assign water absorption bands to discrete H-bonding modes. DODAX (X = F, Cl, Br, I) halides with ions other than bromide were produced by substituting bromide in DODAB by other halide ions, purified, and analytically characterized. Polarized ATR FTIR spectroscopy is a powerful tool to investigate molecular orientation and ordering of membranes and associated water. Complementary information was obtained from molecular dynamics (MD) simulations of the DODAB/water system.

The lipid's phase behavior was characterized as it constitutes the matrix for the interfacial water. Chain-melting temperatures and chain order parameters were determined form the discontinuous change of the CH_2-stretching vibration absorption [1]. Further the symmetric CNC-stretching vibration attributed to DODAX head groups showed a direct interaction with interbilayer water. To study the structure of both H_2O and D_2O adhered to DODAX membranes, ATR spectra were measured at low hydration (1-2 molecules/lipid). The stretch absorptions demonstrate clearly visible subbands which are attributed to differently H-bonded populations. The band-fitting and subsequent analysis of the IR order parameter revealed an anisotropic orientation for the membrane-bound water. The positions of the subbands were compared with those of water stretch bands from aqueous salt solutions and ion-water clusters. The results suggest the presence of small water clusters consisting of one to five water molecules within DODAX membranes. MD simulations of a DODAB bilayer extrapolated from crystal data and water were performed with the GROMACS 3.3.3 software. Water and DODAB were modeled using the simple point charge model and a Berger lipid force field within GROMOS96 (ffG53a6), respectively. Energy minimized DODAB bilayers were used as starting configurations for the MD simulations. They confirmed the existence of differently H-bonded and oriented water along the DODAB bilayer. The water molecules showed relatively slow rotation and confined diffusion. Three major fractions were identified, however a generic correlation between average orientations

of simulated water fractions and experimentally observed water populations was not found, possibly due to effects of molecular coupling. However, by controlling the degree of hydration and through counterion exchange the unusually strong structured water in the proximity of the model lipid membranes was revealed, demonstrating the dramatic extent to which biological assemblies can influence the surrounding water layer, which in turn influences subsequent interfacial events.

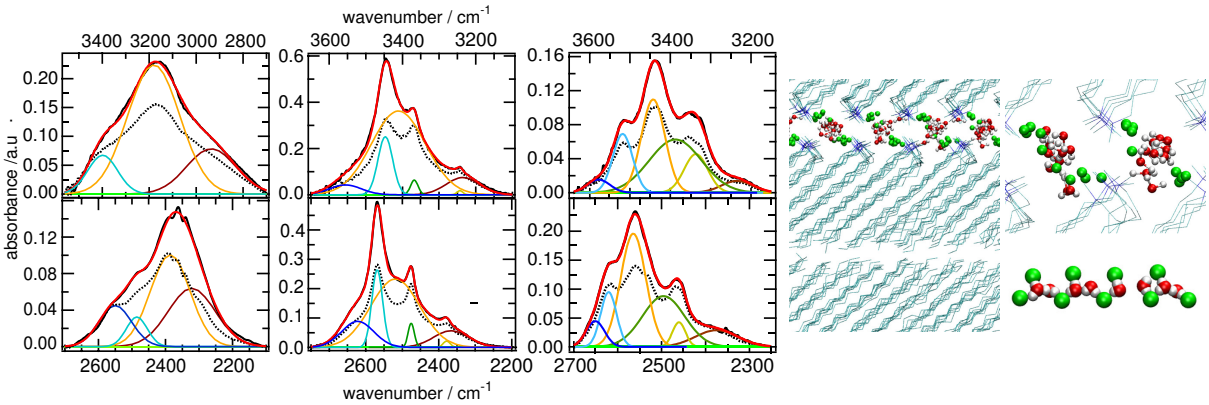

Figure 5.8: Water bound to cationic DODAX model membranes. ATR spectra and band fitting results for OH- (top) and OD- (bottom) stretching bands of water bound to DODAF, DODAC and DODAB from left to right.

[1] L. Woiterski et al.: Langmuir **28**, 4712-4722 (2012)

5.9 Funding

Leipziger Schule der Naturwissenschaften - Bauen mit Molekülen und Nano- Objekten (BuildMona)
Prof. Dr. E. Hey-Hawkins, Prof. Dr. M. Grundmann und Prof. Dr. J. A. Käs
GSC 185/1

InterNeuro
Prof. Dr. J. A. Käs, Mitglied im DFG-Graduiertenkolleg "InterNeuro", Projekte 5 und 7
GRK 1097

Optical Stretcher Methode zur Krebsdiagnose an Biopsien
Prof. Dr. J. A. Käs
EXPRIMAGE-Forschungsverbund

Zuverlässige Untersuchung und gezielte Modifikation der mechanischen Eigenschaften retinaler Zellen bei Netzhauterkrankungen und in Glianarben
Prof. Dr. J. A. Käs, Prof. Dr. A. Reichenbach et al.
Teilprojekt 2 / SAB-Förderung

Optische Messung zellulärer Materialeigenschaften für pharmakologische Hochdurchsatz-Technologie ("Agescreen")
Prof. Dr. J. A. Käs
BMBF-Projekt, 13N109 35

Von lokalen Einschränkungen bis zum makroskopischen Transport - From local constraints to macroscopic transport
Prof. Dr. J. Käs, Dr. Stephan Diez et al.
DFG Forschergruppe FOR 877, Teilprojekt 6, KA 1116/ 7-1

Light propagation through the retina: Vertebrate retinal optics
Prof. Dr. J. A. Käs, Prof. Dr. A. Reichenbach et al.
DFG, RE 849/15-1

Untersuchung funktioneller Änderungen von Tumorzellen als Ursache unsymmetrischer Verteilungsfunktionen des Zelldeformationsverhaltens
Prof. Dr. J. A. Käs, Dr. M. Zink
DFG, KA 1116/9-1

Rezidivprognose zur Entwicklung von effektiven Brusttumortherapeutika
Prof. Dr. J. A. Käs, Prof. Dr. A. Beck-Sickinger, Prof. Dr. E. Hey-Hawkins
SAB, 33707045

Nanostrukturierte Substrate zur organotypischen Langzeitkultivierung adulter Gewebe: Neuartige Verfahren für in vitro Wirkstoffscreening am Beispiel von Augenerkrankungen
Dr. M. Zink, Prof. Dr. J. A. Käs, Prof. Dr. A. Robitzki (BBZ)
SAB, 33707049

5.10 Organizational Duties

Prof. J. A. Käs

- Direktor des Instituts für Experimentelle Physik I
- PWM Winterschool Spindlermühle CZ, February 2012
- Member of the Organizing Committee: 3rd Annual Symposium - Physics of Cancer, Leipzig, November 2012
  involved organizers: Prof. Dr. C. T. Mierke, Prof. Dr. S. Köster, Prof. Dr. H. Herrmann
- Modul der Graduierten-Schule BuildMona "Chemical Biology and Biophysics of Cancer", November 2012
- Journal review: Nature, Physical Review Letters, Physical Review E, Biophysical Journal, Biophysica and Biochemica Acta, Biochemistry, Proceedings of the National Academy of Science, European Biophysical Journal, Langmuir
- Grant review: National Science Foundation, Div. of Materials Research; National Science Foundation, Div. of Cellular Organization; National Science Foundation, Div. of Computational Biology; National Science Foundation, Div. of Physics, Special Programs; Deutsche Forschungsgemeinschaft, Alexander von Humboldt Foundation, Deutsche Studienstiftung, Centre National de Recherche

Dr. C. Fütterer
- Dynamics of Tissue and Multicellular Systems
  Deutsch-Französische Hochschule, December 2012

5.11 External Cooperations

Academic

- Institute Curie, Paris, France
  Prof. Dr. J.-F. Joanny
- ESPCI, Paris, France
  Prof. Dr. J. Prost
- Cea Saclay, France
  Prof. Dr. M.-F. Carlier
- Princeton University, USA
  Prof. Dr. R. Austin
- Albert Einstein Institute of Medicine, U.S.A.
  Prof. Dr. J. Condeelis
- Deutsche Gesellschaft für Zellbiologie (DGZ)
  Prof. Dr. H. Herrmann
- Georg August University Göttingen
  Prof. Dr. S. Köster
- Physikalisch-Technische Bundesanstalt
  Prof. Dr. M. Bär
- Max-Delbrück-Zentrum für molekulare Medizin
  Dr. M. Falcke
- MPI for Colloids and Interfaces, Potsdam-Golm
  Prof. Dr. R. Lipowsky
- Deutsches Krebsforschungszentrum
  Prof. Dr. R. Eills
- Universität Leipzig, Klinik u. Poliklinik für Frauenheilkunde
  Prof. Dr. M. Höckel
- Universität Leipzig, Institut für Pathologie
  Prof. Dr. L.-C. Horn
- Universität Leipzig, Institut für Anorganische Chemie
  Prof. Dr. E. Hey-Hawkins
- Universität Leipzig, Institut für Biochemie
  Prof. Dr. A. Beck-Sickinger
- Universität Leipzig, Klinik u. Poliklinik f. Mund-, Kiefer- u. Plastische Gesichtschirurgie
  Dr. T. Remmerbach

- Westfälische Wilhelms-Universität Münster
  Dr. J. Schnekenburger
- Technische Universität Dresden
  Prof. Dr. J. Guck
- Charité Berlin, MR Elastographie
  Prof. Dr. I. Sack

Industry

- Beiersdorf AG, Hamburg
  Dr. C. Schulze
- JPK Instruments, Berlin
  Dr. T. Müller
- Niendorf & Hamper, Hamburg
  Prof. A. Niendorf
- ibidi GmbH, Martinsried
  Dr. V. Kahl
- Inventages, London, GB
  Prof. Dr. T. Bayerl

5.12 Publications

Journals

K. El-Laithy, M. Knorr, J. A. Käs, M. Bogdan: *Digital detection and analysis of branching and cell contacts in neural cell cultures*, Journal Neuroscience Methods **210**, Issue 2, 206-219 (2012)

C. Kappel, N. Dölker, R. Kumar, M. Zink, U. Zachariae, H. Grubmüller: *Universal Relaxation Governs the Nonequilibrium Elasticity of Biomolecules*, Physical Review Letters **109**, 118304 (2012)

K. D. Nnetu, M. Knorr, J. A. Käs, M. Zink: *The impact of jamming on boundaries of collectively moving weak-interacting cells*, New Journal of Physics **14**, 115012 (2012)

K. D. Nnetu, M. Knorr, D. Strehle, M. Zink, J. A. Käs: *Directed persistent motions maintain sheet integrity during multi-cellular spreading and migration*, Soft Matter **8**, Issue 26, 2913-2921 (2012)

M. Martin, K. Müller, C. Cadenas, M. Hermes, M. Zink, J. G. Hengstler, J. A. Käs: *ERBB2 overexpression triggers transient high mechanoactivity of breast tumor cells*, Cytoskeleton **69**, Issue 5, 267-277 (2012)

V. Dallacasagrande, M. Zink, S. Huth, A. Jakob, M. Müller, A. Reichenbach, J. A. Käs, S. G. Mayr: *Tailoring Substrates for Long-Term Organotypic Culture of Adult Neuronal Tissue*, Advanced Materials **24**, Issue 18, 2399-2403 (2012)

L.Woiterski, D. W. Britt, J. A. Käs, C. Selle: *Oriented Confined Water Induced by Cationic Lipids*, Langmuir **28**, Issue 10, 4712-4722 (2012)

A. Leal-Egaña, A. Fritsch, F. Heidebrecht, A. Diaz-Cuenca, M. Nowicki, A. Bader, J. A. Käs: *Tuning liver stiffness against tumours: An in vitro study using entrapped cells in tumour-like microcapsules*, Journal of the Mechanical Behavior of Biomedical Materials **9**, 113-121 (2012)

J. Zimmermann, C. Brunner, M. Enculescu, M. Goegler, A. Ehrlicher, J. A. Käs, M. Falcke: *Actin Filament Elasticity and Retrograde Flow Shape the Force-Velocity Relation of Motile Cells*, Biophysical Journal **102**, Issue 2, 287-295 (2012)

F. Huber, D. Strehle, J. A. Käs: *Counterion-induced formation of regular actin bundle networks*, Soft Matter **8**, Issue 4, 931-936 (2012)

in press

M. Zink, F. Szillat, U. Allenstein, S. G. Mayr: *Interaction of Ferromagnetic Shape Memory Alloys and RGD Peptides for Mechanical Coupling to Cells: from Ab Initio Calculations to Cell Studies*, Advanced Functional Materials

T. Fuhs, L. Reuter, I. Vonderhaid, T. Claudepierre, J. A. Käs: *Inherently slow and weak forward forces of neuronal growth cones measured by a drift-stabilized atomic force microscope*, Cytoskeleton

Talks

J. A. Käs *Are Biomechanical Changes Necessary for Tumor Progression?*, 2012 Aspen Winter Conference on Form and Growth: Pattern Formation in Biology, Aspen (USA) January 2012 (invited talk)

A. Fritsch, T. Kießling, R. Stange, J. A. Käs *Temperature dependence of optically induced cell deformations*, APS Spring Meeting Boston (USA) February 2012

M. Zink, V. Dallacasagrande, S. Huth, A. Jakob, M. Müller, A. Reichenbach, J. Käs, and S.G. Mayr *Longterm organotypic culture of adult neuronal tissue*, Gruppenseminar Neuroanatomie, Prof. I. Bechmann, Universität Leipzig, February 2012 (invited talk)

J. Lippoldt, C. Händel, B. Käßemodel, U. Dietrich, and J. A. Käs *Pattern Formation in Biomimetic Membranes*, 16. Harzseminar - Strukturbildung in Chemie und Biophysik in Hahnenklee, February 2012

J. A. Käs *Are Biomechanical Changes Necessary for Tumor Progression?*, Albert-Einstein-College of Medicine, Yeshiva University, New York (USA) February 2012 (invited talk)

U. Allenstein, Y. Ma, A. Arabi-Hashemi, S. G. Mayr, and M. Zink *Biocompatibility of $Fe_{70}Pd_{30}$ ferromagnetic shape memory films for cell actuation*, DPG Spring Meeting, Berlin, March 2012

T. Kießling, A. Fritsch, R. Stange, J. A. Käs *Thermorheology of single living cells*, DPG Spring Meeting, Berlin, March 2012

T. Fuhs, L. Reuter, I. Vonderhaid, T. Claudepierre, and J. A. Käs *Inherently slow and weak forward forces of neuronal growth cones measured by a drift-stabilized Atomic Force Microscope*, DPG Spring Meeting, Berlin, March 2012

J. A. KäsFrom Nano-scaffolds and Nano-motors to Metastasis and Nerve Regeneration, Göttinger Biophysik Kolloquium, Georg-August-Universität Göttingen, March 2012 (invited talk)

M. Zink *Nanostrukturierte Substrate zur organotypischen Langzeitkultivierung adulter Gewebe: Neuartige Verfahren für in vitro Wirkstoffscreening am Beispiel von Augenerkrankungen*, Statusseminar Biotechnologisch-Biomedizinisches Zentrum, Universität Leipzig, April 2012 (invited talk)

A. Fritsch *From single cells to cell aggregates: Biomechanical studies*, Lunch Seminar: Soft Matter and Biophysics LMU München, May 2012

J. A. Käs *Physics of Cancer*, Systembiologie Netzwerk Leipzig, Informelles Treffen im UFZ, May 2012 (invited talk)

J. A. Käs *Are Fundamental Changes in a Cell's Material Properties Necessary for Tumor Progressions?* Conference on Active Jammed Systems, New York (USA) May 2012 (invited talk)

T. Händler, S. Pawlizak, and J. A. Käs *Probing the mechanosensing of neurons with magnetic tweezers*, Saxon Biotechnology Symposium, June 2012

P. Heine, and J. A. Käs *Optical Neuronal Guidance revisited Lighting the way at every turn*, InterNeuro Colloquium B, June 2012

C. Händel, U. Dietrich, S. Alonso, M. Bär, and J. Käs *Chemical Oscillations in Cell Membranes*, 2nd EBSA Biophysics Course: Membrane Biophysics and Lipid-Protein Interaction, Bordeaux-Lacanau (France) June 2012

J. A. Käs *Contractile Force Generation by Entropic Softening of Actin Networks*, Trilateral Russia-German-France Workshop "Oncology: on the Frontiers of Molecular Genetics, Biophysics and Medicine", Perm (Russia) June 2012 (invited talk)

J. A. Käs *AgeScreen*, International Congress on Biophotonics Ð ICOB 2012, 7. Statustreffen des Forschungsschwerpunktes Biophotonik, Jena, June 2012 (invited talk)

M. Zink *Von dünnen Schichten und Nanoröhren: Biokompatibilität neuer Materialien für die Medizin*, Lange Nacht der Wissenschaften, Leipzig, June 2012 (invited talk)

C. Fütterer, M. Krahe, I. Wenzel, K.-N. Lin, and J. Fischer *Physikalische Kräfte bei der Regeneration von Gewebe: Kritische Phänomene und neue Technologien*, Universität Magdeburg, July 2012

J. A. Käs *Are Fundamental Changes in a Cell's Material Properties Necessary for Tumor Progressions?* Seminar für GRK 1558, Technische Universität Berlin, July 2012 (invited talk)

J. A. Käs *Do tumor cells care about physics?*, 4th Conference on Systems Biology of Mammalian Cells, Leipzig, July 2012 (invited talk)

J. A. Käs *Are Fundamental Changes in a Cell's Material Properties Necessary for Tumor Progressions?* Conference on "Tissue Growth and Morphogenesis: From Genetics to Mechanics and Back", Banff (Canada) July 2012 (invited talk)

J. A. Käs *Are Fundamental Changes in a Cell's Material Properties Necessary for Tumor Progressions?*, Conference 8458: Optical Trapping and Optical Micromanipulation IX (OTOM), SPIE-Optics + Photonics, San Diego (USA) August 2012 (invited talk)

J. A. Käs *Are Fundamental Changes in a Cell's Material Properties Necessary for Tumor Progressions?*, XI. International Conference on Nanostructured Material (NANO 2012), Rhodes (Greece) August 2012 (invited talk)

J. Schnauß, F. Huber, D. Strehle, and J. A. Käs *Actin bundle assembly in higher ordered structures - a new liquid crystal phase?* 5th BuildMoNa Workshop for Doctoral Candidates, September 2012

C. Händel, U. Dietrich, S. Alonso, M. Bär, and J. Käs *Chemical Oscillations in Cell Membranes*, 5th BuildMoNa Workshop for Doctoral Candidates, September 2012

F. Rämisch, and C. Fütterer *Dynamik von magnetischen Mikropartikel in Mikrokanälen*, Meeting zum BMBF Projekt "Minolab", September 2012

C. Fütterer, M. Krahe, I. Wenzel, K.-N. Lin, and J. Fischer *Kräfte bei der Regeneration von Hydra Gewebe*, Herzzentrum Leipzig, Gruppe Prof. Dhein, September 2012

M. Zink and S.G. Mayr *Fe-Pd Based Ferromagnetic Shape Memory Alloy Membranes as Sensors and Actuators in Biomedical Applications - Fundamentals, Applications and Challenges*, Department of Engineering, Cambridge University (GB), September 2012 (invited talk from Dr. A. Markaki)

J. A. Käs *Are Fundamental Changes in a Cell's Material Properties Necessary for Tumor Progressions?* Conference on Optogenetics, The Rank Prize Funds (GB) September 2012 (invited talk)

J. A. Käs *Physics of Cancer*, ESF Exploratory Workshop on "Physics of Cancer", Varenna (Italy) September 2012 (invited talk)

C. Schuldt, T. Golde, J. A. Käs *Contractile Force Generation by Entropic Softening of Actin Networks*, Trilateral Oncology Workshop, Perm (Russia), June 2012; Sächsische Forschergruppe Symposium, Dresden, September 2012; BuildMoNa Workshop, September 2012

T. Kießling, A. Fritsch, E. Warmt, R. Stange, and J. A. Käs *The Impact of Temperature Variations on Cell Mechanics*, Institut Curie, Paris (France) November 2012

J. Schnauß, F. Huber, D. Strehle, M. Glaser and J. A. Käs *Actin bundle assembly in higher ordered structures - a new liquid crystal phase?* 3rd Annual Symposium - Physics of Cancer; Leipzig, November 2012

M. Zink, U. Allenstein, Y. Ma, and S.G. Mayr *Fe-Pd ferromagnetic shape memory foils for biomedical applications - fundamentals, applications, challenges* Annual Meeting of the German Biophysical Society, September 2012; Materials Research Society Meeting, Boston (USA) November 2012

C. Fütterer, M. Krahe, I. Wenzel, K.-N. Lin, and J. Fischer *Fluctuations and symmetry breaking during regeneration of Hydra vulgaris tissue toroids*, Conference Dynamics of tissues and multicellular systems, Leipzig, December 2012

J. A. Käs *Do tumor cells care about physics?* Seminarvortrag am Max-Planck-Institut für Intelligente Systeme, Stuttgart, Dezember 2012 (invited talk)

Posters

A. Fritsch , S. Pawlizak , M. Zink , J. A. Käs *The mechanics of cellular compartmentalization as a model for tumor spreading*, APS Spring Meeting Boston (USA), February 2012

J. Schnauß, F. Huber, M. Steinhagen, and J. Käs *Actin network growth at oil-water interphases*, 5th Scientific Symposium of the Graduate School BuildMoNa, March 2012

M. Knorr and J. A. Käs *Filopodia-Lamellipodia Interaction Dynamics in Neuronal Growth Cones*, DPG Spring Meeting, Berlin, March 2012

P. Rauch, P. Heine, B. Goettgens, J. A. Käs *When Folding does not Imply Pullout: Different Modes of Growth Cone*, DPG Spring Meeting, Berlin, March 2012

F. Huber, D. Strehle, J. Schnauß, M. Gralka, J. A. Käs *Formation of regular actin bundle networks by counter-ion condensation and entropic forces*, DPG Spring Meeting, Berlin, March 2012

E. Warmt, T. Kießling, A. Fritsch, R. Stange, and J. A. Käs *Impact of Temperature on Cell Nuclei Integrity in the Optical Stretcher*, DPG Spring Meeting, Berlin, March 2012

C. Händel, U. Dietrich, S. Alonso, M. Bär, and J. Käs *Chemical Oscillations in Cell Membranes*, 4th BuildMoNa Workshop for Doctoral Candidates, March 2012

A. Fritsch, S. Pawlizak, R. Stange, and J. A. Käs *The mechanics of cellular compartmentalization as a model for tumor spreading*, Active Jammed Systems, New York (USA), May 2012

T. Händler, B. Kohlstrunk, and J. Käs *Probing the mechanosensing of neurons with magnetic tweezers*, Saxon Biotechnology Symposium, June 2012

J. Schnauß, F. Huber, D. Strehle, M. Glaser, and J. A. Käs *Higher ordered actin bundle assembly induced by counterions and crowding agents*, Active Soft and Biological Matter: A Conference in honour of Jacques Prost, Les Houches (France), October 2012; 3rd Annual Symposium - Physics of Cancer, Leipzig, November 2012

C. Schuldt, T. Golde, D. Strehle, J. Schnauß, J. A. Käs *Mechanics of actin bundles: Bending & Contraction*, Active Soft and Biological Matter: A Conference in honour of Jacques Prost, Les Houches (France), October 2012

C. Schuldt, T. Golde, J. A. Käs *Contractile Force Generation by Entropic Softening of Actin Networks*, 5th Scientific Symposium of the Graduate School BuildMoNa, March 2012; DPG Spring Meeting, Berlin, March 2012; 3rd Annual Symposium - Physics of Cancer, Leipzig, November 2012

A. Fritsch, S. Pawlizak, M. Höckel, J. A. Käs *Biomechanical studies on human primary cervix cells*, 3rd Annual Symposium - Physics of Cancer, Leipzig, November 2012

V. Dallacasagrande, M. Zink, S. Huth, A. Jakob, M. Müller, J. Käs, S.G. Mayr, and A. Reichenbach *Tailoring Substrates for Long-term Organotypic Culture of Adult Neuronal Tissue*, Neuroscience 2012, New Orleans (USA), October 2012

T. Fuhs, L. Reuter, I. Vonderhaid, T. Claudepierre, and J. A. Käs *Inherently slow and weak forward forces of neuronal growth cones measured by a drift-stabilized Atomic Force Microscope*, 3rd Annual Symposium - Physics of Cancer, Leipzig, November 2012

M. Zink, V. Dallacasagrande, S. Huth, A. Jakob, M. Müller, A. Reichenbach, J. Käs and S.G. Mayr *Tailoring Substrates for Long-term Organotypic Culture of Adult Neuronal Tissue*, Annual Meeting of the German Biophysical Society, Göttingen, September 2012; Materials Research Society Meeting, Boston (USA), November 2012

T. Kießling, A. Fritsch, R. Stange, and J. A. Käs *Thermorheology of living cells*, Annual Meeting of the American Society of Cell Biology, San Francisco (USA), December 2012

M. Knorr, M. Ilse, T. Claudepierre, and J. A. Käs *How growth cone leading edge dynamics alters with substrate adhesion*, Annual Meeting of the American Society of Cell Biology, San Francisco (USA), December 2012

M. Krahe, I. Wenzel, K.-N. Lin, J. Fischer, and C. Fütterer *The mechanics of regeneration and healing of Hydra vulgaris tissues*, Conference Dynamics of tissues and multicellular systems, Leipzig, December 2012

H. Kubitschke, and C. Fütterer *Protocells: From a Closed to an Opened System*, Conference Dynamics of tissues and multicellular systems, Leipzig, December 2012

5.13 Graduations

Doctorate

- Florian Huber
  Emergent structure formation of the actin cytoskeleton
  March 2012
- Katja Taute
  Microtubule mechanics and the implications for their assembly
  May 2012

Diploma

- Bernd Käßemodel
  Non-Linear Pattern Formation in Biomimetic Lipid Membranes
  December 2012

Master

- Martin Glaser
  Actin Bundle Mechanics
  October 2012
- Tom Golde
  Polymerization Effects in Actin Networks
  October 2012
- Hans Kubitschke
  On the Influence of Mitotic Inhibitors on Cells - Modeling the Toxicity of Paclitaxel
  October 2012
- Jürgen Lippoldt
  Nonlinear dynamics in lipid membranes
  November 2012
- Wolfram Pönisch
  Chemical Guidance and Chemotaxis of Neurons
  Novenber 2012

Bachelor

- Iris Wenzel
  Hydra Regeneration under Mechanical Confinement
  February 2012
- Tobias Eggebrecht
  The physics of tumor cell motility
  February 2012
- Kao-Nung Lin
  Fundamental experiments and observations of behavior of hydra ring and inhibitor treatment on hydra ring
  June 2012
- Maximilian Ilse
  Role of Substrate Adhesion in Actin Dynamicsof Neuronal Growth Cones
  September 2012
- Julia Fischer
  Zellübergreifende Aktinstrukturen und kollektives Zellverhalten in Gewebe von Hydra vulgaris infolge mechanischer Stimulation
  September 2012
- Stefanie Riedel
  Cell-Cell Adhesion Forces of Human Breast Carcinoma
  October 2012
- Dave Ahrens
  Cell-Cell Adhesion Forces in the Mammary Carcinoma Cell Line MDA-MB 231
  December 2012

5.14 Guests

- Valentina Dallacasagrande M. Sc.
  EU-research assistant at the Paul-Flechsig-Institut for brain research and the Dept. Softmatter Physics, Universität Leipzig, March 2010 - approx. 2013

II

Institute for Experimental Physics II

6

Magnetic Resonance of Complex Quantum Solids

6.1 Introduction

The electronic properties of quantum-solids in which the electrons exhibit strong correlations with each other or with the lattice are particularly rich and will be of special importance in future functional materials. In addition, such solids are challenging for experiment, as well as theory, as the more than twenty-year history of high-temperature superconductivity shows: we still do not understand the electronic structure of these systems. One particular aspect of strongly correlated electronic materials is their tendency towards nano-scale electronic phase separation. Even in perfect lattices, electronic nano-structures can form. The investigation of such materials requires the use of methods that can give detailed information. Here, magnetic resonance, on nuclei and electrons, is of particular interest as they not only have atomic scale resolution, but also yield bulk information in contrast to surface techniques. We explore the properties of these materials with tailored new techniques of magnetic resonance.

Jürgen Haase

6.2 Nuclear magnetic resonance apparatus for pulsed high magnetic fields

B. Meier, J. Kohlrautz, J. Haase, M. Braun [*], F. Wolff-Fabris [†], E. Kampert [†], T. Herrmannsdörfer [†], J. Wosnitza [†],

[*]NMR-Service, Erfurt

[†]Dresden High Magnetic Field Laboratory, Forschungszentrum Dresden-Rossendorf

A nuclear magnetic resonance apparatus for experiments in pulsed high magnetic fields is described. The magnetic field pulses created together with various magnet coils determine the requirements such an apparatus has to fulfill to be operated successfully in pulsed fields. Independent of the chosen coil it is desirable to operate the entire experiment at the highest possible bandwidth such that a correspondingly large

temporal fraction of the magnetic field pulse can be used to probe a given sample. Our apparatus offers a bandwidth of up to 20 MHz and has been tested successfully at the Hochfeld-Magnetlabor Dresden, even in a very fast dual coil magnet that has produced a peak field of 94,2 T. Using a medium-sized single coil with a significantly slower dependence, it is possible to perform advanced multi-pulse nuclear magnetic resonance experiments. As an example we discuss a Carr-Purcell spin echo sequence at a field of 62 T.

6.3 Eigenmodes in the Long-Time Behavior of a Coupled Spin System Measured with Nuclear Magnetic Resonance

B. Meier, J. Kohlrautz, J. Haase,

The many-body quantum dynamics of dipolar coupled nuclear spins I=1/2 on an otherwise isolated cubic lattice are studied with nuclear magnetic resonance. By increasing the signal-to-noise ratio by 2 orders of magnitude compared with previous reports for the free induction decay (FID) of ^{19}F in CaF_2] we obtain new insight into its long-time behavior. We confirm that the tail of the FID is an exponentially decaying cosine, but our measurements reveal a second decay mode with comparable frequency but twice the decay constant. This result is in agreement with a recent theoretical prediction for the FID in terms of eigenvalues for the time evolution of chaotic many-body quantum systems.

6.4 Two-component uniform spin susceptibility in superconducting $HgBa_2CuO_{4+\delta}$ single crystals measured using ^{63}Cu and ^{199}Hg nucleear magnetic resonance

J. Haase, D. Rybicki, C.P. Slichter*, M. Greven†, G. Yu†, Y. Li†, X. Zhao†,

*University of Illinois at Urbana-Champaign, Department of Physics, USA
†University of Minnesota, School of Physics and Astronomy, USA

^{63}Cu and ^{199}Hg NMR shifts for an optimally and underdoped $HgBa_2CuO_{4+\delta}$ single crystal are reported, and the temperature dependence dictates a two-component description of the uniform spin susceptibility. The first component, associated with the pseudogap phenomenon in the NMR shifts, decreases already at room temperature and continues to drop as the temperature is lowered, without a drastic change at the transition temperature into the superconducting state. The second component is temperature independent above the superconducting transition temperature and vanishes rapidly below it. It increases with doping and is a substantial part of the total spin susceptibility measured at both nuclei.

6.5 Highly proton conducting sulfonic acid functionalized mesoporous materials studied by impedance spectroscopy, MAS NMR spectroscopy and MAS PFG NMR diffusometry Microporous Mesoporous Mater

M. Sharifi*, M. Wark*, D. Freude, J. Haase,

*Ruhr-University Bochum, Laboratory of Industrial Chemistry, Germany

Proton conducting mesoporous Si-MCM-41 materials with different amounts of SO_3H-groups were prepared by the co-condensation method and investigated by NMR spectroscopy, NMR diffusometry and impedance spectroscopy. The successful incorporation of mercaptopropyltrimethoxysilane (MPMS) into the mesoporous framework was proven by ^{29}Si NMR measurements. The deconvolution of the ^{29}Si MAS NMR spectra shows that Si atoms of the functionalizing silane are linked to the MCM-41 framework via three or two ≡Si-O-Si≡ bonds. ^{29}Si MAS NMR proves that almost all MPMS was incorporated into the mesoporous framework, since 36.9% of the signal belongs to T groups, whereas the concentration of MPMS in the synthesis solution amounts 40%. ^{13}C CP MAS spectroscopy confirms that the majority of the organic functional groups remained intact after the oxidation in 30 wt.-% H_2O_2.

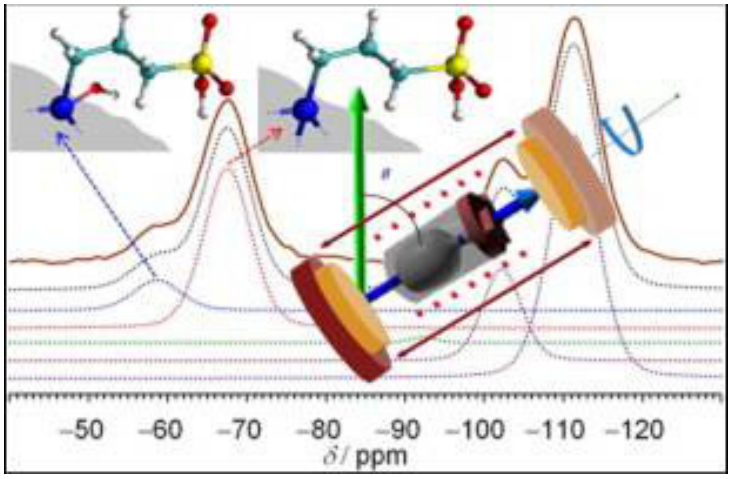

Figure 6.1: Highly proton conducting sulfonic acid functionalized mesoporous materials studied by impedance spectroscopy, MAS NMR spectroscopy and MAS PFG NMR diffusometry

The proton conductivity was investigated by impedance spectroscopy (IS). Drastic differences were found for different degrees of functionalization. The maximum conductivity was found for the sample with maximum loading of sulfonic acid groups (40% functionalization) as $\sigma_{dc} = 0.19\ S\ cm^{-1}$ at 413 K. The large conductivity differences between 20% and 40% functionalization result in large differences in the diffusion coefficients of the charge carrier by application of the Nernst-Einstein equation. But only small differences of the water self-diffusion coefficients were measured by magic-angle spinning pulsed field gradient (MAS PFG) NMR diffusometry. The comparison of IS and MAS PFG NMR results allows the determination of the Haven factor, which amounts

5 660 for 20% and 329 for 40% functionalization. We explain the proton conductivity in functionalized MCM-41 by structure diffusion. The drastic increase of conductivity (at 353 K from 9.51 to 260 x 10^{-5} S cm^{-1}) from 20% to 40% functionalization is caused by the reduction of the activation energy of the charge relocation in a denser lattice of proton donator sites.

6.6 Two-Component Behavior of Cuprate Superconductors from NMR Shifts

D. Rybicki, M. Greven*, J. Haase, T. Meissner, S.K. Goh †, G.V.M. Williams ‡,

*University of Minnesota, School of Physics and Astronomy, USA
†Department of Physics, Cavendish Laboratory, University of Cambridge, United Kingdom
‡Victoria University, Physics Department, Wellington, New Zealand

NMR spin shift data of $La_{1:85}Sr_{0:15}CuO_4$, $HgBa_2CuO_{4+\delta}$ at ambient pressure, and of $YBa_2Cu_4O_8$ at pressure up to 63 kbar are discussed that fail the traditional single-electronic fluid picture used for the discussion of NMR data. Instead the results point to a common explanation for all three systems in terms of two electronic components. One of them has a temperature-dependent magnetic susceptibility while the second component, as well as its coupling to the first component, are constant above the superconducting transition temperature Tc. All susceptibilities vanish below Tc.

6.7 Simultaneous 3D localization of multiple MR-visible markers in fully reconstructed MR images: proof-of-concept for sub-second position tracking

G. Thörmer, N. Garnov* M. Moche*, J. Haase, T. Kahn*, H. Busse*,

*Department of Diagnostic and Interventional Radiology, Leipzig University Hospital, Leipzig, Germany

To determine whether a greatly reduced spatial resolution of fully reconstructed projection MR images can be used for the simultaneous 3D localization of multiple MR-visible markers and to assess the feasibility of a subsecond position tracking for clinical purposes. Miniature, inductively coupled RF coils were imaged in three orthogonal planes with a balanced steady-state free precession (SSFP) sequence and automatically localized using a two-dimensional template fitting and a subsequent three-dimensional (3D) matching of the coordinates. Precision, accuracy, speed and robustness of 3D localization were assessed for decreasing in-plane resolutions (0.6-4.7 mm). The feasibility of marker tracking was evaluated at the lowest resolution by following a robotically driven needle on a complex 3D trajectory. Average 3D precision and accuracy, sensitivity and specificity of localization ranged between 0.1 and 0.4 mm, 0.5 and 1.0 mm, 100% and 95%, and 100% and 96%, respectively. At the lowest resolution, imaging and localization took $\approx 350ms$ and provided an accuracy of $\approx 1.0mm$. In the tracking experiment, the needle was clearly depicted on the oblique scan planes defined by the markers.

Image-based marker localization at a greatly reduced spatial resolution is considered a feasible approach to monitor reference points or rigid instruments at subsecond update rates.

6.8 Formation of Mixed Metal $Cu_{3-x}Zn_x(btc)_2$ Frameworks with Different Zinc Contents: Incorporation of Zn^{2+} into the MOF Structure as Studied by Solid-State NMR

F. Gul-E-Noor, B. Jee, M. Mendt, D. Himsl*, A. Pöppl M. Hartmann *, J. Haase, H. Krautscheid† M. Bertmer

*Erlangen Catalysis Resource Center, University Erlangen-Nuremberg
†Chemistry and Mineralogy, Leipzig University

Incorporation of Zn^{2+} into the $Cu_3(btc)_2$ metal-organic framework (HKUST-1) was successfully done with Zn^{2+} replacing Cu^{2+} in the paddle wheel unit up to 21% zinc. Detailed spectroscopic characterization of the resulting binuclear Cu-Zn paddle wheel units was carried out by ^1H and ^{13}C solid-state nuclear magnetic resonance (SSNMR). By intensity analysis of the NMR signals a quantitative determination of the Zn^{2+} content incorporated into the $Cu_3(btc)_2$ framework is possible. X-ray and EPR data verify the analysis. Surface areas were determined for the different samples that indicate a decreasing porosity with increasing zinc content. Water molecules coordinated to the zinc atoms remain in the structure even after evacuation. Their assignment was also confirmed by calculation of the pseudocontact or dipolar shift contribution from all unpaired electrons of surrounding paddle wheels.

6.9 Electronic structure of the nitrogen donors in 6H SiC as studied by pulsed ENDOR and TRIPLE ENDOR spectroscopy

DariyaV. Savchenko *, EkaterinaN. Kalabukhova †, BelaD. Shanina †, A. Pöppl

*Institute of Physics, AS CR, Na Slovance 2, 18221, Praha 8, Czech Republic
†V.E. Lashkaryov Institute of Semiconductor Physics, NASU, Pr. Nauki 45, 03028, Kiev, Ukraine

The nitrogen (N) donors in 6H SiC were investigated by field sweep electron spin echo (FS ESE), pulsed electron nuclear double resonance (ENDOR) and pulsed General TRIPLE ENDOR spectroscopy [1]. The ^{29}Si and ^{13}C superhyperfine (shf) lines observed in the FS ESE and ENDOR spectra of N in n-type 6H SiC were assigned by pulsed General TRIPLE resonance spectroscopy to the specific carbon (C) and silicon (Si) atoms located in the environment of N donors residing at two quasi-cubic lattice sites (N_{k1}, N_{k2}) in 6H SiC. As a result, the largest value of the shf interaction was found with Si atoms for the N donors at the hexagonal (N_h) and quasi-cubic site N_{k1}, while

for N_{k2} the largest value of the shf interaction was found with C atoms. It gives us the argument to consider that N substitute different lattice sites in 6H SiC lattice. The relative signs of the shf interaction (shfi) constants for N_{k1} and N_{k2} with ^{29}Si and ^{13}C nuclei located in the nearest-neighbor, next nearest-neighbor and outer shells are found from the TRIPLE ENDOR spectra to be positive for C atoms and negative for Si atoms. From the comparison of the experimentally obtained shfi constants with the theory, the electronic spin-density distribution over the ^{29}Si and ^{13}C nuclei located in the nearest neighbor shells of N donors has been obtained taking into account the Kohn-Luttinger interference effect. The position of the conduction band minimum along the ML-line was determined to be at $k_{0z}/k_{max} = 0.2 \pm 0.05$.

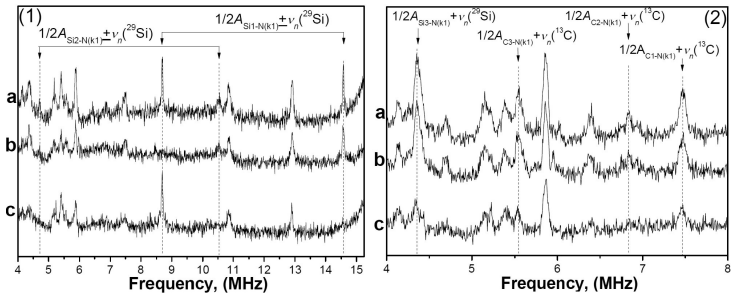

Figure 6.2: X-band pulsed Davies ENDOR (a) and General TRIPLE-ENDOR spectra (b, c) measured in n-type 6H SiC samples when low-frequency (b) and high-frequency (c) ENDOR lines of N_{k1} at 15.653 MHz and 17.867 MHz were "pumped", respectively. B_0 = 346.94 mT (1), B_0 = 346.85 mT (2). B ⊥ c, T = 6 K.

6.10 A novel Zn_4O-based triazolyl benzoate MOF: synthesis, crystal structure, adsorption properties and solid state ^{13}C NMR investigations

J. Lincke* D. Lässig*, K. Stein*, J. Möllmer† A. ViswanathKuttatheyil, Ch. Reichenbach†, A. Moeller†, R. Staudt‡ G. Kalies M. Bertmer H. Krautscheid*,

*Chemistry and Mineralogy, Leipzig University
†Institut für Nichtklassische Chemie e. V., Leipzig
‡Fakultät für Maschinenbau und Verfahrenstechnik, Hochschule Offenburg

The newly synthesized Zn_4O-based MOF $^3_\infty[Zn_4(\mu_4\text{-O})(\text{Metrz-pba})_2\text{mPh}_3]\cdot 8\text{DMF}(1\cdot 8\text{DMF})$of rare tungsten carbide (acs) topology exhibits a porosity of 43% and remarkably high thermal stability up to 430 °C. Single crystal X-ray structure analyses could be performed using as-synthesized as well as desolvated crystals. Besides the solvothermal synthesis of single crystals a scalable synthesis of microcrystalline material of the MOF is reported. Combined TG-MS and solid state NMR measurements reveal the presence of mobile DMF molecules in the pore system of the framework. Adsorption measurements confirm that the pore structure is fully accessible for nitrogen molecules at 77 K. The adsorptive pore volume of 0.41 $cm^3\ g^{-1}$ correlates well with the pore volume of 0.43 $cm^3\ g^{-1}$ estimated from the single crystal structure.

6.11 Effects of Aromatic Substitution on the Photodimerization Kinetics of β-trans Cinnamic Acid Derivatives Studied with ^{13}C Solid-State NMR

I. Fonseca*, M. Baias†, S.E. Hayes‡, Ch.J. Pickard†, M. Bertmer

*Macromolecular Chemistry, Aachen University of Technology
†Department of Physics & Astronomy, University College London
‡Department of Chemistry, Washington University in St. Louis, St. Louis, MO

In our efforts to study photodimerizations in the solid state, we present data on the influence of the position of aromatic substitution by bromine on the photodimerization rate in cinnamic acid derivatives. Results were obtained by ^{13}C CPMAS NMR spectroscopy together with chemical shift tensor analysis, DFT calculations using the NMR-CASTEP program, and crystal structure data. Reaction rates are highest for para bromo substitution, whose parent crystal structure was solved in this work. To explain the di?erences in photoreaction rate, several factors such as distance between double bonds, best π-orbital overlap of the reacting C=C double bonds, and CSA tensor analysis (using 2D PASS) were taken into account. Calculations of ^{13}C chemical shifts and chemical shift anisotropy tensor parameters show very good agreement with experimental data, including the carboxylic carbon that is hydrogen bonded to the neighboring cinnamic acid molecule. For the cinnamic acid photodimerization, the best angle between reacting double bonds and the smallest degree of molecular reorientation favor faster photoreaction.

6.12 pH-Specific Structural Speciation of the Ternary V(V)-Peroxido-Betaine System: A Chemical Reactivity-Structure Correlation

C. Gabriel*, E. Kioseoglou*, J. Venetis*, V. Psycharis†, C.P. Raptopoulou†, A. Terzis†, G. Voyiatzis‡, M. Bertmer C. Mateescu§, A. Salifoglu*,

*Laboratory of Inorganic Chemistry, Aristotle University of Thessaloniki, Greece
†Institute of Materials Science, NCSR Demokritos, Attiki, Greece
‡Institute of Chemical Engineering and High Temperature Chemical Processes, Patras, Greece
§Banat's University of Agricultural Sciences and Veterinary Medicine, Timisoara, Romania

Vanadium involvement in cellular processes requires deep understanding of the nature and properties of its soluble and bioavailable forms arising in aqueous speciations of binary and ternary systems. In an e?ort to understand the ternary vanadium-H_2O_2-ligand interactions relevant to that metal ions biological role, synthetic efforts were launched involving the physiological ligands betaine ($Me_3N^+CH_2CO_2^-$) and H_2O_2. In a pH-specific fashion, V_2O_5, betaine, and H_2O_2 reacted and afforded three new, unusual, and unique compounds, consistent with the molecular formulation $K_2[V_2O_2(O_2)_4(CH_3)_3NCH_2CO_2)]\cdot H_2O(1)$, $(NH_4)_2[V_2O_2(O_2)_4(CH_3)_3\text{-}NCH_2CO_2)]\cdot 0.75H_2O$

(2), and Na_2 $[V_2O_2(O_2)_4(CH_3)_3\text{-}NCH_2CO_2)_2]n{\cdot}4nH_2O$ (3). All complexes 1-3 were characterized by elemental analysis; UV/visible, FT-IR, Raman, and NMR spectroscopy in solution and the solid state; cyclic voltammetry; TGA-DTG; and X-ray crystallography. The structures of 1 and 2 reveal the presence of unusual ternary dinuclear vanadium-tetraperoxido-betaine complexes containing $[(V^{V}{=}O)(O_2)_2]$ units interacting through long V-O bonds. The two V(V) ions are bridged through the oxygen terminal of one of the peroxide groups bound to the vanadium centers. The betaine ligand binds only one of the two V(V) ions. In the case of the third complex 3, the two vanadium centers are not immediate neighbors, with Na^+ ions (a) acting as effcient oxygen anchors and through Na-O bonds holding the two vanadium ions in place and (b) providing for oxygen-containing ligand binding leading to a polymeric lattice. In 1 and 3, interesting 2D (honeycomb) and 1D (zigzag chains) topologies of potassium nine-coordinate polyhedra (1) and sodium octahedra (3), respectively, form. The collective physicochemical properties of the three ternary species 1-3 project the chemical role of the low molecular mass biosubstrate betaine in binding V(V)-diperoxido units, thereby stabilizing a dinuclear V(V)- tetraperoxido dianion. Structural comparisons of the anions in 1-3 with other known dinuclear V(V)-tetraperoxido binary anionic species provide insight into the chemical reactivity of V(V)-diperoxido systems and their potential link to cellular events such as insulin mimesis and anitumorigenicity modulated by the presence of betaine.

6.13 ph-Specific Hydrothermal Assembly of Binary and Ternary Pb(II)-(O,N-Carboxylic Acid) Metal Organic Framework Compounds: Correlation of Aqueous Solution Speciation with Variable Dimensionality Solid-State Lattice Architecture and Spectroscopic Signatures

C. Gabriel[*], M. Perikli[*], C.P. Raptopoulou[†], A. Terzis[†], V. Psycharis[†], C. Mateescu[‡], T. Jakusch[§] T. Kiss[§], M. Bertmer A. Salifoglu[*],

[*]Laboratory of Inorganic Chemistry, Aristotle University of Thessaloniki, Greece
[†]Institute of Materials Science, NCSR Demokritos, Attiki, Greece
[‡]Banat's University of Agricultural Sciences and Veterinary Medicine, Timisoara, Romania
[§]Department of Inorganic and Analytical Chemistry, University of Szeged, Hungary

Hydrothermal pH-specific reactivity in the binary/ ternary systems of Pb(II) with the carboxylic acids N-hydroxyethyl- iminodiacetic acid (Heida), 1,3-diamino-2-hydroxypropane-N,N,N′, N′-tetraacetic acid (Dpot), and 1,10-phenanthroline (Phen) a?orded the new well-de?ned crystalline compounds $[Pb(Heida)]_n{\cdot}nH_2O$ (1), $[Pb(Phen)(Heida)]{\cdot}4H_2O$ (2), and $[Pb_3(NO_3)(Dpot)]_n$ (3). All com- pounds were characterized by elemental analysis, FT-IR, solution or/ and solid-state NMR, and single-crystal X-ray di?raction. The structures in 1-2 reveal the presence of a Pb(II) center coordinated to one Heida ligand, with 1 exhibiting a two-dimensional (2D) lattice extending to a three-dimensional

(3D) one through H-bonding interactions. The con- current aqueous speciation study of the binary Pb(II)-Heida system projects species complementing the synthetic e?orts, thereby lending credence to a global structural speciation strategy in investigating binary/ternary Pb(II)-Heida/Phen systems. The involvement of Phen in 2 projects the signi?cance of nature and reactivity potential of N-aromatic chelators, disrupting the binary lattice in 1 and in?uencing the nature of the ultimately arising ternary 3D lattice. 3 is a ternary coordination polymer, where Pb(II)-Dpot coordination leads to a 2D metal-organic-framework material with unique architecture. The collective physicochemical properties of 1-3 formulate the salient features of variable dimensionality metal-organic-framework lattices in binary/ternary Pb(II)-(hydroxy- carboxylate) structures, based on which new Pb(II) materials with distinct architecture and spectroscopic signature can be rationally designed and pursued synthetically.

6.14 Paramagnetic hole centers in natural zircon and zircon colouration

M. Klinger [*], U. Kempe [*], A. Pöppl, R. Böttcher, M. Trinkler [†],

[*]Institute of Mineralogy, TU Berakademie Freiberg, Germany
[†]alpha Geoservice GbR, Bobritzsch, Germany

Paramagnetic defect centres and their relation to variable types of colouration were studied for eleven natural zircon crystals from three localities in North Carolina (USA), Massif Central (France), and Ural Mountains (Russia) using electron paramagnetic resonance (EPR) and optical absorption spectroscopy. The presence of tetragonal centres of trivalent rare-earth elements (REE^{3+}) and niobium (Nb^{4+}) irrespective of the colouration type and also in colourless grains suggests that these defects are not directly related to any specific zircon colouration. In contrast, the occurrence of two hole centres in crystals from North Carolina and the Massif Central correlates with the formation of specific broad bands in the absorption spectra. The appearance of pink colouration corresponds to the occurrence of a hole located at an oxygen nearest to Y^{3+} on zirconiumsite. This defect displays a single line at g = 2.006 in the EPR spectra for external magnetic field orientations parallel to the tetragonal crystal axis c. The related broad band in the optical absorption spectra peaks at 340-350 nm and its low-energy wing extends into the visible range. Reddish colour results from an intense broad absorption feature around 510-515 nm caused by a hole located at an oxygen next nearest to Y^{3+} substituting for Zr^{4+}. A single line at g = 2.011 related to this "red" hole centre is observed in the EPR spectra in magnetic field orientation parallel c. The nature of the two paramagnetic centres was verified by their angular dependencies. Reddish-brownish and orange colour of zircon may appear for certain intensity relations between the two absorption bands with possible additional influence from charge transfer bands caused by Tb4þ centres. Yellowish-brownish colouration of zircon from the Ural Mountains is essentially different in nature. Several other paramagnetic defects with spin S=1/2 were found in zircon from this locality besides the "red" hole centre, Tb^{4+}, and REE^{3+} defects. There is a characteristic set of four bands in the optical absorption spectra. Additional heating and irradiation experiments are necessary for a correct assignment

of paramagnetic defects to specific colour centres in this case.

6.15 Funding

EuroMagNET, JRA NMR
Prof. J. Haase
EU, RII3CT-2004-506239.

Nanocomposites, ferroelectric nanostructures
Prof. J. Haase, Prof. Dr. Cheng Tien
DAAD, 50750765.

Investigation of the mechanism of the proton conductivity in functionalized organosilicates and composite membranes by means of NMR spectroscopy and NMR diffusometry
Prof. J. Haase, Prof. Dr. Michael Wark
DFG, HA 1893/9-1.

Magnetic Ground State and Dynamics in High-Temperature Superconductors
Prof. J. Haase, Prof. O.P. Sushkov, Prof. B. Keimer
EU, DP0881336.

MOF as carrier for nitric oxide delivery in biological systems, microscopic fundamentals of adsorption and controlled release studied by infrared and electron and nuclear spin spectroscopy
Prof. A. Pöppl
DFG, PO 426/8-2.

Paramagnetic adsorption sites in microporous crystalline solids studied by electron paramagnetic resonance spectroscopy-from single crystals to oriented thin films
Prof. A. Pöppl
DFG, PO 426/11-1.

Funding for the Initiation and Enhancement of Bilateral Cooperation - Investigation of trivalent ion doping in nanocrystalline ceria by cw and pulsed EPR spectroscopy
Prof. A. Pöppl
DFG, PO 426/9-1.

Investigation of trivalent ion doping in nanocrystalline ceria by cw and pulsed EPR spectroscopy
Prof. A. Pöppl
DFG, PO 426/10-1.

Characterization of the [2+2] photodimerization of photo-active substances based on cinnamic acid incorporated in polymers and supramolecular structures with solid-state NMR
Dr. M. Bertmer
DFG BE 2434/2-3.

MOF as carrier for nitric oxide delivery in biological systems, microscopic fundamentals of adsorption and controlled release studied by infrared and electron and nuclear spin spectroscopy
Dr. M. Bertmer
DFG BE 2434/4-2.

SOM-AGING II. Hydration-dehydration mechanisms at Biogeochemical Interfaces
Dr. M. Bertmer
within SPP 1315.

Microstructure and molecular mobility in aqueous solutions of organic molecules
Prof. D. Michel, Prof. V. I. Chizhik
DFG Mi 390/23-1.

Fabrication and physical properties of ferroelectrics confined in nanoporous materials
Prof. D. Michel, Prof. E. V. Charnaya
DFG Mi 390/25-1.

6.16 Organizational Duties

J. Haase
- Dean of Faculty
- Vice Director of the Magnetic Resonance Center Leipzig (MRZ)
- Referee: Physical Review, GIF

A. Pöppl
- Referee: Journal of Magnetic Resonance, Journal of American Chemical Society, Physical Chemistry Chemical Physics, Chemical Physics Letters
- Project Reviewer: German-Israel-Foundation for Scientific Research and Development (GIF)

M. Bertmer
- Referee: Angewandte Chemie, Chemistry of Materials, Journal of Physical Chemistry, Solid State Nuclear Magnetic Resonance

D. Michel
- Referee: Physical Review, Journal of Physics: Condensed Matter, Langmuir, Journal of Magnetic Resonance, Phys. Stat. Sol., Materials Chemistry and Physics, GIF

R.-M. Böttcher
- Referee: Physical Review, Journal of Physics: Condensed Matter, Langmuir, Journal of Magnetic Resonance

6.17 External Cooperations

Academic

- Laboratoire National des Champs Magnétiques Pulsés Toulouse, France
  Prof. Dr. Geert Rikken
- University of Illinois at Urbana-Champaign, Department of Physics, USA
  Prof. Dr. Charles P. Slichter
- University of New South Wales Australia, School of Physics, Sydney, Australia
  Prof. Dr. Oleg P. Sushkov
- University of Minnesota, School of Physics and Astronomy, USA
  Prof. Dr. Martin Greven
- Victoria University, Physics Department, Wellington, New Zealand
  Dr. Grant V. M. Williams
- Dresden High Magnetic Field Laboratory, Helmholtz-Zentrum Dresden-Rossendorf, Germany
  Prof. Dr. Joachim Wosnitza
- Walther-Meissner-Institute for Low Temperature Research, Bavarian Academy of Sciences and Humanities, Munich, Germany
  Dr. Andreas Erb
- Georgetown University, Department of Chemistry, Washington DC, USA
  Prof. Dr. YuYe Tong
- Leiden University Medical Center, Leiden, Netherlands
  Prof. Dr. Andrew G. Webb
- University of Illinois at Chicago, University of Chicago, USA
  Prof. Dr. D. K. Morr
- MPI Festkörperforschung, Stuttgart, Germany
  Prof. Dr. B. Keimer
- Cavendish Laboratory, Cambridge, UK
  Dr. S. Goh, Dr. P. Alireza
- Washington University, St. Louis MO, USA
  Prof. Dr. J. Schilling, Prof. Dr. M. Conradi
- Argonne National Laboratory, Illinois, USA
  Prof. Dr. P. Littlewood
- IFW-Dresden, Germany
  Dr. M. Richter
- Washington University, St. Louis, MO, USA, Department of Chemistry
  Sophia E. Hayes
- Universität Koblenz-Landau, Koblenz, Abteiltung Chemie
  Gabriele E. Schaumann
- Martin-Luther-Universität Halle-Wittenberg, Physikalisches Institut
  Dr. H. T. Langhammer
- Universität Augsburg, Advanced Materials Science, Institut für Physik
  Prof. Dr. M. Hartmann

- NASU, Institute of Semiconductor Physics, Kiev, Ukraine
  Prof. Dr. E. N. Kalabukhovaa
- Staatliche Universität Kazan, Tartastan, Russische Förderation
  Prof. Dr. E. N. Kalabukhovaa
- Université du Maine, Faculté des Sciences, Laboratoire de Physique de l'Etat Condenseé, Le Mans, France
  Prof. Dr. A. Kassiba
- University of Vilnius, Faculty of Physics, Lithuania
  Prof. Dr. J. Banys
- Technische Universität München, Anorganisch-chemisches Institut
  Prof. Dr. K. Köhler

Industry

- NMR-Service, Erfurt
  M. Braun
- Bruker BioSpin, Rheinstetten
  F. Engelke

6.18 Publications

Journals

B. Meier, J. Kohlrautz, J. Haase:*Eigenmodes in the long-time behavior of a coupled spin system measured with nuclear magnetic resonance*, Phys. Rev. Lett.: **108**, 177602 (2012)

B. Meier, J. Kohlrautz, J. Haase, M. Braun, F. Wolff-Fabris, E. Kampert, T. Herrmannsdörfer, J. Wosnitza:*Nuclear magnetic resonance apparatus for pulsed high magnetic fields*, Rev. Sci. Instrum.:**83**, 083113 (2012)

M. Klinger, U. Kempe, A. Pöppl, R. Böttcher, M. Trinkler:*Paramagnetic hole centres in natural zircon and zircon colouration*, Eur. J. Mineral.:**24**, 1005-1016 (2012)

D. V. Savchenko, E.N. Kalabukhova, A. Pöppl, B. D. Shanina:*Electronic structure of the nitrogen donors in 6H SiC as studied by pulsed ENDOR and TRIPLE ENDOR spectroscopy*, Phys. Status Solidi.:**249**, 2167-2178 (2012)

F. Weickert, B. Meier, S. Zherlitsyn, T. Herrmannsdörfer, R. Daou, M. Nicklas, J. Haase, F. Steglich, J. Wosnitza:*Implementation of specific-heat and NMR experiments in the 1500 ms long-pulse magnet at the Hochfeld-Magnetlabor Dresden*, Meas. Sci. Technol.:**23**, 105001 (2012)

D. Rybicki, M. Greven, J. Haase, T. Meissner, S.K. Goh, G.V.M. Williams:*Two-Component Behavior of Cuprate Superconductors from NMR Shifts*, Mater. Sci. Forum.:**700**, 1-6 (2012)

O. Kozachuk, K. Khaletskaya, M. Halbherr, A. Bétard, M. Meilikhov, R. S. Seidel, B. Jee, A. Pöppl, R. A. Fischer:*Microporous Mixed-Metal Layer-Pillared [Zn1-xCux(bdc)(dabco)0.5] MOFs: Preparation and Characterization*, Eur. J. Inorg. Chem.:**49**, 1688-1695 (2012)

C. Chmelik, D. Freude, H. Bux, J. Haase:*Ethene/ethane mixture diffusion in the MOF sieve ZIF-8 studied by MAS PFG NMR diffusometry*, Microporous Mesoporous Mater.:**147**, 135-141 (2012)

G. Thörmer, N. Garnov, M. Moche, J. Haase, T. Kahn, H. Busse :*Simultaneous 3D localization of multiple MR-visible markers in fully reconstructed MR images: proof-of-concept for subsecond position tracking*, Magn. Reson. Imaging **30** 371-381 (2012)

M. Sharifi, M. Wark, D. Freude, J. Haase:*Highly proton conducting sulfonic acid functionalized mesoporous materials studied by impedance spectroscopy, MAS NMR spectroscopy and MAS PFG NMR diffusometry*, Microporous Mesoporous Mater.:**156**, 80-89 (2012)

J. Haase, D. Rybicki, C. P. Slichter, M. Greven, G. Yu, Y. Li, X. Zhao:*Two-component uniform spin susceptibility in superconducting $HgBa_2CuO_{4+\delta}$ single crystals measured using ^{63}Cu and ^{199}Hg nuclear magnetic resonance*, Microporous Mesoporous Mater.:**85**, 104517 (2012)

Jörg Lincke, Daniel Lässig, Karolin Stein, Jens Moellmer, Anusree Viswanath Kuttatheyil, Christian Reichenbach, Andreas Moeller, Reiner Staudt, Grit Kalies, Marko Bertmer, Harald Krautscheid: *A novel Zn4O-based triazolyl benzoate MOF: synthesis, crystal structure, adsorption properties and solid state 13C NMR investigations*, Dalton Trans.: **41**, 817-824 (2012).

Isa Fonseca, Maria Baias, Sophia E. Hayes, Chris J. Pickard, M. Bertmer: *Effects of Aromatic Substitution on the Photodimerization Kinetics of beta-trans Cinnamic Acid Derivatives Studied with 13C Solid-State NMR*, J. Phys. Chem. C: **116**, 12212-12218 (2012).

C. Gabriel, E. Kioseoglou, J. Venetis, V. Psycharis, C. P. Raptopoulou, A. Terzis, G. Voyiatzis, M. Bertmer, C. Mateescu, A. Salifoglu: *pH-Specific Structural Speciation of the Ternary V(V)-Peroxido-Betaine System: A Chemical Reactivity-Structure Correlation*, Inorg. Chem.: **51**, 6056-6069 (2012).

C. Gabriel, M. Perikli, C. P. Raptopoulou, A. Terzis, V. Psycharis, C. Mateescu, T. Jakusch, T. Kiss, M. Bertmer, A. Salifoglu: *pH-Specific Hydrothermal Assembly of Binary and Ternary Pb(II)-(O,N-Carboxylic Acid) Metal Organic Framework Compounds: Correlation of Aqueous Solution Speciation with Variable Dimensionality Solid-State Lattice Architecture and Spectroscopic Signatures*, Inorg. Chem.: **51**, 9282-9296 (2012).

Farhana Gul-E-Noor, Bettina Jee, Matthias Mendt, Dieter Himsl, A. Pöppl, Martin Hartmann, Jürgen Haase, Harald Krautscheid, Marko Bertmer: *Formation of Mixed Metal Cu3-xZnx(btc)2 Frameworks with Different Zinc Contents: Incorporation of Zn2+ into the MOF Structure as Studied by Solid-State NMR*, J. Phys. Chem. C: **116**, 20866-20873 (2012).

Talks

T. Meissner, S.K. Goh, J. Haase, G.V.M. Williams: *High Pressure Changes of the ^{17}O NMR Spin Shift Pseudo-Gap of $YBa_2Cu_4O_8$*, 25.03.-30.03.2012 DPG Spring Meeting, Berlin

B. Meier: *NMR in pulsed high magnetic fields*, Seminar, Freiburg Institute for Advanced Studies (FRIAS), 22.03.2012 Freiburg

B. Meier, J. Kohlrautz, J. Haase: *Eigenmodes in the long-time behavior of a coupled spin system measured with NMR*, 25.03.-30.03.2012 DPG Spring Meeting, Berlin

A. Pöppl: *Pulsed EPR spectroscopy of paramagnetic adsorption complexes in porous materials 15th Workshop of the International Research Training Group "Diffusion in Porous Materials"*, 02.04.-04.04.2012, Leipzig

J. Haase: *Inhomogeneities in the Cuprate Superconductors from NMR Phase Separation and super stripes in high temperature superconductors and related materials*, SUPERSTRIPES, 11.07-17.07.2012, Erice, Italy

J. Haase: *High-Sensitivity Giga-Pascal NMR*, 54th Rocky Mountain Conference on Analytical Chemistry, 15.07-19.07.2012, Copper Mountain, USA

J. Haase: *Elektronisches Leben in Festkörpern - Leipziger Einblicke und Ansichten*, Plenarsitzung der Sächsischen Akademie der Wissenschaften, 09.03.2012, Leipzig

J. Haase: *Extreme NMR - Strukturaufklärung mit Magnetischer Kernresonanz unter höchsten Drücken und magnetischen Feldern*, GDCH-Kolloquium, TU Bergakademie Freiberg, 02.05.2012, Freiberg

N. Georgieva: *Properties of topological insulators, First look with nuclear magnetic resonance*, 5th BuildMoNa Workshop for Doctoral Candidates, 24.09-25.09.2012, Burgstädt

M. Mendt, F. Debatin, F. Gul-E-Noor, M. Bertmer, M. Hartmann, M. Fröba, H.-J. Holdt, A. Pöppl: *Electron paramagnetic resonance spectroscopy introduced as a method to investigate the adsorption sites of nitric oxide in metal-organic frameworks*, GDCH-Tagung 18.09.-22.09.2012, Halle

S. Reichardt: *Towards NMR shift measurements in pulsed magnetic fields*, EuroMagNET Summer School, 30.09-07.10.2012, Rügen

K. Peikert, M. Mendt: *MOFs as carrier for nitric oxide delivery in biological systems*, MOF Status Report Meeting, 28.11.2012, Dresden

M. Bertmer: *Structure of MOFs and Adsorption of Small Molecules studied by Solid-State NMR*, Max-Planck-Institut für Polymerforschung, 08.02.2012, Mainz

M. Bertmer, A. Jäger: *One and Two Dimensional Solid State NMR Techniques Applied to Study the Structure and Rigidity of Soil Organic Matter (SOM)*, 4th International Congress EUROSOIL 2012, 02.07.-06.07.2012, Bari, Italy

Posters

B. Meier, J. Kohlrautz, J. Haase, F. Wolff-Fabris, T. Herrmannsdörfer, J. Wosnitza: *NMR spectroscopy in pulsed high magnetic fields*, DPG Spring Meeting, 25.03.-30.03.2012, Berlin

B. Meier: *NMR Signal Averaging in 62 Tesla Pulsed Fields*, Gordon Research Conference, 12.06.-17.06.2012, Biddeford, USA

M. Bertmer: *How water dynamics affect soil organic matter (SOM) - a combined 1H solid state NMR and DSC study*, 4th International Congress EUROSOIL 2012, 02.07.-06.07.2012, Bari, Italy

S. Friedländer, R. Böttcher, M. Lorenz, H. Hochmuth, M. Grundmann, O. Ovchar, A. Belous, A. Pöppl: *EPR spectroscopy of semiconducting ZnO films and porous HKUST-1 thin layers*, DFG Priority Program SPP 1601 Meeting - GDCh FGMR 34th Annual Discussion Meeting, 17.09.-20.9.2012, Halle (Saale)

6.19 Graduations

Doctorate

- Dimo Ivanov
  Functional mapping of hemodynamic parameters and oxygen utilization in human brain using magnetic resonance imaging techniques at 7 Tesla
  17.09.2012
- Benno Meier
  Nuclear Magnetic Resonance in pulsed high magnetic fields
  19.11.2012
- Ingo Hilschenz
  Design of a Low Field Magnetic Resonance Imaging Measurement System working below one Kilohertz
  19.11.2012

Master

- Thomas Meier
  Giga-Pascal NMR in Solids
  21.02.2012
- Steven Reichardt
  NMR-Double Resonance in a High Temperature Superconductor
  15.06.2012
- Emmanouil Veroutis
  ^{63}Cu and ^{17}O Nuclear Magnetic Resonance studies of the electron doped high-Tc superconductor $Pr_{1.8}Ce_{0.2}CuO_4$
  19.11.2012

Bachelor

- Robin Gühne
  ^{17}O-NMR an Pr_2CuO_4 Einkristallen
  12.03.2012

6.20 Guests

- Dr. Sergei A. Dontsov
  St. Petersburg State University, Institute of Physics, Petrodvorets, Russia
  10.01.-10.02.2012
- Mikhail Andreevich Vovk
  St. Petersburg State University, Institute of Physics, Petrodvorets, Russia
  10.01.-10.02.2012
- Prof. Dr. Hiroshi Yasuoka
  Japan Atomic Energy Agency, Advanced Science Research Center, Research Group for Spin Manipulation and Material Design by Combining Spintronics and High-Speed Rotation Technique, Japan
  14.03.-15.03.2012
- Prof. Dr. Lieh-Jeng Chang
  National Cheng Kung University, NSC Instrument Center, Tainan, Taiwan
  28.03.-31.03.2012
- Prof. Dr. Wojciech Grochala
  Warsaw University, Department of Chemistry, Warsaw, Poland
  23.04.-25.04.2012
- Dmitry Yurievich Podorozhkin
  St. Petersburg State University, Institute of Physics, St. Petersburg, Russia
  16.04.-09.05.2012
- Denis Yurievich Nefedov
  St. Petersburg State University, Institute of Physics, St. Petersburg, Russia
  16.04.-15.05.2012
- Prof. Dr. Elena Charnaya
  St. Petersburg State University, Institute of Physics, St. Petersburg, Russia
  11.05.-24.05.2012
- G.V.M Williams, PhD
  Viktoria University of Wellington, School of Chemical and Physical Sciences, Wellington, New Zealand
  15.08.-18.09.2009
- Dr. Min Kai Lee
  National Cheng Kung University, NSC Instrument Center, Tainan, Taiwan
  24.10.-09.11.2012

7

Nuclear Solid State Physics

7.1 Introduction

The division of Nuclear Solid State Physics continued research in material and life sciences with the high-energy ion-nanoprobe LIPSION being the working horse.
An important branch is ion beam analysis of solid objects, e.g. semiconductors or meteorites, as well as a broad range of biomedical samples from tissue sections down to single cells using Particle Induced X-Ray Emission (PIXE) and Rutherford Backscattering Spectrometry (RBS) with lateral resolutions down to about 300 nm, and Scanning Transmission Ion Microscopy (STIM) with lateral resolutions down to 100 nm. Technical improvements to enhance the analytical capabilities include new 300 mm^2 and 50 mm^2 RBS detector setups with in-vacuum pre-amplifiers that achieve outstanding energy resolutions of 10.6 keV and 5.1 keV, respectively, for 2.29 MeV protons as well as a system for measuring the dead-time of the detector electronics on a pixel by pixel basis allowing quantitative elemental imaging in laterally strongly inhomogeneous samples like meteorites. In addition, a compact, fully digital data acquisition system is currently under development in close collaboration with the University of North Texas that will significantly increase the flexibility and rate of data processing which helps to reduce analysis time.
The second important branch of research is materials modification, e.g. for the study of defect-related phenomena in solid state physics like defect-induced magnetism (DIM) and Proton Beam Writing (PBW) and Sculpting. With protons, H_2^+, and He-ions 3D-structures in a variety of photoresists and semiconductors can be created – even arbitrary height profiles are possible as could be demonstrated with greyscale PBW on p-type GaAs.
The financial support of our research by the Deutsche Forschungsgemeinschaft and the Federal German Excellence Initiative and the cooperation with academic and industrial partners is gratefully acknowledged.
As already done in 2011, we opened the doors of the LIPSION laboratory to the public on the 3rd of Octobre, 2012 – an event called "MausTag" initiated by the Westdeutscher Rundfunk (WDR). In total 105 "MausFans" (62 children and 43 adults) took the opportunity to visit the lab and do simple experiments on elastic collisions, electrostatics, deflection of charged particles in magnetic fields as well as tomography – a representation of some of the fundamental processes and techniques that are used in the daily work of the lab.

Since January 2013, Prof. Jan Meijer is leading the Nuclear Solid State Physics group. I would like to take this opportunity to express my sincere gratitude to all present and former group members for their dedicated work in the past years which helped to make it a well-respected group in the ion beam community worldwide and to wish Jan all the best and the group a prospering future.

Daniel Spemann

7.2 An outstanding contribution of Leipzig physicists to the German uranium project between 1940 and 1942 – A historical study

D. Lehmann

In 2012 was the 70th anniversary of the first experimental proof of the neutron multiplication in a subcritical, heterogeneous uranium moderator arrangement.

At the end of 1939 Werner Heisenberg (at that time the Director of the Institute for Theoretical Physics at Leipzig University) sketched in a report of 25 type-written pages on behalf of "Heereswaffenamt" the possibilities of the technical energy gain with uranium fission [1]. The best results he hoped to achieve with a layered structure of moderator and uranium. Heavy water seemed to him the optimum material for the neutron moderation, but the permanent stringency of D_2O and at the beginning also of uranium forced Heisenberg to replace the one-dimensional lattice structure by spherical shells like an onion.

Since 1940 there was a fruitful cooperation at Leipzig University between Heisenberg and the experimental nuclear physicist Robert Döpel, who designed ingenious devices realizing the ideas of Heisenberg. In May of 1942 Döpel was for the first time successful in observing the unambiguous experimental result of neutron multiplication due to uranium fission in such a spherical shells device [2]. His apparatus (with the notation L4) consisted of four shells filled with in total 3/4 metric tons of metallic uranium powder and only 140 kg of heavy water in spherical chamber shells made from technical pure Al metal (together 30 kg).

The quantity of interest was the so called neutron production coefficient ν_{eff}, the German pendant of Fermi's k_∞. The evaluation of the measurements gave a value of $+208\,\text{s}^{-1}$. By omission of the Al shells (which was outside of each reality) a 100% increase in ν_{eff} seemed to be possible. Later experiments were therefore planned only with layers made from uranium metal cast, thus without Al.

Without an exact calculation Heisenberg and Döpel gave an estimate of the critical mass of such a device (so called "Uranmaschine") with a minimum of 10 metric tons of uranium and 5 tons of heavy water. An evaluation with todays more precise nuclear parameters is in preparation.

On June 23, 1942, at the beginning of the planned dismantling of the apparatus L4 the pyrophoric behaviour of the uranium powder initiated an ignition of the uranium content with bursts of sparkling uranium dust as a result of the sudden contact with air within the outer shell. Three hours after the beginning, a strong explosion took place with bursts of flames. The Fire Police was called but the fire continued for further 42

hours. As a consequence, the whole apparatus was destroyed [3]. This was probably the first serious incident in the history of mankind's development of nuclear power around the world. Today the L4 event could be assessed with step "3" at maximum according to the International Nuclear Event Scale (INES) of the International Atomic Energy Agency (IAEA) [4].

After the accident Döpel had reduced his activities within the German uranium project.

[1] W. Heisenberg, Die Möglichkeit der technischen Energiegewinnung aus der Uranspaltung (vom 06.12.1939), In: "Werner Heisenberg, Gesammelte Werke" (Hg. W. Blum, H.-P. Dürr, H. Rechenberg), Serie AII, Springer-V. Berlin / Heidelberg / New York (1989) 378–96.
[2] R. Döpel, K. Döpel, and W. Heisenberg, Der experimentelle Nachweis der effektiven Neutronenvermehrung in einem Kugel-Schichten-System aus D_2O und Uran-Metall, In: "Werner Heisenberg, Gesammelte Werke" (Hg. W. Blum, H.-P. Dürr, H. Rechenberg), Serie AII, Springer-V. Berlin / Heidelberg / New York (1989) 536–43.
[3] R. Döpel, Bericht über zwei Unfälle beim Umgang mit Uranmetall, In: "Werner Heisenberg in Leipzig 1927 - 1942" (Hg. Ch. Kleint, G. Wiemers), Abh. Sächs. Akad. Wiss. z. Leipzig, Math.-Nat. Klasse, Berlin **58** (1993), 2, S.62–67.
[4] INES. The International Nuclear and Radiological Event Scale. User's Manual, 2008 Edition (Revised), IAEA, Vienna, 2012.

7.3 Optimizing the Rutherford Backscattering Spectrometry setup in a nuclear microprobe

N. Klingner, J. Vogt, D. Spemann

Rutherford Backscattering Spectrometry (RBS) as one of the standard techniques of ion beam analysis for non-destructive quantification of film thicknesses and elemental concentrations, in general requires a good mass separation and energy resolution. In nuclear microprobes large solid angles of detection of ~ 100 msr are necessary to compensate for the comparably low beam current. However, under these conditions geometrical straggling effects cannot be neglected anymore. Therefore, in order to optimize the RBS detection setup, the geometrical straggling was calculated for circular detectors and the noise contributions to the signal generation and amplification analyzed. The analysis shows that an annular RBS detector should be used directly connected to a dedicated in-vacuum preamplifier (Fig. 7.1). In this way, as is demonstrated in this study with preamplifiers based on an Amptek A250 in a very compact, reliable and low-cost package, excellent energy resolutions of (10.6±0.2) keV FWHM can be achieved in 2.29 MeV proton RBS for a 300 mm^2 Canberra PIPS detector mounted under 86 msr solid angle (Fig. 7.2). For smaller detectors even better energy resolutions are obtained, i.e. (5.1±0.2) keV for a 50 mm^2 Canberra PIPS and (5.8±0.2) keV for a Hamamatsu S1223-01 PIN-photodiode detector for 2.29 MeV proton RBS and Scanning Transmission Ion Microscopy, respectively.

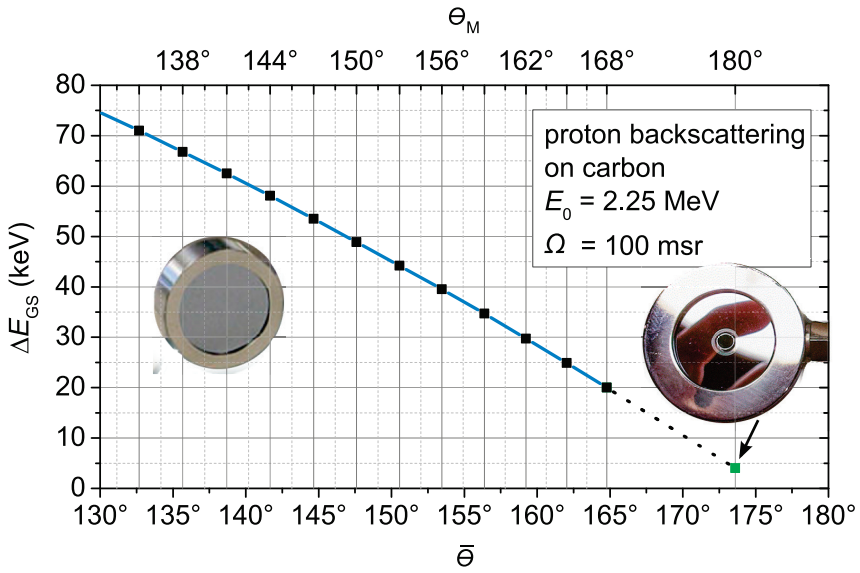

Figure 7.1: Width ΔE_{GS} of energy broadening for different detector positions where θ_M denotes the backscattering angle of the center of the detector. In contrast, $\overline{\theta}$ is the angle averaged by the ion yield. The black squares reflect calculations for standard circular detectors, whereas the green square at $\theta_M = 180°$ is the case of the annular detector. The gap in between is the region where a 100 msr detector cuts off the incoming ion beam (dashed line).

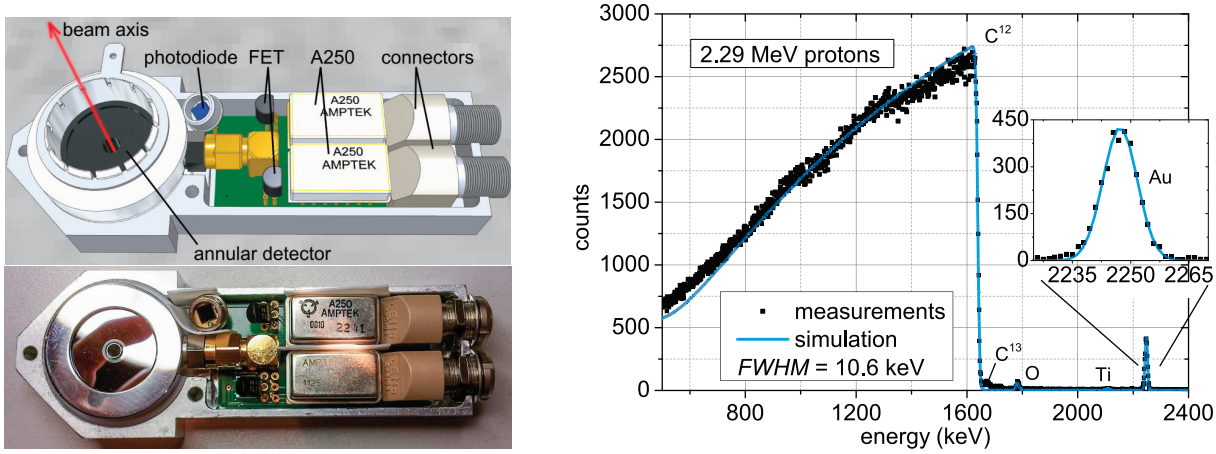

Figure 7.2: Left: 3D-CAD model and photography of the open casing of the constructed detector system for the LIPSION nanoprobe using a 300 mm^2 annular PIPS detector and a Hamamatsu S1223-01 PIN-photodiode. In the CAD model a metallic ring is visible in front of the detector. This ring (not mounted on the photography) can be biased for suppressing secondary electron emission, thereby allowing an accurate charge integration on the sample.
Right: Spectrum of 2.29 MeV protons backscattered on a 2.5 nm gold layer on top of glassy carbon detected by the new annular detector system with an energy resolution of (10.6±0.2) keV.

7.4 Development of a laterally resolved dead-time correction for quantitative elemental mapping of extraterrestrial material at LIPSION

R. Wunderlich, N. Klingner, J. Vogt, D. Spemann

A simple system for laterally resolved dead-time correction was developed at the Leipzig ion nanoprobe LIPSION in order to investigate diverse meteorite samples. The meteorite building crystals can often be found in close proximity to massive iron-nickel grains which provides a challenge for ion beam analysis methods, like Particle Induced X-ray Emission (PIXE) or Rutherford Backscattering Spectrometry (RBS) due to the strongly varying dead-time of the detector electronics on such inhomogeneous samples. This leads to incorrect concentration mapping on a local scale. In order to account for this problem, a noise-triggered setup was developed that generates defined pulses statistically in time which are fed into the preamplifiers of the detector electronics and act as pseudo events in the data processing (Fig. 7.3).

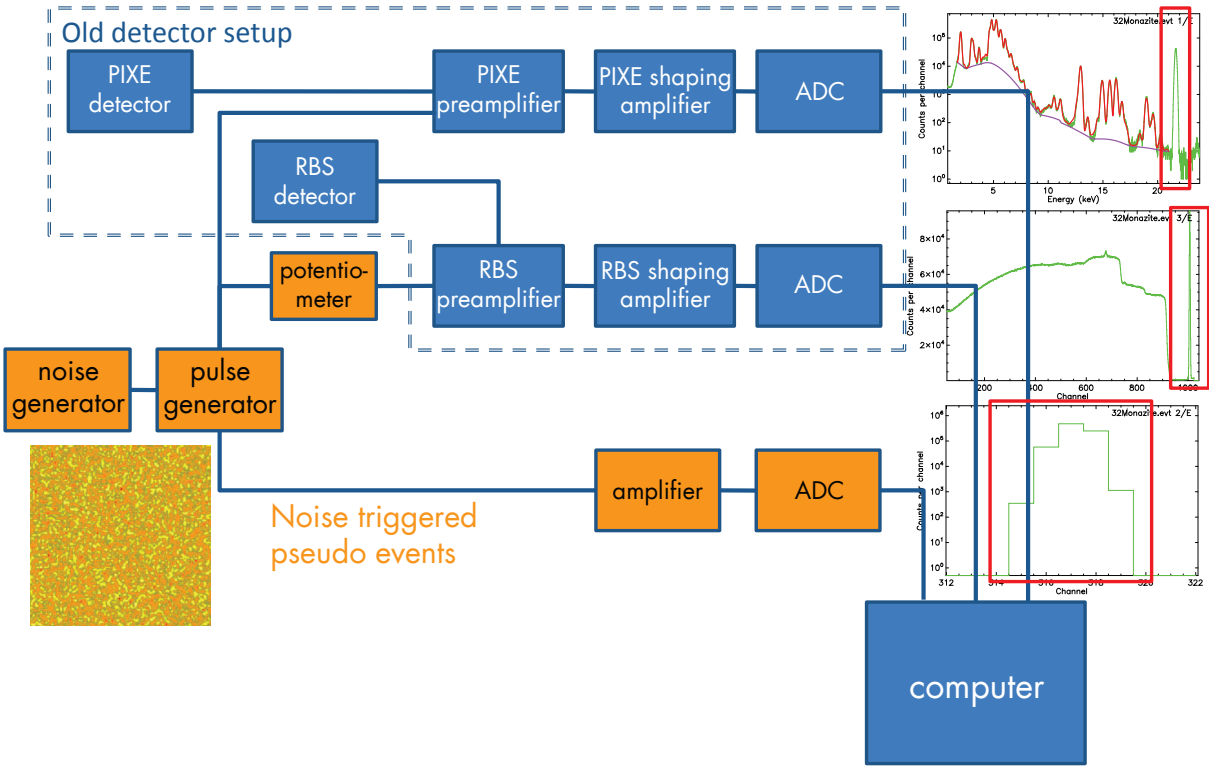

Figure 7.3: Modified detector setup for lateral dead-time mapping functionality. For each pixel the number of generated and processed pseudo events is recorded. The red boxes mark the peaks of the pseudo events produced by the processed pulses in each spectrum. The map in the lower left shows that the noise-triggering of the pulse generator leads to an uniform pseudo event map.

A comparison of the number of generated and processed pulses allows the computation of a dead-time map and thereby a correction of the collected spectrum on a pixel per

pixel basis. The proper function of this technique was verified by measurements on a simple test specimen and a chondrule of the Acfer 094 meteorite (Fig. 7.4).

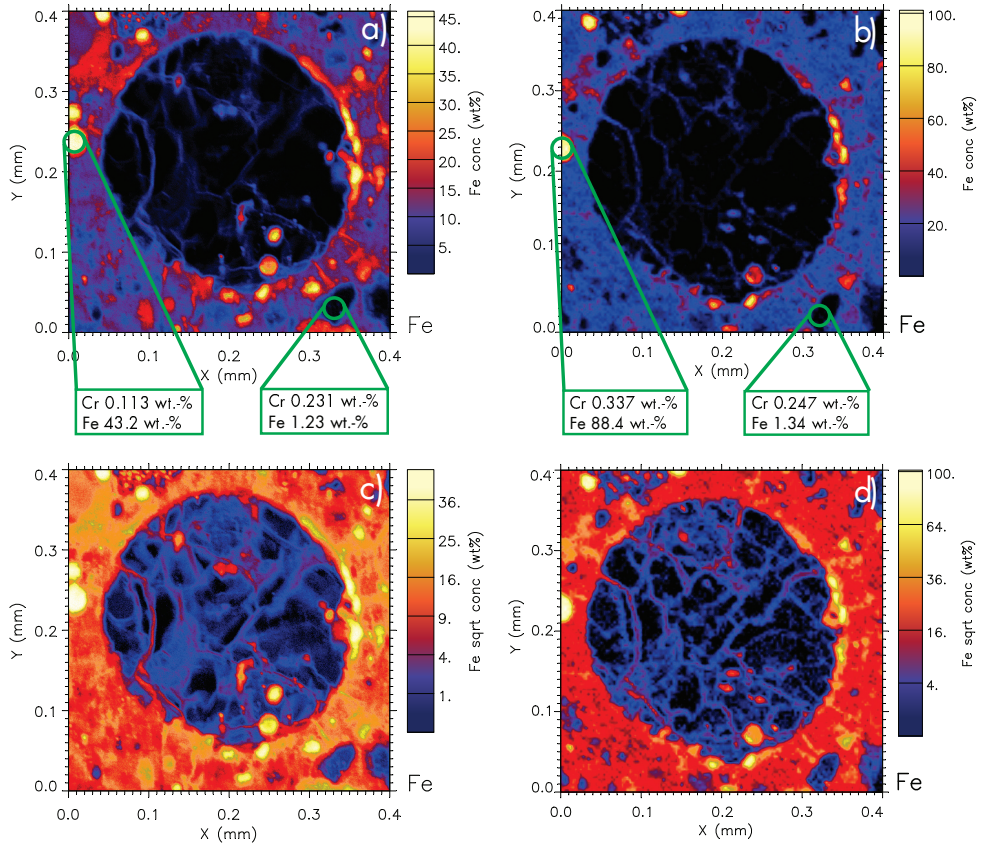

Figure 7.4: Iron map of a chondrule of Acfer 094: (a and c) uncorrected elemental concentrations in a linear and square root false color scale, respectively; (b and d) dead-time corrected elemental concentrations in a linear and square root false color scale, respectively.

7.5 Scalable multi-detector digital spectrometer and data acquisition system for a nuclear microprobe

M. Jäger*, T. Reinert†, J. Vogt, M. Bogdan*

*Fakultät für Mathematik und Informatik, Universität Leipzig
†Ion Beam Modification and Analysis Laboratory, Dept. of Physics, University of North Texas, Denton, Texas, USA

A reasonable evolution of ion beam analytical spectrometers and data acquisition systems is the combination of detector pulse height/timing analysis and data acquisition with beam control in a compact digital system. The advantage lies in the replacement of slower and in sum costlier analog electronics by signal digitizers and flexible and optimized digital pulse processors (DPP), which leads to higher performances in energy resolution and pulse rate capability. The new system is based on the ADQ412

four-channel, 12 bit, 1 GHz sampling frequency digitizer module with an on-board Xilinx Virtex 6 LX240T FPGA (Field Programmable Gate Array) for signal handling and pulse processing, and the X3-25M module with an on-board Xilinx Spartan 3A DSP FPGA serving two analogue output channels via 50 Mega-samples per second, 16-bit D/A converters and additional digital inputs/outputs for ion beam scanning and data acquisition control. The host for the modules is the PXI-1062Q chassis that is connected to a control PC. Since an ion beam analysis set-up for PIXE, RBS, STIM, PIGE, SE, etc. uses several different detector types, the digital filters for the pulse processing should be chosen and optimized individually for the different signal shapes to achieve the digital filter response (DFR), i.e. the pulse shaping with best performance. The implementation of an infinite impulse response (IIR) filter provides the means to realize the optimum DFR for any given input signal and achieves a high flexibility to adapt the DPP to different detector characteristics. The spectrometer system is designed to handle multiple ADQ412 modules, each of which being able to process four detector signals.

7.6 Greyscale Proton Beam writing in p-type GaAs

D. Diering, D. Spemann, J. Lenzner*, T. Böntgen*, St. Müller*, H. von Wenckstern*

*Halbleiterphysik, Institut für Experimentelle Physik II, Universität Leipzig

Proton Beam Writing (PBW) is a well known direct-write technique for micromachining, e.g. of semiconductors. Up to now, only few indication is given on how the resulting structure height in micromachined semiconductors can be controlled by means of fluence variation [1–3]. Fluence variation is a fast method and realized mainly by changing the integrated dwell time of the ion beam on a specific area of the substrate. This approach, called Greyscale PBW, for 3D-microstructuring was successfully demonstrated for negative photoresists [4].

In this study, (100) p-type Gallium Arsenide (GaAs) was irradiated with 2.28 MeV protons and fluences in the range from 1.5×10^{14} H^+/cm^2 to 2.4×10^{17} H^+/cm^2 at the ion beam laboratory LIPSION and subsequently electrochemically etched with 10%-KOH. On a series of irradiated square patterns of 30 $\mu m \times 30$ μm size the dependency of structure height on ion fluence could be established (Fig. 7.5). As can be seen, the resulting structure height increases linearly with fluence up to 1.7×10^{15} H^+/cm^2 where the full structure height is reached. Making use of this behaviour, pyramid-like structures as well as concave-shaped structures could be created. Furthermore, self-supporting structures were produced by undercutting.

GaAs showed a lateral anisotropic etch behaviour during the development step, depending on the substrate orientation. Atomic force microscopy measurements yielded a increased surface roughness after etching for areas which were exposed to higher fluences. Scanning electron microscopy (SEM) and scanning capacitance microscopy (SCM) measurements approved a local fluence-dependent modification of the conductivity of the irradiated material (Fig. 7.6).

[1] M.B.H. Breese, F.J.T. Champeaux, E.J. Teo, A.A. Bettiol, D.J. Blackwood, Phys. Rev. B **73** 035428 (2006).

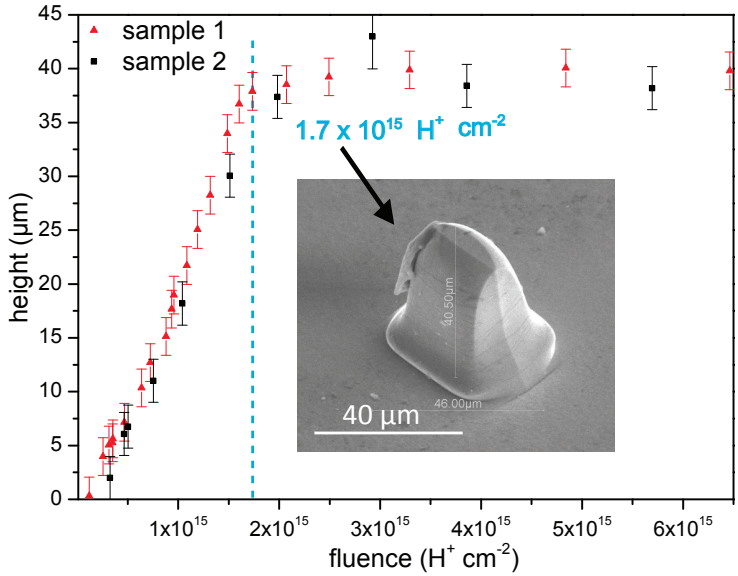

Figure 7.5: Feature height-fluence dependency for two different irradiation series (sample 1, red; sample 2, black) after irradiation with 2.28 MeV H^+ and electrochemical anodisation.

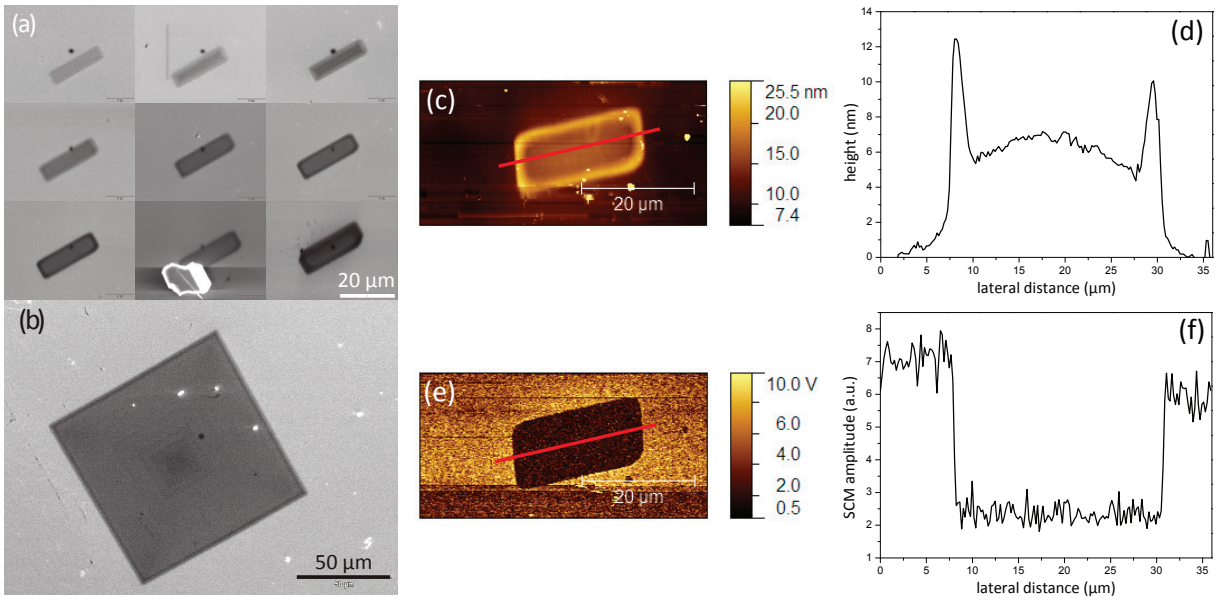

Figure 7.6: Results from SEM and SCM measurements: **(a, b)** SEM images of irradiated p-type GaAs – **(a)** Rectangles 20 µm × 5 µm with increasing fluences from ~ 2.5×10^{15} H^+ cm^{-2} to 1.0×10^{18} H^+ cm^{-2} (top left to bottom right); **(b)** Pyramid pattern with increasing fluence towards the centre. **(c–f)** SCM images and profiles of the rectangle irradiated with 1.0×10^{18} H^+ cm^{-2} – **(c)** topography, **(d)** topographic profile, **(e)** capacitance amplitude, **(f)** capacitance amplitude profile. The profiles were obtained along the red lines.

[2] E.J. Teo, E.P. Tavernier, M.B.H. Breese, A.A. Bettiol, F. Watt, M.H. Liu, D.J. Blackwood, Nucl. Instr. and Meth. B **222**, 513 (2004).
[3] M. Schulte-Borchers, U. Vetter, T. Koppe, H. Hofsäss, J. Micromech. and Microeng. **22**, 025011 (2012).
[4] F. Menzel, D. Spemann, T. Koal, T. Butz, Nucl. Instr. and Meth. B **269**, 2427 (2011).

7.7 About the coupling of magnetic and structural properties in Ni-Mn-Ga ferromagnetic shape memory thin films

A.M. Jakob[*] [†], M. Hennes[†], M. Müller[†], D. Spemann, S.G. Mayr[*] [†] [‡]

[*]Translationszentrum für Regenerative Medizin Leipzig, Universität Leipzig
[†]Leibnitz-Institut für Oberflächenmodifizierung e.V., Leipzig
[‡]Fakultät für Physik und Geowissenschaften, Universität Leipzig

Yielding the ability of large strains up to 10% at moderate external magnetic fields below 1 T, martensite Ni-Mn-Ga has become an attractive material for industrial applications [1–3]. Especially thin films of this ferromagnetic shape memory alloy (FSMA) yield promising future applicability in miniaturized sensor- and actuator systems and are focus of recent scientific research since mechanical and magnetic properties at the micro- and nanoscale differ from their bulk counterparts. We investigated the appearance and evolution of micro-magnetic domain structure by means of temperature dependent Magnetic Force Microscopy (MFM) [4]. Experiments are compared to three-dimensional numerical simulations as exemplarily shown in 7.7. Influences arising

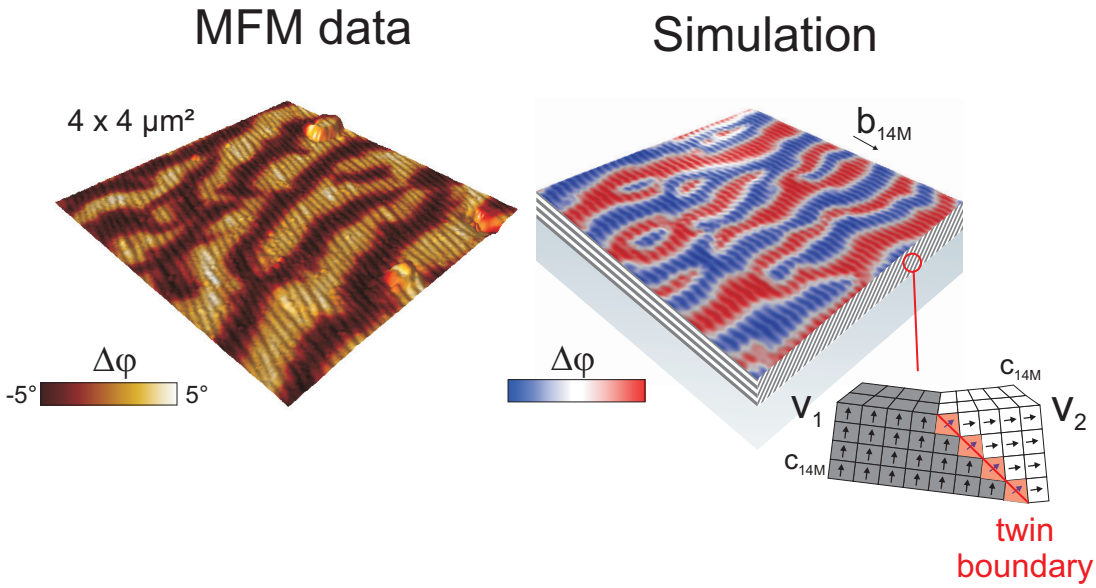

Figure 7.7: Left: Experimentally obtained AFM/MFM micrograph (3D view: height, color map overlay: magnetic information) of a nano-twinned 14M martensite Ni-Mn-Ga thin film. Right: Three-dimensional numerical micro-magnetic simulation considering known structural characteristics as well as material specific magneto-crystalline anisotropy, saturation magnetization and exchange interaction.

from film thickness and variant twinning are predicted correctly by the computational approach. Thermal stresses are identified to cause a deviation from the cubic magneto-crystalline anisotropy, usually occurring in the parental austenite phase. The corresponding stress induced anisotropy constant K_{stress} was estimated by introducing an analytical model of partial flux closuring. A shallow potential energy landscape

coming along with K_{stress} can explain the presence of a temperature hysteresis between two metastable domain configurations

[1] V.V. Kokorin and V.A. Chernenko, Fiz. Met. Metalloved **6**, 1157 (1989).
[2] V.A. Chernenko, E. Cesari, V.V. Kokorin, I.N. Vitenko, Scripta Metallurgica et Materialia **33**, 1239 (1995).
[3] K. Ullakko, Journal of Materials Engineering and Performance **5**, 405 (1996).
[4] A.M. Jakob, M. Hennes, M. Müller, D. Spemann, S.G. Mayr, Adv. Funct. Mat., DOI: adfm.201300165 (2013).

7.8 Investigation of intracellular multilayer decomposition of Layer-by-Layer self-assembled particles by means of ion beam analysis

O. Naumov[*] [†], St. Jankuhn, U. Reibetanz[*]

[*]Institut für Medizinische Physik und Biophysik, Universität Leipzig
[†]Nukleare Festkörperphysik, Institut für Experimentelle Physik II, Universität Leipzig

Layer-by-Layer (LbL) coated microcarriers represent a novel group of drug delivery systems which is gaining greater recognition in medical applications. The modular design of the polymer multilayer provides a multifunctional transport system: The step-by-step assembly of oppositely charged biocompatible and biodegradable polyelectrolytes on a dissolvable core allows the fabrication of polyelectrolyte multilayer capsules and simultaneous integration of active substances. Due to surface modifications the particle- or capsule-based delivery systems permit a local, target-oriented transport and time-controlled release of active agents, e.g. cancer therapeutics or anti-inflammatory substances, into certain cells or tissues. The possibility to adjust the amount of transported active agents allows to minimize side-effects of therapeutics [1].

The understanding of uptake and processing of the carriers in cells and organs play a major role concerning the development of new drug delivery systems. Hence, in the first part of this project the design of a microcarrier system for visualization of cytoplasmic processing is focused using nanoparticles as reporters. Finally, uptake, delayed release of the reporters, and their intracellular distribution within the cell will be investigated providing information about the effective transport of active agents.

Spherical cores ($CaCO_3$) were coated with protamine/dextrane sulfate (PRM/DXS) basis multilayer and Fe_3O_4-magnetite nanoparticles (MNPs). MNPs were successfully integrated into the multilayers in different layer depths and layer numbers to demonstrate the variety of transportation of active agents. Via ion beam analysis (PIXE, RBS) the increase of MNP concentration in dependence of coating parameters was measured (Fig. 7.8). After co-incubation with Vero cells for 24 h, 48 h, and 72 h microcarriers were detected by means of confocal laser scanning microscopy (CLSM) (Fig. 7.9). The direct localization of the carriers within the cytoplasm is supported by staining of cell compartments or core of the microcarrier. Here, the use of a highly effective staining for lysosomes enables the detection of microcarriers in endolysosomes [2]. In comparison,

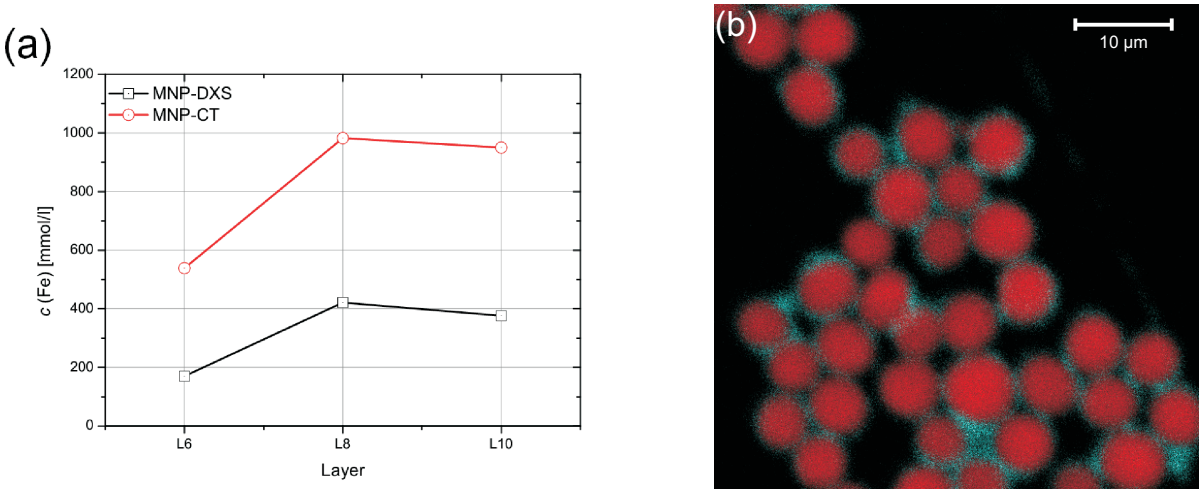

Figure 7.8: Preparation and PIXE analysis of LbL-coated $CaCO_3$ cores (size (5±1) µm). (a) After coating of five layers PRM/DXS magnetite nanoparticles were integrated in layers 6 and 8. An increase of MNP layers leads to increasing Fe-concentrations. Further coating with PRM/DXS shows relative stability of LbL-coated microcarriers. (b) Map of overlayed elemental distributions of Ca (core, red) and Fe (MNP, blue) of LbL-coated microcarriers.

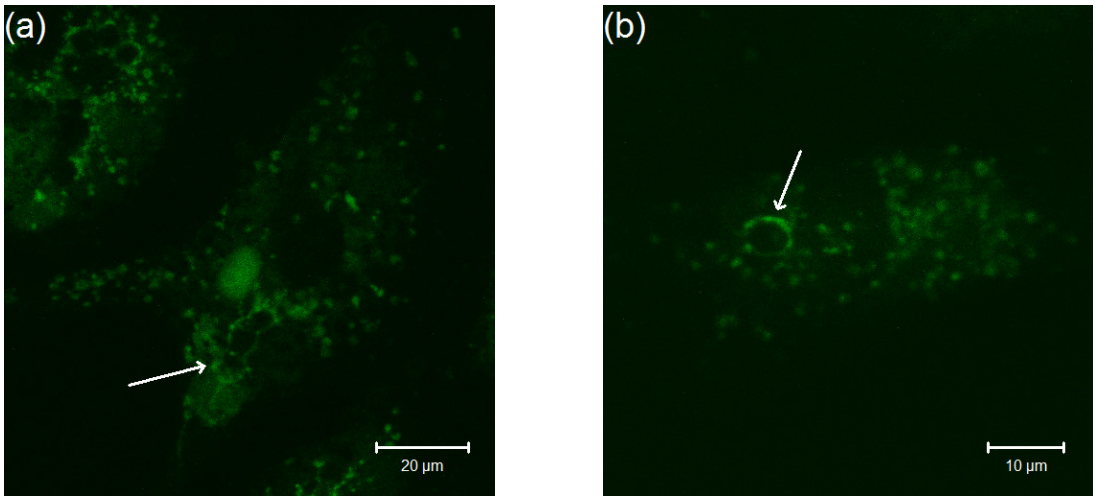

Figure 7.9: CLSM images of spherical microcarriers after 48 h co-incubation with Vero cells. Staining with Lysotracker-FITC visualizes microcarriers in endolysosomes (arrows).

the decomposition of the multilayers in cytoplasm will be then visualized via ion beam analysis (PIXE, RBS) to show the advantage of multi-layered transport of active agents over single application [3].

[1] L.J. De Cock et al., Angew. Chem. Int. Edit. **49**, 6954 (2010), doi:10.1002/anie.200906266
[2] S. Rathmann et al., Cytometry Part A **79A**, 979 (2011), doi:10.1002/cyto.a.21145
[3] U. Reibetanz et al., Nucl. Instrum. Meth. Phys. Res. B **269**, 2281 (2011), doi:10.1016/j.nimb.2011.02.064

7.9 Quantification of NP uptake and distribution in culture cells and animal tissues

I. Estrela-Lopis*, M. Dorn*, L. Cuellar*, D. Spemann, J. Vogt, E. Donath*

*Institut für Medizinische Physik und Biophysik, Universität Leipzig

In the last decade research in nanotechnology lead to numerous new applications in medicine, engineering and even in private households. Therefore the investigation of potential health impacts and risk assessment is crucial to establish new policies and laws. Uptake, distribution and localisation of nanoparticles in human culture cells and animal tissue are key points for estimating the toxic potential of nanoparticles (NPs). Especially the quantification of toxic doses in cells and tissues is important with regard to regulatory issues of nanomaterials. Establishing the relations between exposure-dose and dose-response *in-vitro* and *in-vivo* are the prerequisite for the validation of *in-vitro* tests concerning their relevance for *in-vivo* tests. Ion Beam Microscopy (IBM) was employed to measure uptake and distribution of metal oxide nanoparticles in culture cells and tissues from exposed animals. The uptake of CeO_2, ZnO, TiO_2 und FeO_2 NPs was visualized and quantified in single lung cells (A549) and mouse lung tissues (Fig. 7.10 A) by means of Particle Induced X-ray Emission (PIXE). The nanoparticle distribution has been quantified in their natural environment down to the resolution of single alveoli. Complementary toxicological investigations allowed for the first time, to constitute a correlation between exposure dose, intracellular concentration and toxic effect of nanomaterials (Fig. 7.10 B).

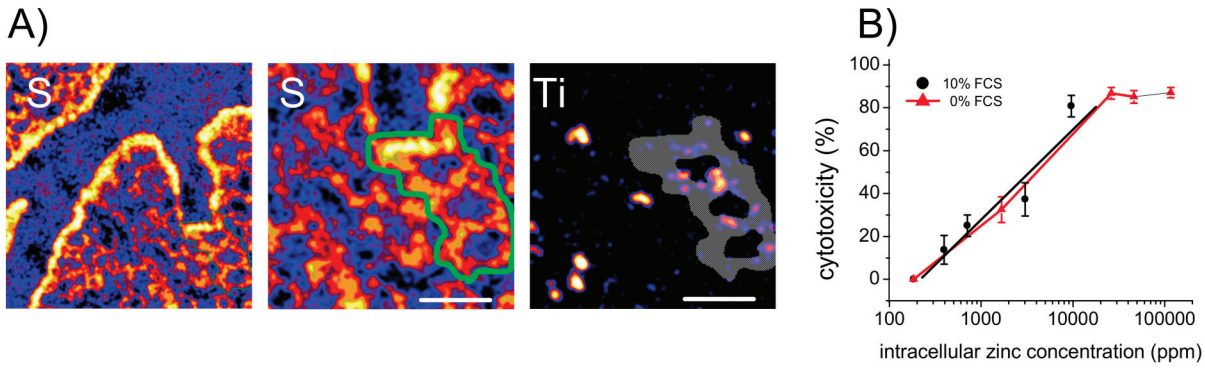

Figure 7.10: Verification and risk assessment of metal oxide nanoparticles: A) Distribution of TiO_2-nanoparticles (24 h, 271 mg/m^3 aerosol) in alveoli of mouse lung tissue. Bar represents 25 µm, respectively; B) Relationship between genuine zinc dose and toxicity (MTT-Test). Culture cells (A549) were exposed to protein surface modified and unmodified ZnO-nanoparticles for 48 h in presence (10 %) and absence (0 %) of fetal calf serum (FCS) in culture media (RPMI 1640), respectively.

7.10 Trace element analysis of nerve cells in the rat model of peripheral diabetic polyneuropathy

I. Estrela-Lopis*, M. Dorn*, L. Cuellar*, D. Spemann, J. Vogt, M. Nowicki†, I. Bechmann†, E. Donath*

*Institut für Medizinische Physik und Biophysik, Universität Leipzig
†Institut für Anatomie, Universität Leipzig

Iron content and metabolism plays a major role in many diseases. It has been suggested that the iron content in nerve cells is related to the development and progression of peripheral diabetic polyneuropathy (PDP). Ion Beam Microscopy (IBM) was used to measure iron content and distribution in the sciatic nerve of control and diabetic rats. Ganglion cells, neurons of the sciatic nerve and the arterioles of the sciatic nerve were investigated by Particle Induced X-ray Emission (PIXE). Ganglion cells and the associated satellite cells could be easily identified by their phosphorous and sulfur signal. In comparison to ganglion cells, satellite cells showed an iron concentration which was approximately increased by factor two (Fig. 7.11 B). Neurons of the sciatic nerve were also clearly identified by their phosphorous and sulfur signal. The sciatic nerve arterioli were identified by visualizing erythrocytes on the basis of their sulfur and particularly their iron signal. IBM was shown to be a proper method, to verify the supposed correlation between peripheral diabetic polyneuropathy and deviations of the trace elemental concentration distribution.

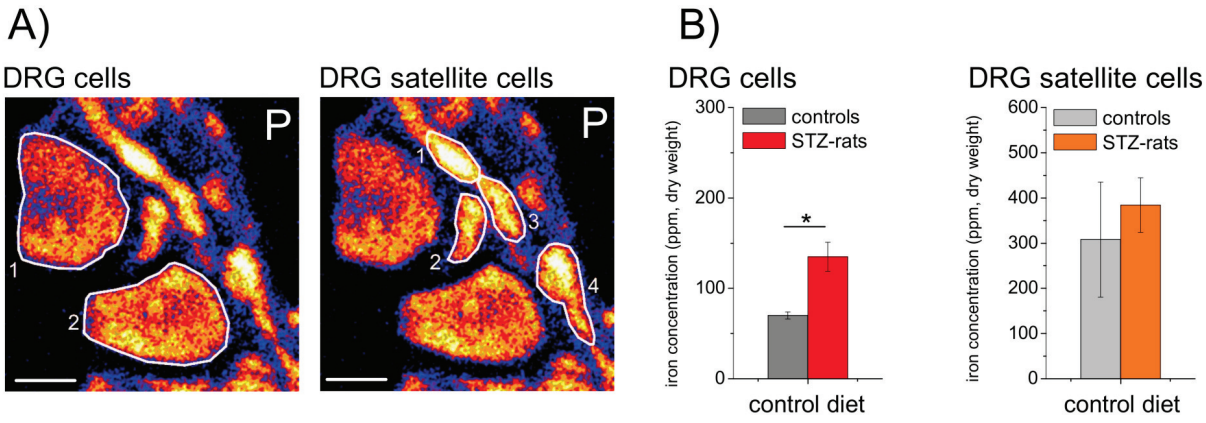

Figure 7.11: Iron quantification in Dorsal Root Ganglion (DRG) and associated satellite cells. A) Visualisation of ganglion cells (left) and satellite cells (right) on the basis of the phosphorous signal. Bar represents 10 μm, respectively. B) DRG and satellite cells of streptozotocin (STZ)-induced diabetic rats (STZ-rats) contain a significantly higher amount of iron per single cell. ($^\star p < 0.05$)

7.11 Lateral and transversal elemental distribution in nanofiltration membranes for water purification

E. Donath*, L. Cuellar*, M. Dorn*, I. Estrela-Lopis*, D. Spemann, J. Vogt

*Institut für Medizinische Physik und Biophysik, Universität Leipzig

The mechanism of nanofiltration for water purification is based in the deceleration of cations through interaction with sulfonates in the membrane matrix. Besides that, the effect of the sieve itself is important for the retention of organic molecules. In the membrane manufacturing process a compromise between flow rate and filtration has to be made, which can be achieved by an asymmetrical pore size distribution. Pore size should increase with membrane depth; whereas sulfonate groups should show a high concentration at the entrance of the pores. These challenging requirements concerning the membrane composition and structure can be achieved by properly adjusting the parameters of the membrane fabrication process. Until recently the optimisation of these parameters was based on empirical experience alone. Ion Beam Microscopy offers a unique opportunity to study the distribution of elements within the membranes both in the vertical and in the lateral dimension. Rutherford Backscattering Spectrometry (RBS) combined with a simulation approach revealed the transversal elemental distribution of sulphur, nitrogen, and oxygen. By means of Particle Induced X-ray Emission (PIXE) the lateral elemental distribution of sulphur was investigated. In conclusion, this approach allows optimizing the performance of nanofiltration membranes on a rational basis.

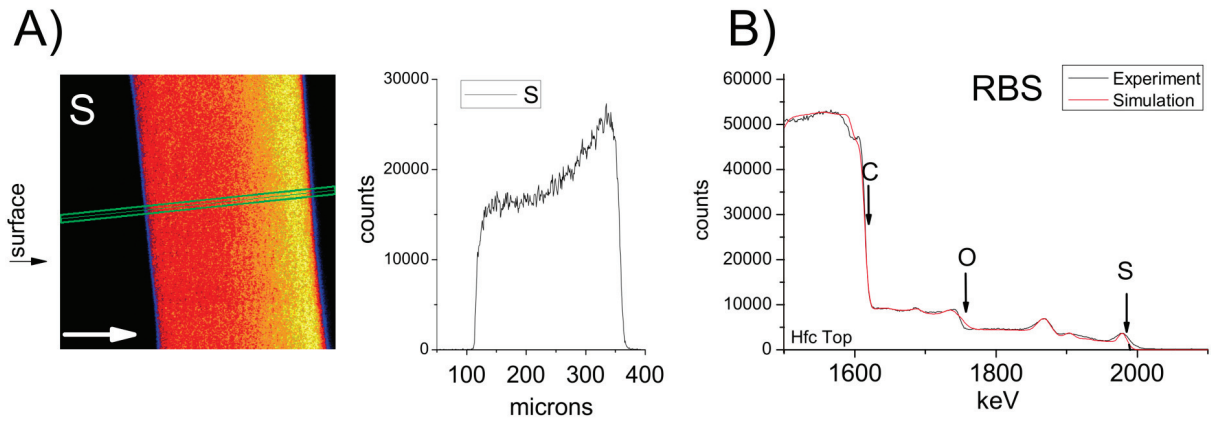

Figure 7.12: Elemental distribution in nanofiltration membranes: A) PIXE study of the transversal distribution of sulphur in the membrane profile. ROI (green) demonstrates a higher sulphur concentration with increasing membrane depth. B) RBS spectrum of nanofiltration membranes.The spectrum can be used to obtain the elemental profile in the z-direction.

7.12 Funding

Leipzig School of Natural Sciences - Building with Molecules and Nano-objects (BuildMona)
Prof. Dr. T. Butz
GSC 185/1

7.13 Organizational Duties

D. Spemann

- Referee: J. Appl. Phys., Nucl. Instrum. Meth. B, The Electrochemical Society, Fundação para a Ciência e a Tecnologia, The Leverhulme Trust

7.14 External Cooperations

Academic

- IOM Leipzig
  Dr. F. Frost, Prof. S.G. Mayr, Dr. K. Zimmer
- University of Amsterdam, Cognitive Science Centre, Netherlands
  Dr. B. Forstmann
- National University of Singapore
  Center for Ion Beam Applications, Prof. M. Breese, Dr. T. Osipowicz, Prof. F. Watt
- Universität Leipzig, Medizinische Fakultät
  Paul-Flechsig-Institut, Prof. T. Arendt, Dr. M. Morawski
- Universität Leipzig, Medizinische Fakultät
  Institut für Rechtsmedizin, Dr. M. Weber, S. Wernecke
- Universität Leipzig, Medizinische Fakultät
  Institut für Laboratoriumsmedizin, Kl. Chemie und Mol. Diagnostik, Prof. J. Thiery, Dr. D. Teupser
- Universität Leipzig, Medizinische Fakultät
  Institut für Medizinische Physik und Biophysik, Prof. E. Donath, Dr. U. Reibetanz, Dr. I. Estrela-Lopis, DBc. M. Dorn
- MPI für Kognitions- und Neurowissenschaften, Leipzig
  Prof. R. Turner
- Universität Leipzig, Fakultät für Mathematik und Informatik
  Prof. M. Bogdan
- The University of Melbourne
  Microanalytical Research Centre, Prof. D. Jamieson
- Universität Hannover
  Arbeitskreis Prof. P. Behrens

- Universität Hannover
  Arbeitskreis Prof. C. Vogt
- Universität Leipzig, Fakuktät für Chemie und Mineralogie, Institut für Technische Chemie
  Prof. R. Gläser
- TU Bergakademie Freiberg, Freiberg
  Prof. J. Heitmann
- University of North Texas, Denton, TX, USA
  Assoc. Prof. T. Reinert

Industry

- Dechema
  Dr. E. Zschau, Self-employed expert in materials research

7.15 Publications

Journals

Matthias Brandt, Michael Bonholzer, Marko Stölzel, Gabriele Benndorf, Daniel Spemann, Michael Lorenz, Marius Grundmann: *Electrical transport in strained $Mg_xZn_{1-x}O$:P thin films grown by pulsed laser deposition on ZnO(000-1)*, phys. stat. sol. B **249**, 82 (2012)
doi:10.1002/pssb.201147212

Markus Jäger, Tilman Butz: *FPGA implementation of digital constant fraction algorithm with fractional delay for optimal time resolution*, Nucl. Instr. and Meth. A **674**, 24 (2012)
doi:10.1016/j.nima.2012.01.022

D. Spemann, M. Rothermel, P. Esquinazi, M. Ramos, Y. Kopelevich, H. Ohldag: *Comment on:"Revealing common artifacts due to ferromagnetic inclusions in highly oriented pyrolytic graphite", by M. Sepioni, R.R. Nair, I.-Ling Tsai, A.K. Geim and I.V. Grigorieva, EPL 97 (2012) 47001*, EPL **98**, 57006 (2012).

M. Jäger and T. Butz: *Perturbed Angular Correlation of the streched cascade in the decay of ^{180m}Hf using a digital spectrometer*, Hyperf. Interact. **211**, 165–172 (2012).

Florian Schmidt, Holger von Wenckstern, Daniel Spemann, Marius Grundmann: *On the radiation hardness of (Mg,Zn)O thin films grown by pulsed-laser deposition*, Appl. Phys. Lett. **101**, 012103 (2012).

J. Michels, J. Vogt, S.N. Gorb: *Tools for crushing diatoms – opal teeth in copepods feature a rubber-like bearing composed of resilin*, Sci. Rep. **2** 465 (2012)
doi:10.1038/srep00465.

T. Butz, R. Vianden: *The temperature dependence of the nuclear quadrupole interaction of $^{44}Ti(EC)^{44}Sc$ in rutile*, Hyperfine Interactions (2012)
doi:10.1007/s10751-012-0675-7.

Michael Lorenz, Christian Schmidt, Gabriele Benndorf, Tammo Böntgen, Holger Hochmuth, Rolf Böttcher, Andreas Pöppl, Daniel Spemann, Marius Grundmann: *Degenerate interface layers in epitaxial Scandium-doped ZnO thin films*, J. Phys. D: Appl. Phys. **46**, 065311 (2013).

D. Diering, D. Spemann, J. Lenzner, St. Müller, T. Böntgen, H. von Wenckstern: *Greyscale Proton Beam Writing in p-type Gallium Arsenide*, Nucl. Instr. and Meth. B **306**, 275 (2013)
doi:10.1016/j.nimb.2012.11.049

N. Klingner, J. Vogt, D. Spemann: *Optimizing the Rutherford Backscattering Spectrometry setup in a nuclear microprobe*, Nucl. Instr. and Meth. B **306**, 44 (2013)
doi:10.1016/j.nimb.2012.12.062

R. Wunderlich, N. Klingner, J. Vogt, D. Spemann: *Quantitative elemental microscopy on lateral highly inhomogeneous meteorite samples using ion beam analysis*, Nucl. Instr. and Meth. B **306**, 85 (2013)
doi:10.1016/j.nimb.2012.11.048

A.M. Jakob, M. Hennes, M. Müller, D. Spemann, S.G. Mayr: *Coupling of micro magnetic and structural properties across the martensite and Curie temperatures in miniaturized Ni-Mn-Ga ferromagnetic shape memory alloys – towards a quantitative physical understanding*, Adv. Func. Mater. (2013)
doi:10.1002/adfm.201300165

Books

T. Butz: *Fouriertransformation für Fußgänger*, 7. Aufl.(Vieweg+Teubner, Wiesbaden 2012), ISBN: 978-3-8348-0946-9

Talks

P. Lorenz, D. Spemann, M. Ehrhardt, K. Zimmer
Laser-induced front side etching (LIFE) of crystalline silica
Frühjahrstagung der DPG, 12.03.–16.03.2012, Stuttgart

F. Schmidt, M. Schmidt, H. von Wenckstern, D. Spemann, M. Grundmann
Ferromagnetic Signals in Nominally Non-magnetic Oxide Single Crystals
Frühjahrstagung der DPG, 25.03.–30.03.2012, Berlin

D. Lehmann, R. Steffler
Die Leipziger Uranmaschine L4 – Zuerst der Forschungserfolg, danach die Katastrophe: Uranbrand am 23.06.1942
Leipziger Schülerakademie, 17.04.12, Leipzig

D. Lehmann
Ionisierende Strahlung: Die unsichtbare Botschaft aus dem Inneren radioaktiver Atome. Eine Zeitreise
Sonntagsvorlesung mit Experimenten an der Fakultät für Physik und Geowissenschaften der Universität Leipzig, 24.06.12, Leipzig

D. Lehmann, R. Steffler
Uranmaschinen-Versuche in Leipzig, (a) 1942: im Mai der Erfolg – im Juni beim Zerlegen ein Uranbrand, (b) der Feuerwehreinsatz vom 23.06.1942 im Vergleich mit KKW-Unfällen
Vortrag an der Fakultät für Physik und Geowissenschaften der Universität Leipzig, 24.06.12, Leipzig

D. Spemann
Die Rolle von Ionenstrahlen bei der Untersuchung des defektinduzierten Magnetismus'
Physikkolloquium, 25.04.2012, TU Bergakademie Freiberg, Freiberg

D. Diering, D. Spemann, J. Lenzner, St. Müller, T. Böntgen, H. von Wenckstern
Greyscale Proton Beam Writing in p-type Gallium Arsenide
Workshop Ionenstrahlphysik, 10.–11.07.2012, Augsburg

N. Klingner, J. Vogt, D. Spemann
Optimizing the Rutherford Backscattering Spectrometry setup in a nuclear microprobe
Workshop Ionenstrahlphysik, 10.–11.07.2012, Augsburg

R. Wunderlich, J. Vogt, D. Spemann
Quantitative IBA microscopy on lateral highly inhomogeneous meteorite samples
Workshop Ionenstrahlphysik, 10.–11.07.2012, Augsburg

D. Lehmann, R. Steffler
Das Uranprojekt in Deutschland 1940–42, Uranmaschinenversuche in Leipzig, Mai 1942: Welterfolg mit L4, am 23.06. dann der Brand
Vortrag am Wilhelm-Ostwald-Gymnasium Leipzig, 17.07.12, Leipzig

M. Engler, S. Müller, F. Frost, R. Feder, D. Spemann, T. Michely
Silicide induced ion beam patterning of silicon(001)
19th International Workshop on Inelastic Ion-Surface Collisions (IISC-19), 16.–21.09.2012, Frauenchiemsee, Germany

Florian Schmidt, Holger von Wenckstern, Daniel Spemann, Marius Grundmann
On the radiation hardness of (Mg,Zn)O PLD thin films
MRS Fall Meeting, 25.–30.11.2012, Boston, MA., USA.

Posters

M. Rothermel, D. Spemann
Alignment tolerances in an ion nanoprobe and octupole abberation corrections
13. International Conference on Nuclear Microprobe Technology and Applications, 23.–27.07.2012, Lissabon, Portugal

T. Andrea, U. Reibetanz, M. Rothermel, T. Butz
3D imaging of cells using limited-angle STIM and PIXE tomography
13. International Conference on Nuclear Microprobe Technology and Applications, 23.–27.07.2012, Lissabon, Portugal

D. Diering, D. Spemann, J. Lenzner, St. Müller, T. Böntgen, H. von Wenckstern
Greyscale Proton Beam Writing in p-type Gallium Arsenide
13. International Conference on Nuclear Microprobe Technology and Applications, 23.–27.07.2012, Lissabon, Portugal

N. Klingner, J. Vogt, D. Spemann
Optimizing the Rutherford Backscattering Spectrometry setup in a nuclear microprobe
13. International Conference on Nuclear Microprobe Technology and Applications, 23.–27.07.2012, Lissabon, Portugal

R. Wunderlich, J. Vogt, D. Spemann
Quantitative elemental microscopy on lateral highly inhomogeneous meteorite samples using ion beam analysis
13. International Conference on Nuclear Microprobe Technology and Applications, 23.–27.07.2012, Lissabon, Portugal

7.16 Graduations

Master

- Nico Klingner
  Entwicklung eines Systems zur hochaufgelösten Rutherford-Rückstreu-Spektrometrie mittels Halbleiterdetektoren
  Septembre 2012
- Ralf Wunderlich
  Methodische Entwicklungen zur quantitativen ortsaufgelösten Ionenstrahlanalytik von lateral stark inhomogenen Meteoritenproben
  June 2012
- Annemarie Sickert
  Ortsaufgelöste ionenstrahlanalytische Untersuchungen atherosklerotischer Ablagerungen
  February 2012

Bachelor

- David Diering
  Greyscale Proton Beam Writing in p-type Gallium Arsenide
  August 2012
- Jeremy Perez
  Energy calibration of the LIPSION accelerator using PIGE and Backscattering Spectrometry
  Octobre 2012
- Pan Zhichao
  Influence of Curved Sample Surfaces on the X-ray dectection in PIXE analysis
  Septembre 2012

8

Semiconductor Physics

8.1 Introduction

In 1907 Karl Bädeker reported in his Habilitation thesis at Universität Leipzig and in [1] the first transparent conductors, CdO and CuI. Cuprous iodide is a zincblende p-type transparent (E_g = 3.1 eV) semiconductor. For modifying its conductivity through the content of copper vacancies, Bädeker is also credited for reporting the first doping of semiconductors. In 2012 we have picked up his process of iodizing copper thin films (Fig. 8.1) and have fabricated p-CuI/n-ZnO heterostructure bipolar diodes with high rectification close to 10^7, larger than any previously reported diode involving oxide materials, only surpassed by our results on p-$ZnCo_2O_4$/n-ZnO diodes reported last year. Further progress in our research on transparent electronics includes normally-off ZnO MISFETs with high-κ WO_3 gate dielectric.

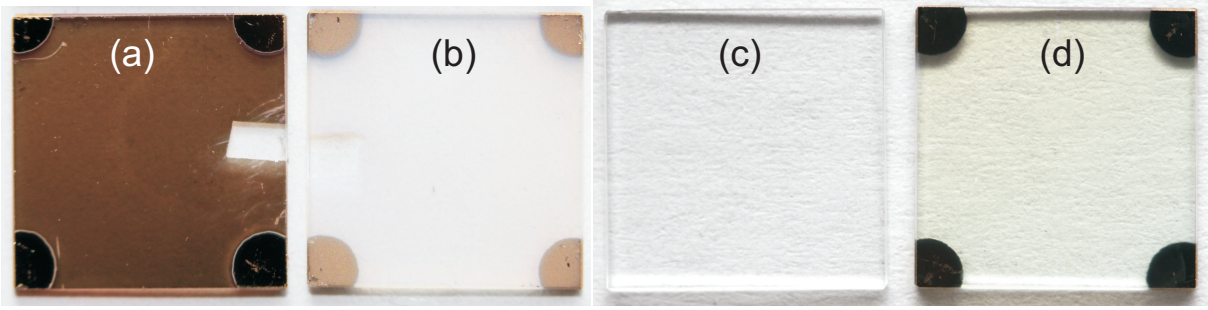

Figure 8.1: (a, b): Evaporated copper thin film on glass (a) before and (b) after vapor iodization. (c) ZnO on sapphire template, (d) CuI/ZnO thin film. Substrate sizes are 1×1 cm^2.

Progress in pulsed laser deposition has been made in the formation of non-polar (Mg,Zn)O/ZnO and (Mg,Zn)O/(Cd,Zn)O quantum well heterostructures around ZnO microwires and the observation of persistent RHEED oscillations and layer-by-layer growth in ZnO homoepitaxy. For ZnO microwires with hexagonal cross-section with sharp corners and very smooth side facets, record low optical pumping threshold at room temperature (70 kW/cm^2) has been found.

We are very grateful to our funding agencies in particular Deutsche Forschungsgemeinschaft (DFG) and European Social Fund (ESF). We are grateful for the continued funding of Sonderforschungsbereich SFB 762 "Functionality of Oxide Interfaces" (2012–

2015) and our project on nanowire heterostructures in the newly established Forschergruppe FOR 1616 "Nanowire Optoelectronics" (2012–2014). Also we thank Sächsische Aufbaubank for support for new work on Ga_2O_3 thin films and oxide solar cells in the framework of EFRE. The generous support of Universität Leipzig allows us to install in 2013 a new high resolution X-ray diffraction setup and a sputter chamber for oxides. The work of our students and researchers together with our academic and industrial partners near and far was fruitful and enjoyable and thus it is with pleasure that the semiconductor physics group presents their progress report.

Marius Grundmann

[1] K. Bädeker, *Über die elektrische Leitfähigkeit und die thermoelektrische Kraft einiger Schwermetallverbindungen*, Ann. Physik **327**, 749–766 (1907)

8.2 Transparent *p*-CuI/*n*-ZnO heterojunction diodes

F.-L. Schein, H. von Wenckstern, M. Grundmann

We have investigated the wide bandgap (E_g = 3.1 eV) *p*-type semiconductor γ-copper(I)-iodide (γ-CuI) [1, 2] as an alternative candidate to *p*-type transparent semiconducting oxides like SnO [3] or $ZnCo_2O_4$ [4]. Room temperature dc-sputtered copper thin films on glass substrates were transformed into CuI by exposing them to iodine vapor. Figure 8.2 (d) depicts such samples before and after iodization. X-ray-diffraction showed that the iodized films are polycrystalline γ-CuI in cubic phase having zinc-blende structure. Hall-effect measurements of these films revealed a hole mobility of about 6 cm^2/Vs, a hole density of 5×10^{18} cm^{-3} and a resistivity of 0.2 Ωcm. These values are comparable to those achieved by other methods like pulsed-laser deposition or rf-dc coupled magnetron sputtering [5]. Despite the wide bandgap and the transparent appearance of the samples to the human eye we measured an optical transmittance of only 49 % for a 500 nm CuI film. This is due to high rms surface roughness of 81 nm as determined by atomic force microscopy causing strong light scattering.

Quite recently the first report of wide bandgap *p*-CuI/*n*-ZnO heterodiodes on rf-magnetron sputtered ZnO grown on CuI single crystals was published [6] but only a small current rectification ratio of about 8 at ±4 V was achieved.

In our approach Cu was dc-sputtered onto pulsed-laser deposited ZnO thin films and vapor iodized afterwards. Figures 8.2 (a)–(c) illustrate the diode fabrication process and the utilization of a degenerately doped ZnO:Al layer as an ohmic back contact [7]. If the Cu is not iodized, a Schottky diode forms which exhibits an ideality factor of η = 1.74 and the ratio between forward and reverse current density is $I_f/I_r = 2\times10^3$ at ±2 V. For iodized Cu the figures of merit for the resulting *p*-CuI/*n*-ZnO heterodiode are η = 2.14 and much higher rectification $I_f/I_r = 6\times10^6$ at ±2 V. The current density j vs. voltage V characteristics of both diodes as well as a photograph of the *pn*-diode are depicted in Fig. 8.2 (e).

Similar wide bandgap heterojunctions with at least one oxidic part mostly have lower I_f/I_r but $\eta > 2$ is also observed in several studies and designated to mechanisms including surface or interface states [5]. The interface region of the polycrystalline and

fairly rough CuI to ZnO presumably has inhomogeneities and defects causing $\eta > 2$ and the small hysteresis in the *pn*-diode *j-V* characteristic.

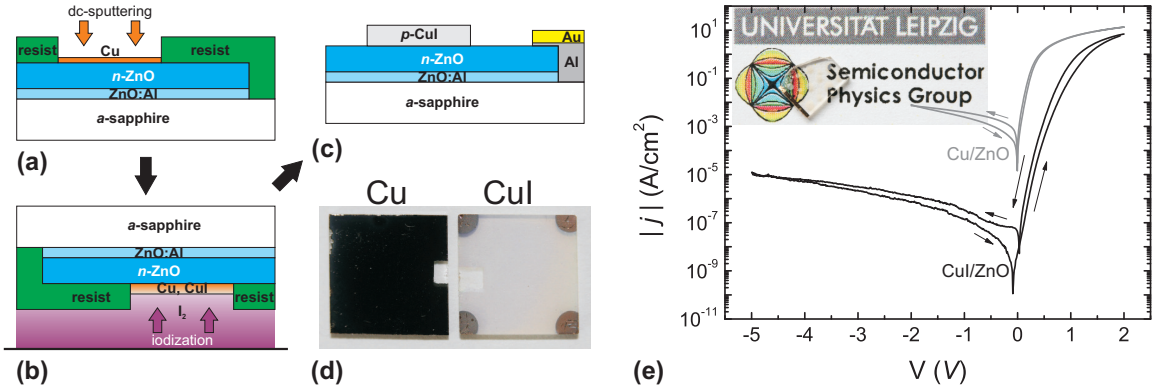

Figure 8.2: Fabrication of CuI/ZnO *pn*-heterodiodes: **(a)** dc-sputtering of circular Cu contacts on ZnO, **(b)** reaction of Cu to CuI by iodine vapor, **(c)** ready-made diode with Au/Al/ZnO:Al back-contact, **(d)** photograph of a Cu thin film without post-treatment (*left*) and after iodization and the deposition of Au contacts (*right*). The notch in both samples was used for thickness determination by means of a profilometer. **(e)** Current density vs. voltage characteristic of a Cu/ZnO Schottkydiode (*grey*) and a CuI/ZnO *pn*-heterodiode (*black*). The *inset* depicts a photograph of the sample with several circular CuI/ZnO diodes lying on a printed logo on paper.

[1] K. Bädeker, Ann. Phys. **327**, 749 (1907), doi:10.1002/andp.19073270409
[2] B.-L. Zhu and X. Z. Zhao, Phys. Status Solidi A **208**, 91 (2011), doi:10.1002/pssa.201026239
[3] E. Fortunato, R. Barros, P. Barquinha, V. Figueiredo, S.-H. Ko Park, C.-S. Hwang and R. Martins, Appl. Phys. Lett. **97**, 052105 (2010), doi:10.1063/1.3469939
[4] F.-L. Schein, H. von Wenckstern, H. Frenzel, and M. Grundmann, IEEE Electron Device Lett. **33**, 676 (2012), doi:10.1109/LED.2012.2187633
[5] F.-L. Schein, H. von Wenckstern, and M. Grundmann, Appl. Phys. Lett. **102**, 092109 (2013) and references therein, doi:10.1063/1.4794532
[6] K. Ding, Q. C. Hu, D. G. Chen, Q. H. Zheng, X. G. Xue, and F. Huang, IEEE Electron Device Lett. **33**, 1750 (2012), doi:10.1109/LED.2012.2218274
[7] H. von Wenckstern, G. Biehne, R. A.. Rahman, H. Hochmuth, M. Lorenz, and M. Grundmann, Appl. Phys. Lett. **88**, 092102 (2006)

8.3 Comparison of ZnO-based JFET, MESFET, and MISFET

F.J. Klüpfel, F.L. Schein, M. Lorenz, H. Frenzel, H. von Wenckstern M. Grundmann

Oxide semiconductor devices are intensely investigated due to prospective applications in displays or sensors. Transistors based on InGaZnO are already integrated in the last generation of flat screen displays [1]. These devices have been optimized for the mentioned application. To open the oxide-based devices to a broader field of applications,

different device types are investigated. Only on the oxide semiconductor ZnO all types of field-effect transistors (FETs), junction FETs (JFETs), metal-semiconductor FETs (MESFETs), and metal-insulator-semiconductor FETs (MISFETs), have been demonstrated [1–4]. We compare these three device types using a common ZnO sample, which was cleaved just before gate deposition. This way we can exclude differences in the device behaviour, which originate in the deposition and structuring of the transistor channel material, and focus on the specific properties introduced by the transistor gates.

The JFET gate consisted of *p*-type $ZnCo_2O_4$, the MESFET Schottky contact was fabricated by reactively sputtered Pt, and the MISFET gate oxide was WO_3, with ZnO:Ga as gate electrode.

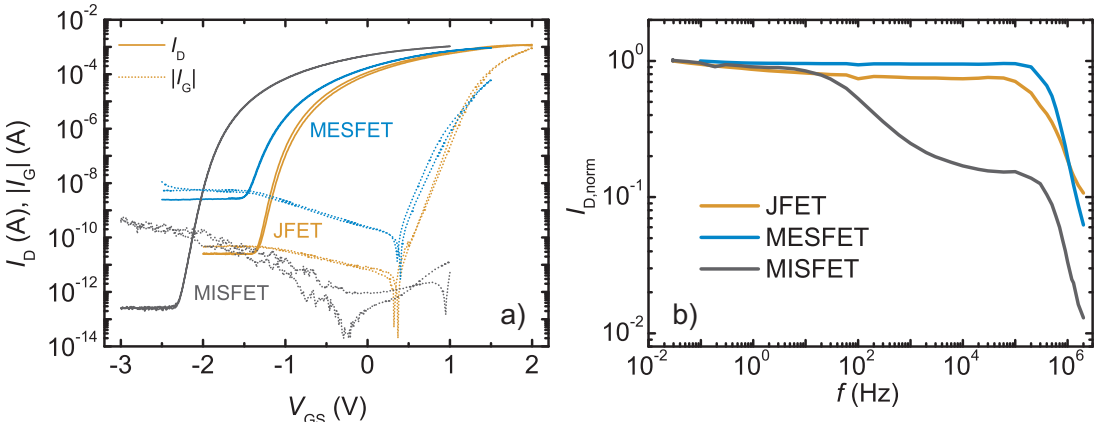

Figure 8.3: a) Transfer characteristics of ZnO-based JFET, MESFET and MISFET for V_{DS} was 2 V. b) Current response in dependence on the switching frequency of the gate voltage (switching between on- and off-state).

Electrical characterization at room temperature, depicted in Fig. 8.3a), demonstrates similar operation voltages for all devices. The characteristics also show differences in the off-current, the on-voltage and the slope of the transfer curves. They can almost entirely be explained by properties of the gate contacts, e.g. by different barrier heights of the JFET and MESFET gates and the voltage drop across the gate insulator of the MISFET. All devices stay functional at temperatures up to 150°C, although some degradation is observed.

Frequency-dependent measurements revealed differences in the switching speed of the transistors, as shown in Fig. 8.3b). Especially the MISFETs exhibit a severe drop in signal strength for frequencies higher than about 10 Hz, which is probably due to trapping processes at the surface of the highly porous insulator.

The identification of the specific strengths of the respective device types can now be used to select the optimal device for specific applications.

[1] Sharp Corporation, Press Release, Apr. 2011 (http://sharpworld.com/corporate/news/110421.html)
[2] H. Frenzel *et al.*, Adv. Mat., 22, 5332 (2010)
[3] F. Schein *et al.*, IEEE Electr. Dev. Lett., 33, 676 (2012)
[4] M. Lorenz *et al.*, Adv. Mat., 23, 5383 (2011)

8.4 Design rules for (Mg,Zn)O-based thin-film transistors with high-κ WO_3 dielectric gates

M. Lorenz, A. Reinhardt, H. von Wenckstern, M. Grundmann

Research and developement on transparent thin-film transistors (TTFTs) is increasingly important since the first demonstration of fully transparent field-effect transistors (FETs) [1]. Beside semiconducting materials like zinc oxide (ZnO) or amorphous gallium-indium-zinc-oxide (a-GIZO) new dielectric materials that cope with requirements like low deposition temperatures ($T < 200$°C), high transparency in the visible spectral range and a high dielectric permittivity κ are currently investigated. Tungsten trioxide was recently demonstrated as high-κ material in combination with excellent electrical properties of ZnO-based metal-insulator-semiconductor field-effect transistors (MISFETs) [2]. In this work the thickness of the gate dielectric has been optimized resulting in a minimized subthreshold slope (SS) and leakage current (j_{off}) in the off-regime of the transfer characterisitic. Furthermore, results on the reduction of the (Mg,Zn)O-channel thickness d and its impact on the turn-on voltage V_{on} are investigated. Depending on the work function of the gate electrode material depletion and enhancement mode devices were fabricated.

Tungsten oxide was grown with a thickness d_{i} between 140 nm and 550 nm by pulsed-laser deposition at room temperature from a WO_3 target at an oxygen pressure of $p(O_2) = 0.2$ mbar. Fig.8.5(a) depicts the dependence of $SS(d_{\mathrm{i}})$. For $d_{\mathrm{i}} \approx 380$ nm an optimal value of $SS = 65$ mV/decade is obtained. For lower dielectric thicknesses the increasing value of j_{off} (see inset of Fig.8.5(a)) prevents an exact determination of the slope. For $d_{\mathrm{i}} > 380$ nm the increasing voltage drop across the insulator inherently leads to a higher value of SS. Furthermore, j_{off} saturates for $d_{\mathrm{i}} \geq 380$ nm. In [1] the reduced leakage-current density j_{off} is explained by the lowered porosity of the WO_3-dielectric with increased insulator thickness giving rise to a much denser film morphology.

The turn-on voltage V_{on} was shifted between $V_{\mathrm{on}} = -1.68$ V and $V_{\mathrm{on}} = -0.27$ V for a thickness of the channel $d = 21$ nm and $d = 8.6$ nm, respectively (Fig.8.5(b)). The highly transparent electrode consisting of ZnO with 4%-wt. Ga_2O_3 (ZGO) has a higher Fermi energy E_{F} than the channel. This gives rise to an accumulation within the semiconductor and in turn invoking depletion mode devices for the thicknesses d as described. For $d = 8.6$ nm the (Mg,Zn)O thin film is not fully coalesced, which leads to an increased resistance of the semiconductor giving rise to an on-current of less than 1 μA. In order to achieve $V_{\mathrm{on}} \geq 0$ V platinum as noble metal with a work function of 5.65 eV was used as metal gate electrode. In combination with a channel thickness of $d = 12$ nm $V_{\mathrm{on}} = 0.19$ V. However, a theoretical calculation of the turn-on voltage according to theory [1] was not successful. A lowered electron concentration was considered in the modeling. Its origin is not fully understood, yet and needs further investigation.

[1] J. Wager: Science **300**, 1245 (2003)
[2] M. Lorenz, H. v. Wenckstern, M. Grundmann: Adv. Mater. **23**, 5383 (2011)
[1] M. Lorenz, A. Reinhardt, H. v. Wenckstern, M. Grundmann: Appl. Phys. Lett. **101**, 183502 (2012)

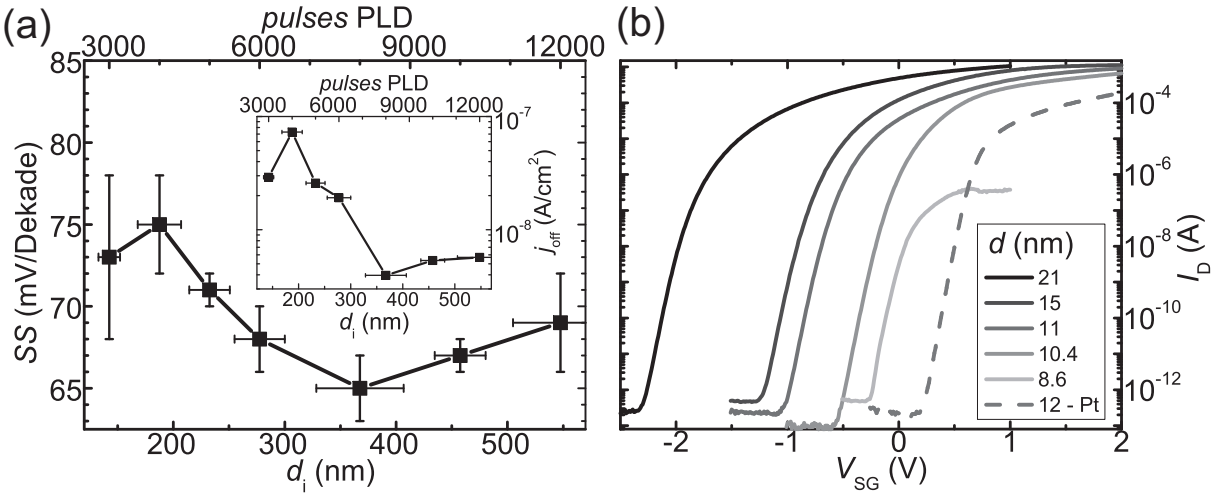

Figure 8.4: (a) Subthreshold slope SS vs. thickness d_i of the WO_3 dielectric. The inset depicts the leakage-current density j_off of the transistor in the off-regime. (b) Transfer characteristics of various TFTs with different channel thicknesses d with a ZGO gate-electrode. For d = 12 nm a Pt gate metal was employed to realize enhancement mode TFTs. For all TFTs W/L = 430/10 and V_SD = 2 V.

8.5 Oxidation state of tungsten oxide thin films used as gate dielectric for zinc oxide based transistors

M. Lorenz, M. Grundmann, S. Wickert*, R. Denecke*

* Wilhelm-Ostwald-Institut für Physikalische und Theoretische Chemie, Fakultät für Chemie und Mineralogie, Universität Leipzig, Linnéstrasse 2, 04103 Leipzig, Germany

Tungsten oxide thin films grown by pulsed-laser deposition (PLD) at room temperature have recently been employed as high-κ gate dielectric in metal-insulator-semiconductor field-effect transistors [1]. The electrical and optical properties depend significantly on the oxygen pressure $p(O_2)$ during the PLD process [2]. X-ray photoelectron spectroscopy (XPS) measurements were carried out in order to investigate the stoichiometric ratio of oxygen and tungsten which presumeably affects the thin-film properties. As highly insulating gate dielectric a WO_x layer with x close to 3 is necessary.

A reference sample consisting of WO_3 powder (purity 3N) is compared to thin-film samples grown at a deposition pressure of $p(O_2)$ = 0.2 mbar and $p(O_2)$ = 0.002 mbar (Fig.8.5). By means of an ESCALAB 220iXL XPS/AES device with a spectral resolution below 1.5 eV, using Al K_α radiation (energy of 1486.6 eV) generated by an Al/Mg dual mode X-ray anode, the XPS measurements were performed ex-situ after the PLD process. Calibration of the spectrometer was performed according to ISO 15472. Furthermore, the signal of the thin-film WO_x-samples was calibrated using the O1s core level due to a shift invoked by a charging of the surface due to the insulating substrate.

The reference sample only shows a signal attributed to WO_3, without the presence of lower oxidized tungsten states. For a low deposition pressure of $p(O_2)$ = 0.002 mbar a significant contribution of WO_2 to the overall signal has to be considered. For this sample the stoichiometric ratio is well below x = 3. For $p(O_2)$ = 0.2 mbar during PLD only

a small fraction of lower oxidized tungsten states is introduced into the thin films and probably stems from the dissociation of WO_3 caused by the high energetic laser fluence or due to different bonding geometries (e.g. at the surface). In summary the different stoichiometric ratio x within the WO_x thin films is used to explain the dependence of the electrical and optical properties on the deposition pressure.

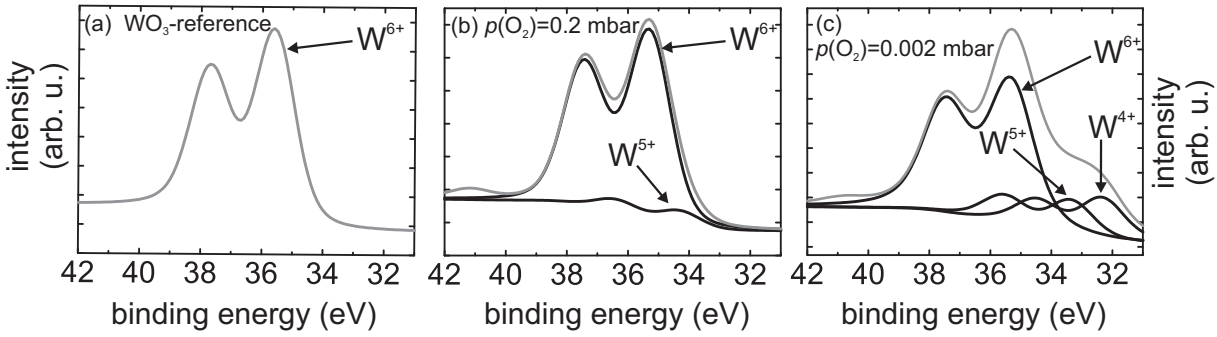

Figure 8.5: (a) XPS spectrum of W4f from the reference sample. XPS spectra in (b) and (c) depict the contributions due to W^{6+}, W^{5+} and W^{4+} (black) fitted to the experimental spectra (grey) of the tungsten oxide thin-film samples. The splitting of the spectra is due to $W4f_{7/2}$ and $W4f_{5/2}$.

[1] M. Lorenz, A. Reinhardt, H. v. Wenckstern, M. Grundmann: Appl. Phys. Lett. **101**, 183502 (2012)
[2] M. Lorenz, H. v. Wenckstern, M. Grundmann: Adv. Mater. **23**, 5383 (2011)
[3] M. Lorenz, M. Grundmann, S. Wickert, R. Denecke: Proc. Mat. Res. Soc. **1494**, 1649 (2013)

8.6 Control of the conductivity of β-Ga_2O_3 thin films via growth temperature and pressure

S. Müller, H. von Wenckstern, D. Splith, F. Schmidt, M. Grundmann

In the past decade oxide semiconductors with large band gap were investigated with a renewed interest. With a band gap of about 4.7 eV β-Ga_2O_3 has unique properties for the realization of solar blind applications and high power devices [1]. Recently, Higashiwaki *et al.* demonstrated the fabrication of the first reproducible working metal-semiconductor field effect transistors on homoepitaxial grown β-Ga_2O_3 thin films [1]. For the realization of β-Ga_2O_3-based application it is important to control the conductivity of β-Ga_2O_3 thin films. So far, the enhancement of conductivity of β-Ga_2O_3 thin film grown by pulsed laser deposition (PLD) was demonstrated by doping of Sn [2–4].
Here, we present the investigation of structural and electrical properties of Si-doped β-Ga_2O_3 thin films grown by pulsed-laser deposition *c*-plane sapphire substrate. The growth temperature and oxygen background pressure both have tremendous influence on crystallinity and the electrical sample properties.
The β-Ga_2O_3 thin film were grown at growth temperatures (T_G) between 510 °C and 650 °C. Additionally, the oxygen partial pressure ($p(O_2)$) was varied between 3×10^{-4} mbar and 2.4×10^{-2} mbar.

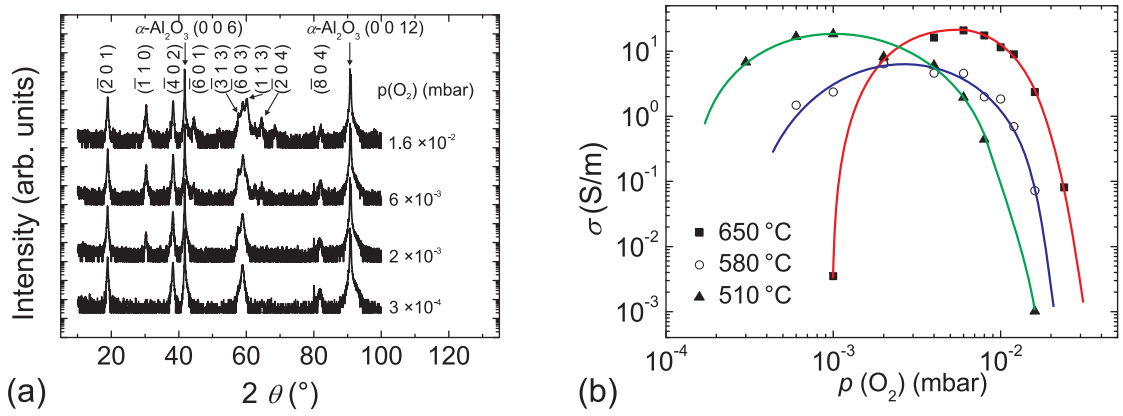

Figure 8.6: (a) X-ray diffraction pattern of β-Ga_2O_3 thin films grown on *c*-plane sapphire substrates at a growth temperature of 650 ℃ and oxygen partial pressures as labeled. (b) Logarithmic conductivity vs the oxygen partial pressure in the PLD-chamber during the deposition of the thin films for different growth temperatures. The solid lines are guides to the eye, respectively.

Figure 8.6 (a) depicts the XRD patterns of β-Ga_2O_3 thin films grown at T_G = 650 ℃. For $p(O_2)$ up to 1×10^{-3} mbar the β-Ga_2O_3 thin films are single phase and $(\bar{2}01)$-oriented. The orientation is indicated by the occurrence of the peaks at 18.9°, 38.4° and 59.2° which correspond to the $(\bar{2}01)$, $(\bar{4}02)$ and $(\bar{6}03)$ planes of β-Ga_2O_3, respectively. With increasing $p(O_2)$ several other peaks occur in the XRD pattern with indicates that the thin films have several not randomly distributed orientations for higher $p(O_2)$. The conductivity in dependence on $p(O_2)$ for different T_G is shown in Figure 8.6 (b). For T_G = 650 ℃ the conductivity first increases with decreasing $p(O_2)$ until it reaches a maximum at $p(O_2) = 6\times10^{-3}$ mbar with 20 S/m. With a further decrease of $p(O_2)$ the conductivity decreases. For lower T_G (580 ℃ and 510 ℃) a similar behavior is visible. The maximal conductivity of the thin films grown at T_G = 580 ℃ (510 ℃) is 6.5 S/m (18.5 S/m) and does not change significantly in dependence on T_G. However, the $p(O_2)$ for which maximal conductivity is reached, shifts with lower T_G to lower $p(O_2)$. For T_G = 580 ℃ (510 ℃) the maximal conductivity is obtained for $p(O_2) = 2\times10^{-3}$ mbar (1×10^{-3} mbar).
This behavior is in contrast to former reports where only a single pair of ($p(O_2)$,T_G) for the highest conductivity was reported [2–4]. The set of ($p(O_2)$,T_G) pairs we report on allows to control the conductivity in dependence on $p(O_2)$ and T_G over several orders of magnitude. Therefore, β-Ga_2O_3 can used as transparent conductive oxide, material for rectifying contacts or as insulating material.

[1] M. Higashiwaki, K. Sasaki, A. Kuramata, T. Masui, and S. Yamakoshi, Appl. Phys. Lett. **100**, 013504 (2012), doi:10.1063/1.3674287
[2] M. Orita, H. Ohta, M. Hirano, and H. Hosono, Appl. Phys. Lett. **77**, 4166 (2000), doi:10.1063/1.1330559
[3] M. Orita, H. Hiramatsu, H. Ohta, M. Hirano, and H. Hosono, Thin Solid Films **411**, 134 (2002), doi:10.1016/S0040-6090(02)00202-X
[4] K. Matsuzaki, H. Hiramatsu, K. Nomura, H. Yanagi, T. Kamiya, M. Hirano, and H. Hosono, Thin Solid Films **496**, 37 (2006), doi:10.1016/j.tsf.2005.08.187

8.7 On the radiation hardness of (Mg,Zn)O PLD thin films

F. Schmidt, H. von Wenckstern, D. Spemann, M. Grundmann

(Mg,Zn)O and related compounds are a potential material systems for optoelectronic devices working in the near UV and a viable alternative to GaN. If used within detectors in outer space, (Mg,Zn)O-based active material must fulfill specific requirements, such as durability, operation in a wide temperature range, and resistance against cosmic radiation.

Auret *et al.* showed that a defect labeled E4 can be introduced by proton bombardment in melt grown and vapor phase grown ZnO bulk crystals [1–3]. The authors determined the generation rate η for this defect as $\eta_{\mathrm{MG}} = 13\,\mathrm{cm}^{-1}$ and $\eta_{\mathrm{SCVT}} = 2.4\,\mathrm{cm}^{-1}$ for the melt grown single crystal and the single crystal grown by seeded chemical vapor transport (SCVT), respectively. So far the defect generation in $Mg_xZn_{1-x}O$ by irradiation with high-energy particles has not been investigated. The scope of this study is to systematically investigate the generation rate of E4 in $Mg_xZn_{1-x}O$ thin films under 2.25 MeV proton irradiation.

$Mg_xZn_{1-x}O$ thin films were grown on *a*-plane sapphire substrates by pulsed-laser deposition (PLD). The respective ceramic MgO/ZnO targets used for sample growth have admixtures of no, 0.10 wt%, 0.25 wt%, 1.00 wt%, and 2.00 wt% MgO. The layers were grown at 650 °C in an oxygen ambient of 0.016 mbar. The Mg-content in the thin films was determined via low temperature photoluminescence from the shift of the energetic position of the I_{6a} line [4], as it is described in Ref. [5]. In order to study samples being similar in the as-grown state, the irradiation with different fluences was conducted at one and the same $10 \times 10\,\mathrm{mm}^2$ sample for each Mg-content.

Prior to the growth of the about 800 nm thick $Mg_xZn_{1-x}O$ layers, a highly conducting aluminum doped (1% wt) ZnO layer was deposited. This layer serves as an ohmic back-contact and leads to Schottky diodes with low series resistance [6]. The Schottky contacts were realized by reactive direct-current (DC) sputtering of palladium (Pd). Subsequently a metallic capping was deposited by DC sputtering of Pd in pure argon [7]. The films were divided into pieces and irradiated through the contacts with protons and fluences D ranging from $1\times10^{13}\,\mathrm{cm}^{-2}$ to $2\times10^{14}\,\mathrm{cm}^{-2}$. All irradiations were carried out at the high energy nanoprobe LIPSION at the University of Leipzig using a focused beam of 2.25 MeV protons with a beam current of approximately 1 nA. The details of the LIPSION laboratory are described in Ref. [8].

Defects with electronic states in the upper third of the ZnO band gap were studied by DLTS in the temperature range from 10 K to 330 K. The DLTS setup is described in Ref. [10]. Similar to previous defects studies on ZnO the defect E4 is also present in our samples. The generation rate of this defect is given by [2] $\eta := \frac{\Delta N_\mathrm{t}}{D}$. The defect concentration N_t can be obtained by evaluating the peak height of a DLTS scan according to [9]. The signals of E3 and E5 are also detectable in the temperature range in which the peak of E4 occurs and increase the baseline and therefore contribute to the height of the E4 peak. The modelled overall signal is depicted in Fig. 8.7 (a) for a sample with $x = 0.002$ and a fluence of $D = 4.6 \times 10^{13}\,\mathrm{cm}^{-2}$. The solid line corresponds to the measurement, the dashed line is the result of the calculation.

Repeating the procedure for all samples, we were able to determine the generation

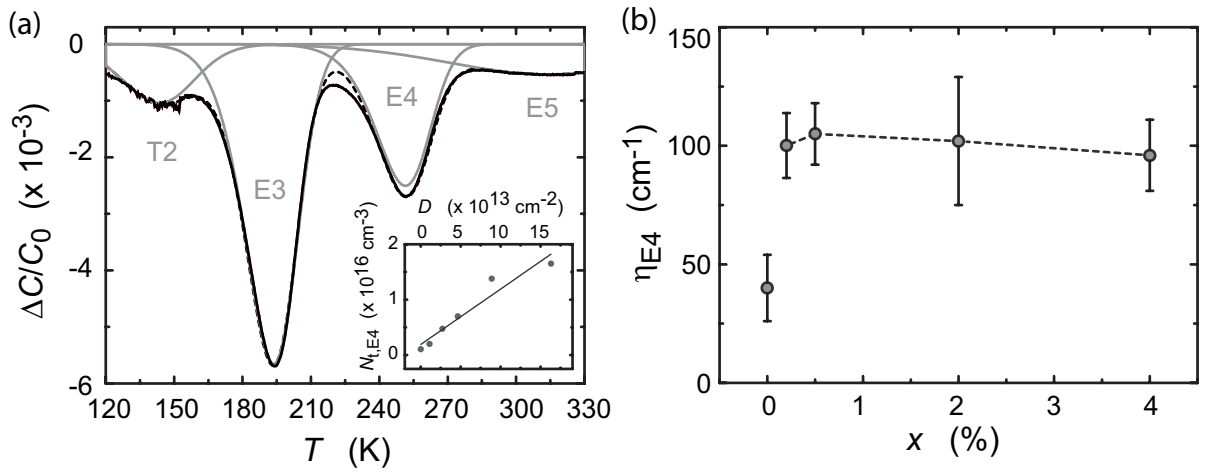

Figure 8.7: (a) DLTS scan of a sample with $x = 0.002$ measured at $V = -2\,\mathrm{V}$ using a pulse voltage of $V_\mathrm{p} = 2.5\,\mathrm{V}$ and a rate window of 125 Hz. The dashed line represents the modeled signal. The inset shows the concentration N_t of E4 vs. the irradiation fluence D for $x = 0.002$. (b) Generation rate η_E4 of E4 over Mg content x obtained from DLTS measurements. Pictures adapted from Ref. [10].

rate η_E4 of E4 as a function of the Mg content x as shown in Fig. 8.7 (b). For the ZnO thin films the generation rate is $\eta = 40 \pm 14\,\mathrm{cm}^{-1}$, which is a factor 3 higher than the value Auret *et al.* obtained from melt-grown ZnO single crystal and a factor of almost 17 higher than that for the SCVT sample. The proton beam Auret *et al.* used for their experiments had an energy of 1.8 MeV and should cause a comparable or at most a slightly higher damage. Evidently the incorporation of E4 is more efficient in ZnO thin films than in ZnO single crystals. The generation rates of E4 for the $\mathrm{Mg}_x\mathrm{Zn}_{1-x}\mathrm{O}$ samples are again about 3 times higher compared to the ZnO thin film. It seems that there is only a minor influence of x itself, since the change of the generation rate with increasing Mg content is small. This demonstrates that the radiation hardness of ZnO thin films is reduced due to the incorporation of Mg. In the present study the generation rate of E4 correlates well with the net-doping density, however in the literature an anti-correlation was observed [1, 2]. Hence a direct connection between $N_\mathrm{d} - N_\mathrm{a}$ and η can be excluded.

[1] M. Hayes *et al.*, Nuclear Instruments and Methods in Physics Research Section B: Beam Interactions with Materials and Atoms **257**, 311 (2007).
[2] F. D. Auret *et al.*, Appl. Phys. Lett. **79**, 3074 (2001).
[3] F. D. Auret *et al.*, Mater. Res. Soc. Symp. Proc. **957** (2007).
[4] B. K. Meyer *et al.*, phys. stat. sol. (b) **241**, 231 (2004).
[5] H. von Wenckstern *et al.*, Journal of Electronic Materials **39**, 584 (2009).
[6] H. von Wenckstern *et al.*, Appl. Phys. Lett. **88**, 092102 (2006).
[7] A. Lajn *et al.*, Journal of Vacuum Science and Technology B **27**, 1769 (2009).
[8] D. Spemann *et al.*, Nuclear Instruments and Methods in Physics Research Section B: Beam Interactions with Materials and Atoms **269**, 2175 (2011).
[9] P. Blood and J. W. Orton, The Electrical Characterization of Semiconductors: Majority Carriers and Electron States (Academic Press, London, 1992).
[10] F. Schmidt *et al.*, Appl. Phys. Lett. **101**, 012103, (2012).

8.8 Implantation-induced gap states in ZnO thin films

F. Schmidt, R. Pickenhain, H. von Wenckstern, S. Müller, S. Geburt*, C. Ronning*, M. Grundmann

*Friedrich-Schiller-Universität Jena, Institute for Solid State Physics

Defects strongly affect various parameters of semiconducting materials such as recombination times, charge carrier lifetimes, deep-level emission and mobility. In order to investigate native defects in ZnO we implanted Ar-ions in ZnO thin films. The films were grown on *a*-plane sapphire substrates by pulsed-laser deposition (PLD) and the implantation was carried out at the Friedrich-Schiller University Jena. The acceleration energies have been varied in a range from 40 keV to 380 keV in order to obtain box-shaped profile with a concentration of $1 \times 10^{16}\ \frac{\text{ions}}{\text{cm}^{-3}}$ Ar-ions within the probed volume.

The samples were investigated by means of deep-level transient spectroscopy (DLTS) and showed signatures of deep levels commonly observed in PLD grown ZnO thin films. Additionally, in a temperature range between 300 K and 340 K we observed a new DLTS signal as illustrated by the dashed line in Fig. 8.8 (a) which is not present in the reference sample (solid line in Fig. 8.8 (a)). The activation energy and apparent capture cross-section of the Ar-implantation induced deep level are 950 meV and $1.3 \times 10^{-13}\ \text{cm}^2$, respectively, which is in accordance with a defect level $E\alpha 2$ found by Nel *et al.* in ZnO single crystals after bombardment with 5.4 MeV α-particles [1] (cmp. Fig. 8.8 (c)). The defect can be fully removed by annealing the sample at 900°C at an oxygen ambient of 700 mbar as shown by the doted line in Fig. 8.8 (a). The concentration of the Ar-induced defect was determined by the peak height of the DLTS signal to be $1 \times 10^{16}\ \text{cm}^{-3}$.

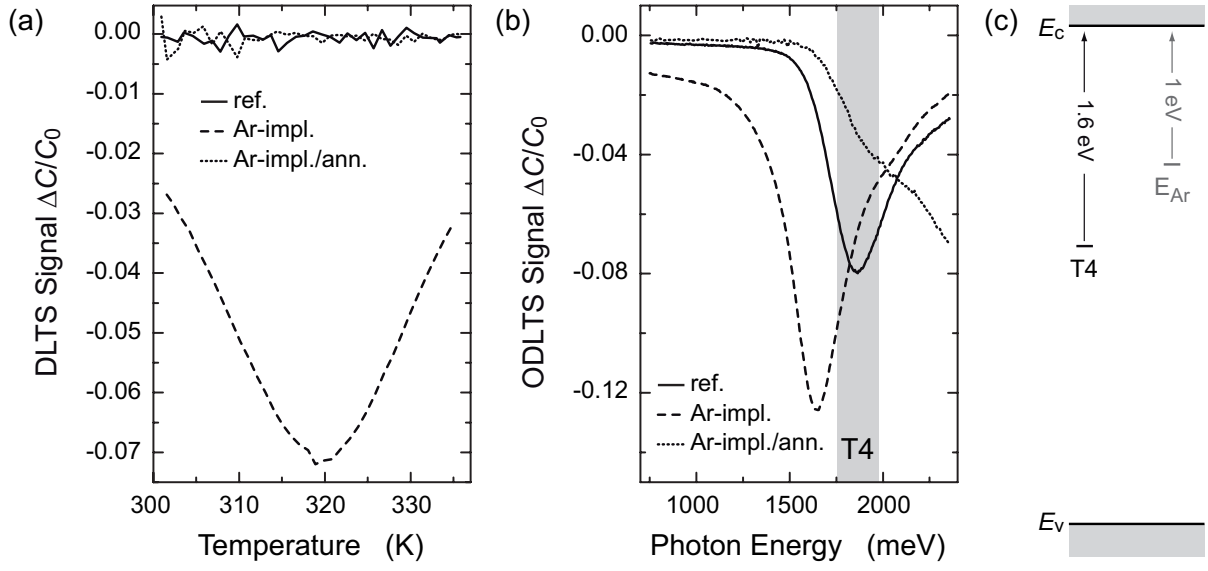

Figure 8.8: (a) DLTS scan and (b) ODLTS spectrum of the untreated (solid line), the Ar-implanted (dashed line) and the annealed Ar-implanted (doted line) ZnO thin film. (c) Schematic band diagram with the energetic positions of the midgap-level T4 and the Ar-introduced defect-level E_{Ar}.

The optical DLTS spectrum of the reference sample (Fig. 8.8 (b)) shows a signal

starting at approximately 1.6 eV which stems from the midgap-level T4 [2]. In the Ar-implanted sample a new feature contributes to the ODLTS signal which already occurs under irradiation with photons having an energy of approximately 1 eV. At 1.6 eV the contribution of T4 is still visible as a shoulder. After annealing the ODLTS signal below 1.6 eV has vanished, which is consistent with the anneal out of the deep level observed in the thermal DLTS measurement. However, the concentration of T4 is reduced in the annealed sample while an increase of the ODLTS signal is observed for photon energies above 2.0eV, indicating that during the annealing E_{Ar} is removed while a defect lying below T4 is introduced.

[1] J.M. Nel *et al.*, Sensors and Actuators B **100**, 270 (2004).
[2] M. Schmidt *et al.*, Sol. State Electron. **75** 48 (2012).

8.9 Defect properties of hydrothermal ZnO with low lithium contamination

R. Heinhold*, H.-S. Kim*, F. Schmidt, H. von Wenckstern, M. Grundmann, R.J. Mendelsberg†, R.J. Reeves*, S.M. Durbin‡ M.W. Allen*

*The MacDiarmid Institute for Advanced Materials and Nanotechnology,
University of Canterbury, Christchurch 8043, New Zealand
†Lawrence Berkeley National Laboratory,
Plasma Applications Group, Berkeley, California 94720, USA
‡Department of Electrical Engineering and Department of Physics,
University at Buffalo, Buffalo, New York 14260, USA

The conductivity of hydrothermal (HT) grown ZnO is strongly influenced by the presence of lithium, introduced via the alkaline mineralizer (LiOH) used to increase the solubility of ZnO precursor material [1–4]. Lithium with typical concentrations of $10^{17} - 10^{18}$ acts as a shallow acceptor on the substitutional Zn site (Li_{Zn}) and appears to effectively compensate the shallow donors responsible for the *n*-type conductivity of ZnO. Therefore the HT grown ZnO crystals are usually characterized by a very low carrier concentration in the $10^{13} - 10^{14}\,cm^{-3}$ range and a high resistivity of $10^2 - 10^3\,\Omega$cm [2, 3]. The removal of Li results in less compensated, lower resistivity *n*-type material desirable for improved device characteristics and reduced impurity diffusion during homoepitaxy. Recently, HT ZnO single crystals with low lithium concentrations (< 0.01 ppm) have become available from Tokyo Denpa Co. Ltd. (Japan) prepared by annealing conventionally grown material at high temperatures (1100 – 1400°C) to drive bulk lithium and other impurities to the surface where it is removed by subsequent surface grinding and re-polishing steps. The low-Li HT ZnO material consisted of pairs of Zn-polar (0001) and O-polar ($000\bar{1}$) face samples cut from a $10 \times 10 \times 0.5\,mm^3$ wafer.

We investigated the electrical and defect properties of low-Li HT ZnO using thermal admittance spectroscopy (TAS) and deep level transient spectroscopy (DLTS). TAS was used to investigate shallow majority carrier traps in low-Li HT ZnO. The measurements were performed in dark conditions over a temperature range of 11 – 330 K, using a

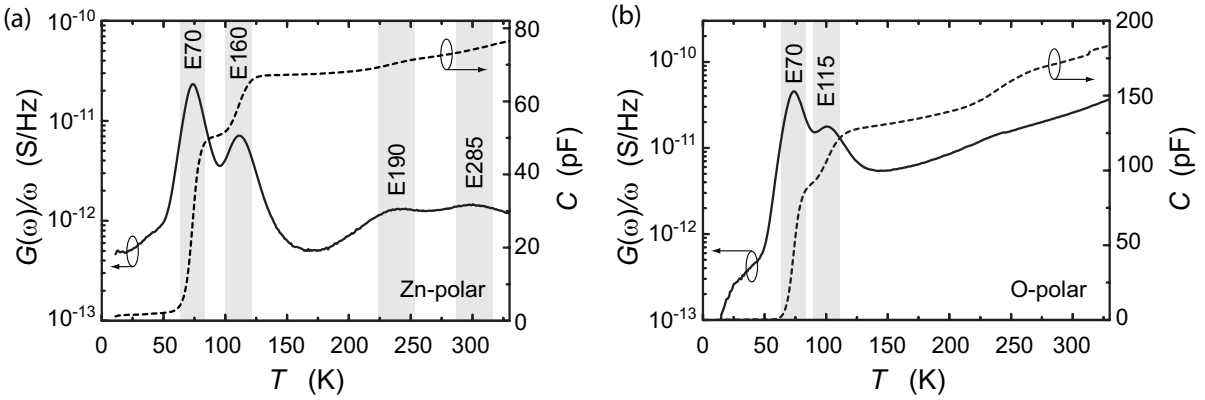

Figure 8.9: Temperature dependence of C and $G(\omega)/\omega$ of the (a) Zn-polar and (b) O-polar ZnO sample, respectively. The samples were measured without external voltage using a fixed test signal frequency of 140 kHz. Pictures adapted from Ref. [9].

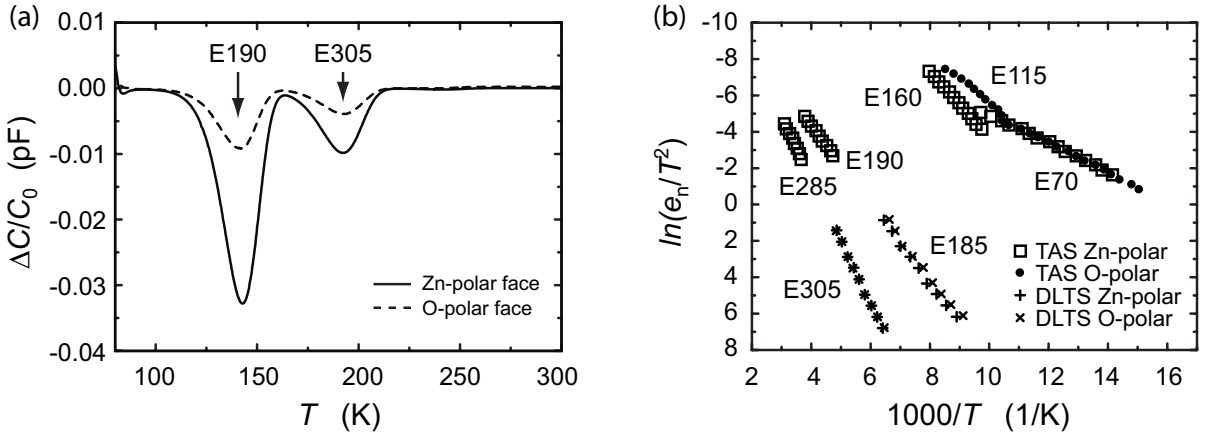

Figure 8.10: (a) DLTS spectra of the Zn-polar and O-polar faces of low-Li HT ZnO (rate window 200 Hz, t_p = 1 ms) and (b) Arrhenius plot of the defect levels obtained from TAS and DLTS. Pictures adapted from Ref. [9].

helium flow cryostat and an Agilent 4294A precision impedance analyzer operated with a test signal of amplitude 50 mV and frequencies from 100 Hz to 10 MHz.

Figure 8.9 shows C vs T and $G(\omega)/\omega$ vs T plots measured with a test signal frequency of 140 KHz. For the Zn-polar face, four distinct electron traps could be observed, which are labeled according to their activation energy in meV. The activation energies and capture cross-sections were extracted via Arrhenius analysis (using the approach of Pautrat *et al.* for the freeze-out peak [5]) as shown in Fig. 8.10 (b). Four different traps E70, E160, E190, and E285 were found on the Zn-polar face, while on the O-polar-face, the same E70 shallow level could be identified along with a different trap E115. E190 and E285 could not be resolved on the O-polar face but this is most likely due to the lower quality of the Schottky contacts on this face since both were observed on the O-polar face using DLTS.

The shallowest donor E17 in conventional HT ZnO attributed to H was not identified in the low-Li HT ZnO samples, which is perhaps not surprising as H_i and H_O are known to be mobile in ZnO at temperatures significantly lower than 1100°C. The main shallow defect E50 in conventional HT ZnO, which is attributed to substitutional Al,

was replaced by E70 here, which may be due to an alternative effective mass donor, such as In, Fe, or Pt.

The emergence of E160 on the Zn-polar face and E115 on the O-polar face were not observed in conventional HT ZnO [6]. Auret *et al.* reported two similar traps in ZnO films grown by pulsed laser deposition and ex-situ annealed at 750°C, which they assigned to a metastable oxygen-related defect and an unassigned donor-like defect, respectively [7]. Schifano *et al.* observed a negative-U donor-type defect with an activation energy ≈ 30 meV above the dominant shallow donor in a HT ZnO wafer which they tentatively assigned to oxygen vacancies [8].

Figure 8.10 (a) shows the DLTS spectra from the Zn-polar and O-polar faces of low-Li ZnO, while Fig. 8.10 (b) shows the corresponding Arrhenius analysis. Two deep defects E190 and E305 were identified on both polar faces. These were the same as those observed on the Zn-polar face in the TAS measurements. E305 is the ubiquitous trap usually referred to as E3 which is observed in many types of ZnO including conventional HT material where it is present in similar concentrations to those measured here but in the form of two closely lying levels E3 and E30. Although the E3 defect is commonly reported in the literature, its assignment is uncertain with oxygen vacancy complexes, Zn interstitials, Fe and Ni impurities having been proposed. Significantly E190, present on both polar faces in higher concentrations than E305, was not observed in conventional HT ZnO but appears to be similar to a level, observed by Schmidt et al. in thermally annealed ZnO films that were either Zn-implanted or grown in Zn-rich conditions. As such E190 may be related to interstitial zinc.

[1] V. Avrutin *et al.*, Proc. IEEE **98**, 1339 (2010).
[2] K. Maeda *et al.*, Semicond. Sci. Technol. **20**, S49 (2005).
[3] E. Ohshima *et al.*, J. Cryst. Growth **260**, 166 (2004).
[4] A. Laufer *et al.*, J. Appl. Phys. **110**, 094906 (2011).
[5] J. Pautrat *et al.*, Solid-State Electron. **23**, 1159 (1980).
[6] H. von Wenckstern *et al.*, Appl. Phys. Lett. **91**, 022913 (2007).
[7] F. D. Auret *et al.*, J. Phys.: Conf. Ser. **100**, 042038 (2008).
[8] R. Schifano *et al.*, Physica B **404**, 4344 (2009).
[9] R. Heinhold *et al.*, Appl. Phys. Lett. **101**, 062105, (2012).

8.10 A pedestrian's approach to continuous composition spread using pulsed-laser deposition

H. von Wenckstern, Z. P. Zhang and M. Grundmann

Properties of multi-component novel material systems are effectively accessed by characterization of material libraries. Such libraries can be obtained, e.g., from discrete [1] or the more elaborate continuous composition spread techniques (CCS) [2–4]. Several different chemical vapor deposition, solution-based or physical vapor deposition methods have been used to apply composition spread techniques. Among the latter are sputtering techniques and pulsed-laser deposition (PLD) being applied most often. In order to achieve a continuous composition spread using PLD two targets A and B are

ablated sequentially and either a mask is moved in front of the substrate to partially shadow one or the other target [5] or the substrate is moved behind a mask to realize the lateral composition spread [6]. Both approaches yield a linear composition gradient and have approved useful for creating material libraries. However, for both approaches movable parts (shadow mask, substrate holder) have to be introduced to the vacuum chamber and this might not always be convenient, e.g. due to lack of space. In this contribution we use a simple, pedestrian approach for creating continuous composition spreads that can be implemented in any PLD chamber without any change of setup. For that we ablate segmented targets as suggested over 40 years ago by Hanak for sputter deposition [3] and created a one-dimensional continuous composition spread for the ternary alloy $Mg_xZn_{1-x}O$.

The source material for the PLD targets were polycrystalline powders of ZnO (purity 5N5) and MgO (4N). From these powders a ZnO target and a ZnO target containing 10wt.% MgO were prepared by ball milling, cold pressing and sintering. The targets were afterwards cut into two pieces with help of a diamond saw. From these pieces the segmented targets were finally obtained.

A CCS thin film was grown on a 2 inch *a*-plane sapphire wafer at a temperature of 650°C and an oxygen background pressure of 0.016 mbar. Cathodoluminescence measurements (CL) were carried out at room temperature in a CamScan CS44 scanning electron microscope. For CL a 5 keV electron beam is scanned over the sample surface and emitted light is focused by an elliptical mirror on a HR320 monochromater equipped with a liquid nitrogen cooled charge-coupled device.

The dependence of the fundamental bandgap E_g of $Mg_xZn_{1-x}O$ on x is linear in the composition range investigated and hence, a variation of the emission energy of a luminescence spectrum can be directly related to a change of x. A systematic shift of the maximal CL emission energy E_{CL} in dependence on the lateral position was observed by room temperature CL measurements and is depicted in fig. 8.11a). In fig. 8.11b) a line scan of E_{CL} is shown. We observe a linear shift of E_{CL} with position. The distance d_l across which the gradient is linear stretches out over the complete wafer with diameter of about 50 mm. This linear change of composition is similar to results obtained by the more involved shadowing CCS-techniques: for (Mg,Zn)O Takeuchi et al. obtained a linear composition gradient; for other material systems such as $(Ca_{1-x}Ba_x)_3Co_4O_9$ with $d_l \approx 10\,\text{mm}$ [5] or $(Sr_{1-x}Ca_x)RuO$ with $d_l \approx 35\,\text{mm}$, linear composition gradients were reported as well. Our "pedestrians approach" resembles results achieved with multi-target, shadowing PLD techniques and extends d_l to 50 mm.

From the results presented we conclude that our simple CCS-method is well suited for creating material libraries. The elemental concentration changes linearly along the direction of the gradient enabling a fast and cheap exploration of new material systems.

[1] X.-D. Xiang and X. Sun and G. Briceño and Y. Lou and K.-A. Wang and H. Chang and W. Wallace-Freedman and S-.W. Chen and P. G. Schultz, Science **268**, 1738 (1995)
[2] E. Sawatzky and E. Kay, IBM Journal of Research and Development **13**, 696 (1969)
[3] J. J. Hanak, Journal of Materials Science **5**, 964 (1970)
[4] R. B. van Dover AND L. F. Schneemeyer AND R. M. Fleming, Nature **392**, 162 (1998)

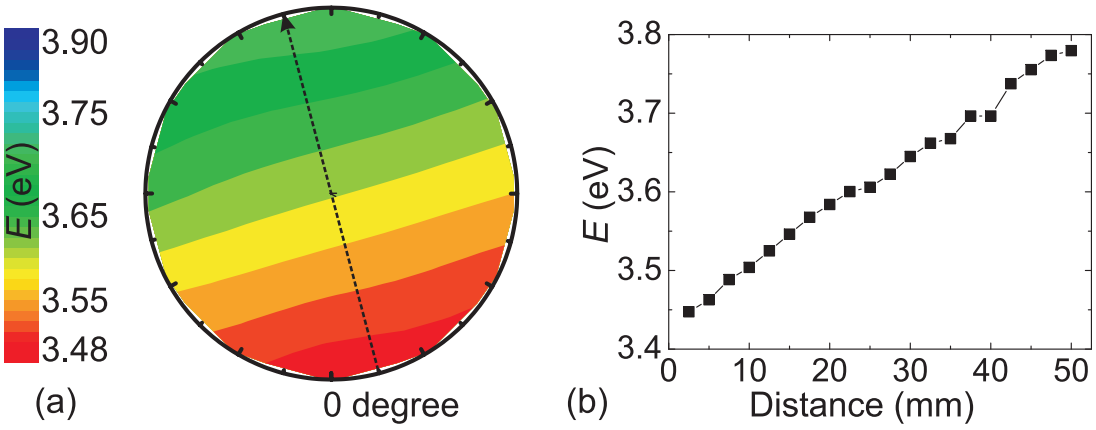

Figure 8.11: a) False color map of the maximum emission energy of room temperature CL measurements. Along the arrow in the figure the line scan shown in b) was acquired.

[5] H. Minami and K. Itaka and H. Kawaji and Q. J. Wang and H. Koinuma and M. Lippmaa, Appl. Surf. Science **197-198**, 442
[6] H. M. Christen and C. M. Rouleau and I. Ohkubo and H.Y. Zhai and H. N. Lee and S. Sathyamurthy and D. H. Lowndes, Review of Scientific Instruments **74**, 4058 (2003)

8.11 Optoelectronic applications of wide-bandgap oxide semiconductors

Z. P. Zhang, R. Karsthof, M. Winter, F-L. Schein, H. von Wenckstern, and M. Grundmann

Transparent semiconducting oxides (TSO) [1] are recently investigated with large effort due to their tremendous potential for applications in transparent electronics. In recent years, ultraviolet (UV) photodetectors (PDs) based on wide-bandgap oxide semiconductors have been developed and find applications for aircraft protection, chemical agent sensing, flame detection and UV-astronomy [2]. We report on the fabrication of photodiodes employing rectifying contacts for transparent optoelectronics based on ZnO [3] and the ternary (Mg,Zn)O system in wurtzite modification utilizing a new concept of a compositionally graded active layer allowing to design visible blind, energy-selective, monolithic multichannel UV-PDs [4]. For transparent photovoltaics we used amorphous p-$ZnCo_2O_4$ (zinc spinels) as a heterojunction on top of a n-ZnO thin film [5].

8.11.1 ZnO-based UV photodetectors

The bandgap (E_g = 3.4 eV) and large binding energy (60 meV) at room temperature makes ZnO a promising candidate for next generation of transparent optoelectronics. Herein, the electrical properties of PdO_y/ZnO Schottky contacts (SCs) and its applicability as visible blind UV-PDs are investigated. First, using pulsed-laser deposition (PLD) a 200 nm thick highly aluminum doped ZnO thin film (10^{21} cm^{-3}) serving as ohmic back

contact [6], and subsequently a nominally undoped ZnO thin film ($10^{16}\,\mathrm{cm}^{-3}$) with a thickness of about 1 µm were deposited on an a-plane sapphire substrate (see inset of Figure 8.12 (a)). The growth temperature and oxygen partial pressure was 650 °C

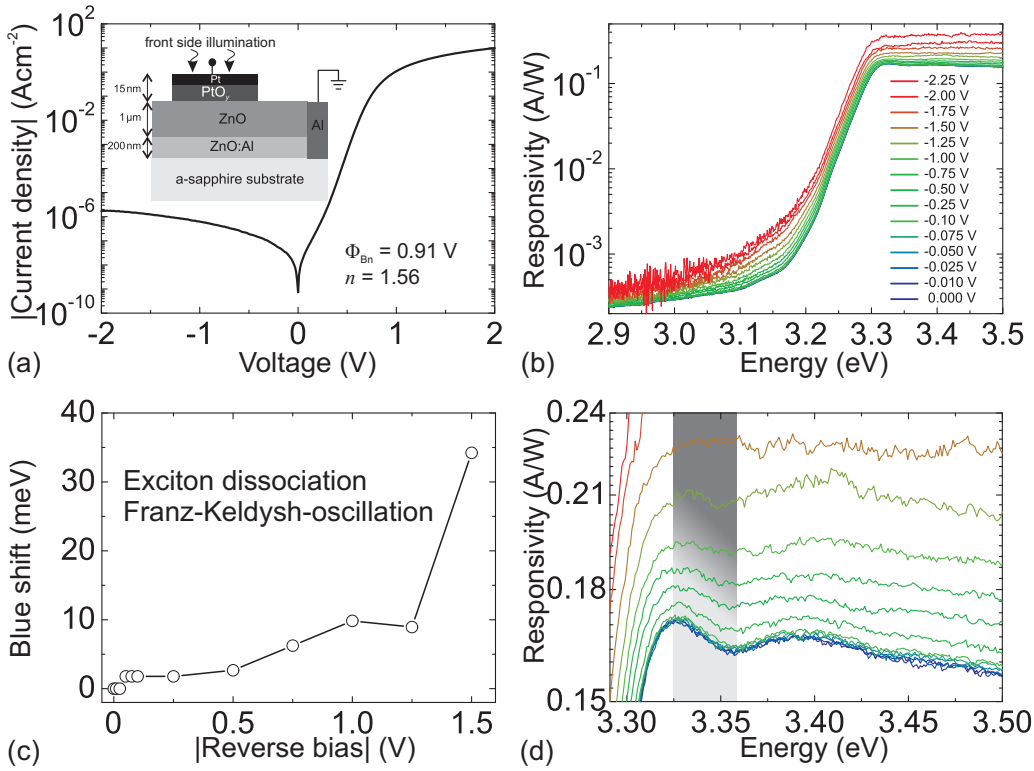

Figure 8.12: (a) *I-V* characteristic of the PdO$_y$/ZnO SC measured in dark conditions, the inset depicts the schematic layout of the device; (b) spectral responsivities of the SC under front side illumination at varying reverse biases; (c) blue shifts of maximum responsivities versus reverse biases up to −1.5 V; (d) a photocurrent modulation by Franz-Keldysh oszillation around fundamental bandgap.

and 0.016 mbar, respectively. Circular SCs were fabricated by reactive DC-sputtering comprising a metallic capping layer [7]. Figure 8.12 (a) shows the current-voltage (*I-V*) characteristic of a PdO$_y$/ZnO SC, which exhibits an effective barrier height of 0.91 V, an ideality factor of 1.56 and a rectification ratio ($|j(-1\,\mathrm{V})/j(+1\,\mathrm{V})|$) of about six orders of magnitude.

The spectral response of the SC under front side illumination in photovoltaic mode (0 V) and at different reverse biases up to −2.25 V are depicted in Figure 8.12 (b). For sub-bandgap illumination photocurrent is strongly suppressed. In particular no photocurrent is generated for illumination with green light. For energies higher than the bandgap a photocurrent is generated, the UV-visible rejection ratio is above 10^3. The SC exhibits an internal gain caused by hole-trapping at PdO$_y$/ZnO-interface (not shown) [4]. Figure 8.12 (d) shows the photo response spectra of Figure **??** (b) with different scale around E_g. For increasing reverse biases up to −1.5 V, we observed blue shift up to 34 meV in transition energies, depicted in Figure 8.12 (c). This behavior is due to Franz-Keldysh oscillation (FKO) [8], which modulates the photocurrent for $E \geq E_g$.

8.11.2 Transparent solar cells based on *p*-$ZnCo_2O_4$/*n*-ZnO heterostructure

For realization of transparent electronics *p*-type and *n*-type material is required. Besides *n*-type ZnO we used *p*-$ZnCo_2O_4$ (zinc spinel), due to its preserved *p*-type conductivity even for amorphous films deposited at room temperature, compared to other promising candidates like $CuAlO_2$ or SnO_x.

First, a metallic conducting *n*-ZnO:Al and a nominally undoped *n*-ZnO layer were grown as the SC of section 8.11.1. Afterwards a 100 nm thin $ZnCo_2O_4$ layer was grown using PLD at room temperature and an oxygen partial pressure of 0.1 mbar followed by deposition of a DC-sputtered gold capping layer in pure argon atmosphere (see inset of Figure 8.13 (a)). The $ZnCo_2O_4$ thin film was X-ray amorphous and its *p*-type

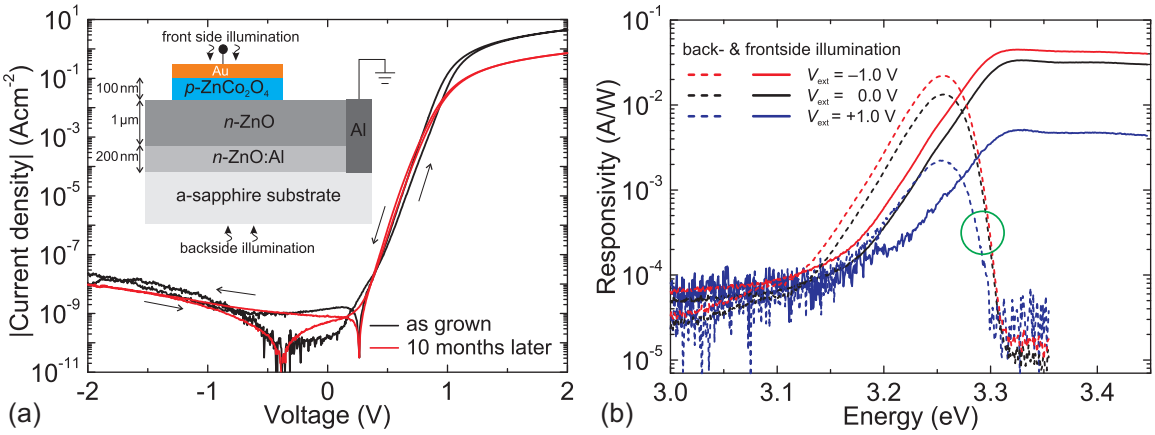

Figure 8.13: (a) Time dependent double-sweep *I-V* characteristics of the *pn*-heterojunction (inset: schematic layout of the device); (b) spectral responsivity of the device under back- and front side illumination measured at 0, ±1 V biases.

conductivity was confirmed by Seebeck-coefficient measurements [5]. Figure 8.13 (a) shows double-sweep *I-V* characteristics of *p*-$ZnCo_2O_4$/*n*-ZnO heterojunction acquired right after fabrication and 10 months after fabrication. It exhibits a clear rectifying behavior with a rectification ratio ($|j(-1\,\mathrm{V})/j(+1\,\mathrm{V})|$) about seven orders of the magnitude. As can be seen from the figure, the current density decreases at high forward biases after 10 months with increasing of ideality factor and series resistance. A small hysteresis ($\Delta V = 0.5\,\mathrm{V}$) due to charge carriers trapping at interface of the junction for both measuring directions is visible.

Figure 8.13 (b) shows the spectral responsivities of this *pn*-junction under back- as well as front side illumination for different bias. The photo response measurements under backside illumination, which are depicted as the dashed lines, a bandpass-like behavior is observed. This is due to light absorption within the ZnO:Al back-contact layer. It absorption edge is because of the Burstein-Moss shift higher than in the nominally undoped ZnO in the active layer. The bandwith is about 47 meV. The responsivities under front side illumination extends expectedly to the deep UV range keeping a constant photo response. In both configuration, the photo response in visible blind region was accompanied with a contrast of more than three orders of magnitude without internal gain effect (not shown) and higher responsivities at reverse biases were achieved due to wider depletion layer. Similar to PdO_y/ZnO SCs,

the photo current here was also modulated by FKO (not shown). For realization of a energy-selective photodiode based on p-$ZnCo_2O_4$/n-ZnO heterojunction, the ternary semiconductor (Mg,Zn)O thin films instead of ZnO role with varying Mg-content can be well suited.

8.11.3 Monolithic multichannel photodiodes based on (Mg,Zn)O

Utilization of ternary semiconductor (Mg,Zn)O system in wurtzite modification enables the construction of visible blind, energy-selective and narrow bandwidth UV-PDs [4]. We demonstrated monolithic multichannel UV-narrowband (Mg,Zn)O-PD arrays based on novel design of continuously changing bandgap of across the spread of active $Mg_yZn_{1-y}O$-layer (see Figure 8.14 (b)), which makes the tuning of cutoff energy and bandwidth possible [9]. In order to achieve a linear continuous composition gradient, we use a segmented PLD-target (see Figure 8.14 (a)). The interdiffusion at

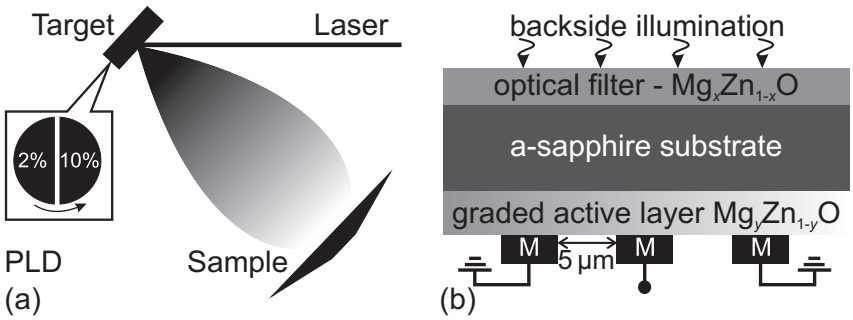

Figure 8.14: (a) PLD-chamber with a discrete target of Mg-contents enabling compositionally graded Mg-profile of active layer of the MSM-PD with (b) a $Mg_yZn_{1-y}O$/a-sapphire/$Mg_xZn_{1-x}O$ structure ($y < x$) under backside illumination.

the interface between filter and active layer of our present design with (Mg,Zn)O-heterostructure [4] and the diffusion of carriers generated within the optical filter layer to the active layer can affect the spectral response of PDs. Therefore, we separate the filter and active layer in order to minimize these effects. Thereby, as the first step of our multichannel arrays, a filter layer with a single Mg-content was grown on a 2 inch double-side polished a-plane sapphire wafer. Subsequently, the active layer with a linear graded Mg-profile was deposited on the other side of the wafer. The growth temperature and oxygen partial pressure was 650 °C and 0.016 mbar, respectively. The lateral variation of the chemical composition was measured by energy dispersive X-ray spectroscopy (not shown).

Figure 8.15 (c) shows room temperature cathodoluminescence (CL) measurements over the sample surface in dependence on the lateral position for both layers. A slight variation of the maximum CL intensity of the filter layer is noticeable, whereas a systematic shift, depending on the lateral position of the active layer, is observed. An obvious linearity of CL intensity of active layer in dependence on the lateral position (depicted as dashed line in Figure 8.15 (a)) is shown in Figure 8.15 (d). The lowering of CL intensity of filter layer in the wafer center is is due to slightly higher growth temperature.

Figure 8.16 (a,b,c) show the normalized responsivities of metal-semiconductor-metal (MSM) PDs versus photon energy for various positions depicted in Figure 8.15 (b).

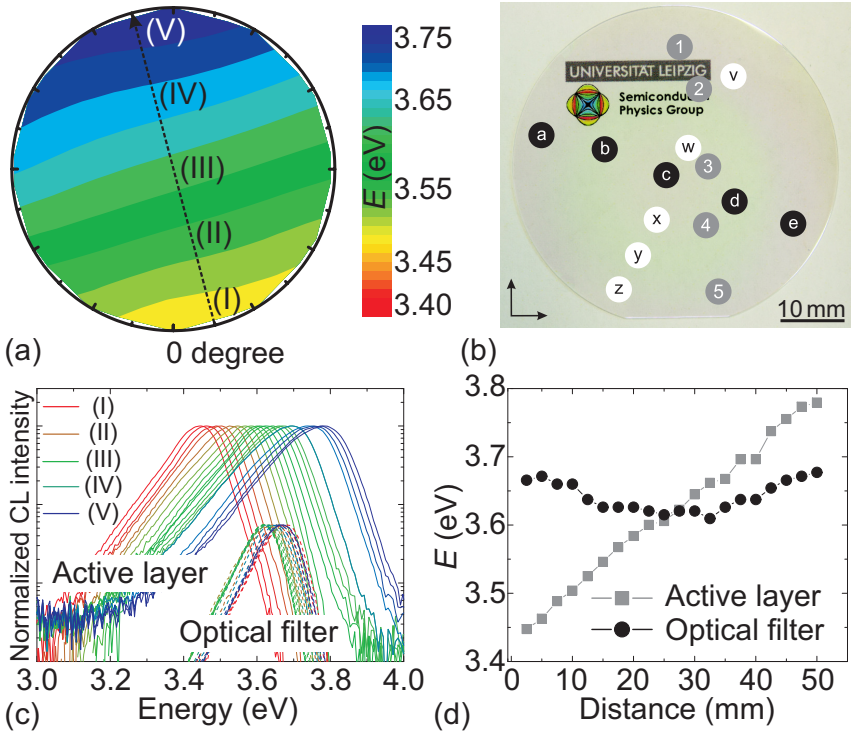

Figure 8.15: (a) Contour plot of the maximum emission energy of the room temperature CL measurements; (b) image of a transparent 2 inch (Mg,Zn)O-wafer, the photo responses were measured at depicted positions; (c,d) CL spectra of both layers along the orientation marked by dashed line of (a).

As can be seen, the high energy cutoffs are due to absorption in the optical filter layer and their slight differences are caused by the small variation of the Mg-content in the filter layer (cf. Figure 8.15). The different low cutoff energies indicate a compositionally graded active layer, which have detect and process signals at different energy simultaneously with in principle high spectral resolution.

Figure 8.16 (e,f,g) show false color maps of cutoff energies and bandwidths of the PDs. As the CL contour plot of Figure 8.15 (a), a longitudinal blue shift of low cutoff energies corresponding the active layer was achieved. Due to the only slightly varied high cutoff energies, a decreasing of bandwidth along the orientation of CL line scans was measured and shown in Figure 8.16 (g). Ideally, an energy selective, narrow-bandwidth multichannel MSM-PD array was fabricated only from sample pieces for which the bandgap satisfies the condition of $E_g^y < E_{ph} < E_g^x$. It means that for $d > 25\,mm$ (cf. Figure 8.15 (d)), the PD should not respond at all, while the measurements was not the case due to insufficient thickness of the filter layer for complete absorption.

[1] M. Grundmann, H. Frenzel, A. Lajn, M. Lorenz, F. Schein, and H. von Wenckstern, phys. stat. sol. (a) **207**, 1437 (2010), doi: 10.1002/pssa.200983771
[2] M. Razeghi and A. Rogalski, J. App. Phys. **79**, 7433 (1996), doi: 10.1063/1.362677
[3] A. Lajn, M. Schmidt, H. von Wenckstern, and M. Grundmann, J. Electron. Mater. **40**, 473 (2011), doi: 10.1007/s11664-010-1395-x
[4] Z. P. Zhang, H. von Wenckstern, M. Schmidt, and M. Grundmann, Appl. Phy. Lett. **99**, 083502 (2011), doi: 10.1063/1.3628338

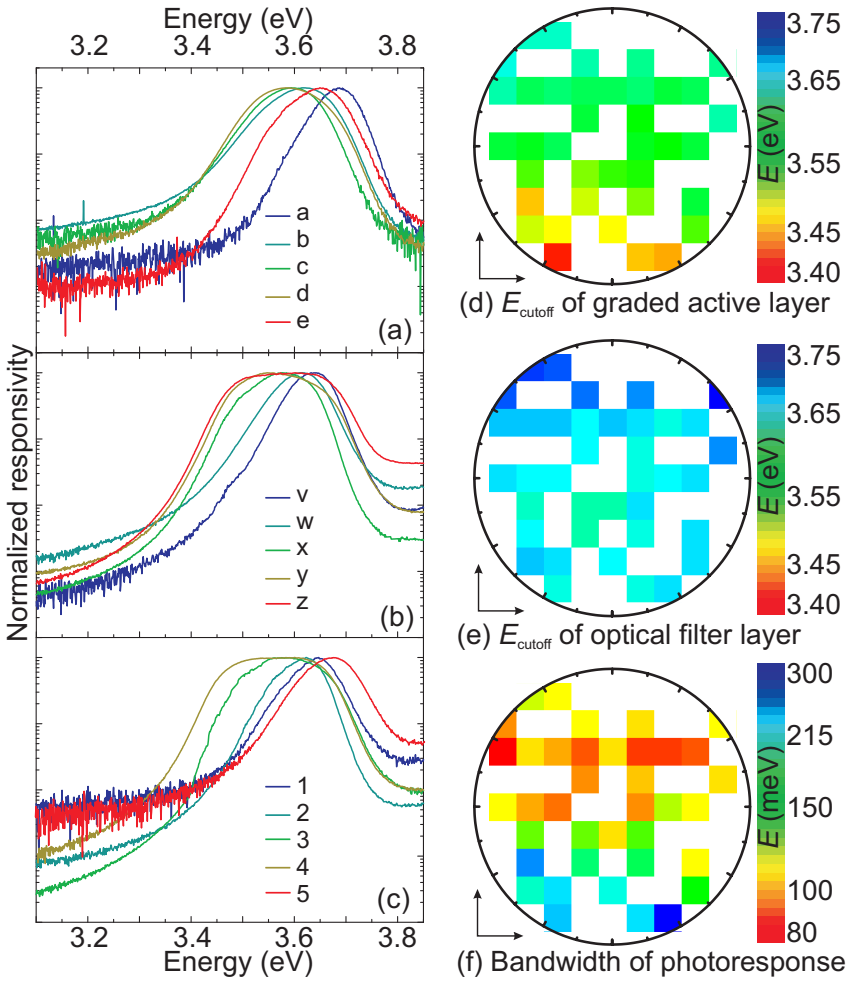

Figure 8.16: (a,b,c) Normalized spectral responsivity of multichannel MSM-PDs as a function of photon energy of different orientations as depicted in Figure 8.15 (a); (e,f) false color maps corresponding the wafer of cutoff energies and (g) bandwidth of photo response.

[5] F-L. Schein, H. von Wenckstern, H. Frenzel, and M. Grundmann, IEEE Electron Lett. **33**, 676 (2012), doi: 10.1109/LED.2012.2187633

[6] H. von Wenckstern, G. Biehne, R. Abdel Rahman, H. Hochmuth, M. Lorenz, and M. Grundmann, Appl. Phys. Lett. **88**, 092102 (2006), doi: 10.1063/1.1638898

[7] A. Lajn, H. von Wenckstern, Z. Zhang, C. Czekalla, G. Biehne, J. Lenzner, H. Hochmuth, M. Lorenz, M. Grundmann, S. Wickert, C. Vogt, and R. Denecke, J. Vac. Sci. Technol. B. **27**, 1769 (2009), doi: 10.1116/1.3086718

[8] H. von Wenckstern, H. Schmidt, R. Pickenhain, and V. Gottschalch, phys. stat. sol. (a) **190**, 709 (2002), doi: 10.1002/1521-396X(200204)190:3<709::AID-PSSA709>3.0.CO;2-7

[9] I. Takeuchi, W. Yang, K.-S. Chang, M. A. Aronova, T. Venkatesan, R. D. Vispute, and L. A. Bendersky, J. App. Phys. **94**, 7336 (2003), doi: 10.1063/1.1623923

8.12 Determination of unscreened single-exciton state in polar ZnO/(Mg,Zn)O quantum wells

M. Stölzel, A. Müller, G. Benndorf, M. Brandt, M. Lorenz and M. Grundmann

We performed low temperature (T = 2 K) time-integrated (TI-) and time-resolved (TR-) photoluminescence (PL) measurements on polar ZnO/(Mg, Zn)O quantum wells (QWs) grown by pulsed laser deposition in an oxygen ambient on a-plane sapphire substrates (T = 650 °C, $p(O_2)$ = 0.004 mbar). Even at moderate excitation densities screening effects have to be considered in these structures [1]. For a ZnO QW with a well width of d_{QW} = 6 nm and a $Mg_{0.3}Zn_{0.7}O$ barrier, for example, an electron-hole pair density as low as 10^{10} cm^{-2} blue-shifts the single-exciton transition energy E_0 due to screening [2]. For well widths larger than the Bohr radius of the exciton, the internal electric field separates electron and hole which leads to decay times up to milliseconds [3]. Therefore an equilibrium between accumulation and recombination (decay time decreases with increasing pair density) establishes. This makes it very hard to determine E_0 directly from continuous-wave (cw) excited PL with a sufficiently high signal-to-noise ratio.

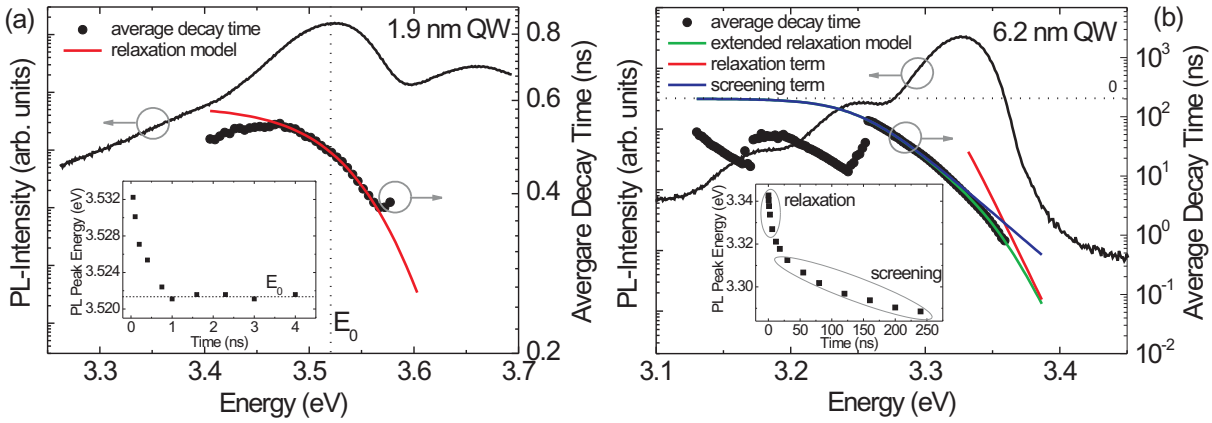

Figure 8.17: Low power TI-PL intensity (left scale) and decay time (right scale) as a function of energy for QWs with (a) 1.9 nm and (b) 6.2 nm well width. The insets show the time-evolution of the respective luminescence maximum determined from the time-delayed spectra.

Figure 8.17 (a) shows exemplarily the dependence of the decay time on emission energy for $d_{QW} \leq 2.5$ nm. It reaches a maximum clearly below the luminescence maximum. The exponential decrease with increasing energy is commonly described by a relaxation model [4] $\tau^{-1}(E) = \tau_0^{-1}(1 + \exp((E - E_{me})/E_t))$ to determine the decay time τ_0 of the single-particle state (E_t represents the depth of the tail states and E_{me} is an energy analogous to a mobility edge). It fits the experimental data well in the region of the luminescence maximum[1] as the influence of the internal electric field is negligible for these well widths. The excitonic transition energy E_0 of the single-particle state can be determined by low power cw excited PL or by the time-evolution of the peak maximum from TR-PL as shown exemplarily for a QW with d_{QW} = 1.9 nm in the inset of Fig. 8.17 (a). Relaxation of hot carriers is visible up to 1 ns after the exciting laser

[1] For high (low) energies the transients are superposed by the barrier (phonon) decay.

pulse. Afterwards the luminescence maximum remains constant over time indicating E_0 of the QW, demonstrating, that E_0 is determined mainly by confinement effects.

Figure 8.17 (b) shows exemplarily the dependence of the decay time on emission energy for $d_{QW} \geq 2.5\,\text{nm}$. To model this dependence to obtain τ_0 of the single-exciton state, we proposed an extended relaxation model $\tau^{-1}(E) = \tau_0^{-1}(1+\exp((E-E_{\text{me}})/E_{\text{t}})+\alpha(E))$ incorporating a screening term $\alpha(E)$. Taking into account an exponential decrease of τ with increasing energy, we assume $\alpha(E) \sim \exp((E-E_1)/E_2)$ analogous to the relaxation term with a characteristic energy E_1 at which τ equals $\tau_0/2$. The relaxation term describes $\tau(E)$ at small decay times and the screening term at larger ones quite well,[2] as can be seen in Fig. 8.17 (b).

The inset in Fig. 8.17 (b) shows the time-evolution of the luminescence maximum of a QW with $d_{QW} = 6.2\,\text{nm}$. Again, carrier relaxation is visible for the first few nanoseconds. Afterwards the transition energy decreases over time due to a restoral of the internal electric field by recombination and diffusion of the excited excitons. E_0 cannot be determined within reasonable time and intensity scales and an analytical function to describe $E(t)$ has not been reported so far.

With this model it is possible to determine the dependence of τ_0 on well width as shown in Fig. 8.18. A numerical simulation [5] of this dependence provides the difference in total polarization between well and barrier material ($\Delta P = x\,\phi$, Mg content x) and fits best for a value of $\phi = 0.026\,\text{C/m}^2$ resulting in an internal electric field of $(1.01 \pm 0.12)\,\text{MV/cm}$. With the internal electric field it is possible to evaluate the dependence of E_0 on well width as shown in Fig. 8.18.

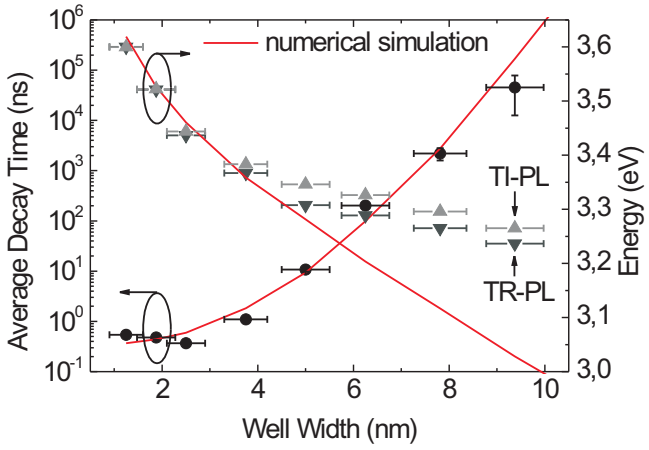

Figure 8.18: Dependence of the single-exciton average decay time and transition energy on the QW width. The numerical simulation fits the decay time very well. Above a QW width of 4 nm, the respective calculated transition energy is lower than the experimentally determined one due to screening effects.

[1] S. Kalusniak et al.: Phys. Rev. B **77**, 113312 (2008).
[2] C. Hall et al.: Phys. Rev. B **80**, 235316 (2009).
[3] C. Morhain et al.: Phys. Rev. B **72**, 241305 (2005).

[2] This holds up to the maximum of the first phonon replica, afterwards the transients are dominated by phonon replica decay and the $\tau(E)$-dependence recurs.

[4] C. Gourdon and P. Lavallard: phys. stat. sol (b) **158**, 641 (1989).
[5] M. Brandt et al.: Appl. Phys. Lett. **97**, 052101 (2010).

8.13 First-order resonant Raman scattering by longitudinal optical phonons in wurtzites

C. Kranert, R. Schmidt-Grund, M. Grundmann

We have investigated the exciton-mediated Raman-scattering in wurtzite crystals excited above the band gap. The first-order scattering by longitudinal optical phonons involves an elastic scattering process breaking the momentum conservation. However its microscopic origin has not been explained conclusively in the literature. Therefore this process is of special interest. We could show that the elastic scattering not only occurs at impurities, but also at the excited surface which is the dominant contribution for crystals with sufficiently low impurity concentrations.

For the theoretical description of this scattering process, we applied the double resonance model of R.M. Martin [1]. The wave vector dependent Raman tensor for Fröhlich interaction was calculated according to the work of C. Trallero-Giner et al. [2]. It consists of three contributions: scattering from a discrete exciton state into another discrete exciton state (*dd*), scattering from a discrete state into a continuum state and vice versa (*dc*) and scattering between two continuum states (*cc*). The result for ZnO excited at 325 nm is shown in Fig. 8.19. It can be seen that the contribution only involving continuum states can be neglected. Thus, scattering mainly occurs via intermediate discrete exciton states.

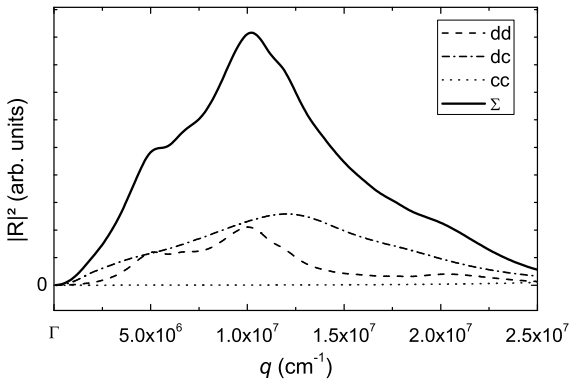

Figure 8.19: Fröhlich Raman tensor element $|R|^2 = |R_{dd} + R_{dc} + R_{cc}|^2$ (*solid line*) and the three individual contributions (see text) calculated for first order LO scattering in ZnO excited at 325 nm.

The calculated Raman tensor can be used to compare simulated spectra for different mechanisms causing the relaxation of momentum conservation, if these show different transition probability profiles in dependence on the wave vector. We simulated spectra for the softening of the wave vector due to absorption and for elastic scattering at the excited surface (Fig. 8.20). The comparison to experiment shows a good agreement

only for elastic scattering at the surface, supporting that this is the dominant scattering mechanism. This is in accordance to previous results obtained by us by measurements in oblique backscattering geometry [3].

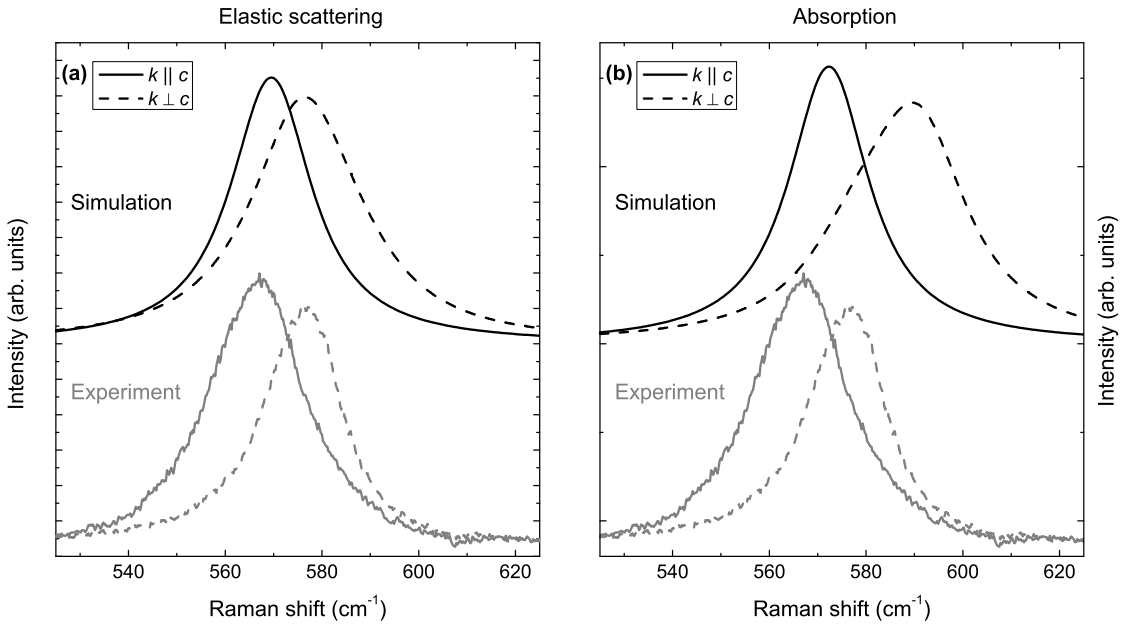

Figure 8.20: Calculated (*black*) and experimental (*grey*) spectra of the 1LO line of ZnO excited at 325 nm for backscattering with normal incidence on the *c*-plane (*solid line*) and on the *a*-plane (*dashed line*), respectively. The calculated spectra assume a relaxation of momentum conservation caused by elastic scattering at the surface **(a)** and the absorption of the incident light **(b)**, respectively. The experimental spectra are the same in both subfigures for comparison.

Another application of the calculations is to explain the discrepancy between the Stokes- and the anti-Stokes spectrum corrected for thermal occupation. The experimental spectra in Fig. 8.21 (a) show an anti-Stokes 1LO line which is lower in intensity than expected and which peaks at a slightly lower Raman shift than its Stokes equivalent. Both these observations can also be found in the simulated spectra in Fig. 8.21 (b). The decreased intensity can be assigned to a decreased contribution of the out-scattering resonance because of the larger energy difference between the anti-Stokes photon and the band gap energy. The spectral shift originates from the involvement of phonons with larger wave vectors in the scattering process.

[1] R.M. Martin: Phys. Rev. B **10**, 2620 (1974).
[2] C. Trallero-Giner et al.: Phys. Rev. B **45**, 6601 (1992).
[3] C. Kranert et al.: in *The Physics Institutes of Universität Leipzig, Report 2011*, M. Grundmann (Ed.), pp. 179, Leipzig, 2012.

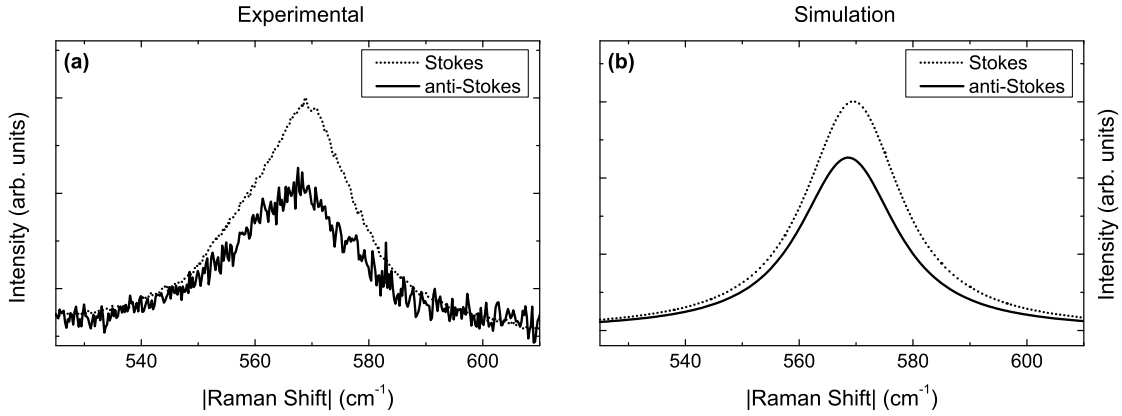

Figure 8.21: Experimental **(a)** and simulated **(b)** spectra of the 1LO-Stokes- (*dotted line*) and anti-Stokes-line (*solid line*). The experimental spectrum has been corrected by the thermal occupation factor at $T = 300$ K.

8.14 Spatially resolved investigations on strained ZnO microwires

S. Lange, T. Michalsky, C.P. Dietrich, J. Lenzner, M. Grundmann

Hexagonal ZnO wires are several ten µm long and a couple of µm thick. When they are bent uniaxially along their crystallographic c-axis they grant the unique opportunity to study the effect of deformation on the band structure of semiconductors since they exhibit both types of strain: compressive strain at the inner (concave) and tensile strain at the outer (convex) side of the bent wire. After growth by means of carbothermal evaporation, the wires were transferred to sapphire substrates and then bent with tweezers (Fig. 8.22 (a)). The optical characterization was done using spatially resolved micro-photoluminescence (µm-PL) and cathodoluminescence (CL) spectroscopy. The experiments showed that for small strains of the order of magnitude of 0.5 % the variation of the band gap energy ΔE_G follows a linear behavior (Fig. 8.22 (b)), $\frac{\partial \Delta E_G}{\partial \varepsilon_{zz}} = (-2.087 \pm 0.053)$ eV, confirming former results [1]. A redshift is observed in the case of tensile strain and a blueshift for compressive strain.

A splitting of the bound exciton lines can be observed in the area of compressive strain (Fig. 8.23 (a)) since in this regime the energetic separation between B and C valence band increases, whereas their energetic spacing remains nearly the same in the presence of tensile strain according to simulations done by Liao et al. [2] (Fig. 8.23 (b)).

For even higher strain (e.g. greater than 1.5 %) the band gap shift becomes more and more nonlinear meaning that the redshift gets stronger than the blueshift as shown in Fig. 8.23 (c). This effect is associated with the strain gradient which causes an additional redshift (also at the neutral fiber) and which has nonlinear influence on the blueshift [3]. The largest gained strain was 3.8 % for a wire with diameter of 1 µm.

[1] C. P. Dietrich et al.: Appl. Phys. Lett. **98**, 031105 (2011).
[2] Z. Liao et al.: Sci. Rep. **2**, 452 (2012).
[3] X. Han et al.: Adv. Mater. **24**, 4707 (2012).

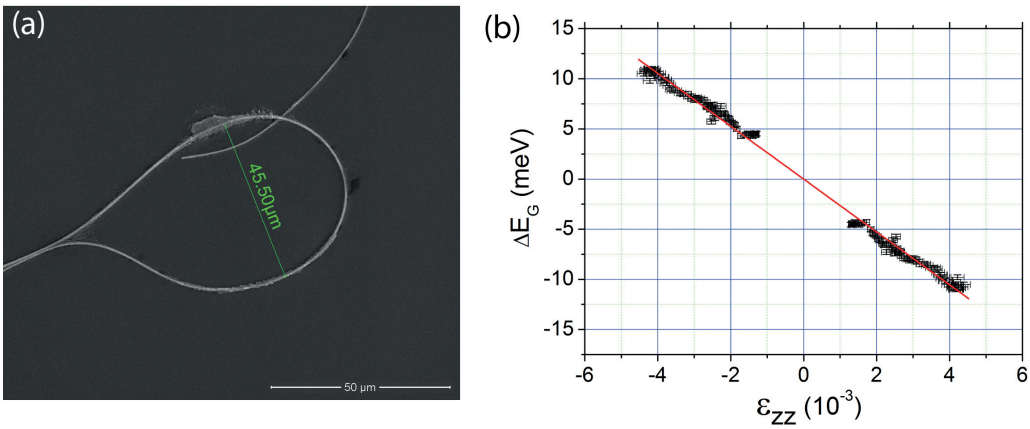

Figure 8.22: (a) Example for an extremely bent microwire on a sapphire substrate. (b) Linear dependence of the energy gap for small strains.

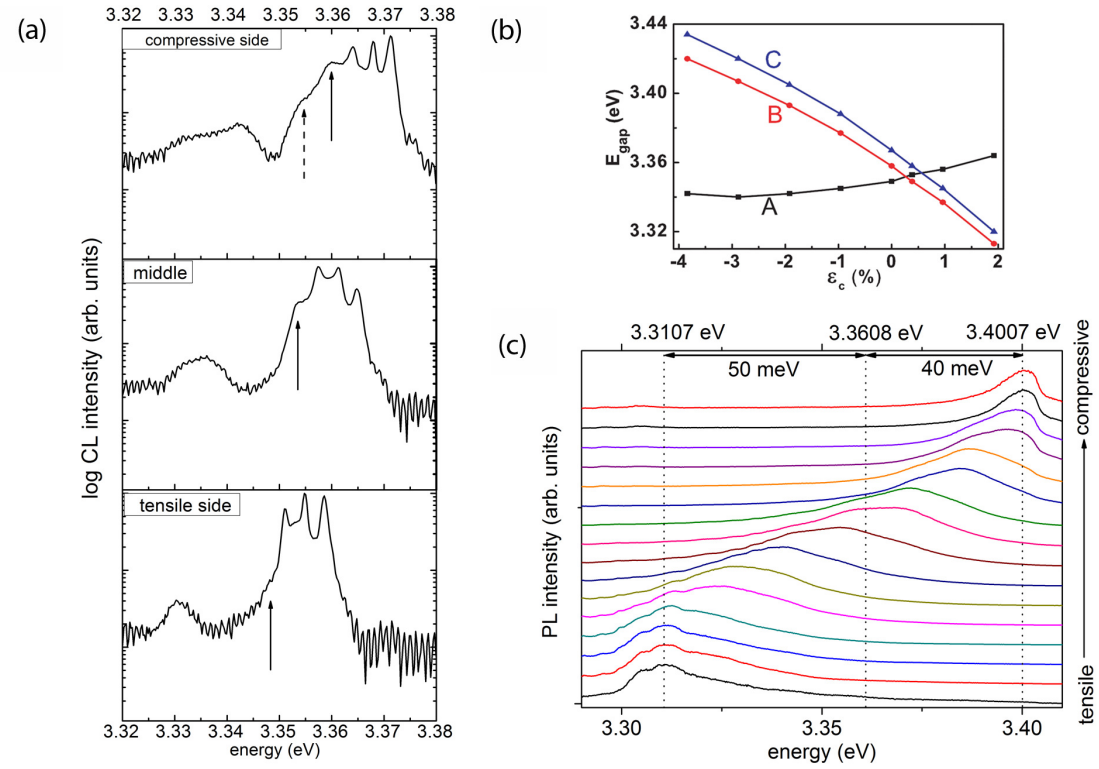

Figure 8.23: (a) Spectra taken from three cross-sectional positions on a microwire showing the appearance of two new peaks due to increasing splitting of the valence bands when going from the tensile to the compressive side. (b) Simulation of the transition energies between conduction band and the three valence bands as a function of uniaxial strain along the c-axis done by Liao et al. [2]. (c) Linescan of a ZnO-microwire along its cross section with maximum strain of (±2.5) % at its outer (+) respectively its inner (-) surface which shows stronger redshift than blueshift with an entire shift of approximately 90 meV.

8.15 Corner effect in hexagonal whispering gallery mode resonators

C.P. Dietrich, M. Lange, T. Böntgen, M. Grundmann

The improvement of light emitters and their optical resonators has become one of the prominent fields of research in recent years due to the increasing demand for photonic and optoelectronic devices. Experimentally, it has been shown that ZnO microwires naturally embody dielectric hexagonal resonators by exhibiting whispering gallery mode (WGMs) signatures in luminescence spectra [1]. Here, we examine the role of the corners of the microwire cross section in light out-coupling, mode quality factor, and threshold of WGM lasing - all crucial parameters for highly efficient laser operation.

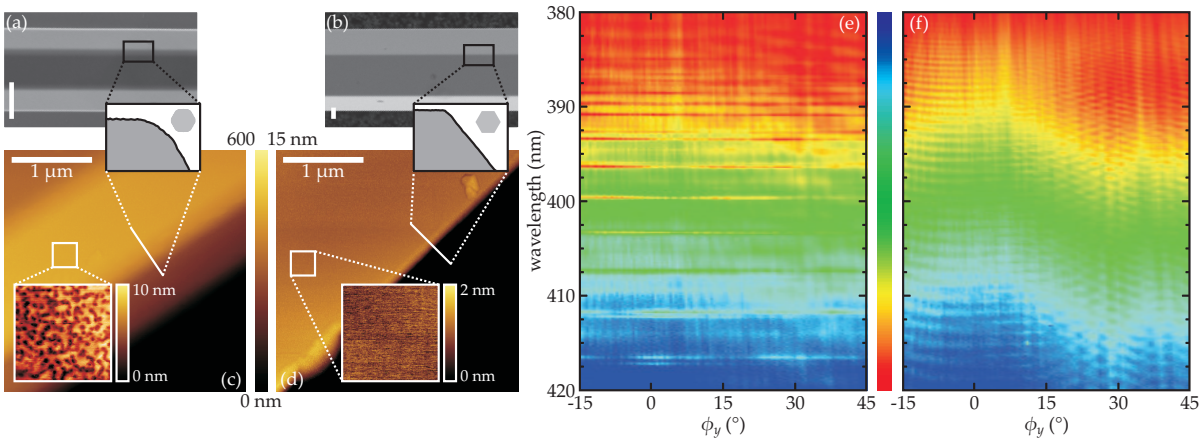

Figure 8.24: SEM (a,b) and AFM (c,d) images of ZnO microwires with blunt (a,c) and sharp (b,d) corners. The length of white bars represents 1 µm. The white squares show magnified sections of the microwire top facets, white lines highlight line scans along microwire corners. Angular-resolved PL spectra along wire cross section (angle ϕ_y) showing WGMs in wires with blunt corners (e) and FPMs in wires with sharp corners (f).

ZnO microwires were grown by carbothermal vapour-phase transport [2] and typically exhibit two different types of morphologies: (i) rough surface ($R_{rms} \approx 6$ nm) and blunt corners (curvature radius $r_C \approx 400$ nm) or (ii) smooth surface ($R_{rms} < 0.25$ nm) and sharp corners ($r_C < 10$ nm) as can be seen by SEM and AFM images in Fig. 8.24 (a-d). We attribute these morphology changes to locally varying material transport or temperature fluctuations during the growth process. Corresponding angular-resolved PL measurements are shown in Fig. 8.24 (e,f) and reveal clear signatures of WGMs for the blunt cornered wires but Fabry-Pérot modes (FPMs) for the wires with sharp corners evidenced by their one- and two-dimensional cavity photon dispersion [3], respectively. In this context, wires with blunt corners exhibit WGMs since these modes effectively couple out at the corners that represent discontinuities for light propagation. The formation of FPMs in that case is unlikely due to the large surface roughness.

We propose that WGM are likewise present in wires with sharp corners but do not exit the resonator due to high photonic confinement provided by the nearly perfect resonator shape. This is proven by excitation dependent PL measurements that reveal WGM signatures in wires with sharp corners both at cryogenic and room temperature

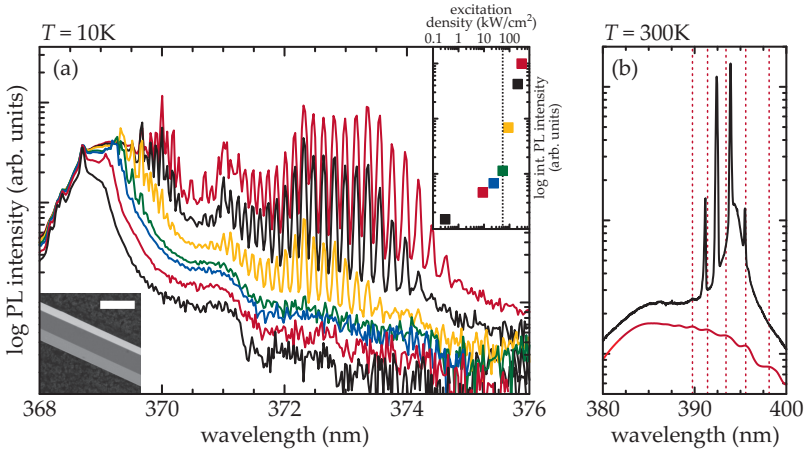

Figure 8.25: Excitation-dependent PL spectra of ZnO microwires with sharp corners at cryogenic (a) and room (b) temperature. Inset at lower left corner in (a): SEM image of investigated microwire, scale bar represent 10 μm. Inset at upper right corner in (a): Integrated PL intensity vs. excitation density (color of dots corresponds to colour of spectra). (b) PL spectra of a microwire below (red line) showing FPMs and above (black line) showing WGMs in lasing regime. Energetic positions of FPMs are highlighted by vertical dashed lines.

(Fig. 8.25). The corresponding lasing thresholds in wires with sharp corners at cryogenic temperatures are a factor of 3 less that in wires with blunt corners which can be ascribed to the smaller optical losses and thus higher optical mode quality of WGMs in sharp cornered wires [4]. At room temperature, the lowest observable WGM lasing threshold in these wires is one order of magnitude smaller than already reported values [5] and therefore demonstrates the necessity to control the resonator shape in order to achieve efficient room-temperature stimulated emission.

[1] T. Nobis et al.: Phys. Rev. Lett. **93**, 103903 (2004).
[2] C.P. Dietrich et al.: J. Appl. Phys. **109**, 013712 (2011).
[3] C.P. Dietrich et al.: New J. Phys. **13**, 103021 (2011).
[4] C.P. Dietrich et al.: Appl. Phys. Lett. **101**, 141116 (2012).
[5] J. Dai et al.: Opt. Mater. **33**, 288 (2011).

8.16 Exciton-polaritons in ZnO-based resonators – bosonic scattering, coherent states and pseudospin

R. Schmidt-Grund, H. Franke, C. Sturm, C.P. Dietrich, T. Michalsky, S. Richter, M. Thunert, A. Janot*, M. Lange, B. Rosenow*, M. Grundmann

*Institute for Theoretical Physics

8.16.1 Introduction

Exciton-polaritons are quasi-particles arising from the strong coupling of excitons and photons confined in a solid state resonator structure. Due to their composite nature,

they combine properties of both constituents. On the one hand, long-range interaction is mediated by the photonic component. On the other hand, the excitonic part provides properties of electronic systems like electric dipole momentum mediating short-range interaction and angular or rather magnetic moments causing together with the photonic polarization the so-called pseudospin (PS) of the exciton-polaritons. Exciton-polaritons are low-mass bosons, thus, quantum mechanical effects can be observed at high temperatures (for ZnO predicted above room temperature). One of the most interesting effects is the so-called bosonic final state stimulation. This type of scattering can cause a massive occupation of a distinct state with exciton-polaritons which can show macroscopic phase coherence, a so-called Bose-Einstein condensate (BEC). Such a BEC can go along with phenomena like lasing or superfluidity. In disordered systems, the superfluid wavefunction can be disturbed and phase transitions from the macroscopic phase- and energy-stiff superfluid state via Bose-glass like states to localized, fully phase-desynchronized states can occur. Further, bosonic scattering mechanisms depend not only on the occupation number of the initial, but also on that of the final states. If the particle density in such a state is high enough, so-called parametric scattering can set in, which also can lead to the creation of entangled exciton-polariton pairs. These interesting properties can be used in applications like information transport or manipulation, quantum information technology, as well as for low-power sources of coherent or entangled light.

All the properties and effects mentioned above depend strongly on and can be manipulated by the design of the properties of the electronic and the photonic system in the resonator structure. The most important here are the systems' dimensionality, the lifetime of the excitons and photons, electronic and photonic disorder, and external or internal electric or magnetic fields or potentials. In the resonators of concern here, the dimensionality of the wave function and thus the particle scattering and propagation (related to the in-plane momentum $k_{||}$) properties are determined by the dimension of the photonic confinement. While two-dimensional quasi particles arise in one-dimensionally confined planar Fabry-Perot microcavities, whispering gallery modes (WGM) in microwires yield one-dimensional exciton-polaritons. The particle lifetime is designed by the strength of the photon confinement and the crystal quality. Potential and fields are manipulated by either laser-spot induced electronic background potentials or by applying external magnetic fields.

In the last years we have established various types of ZnO-based resonators and could reach well controllable photonic mode properties, the strong coupling regime, photon lasing and BEC of exciton-polaritons. But a lot of questions arose which have been in focus of current investigations. In a planar microcavity we have observed polariton BEC [1, 2] showing phenomena like energetical relaxation of propagating BEC when traveling away from regions with a high background potential. New developments in our experimental setup now allows to observe a similar behavior even for uncondensed polaritons, which is a surprising finding and was not reported in literature so far (cf. Sec. 8.16.2, [3]). The BECs further show ballistic propagation as well as fragmentation of the emission pattern,[1, 2] which will be discussed in detail in Sec. 8.16.3 in terms of Bose-glass transition and non-equilibrium theoretical approaches (cf. also Sec. HIER LINK TO JANOT - INST-THEORY). For further understanding of the PS properties of the exciton-polaritons [4] we have applied external magnetic fields to modify the PS orientation (cf. Sec. 8.16.5). Further developed growth techniques

allowed us to grow large area homogeneous (≈ 40 mm in diameter) Bragg reflectors [5] and microcavities showing strong coupling of the excitons with cavity-photons of mode number one up to four at one single sample [1]. A new cavity type was developed by growing the ZnO layer at high temperatures to obtain high-quality electronic properties and subsequently smoothing of their surface by an ion-beam to provide also high-quality photonic properties [1]. In such a cavity we could observe the strong coupling of the confined photons not only to the free and donor bound excitons [6] but also to exciton-phonon complexes (polarons) which provide a huge oscillator strength and thus yield a very high coupling strength of up to twice that of the free excitons [1]. Strong interaction with phonons we have also observed in relaxation processes in microwire WGM resonators (cf. Sec. 8.16.4). Also for this type of resonators, progress in growth (cf. Sec. 8.15, [8]) yields new interesting physics. We have observed BEC in these wires along with relaxation processes of the polaritons showing signatures of parametric inter-branch scattering which will be discussed in Sec. 8.16.4. Mesa structures with diameters in the range of 10 μm etched in planar microcavities provide a potential trap for the photonic system and thus also for the exciton-polaritons [1]. By spatially resolved PL measurements we have observed polariton accumulation within this potential trap and could find some hints for a possible polariton tunnelling process near the potential barrier, i.e. the rim of the mesa [1, 3]. In the following, some aspects will be discussed in more detail.

The resonators under investigation are on the one hand planar Fabry-Perot microcavities consisting of a ZnO bulk cavity as active medium that is sandwiched between two all-oxide Bragg reflectors (BR). Yttria stabilised zirconia and Al_2O_3 are used as BR materials. The samples are grown by means of pulsed laser deposition (PLD) typically at temperatures of (150 – 650) ℃ and an oxygen background pressure of (0.02 – 0.002) mbar on *c*-sapphire substrates. More information on the general properties of the samples and the experimental techniques used can be found elsewhere [1, 6, 7, 9, 10]. The other resonator type is of WGM-type and consists of hexagonal shaped ZnO microwires with diameters in the range (1 – 10) μm, grown by the carbothermal evaporation technique [8, 11]. The mode properties and the emission from the polariton states have been mainly investigated by spatial, energy (E) and angular (Φ) resolved reflectivity and photoluminescence (PL) measurements. The emission angle is directly related to the in-plane momentum $k_{||}$ of the polaritons. By imaging the Fourier plane of a microscope objective in a confocal microscope setup onto a monochromator entrance slit or directly onto a detector array, E-$k_{||}$ space, E-real-space or two-dimensional $k_{||}$- or real-space measurements of the emission are performed with a spatial resolution of ≈ 1 μm. In the macro-PL setup, a compensator and polarizer mounted in the detection path allows for the determination of the complete Stokes vector of the emission.

8.16.2 Discrete relaxation of uncondensed exciton-polaritons in an inhomogeneous potential

We have observed indications, that the energy-stiffness condition in the relaxation and scattering process which we observed in coherent single-phase quantum systems manifest also in a non-coherent single particle ensemble, i.e. well below the BEC threshold. The origin of the energy-stiffness lies in the relaxation process caused by a locally enhanced and spatially inhomogeneous background potential usually induced by the

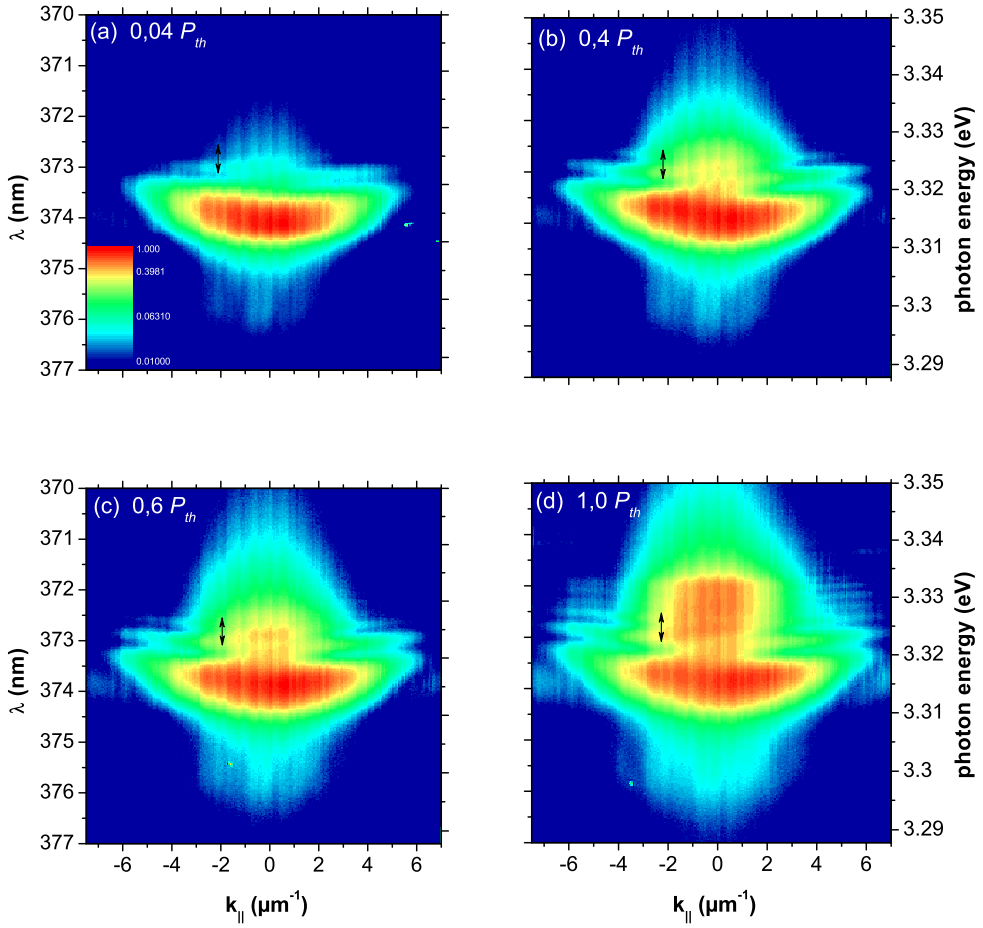

Figure 8.26: Energy-resolved $k_{||}$-space images of the polariton emission for different excitation densities (a-d) below and at the condensation threshold (P_{th}). Image (a) is logarithmic in scale whereas the other images are scaled linearly.

pumping [12]. The conservation of total condensate energy and the compensation of in- and out-scattering rates lead to nearly equally spaced energy levels of the condensate emission in the E-$k_{||}$-space distribution. Surprisingly this particular pattern was also observed for the uncondensed polaritons. E-$k_{||}$-space images of the polariton emission at $T = 10\,\mathrm{K}$ show, that parts of the polariton dispersion appear at different energy levels (Fig. 8.26 (a-d)).

This indicates a propagation of uncondensed polaritons out of the pump area due to the repulsive polariton-polariton interaction and the interaction with hot carriers. This is supported by the polariton distribution in real-space. The observed discrete and fix energy spacing of $\Delta E_{\mathrm{r,uncond}} \sim 3.3\,\mathrm{meV}$ (Fig. 8.27) between the appearing blueshifted dispersion relations supports the assumption that the relaxation process is similar to that of condensate systems, where we have observed $\Delta E_{\mathrm{r,cond}} \sim 0.5 \Delta E_{\mathrm{r,uncond}}$. The factor 0.5 can be attributed to the fact, that the lifetime of the uncondensed polaritons is half that of the condensed ones and therewith the out-scattering rate for uncondensed polariton states is twice as high as for condensate states. This higher loss rate is compensated by the larger ΔE_{r}, as the stimulated in-scattering rate is in first approximation

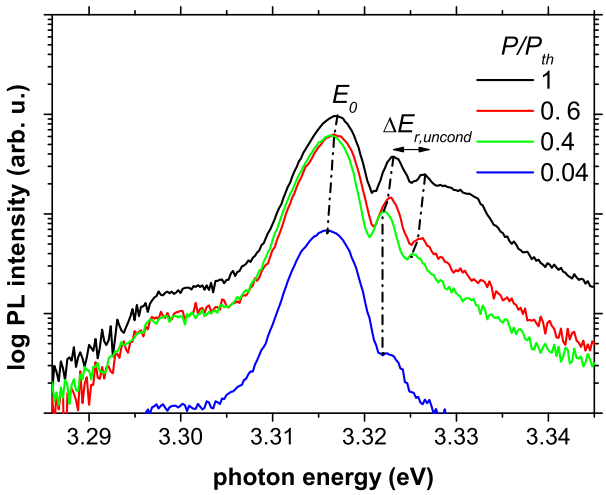

Figure 8.27: $k_{\|} = -2\,\mu\text{m}^{-1}$ spectra from Fig. 8.26 a-d. E_0 represents the polariton emission of the peripheral region of the pump area and $\Delta E_{\text{r,uncond}}$ marks the energy spacing between two emission lines which correspond to blueshifted polariton emissions.

directly proportional to the energy spacing between the initial and the final state of the scattering process [12].

For the experiments discussed here, a pinhole was put additionally in an intermediate image plane of the confocal microscope setup (Fig. 8.28) to cut off the polariton emission from outside the central excitation area of about 3 µm to achieve a strong reduction of the polariton emission of the peripheral region of the pump area (E_0 in Fig. 8.27). Otherwise the fingerprint of the relaxation process is covered from the emission of the vast number of polaritons which could leave the center of the excitation area.

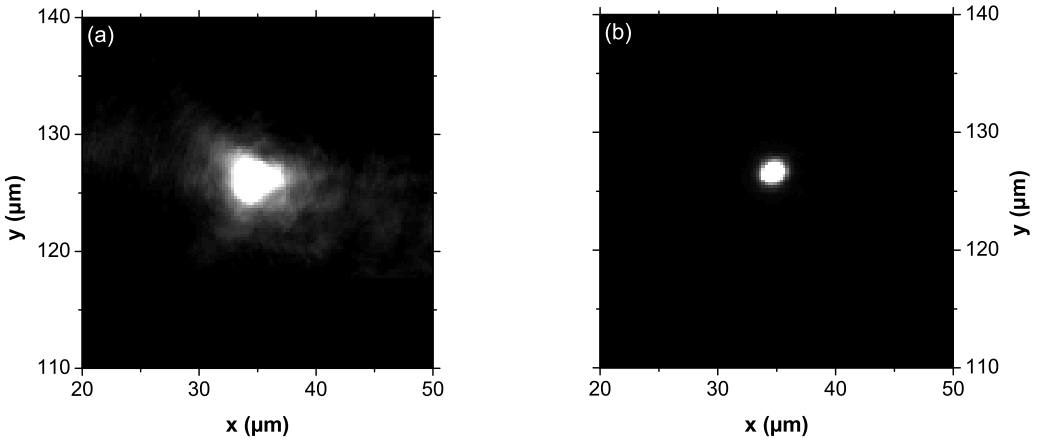

Figure 8.28: Real-space polariton emission pattern without (a) and with (b) the use of a pinhole in an intermediate image plane for the spatial selection of the detection area. Both images are scaled linearly.

8.16.3 Influence of disorder on the propagation of polariton BEC

The BECs in our planar microcavities usually show propagation as well as signatures of disorder induced effects [1, 2, 4]. In previous theoretical [13] and experimental [14] works stabilization of a single-phase condensate was found with increasing polariton density in presence of a disordered background potential landscape. In contrast to this we observed a destabilization, causing a transition from single ballistically propagating to fractionalized condensates (Fig. 8.29 a)).

Structural imperfections in our sample lead to the formation of a spatially inhomogeneous background potential. Due to the composite nature of the polaritons, this background potential is affected by both, the electronic (e.g. inhomogeneous carrier distribution) as well as the photonic (e.g. thickness fluctuations, rough interfaces) disorder which could induce separation, phase breaking or localization of polariton BEC states. This causes a non-homogeneous emission pattern within the energy-momentum-space, which will be denoted as fragmentation (Fig. 8.29 a), $P = 67P_0$), in contrast to propagating condensates, reflected by a spot-like emission exactly at the dispersion branch (Fig. 8.29 a), $P = P_0$).

In order to characterize the non-homogeneous emission pattern we introduce a new quantity, namely the degree of fragmentation. For the determination of this quantity we developed different independent algorithms to extract a condensate fragmentation parameter for a large temperature(T)-detuning(Δ)[3] parameter set. For each method and (T,Δ) data set we found an increase of the fragmentation parameter with increasing pump power, as shown exemplarily in Fig. 8.29 b).

This is also supported by a theoretical prediction where an effective Gross-Pitaevskii equation [15] was employed in a disordered environment. For an externally driven system it turns out that the condensate remains stiff at finite length scales only. This suggests that for an increasing condensate size disorder effects are promoted and should reveal a significant trace in the emission pattern. Thus we find two competing effects: stabilization of the condensate with increasing density and destabilization with increasing effective in-scattering area. The second effect shows a qualitative agreement with our experimental observations. Here, the effective excitation spot size and thus the condensate size increases for increasing pump power leading to a more pronounced disorder effect.

8.16.4 Multimode whispering gallery mode systems

In contrast to planar microcavities, photonic whispering gallery modes (WGM) in hexagonal shaped ZnO microwires [11] cause in the case of strong coupling a multimodal polariton system without a distinct ground state. Since the microwire discussed here has a diameter of about 8 µm (Fig. 8.30), the system exhibits a high spectral mode density and many modes exist between the ZnO free exciton energy and the WGM with mode number one and therefore also the polariton ground state. This allows for a wide variety of relaxation and scattering processes of the polaritons since the energy-momentum conservation can be easily fulfilled.

[3] i.e. the energy difference between the pure cavity photon mode and the free exciton energy at zero in-plane momentum.

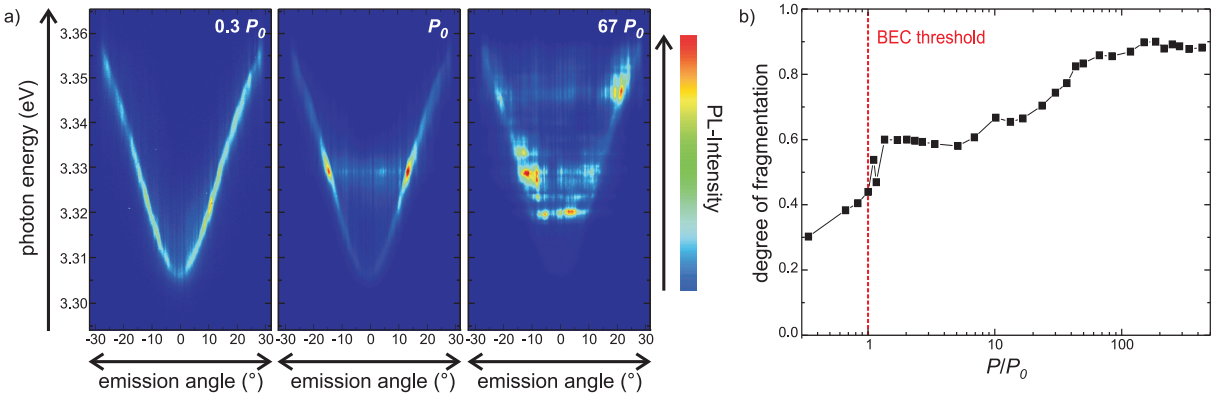

Figure 8.29: (a) From left to right: Fourier images of exciton-polaritons for $T = 10$ K, a detuning of $\Delta \approx -50$ meV and different excitation powers P, normalized to BEC threshold P_0. Increasing the excitation power leads to a transition from uncondensed ($P = 0.3P_0$) to condensed ($P = P_0$) and finally to fractionalized states ($P = 67P_0$), which are affected by disorder. (b) Degree of fragmentation as a function of the normalized excitation power P/P_0 for the same temperature and detuning as in Fig. 8.29 a).

Experimentally we have observed two different regimes by measuring the energy-momentum distribution of the emission (for the geometrical definition cf. Fig. 8.30): At room temperature an LO-phonon assisted relaxation process into low-energy states dominates. At 10 K this process cannot be observed but interbranch polariton-polariton scattering occurs.

Fig. 8.31 shows the energy-momentum distribution of the WGM polariton emission at room temperature for three excitation powers. At very low power (left panel), the dispersion of the WGM or even the polariton branches are observable.[4] Enhancing the excitation power by a factor of six (middle panel), a strong increase of the emission intensity of these modes with energies of one LO-phonon mode energy (≈ 70 meV) below the free exciton emission energy (first low-energy phonon replica) can be observed. A further increase of the excitation power above the threshold power P_0 (right panel) causes a strong non-linear increase of the emission intensity, indicating the transition of the system from a thermal to a coherent regime. These observations reveal a very efficient exciton-phonon or polariton-phonon scattering process.

In the second regime at 10 K, no emission could be observed from modes either close to the free exciton nor to its low-energy phonon replica (Fig. 8.32). Instead, for low excitation powers, strong emission from defect bound excitonic states[5] can be observed (left panels). By increasing the excitation power, one distinct mode becomes more and more pronounced, revealing a strong non-linear intensity increase at P_0 and a transition to the polariton BEC state.[6] Along, a relaxation process of polaritons down to energetically lower states sets in accompanied by a momentum gain of the polaritons.

[4] It cannot conclusively be decided if the system is in the strong or weak coupling regime because of the restricted experimentally accessible momentum range due to the finite aperture of the used microscope objective.

[5] Which are ionized at room temperature and therefore are dark.

[6] In this case, by means of the excitation power evolution of the intensity and energy-momentum distribution of the emission, it can be clearly distinguished between the weak coupling regime, which causes an electron-hole plasma lasing, and the strong coupling regime, causing emission from a polariton BEC.

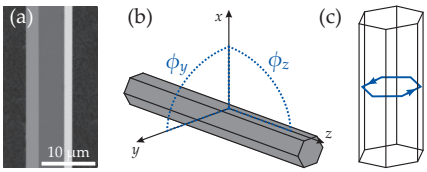

Figure 8.30: (a) Scanning electron microscopy image of the ZnO microwire. (b) Definition of the coordinate system. The polariton dispersion $E(k_{||})$ is measured along the wire axis indicated by the detection angle $\Phi_z \propto k_{||}$. (c) Schematic of a WGM in a hexagonal microwire

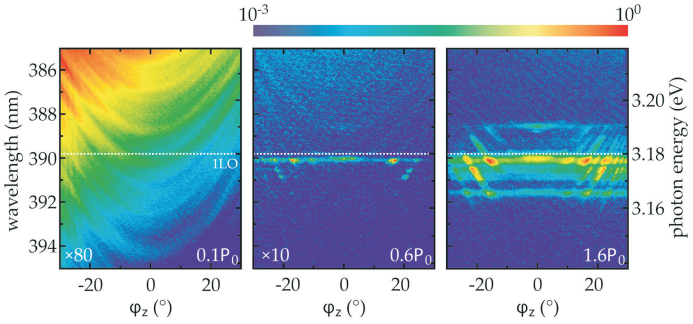

Figure 8.31: False-colour images in a logarithmic intensity scale of the energy-momentum-space distribution of the WGM polariton emission at room temperature for different excitation powers normalized to the lasing threshold power P_0. The intensity scaling factor is indicated in the image. The spectral position of the first LO-phonon replica of the free exciton is indicated by the dashed line.

All these occupied states are separated from each other by equal distances in energy and momentum. If an initial mode reaches a certain occupation, transition into a BEC state can be observed. We ascribe these observations to bosonic parametric scattering processes, that have to be proven further.

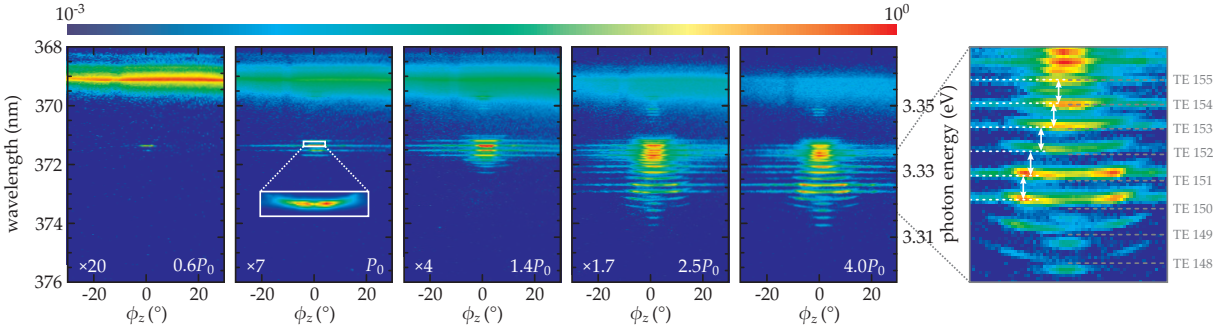

Figure 8.32: Same as in Fig. 8.31 but at 10 K. The very right panel shows an enlarged section in the spectral and momentum range of the condensate emission. The mode numbers of the transversal electric (TE) polarized WGM are indicated by dashed lines.

8.16.5 Pseudospin polarization of exciton-polaritons

The pseudospin (PS) expresses at the same time the mean superposition of the exciton spins and the photonic polarization of an ensemble of exciton-polaritons. Thus, it is directly associated with the light polarization of the polariton emission [16] and can be studied by means of polarization resolved photoluminescence experiments. The emission of the lower polariton branch (LPB) we have studied in the non-condensed regime under non-resonant excitation.

In general, exciton-polaritons in planar microcavities (MC) are supposed to possess two polarization eigenmodes, i.e. TE- and TM-polarization [6]. In contrast to the

conventional planar MC, the energetic splitting between TE- and TM mode of the LPB exceeds 20 meV in the ZnO-based MC investigated. Astonishingly, the emission from the TE and TM modes exhibits an average spin polarization which projection is in maximum about 3° rotated with respect to that expected for the pure TE and TM states. Furthermore, circular polarization contributions of up to 4 % are observed. Both show a dependence on the emission angle which is similar to that of the TE-TM splitting [4]. The dependence on the (negative) detuning Δ is found to be non-monotonic. The origin of this PS rotation is not clear until now. External magnetic fields of 3 T were applied in different configurations (Voigt, Faraday) at the TU Dortmund and yield a strong change in the linear polarization angle or rather the degree of linear polarization (expressed by S_2) and the degree of circular polarization (S_3) (Fig. 8.33).

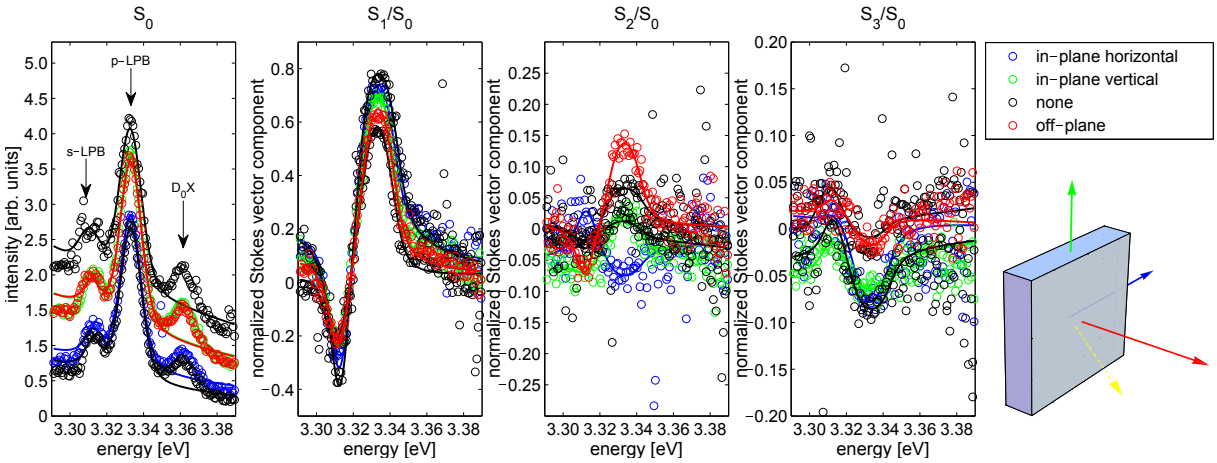

Figure 8.33: Stokes vector components of the LPB emission at an emission angle of approx. 37°, detuning $\Delta = -130$ meV and $T = 30$ K. Colors correspond to the orientation of the applied magnetic fields with respect to the sample (see thick arrows in the schematic on the right), black curves represent measurements without external magnetic field. The dashed yellow arrow in the schematic indicates the investigated emission angle.

For understanding the experimental findings with and without external magnetic field, the particular role of effective magnetic fields was studied in more detail. Effective magnetic fields are associated with any energetic splittings between different PS states. The large TE-TM splitting causes a strong effective field, anisotropies can also cause further effective fields. In analogy to the work of Kavokin *et al.* [17], the solution of the Liouville-von Neumann equations for exciton-polariton PS were applied to calculate the time-averaged PS values under precession of the PS due to the total (external and effective) magnetic fields. However, the model with an reasonable isotropic g-factor, as conventionally assumed in the literature, and a reasonable lifetimecannot explain the experimental observations, even if further internal effective magnetic fields (e.g. caused by structural and thus photonic or electronic anisotropies) are additionally considered. Treating the exciton-polariton g-factor as tensorial is expected to yield a much better description of the experimental results.

Acknowledgement We gratefully acknowledge the fruitful discussion with P. Eastham. For the experimental support during the magnetic field measurements at TU

Dortmund we are grateful to A. Schwan, J.-S. Tempel and M. Bayer. For ion-beam smoothing of the cavity we acknowledge F. Frost and R. Fechner.

[1] H. Franke: Ph.D. thesis, University of Leipzig (2012).
[2] H. Franke et al.: New J. Phys. **14**, 013037 (2012).
[3] T. Michalsky: Master thesis, University of Leipzig (2012).
[4] R. Schmidt-Grund et al.: in *The Physics Institutes of Universität Leipzig, Report 2011*, M. Grundmann (Ed.) pp. 184, Leipzig, 2012.
[5] M. Lorenz et al.: Laser Chemistry **2011**, 140976 (2011).
[6] C. Sturm et al.: New J. Phys. **13**, 033014 (2011).
[7] C. Sturm et al.: New J. Phys. **11**, 073044 (2009).
[8] C.P. Dietrich et al.: Appl. Phys. Lett. **101**, 141116 (2012).
[9] C. Sturm et al.: Phys. Rev. B **83**, 205301 (2011).
[10] R. Schmidt-Grund et al.: in *The Physics Institutes of Universität Leipzig, Report 2010*, M. Grundmann (Ed.), pp. 179, Leipzig, 2011.
[11] C. Czekalla et al.: phys. stat. sol. b **247**, 1282 (2010).
[12] Wouters et al.: Phys. Rev. B **82**, 245315 (2010).
[13] G. Malpuech et al.: Phys. Rev. Lett. **98**, 206402 (2007).
[14] A. Baas et al.: Phys. Rev. Lett. **100**, 170401 (2008).
[15] M.H. Szymanska et al.: Phys. Rev. Lett. **96**, 230602 (2006) and Phys. Rev. B **75**, 195331 (2007); M. Wouters and I. Carusotto: Phys. Rev. Lett. **99**, 140402 (2007).
[16] R.I. Dzhioev et al.: Phys. Rev. B **56**, 13405 (1997).
[17] A. Kavokin et al.: Phys. Rev. Lett. **95**, 136601 (2005).

8.17 NIR-VUV temperature dependent dielectric function of alumina

R. Schmidt-Grund, T. Lühmann, T. Böntgen, H. Franke, M. Grundmann

The dielectric function (DF) of Al_2O_3 thin films was determined for temperatures between 11 K and 300 K and photon energies (1 – 7.5) eV by means of spectroscopic ellipsometry. The thin films have been grown by pulsed laser deposition at room temperature (LT) and 650 °C (HT) on silicon substrates. Both films have been found to be X-ray amorphous. Such Al_2O_3 thin films are important for applications as insulating layers in semiconductor based electric devices, as protective coatings, or even as optical functional layers as e.g. in Bragg Reflectors for ZnO-based microcavities [1–3] (Sec. 8.16).

The experimentally obtained ellipsometry data were analyzed using a model function which describes the onset of the near band-gap absorption by means of a Cody-Lorentz model, which is usually used for amorphous respective micro-crystalline materials or glass [4, 5]. This model considers the lack of long range order in the crystal which causes on the one hand electronic states below the band-gap and on the other hand non-parabolic valence and conduction bands described by the so-called Tauc-Lorentz or Cody-Lorentz oscillators. In this model, an energy $E_g + E_t$ describes the "ideal" absorption edge for parabolic bands, E_g the optical absorption edge, and the Urbach energy E_u an exponentially decaying weak absorption tail below $E_g + E_t$ [6].

It was found that the DF of both, the LT and HT grown thin films, depends only weakly on the temperature (Fig. 8.34). A small red-shift of the onset of the absorption with increasing temperature was observed as expected, reflected also in the temperature dependence of $E_g + E_t$ which follows the Bose-Einstein model [7] (Fig. 8.35, left). The effective phonon energy amounts to ≈ 55 meV (LT) and ≈ 75 meV (HT). The electron-phonon coupling strength was found to be more than a factor of three larger for the HT film. Both findings can be explained by a much better crystal quality of the HT film and thus an enhanced contribution of optical phonons to the electron-phonon interaction. Obviously, the growth temperature strongly influences also the absorption properties and thus the below band-gap real part of the DF and the refractive index as well (Fig. 8.34). Here, the HT film shows much larger values pointing to a much higher oscillator strength of electronic transitions. For the LT grown films, the absorption sets in already at lower photon energies as compared to the HT grown films, which is reflected by a larger E_u (Fig. 8.35, right). While for the HT film no significant temperature dependence of E_u could be found, the higher amorphicity of the LT film causes a strong temperature dependence. We describe $E_u(T)$ following the model proposed by Cheng for glasses [6], which considers a zero point energy distribution of the electronic bands due to disorder E_χ and a temperature dependent coupling to thermal lattice vibrations. For our material, which is more polycrystalline than glassy, we extend this model by a term which considers the coupling to optical phonons using the same Bose-Einstein model parameter set as for $E_g + E_t$. We found that we can neglect the coupling to the thermal lattice vibrations, thus we obtain E_χ from the $T \to 0$ K extrapolation of E_u. We found for the HT and LT film E_χ to be about 170 meV and 200 meV, respectively. $E_u(T)$ scales with some disorder strength parameter which is related to the deformation potential [6] and the electron-phonon coupling strength. As $E_u(T)$ is almost constant for the HT film and its electron-phonon coupling strength is much larger than for the LT film, the disorder strength parameter must be much larger for the LT grown film. We can estimate the ratio of the disorder strength parameters of the LT with respect to the HT films from the ratio of the pre-factors in the Bose-Einstein models for $E_u(T)$ and $E_g + E_t(T)$ to be about ten.

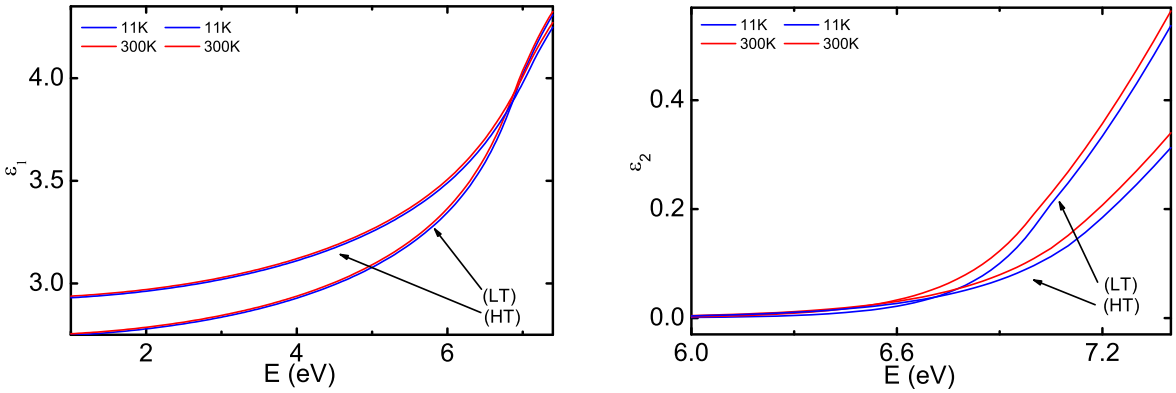

Figure 8.34: Real (ε_1, left panel) and imaginary part (ε_2, right panel) of the dielectric function for temperatures between 11 K and 300 K of Al_2O_3 thin films grown at room temperature (LT) and 650 ℃ (HT). For ε_2, the near band-gap spectral range is shown only.

[1] S.W. Whangbo et al.: J. Mater. Chem. **12**, 2559 (2002).

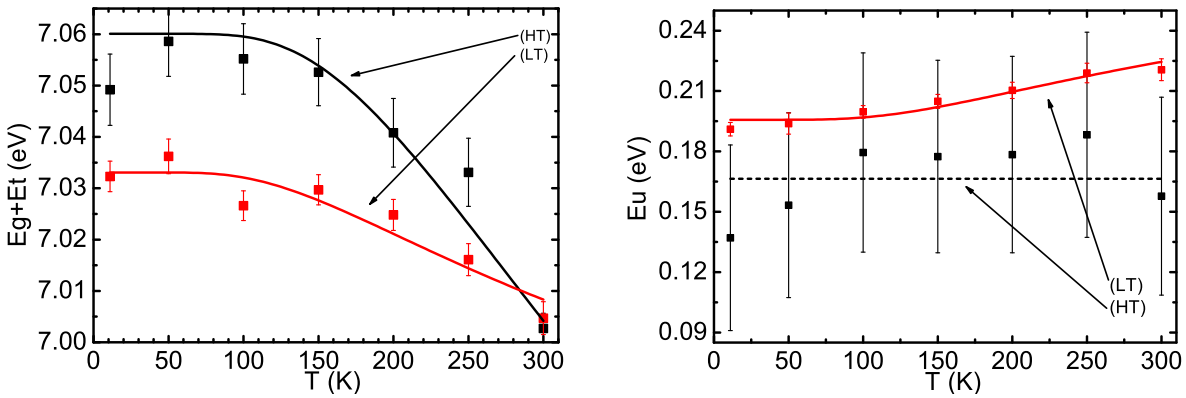

Figure 8.35: Temperature dependence of the effective band-edge energy $E_g + E_t$ (left panel) and the Urbach energy E_u (right panel) for the LT and HT grown thin films. Symbols denote the experimentally obtained data and the lines the Bose-Einstein ($E_g + E_t$) and Cheng (E_u) model approximation.

[2] J. Sellmann et al.: phys. stat. sol. (c) **5**, 1240 (2008).
[3] H. Franke et al.: New J. Phys. **14**, 013037 (2012).
[4] G.D. Cody, in: J.I. Pankove (Ed.), *Semiconductors and Semimetals* **21**, Academic, Orlando, 1984, p. 11.
[5] A.S. Ferlauto et al.: J. Appl. Phys. **92**, 2424 (2002).
[6] S.C. Cheng: Phys. Chem. Glasses: Eur. J. Glass Sci. Technol. B **50**, 329 (2009).
[7] L. Viña et al.: Phys. Rev. B **30**, 1979 (1984).

8.18 Optical properties of spinel oxides

T. Böntgen, V. Zviagin, R. Schmidt-Grund, M. Lorenz, M. Grundmann

We have investigated the optical properties of the spinel type oxides $ZnFe_2O_4$ (ZFO)[1] and $ZnCo_2O_4$ (ZCO). Many inverse spinel oxides (e.g. Fe_3O_4) have long since been in the focus of research interests due to their magnetic and magneto optical properties [2]. Normal spinel oxides (e.g. ZFO, ZCO) on the other hand have only recently gained more interest. This is due to their potential for application in data storage and spintronic devices [3]. By means of pulsed laser deposition we have grown thin films of ZFO and ZCO on *a*-plane sapphire substrates. While ZFO grows with high crystalline quality on sapphire ZCO growth is amorphous. The samples were then investigated using variable angle spectroscopic ellipsometry in a wide spectral range ((0.5 – 9) eV) and a model for the dielectric function was deduced. Since both compounds share a common crystal structure many of the optical transitions observed are expected to be similar. Thus a common model for both materials can be proposed. The main transitions observed take place between the O_{2p} (forming the top of the valence band) and the empty 3d and 4s orbitals of the transition metal ion (Fe/Co) and the 4s orbitals of the Zn ion. Due to the (octahedral) coordination of the Fe/Co ion by oxygen the 3d orbitals exhibit an additional splitting. This results in three transitions from oxygen to the transition metal ($O_{2p} \rightarrow (Fe/Co)_{3d\,t_{2g}}$, $O_{2p} \rightarrow (Fe/Co)_{3d\,e_g}$ and $O_{2p} \rightarrow (Fe/Co)_{4s}$) and one transition from

$O_{2p} \rightarrow Zn_{4s}$. Furthermore for high photon energies an additional transition (likely to Zn) is expected. This model was then employed to model the experimental data. As can be seen the model fits well to the measurements for energies above the absorption edge (Fig. 8.36). However additional transitions are present in the gap region below ≈ 2.5 eV. This is especially true for ZCO. We relate these to transitions between the split 3d orbitals of the transition metal ions. While these transitions are normally forbidden they are readily observed in similar materials and believed to become possible through the disorder in the crystal. Since these transitions depend strongly on the material they have to be modelled independently. The presence of such strong transitions for ZCO might also be a sign for the inferior crystal quality of the material with respect to ZFO.

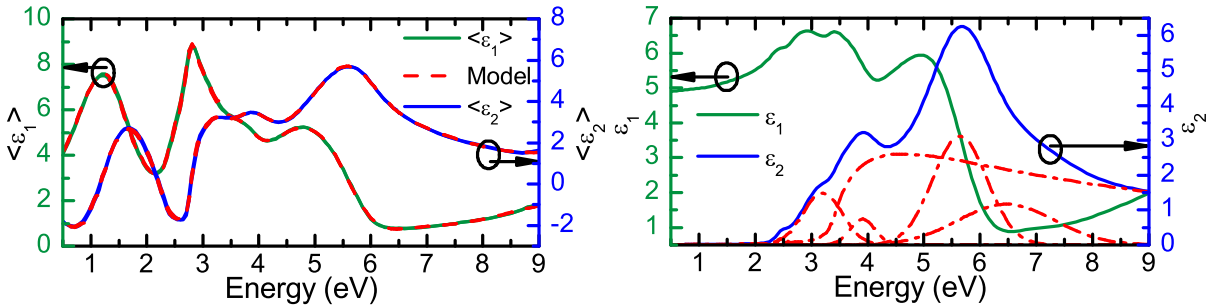

Figure 8.36: Left: pseudo dielectric function measured (green/blue solid lines) and the model fit (red dashed line) for ZFO. Right: dielectric function (green/blue solid lines) calculated from the model and the individual contributions (red dashed lines).

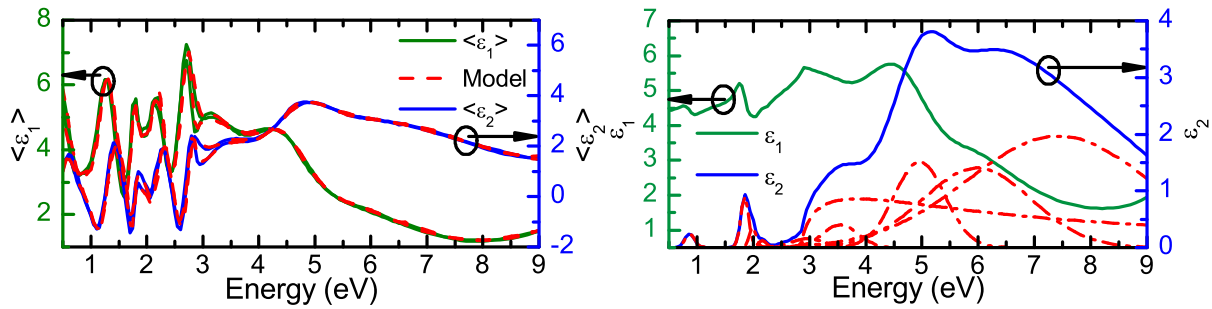

Figure 8.37: The same as in Fig. 8.36, but for ZCO. The transitions below 2.5 eV belong to transitions between the split Co_{3d} orbitals.

[1] T. Böntgen et al.: J. Appl. Phys. **113**, 073503 (2013).
[2] D. L. Camphausen et al.: Phys. Rev. Lett. **29**, 657 (1979).
[3] M. Opel et al.: physica status solidi (a) **208**, 232 (2011).

8.19 In-situ ellipsometry on ZnO single crystal surfaces in vacuum

L. Fricke, T. Böntgen, J. Lorbeer*, R. Schmidt-Grund, M. Grundmann

*Leibniz-Institute for Surface Modification e.V. (IOM), Leipzig

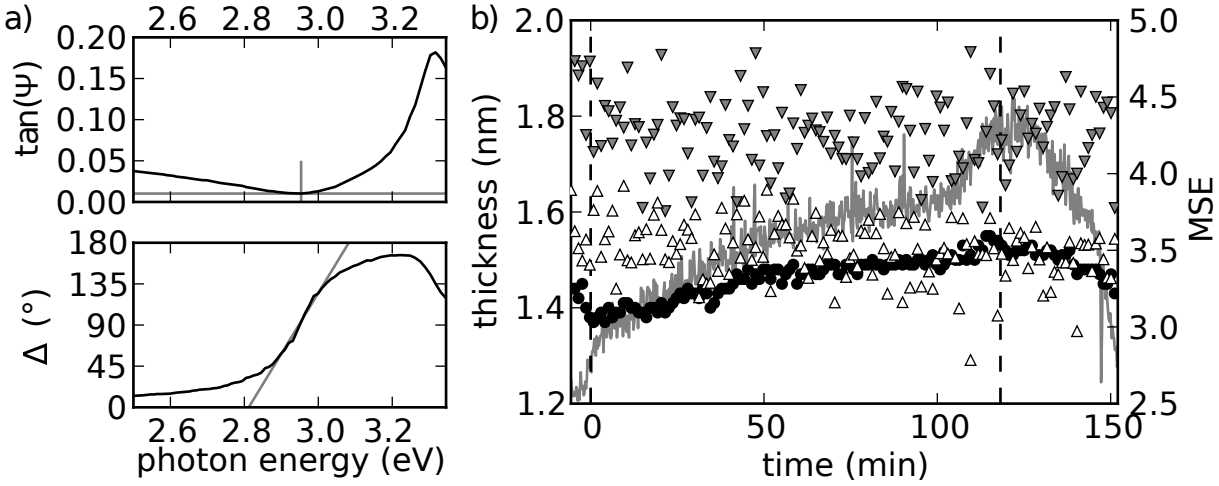

Figure 8.38: a) Ellipsometric spectra taken from an ZnO bulk single crystal before exposure to nitrogen, the slope of Δ around the Brewster angle and the minimum of $\tan\Psi$ are marked in gray. b) Thickness during exposure to nitrogen calculated from the usual method (black circles), from the minimum of $\tan\Psi$ (white upright triangles) and from the slope of Δ (gray downright triangles). The gray line depicts the deviation between modeled and experimental data when using the usual method (MSE).

Ellipsometry is a valuable tool for *in-situ* monitoring of processes, like thin film deposition and surface modification. In the case of only very thin layers on a bulk material the analysis becomes very sensitive to errors. In our setup the sample mount leads to a deviation of the light path while changing samples and evaporating the experimental chamber, so that errors introduced by viewport birefringence and a changing incident angle can not be assessed by reference measurements. Thus the usually employed modelling of the acquired spectra using transfer-matrices includes even for the case of a single layer on top of a substrate 6 parameters (layer thickness, incident angle, 4 window dispersion parameters), of which the 4 parameters for the window dispersion are free parameters.

To model the date taken from an ZnO bulk single crystal, we extended the 3-phase-model by Drude [1] to slightly absorbing media, as it is the case for ZnO in the spectral range slightly below the band gap energy. The minimum of $\tan\Psi$ and the slope of Δ near the Brewster angle are evaluated. Those are marked in the spectra of Fig. 8.38 (a) and yield directly the thickness of the surface layer. This technique is more robust against changes of the alignment and allows a systematic treatment of errors introduced by the windows.

As an example the surface layer thickness evolution of an annealed ZnO single crystal during a two hour exposure to nitrogen atmosphere is shown Fig. 8.38 (b). The

thickness calculated from the usual modelling increases with time. But also the deviation between modelled and experimental spectra increases due to problems mentioned above. Our method does not show these artifacts. But as our method uses only data at single points in the spectra it is noisier and the current determination of the slope of Δ leads to a systematic overestimation of the thickness by approximately 18 %. At the current stage of development the introduced method is best suited as a diagnostic tool to find errors in the usual modelling procedure.

[1] P. Drude: Ann. Phys. **279**, 126 (1891).

8.20 Surface plasmons on nanopatterned surfaces

T. Böntgen, J. Lorbeer*, F. Frost, R. Schmidt-Grund, M. Grundmann

*Leibniz-Institut für Oberflächenmodifizierung Leipzig

We have investigated the anisotropic optical response of surface plasmons on structured SiO_2 surfaces. Flat SiO_2 substrates have been patterned using ion beam erosion under high angles of incidence. This causes the formation of a wave like or rippled surface [1, 2]. The periodicity of the ripples is usually $(40-80)$ nm. Measurements in the far UV with wavelength close to the pattern periodicity have revealed an optical anisotropy due to the structuring. This anisotropy can now be exploited to alter the optical response of surface plasmons excited close to the patterned surface. For this, thin gold films were deposited onto the patterns. By illuminating the sample from the back-side through the SiO_2 substrate surface plasmons at the air-gold interface can be excited (Kretschmann configuration). We have then used a variable angle spectroscopic ellipsometer to measure the optical response. Since plasmons can only be excited by p-polarized light the ellipsometric parameter Ψ will show a strong dip at the plasmon resonance. The spectral position of the plasmon resonance depends on the angle of incidence and is sensitive to the dielectric surroundings. In Fig. 8.39 spectra taken at different angles of incidence and with the beam direction being parallel/perpendicular to the pattern are shown. The distinct dependence on the angle of incidence is well seen for both directions. Additionally the position and the strength of the resonance clearly depend on the orientation of the sample. While this dependence is small for large angles of incidence especially the spectral shift of the resonance becomes strong for smaller angles. For an angle of 40° this causes the plasmon resonance to be shifted completely out of the experimentally investigated spectral range.

[1] D. Flamm et al.: Appl. Surf. Sci. **179**, 96 (2001).
[2] J. Völlner et al.: J. Appl. Phys. **109**, 043501, (2011).

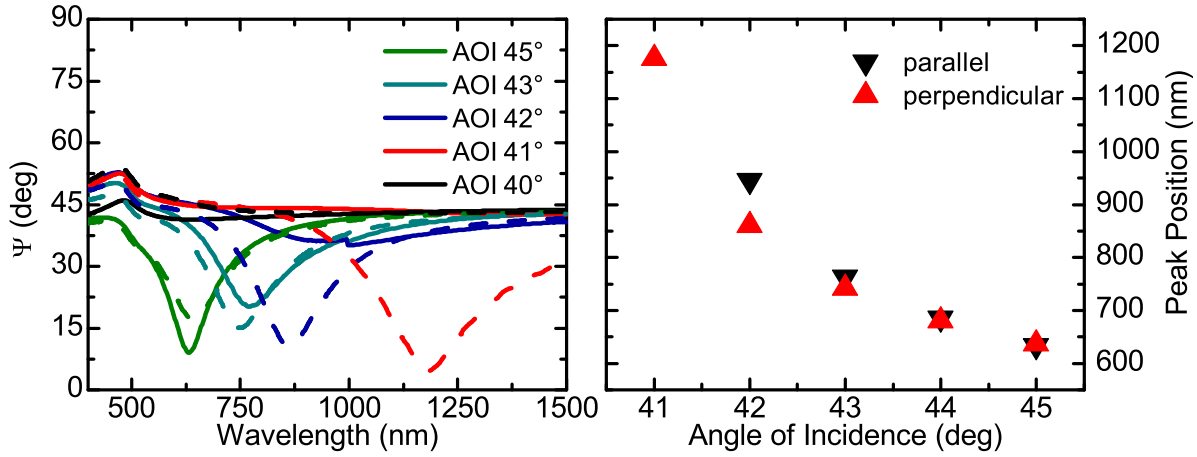

Figure 8.39: Left: Ellipsometric parameter Ψ as a function of wavelength for different angles of incidence. The solid and dashed lines represent measurements with the light beam parallel and perpendicular to the surface pattern, respectively. Right: Position of the plasmon resonance in dependence on the angle of incidence measured parallel (black) and perpendicular (red) to the surface pattern. While the difference is small for large angles it becomes large for smaller ones. For 41° the peak position is outside of the measured spectral range for the parallel configuration.

8.21 Funding

Leipzig School of Natural Sciences - Building with Molecules and Nano-objects (BuildMoNa)
Prof. Dr. M. Grundmann
DFG GS 185/1

Polarisationswechselwirkung in Laser-MBE Wurtzit-Perowskit-Heterostrukturen
Prof. Dr. M. Lorenz
SFB 762/2-2012, TP A2 within SFB 762 *Funktionalität Oxidischer Grenzflächen*

Optische Untersuchungen zu magneto-elektro-optischen Wechselwirkungen in ihrer Dynamik in oxidischen Heterostrukturen
Dr. Rüdiger Schmidt-Grund
SFB 762/2-2012, TP B03 within SFB 762 *Funktionalität Oxidischer Grenzflächen*

Lateraler Transport in oxidischen Feldeffekt-Strukturen
Dr. H. von Wenckstern, Prof. Dr. M. Grundmann
SFB 762/2-2012, TP B04 within SFB 762 *Funktionalität Oxidischer Grenzflächen*

Spinabhängiges Tunneln in oxidischen Heterostrukturen
Prof. Dr. M. Grundmann, Prof. Dr. I. Mertig (Matrin-Luther-Universität Halle-Wittenberg), Dipl.-Phys. M. Lorenz
SFB 762/2-2012, TP B06 within SFB 762 *Funktionalität Oxidischer Grenzflächen*

Bose-Einstein-Kondensation und Supraflüssigkeit von Exziton-Polaritonen bei Raumtemperatur
Prof. Dr. M. Grundmann, Dr. R. Schmidt-Grund
DFG GR 1011/20-2

Extrem verzerrte Nano- und Mikrodrähte
Prof. Dr. M. Grundmann
DFG GR 1011/23-1

Quantum Gases and Liquids in Semiconductor Rods conformally coated with Bragg Mirrors
Dr. R. Schmidt-Grund, Prof. Dr. M. Grundmann
DFG SCHM 2710/2-1, TP P1 within FOR 1616 *Dynamics and Interactions of Semiconductor Nanowires for Optoelectronics*

Oxidische topologische Isolator-Dünnfilme – Darstellung und elektronische Eigenschaften
Prof. Dr. M. Lorenz
DFG LO 790/5-1

Ortsaufgelöste nanomechanische Eigenschaften funktionaler Oberflächen – Experiment und Simulation
Prof. Dr. M. Grundmann, Prof. Dr. Dr. B. Rauschenbach (Leibniz-Institut für Oberflächenmodifizierung e. V.), Prof. Dr. S. Mayr (Leibniz-Intitut für Oberflächenmodifizierung)
SAW-2011-IOM-2

Graduiertenschule: Wolken, Aerosole und Strahlung am Beispiel des Mineralstaubes
Prof. Dr. M. Grundmann, Prof. Dr. A. Macke (Leibniz-Institut für Troposphärenforschung e. V.)
SAW-2012-IfT-4

3D in situ Ellipsometrie
Dr. R. Schmidt-Grund, Dr. K. Bundesmann (Leibniz-Institut für Oberflächenmodifizierung e. V.)
Forschungs- und Entwicklungsvertrag im Rahmen der Förderung aus dem Europäischen Sozialfonds

Transparente photovoltaische Zellen
Prof. Dr. M. Grundmann
Europäischer Fonds für regionale Entwicklung (EFRE) Energie und Klimaschutz – RL EuK 2007

Leistungselektronik auf Basis von Galliumoxid
Prof. Dr. M. Grundmann
Europäischer Fonds für regionale Entwicklung (EFRE) Energie und Klimaschutz – RL EuK 2007

Herstellung und Charakterisierung von transparenten Feldeffekttransistoren
Dipl.-Phys. A. Lajn
Landesinnovationsstipendium des Freistaates Sachsen im Rahmen des Europäischen Sozialfonds

Magnetische Tunnelkontakte
Dipl.-Phys. J. Zippel

Landesinnovationsstipendium des Freistaates Sachsen im Rahmen des Europäischen Sozialfonds

Funktionalisierte Nanosäulen
Prof. Dr. M. Grundmann
ESF-Nachwuchsforschergruppe *Funktionale multiskalige strukturen* des Freistaates Sachsen im Rahmen des Europäischen Sozialfonds

Elektron-Phonon-Wechselwirkung in Mikro- und Nanonadeln
Dipl.-Phys. Christian Kranert
Landesinnovationspromotionsstipendium des Freistaates Sachsen im Rahmen des Europäischen Sozialfonds

Magnetotunnel-Widerstände mit oxidischen Kontakten
Michael Bonholzer, M.Sc.
Landesinnovationspromotionsstipendium des Freistaates Sachsen im Rahmen des Europäischen Sozialfonds

Internationale Zusammenarbeit in Bildung und Forschung mit Neuseeland: Grundlegende Eigenschaften und Anwendungen von MgZnO/ZnO Heterostrukturen
Dr. H. von Wenckstern
NZL 10/010, Deutsches Zentrum für Luft- und Raumfahrt e. V., Internationales Büro des BMBF

Internationale Zusammenarbeit in Bildung und Forschung mit Südafrika: Elektrische Charakterisierung von bei tiefen Temperaturen in ZnO Volumenmaterial und ZnO Nanostrukturen eingebrachten Defekten
Dr. H. von Wenckstern
SUA 09/037, Deutsches Zentrum für Luft- und Raumfahrt e. V., Internationales Büro des BMBF

8.22 Organizational Duties

M. Grundmann

- Direktor des Instituts für Experimentelle Physik II
- Coordinator of the European Network of Excellence on "Self-Assembled semiconductor Nanostructures for new Devices in photonics and Electronics" (SANDiE, http://www.sandie.org)
- Stellvertretender Sprecher der Graduiertenschule "Leipzig School of Natural Sciences - Building with Molecules and Nano-objects" (BuildMoNa), http://www. buildmona.de
- Stellvertretender Sprecher des Sonderforschungsbereiches "Funktionalität Oxidischer Grenzflächen" (SFB762), http://www.physik.uni-halle.de/sfb762
- Sprecher der Fächerübergreifenden Arbeitsgemeinschaft Halbleiterforschung Leipzig (FAHL), http://www.uni-leipzig.de/~fahl
- Mitglied des wissenschaftlichen Beirats des Leibniz-Instituts für Oberflächenmodifizierung e. V., Leipzig (IOM)

- Project Reviewer: Deutsche Forschungsgemeinschaft (DFG), Alexander von Humboldt-Stiftung (AvH), Schweizerischer Nationalfonds zur Förderung der wissenschaftlichen Forschung (FNSNF), Fonds zur Förderung der Wissenschaften (FWF), EU
- Referee: Appl. Phys. Lett., Electr. Lett., J. Appl. Phys., Nature, Physica E, Phys. Rev. B., Phys. Rev. Lett., Phys. Stat. Sol., Adv. Materials, u.a.

M. Lorenz
- Project Reviewer: Deutsche Forschungsgemeinschaft (DFG)
- Referee: Advanced Functional Materials, Applied Physics Letters, Applied Surface Science , Crystal Growth and Design, European Physics Journal, IEEE Transactions on Nuclear Science, Journal of Physical Chemistry, Journal of Physics D: Applied Physics, Japanese Journal of Applied Physics, Materials Science and Engineering, Nanotechnology, Physica Status Solidi (a) and RRL, Thin Solid Films

H. von Wenckstern
- Referee: Appl. Phys. Lett., J. Appl. Phys., Thin Solid Films, Solid State Electron., Phys. Stat. Sol., Superlatt. Microstruct., J. Electron. Mater., Turk. J. Phys., J. Mater. Sci., Mater. Electron., J. Vac. Sci. Technol., Mater. Sci. Eng. B, J. Nanosci. Nanotechnol., Microelectron. Eng., J. Phys. D, J. Cryst. Growth, Surf. Sci.

R. Schmidt-Grund
- Project Reviewer: Deutsche Forschungsgemeinschaft (DFG), US Department of Energy, Basic Energy Science
- Referee: Thin Solid Films, Current Applied Physics, Phys. Stat. Sol. C, Nature Communications, Appl. Phys. Lett., Optics Express, Journal of Electromagnetic Waves and Applications, Opt. Materials, ACS Applied Materials & Interfaces

H. Frenzel
- Referee: IEEE Electronic Device Letters, Thin Solid Films, Applied Physics Letters, ETRI Journal, Journal of Applied Physics, Japanese Journal of Applied Physics, Advanced Materials, physics status solidi (a)

8.23 External Cooperations

Academic

- Leibniz-Institut für Oberflächenmodifizierung e. V., Leipzig, Germany
  Prof. Dr. B. Rauschenbach, Prof. Dr. S. Mayr, Dr. J. Gerlach, Dr. K. Bundesmann
- Universität Leipzig, Fakultät für Chemie und Mineralogie, Germany
  Prof. Dr. H. Krautscheid, Prof. Dr. R. Denecke
- Universität Halle-Wittenberg, Germany
  Prof. Dr. I. Mertig, Prof. Dr. W. Widdra
- Max-Planck-Institut für Mikrostrukturphysik, Halle/Saale, Germany
  Dr. O. Breitenstein, Dr. A. Ernst, Dr. P. Werner, Prof. Dr. D. Hesse
- Forschungszentrum Dresden-Rossendorf, Germany
  Prof. Dr. M. Helm, Dr. K. Potzger

- Technische Universität Berlin, Germany
  Prof. Dr. D. Bimberg, Prof. Dr. A. Hoffmann
- University of Aveiro, Portugal
  Prof. N. A. Sobolev
- Universität Gießen, Germany
  Prof. Dr. B. Meyer
- Universität Magdeburg, Germany
  Prof. Dr. A. Krost, Dr. J. Bläsing, Prof. Dr. J. Christen
- Universität Jena, Germany
  Prof. Dr. C. Ronning
- Göteborg University, Sweden
  Prof. Dr. M. Willander
- NCSR "Demokritos", Institute of Materials Science, Greece
  Prof. Dr. A. Travlos
- University of Pretoria, South Africa
  Prof. F. D. Auret
- University of Canterbury, Christchurch, New Zealand
  Prof. Dr. S. Durbin, Prof. Dr. M. Allen
- University of Nebraska, Lincoln, USA
  Prof. Dr. M. Schubert
- Centre de Recherche sur l' Hétéro-Epitaxie et ses Applications (CNRS-CRHEA), Valbonn, France
  Dr. J. Zúñiga-Pérez
- University at Buffalo, USA
  Prof. Dr. S. M. Durbin

Industry

- Solarion AG, Leipzig Germany
  Dr. Alexander Braun, Dr. Andreas Rahm
- Freiberger Compound Materials GmbH, Freiberg, Germany
  Dr. G. Leibiger
- Q-Cells SE, Thalheim, Germany
  Dr. K. Petter

8.24 Publications

Journals

M. Brandt, M. Bonholzer, M. Stölzel, G. Benndorf, D. Spemann, M. Lorenz, M. Grundmann: *Electrical transport in strained $Mg_xZn_{1-x}O$:P thin films grown by pulsed laser deposition on ZnO (000-1)*, phys. stat. sol. (b) **249**(1), 82-90 (2012)

C.P. Dietrich, M. Lange, T. Böntgen, M. Grundmann: *The corner effect in hexagonal whispering gallery microresonators*, Appl. Phys. Lett. **101**, 141116 (5 pages) (2012)

C.P. Dietrich, M. Lange, M. Stölzel, M. Grundmann: *Microwire (Mg,Zn)O/ZnO and (Mg,Zn)O/(Cd,Zn)O non-polar quantum well heterostructures for cavity applications*, Appl. Phys. Lett. **100**(3), 031110 (4 pages) (2012)

S. Durbin, T. Veal, M. Grundmann, J. Phillips: *Focus Issue on Oxide Semiconductors, Introduction*, J. Mat. Res. **27**(17), 2179 (1 page) (2012) (Materials Research Society, Warrendale, PA, 2012)

H. Franke, C. Sturm, R. Schmidt-Grund, G. Wagner, M. Grundmann: *Ballistic propagation of exciton-polariton condensates in a ZnO-based microcavity*, New J. Phys. **14**, 013037 (12 pages) (2012)

H. Frenzel, M. Lorenz, F.-L. Schein, A. Lajn, F.J. Klüpfel, T. Diez, H. von Wenckstern, M. Grundmann: *Metal-semiconductor field-effect transistors and integrated circuits based on ZnO and related oxides*, Handbook of Zinc Oxide and Related Materials, Vol. 2 Devices and Nano-Engineering, p. 369-434 (2012), Z.C. Feng, ed. (Taylor and Francis/CRC Press, Florida, USA, 2012), ISBN 978-1439855744

M. Grundmann, C.P. Dietrich: *Whispering gallery modes in deformed hexagonal resonators*, phys. stat. sol. (b) **249**(5), 871-879 (2012)

R. Heinhold, H.-S. Kim, F. Schmidt, H. von Wenckstern, M. Grundmann, R.J. Mendelsberg, R.J. Reeves, S.M. Durbin, M.W. Allen: *Optical and defect properties of hydrothermal ZnO with low lithium contamination*, Appl. Phys. Lett. **101**, 062105 (4 pages) (2012)

M. Lange, C.P. Dietrich, K. Brachwitz, T. Böntgen, M. Lorenz, M. Grundmann: *(Zn,Cd)O thin films for the application in heterostructures: structural and optical properties*, J. Appl. Phys. **112**, 103517 (6 pages) (2012)

M. Lange, J. Kupper, C.P. Dietrich, M. Brandt, M. Stölzel, G. Benndorf, M. Lorenz, M. Grundmann: *Exciton localization and phonon sidebands in polar ZnO/MgZnO quantum wells*, Phys. Rev. B **86**(4), 045318 (7 pages) (2012)

M. Lange, C.P. Dietrich, K. Brachwitz, M. Stölzel, M. Lorenz, M. Grundmann: *Visible emission from ZnCdO/ZnO multiple quantum wells*, phys. stat. sol. RRL **6**(1), 31-33 (2012)

M. Lorenz, M. Ziese, G. Wagner, J. Lenzner, C. Kranert, K. Brachwitz, H. Hochmuth, P. Esquinazi, M. Grundmann: *Exchange bias and magnetoelectric coupling effects in $ZnFe_2O_4$-$BaTiO_3$ composite thin films*, CrystEngComm **14**, 6477-6486 (2012)

M. Lorenz, A. Reinhardt, H. von Wenckstern, M. Grundmann: *Design rules of (Mg,Zn)O-based thin-film transistors with high-κ WO_3 dielectric gates*, Appl. Phys. Lett. **101**, 183502 (4 pages) (2012)

S. Müller, H. von Wenckstern, O. Breitenstein, J. Lenzner, M. Grundmann: *Microscopic identification of hot spots in multi-barrier Schottky contacts on pulsed laser deposition grown zinc oxide thin films*, IEEE Transact. Electr. Dev. **59**(3), 536-541 (2012)

M. Noltemeyer, F. Bertram, Th. Hempel, B. Bastek, A. Polyakov, J. Christen, M. Brandt, M. Lorenz, M. Grundmann: *Excitonic Transport in ZnO*, J. Mat. Res. **27**(17), 2225-2231 (2012)

M. Noltemeyer, F. Bertram, T. Hempel, B. Bastek, J. Christen, M. Brandt, M. Lorenz, M. Grundmann: *Excitonic transport in ZnO*, Proc. SPIE **8263**, 82630X (2012)

J.P. Richters, J. Kalden, M. Gnauck, C. Ronning, C.P. Dietrich, H. von Wenckstern, M. Grundmann, J. Gutowski, T. Voss: *Modal gain and its diameter dependence in single ZnO micro- and nanowires*, Semic. Sci. Technol. **27**, 015005 (5 pages) (2012)

F.-L. Schein, H von Wenckstern, H. Frenzel, M. Grundmann: textitZnO-based n-channel junction field-effect transistor with room-temperature fabricated p-type $ZnCo_2O_4$-gate, IEEE Electron Device Letters **33**(5), 676-678 (2012)

F. Schmidt, H. von Wenckstern, D. Spemann, M. Grundmann: *On the radiation hardness of (Mg,Zn)O PLD thin films*, Appl. Phys. Lett. **101**, 012103 (4 pages) (2012)

M. Schmidt, M. Ellguth, R. Karsthof, H. von Wenckstern, R. Pickenhain, M. Grundmann, G. Brauer, F.C.C. Ling: *On the T2 trap in zinc oxide thin films*, phys. stat. sol. (b) **249**(3), 588-595 (2012)

M. Schmidt, H. von Wenckstern, R. Pickenhain, M. Grundmann: *On the investigation of electronic defect states in ZnO thin films by space charge spectroscopy with optical excitation*, Sol. St. Electr. **75**, 48-54 (2012)

M. Stölzel, J. Kupper, M. Brandt, A. Müller, G. Benndorf, M. Lorenz, M. Grundmann: *Electronic and optical properties of ZnO/(Mg,Zn)O quantum wells with and without a distinct QCSE*, J. Appl. Phys. **111**, 063701 (10 pages) (2012)

H. von Wenckstern, R. Schmidt-Grund, C. Bundesmann, A. Müller, C.P. Dietrich, M. Stölzel, M. Lange, M. Grundmann: *The (Mg,Zn)O Alloy*, Handbook of Zinc Oxide and Related Materials, Vol. 1 Materials, p. 257-320 (2012), Z.C. Feng, ed. (Taylor and Francis/CRC Press, Florida, USA, 2012), ISBN 978-1439855706

J. Zippel, M. Lorenz, G. Benndorf, M. Grundmann: *Persistent layer-by-layer growth for pulsed-laser homoepitaxy of (000-1) ZnO*, phys. stat. sol. RRL **6**(11), 433-435 (2012)

Talks

K. Brachwitz, K. Mexner, M. Lorenz, F. Bern, M. Ziese, P. Esquinazi, M. Grundmann: *Zinc ferrite - magnetic thin films with highly tunable conductivity*, 76th Spring Meeting of the German Physical Society 2012, Berlin, Germany, March 2012

K. Brachwitz, M. Lorenz, M. Grundmann: *Defect-induced conduction mechanism in spinel-type ferrites*, MRS Fall Meeting 2012, Boston, Massachusetts, USA, November 2012

M. Bonholzer, K. Brachwitz, J. Zippel, A. Setzer, P. Esquinazi, M. Lorenz, M. Grundmann: *Magnetic tunnel junctions based on zinc ferrite and cobalt*, 76th Spring Meeting of the German Physical Society 2012, Berlin, Germany, March 2012

F. Daume, A. Rahm, M. Grundmann: *Application of series resistance imaging techniques to Cu(In,Ga)Se_2 solar cells*, 3rd International Workshop on CIGS Solar Cell Technology, Berlin, Germany, April 2012

F. Daume, A. Rahm, A. Braun: *Sodium in Cu(In,Ga)Se_2 solar cells: beneficial influences & damp heat stability*, E-MRS spring meeting 2012, Strasbourg, France, May 2012

F. Daume, S. Puttnins, A. Rahm, A. Braun, M. Grundmann: *The Influence of sodium on the long-term stability of Cu(In,Ga)Se_2 solar cells*, 5th BuildMoNa Workshop for Doctoral Candidates, Burgstätt, Germany, September 2012

C.P. Dietrich, M. Lange, M. Stölzel, H. Franke, M. Grundmann: *ZnO microwire quantum well heterostructures*, SPIE Photonics West 2012, San Francisco, CA, USA, January 2012

H. Franke, C. Sturm, R. Schmidt-Grund, T. Michalsky, G. Wagner, M. Grundmann: *Exciton-polariton condensates in a ZnO-based microcavity*, 76th Spring Meeting of the German Physical Society 2012, Berlin, Germany, March 2012

H. Franke, C. Sturm, A. Meißner, R. Schmidt-Grund, M. Grundmann: *ZnO-based microcavities with different dimensionality*, International Conference on Superlattices, Nanostructures, and Nanodevices, Dresden, Germany, July 2012

M. Grundmann: *Amorphous Oxides for Diodes and Transistors*, 4th Intational Symposium on Transparent Conductive Materials (TCM-4), Crete, Greece, October 2012 (invited)

M. Grundmann: *Nanowires Through the Decades or Accidents in Epitaxy*, Honorary Symposium for Prof. Dr. Dr. h.c. Dieter Bimberg, TU Berlin, Germany, 16.11.2012 (invited)

M. Grundmann: *ZnO-based microwire and nanowire quantum well heterostructures for cavity applications*, International Workshop on ZnO and Related Materials (IWZnO 2012), Nice, France, November 2012

M. Grundmann: *Oxide Materials Enabling Novel Device Applications*, MRS Fall Meeting 2012, Boston, Massachusetts, USA, November 2012 (invited)

M. Grundmann: *Neue Oxide für die Dünnfilmtechnik*, Symposium 20 Jahre TGZ, TGZ Bitterfeld, Germany, 15.11.2012

M. Lorenz, M. Ziese, G. Wagner, C. Kranert, K. Brachwitz, P. Esquinazi, M. Grundmann: *Exchange Bias and Magnetodielectric Coupling Effects at Nanocrystalline $ZnFe_2$ O_4 –$BaTiO_3$ Interfaces*, MRS Fall Meeting 2012, Boston, Massachusetts, USA, November 2012

M. Lorenz, H. von Wenckstern, M. Grundmann: *Tungsten oxide as gate dielectric for highly transparent and temperature-stable zinc oxide based thin-film transistors*, 6th Transparent Conductive Materials Conference 2012, Hersonissos, Greece, October 2012

S. Müller, H. von Wenckstern, R. Heinhold, M. Allen, M. Grundmann: textitProperties of high-quality Schottky contacts on PLD-grown ZnO thin films: Rectification, temperature stability and effective Richardson constant, MRS Fall Meeting 2012, Boston, Massachusetts, USA, November 2012

S. Müller, H. von Wenckstern, F. Schmidt, D. Splith, M. Grundmann: *Structural and electrical properties of Si-doped beta-Ga_2O_3 thin films*, MRS Fall Meeting 2012, Boston, Massachusetts, USA, November 2012

A. Reinhardt, M. Lorenz, H. von Wenckstern, M. Grundmann: *Passivation of tungsten trioxide gated MISFETs based on ZnO channel material*, 76th Spring Meeting of the German Physical Society 2012, Berlin, Germany, March 2012

F.-L. Schein, M. Lorenz, H. von Wenckstern, M. Grundmann: *Tungsten oxide as gate dielectric for highly transparent and temperature-stable zinc oxide based thin-film transistors*, 8th International Thin-Film Transistors Conference Lisbon, Portugal, January 2012

F.-L. Schein: *p-leitende Oxide für Transparente Elektronik*, EFDS Workshop "Transparente leitfähige Oxide", Dresden, Germany, May 2012, invited

F.-L. Schein, P. Schlupp, H. von Wenckstern, M. Grundmann: *Amorphous oxides $ZnCo_2O_4$ and ZnSnO - Thin films and devices*, MRS Fall Meeting 2012, Boston, Massachusetts, USA, November 2012

F. Schmidt, H. von Wenckstern, M. Schmidt, D. Spemann, M. Grundmann: *Electrical characterization of proton-irradiated MgZnO thin films*, 76th Spring Meeting of the German Physical Society 2012, Berlin, Germany, March 2012

F. Schmidt, H. von Wenckstern, M. Schmidt, D. Spemann, M. Grundmann: *Electrical characterization of proton-irradiated MgZnO thin films*, Pretorias, South Africa, October 2012, invited

F. Schmidt, R. Pickenhain, H. von Wenckstern, M. Grundmann, S. Geburt, C. Ronning, O. Breitenstein: *Low Rate Deep Level Transient Spectroscopy (LR-DLTS) - A qualitative study on Fe-implanted ZnO thin films*, Jena, Germany, December 2012, invited

F. Schmidt, H. von Wenckstern, D. Spemann, M. Grundmann: *On the Radiation Hardness of (Mg,Zn)O PLD Thin Films*, MRS Fall Meeting 2012, Boston, Massachusetts, USA, November 2012

H. von Wenckstern, F. Schmidt, M. Scheibe, G. Benndorf, M. Grundmann: *Comparative study of c-, a-, and m-planar ZnO thin films*, 7th International Workshop on Zinc Oxide and Related Materials, Nice, France, September 2012

H. von Wenckstern, F. Schmidt, M. Scheibe, G. Benndorf, M. Grundmann: *Comparative study of c-, a-, and m-planar ZnO thin films*, MRS Fall Meeting 2012, Boston, Massachusetts, USA, November 2012

J. Zippel, M. Lorenz, G. Benndorf, M. Grundmann: *Persistent Layer-by-layer Growth for Pulsed Laser Homoepitaxy of (0001) ZnO*, MRS Fall Meeting 2012, Boston, Massachusetts, USA, November 2012

Posters

K. Brachwitz, M. Jenderka, A. Timopheev, A. Azevedo, N. Sobolev, A. Setzer, P. Esquinazi, M. Lorenz, M. Grundmann: *Structural and magnetic properties of zinc ferrite thin films grown by pulsed-laser deposition*, 76th Spring Meeting of the German Physical Society 2012, Berlin, Germany, March 2012

K. Brachwitz, M. Bonholzer, M. Lorenz, M. Ziese, P. Esquinazi, M. Grundmann: *Zinc ferrite - Magnetic thin films with highly tunable conductivity*, Intermag 2012, IEEE International Magnetics Conference, Vancouver, Canada, May 2012

K. Brachwitz, K. Mexner, A. Setzer, M. Lorenz, P. Esquinazi, M. Grundmann: *Zinc ferrite - magnetic thin films with highly tunable conductivity*, 5th Scientific Symposium of the Graduate School BuildMoNa, Leipzig, Germany, March 2012

M. Bonholzer, K. Brachwitz, J. Zippel, A. Setzer, P. Esquinazi, M. Lorenz, M. Grundmann: *Magnetic tunnel junctions based on zinc ferrite and cobalt*, Intermag 2012, IEEE International Magnetics Conference, Vancouver, Canada, May 2012

M. Bonholzer, K. Brachwitz, J. Zippel, A. Setzer, P. Esquinazi, M. Lorenz, M. Grundmann: *Magnetic tunnel junctions based on zinc ferrite and cobalt*, Spintronics Workshop, Regensburg, Germany, September 2012

M. Bonholzer, K. Brachwitz, J. Zippel, A. Setzer, P. Esquinazi, M. Lorenz, M. Grundmann: *Magnetic Tunnel Junctions Based on Zinc Ferrite and Cobalt*, MRS Fall Meeting 2012, Boston, Massachusetts, USA, November 2012

F. Daume, S. Puttnins, C. Scheit, H. Zachmann, A. Rahm, A. Braun, M. Grundmann: *Damp heat treatment of Cu(In,Ga)Se_2 solar cells with different sodium content*, 76th Spring Meeting of the German Physical Society 2012, Berlin, Germany, March 2012

F. Daume, S. Puttnins, A. Rahm, A. Braun, M. Grundmann: *Influence of sodium on flexible Cu(In,Ga)Se_2solar cells under damp heat treatment*, 5th Scientific Symposium of the Graduate School BuildMoNa, Leipzig, Germany, March 2012

C.P. Dietrich, M. Lange, M. Grundmann: *Whispering gallery modes in irregular and inhomogeneous polygonal microcavities*, 5th Scientific Symposium of the Graduate School BuildMoNa, Leipzig, Germany, March 2012

C.P. Dietrich, M. Lange, R. Schmidt-Grund, M. Grundmann: *Whispering gallery modes in irregular and inhomogeneous polygonal microcavities*, ICPS 2012 - 31th International Conference on the Physics of Semiconductors, Zürich, Switzerland, August 2012

H. Franke, A. Janot, C. Sturm, R. Schmidt-Grund, T. Hyart, B. Rosenow, M. Grundmann: *Disorder effects in polariton condensates in a ZnO-based microcavity*, ICPS 2012 - 31th International Conference on the Physics of Semiconductors, Zürich, Switzerland, August 2012

C. Heinrichs, C. Sturm, H. Franke, S. Linke, T. Böntgen, R. Schmidt-Grund, M. Grundmann: *Time Resolved Generalized Ellipsometry*, 76th Spring Meeting of the German Physical Society 2012, Berlin, Germany, March 2012

F.J. Klüpfel, S. Schmidt, A. Lajn, H. Frenze, H. von Wenckstern, J.A. Käs, M. Grundmann: *Transparent active multi-electrode arrays for measuring neuron signals*, 5th Scientific Symposium of the Graduate School BuildMoNa, Leipzig, Germany, March 2012

F.J. Klüpfel, D. Splith, S. Müller, H. von Wenckstern, M. Grundmann: *Passivation of ZnO-based MESFETs*, 76th Spring Meeting of the German Physical Society 2012, Berlin, Germany, March 2012

F.J. Klüpfel, S. Schmidt, A. Lajn, H. Frenze, H. von Wenckstern, J.A. Käs, M. Grundmann: *Transparent active multi-electrode arrays for measuring neuron signals*, Saxon Biotechnology Symposium 2012, Leipzig, Germany, June 2012

C. Kranert, R. Schmidt-Grund, M. Grundmann: *Polarisation dependence of UV Raman scattering in wurtzite semiconductors*, 76th Spring Meeting of the German Physical Society 2012, Berlin, Germany, March 2012

C. Kranert, R. Schmidt-Grund, M. Grundmann: *Exciton-mediated 1LO Raman scattering in wurtzite-structure crystals*, ICPS 2012 - 31th International Conference on the Physics of Semiconductors, Zürich, Switzerland, August 2012

M. Lorenz, H. von Wenckstern, M. Grundmann: *Tungsten trioxide as high-κ gate dielectric for highly transparent and temperature-stable zinc-oxide based thin-film transistors*, 76th Spring Meeting of the German Physical Society 2012, Berlin, Germany, March 2012

S. Müller, H. von Wenckstern, O. Breitenstein, J. Lenzner, M. Grundmann: *Microscopic identification of hot spots in multi-barrier Schottky contacts on pulsed laser deposition grown zinc oxide thin films*, 76th Spring Meeting of the German Physical Society 2012, Berlin, Germany, March 2012

S.Müller, H. von Wenckstern, M. Grundmann: *Properties of high-quality Schottky contacts to ZnO: Rectification, temperature stability and effective Richardson constant*, 7th International workshop on ZnO and related Materials, Nice, France, September 2012

F.-L. Schein, M. Winter, T. Böntgen, J. Lenzner, H. von Wenckstern, H. Frenzel, M. Grundmann: *ZnO-based n-channel junction field-effect transistor with room-temperature fabricated p-type $ZnCo_2O_4$-gate*, 8th International thin-film transistor conference, Lisbon, Portugal, January 2012

F.-L. Schein, M. Winter, T. Böntgen, J. Lenzner, H. von Wenckstern, H. Frenzel, M. Grundmann: *ZnO-based n-channel junction field-effect transistor with room-temperature fabricated p-type $ZnCo_2O_4$-gate*, 76th Spring Meeting of the German Physical Society 2012, Berlin, Germany, March 2012

F.-L. Schein, M. Winter, T. Böntgen, J. Lenzner, H. von Wenckstern, H. Frenzel, M. Grundmann: *ZnO-based n-channel junction field-effect transistor with room-temperature fabricated p-type $ZnCo_2O_4$-gate*, 5th Scientific Symposium of the Graduate School BuildMoNa, Leipzig, Germany, March 2012

F. Schmidt, H. von Wenckstern, M. Schmidt, D. Spemann, M. Grundmann: *Electrical characterization of proton-irradiated MgZnO thin films*, 7th International Workshop on Zinc Oxide and Related Materials, Nice, France, September 2012

M. Thuner, H. Franke, C. Sturm, R. Schmidt-Grund, A. Janot, B. Rosenow, M. Grundmann: *Propagation vs. localization of polariton BEC*, BuildMoNa Minisymposium Quantum Coherence in Nanostructures, Leipzig, Germany, October 2012

H. von Wenckstern, M. Lorenz, A. Reinhardt, M. Grundmann, S. Wickert, R. Denecke: *Tungsten trioxide as gate dielectric for highly transparent zinc-oxide based thin-film transistors*, MRS Fall Meeting 2012, Boston, Massachusetts, USA, November 2012

8.25 Graduations

Doctorate

- Matthias Schmidt
  Space Charge Spectroscopy applied to Defect Studies in Ion-Implanted Zinc Oxide Thin Films
  February 2012
- Alexander Müller
  Einfluss der Mischkristallunordnung auf die Lumineszenz von wurtzitischem MgZnO
  June 2012
- Jan Zippel
  Gepulste Laserabscheidung und Charakterisierung funktionaler oxidischer Dünnfilme und Heterostrukturen
  November 2012
- Christof Peter Dietrich
  Cavity effects in polygonal resonators
  December 2012
- Helena Franke
  PLD-grown ZnO-based Microcavities for Bose-Einstein Condensation of Exciton-Polaritons
  December 2012
- Alexander Lajn
  Transparent rectifying contacts on wide-band gap oxide semiconductors
  December 2012
- Martin Lange
  Herstellung und Charakterisierung von planaren und drahtförmigen Heterostrukturen mit ZnO- und (Zn,Cd)O-Quantengräben
  December 2012

Master

- Steve Linke
  Spinpolarisation der Exciton-Polaritonenemission in ZnO basierten Mikrokavitäten
  February 2012

- Christian Schmidt
  Strukturelle, optische und elektrische Untersuchung von Sc-dotierten ZnO-Dünnfilmen
  May 2012
- Anna Reinhardt
  Untersuchungen zur Passivierung von ZnO-basierten Metall-Isolator-Halbleiter-Feldeffekttransistoren
  October 2012
- Robert Karsthof
  Der Einfluss der Pufferschicht in flexiblen Cu(In,Ga)Se_2 Dünnschicht-Solarzellen
  November 2012
- Tom Michalsky
  Orts- und winkelaufgelöste Photolumineszenzspektroskopie an ZnO basierten Mikroresonatoren
  December 2012
- Markus Jenderka
  Growth and Properties of Na_2IrO_3 Thin Films
  December 2012
- Steffen Richter
  Exciton-Polaritons in ZnO-based Microresonators: Pseudospin and Magnetic Fields
  December 2012

Bachelor

- Martin Klass
  Ladungsträger in multikristallinem Solarsilicium
  January 2012
- Benjamin Oesen
  Investigation and Comparison of different methods of Thickness Measurement of thin organic Layers
  February 2012
- Tobias Lühmann
  Tieftemperatur-Ellipsometrie zur Bestimmung der temperaturabhängigen dielektrischen Funktion von Al_2O_3- uned YSZ-Dünnschichten
  July 2012
- Vitaly Zviagin
  Dielectric Function and Structural Properties of $ZnCo_2O_4$ Thin Films in Dependence on the Growth Conditions
  September 2012
- Stefan Lange
  Ortsaufgelöste Untersuchung von verbogenen Zinkoxid-Mikronadeln
  November 2012
- Katharina Rudisch
  Polarized Photoluminescence of MgZnO Heterostructures
  December 2012

8.26 Guests

- Prof. Dr. Yoshito Ashizawa
  College of Science and Technology, Nihon University, Funabashi, Japan
  16. Junly – 30. September 2012
- Dr. Vera Lazenka
  INPAC, KU Leuven, Leuven, Belgium
  8. October – 20. October 2012
- Wilbert Mtangi
  University of Pretoria, Pretoria, South Africa
  16. September – 24. September 2012
- Johan Janse von Rensburg
  University of Pretoria, Pretoria, South Africa
  18. February – 4. March 2012
- Sherzod Khujanov, M. Sc.
  Academy of Science of Usbekistan, Tashkent, Usbekistan
  Optische Eigenschaften verzerrter Mikrodrähte
  Islamic Development Bank within its Scholarship Programme
  since May 2012
- Abdurashid Mavlonov, M. Sc.
  Academy of Science of Usbekistan, Tashkent, Usbekistan
  Novel oxide materials for economic and efficient solar cells
  Islamic Development Bank within its Scholarship Programme
  since September 2012

9

Superconductivity and Magnetism

9.1 Introduction

The main interests of the group are phenomena related to superconductivity and magnetism in solids. In the last few years the research activities in superconductivity have been mainly focused in searching for its existence in graphite, especially at graphite interfaces between Bernal-like crystalline regions. This research issue started in our division in Leipzig in the year 2000 and became supporting experimental evidence quite recently, indicating the existence of superconductivity at temperatures above 100 K. Future work will be concerned with the localization of the superconducting phases and the increase of the superconducting yield.

Our division was the first to show that atomic lattice defects can produce magnetic order in graphite without the need of magnetic ions. This phenomenon is known nowadays as Defect-Induced Magnetism and it is found in a broad spectrum of different materials. We are involved in a collaborative research project with the aim of triggering this phenomenon in nominally non-magnetic oxides, via vacancies and/or hydrogen doping. Further research topic is the study of the electrical and magnetic properties of oxide multilayers of thickness starting from a few unit cells. Main research issues are related to the magnetic coupling at the interfaces of oxide layers, i.e. exchange bias phenomena, with different magnetic properties as well as the possibility to develop a two-dimensional electron gas at the interfaces.

Pablo Esquinazi

9.2 Can doping graphite trigger room temperature superconductivity?

T. Scheike, W. Böhlmann, P. Esquinazi, J. Barzola-Quiquia, A. Ballestar, A. Setzer

Theoretical studies in the last ten years predict that graphite as well as graphene are good candidates for high-temperature superconductivity. In fact, some reports in the past 38 years suggest its existence in these materials but did not attract the necessary attention or independent verifications were reported. In this study we show reproducible evidence for granular superconductivity in powders of several tens of

micrometers small graphite grains after treatment with pure water. The temperature, magnetic field and time dependence of the magnetic moment of the treated powder provides evidence for the existence of superconducting vortices with some similarities to high-temperature granular superconducting oxides but at much higher temperatures.

[1] T. Scheike, W. Böhlmann, P. Esquinazi, J. Barzola-Quiquia, A. Ballestar and A. Setzer, Adv. Mater. **24**, 58261 (2012)

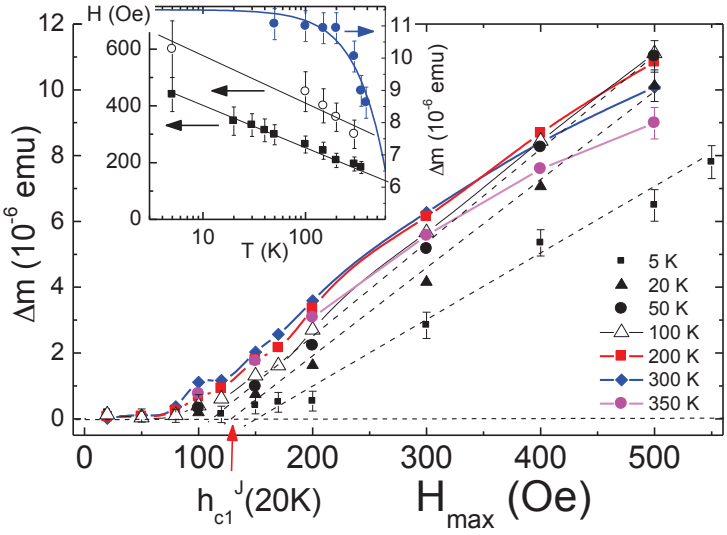

Figure 9.1: (Full remanent ($H = 0$) magnetic moment width Δm of the hysteresis loops measured after cycling the sample (61.5 mg) to a maximum field $H_{\max}$ at different temperatures. The lower Josephson critical field h^J_{c1} is defined at the crossing point between the zero line and the linear increasing lines (dashed straight lines as examples for 5K, 20K and 50K). Similar values and temperature dependence are obtained plotting the data semilogarithmic and defining h^J_{c1} at constant $\Delta m = 3x10^{-7}$ emu. The red arrow shows this field for the curve measured at 20 K. Inset: Temperature dependence of the lower (close squares) and upper (open circles) critical Josephson fields (left y-axis). The measured values of the lower critical field were multiplied by a factor of three in this figure. The right y-axis corresponds to the width Δm of the hysteresis field loop at zero field after cycling the field to $H_{\max} = 500$ Oe.

9.3 Multiferroic behaviour of magnetite (Fe_3O_4)

M. Ziese, P. Esquinazi, D. Pantel*, M. Alexe,* N.M. Nemes†, M. Garcia-Hernández‡

*Max Planck Institute of Microstructure Physics, 06120 Halle, Germany
†GFMC Departamento Física Aplicada III, Universidad Complutense de Madrid, E-28040 Madrid, Spain
‡Instituto de Ciencia de Materiales de Madrid-CSIC, Cantoblanco, E-28049 Madrid, Spain

We investigated the electric polarization, dielectric permittivity, magnetoelectric effect, heat capacity, magnetization and ac susceptibility of magnetite films and polycrystals. Both films and polycrystals showed a magnetoelectric effect. The electric polarization could only be measured for magnetite films and had saturation values between 4 and

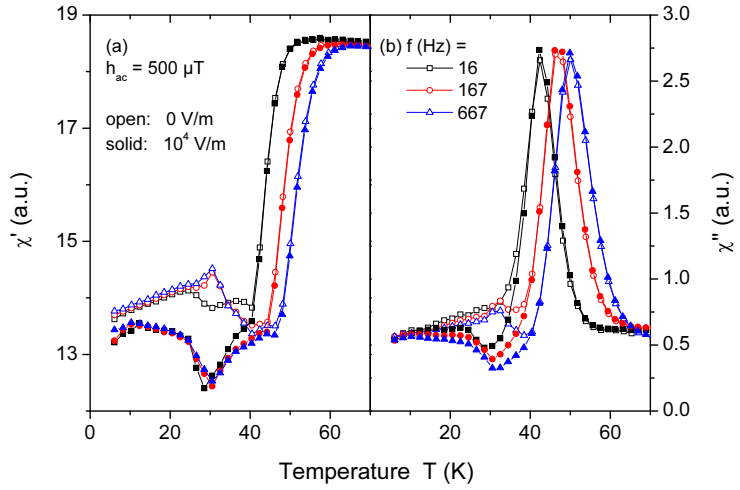

Figure 9.2: (a) Real and (b) loss component of the ac susceptibility of a magnetite polycrystal as a function of temperature. The measurements were made at various frequencies and with (solid symbols) or without (open symbols) an electric field applied across the sample. At low temperatures a magnetoelectric effect was observed.

8 μC cm^{-2}; the electric polarization vanished at a sample dependent temperature between 32 and 38 K, i.e. far below the Verwey transition. The magnetoelectric effects of magnetite films and polycrystals were only found at low temperatures below a frequency-dependent crossover, see Fig. 9.1. This might arise from multiferroic relaxor behavior.

9.4 Stabilization of ferromagnetic order in $La_{0.7}Sr_{0.3}MnO_3$-$SrRuO_3$ superlattices

M. Ziese, F. Bern, E. Pippel*, D. Hesse,* I. Vrejoiu*

*Max Planck Institute of Microstructure Physics, 06120 Halle, Germany

The study of spatially confined complex oxides is of wide interest, since correlated electrons at interfaces might form exotic phases. We have investigated $La_{0.7}Sr_{0.3}MnO_3$ /$SrRuO_3$ superlattices with coherently grown interfaces using structural techniques, magnetization, and magnetotransport measurements. Magnetization measurements showed that ferromagnetic order in ultrathin $La_{0.7}Sr_{0.3}MnO_3$ layers is stabilized in the superlattices down to layer thicknesses of at least two unit cells. This stabilization was destroyed, if the ferromagnetic layers are separated by two unit cell thick $SrTiO_3$ layers. The corresponding values of the Curie temperatures are shown in Fig. 9.2. The resistivity of the superlattices showed metallic behavior and was dominated by the conducting $SrRuO_3$ layers, the Hall resistivity showed an anomalous Hall effect from both $SrRuO_3$ and $La_{0.7}Sr_{0.3}MnO_3$ layers. >From this we infer that the $La_{0.7}Sr_{0.3}MnO_3$ layers are not only ferromagnetic but also highly conducting; probably a conducting hole gas is induced at the interfaces that stabilizes the ferromagnetic order. This result opens up an alternative route for the fabrication of two- dimensional systems with long-range ferromagnetic order.

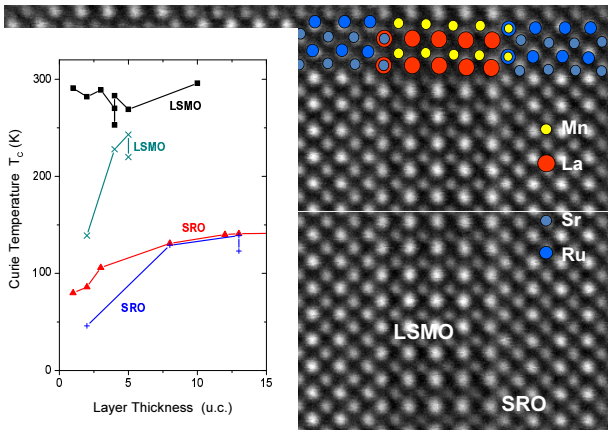

Figure 9.3: High resolution TEM image of a $La_{0.7}Sr_{0.3}MnO_3$ /$SrRuO_3$ superlattice and Curie temperatures of the $La_{0.7}Sr_{0.3}MnO_3$ and $SrTuO_3$ layers in $La_{0.7}Sr_{0.3}MnO_3$ /$SrRuO_3$ (black and red symbols) and $La_{0.7}Sr_{0.3}MnO_3$ /$SrTiO_3$/$SrRuO_3$/$SrTiO_3$ superlattices.

9.5 Hall effect of tetragonal $SrRuO_3$

F. Bern, M. Ziese, K. Dörr,* A. Herklotz,* I. Vrejoiu†

*Institut für Physik, Martin-Luther-Universität Halle-Wittenberg, 06099 Halle, Germany
†Max Planck Institute of Microstructure Physics, 06120 Halle, Germany

The Hall effect of a tetragonal $SrRuO_3$ film was measured and – in contrast to the Hall effect of orthorhombic $SrRuO_3$ – was found to be positive in the ferromagnetic phase. A comparison of the Hall resistivity of tetragonal and orthorhombic $SrRuO_3$ is shown in Fig. 9.3.

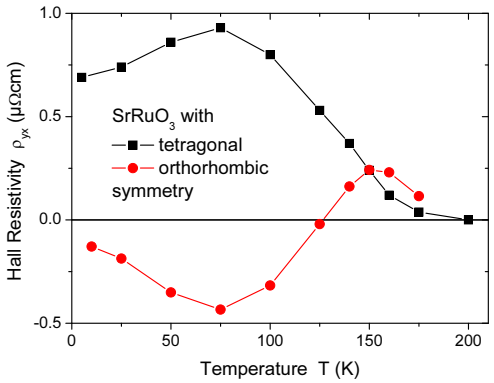

Figure 9.4: Hall resistivity ρ_{yx} of tetragonal and orthorhombic $SrRuO_3$ films at 7 T as a function of temperature.

9.6 Quantum oscillations and ferromagnetic hysteresis observed in iron filled multiwall carbon nanotubes

J. Barzola-Quiquia, N. Klingner, J. Krüger, A. Molle, P. Esquinazi, A. Leonhardt,* M.T. Martinez,†

*IFW Dresden, Helmholtzstrasse 20, 01069 Dresden, Germany
†Institute of Carbochemistry, CSIC, Zaragoza, E-50018, Spain

We report on the electrical transport properties of single multiwall carbon nanotubes with and without an iron filling as a function of temperature and magnetic field. For the iron filled nanotubes the magnetoresistance shows a magnetic behavior induced by iron, which can be explained by taking into account a contribution of s-d hybridization. In particular, ferromagnetic-like hysteresis loops were observed up to 50 K for the iron filled multiwall carbon nanotubes. The magnetoresistance shows quantum interference phenomena such as universal conductance fluctuations and weak localization effects.

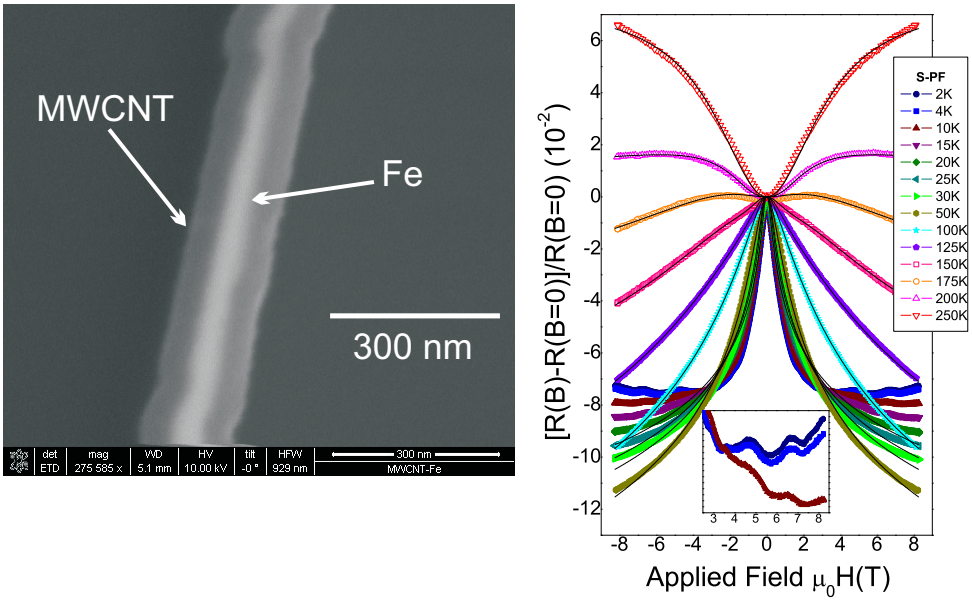

Figure 9.5: Left panel: Scanning electron microscope picture of the investigated sample. Right panel: Magnetoresistance of the Fe filled sample measured at magnetic fields applied perpendicular to the main sample axis. The lines through the data are fits done using a semiempirical equation. The inset shows the Universal Quantum Fluctuations.

9.7 Effect of the dry nanodispersion procedure in the magnetic order of the Co_3O_4 surface

I. Lorite, L. Pérez,* J.J. Romero,† J.F. Fernandez†

*Dept. Física de Materiales, Universidad Complutense de Madrid, 28040 Madrid, Spain
†Instituto de Ceramica y Vidrio, ICV-CISC, 28049 Madrid, Spain

The ferrimagnetism at the interface of the Co_3O_4 nanoparticles and microparticles used as substrate depends on different parameters of nanoparticles dry dispersion methodology. The quantity of nanoparticles, the energy and the time employed in the process play a key role in the dispersion efficiency. A better dispersion of the nanoparticles produces a larger covering of the Al_2O_3 microparticles substrate and larger UV-vis absorbance and M_S. The magnetic order strongly depends on the number of interaction nanoparticle substrate related to dispersion degree. UV-vis absorbance is a good parameter to measure the dispersion and, therefore, a fingerprint of the magnetic order. Due to the relation between UV-vis absorbance and M_S, it was possible to optimize the dry dispersion parameter to obtain the maximum M_S.

9.8 Funding

Study of intrinsic and extrinsic phenomena in the electrical transport properties of multi-graphene
Prof. P. Esquinazi
DFG ES 86/16-1

Defect-induced Magnetism in Oxides
Prof. P. Esquinazi
DFG SFB762 B1

Magnetic and electric properties of oxide superlattices with ultrathin single layers
Dr. M. Ziese and Prof. P. Esquinazi
DFG SFB 762 B5

Untersuchung des Einflusses von Leerstellen und Wasserstoff auf die elektrischen, magnetischen und optischen Eigenschaften von ZnO und $Mg_xZn_{1-x}O$ Nanostrukturen
Prof. P. Esquinazi
DAAD

Development of nanostructured ZnO Biosensors for the detection of very low concentration of analytes in Biomedical Applications
Prof. P. Esquinazi
BMBF

9.9 Organizational Duties

P. Esquinazi

- Dean of Studies
- Project Reviewer: Deutsche Forschungsgemeinschaft (DFG), National Science Foundation (USA), German-Israeli Foundation (GIF), Israel Science Foundation, Department of Energy (Washington), DAAD
- Referee: Phys. Rev. Lett, Phys. Rev. B., Appl. Phys. Lett., Chem. Phys. Lett., Nature Physics, Nature Materials, Physica C, Phys. Lett. A, phys. stat. sol., J. Low Temp. Phys., Carbon, J. Chem. Phys., Eur. J. Phys. B, J. Magn. Magn. Mater.

M. Ziese
- Head of the Undergraduate Physics Laboratory
- Member of the study commission
- Referee: Phys. Rev. Lett., Phys. Rev. B., Adv. Mater., Appl. Phys. A, Current Nanoscience, Eur. Phys. J. B, IEEE Trans. Magn., J. Phys.: Condens. Matter, J. Phys. D: Appl. Phys., J. Alloys Comp., J. Appl. Phys., J. Am. Ceram. Soc., J. Magn. Magn. Mater., J. Mater. Research, J. Mater. Science, Materials Science and Engineering B, Nanotechnology, Nuclear Inst. and Methods in Physics Research B, phys. stat. sol., Thin Solid Films

W. Böhlmann
- Referee: J. Physical Chemistry, J. of American Chemical Society, Microporous and Mesoporous Materials

9.10 External Cooperations

Academic

- State University of Campinas, Campinas, Brazil
  Prof. Dr. Yakov Kopelevich
- Max-Planck Institute of Microstructure Physics, Halle, Germany
  Dr. Ionela Vrejoiu
- Max-Planck Institute of Microstructure Physics, Halle, Germany
  Prof. Dietrich Hesse
- Max-Planck Institute of Microstructure Physics, Halle, Germany
  Dr. Marin Alexe
- Max-Planck Institute of Microstructure Physics, Halle, Germany
  Dr. Arthur Ernst
- Martin-Luther Universität Halle-Wittenberg, Halle, Germany
  Prof. Ingrid Mertig
- Martin-Luther Universität Halle-Wittenberg, Halle, Germany
  Prof. Wolfram Hergert
- Martin-Luther Universität Halle-Wittenberg, Halle, Germany
  Dr. Angelika Chassé
- Martin-Luther Universität Halle-Wittenberg, Halle, Germany
  Dr. Manfred Dubiel
- Stanford Synchrotron Radiation Laboratory, USA
  Dr. Hendrik Ohldag
- Max-Planck-Institut für Metallforschung, Stuttgart, Germany
  Dr. Eberhard Goering
- Laboratorio de Física de Sistemas Pequeños y Nanotecnologíia, Consejo Superior de Investigaciones Científicas, Madrid, Spain
  Prof. N. García (Madrid)

- Forschungszentrum Dresden-Rossendorf e.V., Institut für Ionenstrahlphysik und Materialforschung, Germany
  Dr. W. Anwand
- Forschungszentrum Dresden-Rossendorf e.V., Institut für Ionenstrahlphysik und Materialforschung, Germany
  Dr. G. Brauer
- Tucuman University, Argentina
  Prof. S. P. de Heluani
- University of La Plata, Argentina
  Dr. C. E. Rodriguez Torres
- Universidad Autónoma de Madrid, Spain
  Prof. Dr. Miguel Angel Ramos
- University of Ioannina, Greece, Ioannina, Greece
  Prof. I. Panagiotopoulos

9.11 Publications

Journals

R. Wunderlich, C. Chiliotte, G. Bridoux, T. Maity, Ö. Kocabiyik, A. Setzer, M. Ziese and P. Esquinazi:
Structural, magnetic and electric properties of $HoMnO_3$ films on $SrTiO_3$ (001)
J. Magn. Magn. Mater. **324**, 460 (2012)

J. Barzola-Quiquia, N. Klingner, J. Krüger, A. Molle, P. Esquinazi, A. Leonhardt and M. T. Martínez:
Quantum oscillations and ferromagnetic hysteresis observed in iron filled multiwall carbon nanotubes
Nanotechnology **23**, 015707 (2012)

G. Bridoux, J. Barzola-Quiquia, F. Bern, W. Böhlmann, I. Vrejoiu, M. Ziese and P. Esquinazi:
An alternative route towards micro- and nano-patterning of oxide films
Nanotechnology **23**, 085302 (2012)

M. Ziese, P. D. Esquinazi, D. Pantel, M. Alexe, N. M. Nemes and M. Garcia-Hernández:
Magnetite (Fe_3O_4): a new variant of relaxor multiferroic?
J. Phys.: Condens. Matter **24**, 086007 (2012)

P. Esquinazi, J. Barzola-Quiquia, S. Dusari and N. García:
Length dependence of the resistance in graphite: Influence of ballistic transport
J. Appl. Phys. **111**, 033709 (2012)

Y. Ma, A. Setzer, J. W. Gerlach, F. Frost, P. Esquinazi and S. G. Mayr:
Freestanding Single Crystalline Fe-Pd Ferromagnetic Shape Memory Membranes - Role of Mechanical and Magnetic Constraints Across the Martensite Transition
Adv. Funct. Mater. **22**, 2529 (2012)

M. Khalid and P. Esquinazi:
Hydrogen-induced ferromagnetism in ZnO single crystals investigated by magneto-transport
Phys. Rev. B **85**, 134424 (2012)

N. García, P. Esquinazi, J. Barzola-Quiquia and S. Dusari:
Evidence for semiconducting behavior with a narrow band gap of Bernal graphite
New Journal of Physics **14**, 053015 (2012)

D. Spemann, M. Rothermel, P. Esquinazi, M. A. Ramos, Y. Kopelevich and H. Ohldag:
Comment on "Revealing common artifacts due to ferromagnetic inclusions in highly oriented pyrolytic graphite" by Sepioni M. et al.
Europhys. Lett. **98**, 57006 (2012)

M. Lorenz, M. Ziese, G. Wagner, J. Lenzner, C. Kranert, K. Brachwitz, H. Hochmuth, P. Esquinazi and M. Grundmann:
Exchange bias and magnetodielectric coupling effects in $ZnFe_2O_4$-$BaTiO_3$ composite thin films
CrystEngComm **14**, 6477 (2012)

J. Barzola-Quiquia, A. Lessig, A. Ballestar, C. Zandalazini, G. Bridoux, F. Bern and P. Esquinazi:
Revealing the origin of the vertical hysteresis loop shifts in an exchange biased Co/YMnO3 bilayer
J. Phys.: Condens. Matter **24**, 366006 (2012)

M. Ziese, F. Bern, E. Pippel, D. Hesse and I. Vrejoiu:
Stabilization of Ferromagnetic Order in $La_{0.7}Sr_{0.3}MnO_3$ - $SrRuO_3$ Superlattices
Nano Letters **12**, 4276 (2012)

T. Scheike, W. Böhlmann, P. Esquinazi, J. Barzola-Quiquia, A. Ballestar and A. Setzer:
Can Doping Graphite Trigger Room Temperature Superconductivity? Evidence for Granular High-Temperature Superconductivity in Water-Treated Graphite Powder
Adv. Mater. **24**, 5826 (2012)

in press

F. Bern, M. Ziese, K. Dörr, A. Herklotz and I. Vrejoiu:
Hall effect of tetragonal and orthorhombic $SrRuO_3$ films
DOI 10.1002/pssr.201206500

M. Ziese and I. Vrejoiu:
Properties of manganite/ruthenate superlattices with ultrathin layers
DOI 10.1002/pssr.201307007

Talks

A. Ballestar:
Electric Field induced Superconductivity in Multigraphene
DPG spring meeting, Berlin, March 2012

F. Bern:
Magnetotransport and Hall effect studies of $SrRuO_3/SrTiO_3$ superlattices
JEMS 2012, Parma, Italy, September 2012

F. Bern:
Structural, Magnetic and Magnetotransport Properties of Manganite/Ruthenate Superlattices
WOE19, Apeldoorn, The Netherlands, October 2012

M. Ziese:
Existence of a magnetically ordered hole gas at the $La_{0.7}Sr_{0.3}MnO_3/SrRuO_3$ interface
JEMS 2012, Parma, Italy, September 2012

Posters

A. Ballestar, J. Barzola-Quiquia, S. Dusari, P. Esquinazi, R. da Silva and Y. Kopelevich:
Electric Field induced Superconductivity in Multigraphene
"Correlations and coherence in quantum systems" Conference in Évora, Portugal, October 2012

A. Ballestar, J. Barzola-Quiquia, S. Dusari, P. Esquinazi, R. da Silva and Y. Kopelevich:
Electric Field induced Superconductivity in Multigraphene
5th Scientific Symposium of the Graduate School BuildMoNa, Leipzig, March 2012

Francis Bern, Michael Ziese and Ionela Vrejoiu:
Hall effect in ultrathin LSMO/SRO superlattices
DPG spring meeting, Berlin, March 2012

F. Bern, M. Ziese, I. Vrejoiu, E. Pippel and D. Hesse:
Characterization of $SrRuO_3/SrTiO_3$ Superlattices by Magnetization and Magnetotransport
WOE19, Apeldoorn, The Netherlands, October 2012

I. Lorite, A. Ballestar, J. Barzola-Quiquia and P. Esquinazi:
Study of the transport properties frequency dependence of multilayer graphene by Impedance Spectroscopy
Trends in Nanotechnology 2012 (TNT), Madrid, September 2012

M. Ziese, A. Setzer, R. Wunderlich, C. Zandalazini and P. Esquinazi:
Angular dependence of the magnetoelectric effect in orthorhombic $HoMnO_3$ films
JEMS 2012, Parma, Italy, September 2012

9.12 Graduations

Doctorate

- Srujana Dusari
  Ballistic Transport in Multigraphene Samples
  09.02.2012

- M. Sc. Muhammad Khalid
  Defect-induced magnetism in non-magnetic oxides
  03.04.2012

Master

- Justus Krüger
  Magnetotransport Measurements of Multigraphene Samples at Higher Magnetic Fields
  15.11.2012
- Thomas Scheike
  High Temperature Superconductivity of Water Treated Graphite Powder
  13.12.2012
- Axel Molle
  Some magnetic moment observations on an epitaxial high-temperature-superconductor colossal-magnetoresistance-manganite bilayer
  14.12.2012

Bachelor

- Mahsa Zoraghi
  Raman Spectroscopy of Multi- and Few layers Graphene after Oxygen Plasma Etching
  21.05.2012

9.13 Guests

- Prof. Dr. Silvia Perez
  Universidad Nacional de Tucumán, Argentine
  26.-29.03.2012
- Dr. David Comedi
  Universidad Nacional de Tucumán, Argentine
  10.-21.04.2012
- Gustavo Grinblat
  Universidad Nacional de Tucumán, Argentine
  09.04.-03.06.2012
- Pablo Joaquín Serrano Santos
  Universidad San Francisco de Quito, Ecuador
  25.05.-24.08.2012
- Jacek Wasik
  Politechnika Gdanska, Poland
  29.06.-29.09.2012
- Dr. Rossana Madrid
  Universidad Nacional de Tucumán, Argentine
  14.-27.10.2012

- Dr. Nsoyani Mbekum Beri
  Instituto de Microeletronica de Barcelona, Spain
  22.-26.10.2012
- Luciano Sappia
  Universidad Nacional de Tucumán, Argentine
  14.10.-29.12.2012
- Natalia Cuello
  Centro de Investigacion de Tecnología y Química (CITeQ) Córdoba, Argentine
  01.11.-31.12.2012

III

Institute for Theoretical Physics

10

Computational Quantum Field Theory

10.1 Introduction

The Computational Physics Group performs basic research into classical and quantum statistical physics with special emphasis on phase transitions and critical phenomena. In the centre of interest are the physics of spin glasses, diluted magnets and other materials with quenched, random disorder, soft condensed matter physics with focus on fluctuating paths and interfaces, biologically motivated problems such as protein folding, aggregation and adsoprtion as well as related properties of homopolymers, and the intriguing physics of low-dimensional quantum spin systems. Our investigations of a geometrical approach to the statistical physics of topological defects with applications to superconductors and superfluids and research into fluctuating geometries with applications to quantum gravity, e.g., dynamical triangulations, build on the previous European Research Training Network (RTN) "ENRAGE": *Random Geometry and Random Matrices: From Quantum Gravity to Econophysics*, a collaboration of 13 teams throughout Europe. Moreover, initiated by a bi-national Institute Partnership with the Jagiellonian University in Krakow, Polen, supported by the Alexander von Humboldt (AvH) Foundation the statistical mechanics of complex networks is studied. In April 2012 a new Institute Partnership Grant of the Alexander von Humboldt Foundation with the Institute for Condensed Matter Physics of the National Academy of Sciences in Lviv, Ukraine, commenced with special focus on *Polymers in Porous Environments and on Disordered Substrates*.

The methodology is a combination of analytical and numerical techniques. The numerical tools are currently mainly Monte Carlo computer simulations and exact enumeration techniques. The computational approach to understand physical phenomena is expected to gain more and more importance with the future advances of computer technology, and is likely to become the third cornerstone of physics besides experiment and analytical theory as sketched in Fig. 10.1. Already now it can help to bridge the gap between experiments and the often necessarily approximate calculations of analytical work. To achieve the desired high efficiency of the numerical studies we develop new algorithms, and to guarantee the flexibility required by basic research all computer codes are implemented by ourselves. The technical tools are Fortran, C, and C++ programs running under Unix or Linux operating systems and computer algebra

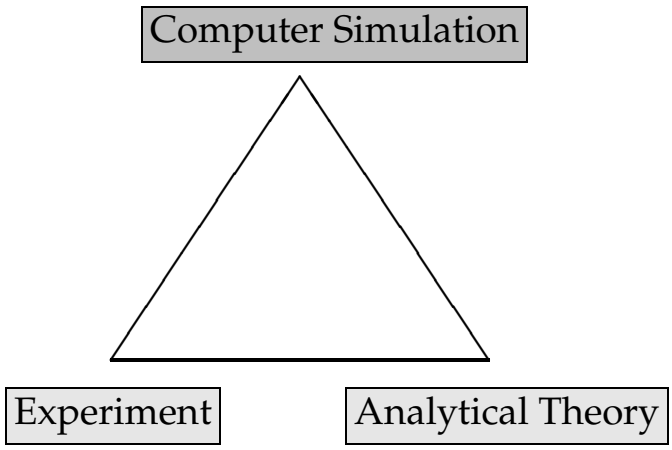

Figure 10.1: Sketch of the relationship between theory, experiment and computer simulation.

using Maple or Mathematica. The software is developed and tested at the Institute on a cluster of PCs and workstations, where also most of the numerical analyses are performed. Currently we are also exploring the possibilities of the rapidly developing graphics card computing, that is computer simulations on graphics processing units (GPUs) with many cores. Large-scale simulations requiring vast amounts of computer time are carried out at the Institute on quite powerful compute servers, at the parallel computers of the University computing center, and, upon successful grant application at the national supercomputing centres in Jülich, Stuttgart and München on parallel supercomputers. This hierarchy of various platforms gives good training opportunities for the students and offers promising job perspectives in many different fields for their future career.

Within the University, our research activities are closely integrated into the Graduate School "BuildMoNa": Leipzig School of Natural Sciences – *Building with Molecules and Nano-objects*, the International Max Planck Research School (IMPRS) *Mathematics in the Sciences* and the international DFH-UFA Graduate School *Statistical Physics of Complex Systems* with Université de Lorraine in Nancy, France, supported by the Deutsch-Französische Hochschule. In the second funding period 2011–2013, Coventry University in England has been integrated as an associated partner. The three Graduate Schools are all "Classes" of the Research Academy Leipzig (RALeipzig), providing the organizational frame for hosting visiting students and senior scientists, offering language courses, organizing childcare and for many other practical matters. At the post-graduate level our research projects are embedded into the "Sächsische DFG-Forschergruppe" FOR877 *From Local Constraints to Macroscopic Transport* and the Sonderforschungsbereich/Transregio SFB/TRR 102 *Polymers under Multiple Constraints: Restricted and Controlled Molecular Order and Mobility* together with Halle University. Our group also actively contributes to two of the top level research areas ("Profilbildende Forschungsbereiche (PbF)") and the Centre for Theoretical Sciences (NTZ) of the University. Beside "BuildMoNa" the latter structures are particularly instrumental for our cooperations with research groups in experimental physics and biochemistry on the one hand and with mathematics and computer science on the other.

On an international scale, our research projects in part initiated by the European RTN "ENRAGE" and the AvH Institute Partnership with the Jagiellonian University in Krakow, Poland, are currently carried out in a wide net of collaborations mainly funded by the German Academic Exchange Service (DAAD) and the Alexander von Humboldt Foundation through the new Institute Partnership with the National Academy of Sciences in Lviv, Ukraine, as well as their Fellowship Programmes. From June 2011 to November 2012 our group has been hosting Professor Handan Arkın-Olgar from Ankara University in Turkey who was awarded an Alexander von Humboldt Fellowship for Experienced Researchers. Further close contacts and collaborations are established with research groups in Armenia, Austria, China, France, Great Britain, Israel, Italy, Japan, Poland, Russia, Spain, Sweden, Taiwan, Turkey, Ukraine, and the United States. These contacts are refreshed and furthered through topical Workshops and Tutorials and our International Workshop series *CompPhys: New Developments in Computational Physics*, taking annually place at the end of November just before the first advent weekend.

Wolfhard Janke

10.2 Grafted vs Nongrafted Polymers near Attractive Substrates

M. Möddel*, M. Bachmann†, W. Janke

*Present address: Basycon Unternehmensberatung, Welserstraße 1, 81373 München, Germany
†Center for Simulational Physics, The University of Georgia, Athens, USA

The statistical properties of a polymer grafted, i.e. firmly attached at one of its ends, to an attractive substrate [1] are significantly different from those of a polymer that can move freely above that substrate [2]. Especially for the adsorption transition such differences were suggested by a microcanonical analysis of a nongrafted polymer which showed first-order like signals for short extended conformations that get more pronounced with increasing translational entropy of desorbed conformations [3, 4]. To systematically compare the two cases, we employed a combination of canonical and microcanonical analyses over a wide range of surface attraction strengths ϵ_s and temperature T [1]. This way not only the adsorption transition, but also the collapse and freezing transitions of an individual self-interacting polymer in solution were covered.

Our analysis is based on a simple bead-stick model with 12-6 Lennard-Jones (LJ) interaction between nonbonded monomers, a weak bending stiffness and an attraction to a flat substrate that is proportional to a parameter ϵ_s which measures the relative strength compared to the monomer-monomer attraction. This surface attraction is a 9-3 LJ potential obtained by integrating the 12-6 LJ potential over a half space. The polymer is once grafted with one end to the substrate and once considered in a box within which it can move freely. All simulations were performed with the parallel tempering Monte Carlo method that allowed to highly parallelize the simulation and obtain good statistics over the whole energy range [5].

It turned out that qualitative differences mainly occur at the adsorption transition where four cases need to be differentiated for finite chains: (1) the adsorption of ex-

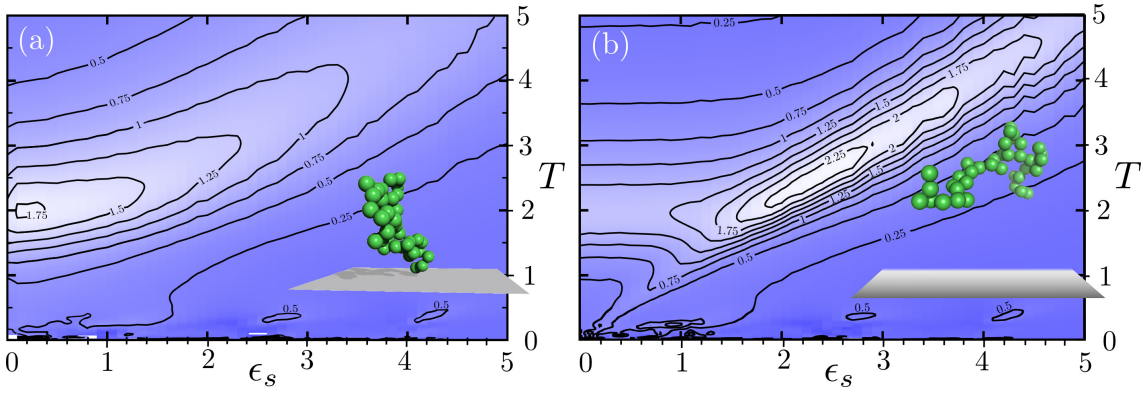

Figure 10.2: Fluctuation of the tensor component of the radius of gyration perpendicular to the substrate $d\left\langle R^2_{\mathrm{gyr},\perp}\right\rangle/dT$ for (a) the grafted and (b) the free polymer as a contour plot versus surface attraction strength ϵ_s and temperature T.

tended nongrafted polymers, (2) the adsorption of extended grafted polymers, (3) the adsorption of globular nongrafted polymers and (4) the adsorption of globular grafted polymers. Only in the first case, the microcanonical entropy, which is proportional to the logarithm of the density of states, gets convex such that the adsorption transition appears first-order-like here. In the cases (2) and (3) a continuous adsorption is observed already for short chains, while in case (4) the adsorption signals get reduced significantly and only a weaker wetting transition is left.

As an example, Fig. 10.2 shows how this is reflected in the temperature derivative of the canonical expectation value of the tensor component of the radius of gyration perpendicular to the substrate. While for the nongrafted polymer a maximum over the whole diagonal $T_{\mathrm{ads}} \propto \epsilon_s$ is visible, this signal is strongly weakened for extended grafted conformations ($\epsilon_s \gtrsim 1.9$, $T \gtrsim 2$) and even disappears for globular grafted conformations ($\epsilon_s \lesssim 1.9$, $T \lesssim 2$). For grafted chains, in this observable only the collapse transition at $T \approx 2$ is signaled for low ϵ_s values. It is among others this necessary distinction between the adsorption of globular and extended conformations that demonstrates that it is not just the difference in translational, but also in conformational entropy that gives rise to the differences. This has been carefully described and explained in Ref. [1].

[1] M. Möddel et al.: Macromolecules **44**, 9013 (2011)
[2] M. Möddel et al.: J. Phys. Chem. B **113**, 3314 (2009)
[3] M. Möddel et al.: Phys. Chem. Chem. Phys. **12**, 11548 (2010)
[4] M. Möddel et al.: Comput. Phys. Commun. **182**, 1961 (2011)
[5] M. Möddel et al.: in Proceedings of the *NIC Symposium 2012*, eds. K. Binder, G. Münster, M. Kremer, John von Neumann Institute for Computing, Jülich, NIC Series, Vol. **45**, p. 277 (2012)

10.3 Polymer Adsorption onto a Stripe-Patterned Substrate

M. Möddel*, M. Bachmann†, W. Janke

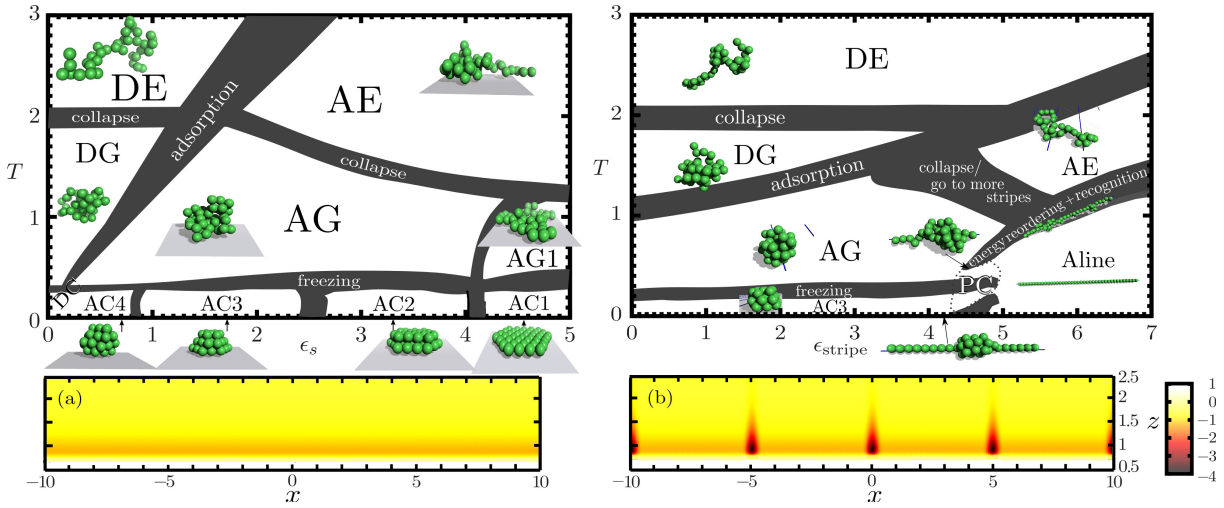

Figure 10.3: (a) On the left the pseudo-phase diagram of the polymer versus temperature and varying ϵ_s for $\epsilon_{\text{stripe}} = 0$ and a heat map of the substrate potential for $\epsilon_s = 1$ is shown – the homogeneous substrate case. (b) On the right the analogous pseudo-phase diagram versus temperature and varying ϵ_{stripe} for $\epsilon_s = 1$ is displayed – the stripe patterned case. Phases with "A/D" are adsorbed/desorbed, while "E", "G", and "C" denote phases with increasing order: expanded, globular, and compact. "PC" is a short form for a region with phase coexistence.

*Present address: Basycon Unternehmensberatung, Welserstraße 1, 81373 München, Germany
†Center for Simulational Physics, The University of Georgia, Athens, Georgia 30602, USA

Naturally occuring substrates almost exclusively exist with heterogeneities not just on the macroscopic, but also on the micro- or nanoscopic level. Consequently, after we developed an in-depth understanding of the statistical equilibrium behaviour of a generic self-attracting polymer model close to an attractive homogeneous substrate in recent years [1–5], the question arose how this behaviour gets modified if hetereogenities are introduced on the substrate.

The goal was to see the influence on the level of the whole pseudo-phase diagram, where "pseudo" refers to the finiteness of the simulated chain length. Since already the phase diagram of the polymer near the homogeneous substrate is very rich in transitions (cf. Fig. 10.3(a)), to extract any meaningful results the chosen surface heterogeneity needs to be easily controllable and preferably simple.

Our choice was to add to the previously investigated [1–5] bulk energy term and 9-3 Lennard-Jones (LJ) attraction between each monomer and the substrate an attractive cosine-square potential of distance $D = 5$ such that the energy of the system in total is

$$E_{\text{bulk}} = 4 \sum_{i=1}^{N-2} \sum_{j=i+2}^{N} \left(r_{ij}^{-12} - r_{ij}^{-6} \right) + \frac{1}{4} \sum_{i=1}^{N-2} (1 - \cos \vartheta_i) \ , \tag{10.1}$$

that is strongly dominated by a 12-6 Lennard-Jones (LJ) attraction between non-neighboring monomers, and

$$E_{\text{sur, stripe}}(x, z) = \begin{cases} \left(\frac{2}{15} z^{-9} - z^{-3}\right) \left[\epsilon_s + \epsilon_{\text{stripe}} \cos^2 \left(\pi \left(\text{mod}\left(x + \frac{D}{2}, D\right) - \frac{D}{2} \right) \right) \right], & \text{if } \left| \text{mod}\left(x + \frac{D}{2}, D\right) - \frac{D}{2} \right| \leq \frac{1}{2} \\ \left(\frac{2}{15} z^{-9} - z^{-3}\right) \epsilon_s, & \text{else.} \end{cases}$$

(10.2)

The impact of those stripes was described in detail with an emphasis on the onset of the "recognition" transition below which the polymer perfectly adapts the shape of the stripe. Despite some striking differences, many conclusions drawn for the adsorption of a single polymer on a homogeneous substrate remain valid in the more general hetereogeneous case [6].

[1] M. Möddel et al.: J. Phys. Chem. B **113**, 3314 (2009)
[2] M. Möddel et al.: Phys. Chem. Chem. Phys. **12**, 11548 (2010)
[3] M. Möddel et al.: Macromolecules **44**, 9013 (2011)
[4] M. Möddel et al.: Comput. Phys. Commun. **182**, 1961 (2011)
[5] M. Möddel et al.: in Proceedings of the *NIC Symposium 2012*, eds. K. Binder, G. Münster, M. Kremer, John von Neumann Institute for Computing, Jülich, NIC Series, Vol. **45**, p. 277 (2012)
[6] M. Möddel et al.: Leipzig preprint, in preparation

10.4 Exact Enumeration of Polymer Adsorption onto a Stripe-Patterned Surface

M. Ivanov, M. Möddel*, W. Janke

*Present address: Basycon Unternehmensberatung, Welserstraße 1, 81373 München, Germany

In recent years, polymers have received a great deal of attention from both experimental and theoretical researchers. However, a complete description of the properties of these materials does not currently exist. Therefore, further research is needed. This particular study is part of an ongoing effort to try to understand these systems and is focused on the adsorption of single polymer chains. Previous theoretical studies have provided phase diagrams that lay the foundations for understanding polymer adsorption. This particular study focuses on a single polymer chain in a confined volume and its adsorption onto a stripe-patterned surface.

A minimalistic simple-cubic lattice model was used where the chain is represented by an interacting self-avoiding walk (ISAW) and was confined between an attractive patterned wall and a steric wall with no interaction whatsoever. The pattern consisted of parallel stripes of defined width and separation. The complete system as well as the patterned surface are illustrated in Fig. 10.4. Besides the pattern parameters, entropy and three energy scales define the phase diagram of the system: chain-surface attraction ϵ_s, chain-pattern attraction ϵ_{str} and chain self-attraction ϵ_m. The energy of the polymer was defined as a function of the different types of contacts $E(n_s, n_{str}, n_m) = -\epsilon_s n_s - \epsilon_{str} n_{str} - \epsilon_m n_m$. One of the coupling constants (ϵ_s) was used to set the scale of the temperature of the system, whereas the other two were expressed as fractions of it. This allowed for the systematic study of a total of four parameters on the properties of the system.

Chains of lengths up to $N = 19$ monomers were studied using the method of exact enumeration. The influence of the energy scales and pattern parameters on the system was analysed with the help of temperature vs. chain-pattern attraction phase diagrams. These diagrams were constructed by means of both canonical and microcanonical

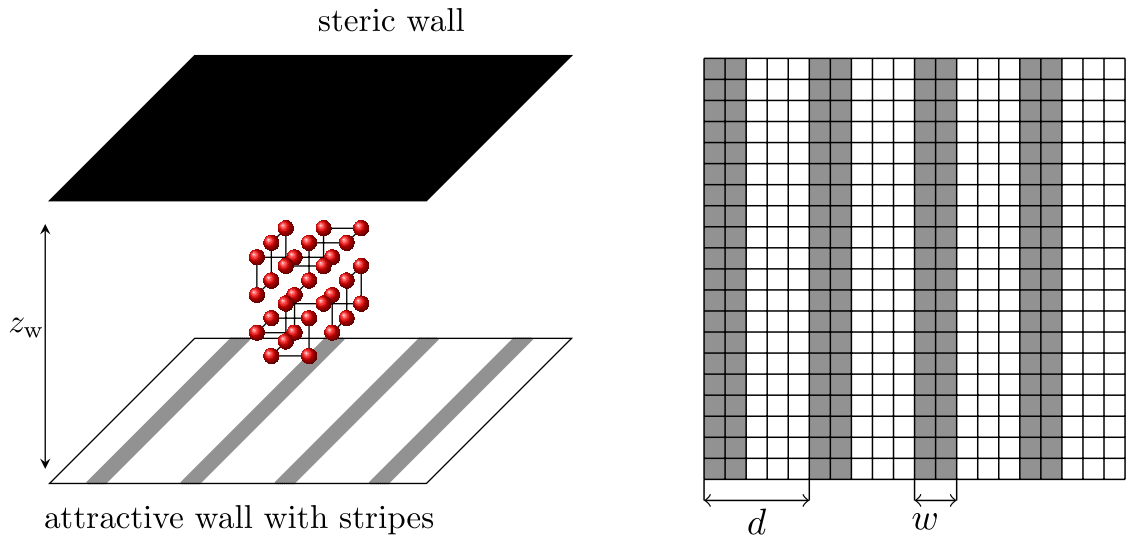

Figure 10.4: Sketch of an ISAW in a cavity of height z_w. The width of the attractive stripes (in grey) is controlled by the parameter w and the stripe distance by the parameter d.

analysis of the simulation data. The results are comparable to those from another study of a similar system using an off-lattice polymer model [1]. Although the two models yield quantitatively different results, both show comparable qualitative behaviour.

The effects of the confinement volume on the phase diagram were found to be considerable when the separation between both walls is $O(N)$. For distances between $O(10\times N)$ and $O(100\times N)$, minor differences of the transition temperatures were found. The results from the non-grafted chain were also compared with the results for a chain grafted to a stripe. However, the grafted chain was considered to be too short and was not analysed in detail.

These findings are important since substantial progress has very recently been made in experimental techniques. More importantly, it is now possible to visualise single chains, enabling the verification of theoretical models against experimental data as part of a future collaborative research.

[1] M. Möddel: *Statistical Equilibrium Behaviour of Finite Polymers Near Attractive Substrates*, PhD thesis, Universität Leipzig (2012)

10.5 Polymers Adsorbing onto a Fractal Surface

V. Blavatska*, W. Janke

*Institute for Condensed Matter Physics, National Academy of Sciences of Ukraine, Lviv, Ukraine

The study of polymers near disordered surfaces is of great importance since most naturally occurring substrates are rough and energetically (or structurally) inhomogeneous and surface heterogeneity is known to have a crucial effect on polymer adsorption phenomena [1]. As most chemical substrates are proved to be of fractal nature, studying the

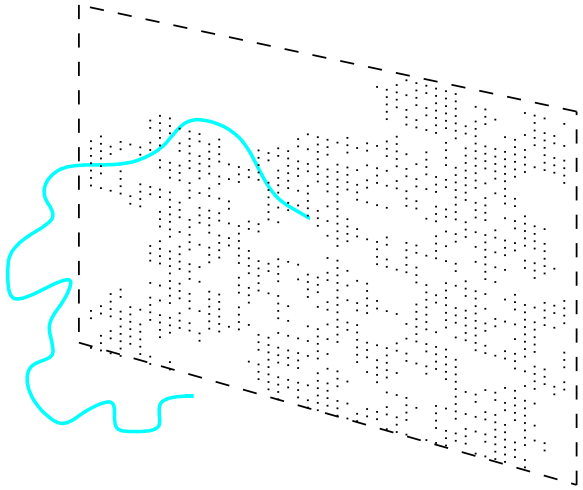

Figure 10.5: Sketch of a polymer grafted to a site of an attractive percolation cluster.

influence of such a non-trivial surface geometry is of particular interest. It is established that the adsorption process is enhanced (diminished) when the fractal dimension of the substrate is larger (smaller) than that of a plain Euclidean surface [2].

As order parameter one considers the fraction of the average number of monomers N_s adsorbed to the surface and the total length N of the polymer chain, obeying for long chains the scaling law $\langle N_s \rangle / N \sim N^{\phi_s - 1}$ where ϕ_s is the surface crossover exponent [3]. In the language of lattice models, where polymers can be represented by self-avoiding random walks (SAWs) [4], disordered surfaces can be modeled as a two-dimensional regular lattice with randomly distributed attractive sites. Fractal properties emerge at the percolation threshold where a spanning percolation cluster of attractive sites with fractal dimension $d_s^{p_c} = 91/49 \approx 1.89 < 2$ appears [5], cf. Fig. 10.5.

We have studied this problem with the help of the pruned-enriched Rosenbluth method (PERM) [6] for simulating the polymer chains. We examined the behaviour of the components of the radius of gyration $\overline{\langle R_{g\parallel}^2 \rangle}$, $\overline{\langle R_{g\perp}^2 \rangle}$ in directions parallel and perpendicular to the surface and obtained $\nu_2^{p_c} = 0.772 \pm 0.006$ [7, 8] for the critical exponent that governs the scaling of the size of a polymer adsorbed onto a fractal substrate. This value is compatible with $\nu_2^{p_c} = 0.782 \pm 0.003$ for a polymer strictly confined onto a two-dimensional percolating cluster [9], but significantly larger than $\nu_2 = 0.742 \pm 0.006 \approx 3/4$ for a plain homogeneous surface [7]. Examining the peak structure of the heat capacity, we estimated for the surface crossover exponent $\phi_s^{p_c} = 0.425 \pm 0.009$, compared to $\phi_s = 0.509 \pm 0.009$ for the plain surface [7]. As expected, the adsorption is diminished, when the fractal dimension of the surface is smaller than that of the plain Euclidean surface due to the smaller number of contacts of monomers with attractive sites.

[1] J. Zierbarth et al.: Macromolecules **40**, 3498 (2007)
[2] E. Bouchaud, J. Vannimenus: J. Physique (France) **50**, 2931 (1989)
[3] E. Eisenriegler et al.: J. Chem. Phys. **77**, 6296 (1982)
[4] C. Vanderzande: *Lattice Models of Polymers* (Cambridge University Press, Cambridge (England) 1998)

[5] S. Havlin, D. Ben Abraham: Adv. Phys. **36**, 155 (1987)
[6] P. Grassberger: Phys. Rev. E **56**, 3682 (1997)
[7] V. Blavatska, W. Janke: J. Chem. Phys. **136**, 104907 (2012)
[8] V. Blavatska, W. Janke: Physics Procedia **34**, 55 (2012)
[9] V. Blavatska, W. Janke: Europhys. Lett. **82**, 66006 (2008); J. Phys. A **42**, 015001 (2009)

10.6 Ground-State Properties of a Polymer Chain Inside an Attractive Sphere Potential

H. Arkın *, W. Janke

*On leave from Department of Physics Engineering, Faculty of Engineering, Ankara University, Tandogan, 06100 Ankara, Turkey

Investigating basic structure formation mechanisms of biomolecules at different interfaces is one of the major challenges of a large variety of modern interdisciplinary research and possible applications in nanotechnology. Knowledge of the origin of structure formation is an important prerequisite for the understanding of polymer adhesion to metals and semiconductors [1], biomedical implants [2], and biosensors [3]. The adsorption behaviour can also influence cellular motion, drug delivery, and other biological processes. The advances in designing and manipulating biomolecules at solid substrates on the nanoscale open new challenges for potential nanotechnological applications of hybrid organic-inorganic interfaces.

Recently, some progress has been achieved in the understanding of general properties of the conformational behaviour of homopolymers and heteropolymers near substrates. In most cases, the substrates are considered to be planar [4]. In this work, we considered a simple off-lattice coarse-grained polymer model inside of an attractive sphere, for which we have recently constructed the finite-temperature phase diagram [5]. Here, we focused on the ground-state properties caused by different attraction strengths ϵ of the sphere within the frame of generalized-ensemble simulations [6]. In a comparative analysis based among others on various (invariant) shape parameters related to the eigenvalues of the gyration tensor, a classification of the structures formed in the accompanying adsorption process has been achieved.

The distributions of all successive pairs of virtual bond angles $\Theta_i = \pi - \vartheta_i$ and torsion angles Φ_i in the low-temperature regime ($T < 0.2$) for different values of the surface attraction strength ϵ are shown in Fig. 10.6. It is one of the most remarkable results of our study that for different parameter values of the polymer-attractive sphere system, we get conformations that fit perfectly to the inner wall of the sphere. A careful comparison with results for flat substrates has recently been presented in Ref. [7].

[1] M. Bachmann et al.: Angew. Chem. Int. Ed. **49**, 9530 (2010)
[2] E. Nakata et al.: J. Am. Chem. Soc. **126**, 490 (2004)
[3] R.F. Service: Science **270**, 230 (1995)
[4] M. Möddel et al.: J. Phys. Chem. B **113**, 3314 (2009); Phys. Chem. Chem. Phys. **12**, 11548 (2010); Comput. Phys. Commun. **182**, 1961 (2011); Macromolecules **44**, 9013 (2011)

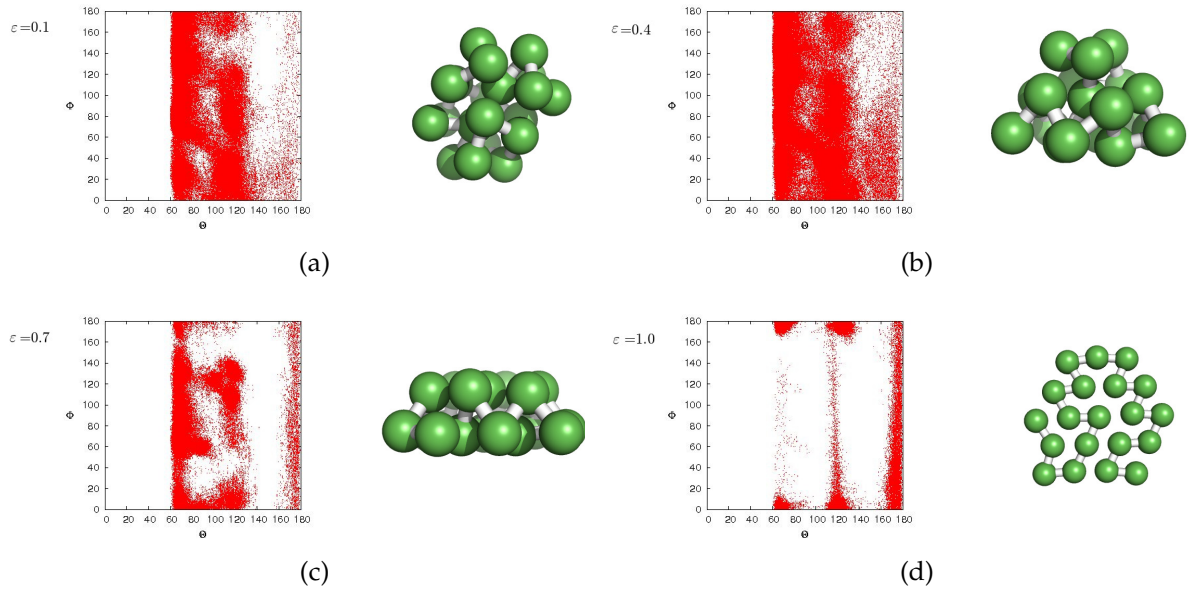

Figure 10.6: Bond and torsion angle distributions for (a) $\epsilon = 0.1$, (b) $\epsilon = 0.4$, (c) $\epsilon = 0.7$, (d) $\epsilon = 1.0$ and the associated conformations of the global energy minimum. The distribution of the torsion angles has reflection symmetry and therefore only the positive interval is shown.

[5] H. Arkın, W. Janke: Phys. Rev. E **85**, 051802 (2012)
[6] H. Arkın, W. Janke: J. Phys. Chem. B **116**, 10379 (2012)
[7] H. Arkın, W. Janke: Eur. Phys. J. – Special Topics **216**, 181 (2013)

10.7 Thermodynamics of a Model Protein in Spherical Confinement

M. Bilsel [*], B. Taşdizen [*], H. Arkın [†], W. Janke

[*]Department of Physics Engineering, Faculty of Engineering,
Ankara University, Tandogan, 06100 Ankara, Turkey
[†]On leave from Department of Physics Engineering, Faculty of Engineering,
Ankara University, Tandogan, 06100 Ankara, Turkey

We have performed Monte Carlo computer simulations in generalized ensembles of a model protein confined in a spherical cage to investigate the dynamics of the folding mechanism [1]. The problem of whether proteins are misfolded or aggregated or, on the contrary, fold properly more promptly in spatial confinement has recently attracted much interest [2, 3]. A detailed understanding of this subject would play a key role for finding treatments to diseases caused by misfolding of proteins. Our goal is thus to analyze the thermodynamics of the folding mechanism and to investigate whether the folding mechanism is controlled or not in a confining environment. To do so we have employed exhaustive multicanonical Monte Carlo simulations by using a minimalistic AB model where hydrophobic residues are labeled by A and the polar or hydrophilic

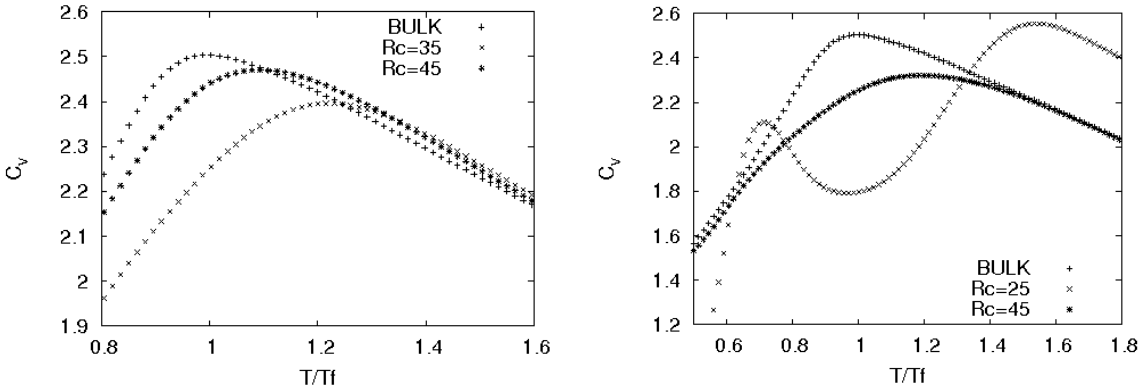

Figure 10.7: Specific heat as a function of temperature for the AB model protein $BA_6BA_4BA_2BA_2B_2$ in a spherical confinement with sphere radius R_c. The temperature T is given in units of the folding temperature T_f in the bulk. *Left:* Purely repulsive potential. *Right:* Attractive potential.

ones by B [4, 5]. Adjacent residues or monomers are connected by rigid covalent bonds. Thus, their distance is kept fixed and set to unity. The contact interaction is replaced by a distance- and residue-dependent $12-6$ Lennard-Jones potential accounting for short-range excluded volume repulsion and long-range interaction. An additional interaction accounts for the bending energy of any pair of successive bonds. In this study, we focused on the folding of a model protein with 20 residues arranged in the sequence $BA_6BA_4BA_2BA_2B_2$.

The model protein is enclosed by a sphere of radius R_c. Apart from the steric hindrance effect, we assumed two different types of wall interactions, one with a purely repulsive wall potential and another that exhibits an attractive part close to the inner sphere wall. By monitoring the specific heat as a function of temperature, we observe in the first, purely repulsive case merely a monotonic finite-size scaling shift of the folding temperature, cf. Fig. 10.7 (left). The second case with attractive wall interaction is much more interesting since here, for small enough sphere radius R_c, the protein is first adsorbed to the (inner) surface of the sphere and in a second step the folding takes place. This is indicated by the two peaks of the specific heat for $R_c = 25$ in Fig. 10.7 (right) [6].

[1] J.A. Hubbell: Curr. Opin. Biotechnol. **10**, 123 (1999); S. Santosa et al.: Nano Lett. **2**, 687 (2002); S. Vauthey et al.: Proc. Natl. Acad. Sci. USA **99**, 5355 (2002)
[2] F. Takagi et al.: Proc. Natl. Acad. Sci. USA **100**, 11367 (2003); N. Rathore et al.: Biophys. J. **90**, 1767 (2006); D. Lu et al.: Biophys. J. **90**, 3224 (2006)
[3] S. Kumar, M.S. Li: Phys. Rep. **486**, 1 (2010)
[4] F.H. Stillinger, T. Head-Gordon: Phys. Rev. E **52**, 2872 (1995); A. Irbäck et al.: Phys. Rev. E **58**, R5249 (1998)
[5] M. Bachmann et al.: Phys. Rev. E **71**, 031906 (2005)
[6] M. Bilsel et al.: in Proceedings of the NIC Workshop *From Computational Biophysics to Systems Biology (CBSB11) – Celebrating Harold Scheraga's 90th Birthday*, eds. P. Carloni, U.H.E. Hansmann, T. Lippert, J.H. Meinke, S. Mo-

hanty, W. Nadler, O. Zimmermann, John von Neumann Institute for Computing, Forschungszentrum Jülich, IAS Series Vol. **8**, p. 21 (2012)

10.8 Effects of Spherical Confinement on Phase Transitions of a Simple Model for Flexible Polymers

M. Marenz, J. Zierenberg, H. Arkın*, W. Janke

*On leave from Department of Physics Engineering, Faculty of Engineering, Ankara University, Tandogan, 06100 Ankara, Turkey

We used our recently developed "Polymer Framework" for Monte Carlo simulations to investigate a simple bead-stick model for a flexible homopolymer. This model features two different pseudo-phase transitions, the collapse transition which distinguishes the random coil and the globular phase and the freezing transition which distinguishes the globular and a crystal like phase. Our model is so simple, that we cannot claim to observe quantities for any specific polymer or biopolymer, but it is also so generic, that it should reflect the qualitative behaviour of any flexible chain-like object. Especially, we are interested in the case where we confine this polymer to a spherical cage as illustrated in Fig. 10.8 and how this confinement influences the two pseudo-phase transitions of our model. On the one hand, confinements are very important for all kind of biopolymers such as proteins, DNA or RNA, because their natural habitat are crowded environments like micelles or chaperon-like cages, where a spherical cage could be considered as a first-order approximation for these environments. For synthetic polymers the behaviour inside a confinement could be also very important for different kinds of technical applications which try to combine polymers with novel materials.

To investigate the thermodynamic behaviour of our model, we need to calculate different thermodynamic observables, such as the energy, the end-to-end distance or the radius of gyration and their thermodynamic derivatives, over a broad temperature range. For this propose we use the parallel tempering Monte Carlo technique [1, 2], which enables us not only to calculate all desired observables over a temperature range, it also helps us to overcome technical problems arising from the complex energy landscape which even such a simple model features [3].

The Hamiltonian of our system is given by a Lennard-Jones potential which corresponds to the excluded-volume and attractive parts of the monomer-monomer interaction, a cosine potential which introduces a bending stiffness to our model and a spherical cage which restricts the phase space of the polymer to a sphere with radius R_S:

$$H = 4\sum_{i=1}^{N-2}\sum_{j=i+2}^{N}\left(\frac{1}{r_{ij}^{12}} - \frac{1}{r_{ij}^{6}}\right) + \kappa\sum_{i=1}^{N-2}(1-\cos\theta_i) \times \begin{cases} 1 & \text{if all } |r_i| < R_S \\ \infty & \text{if any } |r_i| \geq R_S \end{cases} . \tag{10.3}$$

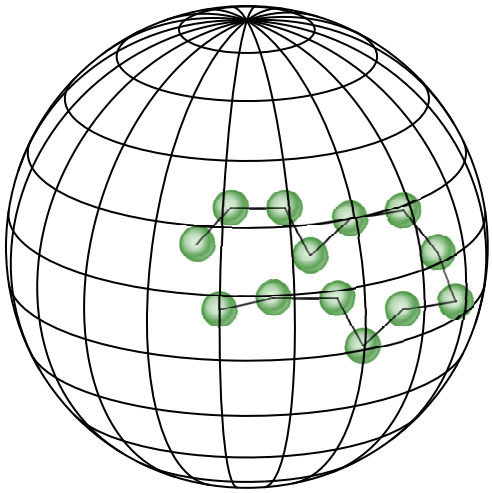

Figure 10.8: Sketch of a polymer fluctuating inside a spherical cage.

Our main goal was to determine the transition temperatures $T_{\max}$ of the pseudo-phase transitions and the dependency of $T_{\max}$ on the radius of the spherical cage. Good indicators for the transition temperature are the maxima of the temperature derivative of several thermodynamic observables, for example of the radius of gyration, $\frac{d}{dT}\langle R^2_{\text{gyr}}\rangle$, see Fig. 10.9. For the freezing transition we observe hardly any change in the position of the phase transition, except for very small radii where the polymer is pressed into very artificial high-energy states due to the repulsive part of the Lennard-Jones potential. In contrast to the freezing transition, the transition temperature of the collapse transition shows a clear dependence on the radius of the sphere. We found the following power law for this dependency, where $T^{\Theta,N}_{\max}$ is the transition temperature in the confined case of the collapse transition for a fixed length N of the polymer and $T^{\Theta,N}_{c}$ is the transition temperature for the free case:

$$|T^{\Theta,N}_{\max} - T^{\Theta,N}_{c}| = A\left(\frac{N^{\frac{1}{2}}}{R_S}\right)^{3.63(15)} . \tag{10.4}$$

The amplitude A is the same for all N. Another notable effect is that the direction of the shift of the transition temperature is opposite to what has been observed in simulations of different realistic models for specific proteins [4–6]. This may depend on the flexibility of the polymer: Our polymer is a very flexible one and most proteins are relatively stiff. The clarification of this question is the objective of further investigations.

[1] K. Hukushima, K. Nemoto: J. Phys. Soc. Japan **65**, 1604 (1996)
[2] C.J. Geyer: in *Computing Science and Statistics*, Proceedings of the 23rd Symposium on the Interface, ed. E.M. Keramidas (Interface Foundation, Fairfax, Virginia 1991), p. 156
[3] M. Marenz et al.: Condens. Matter Phys. **15**, 43008 (2012)
[4] D.K. Klimov et al.: Proc. Natl. Acad. Sci. USA **99**, 8019 (2002)
[5] N. Rathore et al.: Biophys. J. **90**, 1767 (2006)
[6] M. Bilsel et al.: in Proceedings of the NIC Workshop *From Computational Biophysics to Systems Biology (CBSB11) – Celebrating Harold Scheraga's 90th*

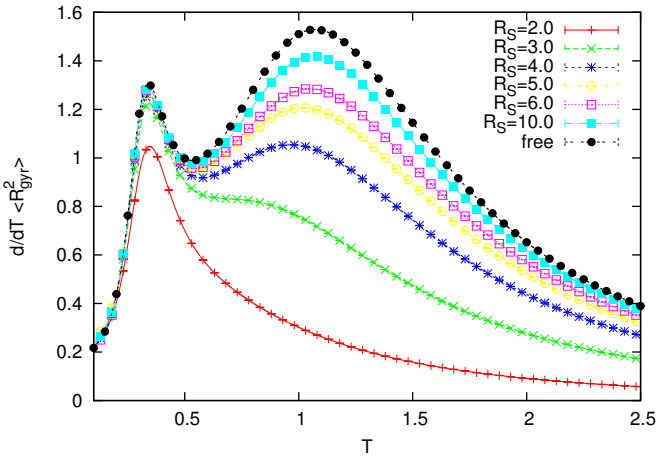

Figure 10.9: The derivative of the radius of gyration, $\frac{d}{dT}\langle R^2_{\text{gyr}}\rangle$, of a 14mer inside spherical cages with different radii.

Birthday, eds. P. Carloni, U.H.E. Hansmann, T. Lippert, J.H. Meinke, S. Mohanty, W. Nadler, O. Zimmermann, John von Neumann Institute for Computing, Forschungszentrum Jülich, IAS Series Vol. **8**, p. 21 (2012)

10.9 Polymer Aggregation Modeled by Interacting Self-Avoiding Walks

J. Zierenberg, A. Tretbar, W. Janke

In order to investigate aggregation of flexible polymers in large systems, we decided to consider interacting self-avoiding walks as a simplified model. This model has been applied to a variety of problems such as protein folding or surface adsorption and yielded good qualitative results. The Hamiltonian of the system is given by

$$\mathcal{H} = -\left(\epsilon_{\text{intra}} n_{\text{intra}} + \epsilon_{\text{inter}} n_{\text{inter}}\right), \tag{10.5}$$

where $n_{\text{intra}}, n_{\text{inter}}$ are the number of contacts of the polymers with themselves and with each other, respectively. This simple but straightforward model allowed to capture the qualitative results for few-polymer aggregation of a coarse-grained model investigated by our group [1].

We applied Metropolis and Parallel Multicanonical [2] simulations to systems with different number of polymers of fixed length and density. It was possible to observe an aggregation process with decreasing temperature, see Fig. 10.10. At the transition temperature, we observed a double peak in the energy distribution with decreasing probability for the intermediate regime, indicating a first-order phase transition. For increasing system sizes, the Metropolis algorithm showed difficulties in the low-temperature regime such that the application of the more sophisticated multicanonical method became more and more necessary. To this end, we successfully applied the "Polymer Framework", developed recently in our group.

(a) (b)

Figure 10.10: Example of the aggregation process for 20 interacting self-avoiding walks of length 13: (a) High-temperature fluctuations and (b) low-temperature aggregation.

The transition temperature of the aggregation was observed to depend on the number of polymers, the length of the polymers and the density. The explicit dependencies are currently under investigations. Still, the rich parameter space combined with the accessible numeric effort promise interesting insight into the aggregation phenomenon of flexible polymers.

[1] C. Junghans et al.: Europhys. Lett. **87**, 40002 (2009)
[2] J. Zierenberg et al.: Comput. Phys. Comm. **184**, 1155 (2013)

10.10 Random Heteropolymer Models

V. Blavatska*, W. Janke

*Institute for Condensed Matter Physics, National Academy of Sciences of Ukraine, Lviv, Ukraine

A subject of great interest in both chemical and biological physics are the conformational properties of long heteropolymer chains. Typical examples are proteins, consisting of sequences of amino acid residues, connected by peptide bonds. The conformations of individual macromolecules are controlled by the type of monomer-monomer interactions. In general, the constituents (monomers) of macromolecules in an aqueous environment can be characterized as hydrophilic or hydrophobic, depending on their chemical structure. Hydrophilic residues tend to form hydrogen bonds with surrounding water molecules, whereas the hydrophobic monomers effectively attract each other and tend to form a dense hydrophobic core.

We studied the conformational transitions in heteropolymers within the frames of a lattice model containing two types of monomers A and B, N_A monomers of type A and $N_B = N - N_A$ monomers of type B. Such a model can describe in particular the sequences of hydrophobic and hydrophilic residues in proteins [1] and polyampholytes with oppositely charged groups [2]. Restricting ourselves only to short-range

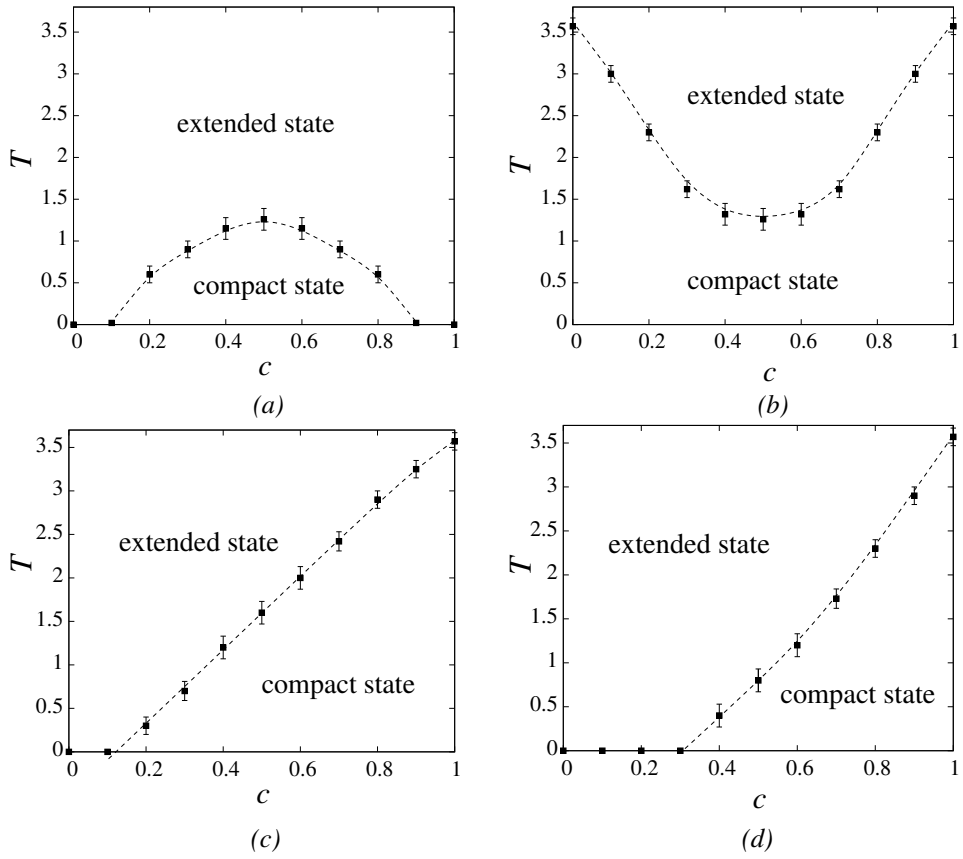

Figure 10.11: Phase diagrams of heterogeneous polymer chains in T-c space. (a) model 1, (b) model 2, (c) model 4, (d) model 5.

interactions between any pair of monomers residing on neighboring lattice sites that are not connected by a covalent bond, we considered 5 different parametrizations of this model. In particular, model 1 ($\varepsilon_{AA} = \varepsilon_{BB} = 1, \varepsilon_{AB} = -1$) where like monomers repel and opposite ones attract each other, refers to strongly screened Coulomb interactions [2]. The model 3 ($\varepsilon_{AA} = 1, \varepsilon_{BB} = \varepsilon_{AB} = 0$) is a particular case of model 1 and corresponds to a polymer chain containing charged (A) and neutral (B) monomers. Model 4 ($\varepsilon_{AA} = -1, \varepsilon_{BB} = \varepsilon_{AB} = 0$) refers to the (minimal) HP model [5] with hydrophobic (A) and hydrophilic (B) monomers. Models 2 ($\varepsilon_{AA} = \varepsilon_{BB} = -1, \varepsilon_{AB} = 1$) and 5 ($\varepsilon_{AA} = -1, \varepsilon_{BB} = 1, \varepsilon_{AB} = 0$) can be considered as generalizations of the two above mentioned cases.

Applying the pruned-enriched Rosenbluth chain-growth algorithm (PERM) [3] we analyzed numerically the transitions from an extended into a compact state as function of the inhomogeneity ratio $c = N_A/N$ for all five heteropolymer chain models [4]. In model 3, unlike the other models, the polymer chain expands its size with lowering the temperature due to the repulsion between monomers, and the polymer chain remains in an extended state at any temperature. As it shown in Figure 10.11, in model 2, the so-called θ-transition between an extended and compact state is always present at any value of inhomogeneity ratio c, whereas models 1, 4 and 5 remain in an extended state when the concentration of attracting monomers is too small to cause a transition into the compact state. Note also that at small concentration of attractive monomers,

the chains can attain the compact state only when they are long enough and have enough attractive nearest-neighbour contacts to overcome the conformational entropy. In the limiting case $c = 1$, models 2, 4 and 5 describe homogeneous polymer chains with nearest-neighbour attractions (for model 2 also $c = 0$) with known value of the transition temperature $T_\theta = 3.717(3)$ [3].

[1] K.A. Dill: Biochemistry **24**, 1501 (1985); K.F. Lau, K.A. Dill: Macromolecules **22**, 3986 (1989)
[2] Y. Kantor, M. Kardar: Europhys. Lett. **28**, 169 (1994)
[3] P. Grassberger: Phys. Rev. E **56**, 3682 (1997)
[4] V. Blavatska, W. Janke: *Conformational transitions in random heteropolymer models*, e-print arXiv:1212.0348 (cond-mat.dis-nn)

10.11 Exact Enumeration of Self-Avoiding Walks on Multidimensional Critical Percolation Clusters

N. Fricke, T. Peschel, W. Janke

The self-avoiding walk (SAW) is one of the most fundamental models in statistical physics. Its asymptotic scaling behaviour is characterized by universal exponents, which are assumed to be valid for a range of systems, from SAWs on a square lattice to flexible polymers in good solvents. The exponents are independent of details such as the lattice type, but they do depend on the dimensionality of the system.

While SAWs on regular lattices are relatively well understood, their behaviour in crowded disordered environments still holds many questions. A paradigmatic case are SAWs on critical percolation clusters, see [1, 2]. At the percolation threshold, the lattice is disordered on all length scales and the clusters have non-integer fractal dimensions. It is natural to assume that the clusters' Hausdorff dimension will take role of the Euclidean dimension for SAWs on regular lattices. However, there are a number of other fractal dimensions that might also be relevant. It has even been argued that only the cluster backbone (Fig. 10.12), the part of the cluster that remains when all singly connected "dangling ends" are removed, should determine the SAW's scaling behaviour. While this is probably not the case, it is clear that the backbone plays a crucial role. Treatment of the problem with standard numerical tools has proved difficult, and the few existing analytical results are controversial.

We recently developed a new method to efficiently enumerate all SAW conformations on a critical cluster or its backbone [3, 4]. Exploiting the clusters' low connectivity and self-similarity, it outperforms the best Monte Carlo methods [5]. We have now generalized the method to systems of arbitrary dimensionality, and recent optimizations have made it possible to handle 10^4 SAW steps with 10^{1000} conformations. Preliminary measurements of SAWs of 10^3 steps already yielded good estimates for the scaling exponents on critical clusters in up to seven dimensions. More extensive simulations, which will shed some light on the role of the fractal dimensions, are ongoing.

[1] B. Barat, B.K. Chakrabarti: Phys. Rep. **258**, 377 (1995)

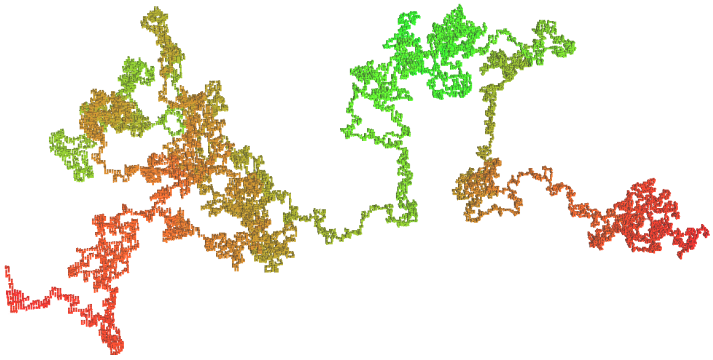

Figure 10.12: Backbone of a three-dimensional critical percolation cluster. Coloring indicates chemical distance to the origin.

[2] V. Blavatska, W. Janke: Europhys. Lett. **82**, 66006 (2008); Phys. Rev. Lett. **101**, 125701 (2008)
[3] N. Fricke, W. Janke: Europhys. Lett. **99**, 56005 (2012)
[4] N. Fricke, W. Janke: in *Computer Simulation Studies in Condensed-Matter Physics XXV*, eds. D.P. Landau, H.-B. Schüttler, S. Lewis, M. Bachmann, Physics Procedia **34**, 39 (2012)
[5] N. Fricke, W. Janke: Eur. Phys. J. – Special Topics **216**, 175 (2013)

10.12 Kinetic Growth Random Walks

J. Bock, N. Fricke, W. Janke

Random walks are a field of interest in statistical physics since the 1950s. They are a basic model of polymers and are investigated in various forms, e.g., the simple random walk, the self-avoiding walk (SAW) or the kinetic growth walk (KGW). A special interest lies in their universal scaling behaviour with respect to their end-to-end distance R and chain length N, $\sqrt{\langle R^2 \rangle} \sim N^{\nu}$, where ν denotes the universal exponent. Measurements were done by our group for self-avoiding walks in two and three dimensions on regular lattices and diluted lattices [1, 2].

We revisited kinetic growth random walks for two reasons in particular: First they have not been under investigation since the early 1990s and the results from that time were to be evaluated by nowadays computational possibilities. Second to compare these results to those of the self-avoiding walks. To this end, two algorithms were used, the Rosenbluth-Rosenbluth and pruned-enriched Rosenbluth chain-growth algorithm (PERM). The results of our work [3] for regular lattices are shown in Fig. 10.13. The difference between KGW and SAW is obvious and quite similar results were obtained on diluted lattices. The comparison with previous results is shown in Table 10.1. For the 2D case, our results are similar to the work done bei Kremer and Lyklema [4] and in 3D we are between Kremer and Lyklema and Majid [5]. Also in the case of diluted lattices we obtained different results for SAW and KGW, hence we can conclude both walks behave differently and are not the same.

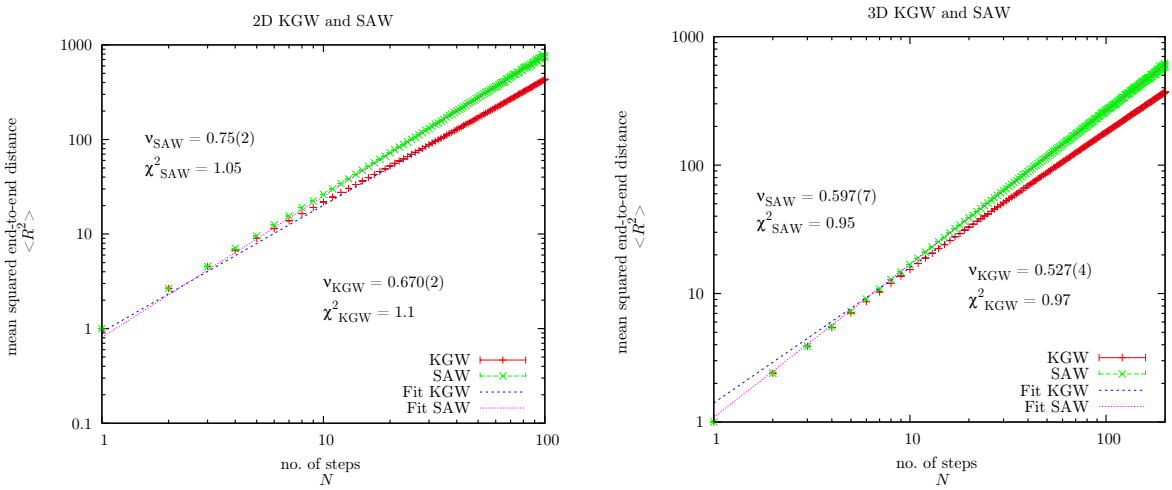

(a) 2D walks of length 250 and fit range (10:250). (b) 3D walks of length 200 and fit range (13:148).

Figure 10.13: Comparison of (a) two-dimensional (2D) and (b) three-dimensional (3D) kinetic growth walks (KGWs) and self-avoiding walks (SAWs).

Table 10.1: Comparison of the exponent ν for KGWs with previous results.

Authors	ν
Majid [5]	$\nu_{2D} = 2/3; \nu_{3D} = 1/2$
Lam, Zhang [6]	$\nu_{2D} = 0.646$
Kremer, Lyklema [4]	$\nu_{2D} = 0.68; \nu_{3D} = 0.525$
Pietronero [7]	$\nu_{2D} = 3/4; \nu_{3D} = 3/5$
our work	$\nu_{2D} = 0.682(2); \nu_{3D} = 0.520(1)$

[1] V. Blavatska, W. Janke: Europhys. Lett. **82**, 66006 (2008); Phys. Rev. Lett. **101**, 125701 (2008)
[2] N. Fricke, W. Janke: Europhys. Lett. **99**, 56005 (2012)
[3] J. Bock: Master Thesis, Universität Leipzig (2013)
[4] K. Kremer, J.W. Lyklema: Phys. Rev. Lett. **55**, 2091 (1985)
[5] I. Majid et al.: Phys. Rev. Lett. **55**, 1257 (1984)
[6] P.M. Lam, Z.Q. Zhang: Z. Phys. B **69**, 65 (1984)
[7] L. Pietronero: Phys. Rev. Lett. **55**, 2025 (1985)

10.13 Semiflexible Polymers in Hard-Disk Disorder

S. Schöbl, J. Zierenberg, W. Janke

The conformational properties of polymers exposed to disordered media are strongly affected by the surrounding disorder potential. For the case of flexible polymers, the impact of disorder on polymers has already been discussed since long [1–3]. The special case of geometrical constraining environments has been investigated recently in, e.g., Ref. [4]. It is expected that geometrical restrictions to chain conformations also play a crucial role for biological systems. In these systems, however, polymers may no

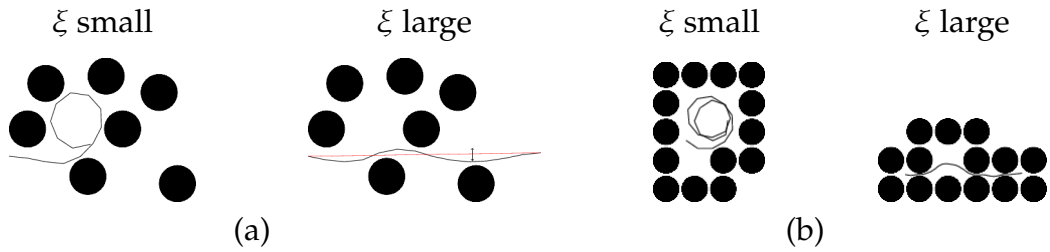

Figure 10.14: Sketch to elucidate the idea of softening and stiffening for polymers with small and large persistence length ξ at (a) low and (b) high occupation probabilities, respectively. The double-headed arrow indicates the width of the thermal fluctuations of the polymer.

longer be assumed flexible and models of moderately stiff polymers, called semiflexible polymers, are introduced. The stiffness is characterized by the persistence length ξ. On length scales shorter than the persistence length, the polymers behave like stiff rods; on longer scales, they exhibit entropic flexibility and random coiling occurs. The geometrical restrictions of the environment along with the intrinsic stiffness of the polymers lead to an interesting phenomenology, which, in contrast to the case of flexible polymers, is to date only partially understood [5, 6].

In this work we used an off-lattice growth algorithm [7] and multicanonical simulations to examine the equilibrium properties of a pinned semiflexible polymer exposed to a quenched random potential consisting of hard disks [8]. The disks are arranged on the sites of a square lattice. We build up on Ref. [4], where flexible polymers exposed to hard-disk disorder assembled on the sites of a square lattice were investigated. We extend the polymer model to comprise bending stiffness. In computer simulations, the appropriate polymer model is the Heisenberg chain model which in the continuum limit becomes the worm-like chain, also called the Kratky-Porod model [9].

We found that the polymer, depending on the ratio of persistence length and void space extension, either crumples up (small ξ) or straightens (large ξ) for increasing density of the potential (see Fig. 10.14). Besides, the periodic structure of the lattice is reflected in the distribution functions of the polymer. Furthermore, we found that the distributions – in the case of pinning the polymer at one end – strongly reflect the local cluster structure of the disorder. Leaving the constraint of pinning lets the polymer escape local cavities and gain entropy in larger void-space clusters. The corresponding distributions for pinned and non-pinned polymers differ considerably. Equipped with this finding, a challenging next step is to investigate the behaviour of semiflexible polymers in hard-disk fluid disorder.

[1] M.T. Bishop et al.: Phys. Rev. Lett. **57**, 1741 (1986)
[2] A. Baumgärtner, M. Muthukumar: J. Chem. Phys. **87**, 3082 (1987)
[3] M.E. Cates, R.C. Ball: J. Physique **49**, 2009 (1988)
[4] S. Schöbl et al.: Phys. Rev. E **84**, 051805 (2011)
[5] H. Hinsch, E. Frey: Chem. Phys. Chem. **10**, 2891 (2009)
[6] P. Cifra: J. Chem. Phys. **136**, 024902 (2012)
[7] T. Garel, H. Orland: J. Phys. A: Math. Gen. **23**, L621 (1990)
[8] S. Schöbl et al.: J. Phys. A: Math. Theor. **45**, 475002 (2012)
[9] O. Kratky, G. Porod: Rec. Trav. Chim. Pays-Bas **68**, 1106 (1949)

10.14 Polymer Framework: A Tool Box for fast Programming of Monte Carlo Simulations

M. Marenz, J. Zierenberg, W. Janke

We have started to create an environment for writing fast and efficient Monte Carlo (MC) simulations for arbitrary polymer models. Simulations of such systems yield a better understanding of the behaviour of polymers in specific circumstances [1], or may provide a good initial guess for creating new ones with specific properties [2]. There are a lot of different Molecular Dynamics (MD) programs available, which are capable of simulating biological or synthetic polymers. However, their abilities to perform MC simulations are rather limited because sophisticated update algorithms are, if at all, implemented only rudimentary. Although MC techniques, in contrast to MD, cannot investigate dynamical properties, they are very convenient for investigating phase transitions and the general character of phase space of arbitrary models in a very efficient manner. The efficiency comes from the broad range of improved MC techniques and the possibility to design a suitable propagation of the system as a Markov process freely.

Unfortunately there exists no widely-used program for MC simulations of polymers. To write a single program which implements all these techniques and possibilities at the same time and still remains efficient is nearly impossible. The alternative, writing a new program from scratch for every demand could be very annoying. That is one reason, why we developed a framework for MC simulations of polymers. The aim of this framework is to provide an environment in the C++ programming language, allowing to perform MC simulations for specific problems in a short time. Another goal of the framework is the expandability. Thus, one can add new methods, potentials, systems and update methods, without adjusting all other parts of the framework. To achieve this goal we divided the problem into single parts, which fit into each other. One can imagine every part as a brick, which can be combined in order to construct a simulation.

There are five basic building blocks: The smallest building blocks are the atoms. The next block is the system, which combines all needed atoms and defines the Hamiltonian of the physical system. On top of the system are the last two main building blocks, the update move and the MC technique. Moves define single updates of the system, propagating from the current state to the next one. Additionally a constraint can be added to every move, in order to simulate a polymer in confinement. An organogram of the simulation framework is sketched in Fig. 10.15.

Until now, we have implemented several MC techniques such as parallel tempering [3], multicanonical [4] and Wang-Landau [5]; for recent reviews, see [6, 7]. As system there are all kinds of linear polymers available, such as simple bead-spring or bead-stick models, with Lennard-Jones, spring, FENE and bending potentials. Adding further pair or bending potentials is extremely simple. We have also implemented confinement constraints such as steric walls, a sphere or a barbell.

As first examples, we are looking at the behaviour of a homopolymer in two different confinements, a polymer inside a sphere and inside a barbell. One important question here is to what extent the confinement modifies the phase transition properties compared to those of a free polymer.

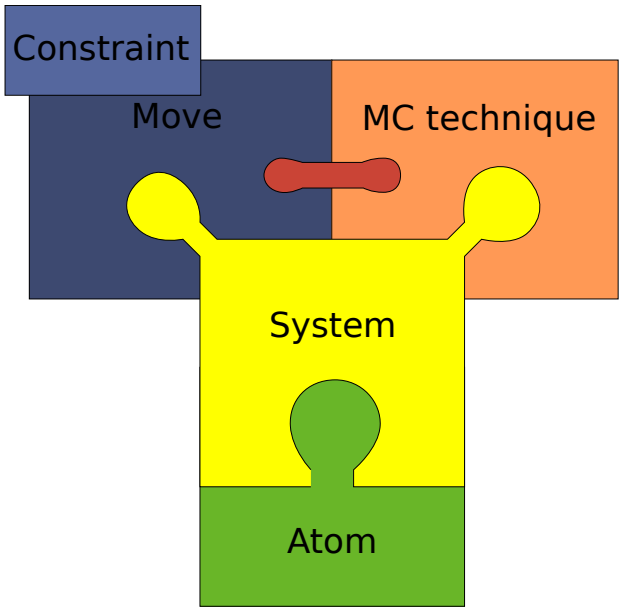

Figure 10.15: The five basic building blocks of the MC simulations framework.

[1] M. Möddel et al.: Phys. Chem. Chem. Phys. **12**, 11548 (2010); Macromolecules **44**, 9013 (2011)
[2] M. Bachmann et al.: Angew. Chem. Int. Ed. **49**, 9530 (2010) [Angew. Chem. **122**, 9721 (2010) (in German)]
[3] K. Hukushima, K. Nemoto: J. Phys. Soc. Japan **65**, 1604 (1996)
[4] B.A. Berg, T. Neuhaus: Phys. Lett. B **267**, 249 (1991); Phys. Rev. Lett. **68**, 9 (1992)
[5] F. Wang, D. P. Landau: Phys. Rev. Lett. **86**, 2050 (2001); Phys. Rev. E **64**, 056101 (2001)
[6] W. Janke: Lect. Notes Phys. **739** (Springer, Berlin 2008), pp. 79-140
[7] W. Janke: in *Order, Disorder and Criticality: Advanced Problems of Phase Transition Theory*, Vol. 3, ed. Y. Holovatch (World Scientific, Singapore 2012), pp. 93–166

10.15 The Effect of Multiple Inherent Time Scales on the Dynamics of the Binary Frustrated Unit

D. Labavić*, H. Nagel, W. Janke, H. Meyer-Ortmanns*

*School of Engineering and Science, Jacobs University Bremen

The motif of a self-activating species A that also activates another species B, which in turn represses its activator A, is often found in biological systems, particularly in those featuring inherent oscillatory behaviour. In such biological systems a source of delay in the interaction is essential for the observed dynamics. Thus different time scales are present in the interaction of the species. In this research, we investigated how such different inherent time scales lead to distinct dynamics in a stochastic description of such a system.

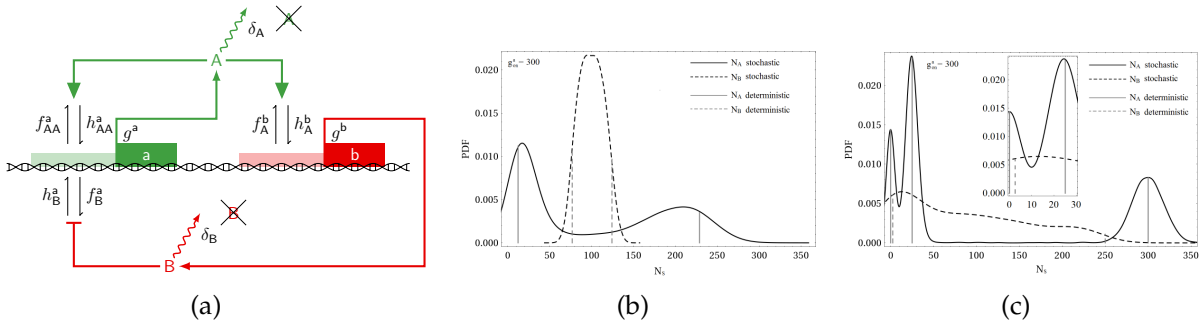

Figure 10.16: (a) Implementation of the basic motif as a genetic circuit. (b), (c) Probability density functions for populations N_A, N_B of species A, B respectively for a fast (b) and slow (c) time scale of gene activation. For slow genes (c) the bifurcation picture changes and attractors split up.

We considered a realization as a genetic circuit where two kinds of a proteins act as species A and B. The mechanism of activation and repression is modeled after genetic promoter sequences encoded before their respective regulated genes: The binding of a specific protein to an activating or inhibiting promoter region respectively increases or decreases the expression rate of the protein associated to that gene, cf. Fig. 10.16.

In previous work [1] we found that one source of delay can be introduced by making the species B-protein expression and decay slower than that of the A-protein and could observe oscillations. Depending on the amount of delay, these oscillations are the consequence of a limit cycle and large excursions from a fixed point in a Hopf–type bifurcation.

Here we identified and investigated the effect of a second source of delay in the activation/repression mechanism itself [2]. The corresponding time scale is defined by the binding rates of the proteins to the genes promoter regions. Employing Monte Carlo simulations as well as coarse-graining methods in the time domain we were able to identify distinct dynamic behaviours when the time scale of activation is much faster than that of species A, as fast as A and as slow as B. The bifurcational patterns change with the inherent time scales, too.

[1] A. Garai et al.: J. Stat. Mech.: Theor. Exp., P01009 (2012)
[2] D. Labavić et al.: *Caveats in modeling a common motif in genetic circuits*, e-print arXiv:1209.0581 (physics.bio-ph), to appear in Phys. Rev. E (2013), in print

10.16 Condensation Shapes in a Stochastic Mass Transport Model

E. Ehrenpreis, H. Nagel, W. Janke

Generic examples for stochastic mass transport processes are traffic flow, force propagation in granular media, aggregation and fragmentation of clusters, and many others [1]. The transport is classically modeled by probabilities for hopping events from one site to another. Since such processes are usually out-of-equilibrium, it is in general

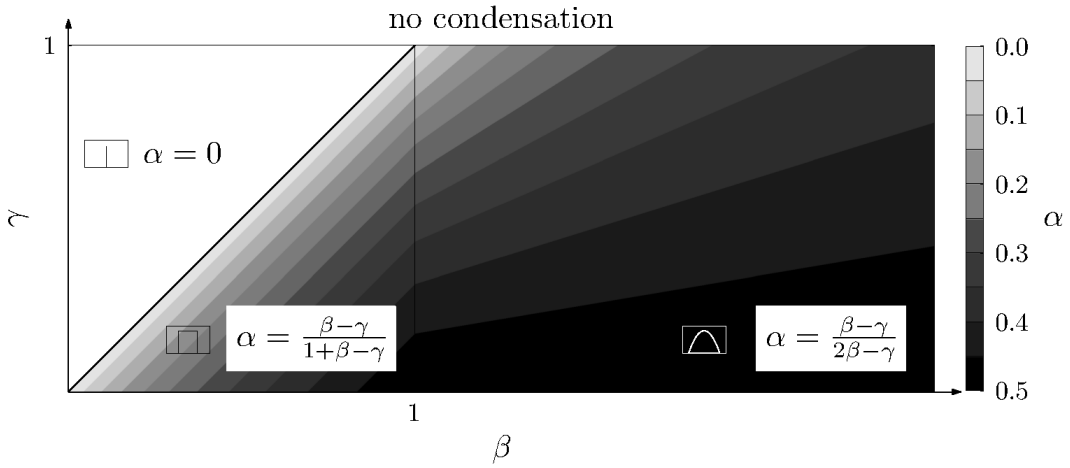

Figure 10.17: Theoretically predicted phase diagram for $K(x) \sim e^{-x^\beta}$ and $p(m) \sim e^{-m^\gamma}$, exhibiting condensed phases with point-like, rectangular and parabolic shapes (from left to right). The predicted value of the exponent α in the scaling law for the condensate extension W with the number M' of condensed particles, $W \simeq M'^\alpha$, is indicated by the gray code.

difficult to predict possible stationary states. Still, under certain circumstances it is possible to identify a transition between a liquid-like phase and a phase with a condensate (e.g., a "traffic jam") that are associated with different stationary states. In the condensate a finite fraction M' of constituent particles condenses onto a finite extension W in space, sometimes even onto a single site. This is an example of spontaneous symmetry breaking which, in contrast to equilibrium systems, can happen here even in a one-dimensional system.

In previous analytical work [2–4] we concentrated on a class of models with steady states that factorize over the links of arbitrary connected graphs, so-called pair-factorized steady states (PFSS). This property enables at least partially an analytic treatment of the transport properties. In one dimension we could predict the critical mass density at the condensation transition and in particular the condensate shape which turned out to be non-universal. Rather, by the competition of local (K) and ultralocal (p) interactions governing the hopping rates, it can be tuned from "extended" to "point-like" [5]. The resulting phase diagram for the choice $K(x) \propto \exp(-x^\beta)$ and $p(m) \propto \exp(-m^\gamma)$ and the analytically predicted exponent α in the scaling law for the condensate extension, $W \sim M'^\alpha$, are shown in Fig. 10.17.

The analytical treatment is based on several approximations. To assess their accuracy, we have performed extensive computer simulations of the hopping events and determined the phase diagram numerically [6]. As a result we find very nice agreement with the theoretical prediction. This is demonstrated in Fig. 10.18 where the measured condensate shapes are displayed in the β-γ plane. By performing power-law fits of the condensate widths W against the number of constituent particles M', we obtain in most parts of the β-γ plane very good agreement with the predicted values of the exponent α at a 1% accuracy level.

[1] M.R. Evans et al.: Phys. Rev. Lett. **97**, 010602 (2006)
[2] B. Wacław et al.: J. Phys. A: Math. Theor. **42**, 315003 (2009)

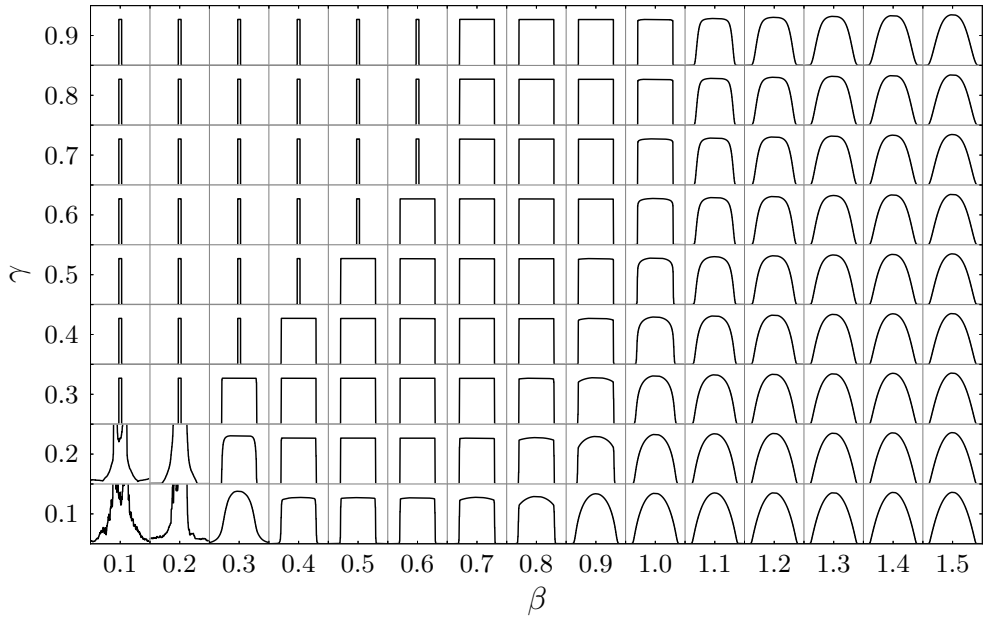

Figure 10.18: Numerically determined characteristic condensate shapes for systems of various β and γ at a condensate volume of about 10^5 masses. The shapes are derived from averages over many measured condensate states. The point-like shapes in the upper left region of the parameter space have not been identified with the present techniques.

[3] B. Wacław et al.: Phys. Rev. Lett. **103**, 080602 (2009)
[4] B. Wacław et al.: J. Stat. Mech. P10021 (2009)
[5] B. Wacław et al.: J. Phys.: Conf. Ser. **246**, 012011 (2010)
[6] E. Ehrenpreis et al.: Leipzig preprint, in preparation

10.17 Mixed Heisenberg Spin Chains: Theory and Quantum Monte Carlo Simulations

R. Bischof, W. Janke

The original Heisenberg model (developed by Heisenberg during his time in Leipzig) and its variants are the basis for understanding quantum magnetism. For instance high-temperature superconducting cuprates can be successfully described as 1D and 2D quantum antiferromagnets at low doping. Depending on the size of the spins and types of coupling mechanisms, the model exhibits a rich variety of zero-temperature quantum critical phenomena. It is well known that uniform chains of half-odd integer spins have no energy gap between the ground state and first excited states (i.e., they are quantum critical), whereas chains with integer spins do show an excitation gap [1]. Moreover by tuning appropriate parameters (such as bond alternation, exchange anisotropy, next-nearest-neighbour interaction, spin-phonon coupling, etc.), spin chains can be driven to or away from criticality.

In this project we consider mixed anisotropic Heisenberg (XXZ) spin chains with bond alternation for which much less is known than for uniform chains. Specifically, our focus is on two different mixed quantum XXZ chains consisting of two different kinds of spins, $S_a = 1/2$ and $S_b = 1$ or $3/2$, that appear alternatingly in pairs [2]. In order to investigate their quantum critical properties we employ self-implemented versions of the continuous time loop algorithm [3] and Lanczos exact diagonalization. By successful generalization of recently proposed quantum reweighting methods [4] to improved estimators of the loop algorithm, we have been able to determine the phase diagram in the XY-like region to high precision and could establish a line of continuously varying critical exponents. This strongly suggests that mixed spin chains are in the Gaussian universality class characterized by a central charge of $c = 1$. Furthermore, we could show the presence of logarithmic corrections in the mixed spin models at the SU(2) symmetric isotropic point. These logarithmic corrections influence the scaling and finite-size scaling behaviour on all length scales, which makes the extraction of critical exponents particularly difficult. It is well known that the homogeneous spin chains of $S = 1$ do exhibit such types of corrections [5].

By invoking conformal field theory, we have identified several scaling dimensions that can all be parametrized in terms of one fundamental parameter, a typical sign of the Gaussian universality class. To this end we proposed novel string-like order parameters as a generalization of the disorder parameters of the quantum Ashkin-Teller model. For the $S = 1$ chain our generalization corresponds to the order parameter of the dimerized phase in contrast to the usual string order parameter of the Haldane phase. These new order parameters offer access to scaling dimensions that differ from those of spin operators. As a consequence, the validity of scaling relations can be tested with higher accuracy [6].

Another exotic order parameter is the twist order parameter [7] that is particularly well suited to signal quantum phase transitions between different valence-bond configurations in 1D chains. Despite its potential to accurately locate pseudo-critical points in quantum Monte Carlo simulations, its scaling behaviour has not yet been studied. Our attempts to identify scaling behaviour seem to fail due to the inherently non-local nature of the twist order parameter [6], even though according to [7] a scaling dimension can be assigned.

[1] F.D.M. Haldane: Phys. Rev. Lett. **50**, 1153 (1983)
[2] K. Takano: Phys. Rev. Lett. **82**, 5124 (1999); Phys. Rev. B **61**, 8863 (2000); Z. Xu et al.: Phys. Rev. B **67**, 214426 (2003)
[3] B.B. Beard, U.J. Wiese: Phys. Rev. Lett. **77**, 5130 (1996); H.G. Evertz: Adv. Phys. **52**, 1 (2003)
[4] M. Troyer et al.: Braz. J. Phys. **34**, 377 (2004)
[5] C.J. Hamer et al.: Phys. Rev. Lett. **68**, 214408 (2003); T. Papenbrock et al.: Phys. Rev. B **68**, 024416 (2003)
[6] R. Bischof, W. Janke: To be published
[7] M. Nakamura, S. Todo: Phys. Rev. Lett. **89**, 077204 (2002)

10.18 Multicanonical Analysis of the Gonihedric Ising Model and its Dual

M. Müller, W. Janke, D.A. Johnston*

*Department of Mathematics and the Maxwell Institute for Mathematical Sciences, Heriot-Watt University, Edinburgh, UK

Models of fluctuating random surfaces are of great interest in various disciplines of physics or biology. Amongst others, they appear in the treatment of complex networks of membranes [1]. The gonihedric Ising model originates from high-energy physics as a possible discretisation of the area swept out by a string worldsheet moving through spacetime [2]. The name comprises the greek words gonia (angle) and hedra (face) as a reminder of the origin.

A two-dimensional surface is considered to be the assembly of plaquettes in the dual lattice of a three-dimensional lattice of spins. Whenever contiguous spins have opposite signs, such a plaquette is introduced separating the two spins. By changing the spin configuration one effectively alters the surface configuration. Modifying the tendency of spins to align by fine-tuning of the Hamiltonian of the spin system therefore induces different properties to the surface [3, 4].

A strong first-order phase transition can be seen in the special case of surfaces that do not suffer an energy penalty upon self-intersection, as well as glassy dynamics upon cooling in simulations. This phase transition has been analysed using canonical Monte Carlo simulations on dual representations of the model [5], leading to inconsistent results introduced by hysteresis effects.

We investigated the discontinuous phase transition in the original model and its dual representation with multicanonical simulations that are tailored to overcome slow dynamics in first-order transitions caused by phase coexistence [6]. In finite systems and a temperature-driven transition, this is reflected by double-peak distributions of the energy as shown in Fig. 10.19. The finite-size scaling needed to extract properties of the infinite system shows a very interesting behaviour. For Potts-like models, there exists a rigorous theory for peak locations of response functions such as the specific heat or Binder's energy cumulant [7, 8]. The leading contribution of the finite-size correction is expected to be of the order of the inverse volume. For the gonihedric Ising model and its dual, our data suggests a finite-size scaling ansatz, where the leading correction is increased by one power of the system size compared to the theory for Potts-like models. Only then we obtain good agreement between the transition temperatures of the original model and its dual representation. We found that the unusual scaling ansatz still coincides with the theory when taking the exponential ground-state degeneracy of the models into account [9].

[1] R. Lipowsky: Nature **349**, 475 (1991)
[2] G.K. Savvidy, F.J. Wegner: Nucl. Phys. B **413**, 605 (1994)
[3] A. Cappi et al.: Nucl. Phys. B **370**, 659 (1992)
[4] R.V. Ambartzumian et al.: Phys. Lett. B **275**, 99 (1992)
[5] D.A. Johnston, R.P.K.C.M. Ranasinghe: J. Phys. A: Math. Theor. **44**, 295004 (2011); e-print arXiv:1106.0325 (2011); e-print arXiv:1106.4664 (2011)
[6] M. Müller: Diplomarbeit, Universität Leipzig (2011)

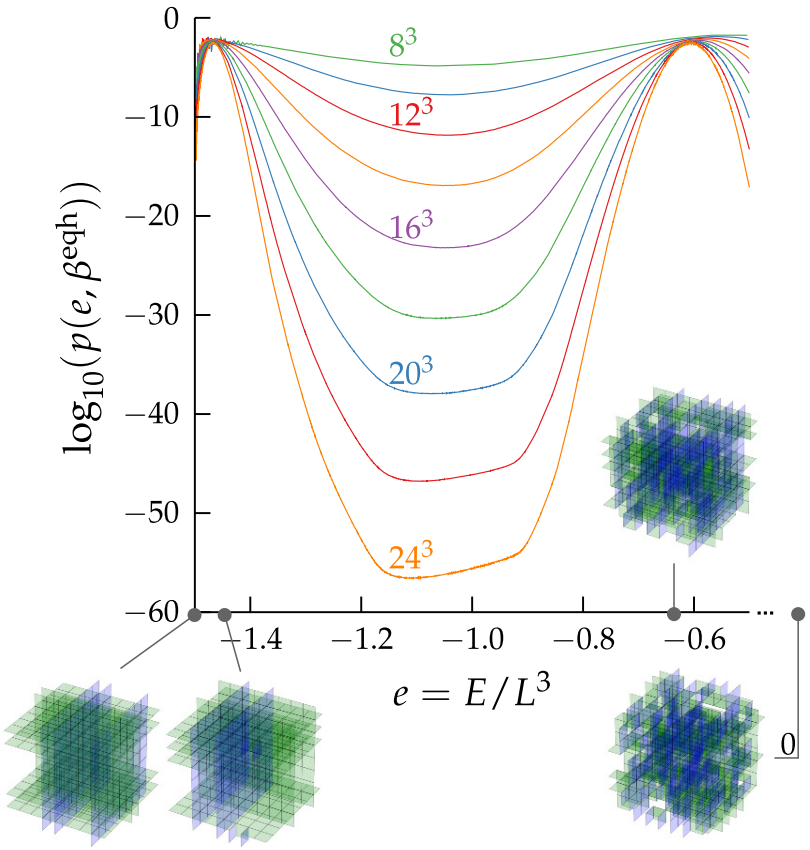

Figure 10.19: Energy probability density of the gonihedric Ising model near the phase transition temperature for various lattice sizes. The rare states between the peaks are strongly suppressed but sufficiently sampled by the multicanonical algorithm. Exemplary configurations for some energies of a cubic lattice with linear size $L = 8$ are depicted as well.

[7] C. Borgs, R. Kotecký: J. Stat. Phys. **61**, 79 (1990)
[8] W. Janke: Phys. Rev. B **47**, 14757 (1993)
[9] M. Müller et al.: Leipzig preprint, in preparation

10.19 Microcanonical Flat-Histogram Sampling

S. Schnabel, W. Janke

Starting from the Metropolis method in 1953 a number of algorithms have been developed to handle complex problems in statistical physics. In many of them estimators of quantities like the density of states or the partition function are in some way derived from histograms, i.e., from measured distributions over a suitable parameter, which is usually the energy of the system. This process can involve the reweighting of a histogram, the determination of the eigenvector of the transition matrix, or – in case of the Wang-Landau method – the adjustment of the algorithm's dynamic at run time while aiming at a flat histogram. Once the density of states is available it can be used

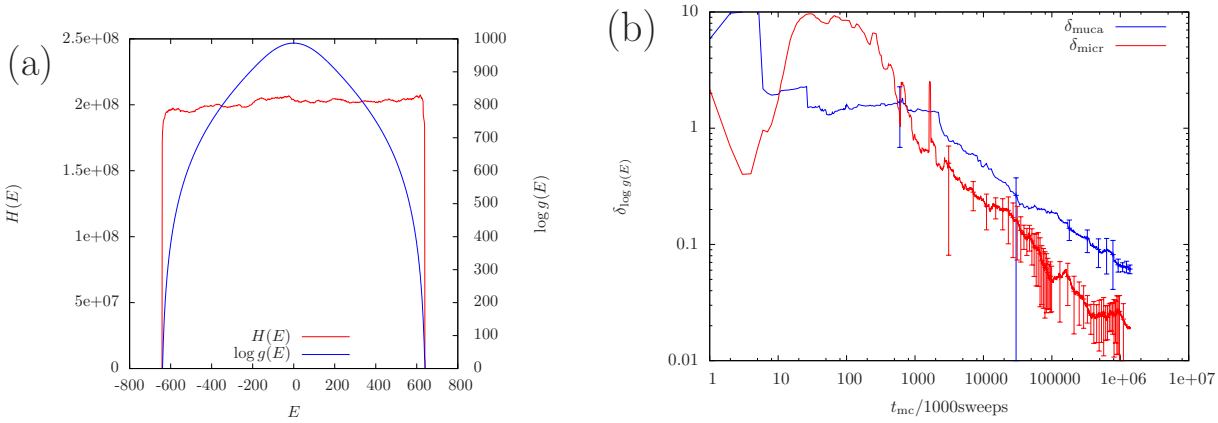

Figure 10.20: (a) The algorithm is able to determine the density of states $g(E)$ over a few hundred orders of magnitude with a high enough precision to produce a flat histogram $H(E)$. (b) Estimating the density of states from microcanonical averages leads to smaller errors (red) compared to a conventional multicanonical simulation (blue).

to obtain thermodynamic quantities like the specific heat or the mean energy. As mentioned, this approach is based on one or more histograms and derived results inherit the comparatively large statistical errors associated with them.

Alternatively, the phase space of a system can as well be analyzed by means of a microcanonical temperature [1] which can be calculated based on gradient and Hessian of the Hamiltonian [2]. It is in principle possible to go one step further and integrate this microcanonical temperature, thus constructing the density of states and use it in turn to drive the Monte Carlo process. This way, shortcomings of the histogram approach would be avoided. However, the calculation of the Hessian is computational expensive and such a method would, therefore, in most cases not be practical.

Using the concept of statistical processes we were able to obtain a slightly different formula where the Hessian is replaced by the Laplacian which can be calculated much faster. The expression becomes particularly simple for spin models with continuous degrees of freedom and we applied the algorithm to the well-known classical Heisenberg model.

We found that the algorithm converges and that the produced histogram is constant over the entire energy range indicating that the estimate of the density of states is accurate [Fig. 10.20(a)]. We consider this an achievement since the main objective of this method is not to balance the histogram but to calculate microcanonical averages. In comparison to established flat-histogram methods our algorithm is faster, i.e. produces results with higher precision in less time. Moreover, even a multicanonical simulation starting with already well-tuned weights (which could be considered a close-to-optimum histogram-based technique) soon has a larger error than the microcanonical sampling [Fig. 10.20(b)].

[1] S. Schnabel et al.: Phys. Rev. E **84**, 011127 (2011)
[2] H.H. Rugh: Phys. Rev. Lett. **78**, 772 (1997)

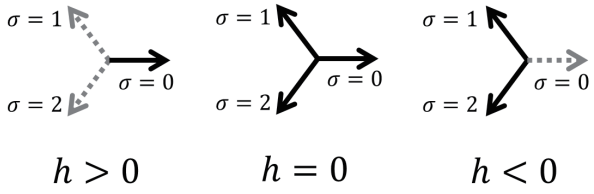

Figure 10.21: Schematic sketch illustrating the behaviour of the spins of the three-state Potts model in an external magnetic field h.

10.20 Simulated Tempering and Magnetizing Simulations of the Three-State Potts Model

T. Nagai*, Y. Okamoto*, W. Janke

*Department of Physics, Graduate School of Science, Nagoya University, Nagoya, Japan

The three-state Potts model in an external magnetic field has several interesting applications in condensed matter physics and serves as an effective model for quantum chromodynamics [1]. When one of the three states per spin is disfavoured in an external (negative) magnetic field (see Fig. 10.21), the other two states exhibit Z_2 symmetry and one expects a crossover from Potts to Ising critical behaviour.

To study such a crossover in a two-dimensional parameter space, generalized-ensemble Monte Carlo simulations are a useful tool [2]. Inspired by recent multi-dimensional generalizations of generalized-ensemble algorithms [3], the "Simulated Tempering and Magnetizing" (STM) method has been proposed by two of us and first tested for the classical Ising model in an external magnetic field [4]. In the conventional simulated tempering (ST) scheme [5] the temperature is considered as an additional dynamical variable besides the spin degrees of freedom. The STM method is a generalization to a two-dimensional parameter space where both the temperature *and* the magnetic field are treated as additional dynamical variables. Recently we have extended this new simulation method to the two-dimensional three-state Potts model and by this means generated accurate numerical data in the temperature-field plane [6].

Our STM simulations were performed for lattice sizes $L = 5, 10, 20, 40, 80$, and 160 with the total number of sweeps varying between about 160×10^6 and 500×10^6, where a sweep consisted of N single-spin updates with the heat-bath algorithm followed by an update of either the temperature T or the field h. By this means one can easily sample a wide range of the two-dimensional parameter space and it is straightforward to compute a two-dimensional map of any thermodynamic quantity that can be expressed in terms of the energy and magnetization. As an example, Fig. 10.22 shows (a) the specific heat and (b) the susceptibility for $L = 80$. We see a line of phase transitions starting at the Potts critical point at $h = 0$, $T_c^{\text{Potts}} = 1/\ln(1+\sqrt{3}) = 0.9950$ which approaches for strong negative magnetic fields the Ising model limit with a critical point at $h \to -\infty$, $T_c^{\text{Ising}} = 1/\ln(1+\sqrt{2}) = 1.1346$. By means of finite-size scaling analyses we confirmed that along this transition line the critical exponents indeed fall

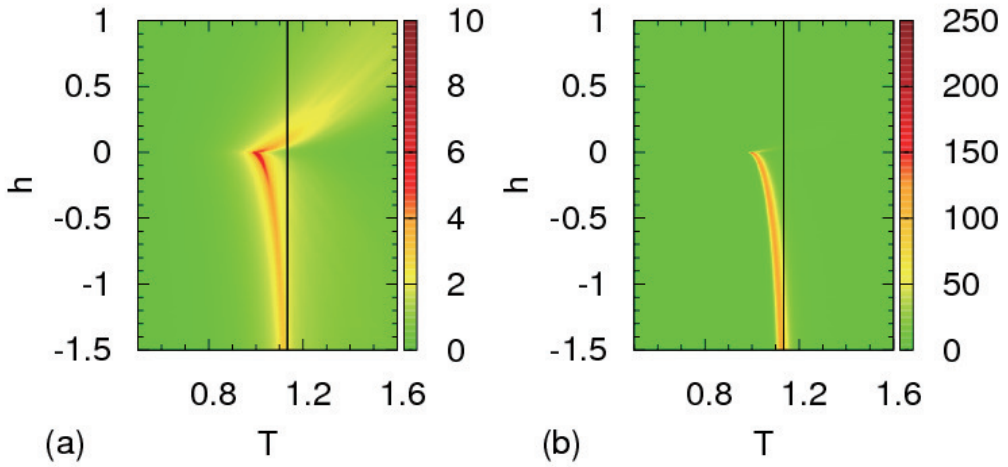

Figure 10.22: (a) Specific heat C/L^2 and (b) magnetic susceptibility χ/L^2 as functions of T and h for $L = 80$. The solid vertical line at $T = 1.1346$ shows the critical temperature of the Ising model (in 2-state Potts model normalization).

into the Ising universality class [6], as expected. For positive magnetic fields, the phase transition disappears altogether.

[1] F.Y. Wu: Rev. Mod. Phys. **54**, 235 (1982)
[2] W. Janke: Physica A **254**, 164 (1998); U.H.E. Hansmann, Y. Okamoto: In *Annual Reviews of Computational Physics VI*, ed. D. Stauffer, (World Scientific, Singapore, 1999), p. 129; W. Janke (ed.): *Rugged Free Energy Landscapes: Common Computational Approaches to Spin Glasses, Structural Glasses and Biological Macromolecules*, Lect. Notes Phys. **736** (Springer, Berlin, 2008)
[3] A. Mitsutake, Y. Okamoto: Phys. Rev. E **79**, 047701 (2009); J. Chem. Phys. **130**, 214105 (2009)
[4] T. Nagai, Y. Okamoto: Phys. Rev. E **86**, 056705 (2012); Physics Procedia **34**, 100 (2012)
[5] A.P. Lyubartsev et al.: J. Chem. Phys. **96**, 1776 (1992); E. Marinari, G. Parisi: Europhys. Lett. **19**, 451 (1992)
[6] T. Nagai et al.: J. Stat. Mech.: Theor. Exp., P02039 (2013); Condens. Matter Phys. **16**, 23605 (2013)

10.21 Scaling Properties of a Parallel Version of the Multicanonical Method

J. Zierenberg, M. Marenz, W. Janke

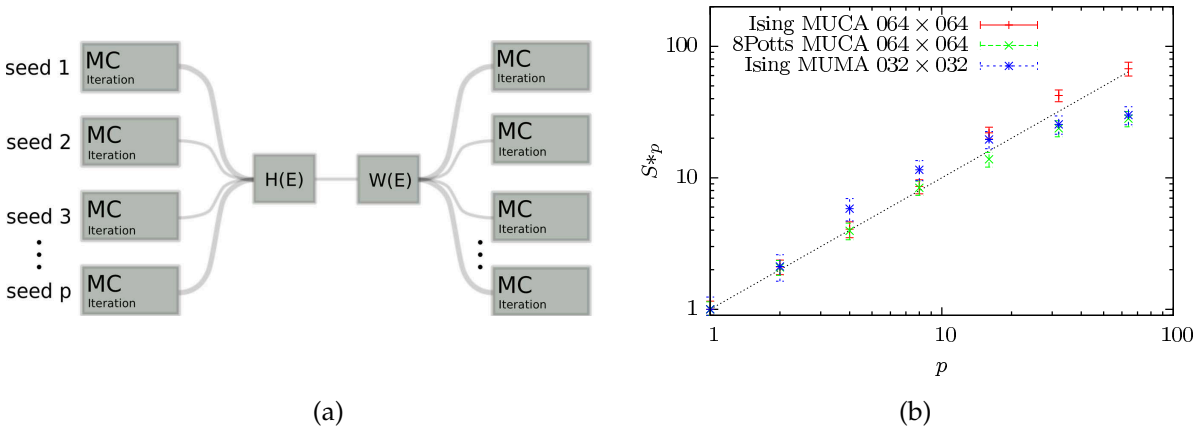

(a) (b)

Figure 10.23: (a) The working principle of the parallel implementation. After each iteration, the histograms of the independent Markov Chains are merged, the consecutive weight function is determined and distributed again onto the independent processes. (b) Statistical speedup for the multicanonical simulation of the Ising and Potts model as well as the multimagnetic simulation of the Ising model.

At times, with computer performance increasing mainly in terms of parallel processing on multi-core architectures, it is crucial to parallelize the applied algorithm. With this in mind, we extended our Monte Carlo tool box by a parallel implementation of the multicanonical method. The parallelization relies on independent equilibrium simulations that only communicate when the multicanonical weight function is updated. That way, the Markov chains efficiently sample the temporary distributions allowing for good estimations of consecutive weight functions. We discovered that similar approaches have been made in the literature [1, 2], without giving a detailed answer to the performance of this parallelization.

We set out to answer this open question for well known simple test systems, namely the two-dimensional Ising model and 8-state Potts model. They exhibit phase transitions of second and first order, respectively. As the parallelization employs independent Markov chains, simulations with different number of cores may not be compared one to one. This demanded a detailed consideration of the involved parameters in order to compare the average optimal performance at each degree of parallelization.

Overall, the parallelization was shown to scale quite well for up to 64 cores [3, 4]. In the case of multicanonical simulations of the 8-state Potts model, the optimal performance is limited due to emerging barriers. The parallelization can be applied also to other flat-histogram simulations, e.g. multimagnetic simulations. It may be pointed out that no greater adjustment to the usual implementation is necessary and that additional modifications may be carried along. This allows a straightforward application of this parallelization to complex systems like (bio) polymers and (spin) glasses.

[1] V.V. Slavin: Low Temp. Phys. **36**, 243 (2010)
[2] A. Ghazisaeidi et al.: J. Lightwave Technol. **28**, 79 (2010)
[3] J. Zierenberg et al.: Comput. Phys. Comm. **184**, 1155 (2013)
[4] J. Zierenberg et al.: *Application of parallel multicanonical simulations to systems*

with first and second order phase transitions, to appear in Physics Procedia (2013), in print

10.22 Funding

Graduate School *"BuildMoNa": Leipzig School of Natural Sciences – Building with Molecules and Nano-objects*
W. Janke (Principal Investigator)
Deutsche Forschungsgemeinschaft (DFG), Excellence Initiative

Graduate School *Statistical Physics of Complex Systems*
W. Janke (with B. Berche, Nancy)
Deutsch-Französische Hochschule, Deutsch-Französisches Doktorandenkollegium (DFDK) with "Co-tutelle de Thèse", jointly with Université de Lorraine, Nancy, France, and Coventry University, UK, as associated partner, Grant No. CDFA-02-07

International Max Planck Research School (IMPRS) *Mathematics in the Sciences*
W. Janke (Scientific Member)
Max Planck Society and Klaus Tschira Foundation

Forschergruppe 877 *From Local Constraints to Macroscopic Transport*
W. Janke (Principal Investigator, project P9 in collaboration with K. Kroy)
Deutsche Forschungsgemeinschaft (DFG), Grant No. JA 483/29-1

Sonderforschungsbereich/Transregio SFB/TRR 102 *Polymers under Multiple Constraints: Restricted and Controlled Molecular Order and Mobility*
W. Janke (Principal Investigator, project B04)
Deutsche Forschungsgemeinschaft (DFG)

Institute Partnership with the Institute for Condensed Matter Physics of the National Academy of Sciences of Ukraine, Lviv, Ukraine, *Polymers in Porous Environments and on Disordered Substrates*
W. Janke (with V. Blavatska, Lviv)
Alexander von Humboldt Foundation

Dynamik und Statik von Spingläsern
W. Janke
Deutsche Forschungsgemeinschaft (DFG), Grant No. JA 483/22-1

Molecular Conformation Mechanics of Proteins and Polymers
W. Janke
Deutsche Forschungsgemeinschaft (DFG), Grant No. JA 483/24-3

Mass Transport Models on Networks
W. Janke (twin project with H. Meyer-Ortmanns, Jacobs University Bremen)
Deutsche Forschungsgemeinschaft (DFG), Grant No. JA 483/27-1

Grafted and Non-Grafted Polymer Adsorption to (Patterned) Substrates
W. Janke and M. Möddel
NIC Jülich (computer time grant for "JUROPA"), Grant No. hlz17

Host of Prof. Dr. Handan Arkın-Olgar (Ankara University, Turkey), *Fellowship for Experienced Researchers*
W. Janke
Alexander von Humboldt Foundation

Host of Buket Taşdizen (Ankara University, Turkey), ERASMUS Fellowship
W. Janke
ERASMUS Programme

10.23 Organizational Duties

Wolfhard Janke

- Director, Institute for Theoretical Physics (ITP), Universität Leipzig
- Director, Naturwissenschaftlich-Theoretisches Zentrum (NTZ), Universität Leipzig
- Member of Department Council ("Fakultätsrat"), Faculty for Physics and Earth Sciences, Universität Leipzig
- Member of the Steering Committee ("Direktorium") of the Graduate Centre *Mathematics/Computer Science and Natural Sciences*, Research Academy Leipzig
- Member Priority Research Area PbF1 *Molecules and Nano-objects*
- Member Priority Research Area PbF2 *Mathematical Sciences*
- Spokesperson of the German-Ukrainian Institute Partnership Leipzig-Lviv of the Alexander von Humboldt Foundation
- Spokesperson of the German-French Graduate College *Statistical Physics of Complex Systems*
- External Member of the Jagiellonian University Graduate School *International Ph.D. Studies in Physics of Complex Systems*, Krakow, Poland
- Chairperson of the Programme Committee "Scientific Computing" of Forschungszentrum Jülich
- Member of the Scientific-Technical-Council of the Supervisory Board ("Aufsichtsrat") of the Forschungszentrum Jülich GmbH
- Permanent Member of the "International Advisory Board", *Conference of the Middle European Cooperation in Statistical Physics (MECO)*
- Member of the Programme Committee for the 4th Conference on *Statistical Physics: Modern Trends and Applications*, Lviv, Ukraine, 03.–06. July 2012
- Member of the International Advisory Board for the XXV IUPAP *Conference on Computational Physics* CCP2013, Moscow, Russia, 20.–24. August 2013
- Co-organizer of the "BuildMoNa"Modul *Basic Concepts in Physics* (with P. Esquinazi and J. Haase), Universität Leipzig, 14. February 2012
- Co-organizer of the AvH Kick-Off Workshop *Polymers in Porous Environments and on Disordered Substrates* (with V. Blavatska), Ivan Franko National University, Lviv, Ukraine, 03. July 2012
- Co-organizer of the "BuildMoNa" Module 2012-M10 *Multifunctional Scaffolds* (with F. Kremer, K. Kroy, and T. Pompe), Universität Leipzig, 27.–28. September 2012
- Organizer of the Workshop *CompPhys12* – 13th International NTZ Workshop on *New Developments in Computational Physics*, ITP, Universität Leipzig, 29. November – 01. December 2012

- Organizer of the Workshop *CompPhys13* – 14th International NTZ Workshop on *New Developments in Computational Physics*, ITP, Universität Leipzig, 28.–30. November 2013
- Editor "Computational Physics", Central European Journal of Physics, Krakow, Poland
- Member of Editorial Board, Condens. Matter Phys., Lviv, Ukraine
- External Reviewer for Humboldt-Stiftung (AvH); Studienstiftung des deutschen Volkes; Deutsche Forschungsgemeinschaft (DFG); "Fond zur Förderung der wissenschaftlichen Forschung (FWF)", Österreich; "The Royal Society", Great Britain; The "Engineering and Physical Sciences Research Council (EPSRC)", Great Britain; Israel Science Foundation, Israel; National Science Foundation (NSF), USA; Natural Sciences and Engineering Research Council of Canada (NSERC), Canada; the Jeffress Memorial Trust, Bank of America, Virginia, USA; Universität Mainz, Germany; The University of Warwick, England, Great Britain; Coventry University, England, Great Britain; CECAM, Lyon, France
- Referee for Physical Review Letters, Physical Review B, Physical Review E, Journal of Chemical Physics, Europhysics Letters, Physics Letters A, Physics Letters B, The European Physical Journal B, Physica A, Proceedings of the Royal Physical Society, Journal of Physics A, Computer Physics Communications, JSTAT, New Journal of Physics, International Journal of Modern Physics C

10.24 External Cooperations

Academic

- Institute of Physics, Jagiellonian University, Kraków, Poland
  Prof. Dr. Piotr Białas, Dr. Leszek Bogacz, Prof. Dr. Zdzisław Burda
- CEA/Saclay, Service de Physique Théorique, France
  Dr. Alain Billoire
- Institut für Physik, Universität Mainz, Germany
  Prof. Dr. Kurt Binder, Dr. Hsiao-Ping Hsu, Andreas Nußbaumer, Prof. Dr. Friderike Schmid
- Institut für Theoretische Physik, Universität Heidelberg, Germany
  Dr. Elmar Bittner
- Laboratoire de Physique des Matériaux (UMR CNRS No 7556), Université de Lorraine, Nancy, France
  Prof. Dr. Bertrand Berche, Dr. Christophe Chatelain, Dr. Olivier Collet, Prof. Dr. Malte Henkel, Prof. Dr. Dragi Karevski
- Groupe de Physique des Matériaux (UMR CNRS No 6634), Université de Rouen, France
  Dr. Pierre-Emmanuel Berche
- SUPA, School of Physics and Astronomy, University of Edinburgh, Scotland, UK
  Dr. Richard A. Blythe, Prof. Dr. Martin R. Evans, Dr. Bartłomiej Wacław

- Istituto Nazionale di Fisica Nucleare, Sezione di Milano-Bicocca, Milano, Italy
  Prof. Dr. Pablo Butera
- Jülich Supercomputing Centre (JSC), Forschungszentrum Jülich, Germany
  Prof. Dr. Peter Grassberger, PD Dr. Thomas Neuhaus
- IAC-1, Universität Stuttgart
  Prof. Dr. Rudolf Hilfer, Anjan Prasad Gantapara
- Complex Systems Division, Department of Theoretical Physics, Lunds Universitet, Lund, Sweden
  Prof. Dr. Anders Irbäck, Simon Mitternacht
- Department of Mathematics and the Maxwell Institute for Mathematical Sciences, Heriot-Watt University, Edinburgh, Scotland, UK
  Prof. Dr. Desmond A. Johnston
- Applied Mathematics Research Centre, Coventry University, England, UK
  Dr. Ralph Kenna, PD Dr. Christian von Ferber, Dr. Martin Weigel
- Inst. für Theoretische Physik, FU Berlin, Germany
  Prof. Dr. Hagen Kleinert
- Max-Planck Institut für Physik komplexer Systeme, Dresden, Germany
  Dr. Andreas Läuchli
- Atominstitut, TU Wien, Austria
  Prof. Dr. Harald Markum, Dr. Rainer Pullirsch
- Jacobs Universität Bremen, Germany
  Dr. Ashok Garai, Prof. Dr. Hildegard Meyer-Ortmanns, Darka Labaviç
- Applied Mathematics, Universitat Pompeu Fabra, Barcelona, Spain
  Dr. Ramon Villanova
- EPF Lausanne, Switzerland
  Dr. Sandro Wenzel
- Department of Engineering of Physics, Ankara University, Turkey
  Prof. Dr. Handan Arkın (Olgar), Mustafa Bilsel, Buket Taşdizen
- Dept. of Physics, Hacettepe University, Ankara, Turkey
  Prof. Dr. Tarik Çelik, Gökhan Gökoğlu
- Institute for Condensed Matter Physics, National Academy of Sciences, Lviv, Ukraine
  Dr. Viktoria Blavatska, Prof. Dr. Yurij Holovatch
- Yerevan Physics Institute, Yerevan, Armenia
  Prof. Dr. David B. Saakian
- Landau Institute for Theoretical Physics, Chernogolovka, Russia
  Prof. Dr. Lev N. Shchur
- Banaras Hindu University, Varanasi, India
  Prof. Dr. Sanjay Kumar
- Center for Simulational Physics, The University of Georgia, Athens, USA
  Prof. Dr. Michael Bachmann, Jonathan Gross, Prof. Dr. David P. Landau, Dr. Thomas Vogel

- Dept. of Physics, Florida State University, Tallahassee, USA
  Prof. Dr. Bernd A. Berg
- Dept. of Physics, Michigan Technological University, Houghton, USA
  Prof. Dr. Ulrich H.E. Hansmann
- Dept. of Physics, Virginia Tech, Blacksburg, USA
  Prof. Dr. Michel Pleimling, Prof. Dr. Royce K.P. Zia
- Physics Department, Carnegie Mellon University, Pittsburgh, USA
  Prof. Dr. Robert H. Swendsen
- The University of Tokyo, Japan
  Prof. Dr. Nobuyasu Ito
- Nagoya University, Japan
  Tetsuro Nagai, Prof. Dr. Yuko Okamoto
- Laboratory of Statistical and Computational Physics, Institute of Physics, Academia Sinica, Nankang, Taipei, Taiwan
  Prof. Dr. Chin-Kun Hu
- Zhejiang Institute of Modern Physics, Zhejiang University, Hangzhou, P.R. China
  Prof. Dr. He-Ping Ying, Prof. Dr. Bo Zheng

10.25 Publications

Journals

H. Arkın, W. Janke: *Structural Behavior of a Polymer Chain Inside an Attractive Sphere*, Phys. Rev. E **85**, 051802-1–9 (2012)

H. Arkın, W. Janke: *Ground-State Properties of a Polymer Chain in an Attractive Sphere*, J. Phys. Chem. B **116**, 10379–10386 (2012)

M. Bilsel, B. Taşdizen, H. Arkın, W. Janke: *Effects of Confinement on the Thermodynamics of a Model Protein*, in Proceedings of the NIC Workshop *From Computational Biophysics to Systems Biology (CBSB11) – Celebrating Harold Scheraga's 90th Birthday*, Forschungszentrum Jülich, Germany, 20–22 July 2011, eds. P. Carloni, U.H.E. Hansmann, T. Lippert, J.H. Meinke, S. Mohanty, W. Nadler, O. Zimmermann, John von Neumann Institute for Computing, Forschungszentrum Jülich, IAS Series Vol. **8**, pp. 21–24 (2012)

V. Blavatska, W. Janke: *Polymer Adsorption on a Fractal Substrate: Numerical Study*, J. Chem. Phys. **136**, 104907-1–8 (2012)

V. Blavatska, W. Janke: *Conformational Properties of Polymers Near a Fractal Surface*, in *Computer Simulation Studies in Condensed-Matter Physics XXV*, eds. D.P. Landau, H.-B. Schüttler, S. Lewis, M. Bachmann, Physics Procedia **34**, 55–59 (2012)

N. Fricke, W. Janke: *Exact Enumeration of Self-Avoiding Walks on Percolation Clusters*, in *Computer Simulation Studies in Condensed-Matter Physics XXV*, eds. D.P. Landau, H.-B. Schüttler, S. Lewis, M. Bachmann, Physics Procedia **34**, 39–43 (2012)

N. Fricke, W. Janke: *Scale-Free Enumeration of Self-Avoiding Walks on Critical Percolation Clusters*, Europhys. Lett. **99**, 56005-1–5 (2012)

A. Garai, B. Waclaw, H. Nagel, H. Meyer-Ortmanns: *Stochastic Description of a Bistable Frustrated Unit*, J. Stat. Mech.: Theor. Exp., P01009-1–28 (2012)

W. Janke: *Monte Carlo Simulations in Statistical Physics – From Basic Principles to Advanced Applications*, in *Order, Disorder and Criticality: Advanced Problems of Phase Transition Theory*, Vol. 3, ed. Y. Holovatch (World Scientific, Singapore, 2012), pp. 93–166

M. Marenz, J. Zierenberg, H. Arkın, W. Janke: *Simple Flexible Polymers in a Spherical Cage*, Condens. Matter Phys. **15**, 43008-1–7 (2012)

M. Möddel, M. Bachmann, W. Janke: *Grafted versus Non-Grafted Polymer Adsorption*, in Proceedings of the *NIC Symposium 2012*, Forschungszentrum Jülich, Germany, 7–8 February 2012, eds. K. Binder, G. Münster, M. Kremer, John von Neumann Institute for Computing, Jülich, NIC Series, Vol. **45**, pp. 277–284 (2012)

S. Schnabel, D.P. Landau: *Fictitious Excitations in the Classical Heisenberg Antiferromagnet on the Kagome Lattice*, Phys. Rev. B **86**, 014413-1–10 (2012)

S. Schöbl, J. Zierenberg, W. Janke: *Influence of Lattice Disorder on the Structure of Persistent Polymer Chains*, J. Phys. A: Math. Theor. **45**, 475002-1–19 (2012)

D.T. Seaton, S. Schnabel, M. Bachmann, D.P. Landau: *Effects of Stiffness on Short, Semiflexible Homopolymer Chains*, Int. J. Mod. Phys. C **23**, 1240004-1–7 (2012)

in press

H. Arkın, W. Janke: *Polymer-Attractive Spherical Cage System*, Eur. Phys. J. – Special Topics **216**, 181–190 (2013)

H. Arkın, W. Janke: *Gyration Tensor Based Analysis of the Shapes of Polymer Chains in an Attractive Spherical Cage*, J. Chem. Phys. **138**, 054904-1–8 (2013)

N. Fricke, W. Janke: *Self-Avoiding Walks on Strongly Diluted Lattices: Chain-Growth Simulations vs Exact Enumeration*, Eur. Phys. J. – Special Topics **216**, 175–179 (2013) [Fig. 1 selected for the cover page of this volume]

D. Labavić, H. Nagel, W. Janke, H. Meyer-Ortmanns: *Caveats in Modeling a Common Motif in Genetic Circuits*, Phys. Rev. E **87**, 062706-1–1 (2013)

T. Nagai, Y. Okamoto, W. Janke: *Application of Simulated Tempering and Magnetizing to a Two-Dimensional Potts Model*, J. Stat. Mech.: Theor. Exp., P02039-1–21 (2013)

T. Nagai, Y. Okamoto, W. Janke: *Crossover Scaling in the Two-Dimensional Three-State Potts Model*, Condens. Matter Phys. **16**, 23605-1–8 (2013)

D.T. Seaton, S. Schnabel, D.P. Landau, M. Bachmann: *From Flexible to Stiff: Systematic Analysis of Structural Phases for Single Semiflexible Polymers*, Phys. Rev. Lett. **110**, 028103-1–5 (2013)

J. Zierenberg, M. Marenz, W. Janke: *Scaling Properties of a Parallel Implementation of the Multicanonical Algorithm*, Comput. Phys. Comm. **184**, 1155–1160 (2013)

J. Zierenberg, M. Marenz, W. Janke: *Application of Parallel Multicanonical Simulations to Systems with First and Second Order Phase Transition*, in *Computer Simulation Studies in Condensed-Matter Physics XXVI*, eds. D.P. Landau, H.-B. Schüttler, S. Lewis, M. Bachmann, to appear in Physics Procedia (2013), in print

Talks

H. Arkın: *Structure Formation of a Polymer Chain in an Attractive Sphere*, CECAM Workshop, Paris, France, 21.–23. May 2012

H. Arkın: *Conformational Behavior of a Polymer Chain in an Attractive Spherical Cage*, SFB/TR102 Fall Meeting Miniworkshop, Brehna, Germany 19. October 2012

H. Arkın: *Thermodynamics of a Polymer Chain in a Spherical Cage*, 13th International NTZ-Workshop on *New Developments in Computational Physics – CompPhys12*, Universität Leipzig, Germany, 29. November – 01. December 2012

N. Fricke: *Scale-Free Enumeration of Self-Avoiding Walks on Percolation Clusters*, 25th Annual CSP Workshop "Recent Developments in Computer Simulation Studies in Condensed Matter Physics", The University of Georgia, Athens, Georgia, USA, 20. February 2012

N. Fricke: *How to Enumerate* 10^{1000} *Self-Avoiding Walks on a Critical Percolation Cluster*, AvH Institute Partnership Leipzig-Lviv Kick-Off Workshop *Polymers in Porous Environments and on Disordered Substrates* (Satellite Workshop of the 4th Conference on *Statistical Physics*), Ivan Franko National University, Lviv, Ukraine, 03. July 2012

N. Fricke: *Self-Avoiding Walks on Disordered Lattices*, 5th BuildMoNa Workshop for Doctoral Candidates, Burgstädt, Germany, 24.–25. September 2012

W. Janke: *Monte Carlo Methods in Classical Statistical Physics*, BuildMoNa Module B3 *Basic Concepts in Physics*, Universität Leipzig, Germany, 14. February 2012

W. Janke: *Formation/Dissolution of Equilibrium Droplets*, Statistical Physics Seminar, Virginia Tech, Blacksburg, USA, 16. February 2012

W. Janke: *Polymer Adsorption on a Fractal Substrate*, 25th CSP Workshop on *Recent Developments in Computer Simulation Studies in Condensed Matter Physics*, The University of Georgia, Athens, Georgia, USA, 20.–24. February 2012

W. Janke: *Polymer Adsorption to a Fluctuating Membrane*, MECO 37 Conference, Tatranské Matliare, High Tatras, Slovakia, 19.–21. March 2012

W. Janke: *Numerical Study of Polymer Adsorption on a Fractal Substrate*, DPG Frühjahrstagung 2012, TU Berlin, Germany, 25.–30. March 2012

W. Janke: *Polymer Adsorption to a Fluctuating Membrane*, Workshop *Statistical Physics and Low Dimensional Systems – SPLDS*, Pont-à-Mousson, France, 29. May – 01. June 2012

W. Janke: *Transition Trajectory for Equilibrium Droplet Formation*, Workshop on *Computation of Transition Trajectories and Rare Events in Non-Equilibrium Systems*, Centre Blaise Pascal, ENS de Lyon, France, 11.–15. June 2012

W. Janke: *Computer Simulations of Polymers in Disordered Media*, BuildMoNa Module 2012-T6 *Hybrid Systems*, Universität Leipzig, Germany, 27. June 2012

W. Janke: *Football Fever: Self-Affirmation Model for Goal Distributions*, Lange Nacht der Wissenschaften, Universität Leipzig, Germany, 29. June 2012

W. Janke: *Polymer Adsorption on a Fractal Substrate*, AvH Institute Partnership Leipzig-Lviv Kick-Off Workshop *Polymers in Porous Environments and on Disordered Substrates* (Satellite Workshop of the 4th Conference on *Statistical Physics*), Ivan Franko National University, Lviv, Ukraine, 03. July 2012

W. Janke: *Polymer Statistics in an Attractive Sphere*, 4th Conference on *Statistical Physics: Modern Trends and Applications*, Ivan Franko National University, Lviv, Ukraine, 03.–06. July 2012

W. Janke: *Computer Simulations of Polymer Adsorption*, IGER International Symposium on *Science of Molecular Assembly and Biomolecular Systems 2012*, Nagoya University, Japan, 04.–05. September 2012

W. Janke: *Computer Simulations of Equilibrium Droplet Formation*, Physics Seminar, Tokyo Metropolitan University, Tokyo, Japan, 07. September 2012

W. Janke: *Generalized Ensemble Simulations of Polymer Adsorption*, International Workshop *Statistical Mechanics: Interplay of Theory and Computer Simulations*, Universität Mainz, Germany, 19.–21. September 2012

W. Janke: *Simulating Polymer Systems on GPU*, MPI-PKS Dresden IMPRS School 2012 *GPU Computing Methods and Applications in the Natural Sciences*, Wroclaw, Poland, 29. October – 02. November 2012

M. Marenz: *Framework for Off-Lattice Monte Carlo Simulations*, 5th BuildMoNa Workshop for Doctoral Candidates, Burgstädt, Germany, 24.–25. September 2012

M. Müller: *Multicanonical Analysis of the Gonihedric Ising Model*, Seminar of the cdfa-dfdk, Université Lorraine, Nancy, France, 07. November 2012

M. Möddel: *Grafted and Nongrafted Adsorption of Polymers on Different Substrates*, Retreat of the SFB/TRR 102, Bad Blankenburg, Germany, 14.–16. March 2012

M. Möddel: *Influence of Striped Surface-Inhomogeneities on the Conformations of a Single Self-Interacting Polymer near an Attractive Substrate*, DPG Frühjahrstagung 2012, TU Berlin, Germany, 30. March 2012

J. Zierenberg: *Simulating Flexible Polymers in Hard Disk Background Potentials*, Seminar of the cdfa-dfdk, Coventry University, England, 22. February 2012

J. Zierenberg: *Scaling Properties of a Parallel Implementation of the Multicanonical Algorithm*, Seminar of the cdfa-dfdk, Université Lorraine, Nancy, France, 07. November 2012

J. Zierenberg: *Scaling Properties of a Parallel Implementation of the Multicanonical Algorithm*, 13th International NTZ-Workshop on *New Developments in Computational Physics – CompPhys12*, Universität Leipzig, Germany, 30. November 2012

Posters

H. Arkın, W. Janke: *Polymer Chain Inside Confinement*, Network Meeting, Alexander von Humboldt Foundation, Kiel, Germany, 08.–10. February 2012

H. Arkın, W. Janke: *Conformational Phase Diagram of a Polymer Chain Inside an Attractive Sphere*, Conference *Career in Polymers 2012*, Prag, Czech Republic, 28.–30. June 2012

H. Arkın, W. Janke: *Polymer Chain in an Attractive Spherical Confinement*, International Workshop *Statistical Mechanics: Interplay of Theory and Computer Simulations*, Mainz, Germany, 19.–21. September 2012

N. Fricke: *Scale-Free Enumeration of Self-Avoiding Walks on Critical Percolation Clusters*, 5th Scientific Symposium of the Graduate School BuildMoNa, Helmholtz Centre for Environmental Research, Leipzig, Germany, 12. March 2012

N. Fricke, W. Janke: *Scale-Free Enumeration of Self-Avoiding Walks on Percolation Clusters*, Conference of the Middle European Cooperation in Statistical Physics "MECO37", Tatranské Matliare, High Tatras, Slovakia, 19.–21. March 2012

N. Fricke, W. Janke: *Self-Avoiding Walks on Critical Percolation Clusters*, 4th Conference on *Statistical Physics: Modern Trends and Applications*, Ivan Franko National University, Lviv, Ukraine, 03.–06. July 2012

M. Marenz, J. Zierenberg, H. Arkın, W. Janke: *Simple Polymer in a Spherical Cage*, 4th Conference on *Statistical Physics: Modern Trends and Applications*, Ivan Franko National University, Lviv, Ukraine, 03.–06. July 2012

M. Marenz, J. Zierenberg, H. Arkın, W. Janke: *Simple Polymer in a Spherical Cage*, 13th International NTZ-Workshop on *New Developments in Computational Physics – CompPhys12*, Universität Leipzig, Germany, 29. November – 01. December 2012

M. Müller, D.A. Johnston, W. Janke: *Multicanonical Analysis of the Gonihedric Ising Model*, 13th International NTZ-Workshop on *New Developments in Computational Physics – CompPhys12*, Universität Leipzig, Germany, 29. November – 01. December 2012

M. Möddel, W. Janke, M. Bachmann: *Comparison of Grafted and Non-Grafted Polymer Adsorption in Different Ensembles*, Conference of the Middle European Cooperation in Statistical Physics "MECO37", Tatranské Matliare, High Tatras, Slovakia, 19.–21. March 2012

M. Möddel, M. Bachmann, W. Janke: *Comparison of Grafted and Non-Grafted Polymer Adsorption in Different Ensembles*, NIC Symposium 2012, Forschungszentrum Jülich, Germany 07.–08. February 2012

H. Nagel, D. Labaviç, H. Meyer-Ortmanns, W. Janke: *Stochastic Description of a Bistable Frustrated Unit* DPG Frühjahrstagung 2012, TU Berlin, Germany, 26.–30. March 2012

H. Nagel, D. Labaviç, H. Meyer-Ortmanns, W. Janke: *Stochastic Description of a Bistable Frustrated Unit* 13th International NTZ-Workshop on *New Developments in Computational Physics – CompPhys12*, Universität Leipzig, Germany, 29. November – 01. December 2012

E. Ehrenpreis, H. Nagel, W. Janke: *Numerical Survey of the Tunable Condensate Shape and Scaling Laws in Pair-Factorized Steady States* 13th International NTZ-Workshop on *New Developments in Computational Physics – CompPhys12*, Universität Leipzig, Germany, 29. November – 01. December 2012

S. Schöbl, J. Zierenberg, K. Kroy, W. Janke: *Broadscale Examination of the Influence of Disorder on Semiflexible Polymers*, 13th International NTZ-Workshop on *New Developments in Computational Physics – CompPhys12*, Universität Leipzig, Germany, 29. November – 01. December 2012

S. Schöbl, J. Zierenberg, W. Janke: *Simulating Flexible Polymers in a Potential of Randomly Distributed Hard Disks*, Conference of the Middle European Cooperation in Statistical Physics "MECO37", Tatranské Matliare, High Tatras, Slovakia, 19.–21. March 2012

S. Schöbl, J. Zierenberg, W. Janke: *Simulating Flexible Polymers in a Potential of Randomly Distributed Hard Disks*, DPG Frühjahrstagung 2012, TU Berlin, Germany, 26.–30. March 2012

10.26 Graduations

Doctorate

- Monika Möddel
  Statistical Equilibrium Behaviour of Finite Polymers Near Attractive Substrates
  20. June 2012

Diploma

- Max Henner Gerlach
  Directional Ordering in the Classical Compass Model in Two and Three Dimesions
  24. February 2012
- Arnd Tretbar
  Polymer Aggregation on a Simple Cubic Lattice
  03. September 2012

- Thomas Peschel
  Exakte Auszählung von Selbst-Avoiding-Walks auf n-dimensionalen einfach kubischen Gittern
  02. October 2012

Master

- Eugen Ehrenpreis
  Mass Condensation in Driven Stochastic Transport Processes – Interaction- and Potential-Driven Condensation Phenomena
  10. May 2012
- Momchil Ivanov
  Polymer Adsorption onto a Stripe-Patterned Surface
  25. October 2012

10.27 Guests

- Buket Taşdizen
  Ankara University, Turkey
  ERASMUS Programme
  01. December 2011 – 29. February 2012
- Prof. Dr. Sanjay Kumar
  Department of Physics, Banaras Hindu University, Varanasi, India
  NTZ/FOR877 Colloquium
  DNA under Periodic Force: Scaling and Phase Diagram
  07. June 2012
- Tetsuro Nagai
  Nagoya University, Japan
  NTZ Colloquium (12. July 2012)
  The Simulated Tempering and Magnetizing Algorithm 01. May - 31. August 2012
- Jeremi Ochab
  Jagiellonian University, Krakow, Poland
  01. August – 30. September 2012
- Dr. Viktoria Blavatska
  Institute for Condensed Matter Physics, Lviv, Ukraine
  Alexander von Humboldt Foundation Institute Partnership Programme
  Conformational Transitions in Random Heteropolymer Models
  01. September – 30. November 2012
- Kristine Haydukivska
  Institute for Condensed Matter Physics, Lviv, Ukraine
  Alexander von Humboldt Foundation Institute Partnership Programme
  01. – 30. November 2012

- Jeremi Ochab
  Jagiellonian University, Krakow, Poland
  Maximal-Entropy Random Walk, Centrality Measures and Communities
  01. November – 20. December 2012

- Prof. Dr. Peter Young
  University of California, Santa Cruz, USA
  NTZ/DFH-UFA/RALeipzig Colloquium
  Mind the Gap: Solving Optimization Problems on a Quantum Computer
  08. November 2012

- Dr. Nathan Clisby
  University of Melbourne, Australia
  NTZ/FOR877 Colloquium
  There are $7 \times 10^{26\,018\,276}$ *self-avoiding walks of* 38 797 311 *steps on* Z^3
  09. November 2012

- Prof. Dr. Bo Zheng
  Zhejiang University, Hangzhou, China
  NTZ/DFH-UFA/RALeipzig Colloquium
  Physics at Zhejiang University
  09. November 2012

- Prof. Dr. Kurt Binder
  Universität Mainz, Germany
  NTZ-Colloquium
  Contact Angles, Wetting Transition, and Macrosopic Interfacial Fluctuations
  28. – 30. November 2012

- Dr. Lev Barash
  Landau Institute, Chernogolovka, Russia
  Parallel Streams of Pseudorandom Numbers for Monte Carlo Simulations: Using most Reliable Algorithms and Applying Parallelism of Modern CPUs and GPUs
  28. November – 02. December 2012

- Dr. Martin Weigel
  Coventry University, England, UK
  Spin Glasses with Many Components
  27. November – 01. December 2012

- Dr. David Yllanes
  "La Sapienza" Rome, Italy
  Finite-Size Scaling Analysis of the Distributions of Pseudo-Critical Temperatures in Spin Glasses
  28. November – 01. December 2012

- Prof. Dr. Juan J. Ruiz-Lorenzo
  Universidad Extremadura, Badajoz, Spain
  Numerical Test of the Cardy-Jacobsen Conjecture in the Site-Diluted Potts Model in Three Dimensions
  28. November – 01. December 2012

- Prof. Dr. Yu-Cheng Lin
  Chengchi University, Taipei, Taiwan
  Correlated Valence-Bond States
  29. November – 01. December 2012
- Prof. Dr. Alexander Hartmann
  Universität Oldenburg, Germany
  Efficient Simulation of Fractional Brownian Motion for Several Values of the Hurst Exponent
  28.–30. November 2012
- Dr. Hsiao-Ping Hsu
  Universität Mainz, Germany
  Scattering Function of Semiflexible Polymer Chains under Good Solvent Conditions
  28. November – 01. December 2012
- Prof. Dr. Malte Henkel
  Nancy Université, France
  Some Exact Results in Systems of Immobile Interacting Particles
  28. November – 01. December 2012
- Prof. Dr. Ferenc Iglói
  Institute of Theoretical Physics, Research Institute for Solid State Physics and Optics, Budapest, Hungary
  Corner Contribution to Percolation Cluster Numbers
  28. November – 02. December 2012
- Tetsuro Nagai
  Nagoya University, Japan
  Simulated Tempering and Magnetizing Simulations of a Potts Model
  27. November – 07. December 2012
- Marcin Zagórski
  Jagiellonian University, Krakow, Poland
  Emergence of Gene Regulatory Networks under Functional Constraints
  28. November – 02. December 2012
- Dr. Elmar Bittner
  Universität Heidelberg, Germany
  Replica-Exchange Cluster Algorithm
  28. November – 01. December 2012
- PD Dr. Thomas Neuhaus
  Jülich Supercomputing Centre, Forschungszentrum Jülich, Germany
  Spin Correlations in the 3D Ising Model on Infinite Cuboids
  28. November – 06. December 2012
- Dr. Artur Barasiński
  Univ. Zielona Góra, Poland
  NTZ/DFH-UFA/RALeipzig Colloquium (06. December 2012)
  Magnetization-Based Assessment of Correlation Energy in Canted Single-Chain Magnets
  28. November – 07. December 2012

11

Molecular Dynamics / Computer Simulation

11.1 Introduction

The group MDC intends to explore adsorption and diffusion of guest molecules in porous solids by analytical calculations and computer simulations (classical Molecular Dynamics Simulations, Metropolis Monte Carlo Simulations, Gibbs Ensemble Monte Carlo Simulations). The simulations are done on modern workstations and supercomputers like large Linux-PC clusters in the NIC Dresden. The examinations include transport properties (diffusion of guest molecules) and adsorption of small hydrocarbons in frameworks of the new exciting class of porous Metal-Organic-Frameworks (so called MOF's).

Hence, we are interested to understand

- the diffusion behaviour of guest molecules in porous crystals in dependence on thermodynamic parameters, steric conditions, intermolecular potentials and the concentration of the guest molecules,
- phase equilibria of a gase phase with an adsorbed phase of guest molecules in dependence on thermodynamic conditions,
- and the structural details and migration mechanisms that enable to explain the interesting and sometimes surprising findings

in microscopic detail and to compare the results with experimental data.

In general the aim of our group during the last 30 years (some of them under a different group name before the unification of Germany) has always been to form a bridge between analytical theoretical theories and experimental measurements.

PD Dr. rer. nat. habil. Siegfried Fritzsche

11.2 Simulation and Experiments on the Diffusion of short alkane/alkene guest molecules in the Metal Organic Framework ZIF-8

S. Fritzsche[*], T. Chokbunpiam[†], C. Chmelik[‡], J. Caro[§], S. Hannongbua[†], T. Remsungnen[¶],

*Abteilung MDC
†Chulalongkorn University, Bangkok, Thailand
‡Institut für Experimentelle Physik I, Abteilung GFP
§Institut für Anorganische Chemie, Leibniz Universität Hannover, Callinstraße 9, 30167 Hannover, Germany
¶Khon Kaen University, Khon Khaen, Thailand

As a part of the SPP 1362 a consortium, formed by 4 research groups in Germany (2

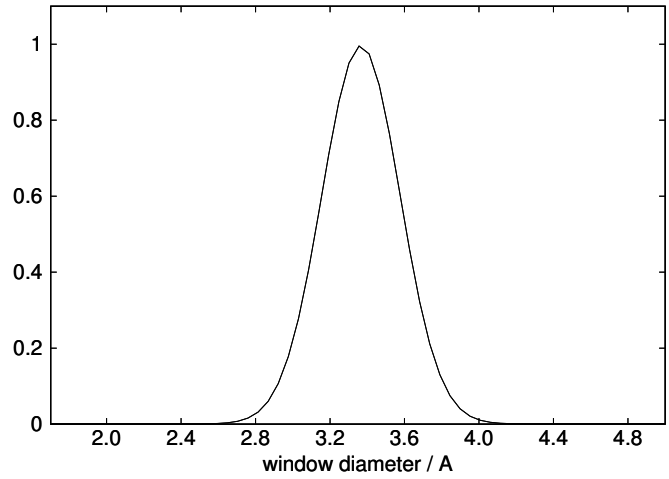

Figure 11.1: The distribution of window diameters in ZIF-8.

in Leipzig, 2 in Hannover) in cooperation with collegues from the Chulalongkorn university, Bangkok and the University of Khon Kaen (both Thailand) the investigation of the transport and adsorption properties of small alkanes ans alkenes within the Metal Organic Framework (MOF) ZIF-8 that led to the publication [1] joining experiment and simulation, has now been extended to ethane, ethene and other small guest molecules.

Particularly, it was the question whether or not the so called 'gate opening' effect could be reproduced by classical MD simulations.

Our classical MD simulations with well established interaction parameters did not show the gate opening effect [2]. This effect is assumed to consist mainly in the rotation of the flexible linker in ZIF-8 which is limiting the window. We did also quantum investigations of this rotational move. The results show [2] that the energy needed do rotate the linker is (under the conditions investigated) to large to be caused by the impact of an arriving guest molecule. These conditions are: a) because of to high computational effort only the linker was flexible, keeping the remaining parts of the lattice rigid. b) The linker rotation was investigated in absence of guest molecules.

The investigations are now continued with other guest molecules (ethene, nitrogen) and modified quantum calculations. There are some hints in [3] that the gate opening is essentially a collective quantum chemical effect.

Additionally, we will start now to investigate adsorption properties of ZIF-8 by own developed software. These simulations are basing on Gibbs ensemble Monte–Carlo simulations. In such simulations the equilibrium between adsorbed phase inside the MOF crystal and the gas phase outside is simulated directly.

[1] L. Hertäg, J. Caro, H. Bux, C. Chmelik, T. Remsungnen, M. Knauth, S. Fritzsche, Journal of Membrane Science **377** (2011) 36–41

[2] T. Chokbunpiam, R. Chanajaree, O. Saengsawang, S. Reimann, C. Chmelik, S. Fritzsche, J. Caro, T. Remsungnen and S. Hannongbua, *The Importance of Lattice Flexibility for the Migration of Ethane in ZIF-8: Molecular Dynamics Simulations*, Microporous and Mesoporous Materials, in press, online available at DOI 10.1016/j.micromeso.2012.12.047

[3] J. van den Bergh, C. Gücüyener, E. A. Pidko, E. J. M. Hensen, J. Gascon and, F. Kapteijn, Chem. Eur. J. **17** (2011) 8832–8840

11.3 Diffusion of carbon dioxide and methane in the Metal Organic Framework ZIF-78

S. Fritzsche[*], S. Phuangjumpee[†], V. Parasuk[†] S. Hannongbua[‡], O. Saengsawang[‡], R. Channajaree[‡], J. Kärger[§],

[*]Abteilung MDC

[†]Petrochemical and Polymer Science Program, Chulalongkorn University, Bangkok, Thailand

[‡]Chulalongkorn University, Bangkok, Thailand

[§]Institut für Experimentelle Physik I, Abteilung GFP

The removal of CO_2 from natural gas that mainly consists of CH_4 is a most important elementary step in upstream petroleum industry. ZIF-78 is found to be a promising material for the separation of CO_2 from CO_2 gas mixtures.

Therefore, the adsorption and diffusion of carbon dioxide and methane is being investigated in this project.

The molecular interaction parameters are taken from the literature. They are improved by Grand Canonical Monte-Carlo simulations (GCMC) and chosing modifications to meet adsorption data from the literatur. The parameters that reproduce the adsorption data best, are then used for Molecular Dynamics simulations of the diffusion behavior.

Some results of this project are published in [1].

[1] S. Phuangjumpee, O. Saengsawang, R. Channajaree, S. Fritzsche, J. Kärger, V. Parasuk and S. Hannongbua, *Investigating Adsorption and Selectivity of CO_2 on Zeolitic Imidazolate Framework-78 Using Molecular Dynamic Simulations*, submitted to Microporous and Mesoporous Materials, under revision

11.4 Adsorption and diffusion of hydrogen in the Metal Organic Framework ZIF-11

S. Fritzsche[*], P. Schierz[*], W. Janke[†], S. Hannongbua[‡], C. Chmelik[§],

[*]Abteilung MDC

[†]Inst. of Theoretical Physics, University of Leipzig

[‡]Chulalongkorn University, Bangkok, Thailand

[§]Institut für Experimentelle Physik I, Abteilung GFP

Metal Organic Frameworks (MOFs) are promising materials for gas separation, gas storage and catalysis. One of the scientific problems at our time is to find a way to store hydrogen in a tank to use it as fuel for cars and in many industrial applications it is necessary to divide a gas mixture into its compounds. These are only two example where the Metal Organic Frameworks are a subject of interest.

To make catalysts, molecular sieves etc. efficient a lot of knowledge about details of adsorption and diffusion is necessary.

Computer simulations are a relatively cheap and effective tool to get inside into molecular processes.

First aim of the project was to develop a force field for hydrogen in ZIF-11 that reproduces existing measurements and afterward this force field was used to calculate the values of unknown observables especially the self-diffusion coefficient.

The recent results are gathered together in the master thesis [1].

[1] P. Schierz, *Investigation of adsorption and diffusion of hydrogen guest molecules in the Metal-Organic Framework ZIF-11 by computer simulations*, master thesis, University of Leipzig, 2012

11.5 Adsorption of small molecules in the Metal Organic Framework ZIF-7

S. Fritzsche[*], P. Pilvar[*], P. Schierz[*], S. Hannongbua[†], C. Chmelik[‡],

[*]Abteilung MDC
[†]Chulalongkorn University, Bangkok, Thailand
[‡]Institut für Experimentelle Physik I, Abteilung GFP

Some effects observed in measurements of adsorption of guest molecules in the Metal

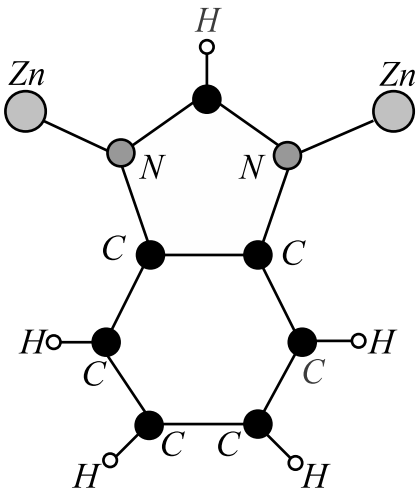

Figure 11.2: The benzimidazolate linker in ZIF-7.

Organic Framework ZIF-7 looked very strange. Molecules much larger than the windows connecting adjacent cavities have been found to be adsorbed in ZIF-7. Hence, this MOF became subject of several experimental and theoretical investigations (see e.g. [1]).

We started classical MD simulations in order to understand this effect. The windows that guest molecules have to pass to penetrate into the MOF crystal are limited by organic linkers connecting Zn metal atoms. One such linker (benzimidazolate) can be seen in figure 11.2.

These linkers are assumed to rotate around the Zn–N bonds when guest molecules are aproaching 'opening the gate'. But, this picture is, maybe, to simple. Density functional simulations in [1] suggest that the possibility for larger molecules to pass the narrow window relies on complex many body quantum effects.

We started our investigations with hydrogen which is small so that gate opening is not essential for the diffusion to become possible.

First results have been presented in [2].

[1] J. van den Bergh, C. Gücüyener, E. A. Pidko, E. J. M. Hensen, J. Gascon and, F. Kapteijn, Chem. Eur. J. **17** (2011) 8832–8840

[2] P. Pilvar, *Investigation of the Diffusion of Small Guest Molecules in ZIF-7 Lattice Using Molecular Dynamics Simulations*, talk at the workshop of the International Research Training Group, DFG IRTG 1056, Leipzig, 3rd of April 2012

11.6 Adsorption and diffusion of methane, hydrogen and carbon dioxide guest molecules in the Metal Organic Framework ZIF-22

S. Fritzsche[*], U. Arsawang,2[*], S. Hannongbua[†], O. Saengsawang[†], R. Channajaree[†],

[*]Abteilung MDC

[†]Chulalongkorn University, Bangkok, Thailand

In experiments it has been shown that ZIF-22 can separate effectively hydrogen from carbon dioxide and methane. Therefore, this project intends to investigate the mechanism of adsorption and transport of these guest molecules within ZIF-22. The structure of ZIF-22 can be seen in Figure 11.3. The adsorption will be investigated by Gibbs ensemble Monte Carlo and the migration of the guest molecules is investigated by Molecular Dynamics using the program package DLPOLY. The results will be compared with the experiments published in [1].

The authors of [1] are our partners in a consortium within the framework of the SPP 1362.

[1] A. Huang, H. Bux, F. Steinbach and, J. Caro, Angewandte Chemie International Edition **49**(2010) 4958–4961

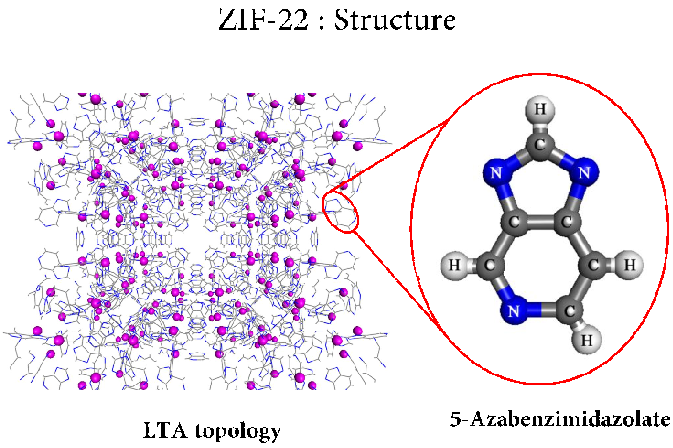

Figure 11.3: The structure of ZIF-22.

11.7 Analytical Treatment and Computer Simulations of the influence of the crystal surface on the exchange of guest molecules between zeolite nanocrystals and the surrounding gas phase

S. Fritzsche[*], O. Saengsawang[†], T. Nanok[‡], S. Vasenkov[§]

[*]Abteilung MDC
[†]Chulalongkorn University, Bangkok, Thailand
[‡]Kasetsart University, Bangkok
[§]University of Florida, Gainesville, USA

Our research about the influence of adsorption barriers and the interplay of diffusion within porous crystals and surface effects were finished in 2012. The results of the years during which our research took place in the framework of the DFG priority program SPP 1155 have been gathered together in a final publication [1].

[1] O. Saengsawang, T. Nanok, S. Vasenkov and S. Fritzsche, Soft Materials **10** (2012) 202-215

11.8 Funding

Adsorption of small molecules in the Metal Organic Framework ZIF-7
S. Fritzsche, P. Pilvar
International Research Training Group, DFG IRTG 1056

Adsorption and diffusion of methane, hydrogen and carbon dioxide guest molecules in the Metal Organic Framework ZIF-22
S. Fritzsche, U. Arsawang
DFG SPP 1362, project code FR 1486/5-1

Simulation and Experiments on the Diffusion of short alkane/alkene guest molecules in the Metal Organic Framework ZIF-8
S. Fritzsche, T. Chokbunpiam
DFG SPP 1362, project code FR 1486/5-1 and a stipend from the Commission on Higher Education for Sandwich Ph.D. Program (CHE-PHD-SW) scholarship and Petroleum, Petrochemicals, and Advanced Materials departement of the Chulalongkorn University, Bangkok, Thailand

Adsorption and diffusion of hydrogen in the Metal Organic Framework ZIF-11,
S. Fritzsche, P. Schierz,
DFG SPP 1362, project code FR 1486/5-1

Analytical Treatment and Computer Simulations of the influence of the crystal surface on the exchange of guest molecules between zeolite nanocrystals and the surrounding gas phase
S. Fritzsche, S. Vasenkov
DFG SPP 1155, project code FR 1486/2-3

11.9 Organizational Duties

S. Fritzsche

- speaker of the workgroup MDC
- project leader of a project within the International Research Training Group, DFG IRTG 1056
- project leader of a project within the DFG SPP 1362

11.10 External Cooperations

Academic

- Chulalongkorn University, Bangkok, Thailand
  Prof. Dr. S. Hannongbua, Dr. O. Saengsawang, Dr. R. Channajaree
- University of Leipzig, Institut für Experimentelle Physik I, Abteilung GFP
  Prof. Dr. J. Kärger, Dr. C. Chmelik

- University of Hannover
  Prof. Dr. J. Caro, Prof. Dr. Wiebcke
- University of Khon Kaen
  Prof. Dr. T. Remsungnen
- University of Bordeaux
  Prof. Dr. P. Bopp

11.11 Publications

Journals

O. Saengsawang, V. Vchirawongkwin, T. Remsungnen, M. Wiebcke, S. Fritzsche and, S. Hannongbua, *Rotational flexibility of bridging ligands in paddle-wheel layer-pillar metal-organic frameworks studied by quantum calculations*, Computational and Theoretical Chemistry **1001** (2012) 33–38

O. Saengsawang, T. Nanok, S. Vasenkov and S. Fritzsche, *Relationship Between Sorbate Transport Inside and at the Margins of Zeolite Crystals*, Soft Materials **10** (2012) 202–215

in press

T. Chokbunpiam, R. Chanajaree, O. Saengsawang, S. Reimann, C. Chmelik, S. Fritzsche, J. Caro, T. Remsungnen and S. Hannongbua, *The Importance of Lattice Flexibility for the Migration of Ethane in ZIF-8: Molecular Dynamics Simulations*, , Microporous and Mesoporous Materials, in press, online available at DOI 10.1016/j.micromeso.2012.12.047

Talks

S. Fritzsche, *Basics of Gibbs ensemble - Monte Carlo Simulations*, Talk February 22nd 2012 at the Chulalongkorn University, Bangkok, Thailand

S. Fritzsche, P. Schierz, *Fugacity Expansion for Adsorption of Guest Molecules in MOF*, Talk March 14th 2012 at the Chulalongkorn University, Bangkok, Thailand

S. Fritzsche, P. Schierz, *Adsorption of Guest Molecules in Pores - Some Theory and Gibbs Simulations*, Talk June 5th 2012 at the IRTG, Leipzig, Inst. f. Exp. Physik I, Leipzig

S. Fritzsche, *Importance of Lattice Flexibility for Adsorption and Diffusion of Guest Molecules in ZIF Frameworks*, Talk August 8th 2012 at the Chulalongkorn University, Bangkok, Thailand

P. Pilvar, *Investigation of the Diffusion of Small Guest Molecules in ZIF-7 Lattice Using Molecular Dynamics Simulations*, talk at the workshop of the International Research Training Group, DFG IRTG 1056, Leipzig, 3rd of April 2012

11.12 Graduations

Master

- Bsc. P. Schierz
  Investigation of adsorption and diffusion of hydrogen guest molecules in the Metal-Organic Framework ZIF-11 by computer simulations
  University of Leipzig, December 2012

12

Quantum Field Theory and Gravity

12.1 Temperature Dependence of the Casimir Force

M. Bordag

The vacuum of quantum fields shows a response to changes in external conditions with measurable consequences. The most prominent manifestation is the Casimir effect. It belongs to the few number of macroscopic quantum effects and it is of big importance in nanometer sizes systems. At present, the problem of the dependence of the Casimir forces on temperature is in the focus of actual interest. There are two reasons for, the possibility to measure these forces due to improved experimental techniques and the more theoretical question on the violation of the third law of thermodynamics observed in a certain model.
Actual research was on the temperature dependent Casimir force between a sphere and a plane and on media with temporal dispersion, [1, 2].

[1] M. Bordag and I. G. Pirozhenko. On the Casimir entropy for a ball in front of a plane. *Phys. Rev. D*, 82:125016, 2010.
[2] M. Bordag, B. Geyer, G. L. Klimchitskaya, and V. M. Mostepanenko. On the definition of dielectric permittivity for media with temporal dispersion in the presence of free charge carriers. *J. Phys.*, A43:015402, 2010.

12.2 Higher order correlation corrections to color ferromagnetic vacuum state at finite temperature

M. Bordag, V. Skalozub*

*U Dnepropetrovsk

Topic of the investigation is the stability of the ground state of QCD with temperature and color magnetic background field by means of the calculation of the polarization tensor of the gluon field. Special attention was devoted to the investigation of the polarization tensor for the color charged gluons at finite temperature. A new technique for a parametric representation was found which allowed for an explicit separation of

the Debye and the magnetic masses and, for instance, for an easy calculation of the Debye mass's field and temperature dependence [1].
Another line of research in this collaboration was on long range magnetic fields.

[1] M. Bordag, V. Demchik, and V.Skalozub. Characteristics of gluon plasma in chromomagnetic field at high temperature. In K.A. Milton and M. Bordag, editors, *Proceedings of the 9th Conference on Quantum Field Theory Under the Influence of External Conditions (QFEXT09)*. World Scientific, Singapore, 2010.

12.3 Structure of the gauge orbit space and study of gauge theoretical models

G. Rudolph, Sz. Charzynski[*], E. Fuchs, H. Grundling[†], J. Huebschmann[‡], P. Jarvis[§], J. Kijowski[*], M. Schmidt

[*]U Warsaw
[†]U Sydney
[‡]U Lille
[§]U Hobart

The investigation of gauge theories in the Hamiltonian approach on finite lattices with emphasis on the role of nongeneric strata was continued.

As a first step towards a generalization of the results of [1] on stratified Kähler quantization to larger gauge groups, the defining relations for arbitrary compact semisimple gauge group have been derived [2]. E. Fuchs worked on the generalization of stratified Kähler quantization to larger lattices.

Based on [3], in collaboration with H. Grundling, the investigation of the structure of the algebra of observables and its representations for specific models of quantum lattice gauge theory in terms of gauge invariant quantities was continued. In [4], the observable algebra for an infinite lattice was constructed.

[1] J. Huebschmann, G. Rudolph, M. Schmidt, Commun. Math. Phys. **286**, Nr. 2 (2009) 459–494
[2] M. Hofmann, G. Rudolph, M. Schmidt: On the Reflection Type Decomposition of the Adjoint Reduced Phase Space of a Compact Semisimple Lie group. arXiv:1302.6118, submitted to J. Math. Phys.
[3] J. Kijowski, G. Rudolph, J. Math. Phys. **43** (2002) 1796–1808;
J. Kijowski, G. Rudolph, J. Math. Phys. **46** (2005) 032303; Rep. Math. Phys. **55** (2005) 199
P. Jarvis, J. Kijowski, G. Rudolph, J. Phys. A **38** (2005) 5359
[4] Commun. Math. Phys. 318 (2013) 717-766

12.4 Quantum field theory on non-commutative geometries, quantum field theory and cosmology, generally covariant quantum field theory

R. Verch, z. Avetisyan, T. Ludwig, M. Gransee, B. Eltzner, J. Zschoche

In non-commutative quantum field theory, the relation between the Euclidean and Lorentzian approach is investigated with T. Ludwig, in collaboration with H. Grosse and G. Lechner, with a focus on the non-commutative Wick-rotation
In collaboration with C.J. Fewster it is investigated how to specify that quantum field theories are the same on all spacetimes, which is an extension of the framework of generally covariant quantum field theory. This connects to the new concept of dynamical locality.
Recently, some new classes of distinguished states have been proposed in quantum field theory in curved spacetimes. In collaboration with C.J. Fewster it was shown that such classes of states have problematic properties and cannot be viewed as physically reasonable states in general.
A further line of investigation in quantum field theory in curved spacetime centers around foundational issues in cosmology. This relates to questions of local thermodynamic equilibrium in cosmological spacetimes (M. Gransee), quantization of fluctuations in the early universe (B. Eltzner), and quantum pressure behaviour and the Chaplygin gas (J. Zschoche), and aspects of group representation theory and harmonic analysis on homogeneous spacetime (Z. Avetisyan)

12.5 Funding

Spectral Zeta Functions and Heat Kernel Technique in Quantum Field Theory with Nonstandard Boundary Condition
M. Bordag
Heisenberg-Landau programme

New Trends and Applications of the Casimir Effect (CASIMIR)
Research Networking Program der ESF (European Research Foundation)
M. Bordag, member of the Steering Committee

Deformations of quantum field theories
G. Lechner, external collaborators at Vienna University
FWF project P22929-N16

Universität Münster, research visit May 2012
R. Verch

ISI Torino, research visit, Sep 2012
R. Verch

31st LQP Workshop "Foundations and Constructive Aspects of QFT", ITP, University of Leipzig, Nov. 23-24, 2012
Ev. Studienwerk Villigst, RALeipzig, PbF2

Quantum field theory and locally noncommutative structures
A. Andersson
IMPRS fellowship

Group theory and harmonic analysis in cosmological spacetimes Z. Avetisyan
IMPRS fellowship

Foundational aspects of cosmology
B. Eltzner, M. Gransee, J. Zschoche
IMPRS fellowship

Quantum Theory of Lattice Gauge models
E. Fuchs
IMPRS fellowship

Non-commutative quantum field theory
T. Ludwig
IMPRS fellowship

12.6 Organizational Duties

Priv.-Doz. Dr. Michael Bordag
- Referee: J. Phys. A, Phys. Rev. D, J. Math. Phys.
- Member of the Steering Committee of the ESF Research Networking Program *New Trends and Applications of the Casimir Effect (CASIMIR)*

Dr. Gandalf Lechner
- Referee for Foundations of Physics, Communications in Mathematical Physics, the Templeton Foundation, and mathscinet
- Organizer of Workshop "LQP 31 – Workshop Foundations and Constructive Aspects of QFT", Universität Leipzig, November 2012

Dr. J. Muñoz-Castañeda
- Organizer of the conference "Mathematical Structures in Quantum Systems", Benasque Centre for Science (Spain), July 2012. Editor of the proceedings, published in Nuovo Cimento C

Prof. Dr. G. Rudolph
- Referee: Class. Quant. Grav., J. Math. Phys., J. Geom. Phys., J. Phys. A, Rep. Math. Phys., Commun. Math. Phys.
- Referee for the German Research Council (DFG) and the Alexander von Humboldt Foundation

Dr. Matthias Schmidt
- Referee: J. Phys. A, Int. J. Mod. Phys. A, Class. Quant. Grav.

Prof. Dr. Rainer Verch
- Speaker, Profilbildender Forschungsbereich 2
- Quality Assurance Officer, Faculty of Physics and Earth Sciences

- Chairman of Examining Board, Physics and Meteorology
- Associate Editor, Journal of General Relativity and Gravitation
- Book Series Editor, Fundamental Theories of Physics (Springer)
- IMPRS Board Member
- Referee for the Alexander von Humboldt Foundation
- Referee: Commun. Math. Phys., J. Math. Phys., JHEP, Rev. Math. Phys., Class. Quantum Grav., Gen. Rel. Grav.
- Organizer, 31st LQP Workshop "Foundations and Constructive Aspects of QFT", ITP, University of Leipzig, Nov. 23-24, 2012

12.7 External Cooperations

Academic

- II. Inst. f. Theoretische Physik, Universität Hamburg
  Prof. Dr. K. Fredenhagen
- Universität Göttingen
  Prof. Dr. D. Bahns, Dr. Y. Tanimoto
- Universität Erlangen
  Prof. Dr. S. Waldmann
- Mathematisches Institut, Universität Münster
  Prof. Dr. R. Wulkenhaar
- Institut für Mathematik, Universität Paderborn
  Dr. Ch. Fleischhack
- Universität Wien
  S. Alazzawi, Prof. Dr. H. Grosse, Dr. J. Schlemmer, C. Schützenhofer
- Department of Mathematics, University of York, England
  Dr. C.J. Fewster
- Universitá di Roma "Tor Vergata"
  Prof. Dr. R. Longo
- Dipartimento di Science, Universitá di Trento, Italy
  Prof. Dr. V. Moretti
- Dipartimento di Matematica, Universitá di Genova, Italy
  Prof. Dr. N. Pinamonti
- Université des Sciences et Technologies de Lille
  Prof. Dr. J. Huebschmann
- Polish Academy of Sciences, Center for Theoretical Physics, Warsaw
  Prof. Dr. J. Kijowski
  Dr. Sz. Charzynski
- National University, Dnepropetrovsk
  Prof. V. Skalozub

- St. Petersburg University
  Prof. Yu.V. Novozhilov
- VIK Dubna
  Dr. V. Nesterenko, Dr. I. Pirozhenko
- University of Tasmania, Hobart
  Prof. Dr. P. Jarvis
- University of New South Wales, Sydney
  Prof. H. Grundling

12.8 Publications

Journals

M. Asorey, J. Muñoz-Castañeda
Quantum vacuum interaction between two sine-Gordon kinks.
J. Phys. A **45** (2012) 374012

M. Asorey, J. Muñoz-Castañeda
Boundary effects in quantum physics
Int. J. Geom. Meth. Mod. Phys. **9** (2012) 1260017

C.J. Fewster, R. Verch
On a recent construction of "vacuum-like" quantum field states in curved spacetime
Class. Quantum Grav. **29** (2012) 205017

C.J. Fewster, R. Verch
Dynamical locality and covariance: What makes a physical theory the same in all spacetimes?
Annales Henri Poincaré **13** (2012) 1613–1674

C.J. Fewster, R. Verch
Dynamical locality of the free scalar field
Annales Henri Poincaré **13** (2012) 1675–1709

Books

G. Rudolph, M. Schmidt
Differential Geometry and Mathematical Physics. Part I. Manifolds, Lie Groups and Hamiltonian Systems.
Springer Series in Theoretical and Mathematical Physics, 2013, 759 p. Available online since November 2012

In press

H. Grosse, G. Lechner, T. Ludwig, R. Verch
Wick rotation for quantum field theories on degenerate Moyal space(-time)
arXiv:1111.6856, in press with J. Math. Phys.

H. Grundling, G. Rudolph
QCD on an infinite lattice
Commun. Math. Phys. **318** (2013) 717–766

G. Lechner, J. Schlemmer, Y. Tanimoto
On the equivalence of two deformation schemes in quantum field theory
Lett. Math. Phys., available online, in press, arXiv:1209.2547

G. Lechner, C. Schützenhofer
Towards an operator-algebraic construction of integrable global gauge theories
Preprint, arXiv:1208.2366

Talks

G. Lechner
Locally Noncommutative Spacetimes and Quantum Field Theory (inv. T)
Conference Planckland - Quantum Geometry and Matter, SISSA, Trieste, February 13-18 2012

G. Lechner
Constructive algebraic quantum field theory at the example of integrable models (inv. T)
Conference Mathematical Aspects of Quantum Field Theory and Quantum Statistical Mechanics, DESY, Hamburg, July 30 - August 1, 2012

G. Lechner
Thermal Equilibrium States for QFTs on Moyal Minkowski Spacetime (T)
Congress ICMP 2012, Aalborg, August 6-11 2012

G. Lechner
KMS states of deformed quantum field theories (inv. T)
Workshop Algebraic Quantum Field Theory and Local Symmetries
Hausdorff Research Institute for Mathematics, Bonn, September 2012

J. Muñoz-Castañeda
Dirac delta configurations, boundary conditions and quantum fluctuations of scalar fields.
Mathematical Structures in Quantum Systems, Benasque Centre for science, July 2012

J. Muñoz-Castañeda
Quantum interaction between kinks.
Zaragoza University, February 2012

J. Muñoz-Castañeda
Quantum fluctuations and Casimir force in the background of two s-G kinks 1
Salamanca University, March 2012

J. Muñoz-Castañeda
Quantum fluctuations and Casimir force in the background of two s-G kinks 2
Salamanca University, July 2012.

G. Rudolph
On the geometry of quantization (2 lectures)
IMPRS, December 2012

R. Verch
Dirac Field on Lorentzian Non-Commutative Spacetime (T)
Workshop Planckland: Quantum Geometry and Matter, SISSA, Trieste, Feb 13-18, 2012

R. Verch
On a Recent Construction of "Vacuum-like" Quantum Field States in Curved Spacetime (T)
Workshop New Trends in Algebraic Quantum Field Theory, Centre for Mathematics and Theoretical Physics, Frascati, Sep 12-14, 2012

Doctorate

- Eric Morfa-Morales (Fakultät für Physik, Universität Wien, supervisors: G. Lechner and J. Yngvason)
  Deformations of Quantum Field Theories on Curved Spacetimes
  February 2012

Diploma

- Albert Huber (Fakultät für Physik, Universität Wien, supervisors: G. Lechner and J. Yngvason)
  Thermal Equilibrium States in Deformed Quantum Field Theory
  April 2012

Bachelor

- Tobias Diez
  Geometrische Quantisierung und semiklassische Näherung
  January, 2012
- Richard Busch
  Quantenmechanische Streuprozesse. Das Coulombpotential
  March, 2012
- Danny Krause
  Die irreduziblen Darstellungen der Poincaré-Gruppe und ihre Bedeutung für die Quantentheorie
  August, 2012

12.9 Guests

- Dr. Yoh Tanimoto (Universität Göttingen)
  April 30–May 3, 2012
- Dr. Jan Schlemmer (Universität Wien)
  April 30–May 3, 2012

- Michael Keyl (ISI Foundation Turin)
  May 29–June 1
- Prof. Dr. Jerzy Kijowski
  September 01–30, 2012

13

Statistical Physics

13.1 Introduction

The focus of research in the STP group is on low-dimensional and mesoscopic interacting systems. These systems are fascinating because on the one hand they allow to study fundamental questions of quantum statistical mechanics, and on the other hand they have a great potential for technological applications. The interplay of a reduced dimensionality with enhanced interaction effects, non-equilibrium physics, and possibly disorder allows the observation of many interesting phenomena, which pose a stimulating challenge for theoretical analysis. The mathematical language used for the description of these systems is quantum field theory, including techniques like functional integrals, renormalization group, instanton calculus, the Keldysh technique for non-equilibrium situations, and the replica method for disordered systems. These analytical tools are supplemented by the use of computer algebra (Mathematica) and numerical calculations (Matlab, Perl, C++). We try to combine the analysis of theoretically interesting problems with relevance to experiments on nanostructures.

Fractional quantum Hall (QH) systems display perhaps the richest and most beautiful physics of all condensed matter systems. They are a prime example for the idea that the whole is more than the sum of its parts, as low lying excitations of a fractional QH fluid carry only a fraction of the electron charge and are thus qualitatively different from the system constituents. Recently, interest in fractional QH physics has been reinvigorated by the prospect that quasiparticles (QPs) of the fractional QH state at filling fraction 5/2 may be non-abelian anyons, i.e. their braiding may not only gives rise to a multiplication of the wave function with a complex phase, but in addition corresponds to a unitary transformation of the highly degenerate ground state. Due to the topological nature of braiding, these unitary transformations are robust against local perturbations and guarantee a high degree of stability of the quantum weave of braids, lending it to the construction of topological quantum bits. Future research in this field will concentrate on both the analysis of qualitative properties of topologically ordered systems and the description of experimentally relevant consequences in nanostructured systems.

Similarly to the edge states of QH systems, in single channel nanowires interactions strongly modify the dynamics of electrons. In the presence of strong spin-orbit coupling and in proximity to a superconductor, nanowires can support a topologically ordered state suitable for the formation of topological quantum bits. In multimode nanowires,

a quantum phase transition between superconductor and diffusive metal can occur, which is tuned by an external magnetic field and is experimentally realized in niobium and molybdenum-germanium systems. Comparatively small changes in the external magnetic field can give rise to a large change in conductivity. Quantum mechanical fluctuations of the superconducting phase can restore part of the the density of states, which is reduced due to scattering of electrons off the superconducting order parameter.

B. Rosenow

13.2 Proposed Detection of the Topological Phase in Ring-Shaped Semiconductor-Superconductor Nanowires Using Coulomb Blockade Transport

B. Zocher[*†], M. Horsdal[*‡], B. Rosenow[*]

[*]Institut für Theoretische Physik, Universität Leipzig
[†]Max-Planck-Institute for Mathematics in the Sciences, Leipzig
[‡]Max-Planck-Institute for Solid State Research, Stuttgart

Topological phases are quantum phases which cannot be described by a local order parameter. Instead, the defining characteristic of topological phases is a pattern of long-range quantum entanglement which is called topological order. One property of topological order is the dependence of the ground-state degeneracy on the topology of the manifold on which the system is defined [1, 2]. Recently, there is much interest in topological phases due to their possible application in topological quantum computation. However, these phases are also of fundamental scientific interest for their ability to support exotic quasiparticle excitations with abelian and even nonabelian quantum statistics.

One particularly interesting class of topological phases are topological superconductors, which have been predicted to host Majorana bound states [1]. The $p_x + ip_y$ superconductor for spinless fermions is a prototype system for a topological superconductor. In particular, the grand canonical ground state of the $p_x + ip_y$ superconductor on the torus depends on boundary conditions for each of the two fundamental cycles [2]. Here, the ground state with only periodic boundary conditions is special and shows an odd parity, while the three ground states with at least one antiperiodic boundary condition are characterized by an even parity. In contrast, the ordinary s-wave superconductor on the torus possess a fourfold degenerate even parity ground state. Promising candidates for topological superconductors are semiconductor nanowires with strong Rashba spin-orbit coupling, such as InAs and InSb, in a magnetic field and proximity coupled to an s-wave superconductor [3].

In Ref. [4], we considered a ring shaped one-dimensional semiconductor-superconductor hybrid system in the limit where the gap Δ is much larger than the single-particle level spacing d, see Fig. 13.1. In the Coulomb blockade regime with a fixed particle number N, the degeneracy of grand-canonical ground states on the torus is reflected in the excitation spectrum, which can be observed in nonlinear transport. In a trivial SC, the lowest excitation above a ground state with even N breaks a Cooper pair and hence costs the

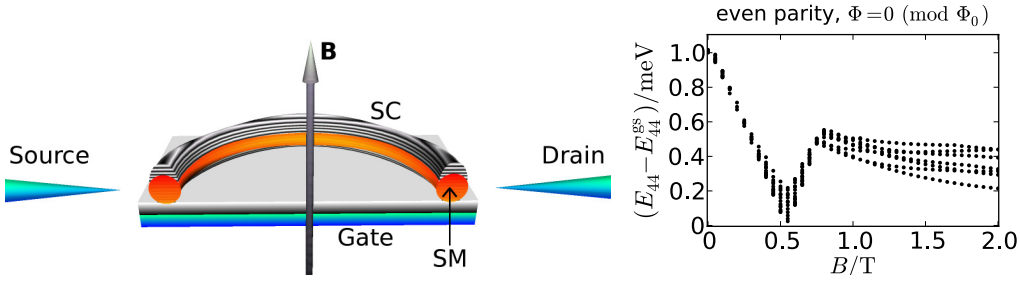

Figure 13.1: Left panel: Cross section of the experimental setup for a ring shaped semiconductor-superconductor hybrid system. The superconductor is sputtered on top of the semiconductor which itself is deposited on a gate electrode. Right panel: Magnetic field dependence of the excitation energies for even parity and mean particle number $N = 44$.

energy $\delta E \approx 2\Delta$. When changing the boundary condition by varying the flux through the ring, δE oscillates with a small amplitude d^2/Δ, i.e. is essentially flux independent. The ground state for odd N has an unpaired particle, and hence $\delta E \approx d^2/\Delta$ with oscillations of the same magnitude. For nontrivial superconductors however, ground states without an unpaired particle have even N for anti-periodic boundary condition, and odd N for periodic boundary condition. As a consequence, δE oscillates between d^2/Δ and 2Δ with a flux period of h/e, very different from the trivial case. In the right panel in Fig. 13.1 the phase transition between the normal phase (low magnetic field) and the nontrivial phase (high magnetic field) can be seen as the closing and reopening of the excitation gap.

[1] N. Read and D. Green, Phys. Rev. B **61**, 10267 (2000).
[2] M. Oshikawa, Y. B. Kim, K. Shtengel, C. Nayak, and S. Tewari, Ann. Phys. **322**, 1477 (2007).
[3] R. M. Lutchyn, J. D. Sau, and S. Das Sarma, Phys. Rev. Lett. **105**, 077001 (2010).
[4] B. Zocher, M. Horsdal, and B. Rosenow, Phys. Rev. Lett. **109**, 227001 (2013).

13.3 Influence of Topological Excitations on Shapiro Steps and Microwave Dynamical Conductance in Bilayer Exciton Condensates

T. Hyart, B. Rosenow

The quantum Hall state at total filling factor $\nu_T = 1$ in bilayer systems realizes an exciton condensate and exhibits a zero-bias tunneling anomaly, similar to the Josephson effect in the presence of fluctuations. In contrast to conventional Josephson junctions, no Fraunhofer diffraction pattern has been observed, due to disorder induced topological defects, so-called merons. We consider interlayer tunneling in the presence of microwave radiation, and predict Shapiro steps in the tunneling current-voltage characteristic despite the presence of merons. Moreover, the Josephson oscillations can also be observed as resonant features in the microwave dynamical conductance.

[1] T. Hyart and B. Rosenow, Phys. Rev. Lett. 110, 076806 (2013)

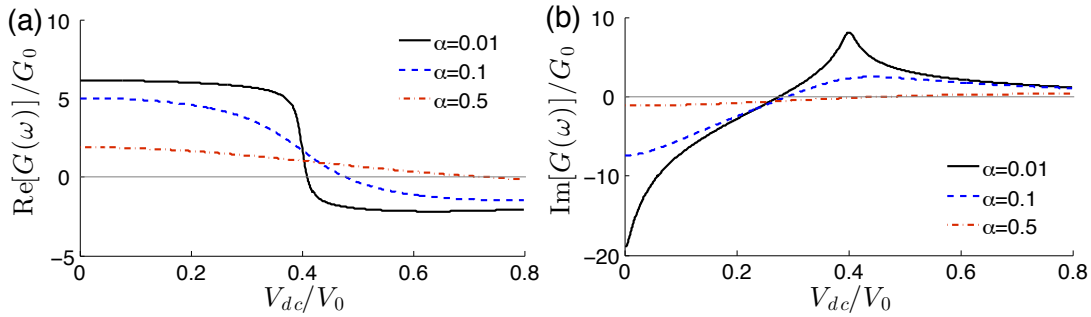

Figure 13.2: (a) Real and (b) imaginary parts of the small signal dynamical conductance for $\hbar\omega/eV_0 = 0.4$ and different dissipation strengths α. The conductance is given in units $G_0 = I_0/V_0$. Re$[G(\omega)] = 0$ and Im$[G(\omega)] = 0$ are marked with a thin gray line.

13.4 Splitting of roton minimum in the $\nu = 5/2$ Moore-Read state

A.R. Wright, B. Rosenow

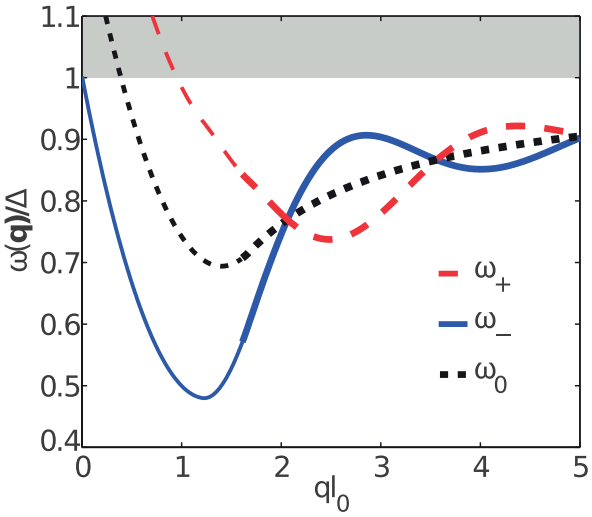

Figure 13.3: The expected roton dispersion. The thick lines constitute the dipole approximation, valid for q beyond the roton minimum, which occurs near $ql_0 \approx 1.4$. The usual single roton mode (shown with black dots) has split into two branches with distinct extrema, denoted ω_+ and ω_-, where $\omega_+ - \omega_- = 2E(2l_0^2 q)$. ω_- is the brighter primary branch, and ω_+ is the secondary split-off branch. In the the small q-regime, the dipole Hamiltonian is no longer valid and the roton minimum is taken to be parabolic with appropriate parameters used as outlined in the text. This regime is plotted with thin lines. $\Delta \approx 0.025e^2/\epsilon l_0$ is the $\nu = 5/2$ exciton gap. The grey shaded region denotes the two-roton continuum.

The quasiparticles and quasiholes in the Moore-Read state of the $\nu = 5/2$ fractional quantum Hall system have an internal Majorana degree of freedom. A qp-qh pair, therefore, has a fermionic degree of freedom which can be either empty or occupied, and leads to a splitting of the roton mode, which is a minimum in the charge density collective excitation spectrum. We demonstrated that the observation of this splitting by

means of finite wavelength optical spectroscopy could provide evidence for Majorana modes in the $\nu = 5/2$ fractional quantum Hall state.

[1] A. R. Wright and B. Rosenow, Phys. Rev. B **86**, 115329 (2012).

13.5 Zero temperature Dephasing and the Friedel Sum Rule

B. Rosenow *, Y. Gefen†

*Institut für Theoretische Physik, Universität Leipzig
†Department of Condensed Matter Physics, Weizmann Institute of Science

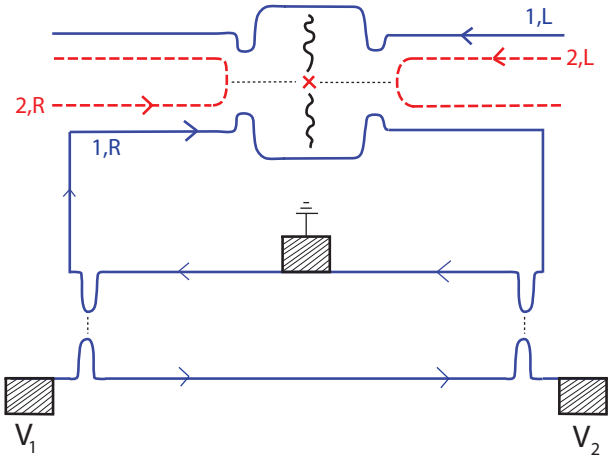

Figure 13.4: Mach-Zehnder interferometer with a quantum dot in its upper arm. The outer edge channel (full line, blue) is fully trasmitted through the dot, the inner edge channel (dashes line, red) has a weak tunnel coupling to the localized state in the dot. If the charge on the localized state is increased by one, the number of electrons on the outer edge is accordingly reduced, giving rise to a phase shift δ . If screening by the two outer edge channels is symmetric, then $\delta = \pi$ and the interference visibility is reduced to zero when the localized level is half filled.

Detecting the passage of an interfering particle through one of the interferometer's arms, known as "which path" measurement, gives rise to interference visibility degradation (dephasing). Here we consider a detector at *equilibrium*. At finite temperature dephasing is caused by thermal fluctuations of the detector. More interestingly, in the zero temperature limit, equilibrium quantum fluctuations of the detector give rise to dephasing of the out-of-equilibrium interferometer. This dephasing is a manifestation of an orthogonality catastrophe which differs qualitatively from Anderson's. Its magnitude is directly related to the Friedel sum rule.

We condsider an electronic Mach-Zehnder interferometer, one arm of which is coupled electrostatically to a detector. The interferometer is defined by the outer edge channel of a $\nu = 2$ quantum Hall setup while the detector consists of localized electronic state, which is tunnel coupled to the inner edge. Our main findings are (i) Thermal fluctuations of the occupancy of the localized state lead to dephasing through statistical

averaging over shifted interference patterns [1]; (ii) In the limit of zero temperature the passage of an electron through the upper arm of the MZI modifies the many-body state of the detector. In similitude to the Anderson orthogonality catastrophy [2, 3], the scalar product of the states before and after this modification has taken place, S_{fi}, plays the role of the visibility suppression factor. However, by contrast to the Anderson orthogonality catastrophy, S_{fi} does NOT scale with the detector's size. Nevertheless, by tuning the gate voltage on the localized impurity, complete dephasing can be achieved. (iii) The degree of dephasing depends on both the magnitude of the system-detector coupling, and the strength of quantum fluctuations in the detector. The former can be expressed through the Friedel sum rule. By changing an external gate voltage, the occupancy of the localized state and the amount of equilibrium charge fluctuations can be tuned. (iv) We briefly discuss the implementation of the Friedel sum rule in the presence of tunnel and/or electrostatic coupling to the localized state whose occupation is varied.

We stress that our dephasing protocol [4] involves energy transfer from the system (MZI) to the detector. The results (ii) and (iii) provide a conceptual and technically workable framework for dealing with tunable zero temperature dephasing.

[1] E. Weisz, H.K. Choi, M. Heiblum, Y. Gefen, V. Umansky, and D. Mahalu, unpublished.
[2] P.W. Anderson, Phys. Rev. Lett. **18**, 1049 (1967).
[3] I. L. Aleiner, N.S. Wingreen, and Y. Meir, Phys. Rev. Lett. 79, 3740 (1997).
[4] B. Rosenow and Y. Gefen, Phys. Rev. Lett. **108**, 256805 (2012).

13.6 Incoherent scatterer in a Luttinger liquid: a new paradigmatic limit

A. Altland [*], Y. Gefen [†], B. Rosenow[‡]

[*]Institut für Theoretische Physik, Universität zu Köln
[†]Department of Condensed Matter Physics, Weizmann Institute of Science
[‡]Institut für Theoretische Physik, Universität Leipzig

We address the problem of a Luttinger liquid with a scatterer that allows for both coherent and incoherent scattering channels. The asymptotic behavior at zero temperature is governed by a new stable fixed point: a Goldstone mode dominates the low energy dynamics, leading to a universal behavior. This limit is marked by equal probabilities for forward and backward scattering. Notwithstanding this non-trivial scattering pattern, we find that the shot noise as well as zero cross-current correlations vanish [1]. We thus present a paradigmatic picture of an impurity in the Luttinger model, alternative to the Kane-Fisher picture.

[1] A. Altland, Y. Gefen, B. Rosenow, Phys. Rev. Lett. **108**, 136401 (2012).

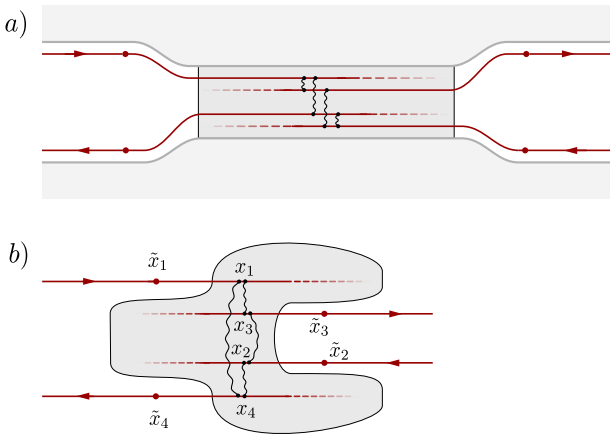

Figure 13.5: Quantum wire comprising two incoming ($l = 1, 2$) and two outgoing ($l = 3, 4$) chiral modes connecting to an extended scattering region. Wiggly lines denote coherent scattering channels, dark shading represents a region of capacitive charging (the quantum dot). (a) Cartoon of possible real space structure in FQHE geometry subject to gating, (b) alternative view adjusted to our modeling with its tunneling 'hot-spots' x_i and lead observation points $\tilde{x}_l$.

13.7 Telegraph noise and the Fabry-Perot quantum Hall interferometer

B. Rosenow*, S.H. Simon †

*Institut für Theoretische Physik, Universität Leipzig
†Institut für Rudolf Peierls Centre for Theoretical Physics, Oxford University

We consider signatures of abelian and nonabelian quasiparticle statistics in quantum Hall Fabry-Perot interferometers. When quasiparticles enter and exit the interference cell, for instance due to glassy motion in the dopant layer, the anyonic phase can be observed in phase jumps [1]. In the case of the nonabelian $\nu = 5/2$ state, if the interferometer is small, we argue that free Majoranas in the interference cell are either strongly coupled to one another or are strongly coupled to the edge. We analyze the expected phase jumps and in particular suggest that changes in the fermionic parity of the ground state should gives rise to characteristic jumps of π in the interference phase.

[1] B. Rosenow and S. H. Simon, Phys. Rev. B **85**, 201302(R) (2012).

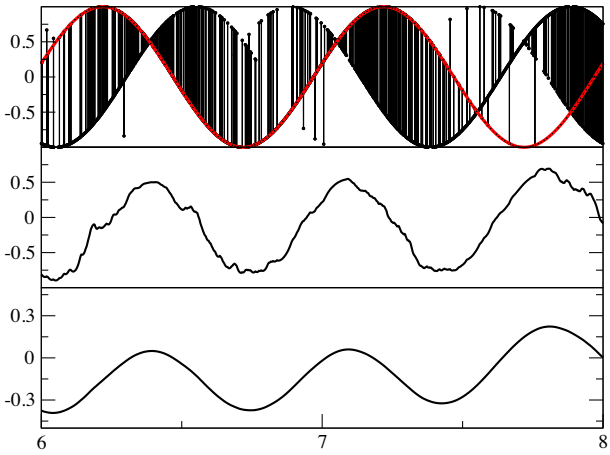

Figure 13.6: A simulation of random telegraph noise during a scan of a $\nu = 1/3$ (or 7/3) Fabry-Perot interferometer. Vertical axis is $\cos(2\pi t + 2\pi N_L/3)$ where $t = e^*\beta V_G$ is the horizontal axis which we can think of as time assume constant voltage sweep rate. Here $N_L = \lfloor \eta t + \xi r \rfloor$ with $\lfloor x \rfloor$ denoting the greatest integer smaller or equal to x, and r being a gaussian random variable with unit variance. The analytic results are then passed through a simulated lock-in amplifier with an averaging time τ. Here $\eta = 1.25$ means roughly 1.25 quasiparticles is added to the dot per cycle and $\xi = .3$ is the amplitude of the noise in units of quasiparticle number. The correlation "time" of the noise constant of the gaussian noise is $\tau_c = .001$ in the above units (Top) observed conductance with an averaging time shorter than the noise correlation time. Red curve is a pure sine wave for reference (Middle) Observed conductance using an averaging time $\tau = .0066$ larger than τ_c. (Bottom) Observed conductance using a very long averaging time $\tau = .066$. Note that the period of oscillation is distorted towards smaller values.

13.8 Funding

Untersuchungen zum topologischen Quanten-Computing
B. Rosenow together with J. Smet (MPI FKF) and W. Dietsche (MPI FKF)
BMBF 01BM0900

13.9 Organizational Duties

B. Rosenow

- Member of the Studienkommission of the Faculty of Physics and Earth Science
- Referee for Science, Phys. Rev. Lett., Phys. Rev. B, Europhys. Lett., Adv. Cond. Matter, JSTAT, Physica A, NSF, Studienstiftung des Deutschen Volkes

13.10 External Cooperations

Academic

- MPI für Festkörperforschung Stuttgart
  Prof. W. Dietsche, Dr. J. Smet, Prof. K. von Klitzing

- Harvard University
  Prof. B.I. Halperin, Prof. C.M. Marcus, Prof. S. Sachdev
- Weizmann Institute for Science
  Prof. Y. Gefen, Prof. A. Stern, Prof. Y. Oreg
- Oxford University
  Prof. S. Simon
- California Institute of Technology
  Prof. G. Refael
- Universität zu Köln
  Prof. A. Altland
- Missouri University of Science and Technology
  Prof. T. Vojta
- Universidade de Sao Paulo
  Prof. J.A. Hoyos
- UBC Vancouver
  Dr. A. Del Maestro
- The University of Maryland College Park
  Dr. S. Takei
- FU Berlin
  Dr. D. Meidan

13.11 Publications

Journals

B. Zocher, M. Horsdal, and B. Rosenow, *Proposed detection of the topological phase in ring-shaped semiconductor-superconductor nanowires using Coulomb blockade transport*, Phys. Rev. Lett. **109**, 227001 (2012).

A. R. Wright and B. Rosenow, *Splitting of roton minimum in the $\nu = 5/2$ Moore-Read state*, Phys. Rev. B **86**, 115329 (2012).

B. Rosenow and Y. Gefen, *Zero temperature Dephasing and the Friedel Sum Rule*, Phys. Rev. Lett. **108**, 256805 (2012).

B. Rosenow and S. H. Simon, *Telegraph noise and the Fabry-Perot quantum Hall interferometer*, Phys. Rev. B **85**, 201302(R) (2012).

T. Hyart, T. Wright, G. Khaliullin und B. Rosenow, *Competition between d-wave and topological p-wave superconductivity in the doped Kitaev-Heisenberg model*, Phys. Rev. B **85**, 140510(R) (2012).

A. Altland, Y. Gefen, and B. Rosenow, *Incoherent scatterer in a Luttinger liquid: a new paradigmatic limit*, Rev. Lett. **108**, 136401 (2012).

J. Nuebler, B. Friess, V. Umansky, B. Rosenow, M. Heiblum, K. v. Klitzing, and J. Smet, *A Quantized $\nu = 5/2$ State in a Two-Subband Quantum Hall System*, Phys. Rev. Lett. **108**, 046804 (2012).

in press

T. Hyart and B. Rosenow, *Influence of topological excitations on Shapiro steps and microwave dynamical conductance in bilayer exciton condensates*, Phys. Rev. Lett. **110**, 076806 (2013).

Talks

B. Zocher, *Coulomb blockade signatures of the topological phase transition in semiconductor-superconductor nanowires*, DPG Spring Meeting of the Condensed Matter Section meeting, Berlin, March 2012.

M. Horsdal, *Charge fractionalization on quantum Hall edges*, DPG Spring Meeting of the Condensed Matter Section, Berlin, March 2012.

T. Hyart, *Competition between d-wave and topological p-wave superconductivity in the doped Kitaev-Heisenberg model*, DPG Spring Meeting of the Condensed Matter Section, Berlin, March 2012.

T. Hyart, *Competition between d-wave and topological p-wave superconductivity in the doped Kitaev-Heisenberg model*, Itinerant Spin-Orbital Systems: From Magnetic Frustration to Novel Superconductivity, Dresden, May 2012.

T. Hyart, *Competition between d-wave and topological p-wave superconductivity in the doped Kitaev-Heisenberg model*, Topological States of Matter, Nordita, Stockholm, August 2012.

M. Horsdal, *Signatures of topological order in Coulomb blockaded transport through semiconductor-superconductor nanowire rings*, Nordita program, Stockholm, August 2012.

B. Zocher, *Crossed Andreev reflection and noise through Majorana bound states*, Ringberg meeting of the von Klitzing department, September 2012.

A. Janot, *Depletion of Superfluidity in a disordered non-equilibrium Polariton Condensate*, BuildMoNa Workshop, Burgstädt, September 2012.

B. Zocher, *Crossed Andreev reflection and noise through Majorana bound states*, Group seminar, TU Dresden, October 2012.

B. Rosenow, Condensed Matter Theory Seminar, IFW Dresden, April 2012.

B. Rosenow, Condensed Matter Seminar, University of Louvain, May 2012.

B. Rosenow Theoretical Physics Colloqium, Cologne University, December 2012.

B. Rosenow Theoretical Condensed Matter Seminar, University of Augsburg, January 2012.

B. Rosenow Theoretical Condensed Matter Seminar, Karlsruhe Institute of Technology, January 2012.

B. Rosenow Condensed Matter Seminar, Niels Bohr Institute, Copenhagen, September 2012.

B. Rosenow Workshop The Science of Nanostructures: New Frontiers in the Physics of Quantum Dots, Chernogolovka, September 2012.

B. Rosenow Workshop Quantum Transport in Correlated Systems, KIAS Seoul, August 2012.

B. Rosenow Conference Quantum Matter from the Nano- to the Macroscale, Max-Planck Institute for Complex Systems Dresden, July 2012.

Posters

A. Janot, *Disorder effects in a non-equilibrium polariton condensate*, BuildMoNa Symposium, Leipzig, March 2012.

M. Treffkorn, *Interference in single quantum Hall point contacts*, DPG Spring Meeting of the Condensed Matter Section, Berlin, March 2012.

L. Kimme, *Topological superconductivity in the Kitaev-Heisenberg model and the effect of impurities*, DPG Spring Meeting of the Condensed Matter Section, Berlin, March 2012.

B. Zocher, *Proposed detection of a topological phase transition in semiconductor-superconductor nanowires using Coulomb blockade transport*, Workshop, Max-Planck Institute for Physics of Complex Systems, Dresden, June 2012.

A. Janot, *Disorder effects in polariton condensates in a ZnO-based microcavity*, International Conference on the Physics of Semiconductors, Zürich, Switzerland, August 2012.

A. Janot, *Depletion of Superfluidity in a disordered non-equilibrium Quantum Condensate*, Symposium: Quantum Coherence in Nanostructures, Leipzig, October 2012.

B. Zocher, *Proposed detection of a topological phase transition in semiconductor-superconductor nanowires using Coulomb blockade transport*, Symposium Quantum Coherence in Nanostructures, Leipzig, October 2012.

13.12 Graduations

Master

- Lukas Kimme
  The effect of impurities in the Kitaev-Heisenberg model
  September 27

Bachelor

- Alexander Uhlig
  Empirical analysis of price impact based on Island ECN order book data
  November 2

13.13 Guests

- Dr. Maria Hermanns
  Princeton University
  January 4-6
- Prof. Giniyat Khaliullin
  MPI FKF Stuttgart
  January 26 and November 15-16
- Prof. Werner Dietsche
  MPI FKF Stuttgart
  February 2-3
- Benedikt Frieß
  MPI FKF Stuttgart
  February 2-3
- Prof. Madeleine Msall
  Bowdoin College, Brunswick
  February 2-3
- Johannes Nuebler
  MPI FKF Stuttgart
  February 2-3
- Ding Zhang
  MPI FKF Stuttgart
  February 2-3
- Prof. Adrian Del Maestro
  University of Vermont
  March 3-11 and July 10-18
- Prof. Paul Eastham
  Trinity College Dublin
  May 7-9 and October 2-5
- Prof. Kirill Shtengel
  University of California Riverside
  June 14
- Prof. Jochen Guck
  TU Dresden
  July 17
- Prof. Woowon Kang
  University of Chicago
  August 16-18

- Dr. Tony Wright
  University of Queensland
  August 26 to September 7
- Prof. Steve Simon
  University of Oxford
  October 15-17
- Dr. Laila Hormozi
  NUI Maynooth, Ireland
  October 24-26
- Dr. Timo Hyart
  Leiden University
  November 12-17
- Prof. Arne Brataas
  Norwegian University of Science and Technology
  November 19-22

14

Theory of Condensed Matter

14.1 Introduction

Major research topics of our groups include nonequilibrium phenomena and pattern formation in systems of various nature, e.g. in soft condensed matter and in biological systems. Modern analytic methods of statistical physics and computer simulations complement and stimulate each other. Cooperations with mathematicians, theoretical and experimental physicists, biologists and medical researchers in Germany, Europe and around the world are well established. Specifically we are interested in the following problems.

Stochastics and pattern formation (Behn). Noise induced phenomena like nonequilibrium phase transitions are studied with analytical and cumputational methods in stochastically driven nonlinear systems with many degrees of freedom. Methods of nonlinear dynamics and statistical physics are used to formulate and investigate mathematical models of the adaptive immune system. We describe the random evolution of idiotypic networks of the B-lymphocyte subsystem, and investigate the regulation of balance in the T- Lymphocyte subsystem in allergy and during hyposensitization (cooperation with G. Metzner, Clinical Immunology), and the lineage committment and plasticity of $CD4^+$ T cells.

Non-equilibrium dynamics in soft-condensed-matter systems (Kroy). Our work is devoted to the theoretical analysis of various soft condensed matter systems: from desert dunes spontaneously developing as a generic consequence of aeolian sand transport, through non-equilibrium dynamics of colloids, proteins and polymers, the viscoelastic and inelastic mechanics of the cytoskeleton, to the tension propagation in single DNA molecules under strong external fields. (Related experimental work is currently in progress at EXP1: MON, MOP, PWM.) Much of what we do can be summarized as Soft Mesoscopics. A common feature is the presence of strong fluctuations and stochastic dynamics on the microscale. The emergence of the mesoscopic structure and transport is to be understood. The applied methods comprise a broad statistical mechanics toolbox including stochastic (integro-)differential equations, liquid-state theories, effective hydrodynamic equations, various systematic coarse-graining techniques, and massively parallel numerical simulations on GPUs.

Ulrich Behn, Klaus Kroy

14.2 Stochastic Phenomena in Systems with Many Degrees of Freedom

U. Behn, M. Höll, R. Kürsten

Arrays of coupled nonlinear dynamical systems subject to multiplicative or additive noise show close analogies to phase transitions in equilibrium [1]. Concepts such as ergodicity breaking, order parameter, critical behaviour, critical exponents etc. developed to describe equilibrium phase transitions can be transfered to noise induced nonequilibrium phase transitions.

In the limit of strong coupling between the constituents there is a clear separation of time scales: The fast degrees of freedom of the relative coordinates r_i are enslaved by the slow center of mass coordinate R which exhibits a critical behaviour [2]. For large, but finite coupling we developed self-consistent mean field theories to determine the probability distributions of both center of mass and relative coordinates, where the mean value $\langle R \rangle$ and the variance $\langle r_i^2 \rangle$ serve as order parameters. Applications include systems with additive [3] and multiplicative noise [4] where the inverse coupling strength and the inverse system size are considered as small parameters.

For an infinite array with additive noise we proved the existence of a well-behaved critical manifold in the parameter space [5]. The critical parameter is bounded by values which are asymptotically reached in the limits of strong and weak noise, respectively. In these limits the mechanism of symmetry breaking is qualitatively different, see Fig. 14.1.

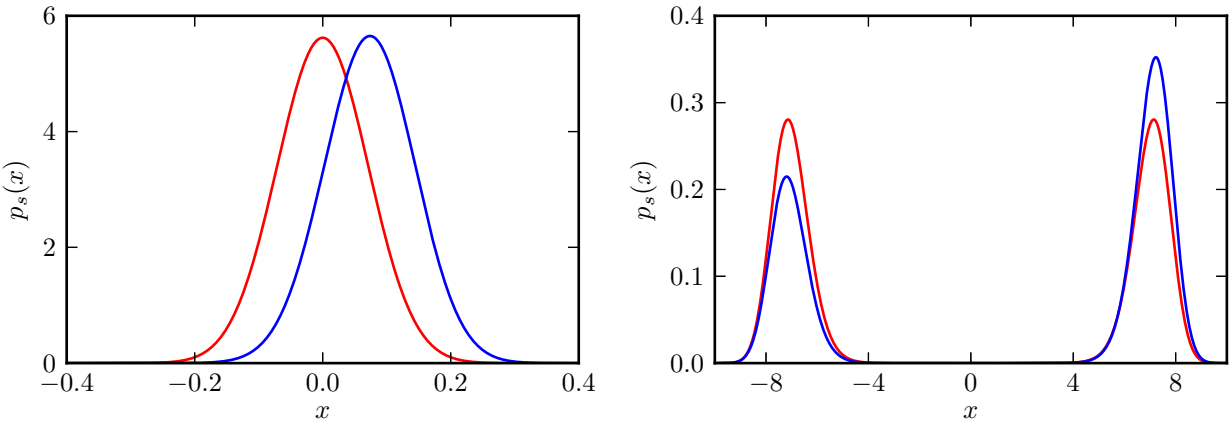

Figure 14.1: Mechanism of symmetry breaking for weak noise (left) and for strong noise (right). Stationary probability distribution $p_s(x)$ at the critical point (red) and just above (blue). For weak noise ($\sigma = 0.1$) the distribution is a Gaussian centered around zero at $a = a_c = 0.0149$ and rigidly shifted to the right for $a = 0.02$. For strong noise ($\sigma = 10$) the distribution is bimodal with sharp peaks located symmetrically with respect to zero, with equal weights for $a = a_c = 52.04$ and with different weights for $a = 53$. Coupling strength $D = 1$. From [5]

[1] F. Sagués, J. García-Ojalvo, J.M. Sancho: Rev. Mod. Phys. **79**, 829 (2007)
[2] F. Senf et al.: New J. Phys. **11**, 063010 (2009)
[3] R. Kürsten: Masterarbeit, Universität Leipzig, 2012

[4] M. Höll: Diplomarbeit, Universität Leipzig, 2012
[5] R. Kürsten, S. Gütter, U. Behn: *Critical manifold of globally coupled overdamped anharmonic oscillators driven by additive Gaussian white noise*, arXiv:1305.3116 (2013), 14 pp.

14.3 Randomly Evolving Idiotypic Networks

U. Behn, H. Schmidtchen, H. Sachsenweger, R. Schulz

The paradigm of idiotypic networks developed few decades ago by Jerne [1] finds today a renewed interest mainly from the side of system biology and from clinical research. A review with focus on modeling is given in [2], biological concepts and clinical applications are discussed in [3]. B-cells express receptors (antibodies) of a given idiotype. Crosslinking these receptors by complementary structures (antigen or antibodies) stimulates the lymphocyte to proliferate; unstimulated B-cells die. Thus a macroscopically large, though finite, functional network of lymphocytes, the idiotypic network emerges. The dynamics is driven by the influx of new idiotypes randomly produced in the bone marrow and by the population dynamics of the lymphocytes themself. In our minimalistic model [4] idiotypes are represented by bitstrings. The model network evolves towards a highly organized architecture where groups of nodes which share statistical characteristics can be identified. We can analytically compute size and connectivity of these groups [5] and calculate in a modular mean field theory mean occupation, and mean life time of the nodes [6].

The idiotypic network is thought to play an essential role in controling self antibodies which recognize self antigen. We therefore investigated in simulations the case that one [7] or several nodes of the network, playing the role of self, are permanently occupied. We observe that the group structure of the architecture is very similar to the case without self antigen, see Fig. 14.2, but organized such that the neighbors of the self are only weakly occupied, thus providing self-tolerance [9]. We also treated this situation in mean field theory in good agreement with data from simulation (Schulz).

Automatization of the real time pattern identification and optimizing the code allowed systematic simulation of networks with about 2^{20} nodes [8]. The findings can be explained by generalizing the pattern module concept and a corresponding mean field theory (Schulz).

[1] N.K. Jerne: Ann. Inst. Pasteur Immunol. **125C**, 373 (1974)
[2] U. Behn: Immunol. Rev. **216** 142 (2007)
[3] U. Behn: *Idiotype Network*, in: Encyclopedia of Life Sciences, John Wiley & Sons, Ltd, Chichester, doi:10.1002/9780470015902.a0000954.pub2 (2011)
[4] M. Brede, U. Behn: Phys. Rev. E **67**, 031920 (2003)
[5] H. Schmidtchen, M. Thüne, U. Behn: Phys. Rev. E **86**, 011930 (2012), 18 pp
[6] H. Schmidtchen, U. Behn: Phys. Rev. E **86**, 011931 (2012), 13 pp
[7] B. Werner: Diplomarbeit, Universität Leipzig, 2010
[8] H. Sachsenweger: Master thesis, Universität Leipzig, 2012
[9] R. Schulz, B. Werner, U. Behn: *Architecture of the idiotypic network in the presence of self antigen*, in preparation

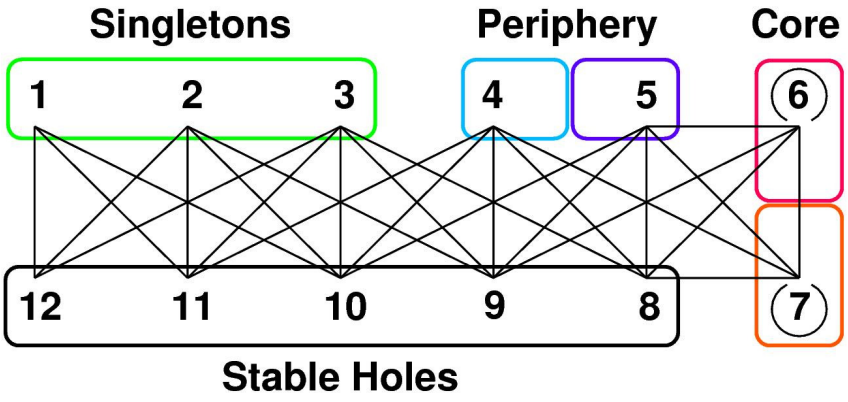

Figure 14.2: Architecture of the idiotypic network for the model with bitstrings of length 12. There are 12 groups of nodes with similar statistical properties which include *singletons* surrounded only by *holes* (unoccupied nodes), weakly occupied *core* groups, and higher occupied *periphery* groups. The lines indicate the possible links between nodes of these groups. Figure from [5]. If nodes are permanently occupied, playing the role of self, the networks evolves such that these nodes belong to the peripheral groups which have only links to the weakly occupied (or empty) core and hole groups, thus providing self-tolerance [9].

14.4 T Cell Regulation, Differentiation, and Plasticity

U. Behn, R. Pfaller, G. Metzner*

*Institute of Clinical Immunology, University Leipzig

T helper cells play a significant role in immune responses to allergenic substances. There are several subtypes which differ in function according to their cytokine profiles. Immunologists distinguish four major lineages: Th1, Th2, Th17 and regulatory T cells (Treg). Among these, mainly specific Th2cells are responsible for allergic reactions since they activate the production of IgE antibodies which provoke the well-known allergic symptoms. Allergen-specific immunotherapy consists of repeated injections of allergens aiming to induce a state of tolerance in the allergic individual. Specific immunotherapy has been carried out for more than one century based entirely on empirical grounds.

We developed a mathematical model describing the nonlinear dynamics of Tregs, naive T helper cells, Th1 and Th2 subsets, and their major cytokines [1]. Administration of allergen according to empirical protocols is targeting the model to a tolerant state. The complexity of the model is reduced by investigating a stroboscobic map describing the maintenance phase of the therapy. One of the stable fixed points of this map describes the state after a successful therapy.

There are other (experimental) systems with a skewed T-cell balance where the novel Th-subtype Th17 is suspected to play a decisive role. They include allergic asthma, Crohn's disease and ulcerative colitis, rheumatoid arthritis, and many others. Th17 cells have a much higher plasticity compared to Th1 and Th2 cells.

To describe the lineage committment and the plasticity of $CD4^+$ T cells we developed a minimalistic model [3]of the network of cytokines and transcription factors [2] based on Boolean cellular automata. The Boolean network has attractors which de-

scribe Th1, Th2, Treg, and Th17 phenotypes and hybrids such as Th1/Th17, Th2/Th17, and Treg/Th17 and reproduces, for example, the high plasticity of Th17 cells. There is ongoing research to further investigate the properties of the model and to develop a multi-scale description of T-cell regulation.

[1] F. Groß, G. Metzner, U. Behn: J. Theor. Biol. **269**, 70-78 (2011)
[2] J. Zhu, W.E. Paul: Immunol. Rev. **238**, 247-262 (2010)
[3] D. Kröber: Masterarbeit, Universität Leipzig, 2011

14.5 Inelastic mechanics of biopolymer networks and cells

L. Wolff, P. Fernandez*, K. Kroy

*Department of Physics, TU München, Garching, Germany

The mechanical state of biological cells is governed by the *cytoskeleton*, a complex biopolymer network. Intriguingly, this mechanical state does not only determine the response of the cell to mechanical agitation, but also influences inherently biological processes, from cell spreading and crawling to stem cell differentiation.

To shed light on the physical mechanisms governing cell mechanics, we study the physics of biopolymer networks. We use shear rheometry on reconstituted actin/HMM networks to experimentally demonstrate that transiently cross-linked actin networks share many unintuitive mechanical phenomena with cells, comprising such apparently contradictory effects as stress stiffening and softening, fluidization, and shake down. We resolve the apparent stiffening-softening paradox using the inelastic glassy wormlike chain model, a phenomenological microscopic model for transiently cross-linked biopolymer networks.

We theoretically identify two distinct underlying physical mechanisms, (i) the stiffening attributable to the stretching response of single polymers and (ii) the softening caused by the transient breaking of weak bonds. The complex interaction of these two basic mechanisms generates a multitude of response patterns (qualitatively summarized as a "constitutive diagram" in figure 14.3). In particular, we can trace back the apparent softening-stiffening paradox to a time scale separation of slow bond breaking and fast single-polymer stiffening. We also derive a set of analytical constitutive material equations that demonstrate the oportunities and limits of the analogy between cells and plastically deforming materials. Finally, we render the model more realistic by showing how biologically relevant feedback mechanisms, such as actively generated stresses or catch bonds, can be incorporated.

[1] L. Wolff, P. Fernandez, K. Kroy: PLoS ONE **7**, e40063 (2012), doi:10.1371/journal.pone.0040063

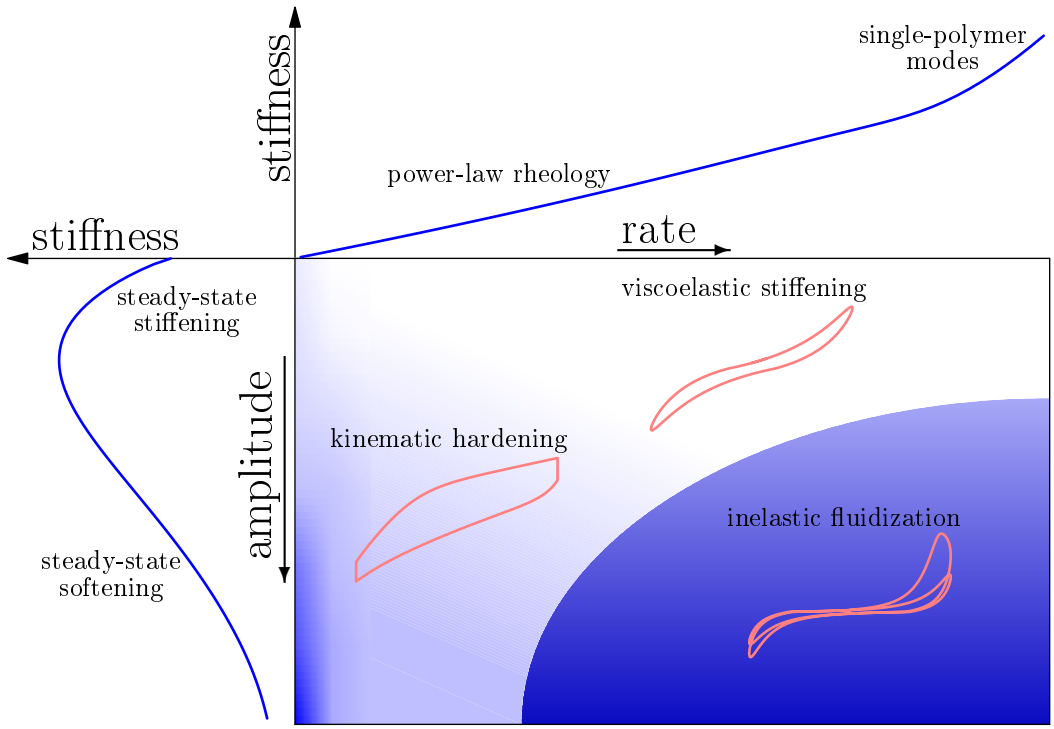

Figure 14.3: Constitutive diagram for the inelastic glassy wormlike chain. The diagram gives a qualitative graphical summary of the mechanical response predicted by the model as a function of the amplitude and characteristic rate of an imposed deformation pulse. At low amplitudes, in the linear regime, it exhibits power-law rheology (upper panel, log-log scale). At low rates, in the quasistatic regime, it exhibits stiffening at low amplitudes, where entropic stiffening of the polymer backbone dominates, and softening at high amplitudes, where the stiffening is eventually overruled by the exponential bond softening (left panel, linear scale). At high rates and high amplitudes, a steep initial stiffening with subsequent fluidization and slow recovery governs the response (central panel). The schematic stress-strain curves for oscillatory driving exemplify the salient features of the nonlinear response in the various parameter regions. [1]

14.6 Rotational hot Brownian motion

D. Rings, D. Chakraborty, S. Auschra, G. Falasco, K. Kroy

The theory of hot Brownian motion describes the Brownian motion of nanoscopic colloidal particles that have an elevated temperature compared to their solvent [1]. While the theory was first developed for the translational degrees of freedom, we recently complemented it with an effective Markov theory for the rotational Brownian motion of hot nanobeads and nanorods [2]. We have derived compact analytical expressions for the effective temperature and friction from the fluctuating hydrodynamic equations of motion. They were verified by comparison with recent measurements [3] and with parallel molecular dynamics simulations over a wide temperature range. This provides unique insights into the physics of hot Brownian motion and an excellent starting point for further experimental tests and applications involving laser-heated nanobeads,

nanorods and Janus particles. The video abstract [4] accompanying our publication [3] was a joint project with the "Zentrum für Medien und Kommunikation" and was promoted to the quarterly top ten list of submitted video abstracts.

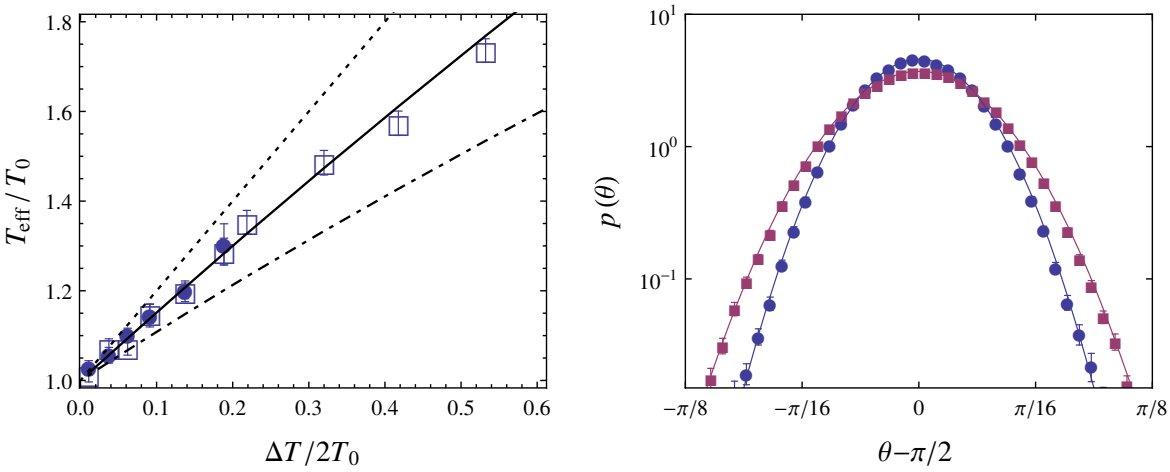

Figure 14.4: Left: Effective temperature of rotational hot Brownian motion. The simulation results for $T^{\theta}_{\rm HBM}$ (●) were deduced from the numerically measured $\zeta^{\theta}_{\rm HBM}$ and $D^{\theta}_{\rm HBM}$ using the generalized Einstein relation $D^{\theta}_{\rm HBM} = k_{\rm B}T^{\theta}_{\rm HBM}/\zeta^{\theta}_{\rm HBM}$. An alternative estimation of $T^{\theta}_{\rm HBM}$ (□) was obtained from the Boltzmann distribution of the inclination angle θ in a harmonic angular confinement (right panel). The theoretical prediction (solid line) was evaluated within the idealized theory for an incompressible fluid using the radial viscosity and temperature profiles $\eta(r)$ and $T(r)$ determined in the MD simulation. For comparison, the effective temperature $T^{x}_{\rm HBM}$ for the translational degrees of freedom (dot-dashed line) and the solvent temperature at the particle surface (dotted line) are shown. **Right:** The measured distribution of the inclination angle θ in a harmonic angular confinement potential for nanoparticle temperatures $T_{\rm p} = 0.8\,\epsilon/k_{\rm B}$ (●), $1.25\,\epsilon/k_{\rm B}$ (■) and the corresponding distribution $p(\theta) \sim e^{-\beta V(\theta)}$ with $\beta^{-1} = k_{\rm B}T^{\theta}_{\rm HBM}$ depicted by the solid lines. (ϵ sets the Lennrad-Jones energy scale). The plots are taken from [2].

[1] D. Rings et al.: Phys. Rev. Lett. **105**, 090604 (2010), doi:10.1103/PhysRevLett.105.090604
[2] D. Rings et al.: New J. P. **14**, 053012 (2012), doi:10.1088/1367-2630/14/5/053012
[3] P. V. Ruijgrok et al.: Phys. Rev. Lett. **107**(3), 037401 (2011), doi:10.1103/PhysRevLett.107.037401
[4] http://iopscience.iop.org/1367-2630/14/5/053012/video/abstract

14.7 Melting of pectin gels

A. Kramer, R.R.R. Vincent*, B.W. Mansel†, K. Kroy, M.A.K. Williams†

*Institute for Bioengineering of Catalonia, University of Barcelona, Spain
†Institute of Fundamental Sciences, Massey University, New Zealand

Pectin gels are the major scaffolding structures responsible for the mechanical stability of plant cells. We have analyzed their slow dynamics and linear and nonlinear viscoelasticity as a function of temperature, using various (micro-)rheological techniques

and theory [1]. The nonlinear mechanical response is found to be much more sensitive to temperature changes than the linear response, a property that is also observed in F-actin networks [2]. These effects can be accounted for by the glassy wormlike chain (GWLC) model of self-assembled semiflexible filaments with some additional assumptions.

Whereas the temperature effects observed in the linear response can be explained by assuming that the solvent viscosity decreases with temperature according to the Vogel-Fulcher equation, for nonlinear measurements structural properties of the network become more important. The pronounced temperature effects in the nonlinear differential shear modulus in Figure 14.5 are dominated by the bond length, which we assume to increase linearly with temperature.

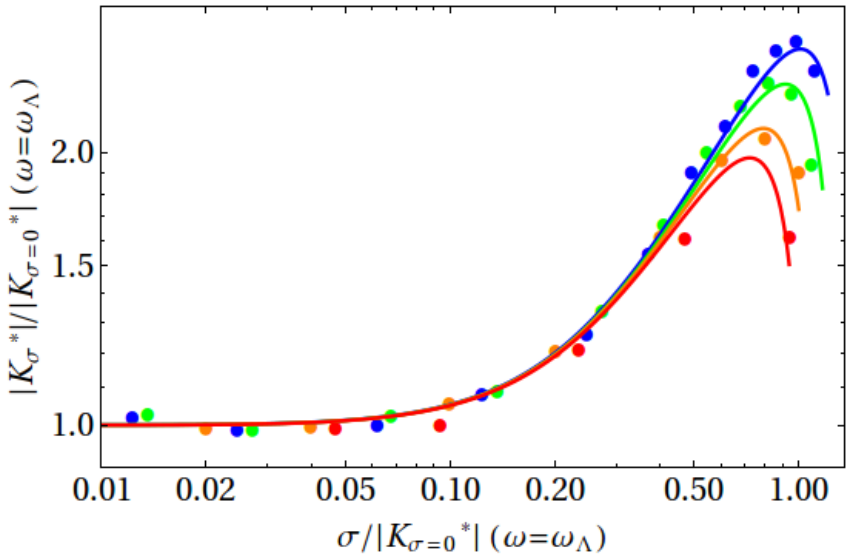

Figure 14.5: Scaled normalized differential modulus plotted against the scaled prestress for a 1 % w/w pectin solution at different temperatures T[°C] = 10, 20, 30, 40 (top to bottom). The lines are fits with the GWLC and additional assumptions described in the text.[1]

[1] R. R. R. Vincent, et al.: New J. Phys. **15**, 1035002 (2013), doi:10.1088/1367-2630/15/3/035002
[2] C. Semmrich et al.: PNAS **51**, 20199 (2007), doi:10.1073/pnas.0705513104

14.8 Wind driven sand transport. A two-species continuum model of aeolian sand transport

M. Lämmel, D. Rings, A. Meiwald, K. Kroy,

The emergence of macroscopic structures and patterns from initially almost homogeneous systems by a microscopic mechanism is a fascinating and frequently addressed phenomenon in physics—such as in the formation of sand ripples and dunes by aeolian sand transport. Understanding the physics of these large objects made of myriad sand

grains requires a deep insight and a reasonable, physically motivated description of how granular material is transported by turbulent air flow. In Ref. [1] we formulated a new, analytically treatable transport model for wind driven sand. The main idea of our description is to divide the transported grains into two populations that we call "saltating" and "reptating" grain species. Highly energetic saltating grains make a dominant contribution to the overall mass transport. When impacting on the sand bed, they dissipate some of their energy in a complex process called splash, ejecting a cloud of reptating grains (Fig. 14.6, see also the video abstract accompanying our publication on http://youtu.be/YFqmb_fSPYI). Based on this picture we were able to derive a closed set of equations providing an analytically tractable, numerically precise, and computationally efficient model, which may deal as a starting point for applications addressing a wealth of phenomena, e.g. sand grading and its influence on ripple formation.

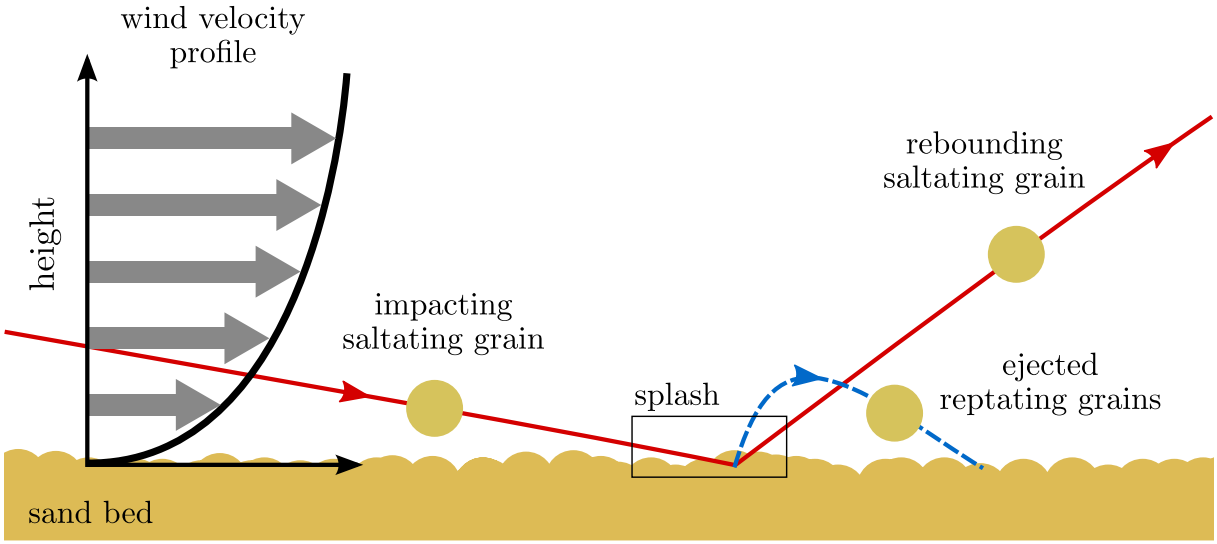

Figure 14.6: The two-species picture of aeolian sand transport: Driven by the wind, high energy grains rebound upon impact and eject a certain number of low energy grains. In our model we map the whole ensemble of trajectories onto one for the rebounded "saltating" grain and a second one for all the ejected "reptating" grains.[1]

[1] M. Lämmel, D. Rings, K. Kroy: New J. Phys. **14**, 093037 (2012) doi:10.1088/1367-2630/14/9/093037

14.9 Rapid force spectroscopy: linker dynamics

S. Sturm, O. Otto*, N. Laohakunakorn*, U.F. Keyser*, K. Kroy

*Cavendish Laboratory, University of Cambridge, UK

The experimental investigation of biomolecules through single molecule manipulation techniques often relies on DNA or other semiflexible polymers as mechanically well-characterized, readily available linkers that easily bind both to other biological

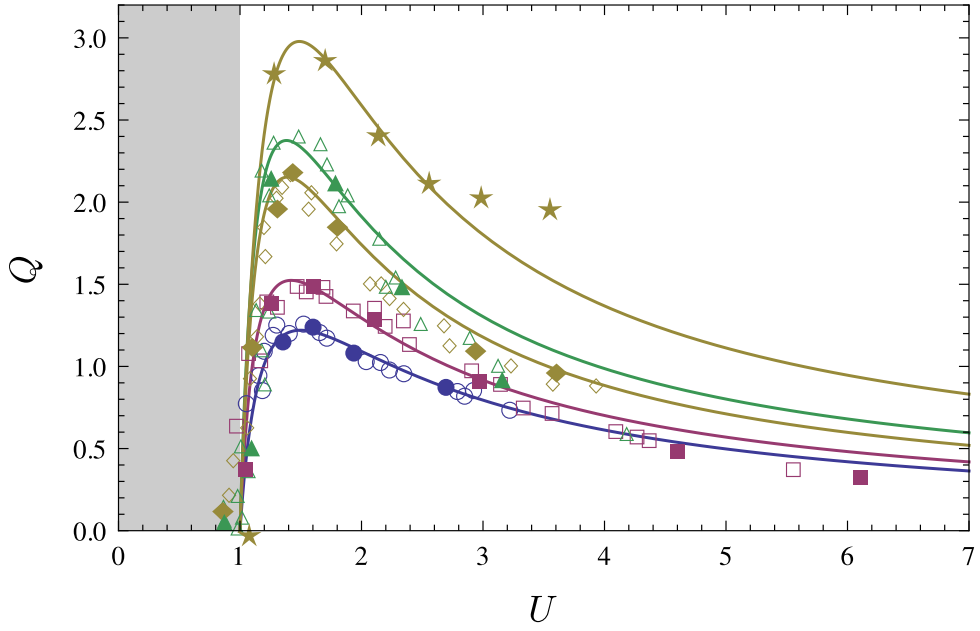

Figure 14.7: The stationary sand flux law (rescaled flux as a function of the wind strength) predicted by the two-species model in comparison to experimental data (symbols). The plot is taken from Ref. [1]

molecules and man-made structures. Whereas the strongly nonlinear stretching behaviour of semiflexible polymers is routinely taken into account, the anomalously large friction that may be generated through internal polymer dynamics has so far not been considered, although it may become a relevant factor for the analysis of high-speed force spectroscopy assays. In cooperation with experimentalists from the University of Cambridge, we provide measurements of, and a theoretical description for, the apparent relaxation timescale of a retracting "DNA handle" held on one end by an optical trap. Based on the theory of tension propagation [1] in semiflexible polymers, we also obtain a semi-empirical formula for the effective relaxation timescale that should hold for all values of polymer length, polymer stiffness, solvent viscosity or trap strength and may be used as a convenient tool for the rational design of high-speed dynamic force spectroscopy setups.

14.10 Rapid force spectroscopy: bond dynamics

J.T. Bullerjahn, S. Sturm, K. Kroy

The forcible separation of non-covalent bonds, such as in protein unfolding and ligand dissociation, can be regarded as a transition between a bound and an unbound state [2]. This two-state system can be modelled by a test particle moving in an effective free energy landscape, trying to overcome an energy barrier separating the two states. Due to external loading the unbound state is favored, which makes the escape practically irreversible. However, established models of such forced rupture [2, 3] are restricted to the adiabatic limit of small loading rates, thus making it impossible to apply them to all-atom simulations.

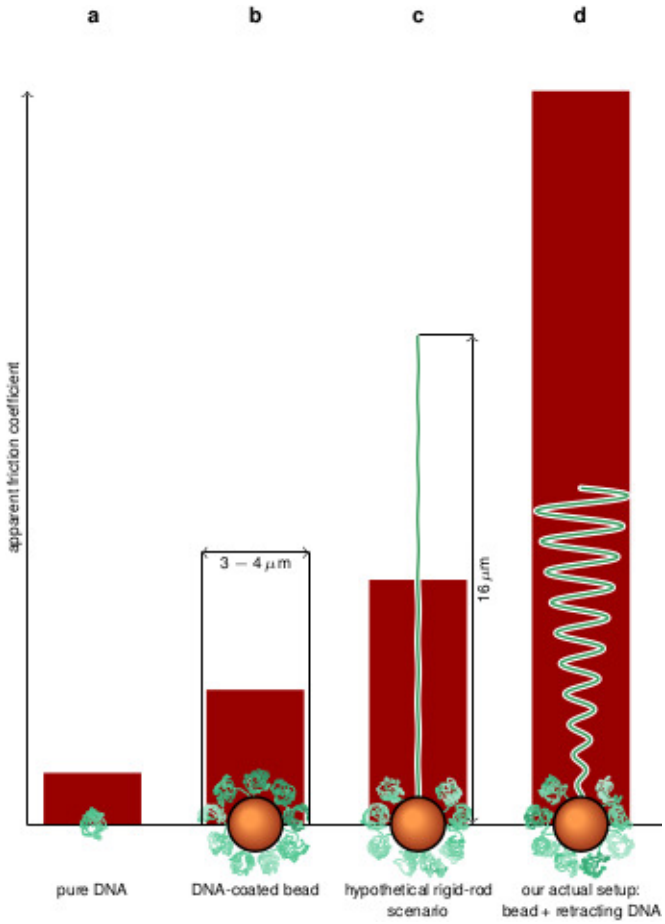

Figure 14.8: A DNA-coated, optically trapped bead relaxes exponentially upon displacement from its stable minimum position; its relaxation timescale (b) is often dominated by the bead itself, as isolated DNA winds up tightly in equilibrium, forming coils of a much smaller hydrodynamic radius than the micrometer-sized beads typically used for optical trapping and thus generating far less drag resistance (a). Fully stretching the attached DNA could increase the static friction coefficient of the DNA-coated bead and thus slow down relaxation considerably (c); a far stronger slowdown, however, is observed upon free relaxation of the attached DNA molecule (d). The plot is taken from [5] (under review).

Starting from the test particle's equation of motion, we describe its irreversible escape from a potential well, driven by a time-dependent external force protocol. Our model is analytically tractable and yields an expression for the rupture force distribution measured in dynamic force spectroscopy experiments [4], which holds for small and large loading rates alike. It can be extended to non-Markovian processes with arbitrary memory kernels and reduces to the main result of [3] in the limit of small loading rates.

[1] O. Hallatschek, E. Frey, K. Kroy: Phys. Rev. E, **75**, 031905 (2007), doi:10.1103/PhysRevE.75.031905
[2] E. Evans, K. Ritchie: Biophys. J. **72**, 1541 (1997), doi:10.1016/S0006-3495(97)78802-7
[3] O. K. Dudko et al.: Phys. Rev. Lett. **96**, 108101 (2006), doi:10.1103/PhysRevLett.96.108101
[4] M. Carrion-Vazquez et al.: Proc. Natl. Acad. Sci. **96**, 3694 (1999), doi:10.1073/pnas.96.7.3694

[5] O. Otto et al.: Nat. Commun. (under review)

14.11 Funding

Leipzig School of Natural Sciences - Building with Molecules and Nano-objects (BuildMoNa)
Prof. Dr. K. Kroy (Principal Investigator)
DFG GS 185/1

DFG FOR 877 "From Local Constraints to Macroscopic Transport"
Prof. Dr. K. Kroy (Principal Investigator)
KR 3381/2-2 and KR 3381/3-1

Landesinnovationsstipendium des Freistaates Sachsen im Rahmen des Europäischen Sozialfonds
Dipl.-Phys. J. T. Bullerjahn, Dipl.-Phys. M. Lämmel

Nonlinear Stochastically Driven Systems with Many Degrees of Freedom
R. Kürsten, M.Sc.
IMPRS Fellowship

14.12 Organizational Duties

U. Behn

- Speaker of the Condensed Matter Theory Group
- Vertrauensdozent für die Nobelpreisträgertagungen in Lindau
- Bibliotheksbeauftragter of the Faculty
- Member of PbF2
- Scientific Member of the International Max Planck Research School "Mathematics in the Sciences"
- Referee: J. Theor. Biology, Math. Biosciences and Engineering
- Reviewer: Life Science Zurich Graduate School, GK Nonequilibrium Collective Dynamics in Condensed Matter and Biological Systems TU Berlin, Institut für Kommunikation und Navigation DLR, The School of Physics Astronomy University of Manchester

K. Kroy

- Member of the graduation committee
- Study counselor for physics
- Member of PbF1 and PbF2
- PI in DFG FOR 877 and Leipzig School of Natural Sciences Building with Molecules and Nano-objects (BuildMoNa)
- Scientific Member of the International Max Planck Research School "Mathematics in the Sciences"
- Referee: Phys. Rev. Lett., Rep. Prog. Phys., Phys. Rev. E, Soft Matter, Eur. Phys. J. E., Geomorphology etc.

A. Kramer
- Scientific Coordinator DFG Research Unit 877 “From Local Constraints to Macroscopic Transport"
- Scientific Manager Graduate School BuildMoNa

14.13 External Cooperations

Academic

- Max-Planck-Institute for Mathematics in the Sciences, Leipzig
  Prof. F. Otto, M. V. Gnann
- Max-Planck-Institute for Intelligent Systems, Stuttgart
  Dr. D. Chakraborty
- University of Barcelona
  Dr. R.R.R. Vincent
- Massey University
  Prof. Dr. M.A.K. Williams, B.W. Mansel
- Cavendish Laboratory, University of Cambridge, UK
  Dr. U. Keyser, Dr. O. Otto, N. Laohakunakorn
- Joint Institute for Nuclear Research, Dubna, Russia
  Prof. Dr. N.M. Plakida
- Ernst-Moritz-Arndt-Universität Greifswald
  Prof. Dr. H. Fehske
- Institut für Klinische Immunologie
  Prof. Dr. G. Metzner

14.14 Publications

Journals

M. Lämmel, D. Rings, K. Kroy: *A two-species continuum model of aeolian sand transport*, New J. Phys. **14**, 093037 (2012)

D. Rings, D. Chakraborty, K. Kroy: *Rotational hot Brownian motion*, New J. Phys. **14**, 053012 (2012).

H. Schmidtchen, M. Thüne, U. Behn: *Randomly Evolving Idiotypic Networks: Structural Properties and Architecture*, Phys. Rev. E **86**, 011930 (2012), 18 pp

H. Schmidtchen, U. Behn: *Randomly Evolving Idiotypic Networks: Modular Mean Field Theory*, Phys. Rev. E **86**, 011931 (2012), 13 pp.

A.A. Vladimirov, D. Ihle, N.M. Plakida: *Optical and dc conductivities of cuprates: Spin fluctuation scattering in the t–J model*, Phys. Rev. B **85**, 224536 (2012)

L. Wolff, P. Fernandez, K. Kroy: *Resolving the Stiffening-Softening Paradox in Cell Mechanics*, PLoS ONE **7**, e40063, (2012), doi:10.1371/journal.pone.0040063

L. Wolff, K. Kroy, *Minimal model for the inelastic mechanics of biopolymer networks and cells*, Phys. Rew. E **86**, 040901, (2012), doi:10.1103/PhysRevE.86.040901

B. Zenker, D. Ihle, F.X. Bronold, H. Fehske: *Electron-hole pair condensation at the semimetal-semiconductor transition: A BCS-BEC crossover scenario*, Phys. Rev. B **85**, 121102(R) (2012)

Books

M. Brede, U. Behn, *Random Evolution of Idiotypic Networks: Dynamics and Architecture*, in: Unifying Themes in Complex Systems, ed. by A. Minai, D. Braha, Y. Bar-Yam (Springer Berlin Heidelberg New York 2011), 49-56.

in press

O. Otto, S. Sturm, N. Laohakunakorn, U. F. Keyser, K. Kroy: *Rapid internal contraction boosts DNA friction*, Nat. Commun. (under review)

R. R. R. Vincent, B. W. Manzel, A. Kramer, K. Kroy, M. A. K. Williams: *Micro-rheological behaviour and nonlinear rheology of networks assembled from polysaccharides from the plant cell wall* New J. Phys. **15**, 1035002 (2013), doi:10.1088/1367-2630/15/3/035002

Talks

U. Behn: *Evolution of Idiotypic Networks*, Theorie-Kolloquium, Physik Department, TU München, June 13, 2012, invited

U. Behn: *Evolution of Idiotypic Networks*, International Seminar Multi-Scale Physics of Lymphocyte Development, August 6-31, 2012, MPI PKS Dresden, August 6, 2012, invited

U. Behn: *Kickoff speach: Holism vs Reductionism, Repertoire, and Architecture of Networks*, International Seminar, Multi-Scale Physics of Lymphocyte Development, August 6-31, 2012, MPI PKS Dresden, August 6, 2012, invited

J. T. Bullerjahn: *Improved modelling of forced Kramers escape*, 5th BuildMoNa workshop for doctoral candidates, Burgstädt b. Chemnitz, Germany, September 24, 2012

K. Kroy: *Plasticity of Cells and Biopolymer Networks*, Plasticity Conference, Puerto Rico, January 2-8 2012

K. Kroy: *Hot Brownian Motion*, Theory Colloquium, Universität Erlangen, Germany, February 7, 2012

K. Kroy: *Hot Brownian Motion*, Universität Innsbruck, Austria, February 20, 2012

K. Kroy: *Stress Relaxation in Polymers*, Focus Session, DPG Früjahrestagung, Berlin, March 29, 2012

K. Kroy: *Windblown Sand, Dunes, and Dust*, Meteorologisches Kolloquium, Universität Leipzig, Mai 3, 2012

K. Kroy: *Hot Brownian Motion*, CeNS Workshop, Venezia, Italy, September 17-21, 2012

K. Kroy: *Hot Brownian Motion*, Workshop on Physics of Active Soft Matter, Universität Heidelberg, September 24-25, 2012

K. Kroy: *Hot Brownian Motion*, Theorieseminar, Universität Augsburg, Germany

K. Kroy: *Soft Mechanics - From Biopolymers to Cells*, Biochemisches Kolloquium, Universität Leipzig, October 17, 2012

K. Kroy: *The stiffening-softening paradox in cell mechanics*, Workshop on Dynamics of Tissues and Multicellular Systems, Universität Leipzig, December 14-16, 2012

M. Lämmel: *A two-species continuum model of aeolian sand transport*, DPG Frühjahrestagung, Berlin, March 28, 2012

M. Lämmel: *Nematic microstructure in gels*, 5th BuildMoNa Workshop for Doctoral Candidates, Burgstädt b. Chemnitz, Germany, September 25, 2012

M. Lämmel: *Grasping the microstructure of F-actin solutions by the tube model*, Forschungszentrum Jülich GmbH (ICS-7-Seminar), Jülich, Germany, November 12, 2012, invited

D. Rings: *Hot Brownian Motion*, Interview presentation, University of Leeds, Leeds, UK, October 10, 2012

D. Rings: *Middle world – Die langsame Revolution*, 11. MinD-Akademie, Würzburg, Germany, October 3-7, 2012

D. Rings: *Mathematica and LaTeX in Science*, SFG PhD-symposium, Meißen, June 20-22, 2012

D. Rings: *Hot Brownian motion*, Complex systems and Biological physics seminar, NORDITA, Stockholm, November 6, 2012

D. Rings: *Effective temperatures for hot Brownian particles*, SFG meeting, Chemnitz, March 20, 2012

Posters

J. T. Bullerjahn: *Forced Kramers escape with memory friction*, 5th scientific symposium of the graduate school BuildMoNa, Leipzig, March 12, 2012

J. T. Bullerjahn: *Forced Kramers escape with memory friction*, 76. DPG Frühjahrstagung, Berlin, March 25-30, 2012

J. T. Bullerjahn: *Forced Kramers escape with memory friction*, 512. WEH-Seminar Single molecule kinetics, Bad Honnef, July 29 - August 1st, 2012

F. Groß, G. Metzner, U. Behn, *Mathematical modeling of T cell regulation in allergy and specific immunotherapy*, International Seminar Multi-Scale Physics of Lymphocyte Development, August 6-31, 2012, MPI PKS Dresden

A. Kramer, R.R.R. Vincent, B.W. Mansel, K. Kroy, M.A.K. Williams *Melting of pectin gels*, Dynamics of Tissues and Multicellular Systems, Leipzig, December 14-16 , 2012

M. Lämmel, K. Kroy: *Nematic microstructure in gels*, Jülich Soft Matter Days 2012, Bad Honnef, Germany, November 13-16, 2012

M. Lämmel, K. Kroy: *Curvature distribution of entangled semiflexible biopolymers*, Fluid-Structure Interactions in Soft-Matter Systems: From the Mesoscale to the Macroscale, Prato, Italy, November 26-30, 2012

S. Sturm: *How a polymer breaks a bond*, 76. DPG Frühjahrstagung, Berlin, March 25-30, 2012

14.15 Graduations

Doctorate

- Daniel Rings
  Hot Brownian Motion
  December 2012

Diploma

- Marc Höll
  Global gekoppelte Stratonovichmodelle: Selbstkonsistente Beschreibung von Phasenübergängen im Nichtgleichgewicht
  June 2012

Master

- Rüdiger Kürsten
  Coupled Nonlinear Systems with Additive Noise: A Self-Consistent Theory
  February 2012
- Heinz Sachsenweger
  Bitstring Model for the Idiotypic Network: Automatized Pattern Identification and Simulation of Large Systems
  September 2012

Bachelor

- Sven Auschra
  Molekulardynamische Simulation heißer Brownscher Teilchen
  October 2012

14.16 Guests

- Prof. Dr. Robert Magerle
  TU Chemnitz
  November 28
- Dr. Nicholas Kurniawan
  Nat. Univ. Singapore
  September 9

15

Theory of Elementary Particles

15.1 Introduction

The Particle Physics Group performs basic research on different aspects of quantized field theories, including the description of elementary particles and in phenomenology, and their relation to gravity. Topics of current interest are, for example (the order does not indicate preference):

1) the formulation of quantum field theories on curved spacetime manifolds, including applications to cosmology, and the formulation of models which realize noncommutative geometry,

2) renormalization problems, electroweak matter at finite temperature, the lattice formulation of gauge theories, the derivation of Regge behaviour of scattering amplitudes from Quantum Chromodynamics and the related study of integrable models with and without supersymmetry,

3) higher dimensional theories of gravity, including the theory of black holes, and their holographic relationship to quantum field theories,

4) conformal symmetry and its breaking in the context of supersymmetric theories, including on curved spacetime manifolds.

A broad range of methods is applied to attack the respective questions. In perturbative quantum field theory, and for differential geometric question related to field theories on manifolds, the work is essentially analytic, using computers only occasionally as a helpful tool. Lattice Monte Carlo simulations on the other hand are based on computers as an indispensable instrument.

The respective scientific communities are organized correspondingly in a somewhat different fashion: in analytical work usually very few people collaborate, whereas e.g. in the lattice community, rather big collaborations are the rule. Our group is involved in many cooperations on the national and international level (Germany: AEI Golm, Göttingen, DESY Hamburg/Zeuthen, MPI Munich; Internationally: Armenia, France, Japan, Russia, UK, USA).

Particle theory has a noticeable impact on other branches of physics e.g. by its power of providing new methodological insight. For a student specializing in this field, an important benefit is her/his training in analysing complex situations and in developing and applying quantitative tools of mathematical nature which are appropriate for the respective problem. A background in particle physics provides a highly useful base for a broad range of employments, including in the financial industry, engineering,

consulting, insurance, and the government. Consequently, graduate students are typically highly sought after by prospective employers and hence very well-placed on the labor market. Academic jobs in particle physics are typically at universities and corresponding research institutes.

Group Leader Prof. Dr. (PhD) S. Hollands

15.2 Wilson loops of pure lattice QCD in numerical stochastic perturbation theory

H. Perlt, A. Schiller

In collaboration with authors from different locations we have continued our research programme using numerical stochastic perturbation theory (NSPT).

It is well known that lattice perturbation theory (LPT) is much more involved compared to its continuum QCD counterpart. The complexity of diagrammatic approaches increases rapidly beyond the one-loop approximation. By now only a limited number of results up to two-loop accuracy have been obtained.

Applying the standard Langevin dynamics [1, 2] to the problem of weak coupling expansions for lattice QCD, a powerful numerical approach for higher loop calculations – called numerical stochastic perturbation theory (NSPT) – has been proposed in [3]. In collaboration with the Parma and Berlin group we applied that technique to find higher loop contributions to ghost and gluon propagators in SU(3) Lattice Gauge Theory [4–6].

With collegues from the QCDSF collaboration we have calculated Wilson loops of various sizes up to 20 loops in SU(3) pure lattice gauge theory at different lattice sizes for Wilson gauge action using the technique of numerical stochastic perturbation theory [7, 8]. This allows us to investigate the perturbative series for various Wilson loops at high loop orders.

We observe differences in the behavior of those series as function of the loop order. Up to $n = 20$ we do not find evidence for the factorial growth of the expansion coefficients often assumed to characterize an asymptotic series. Based on the actually observed behavior we sum the series in a model parametrized by hypergeometric functions. Alternatively we estimate the total series in boosted perturbation theory using information from the first 14 loops. We introduce generalized ratios of Wilson loops of different sizes. Together with the corresponding Wilson loops from standard Monte Carlo measurements they enable us to assess their non-perturbative parts.

Our estimated value for the gluon condensate $\langle \frac{\alpha}{\pi} G\,G \rangle = 0.028(3)\,\mathrm{GeV}^4$ is is somewhat larger than that in the phenomenological SVZ sum rule approach [9] – at least for our 12^4 lattice. Our number agrees within errors with the estimate $0.024(8)\,\mathrm{GeV}^4$ presented by Narison in [10] which is based on a study of heavy quarkonia mass splittings.

On the basis of our present results, *nota bene* - we conclude that the perturbative series of the Wilson loops carry no information on the confining properties of the theory and the non-trivial features of the QCD vacuum. The positive aspect of this result is that the perturbative tail can be cleanly separated from the Monte Carlo results for the plaquette.

[1] G. Parisi and Y. s. Wu, Sci. Sin. **24** (1981) 483.

[2] G. G. Batrouni, G. R. Katz, A. S. Kronfeld, G. P. Lepage, B. Svetitsky and K. G. Wilson, Phys. Rev. D **32** (1985) 2736.
[3] F. Di Renzo, E. Onofri, G. Marchesini and P. Marenzoni, Nucl. Phys. B **426** (1994) 675 [arXiv:hep-lat/9405019].
[4] F. Di Renzo, E. -M. Ilgenfritz, H. Perlt, A. Schiller and C. Torrero, (I) The ghost propagator in Landau gauge," Nucl. Phys. B **831** (2010) 262 [arXiv:0912.4152 [hep-lat]].
[5] F. Di Renzo, E. -M. Ilgenfritz, H. Perlt, A. Schiller and C. Torrero, Nucl. Phys. B **842** (2011) 122 [arXiv:1008.2617 [hep-lat]].
[6] E. -M. Ilgenfritz, C. Menz, M. Muller-Preussker, A. Schiller and A. Sternbeck, Phys. Rev. D **83** (2011) 054506 [arXiv:1010.5120 [hep-lat]].
[7] R. Horsley, G. Hotzel, E. -M. Ilgenfritz, Y. Nakamura, H. Perlt, P. E. L. Rakow, G. Schierholz and A. Schiller, PoS LATTICE **2010** (2010) 264 [arXiv:1010.4674 [hep-lat]].
[8] R. Horsley, G. Hotzel, E.-M. Ilgenfritz, R. Millo, Y. Nakamura, H. Perlt, P. E. L. Rakow, G. Schierholz and A. Schiller, Phys. Rev. D **86** (2012) 054502 [arXiv:1205.1659 [hep-lat]].
[9] M. A. Shifman, A. I. Vainshtein and V. I. Zakharov, Nucl. Phys. B **147** (1979) 385.
[10] S. Narison, Phys. Lett. B **387** (1996) 162 [arXiv:hep-ph/9512348].

15.3 Perturbative subtraction of lattice artifacts in the computation of renormalization constants

H. Perlt, A. Schiller

The determination of renormalization factors is of crucial importance. They relate the observables obtained on finite, discrete lattices to their measured counterparts in the continuum in a suitable renormalization scheme. Therefore, they have to be computed as precisely as possible. A widely used approach is the nonperturbative Rome-Southampton method [1]. It requires, however, a careful treatment of lattice artifacts. They are always present because simulations are done at lattice spacings a and momenta p with ap not necessarily small.

In collaboration with people from QCDSF and Cyprus university we have started an investigation to to suppress these artifacts by subtraction of one-loop contributions in lattice perturbation theory. We compare results obtained from a complete one-loop subtraction made earlier by our collaboration [2] with those calculated for a subtraction of $O(a^2)$ [3–5]. First results have been presented at the Lattice conference 2012 [6]. A detailed report is in preparation.

[1] G. Martinelli, C. Pittori, C. T. Sachrajda, M. Testa and A. Vladikas, Nucl. Phys. B **445** (1995) 81 [arXiv:hep-lat/9411010].
[2] M. Göckeler *et al.*, Phys. Rev. D **82** (2010) 114511 [Erratum-ibid. D **86** (2012) 099903] [arXiv:1003.5756 [hep-lat]].
[3] M. Constantinou, V. Lubicz, H. Panagopoulos and F. Stylianou, JHEP **0910** (2009) 064 [arXiv:0907.0381 [hep-lat]].

[4] A. Skouroupathis and H. Panagopoulos, PoS LATTICE **2010**, 240 (2010).
[5] C. Alexandrou, M. Constantinou, T. Korzec, H. Panagopoulos and F. Stylianou, Phys. Rev. D **86** (2012) 014505 [arXiv:1201.5025 [hep-lat]].
[6] M. Constantinou, M. Costa, M. Göckeler, R. Horsley, H. Panagopoulos, H. Perlt, P. E. L. Rakow, G. Schierholz and A. Schiller, PoS LATTICE **2012** (2012) 239 [arXiv:1210.7737 [hep-lat]].

15.4 Symmetries and integrability in gauge field theories

R. Kirschner

Integrable quantum systems are applied successfully to the study of the high-energy asymptotics and of the renormalization of composite operators in gauge theories [1–4]. These application stimulated the development of the methods of integrable quantum systems.

Continuing the investigation of Baxter operator constructions of last year we studied the cases of trigonometrically and elliptically deformed symmetry and presented in [5] the constructions with and without deformations in a uniform way. The results have been formulated in explicit expressions allowing to derive the physical quantities of integrable quantum systems with rank 1 symmetry.

A simple treatment of higher rank integrable systems has been worked out in the restricted case of Jordan-Schwinger type representations [6]. In many physical applications these restriction are applicable. The calculation of perturbative scattering amplitudes is the application of much recent interest.

New attempts for the cases of symmetries based on non-simply laced algebras have been pursued in [7].

[1] L.N. Lipatov, *High-energy asymptotics of QCD and exactly solvable lattice models* Padova preprint DFPD-93-TH-70B; and
JETP Lett. B342 (1994)596.
[2] L. D. Faddeev and G. P. Korchemsky, "High-energy QCD as a completely integrable model," Phys. Lett. B **342** (1995) 311 [arXiv:hep-th/9404173].
[3] V. M. Braun, S. E. Derkachov and A. N. Manashov, "Integrability of three-particle evolution equations in QCD," Phys. Rev. Lett. **81** (1998) 2020 [arXiv:hep-ph/9805225].
[4] N. Beisert, Phys. Rept. **407** (2004) 1.
[5] D. Chicherin, S. Derkachov, D. Karakhanyan and R. Kirschner, "Baxter operators with deformed symmetry," Nucl. Phys. B **868** (2013) 652 [arXiv:1211.2965 [math-ph]].
[6] R. Kirschner, "Integrable chains with Jordan-Schwinger representations," J. Phys. Conf. Ser. **411** (2013) 012018.
[7] D. Chicherin, S. Derkachov, A. P. Isaev, "Conformal group: R-matrix and star-triangle relation," arXiv:1206.4150 [math-ph].

15.5 Overview of some research projects

S. Hollands

a) **Quantum field theories on spacetime manifolds**. Quantum field theories are normally considered on flat Minkowski spacetime. This is physically reasonable in many situations of interest, because the the spatio-temporal scales associated with reactions of elementary particles are typically much shorter than the scales set by the curvature of the universe. However, in certain situation, this is no longer the case, for example during the inflationary epoch of the Universe, or for extremely long-wavelenght "modes" comparable to the Hubble radius. In such cases, it becomes essential to study quantized field theories on curved spacetimes. An interesting background in this case is deSitter space, due to its relevance in cosmology. There have recently been some interesting controversies about the behavior of QFT's and a correspondingly large number of papers in the community. I have contributed to this with a series of foundational papers on the perturbative formulation of QFT's in this background with a particular view on questions related to long-range correlation or "quantum no-hair", which is one of the most fundamental properties in the setup.

Most recently, I have also been interested in supersymmetric versions of quantum field theories on curved manifolds. The standard approach is to proceed to supergravity theories, but these are rather problematic at the quantum level due to their "non-renormalizable character". Recently, an interesting "hybrid" situation was identified wherein one studies supersymmetric theories on certain, rather special, "supersymmetric backgrounds". In a joint work with P. deMedeiros, we have contributed e.g. towards the proper understanding of the algebraic structure underlying these symmetries.

b) **Higher dimensional gravity theories:** The modern description of (classical) gravity theory is, following Einstein, of a geometric nature, wherein gravity is viewed as a manifestation of the curvature of spacetime ("General Relativity"). Usually, and for obvious reasons, the dimension of spacetime is four (one time plus three space dimensions). However, there has been interest in the study of Einstein's equations in d dimensions almost from the beginning of General Relativity Theory. One reason is that extra dimensions arise very naturally in attempts to describe matter in a unified manner as higher excitations (modes) of the extra dimensions, via the so-called "Kaluza-Klein mechanism" and its many generalizations. In the original version of this proposal, extra dimensions remain essentially invisible because they are compact and very small in size, but other scenarios ("brane worlds") with large, yet unobservable, extra dimensions have also been proposed. Yet another, more recent, motivation for higher dimensional models arises from ideas about holography, such as the celebrated "AdS-CFT"-correspondence. At any rate, if these scenarios are to be taken seriously, then it is of interest to understand the dynamics of higher dimensional General Relativity, in particular of black holes within such theories. This has by now become a topic major in the international community. My own work has been dedicated mostly towards the important, but very complicated, problem of finding a classification of higher dimensional black hole solutions.

Recent papers:

[1] P. de Medeiros and S. Hollands, arXiv:1302.7269 [hep-th].
okular(26608)/kdecore (services) KMimeTypeFactory::parseMagic: Now parsing "/home/schiller/.local/share/mi
[2] S. Hollands, AIP Conf. Proc. **1458**, 146 (2011).
[3] S. Hollands and A. Ishibashi, Class. Quant. Grav. **29**, 163001 (2012) [arXiv:1206.1164 [gr-qc]].
[4] J. Holland and S. Hollands, arXiv:1205.4904 [math-ph].
[5] S. Hollands, Class. Quant. Grav. **29**, 205009 (2012) [arXiv:1204.3421 [gr-qc]].
[6] S. Hollands and R. M. Wald, arXiv:1201.0463 [gr-qc].
[7] S. Hollands, Class. Quant. Grav. **29**, 065006 (2012) [arXiv:1110.5814 [gr-qc]].
[8] S. Hollands and C. Kopper, Commun. Math. Phys. **313**, 257 (2012) [arXiv:1105.3375 [hep-th]].
[9] S. Hollands, Annales Henri Poincare **13**, 1039 (2012) [arXiv:1105.1996 [gr-qc]].
[10] S. Hollands, Commun. Math. Phys. **319**, 1 (2013) [arXiv:1010.5367 [gr-qc]].
[11] S. Hollands and G. Leiler, arXiv:1003.1621 [cond-mat.stat-mech].
[12] S. Hollands, J. Holland and A. Ishibashi, Annales Henri Poincare **12**, 279 (2011) [arXiv:1002.0490 [gr-qc]].
[13] S. Hollands and A. Ishibashi, Annales Henri Poincare **10**, 1537 (2010) [arXiv:0909.3462 [gr-qc]].
[14] S. Hollands and H. Olbermann, J. Math. Phys. **50**, 112304 (2009) [arXiv:0906.5313 [math-ph]].
[15] S. Hollands and R. M. Wald, Commun. Math. Phys. **293**, 85 (2010) [arXiv:0803.2003 [gr-qc]].
[16] S. Hollands and S. Yazadjiev, Commun. Math. Phys. **302**, 631 (2011) [arXiv:0812.3036 [gr-qc]].

15.6 Funding

Quantum fields and curvature
ERC-Starting Grant, 2011-2016

Higher dimensional gravity theories
Leverhulme Trust Grant (UK), 2011-2013

Wilson loops of pure lattice QCD in numerical stochastic perturbation theory
Supported partly by DFG under contract SCHI 422/8-1

Perturbative subtraction of lattice artifacts in the computation of renormalization constants
Supported partly by DFG under contract SCHI 422/8-1 and by the EU grant 283286 (HadronPhysics3)

Symmetry and integrability in gauge field theories
Supported by DAAD, university partnership with St. Petersburg

15.7 Organizational Duties

A. Schiller

- Referee: Phys. Rev. D

R. Kirschner

- Referee: Phys. Rev. D, Phys. Letters B
- Member of the PhD commission of the faculty

15.8 External Cooperations

Academic

- St. Petersburg, Nuclear Physics Institute
  Prof. L.N. Lipatov
- St. Petersburg, St. Petersburg branch of Steklov Mathematical Institute
  Dr. S.E. Derkachov
- Yerevan Physics Institute, Theory Dept.
  Prof. Ara Sedrakyan
- Soltan Institut of Nucl. Studies, Warsaw
  Dr. Lech Szymanowski
- Universität Regensburg, Inst.f. Theor. Physik
  Prof. A. Schäfer, Prof. V. Braun, Dr. M. Göckeler, Dr. A. Sternbeck
- Humboldt- Universität zu Berlin
  Prof. M. Müller-Preussker
- DESY, Hamburg
  Prof. G. Schierholz
- Edinburgh University, UK
  Dr. R. Horsley
- Department of Mathematics, Liverpool University, UK
  Dr. P.E.L. Rakow, Dr. R. Millo
- Parma University
  Prof. F. Di Renzo
- Cyprus University Nikosia
  Prof. H. Panagopoulos and collaborators
- RIKE AIS, Kobe, Japan
  Dr. Y. Nakamura
- Dubna, Russia
  Dr. E.-M. Ilgenfritz

15.9 Publications

Journals

R. Horsley, Y. Nakamura, H. Perlt, D. Pleiter, P. E. L. Rakow, G. Schierholz, A. Schiller, H. Stuben, F. Winter and J. M. Zanotti,
"Hyperon sigma terms for 2+1 quark flavours,"
Phys. Rev. D **85** (2012) 034506 [arXiv:1110.4971 [hep-lat]].

R. Horsley, G. Hotzel, E.-M. Ilgenfritz, R. Millo, Y. Nakamura, H. Perlt, P. E. L. Rakow, G. Schierholz and A. Schiller,
"Wilson loops to 20th order numerical stochastic perturbation theory,"
Phys. Rev. D **86** (2012) 054502 [arXiv:1205.1659 [hep-lat]].

R. Horsley, R. Millo, Y. Nakamura, H. Perlt, D. Pleiter, P. E. L Rakow, G. Schierholz, A. Schiller, F. Winter and J. M. Zanotti [QCDSF and UKQCD Collaborations],
"A Lattice Study of the Glue in the Nucleon,"
Phys. Lett. B **714** (2012) 312 [arXiv:1205.6410 [hep-lat]].

D. Chicherin, S. Derkachov, D. Karakhanyan and R. Kirschner,
"Baxter operators for arbitrary spin,"
Nucl. Phys. B **854** (2012) 393 [arXiv:1106.4991 [hep-th]].

D. Chicherin, S. Derkachov, D. Karakhanyan and R. Kirschner,
"Baxter operators for arbitrary spin II,"
Nucl. Phys. B **854** (2012) 433 [arXiv:1107.0643 [hep-th]].

D. Chicherin, S. Derkachov, D. Karakhanyan and R. Kirschner,
"Baxter operators with deformed symmetry,"
Nucl. Phys. B **868** (2013) 652 [arXiv:1211.2965 [math-ph]].

Proceedings

M. Constantinou, M. Costa, M. Göckeler, R. Horsley, H. Panagopoulos, H. Perlt, P. E. L. Rakow, G. Schierholz and A. Schiller,
"Perturbative subtraction of lattice artifacts in the computation of renormalization constants,"
PoS LATTICE **2012** (2012) 239 [arXiv:1210.7737 [hep-lat]].

R. Kirschner,
"Integrable chains with Jordan-Schwinger representations,"
J. Phys. Conf. Ser. **411** (2013) 012018.

Author Index

E

F

G

H

I

J

K

L

M

N

O

P

R

S

T

U

V

W

Y

Z

Jörg Kärger, Douglas M. Ruthven,
Doros N. Theodorou

WILEY-VCH

Diffusion in Nanoporous Materials

Volume 1

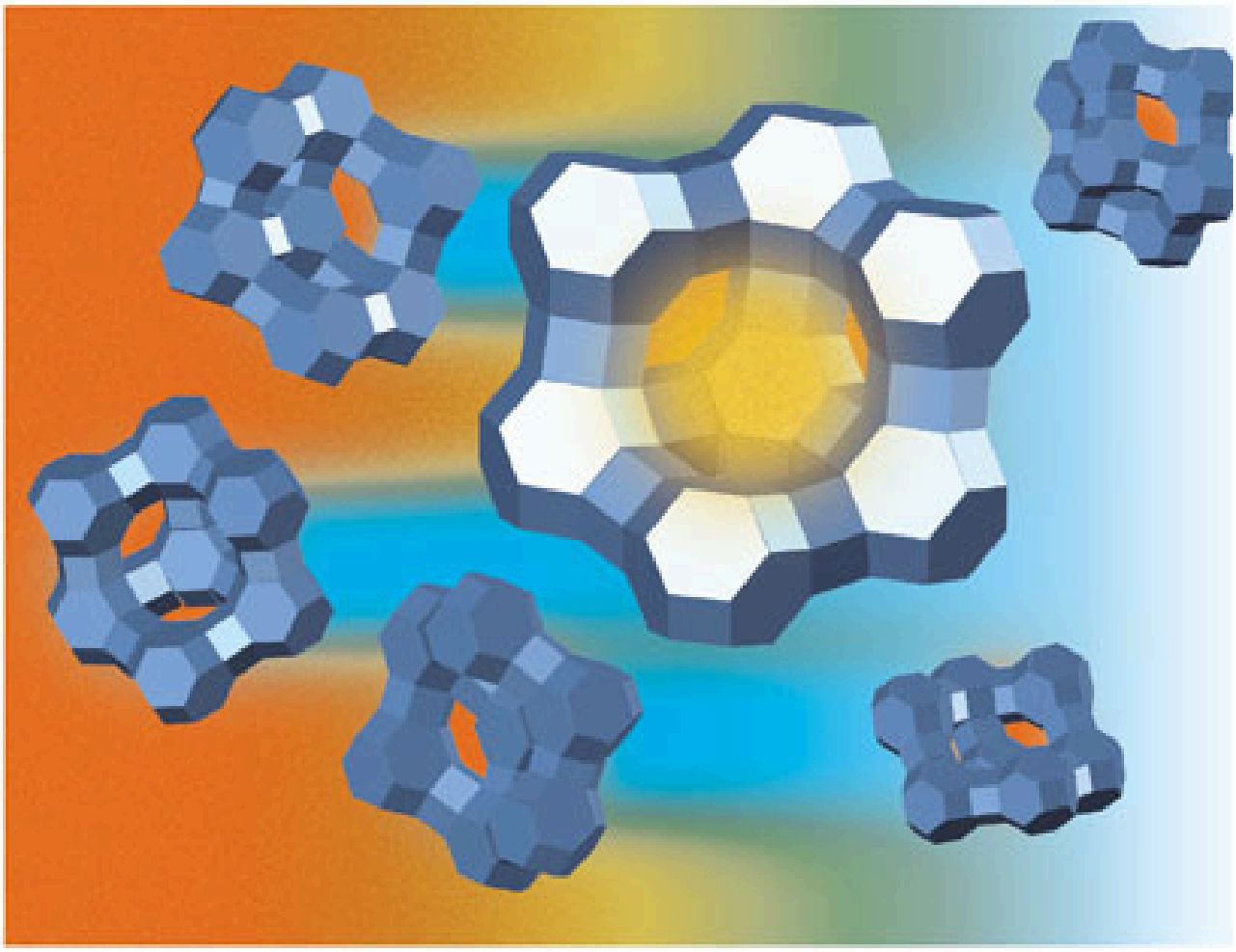

The European Physical Journal

volume 216 · January II · 2013

EPJ ST

Recognized by European Physical Society

Special Topics

C. von Ferber, Yu. Holovatch, I. Mryglod and G. Oshanin (Eds.)

From Brownian Motion to Self-Avoiding Walks and Lévy Flights

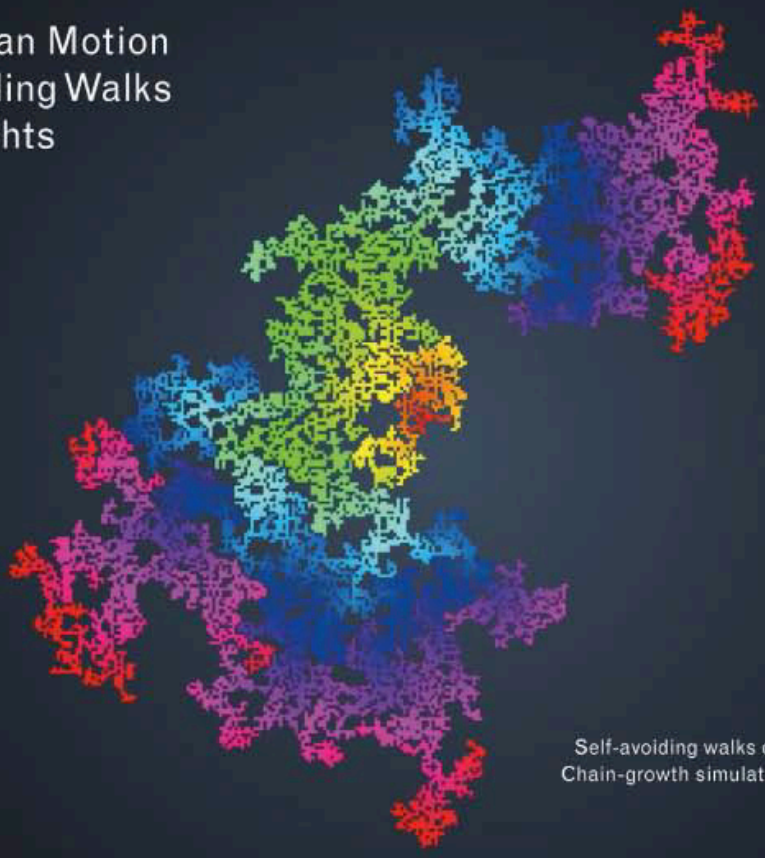

Self-avoiding walks on strongly diluted lattices: Chain-growth simulations vs. exact enumeration
p. 176
by N. Fricke and W. Janke

edp sciences

Springer